# Solution-state Anion Binding Studies of Urea- and Amide-based Hydrogen-bonding Receptors for the Design of Supramolecular Assemblies

**Dermot Gillen B.A. (Mod.)**

2019

**Trinity College Dublin**

**The University of Dublin**

*A thesis submitted to the School of Chemistry,*

*Trinity College Dublin, the University of Dublin*

*for the degree of Doctor of Philosophy*

Based on research carried out under the direction of

**Prof. Thorfinnur Gunnlaugsson**

# Declaration

I declare that this thesis has not been submitted as an exercise for a degree at this or any other university and it is entirely my own work. I agree to deposit this thesis in the University's open access institutional repository or allow the Library to do so on my behalf, subject to Irish Copyright Legislation and Trinity College Library conditions of use and acknowledgement.

Signed: _____

# Abstract

This work investigates urea- and amide-based hydrogen-binding systems as small-molecule anion-binding receptors, as part of a project in the Gunnlaugsson group to develop complex molecular assemblies built around the urea–anion interaction. Chapter 1 introduces the concepts of anion binding, templating and directing, and discusses the utility of molecular assemblies, interlocked structures and urea-based anion-binding receptors, specifically in the context of recent advancements in supramolecular chemistry. An overview of anion–receptor clusters is provided, with a focus on helicates and barrels.

In Chapter 2, the anion binding behaviour of a series of novel electron-rich derivatives of the *meta*-phenylene bis(phenylurea) motif is analysed in detail through $^1$H NMR titrations with the tetrabutylammonium salts of a range of anions. The *meta*-phenylene bis(phenylurea) motif is shown to bind anions such as dihydrogenphosphate, benzoate and acetate in 1:2 host–guest stoichiometries. No electronic effect due to the substitution patterns on the distal aromatic rings is observed. The adducts of these receptors with phosphate and acetate anions in the crystalline-phase is discussed, including a novel triple stranded phosphate-centred helicate. Part of Chapter 2 has been published in *The Journal of Organic Chemistry* (**2018**, *83*, 10398–10408).

Chapter 3 investigates the trends in binding behaviour of the simple di(3-amidophenyl)urea motif with varying aliphatic chain length. Two new receptors are developed as negative controls in this experiment. The titrations of the 3-, 6- and 11-carbon chain receptors with dihydrogenphosphate, benzoate and sulfate are discussed in detail, and in comparison to preliminary results which have been previously reported.

In Chapter 4, the synthesis and characterisation of two classes of $H_6$–hexadentate receptor molecules is presented, which combine the structural elements of the receptors studied in Chapters 2 and 3. The attempted syntheses of macrocyclic derivatives of the *ortho* isomers is also discussed. The binding affinities of these molecules towards dihydrogenphosphate and benzoate anions is quantified and compared. The *ortho* isomers are shown to bind both anions in the expected 1:1 host–guest stoichiometry, while this is 1:2 for the *meta* isomer. A discussion on the complexation-induced shift of the latter is also featured.

The conclusions for this work are presented in Chapter 5, while Chapter 6 describes the experimental details of the work presented herein. The combined references for this thesis are found in Chapter 7. Additional details may be found in the appendices, including synthesis and characterisation (A1), titration and fitting data (A2) and publications (A3).

*Two things to remember Dermot:*

*only answer the question you're asked;*

*and above all, enjoy yourself!*

— My mother, before every exam I've ever walked in to.

# Acknowledgements

positivity, and for letting me steal your couch in Switzerland. Speaking of Swizerland and veritable fountains of positivity, Gearóid, I owe so much for your crash-courses in lanthanide $m_j$ states and magnetic anisotropy tensors during the halcyon days of review-writing. I hope that Switzerland and its food are keeping you sane. Meanwhile, I think I'm going to take you up on your advice and go smash some plates after this!

Sam, I've asked so much of you these past years, and you've always done so much more. I don't know what I would have done without your insight and assistance. Thank you for correcting well-over half of this thesis, and for flying in from Italy with the corrections for the Introduction. Thank you Anna, for sending important papers my way, for our emergency brainstorming sessions on how best to do a titration, and for the conversations on food and gardening – which is of course the most important, because if you want to write a thesis, «*ci vuole un fiore*». 🎵 I wish both of you every happiness in your journey through life together.

"Gracias, mi amiga Sandra, eres la mejor química del ~~universidad entera~~." Perhaps the [*universo entero (sorry Fergus)*] only person I know who actually uses the 🍆 emoji to mean "aubergine", you are sweet and thoughtful and ridiculously hard-working. Amy, from my unsubtle hints in First Year, *via* the hand-in-face incident, through to angry WhatsApp messages, the "let's just buy Camile" dinner invitations, and finally forgetting to buy the tequila for your submission; you sure have had to put up with a lot from me. Hopefully I can make us even on our trip to visit Sandra in Madrid! It's with great sadness that Espandramot/Dermamy/Dermandramy must now go our separate ways. It's been fun with phen, derpy with terpy, and maybe even trippy with bpy. Let's never be strangers. 😊

*Heeeeeeey* Elena, thanks for your assurances when times were tough, and for accidentally teaching me the more important parts of my Spanish vocabulary. Jason, it was a II-2. Emanuele, they're all called oranges. Sachi, you're the most generous person I know, thanks for the tea, and the loan of your laptop! June, I promise I'll have you over for dinner soon! Isabel, I hope that you had a good time in Athlone, make sure to make a return visit sometime so I can show you the sights (read: Sean's Bar)! Thank you for your timely suggestion of the rewrite of Chapter 3. It's something I can be much more proud of now. I'm glad you're back to keep Hannah company, and Bruno never started wearing that wig to act as replacement. Hannah, sorry I broke your heart with my terrible terrible crystal, best of luck in this last stretch. Bruno… *behave yourself*, be the Glupaya Czarevna you know in your heart you are. Thanks and sorry to Shauna and Deirdre for leaving you out of this first time round #totesawks Thanks to "Baby Niamh" Murphy, for being a great student and keeping in touch! Irene, sorry I couldn't help you out when you started, hopefully this thesis

acts as a guidebook. Fergus, congratulations! I'm so happy for you guys. You've always been a great friend/lab mate, even so far as to put up with me singing *Oklahoma* at the top of my voice in the evenings. I still consider myself invited over for dinner…

Keith, we made it through the four years! Apparently, there's nothing like trying not to laugh at silly jokes in the library to kindle a friendship, and nothing like doing a PhD at the same time to cement it. Best of luck in your Post-doc! Thanks to David Alexander Robinson for allaying my fears of "looking like a pretentious w****r" for including the *Ozymandias* quote. Although, considering we know each other through Schols, that's not saying much, is it!? Nathan, thanks for what were a great two years. Best of luck with getting through this; if I can do it, you definitely can too.

To the editing team: Chris Hawes, Samuel Bradberry, Isabel Hegarty, Hannah Dalton (Garamond, you say?), Savyasachi Aramballi Jayanth, Jason Delente (even though I lost your corrections), Dawn Barry, Emanuele Cappello, Adam Henwood, Samuel Bradberry again, June Lovitt, and finally Samuel Bradberry. For your help, insight and support, I give 200 points each to Ravenclaw. To the Tea Tuesday group: with permanent members Donal Eile Foley🐘 and The Malevolent Entity, Ciara [pronoun] McGlynn🕷; sometime members Aoife McCloskey🦒, Emmet Sheerin🐑 and Felim Vajda🦊; and members emeriti Robbie Noonan and Aaron Benson🐻. For keeping me sane and keeping me around, five points per person-day go to Hufflepuff. Let's call it a tie. Kim🐧, Lorcán🐁, Árann🐵– even though I haven't visited you all, I promise I still hope to do it soon!

Thanks Mum, you've been my biggest supporter all the way and it's meant the world to me. From the early days of popping out for lunch during the Junior Cert exams, you've always instilled in me the importance of both doing the job well, and somehow enjoying myself. Thanks for always thinking of me and for the little packages for bringing back up to Dublin. Sorry about the delay on that congratulations card you have sitting at home for me, I know you've been looking forward to celebrating! I hereby give you free rein to make endless jokes about me being two months late for everything. Sean – I'm joining you as Little Doc! Whoop-whoop! Now we can make fun of Ang for being No Doc… OK, I know you're the real one. Thanks for trekking across the world the last few years to spend Christmas with us, you being there has really made home that bit more special. Thanks for your generosity, and the thoughtful hand-made gifts. Best of luck with the upcoming exams, I believe in you! Angela, thanks for being the sensible big sister who's always there on the other end of the phone, and who's always welcomed me to visit. Thanks for engaging Cranky Boss Face 👹 ™ when it was needed, and for the most wonderful birthday in Kyoto (and all around Japan!

# Dedication

Throughout my life, there have been many people who helped me along the way. Regrettably, some of these people have recently passed away. This thesis is dedicated to all those who have made me who I am today, but particularly in memory of Dr Paraic James (DCU), Ms Maureen Dooley (Marist College Athlone) and my dear father, Patrick Gillen. It's hard to find a fitting tribute to the memory of my Dad; hopefully this thesis, and the four years of work that went into it, will do. You'll forever be in my heart,

With love,
Dermot

# Abbreviations

Compound abbreviations, and SI accepted units and prefixes have been omitted.

| | |
|---|---|
| A | Hydrogen-bond acceptor |
| *ca.* | *Circa*; approximately |
| *cf.* | *Confer*; compare |
| CD | Circular dichroism |
| CN | Coordination number |
| CPL | Circularly polarised luminescence |
| D | Hydrogen-bond donor |
| dec | Decomposed |
| *e.g.* | *Exempli gratia*; for example |
| *et al.* | *Et alii*; and co-workers |
| *etc.* | *Et cetera*; and so on |
| FWHM | Full width at half-maximum |
| $h\nu$ | Light radiation; $E = h\nu$ |
| H:G | Host–guest stoichiometry |
| *i.e.* | *Id est*; in other words |
| *in vacuo* | Under vacuum |
| LAG | Liquid-assisted grinding |
| lit. | Literature value |
| lp | Lone pair of electrons |
| *m* | *Meta* |
| MOF | Metal–organic framework |
| m.p. | Melting point |
| *o* | *Ortho* |
| *p* | *Para* |
| Ref. | Reference |
| rt | Room temperature |
| sat. | Saturated |
| UV | Ultraviolet |
| *via* | By means of |
| $2\theta$ | X-ray scattering angle |

**Thermodynamics:**

| | |
|---|---|
| *a* | Thermodynamic activity |
| *G* | Gibbs free energy |
| *K* | Stepwise stability constant |
| $K_a$ | Acid dissociation constant |
| $K_{aH}$ | Dissociation constant of the conjugate acid |
| $K_b$ | Base dissociation constant |
| pH | $-\log_{10} a_{H_3O^+} \approx$ $-\log_{10}[H_3O^+]$ |
| $pK_a$ | $-\log_{10} K_a$ |
| $pK_{aH}$ | $-\log_{10} K_{aH}$ |
| $pK_b$ | $-\log_{10} K_b = 14 - pK_{aH}$ |
| $\alpha$ | Cooperativity constant |
| $\beta$ | Cumulative stability constant |
| $\sigma_m / \sigma_p$ | Hammet substitution parameter |

**Computational Chemistry:**

| | |
|---|---|
| DFT | Density functional theory |
| MMFF94 | Merck molecular force field, 1994 |
| MM2 | Second molecular mechanics force field |

**Statistics:**

| | |
|---|---|
| $\nu$ | Statistical degrees of freedom |
| $\rho$ | Correlation coefficient |
| $\sigma$ | Standard deviation of the sample |

| **MS** | **Mass Spectrometry** |
|---|---|
| APCI | Atmospheric pressure chemical ionisation |
| calcd | Calculated |
| ESI | Electrospray ionisation |
| HRMS | High-resolution mass spectrometry |
| M | Molecular/Parent ion |
| $m/z$ | Mass to charge ratio |
| TOF | Time of flight |

| **NMR** | **Nuclear Magnetic Resonance** |
|---|---|
| app | Apparent peak shape |
| COSY | Correlation spectroscopy |
| d | Doublet |
| DEPT | Distortionless enhancement by polarisation transfer |
| HMBC | Homonuclear multiple bond correlation |
| HSQC | Heteronuclear single quantum coherence |
| *J* | Coupling constant |
| m | Multiplet |
| NOE(SY) | Nuclear Overhauser effect (spectroscopy) |
| q | Quartet |
| quat. | Quaternary carbon |
| ROE(SY) | Rotating-frame nuclear Overhauser effect (spectroscopy) |
| s | Singlet |
| t | Triplet |
| $\delta$ | Chemical shift |
| $\Delta$ | Overall change (as in $\Delta\delta$) |

| | | | | |
|---|---|---|---|---|
| **IR** | **Infra-red** | CTAB | Cetyltrimethylammonium bromide |
| ATR | Attenuated total reflectance | | |
| FTIR | Fourier transform infra-red | DMAP | *N,N*-Dimethylaminopyridine |
| m | Medium | DMF | Dimethylformamide |
| s | Strong | DMSO | Dimethyl sulfoxide |
| str. | Stretch | DMSO-$d_6$ | Hexadeuterodimethyl sulfoxide |
| w | Weak | dpa | Dipicolylamide |
| $\bar{\nu}$ | Wavenumber; $1/\lambda$ | DNA | Deoxyribonucleoic acid |
| $\bar{\nu}_{max}$ | Wavenumber at peak maximum | EDC | 1-Ethyl-3-(3-dimethylamino-propyl)carbodiimide |

**Units:**

| | | | |
|---|---|---|---|
| Å | Ångstrom; $10^{-10}$ m | Et | Ethyl |
| eq. | molar equivalent | Emim$^+$ | 1-Ethyl-3-methylimidazolium cation |
| h | hour | | |
| Hz | Hertz; s$^{-1}$ | en | Ethylene diamine |
| mol% | mole percent | Me | Methyl |
| ppm | parts per million; Hz/MHz | PDI | Perylene diimide |
| ppb | parts per billion; 0.001 ppm | PEG | Poly(ethylene glycol) |
| | | PPi | Pyrophosphate anion |
| | | R | Arbitrary functional group |

**Chemical Abbreviations:**

| | | | |
|---|---|---|---|
| ATP | Adenosine triphosphate | RNA | Ribonucleic acid |
| Ac | Acetyl | TBA$^+$ | Tetrabutylammonium cation |
| Boc | *tert*-Butoxycarbonyl | TFA | Trifluoroacetic acid |
| btp | Bistriazolyl pyridine | THF | Tetrahydrofuran |
| Bz | Benzoyl | TMA$^+$ | Tetramethylammonium cation |
| CBPQT | Cyclobis(paraquat-*p*-phenylene) | tren | Tri(2-aminoethyl)amine |
| CD | Cyclodextrin | trigol | Tri(ethylene glycol) |
| | | UPy | Ureidopyrimidine |
| | | X | Arbitrary halogen or chalcogen |

# Table of Contents

*The White Rabbit put on his spectacles.*

*"Where shall I begin, please your Majesty?" he asked.*

*"Begin at the beginning," the King said, gravely,*

*"and go on till you come to the end: then stop."*

— Carroll, L. Chapter XII: Alice's Evidence. In *Alice's Adventures in Wonderland;*

McMillan & Co.: London, 1866, p 182.

# Chapter 1

# Introduction

## 1.1   Molecular Assemblies and Interlocked Systems

Supramolecular chemistry provides access to a vast array of molecular assemblies possessing geometries that can be difficult or impossible to achieve through the synthesis of discrete covalent molecules. The potential applications of such supramolecular assemblies are many, including the separation of chemical substances, storage and release of gases, selective catalysis, molecular sensing, controlled drug delivery, and stimuli-responsive materials. These assemblies take the form of metal– and supramolecular–organic frameworks (MOFs, SOFs), cages, soft materials such as gels, and molecular machines, which offer programmed responses to stimuli on the nanoscale. The award of the 2016 Nobel Prize in Chemistry to Sauvage, Stoddart and Feringa for "the design and synthesis of molecular machines" has attracted much interest in the latter.[1] Macroscopic machines may be broken down into 'kinematic pairs', fundamental links in which two components are constrained to defined degrees of freedom such that their motion follows 'useful' paths.[2] The pursuit of molecular machinery has led, inevitably, to attempts at mimicking their macroscopic counterparts through molecular systems capable of undergoing motion constrained through either covalent linkages or the interlocking of components.[3–5]

Interlocked molecules offer familiar examples of constraint in chemical systems. The rotaxane is a direct mimic of a wheel (Latin: *rota*) on an axle (*axis*); and the catenane, a series of rings forming a chain (*catena*). Molecular knots are similarly constrained, and can perform similar functions to rotaxanes and catenanes.[6,7] The natural world provides clues as to the possible uses of such systems. The bacteriophage HK97s capsid is protected from harsh conditions *via* a polycatenane "molecular chainmail" comprised of interlocked protein rings.[8] Topoisomerase enzymes convert DNA between normal (coiled), supercoiled and interlocked (knotted and catenated) topological isomers, thereby modulating the rate of transcription and activity of genes.[9,10] The restriction of the movement of dissolved polymer strands through entanglement or intermolecular interactions can change the physical properties of the bulk medium, and the increase in viscosity due to these supramolecular interactions eventually leads to the gelation of the solution.

The increase in complexity introduced by interlocking or entangling molecular components leads to the use of additional chemical and mathematical notation. The descriptors catenane and rotaxane are normally preceded by the number of interlocked components in square brackets, *i.e.* Figure 1.1a shows a [2]rotaxane. It is occasionally useful to describe knots and links using the Alexander–Briggs notation $M_O^N$ (*M* crossings, *N*
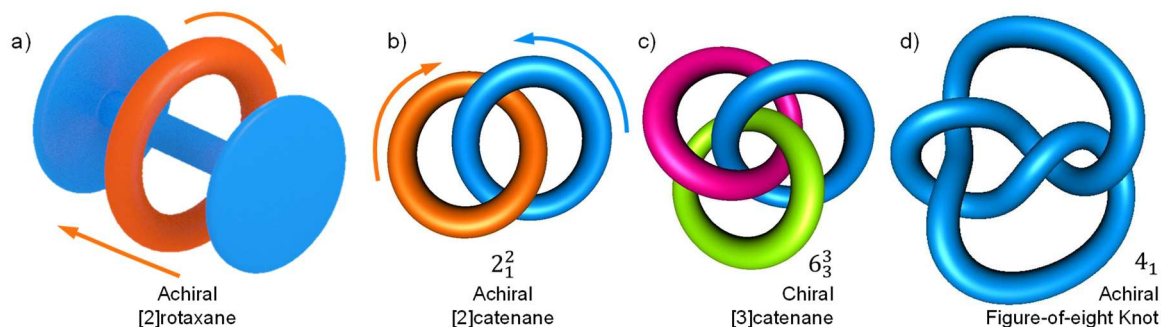
Figure 1.1. Representation of a [2]rotaxane (a), a [2]catenane ($2_1^2$, b), a [3]catenane ($6_3^3$, c), and the figure-of-eight knot ($4_1$, d), showing the inherent topological chirality of each shape. The degrees of freedom in the first two examples are depicted with arrows. Note that if the molecular structures of the [2]rotaxane and [2]catenane possess directionality or asymmetry along the direction defined by these arrows, the assemblies will also become chiral. Knot representations created using KnotPlot.

components and order $O$), and this is explained in a recent review by Gil-Ramirez *et al.*[11] A selection of simple links and knots are shown in Figure 1.1.

The work presented herein is part of a project in the Gunnlaugsson group to develop interlocked structures and complex molecular assemblies, built around the urea–anion interaction. This thesis concerns the synthesis of suitable urea-based receptors for such applications. In the following sections, the utility of interlocked structures, urea-based molecules and anion-binding receptors will be discussed, specifically in the context of recent advancements in supramolecular chemistry.

## 1.1.1 Functionality and Applications of Interlocked and Entangled Systems

The complex topologies of interlocked and entangled molecules also introduce the possibility of other molecular properties and functions which are not present in the individual components, such as pure topological chirality, see Figure 1.1.[12] In particular, two important functions which arise from the entanglement of such molecular assemblies are the manner in which motion may be controlled to perform a particular purpose, and the manner in which a component may 'shield' one that it surrounds from interacting with the bulk medium. These two functions have been used for diverse applications, as set out below.

Lewandowski *et al.* developed a [2]rotaxane machine [**1·2**] that synthesises predetermined peptide sequences through the successive removal of amino acids attached to the rotaxane axle, Scheme 1.1.[13,14] The amino acids act as stoppers, constraining the macrocycle until it performs the next set of reactions, until the eventual slippage of the peptide-linked macrocycle. Useful work therefore occurs along the longitudinal axis of the assembly. This "prismatic" behaviour is shared by two-station molecular shuttles,[4,15,16] and
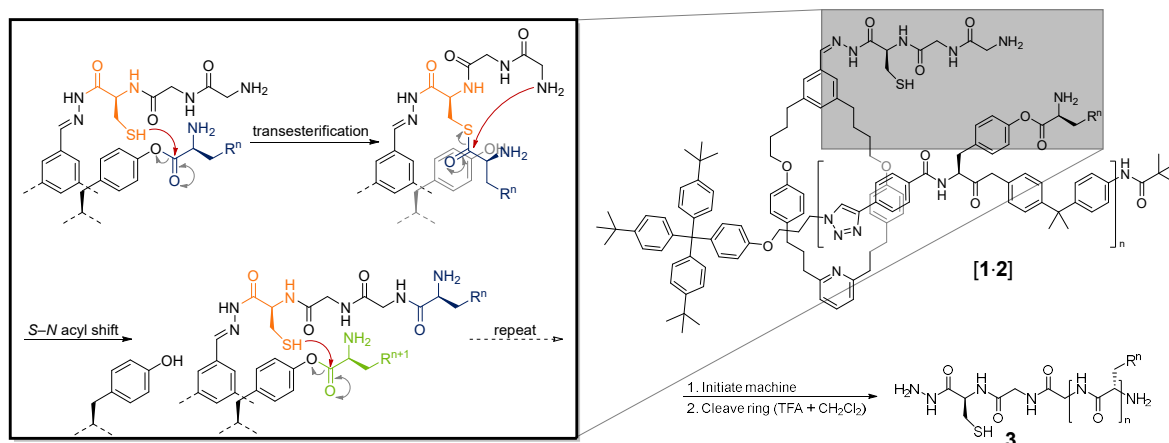
Scheme 1.1. Synthesis of a peptide (**3**) by the rotaxane-based machine [**1·2**].

the extension and contraction of daisy-chain molecules, which are designed as molecular muscle mimics.[7,16]

The conformational freedom of linked β-cyclodextrin (β-CD) units threaded on poly(ethylene glycol) (PEG) chains bestows remarkable bulk properties, Figure 1.2a.[17,18] Similar to the daisy-chain molecules noted above, these polyrotaxane assemblies allow the bulk material to readily change shape. In this case, stress distributes evenly throughout the entirety of the topological material, leading to gels with high swelling power, and
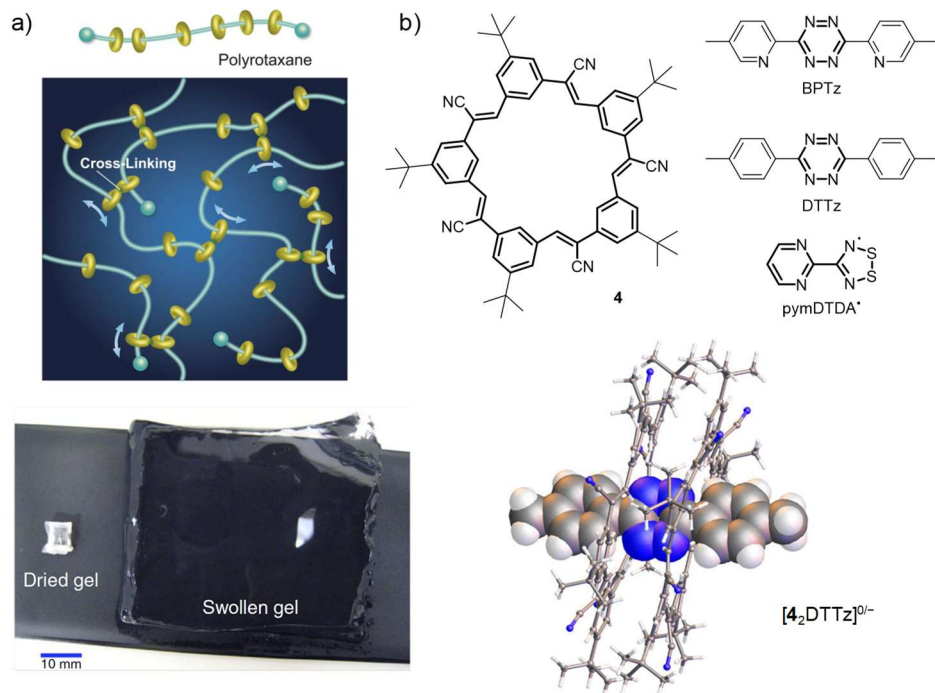


Figure 1.2. a) A schematic of a slide-ring material, and an example of a slide-ring gel, with high swelling power. Figures reproduced in part from reference 17 under a Creative Commons Attribution-NonCommercial-NoDerivs Licence and reference 18 under a Creative Commons Attribution 4.0 International Licence. b) Highly reactive tetrazine (BPTz, DTTz) and dithiadiazolyl (pymDTDA) radical anions are stabilised within the core of the cyanostar-based [3]rotaxane assembly. The crystal structure of [**4**$_2$·DTTz]$^{0/-}$, with unassigned charge. Figure reproduced in part from reference 19, copyright 2016 American Chemical Society

applications such as scratch-resistant coatings. Such properties are impossible to achieve with non-interlocked systems.

Flood and coworkers have exploited the insulating effect that macrocycles have on threaded components to study otherwise unstable tetrazine radical anions within the axle component of a [3]rotaxane, Figure 1.2b.[19] The radical half-life was extended from 2 h to more than 20 days, with electron paramagnetic resonance (EPR) spectroscopy and cyclic voltammetry (CV) experiments being performed on the stabilised species. Tentative results suggested that the radical species was present in crystalline samples of the [3]rotaxane. Similarly, molecular wires can be protected from external interactions by wrapping them in a molecular sheath.[20] Polyrotaxane assemblies of threaded β-cyclodextrins, cucurbit[n]urils or cyclophanes have been used to shield molecular wires, while others have entangled the wire within a helical polymer such as amylose, or grafted a helical chain onto the ends of the wire.[20] As such, the second interlocking moiety may inhibit or disguise the chemical or physical characteristics of a molecule. Chiu *et al.* trapped the perylenediimide (PDI) derived low molecular weight gelator **5** within a photo-degradable rotaxane assembly [**5·6**], producing a liquid system in which the PDI cores cannot interact through π–π stacking. Upon irradiation with light, **5** is released from the assembly, triggering localised gelation, Figure 1.3.[21]

It can be seen from the above examples that interlocked molecules have a broad array of functions and uses. The question of how to achieve such an interlocked system in the first
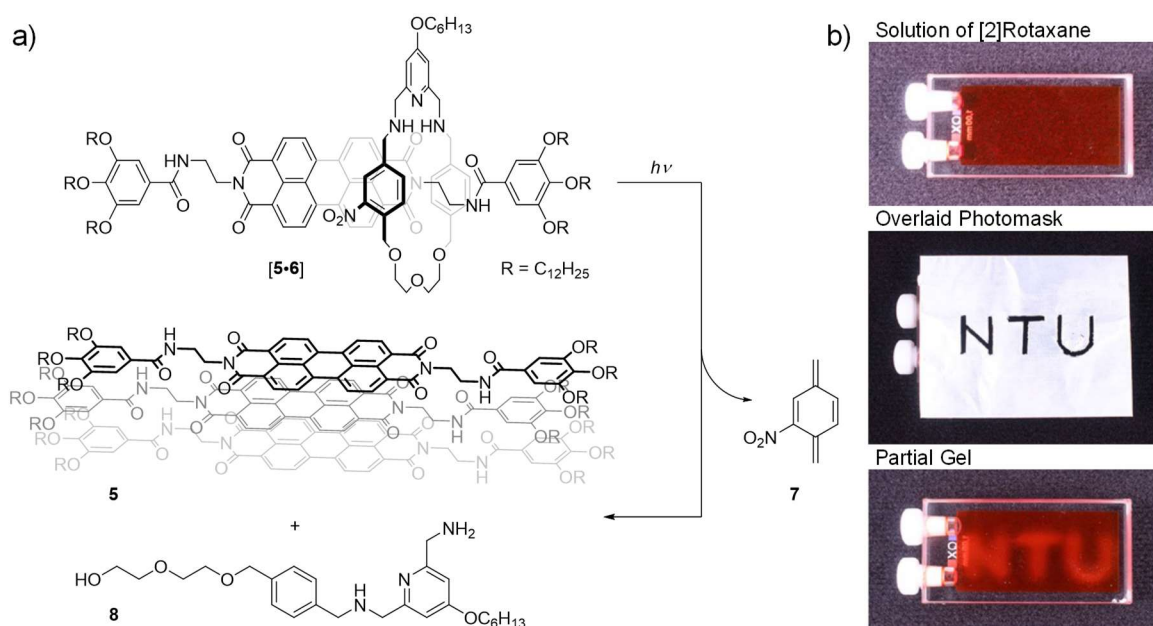


Figure 1.3. a) The rotaxane [**5·6**] undergoes ring opening upon irradiation with light, freeing the perylenedimide gelator **5**. b) Photomasking of a sample of rotaxane-containing solution with paper, and partial gelation in the non-photomasked region. Image adapted from reference 21. Copyright 2018 Wiley-VCH Verlag GmbH & Co. KGaA, Weinheim.

place has yet to be discussed. While the individual components may be locked together through adding bulky terminal groups to one component (stopping) or closing its ends into a ring (clipping), the components must first be brought together. This is the most important step in the formation of the interlocked molecule and several strategies exist to achieve this.

## 1.2   Supramolecular Templates and Directing Effects

Templating or directing effects are required to bring the components together to reliably produce useful quantities of interlocked product. The earliest example of a rotaxane, by Harrison *et al.*, was achieved with a yield of only 6% after seventy reaction cycles, due to the reliance on statistical pseudorotaxane formation.[22] In the context of this thesis, a template is a component which causes the formation of an assembly from discrete parts, and a 'directing effect' is exerted by a component which drives the assembly to assume a particular formation. The formation of these assemblies are achieved by taking advantage of various types of intermolecular interactions.

Lehn reported the Fe(II)-templated $[6]^2$circular helicate $[Fe_6\mathbf{9}_6]^{12+}$ in 1997,[23] see Scheme 1.2b. The presence of $Cl^-$ anions, however, would direct the helicate formation towards the pentamer $[(Cl)(Fe_5\mathbf{9}_5)]^{9+}$.[24] Leigh and coworkers later made subtle changes to the bipyridine-derived ligands to permit the linking of the strands. The aldehyde-terminated ligand **10** and a diamine were assembled with Fe(II) and $Cl^-$ ions using Schiff-base chemistry to yield the complex $[(Cl)(Fe_5\mathbf{11})]^{9+}$. Subsequent removal of the iron template afforded a single-molecule pentafoil knot, Scheme 1.2d.[25] The "Star of David" [2]catenane $[\mathbf{12}_2]$ (a $6_1^2$ link) was synthesised by performing ring-closing metathesis (RCM) on the assembly $[Fe_6\mathbf{13}_6]^{12+}$, formed under chloride-free conditions, and demetallation of the resulting [2]catenate $[Fe_6\mathbf{12}_2]^{12+}$; a catenate is a precursor to a catenane in which the rings remain connected *via* a template.[26] Leigh and coworkers later adapted this RCM procedure for the synthesis of pentafoil knots, which were in turn used as bromide-abstraction reagents due to their high affinity for halide anions.[27] The development of these novel structures was predicated on Lehn's discovery of the circular helicates $[Fe_6\mathbf{9}_6]^{12+}$ and $[(Cl)(Fe_5\mathbf{9}_5)]^{9+}$ several years prior. The availability of a variety of templating and directing strategies transforms an intricate problem of chemical synthesis into one more similar to engineering. The development of new supramolecular synthons into parts of a reliable toolkit is an important step in facilitating the synthesis of novel supramolecular systems and topological materials.

There are a variety of classes of supramolecular interactions which have been used to template or direct the formation of assemblies.[3,11,28,29] For example, the coordination chemistry of *d*-metal ions is well known, and these have found widespread use as templates
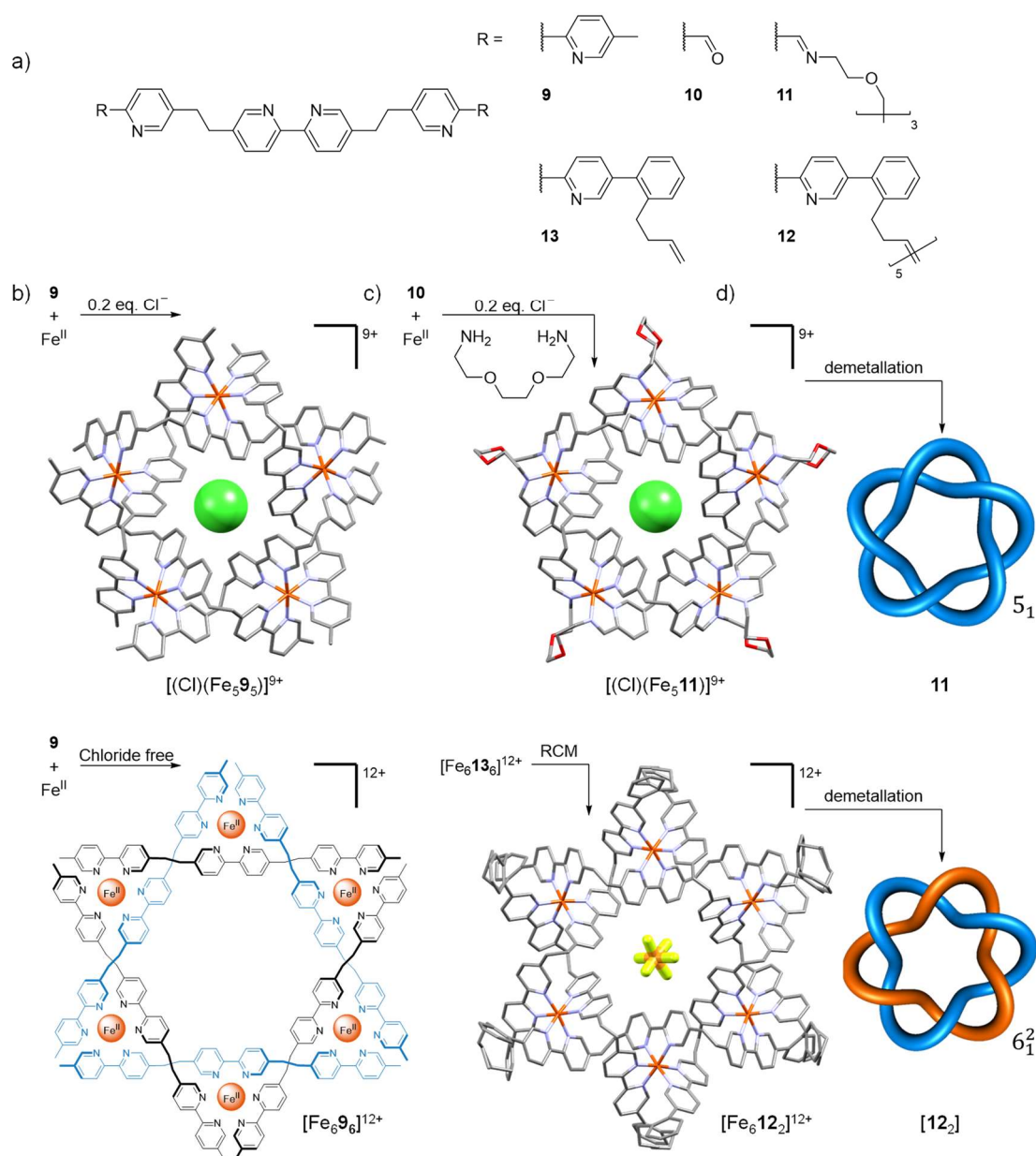
Scheme 1.2. a) Chemical structures of the bipyridine-derived ligands **9**–**13**. b) Synthesis of the five- and six-stranded circular helicates $[(Cl)(Fe_5\mathbf{9}_5)]^{9+}$ and $[Fe_6\mathbf{9}_6]^{12+}$, respectively, first reported by Lehn and coworkers. c) Ring-closing of the assemblies $[(Cl)(Fe_5\mathbf{10}_5)]^{9+}$ and $[Fe_6\mathbf{13}_6]^{12+}$ to yield $[(Cl)(Fe_5\mathbf{11})]^{9+}$ and $[Fe_6\mathbf{12}_2]^{12+}$, respectively. d) Demetallation of the resulting complexes to yield the $5_1$ pentafoil knot **11**, or the $6_1^2$ "Star of David" [2]catenane [**12**$_2$]. Knot representations created using KnotPlot.

for the formation of complex ligand-based structures, Figure 1.4a. Besides the Fe(II)-templated helicates and knots in Scheme 1.2, Fujita and coworkers have produced elaborate geometric assemblies with $[Pd(en)]^{2+}$ cornered complexes,[30,31] while large, multi-porphyrin macrocycles have been synthesised by Anderson and others through pyridine-based templates.[32]

Van der Waals interactions between the interior surfaces of barrel-shaped molecules, such as β-cyclodextrin (β-CD) and cucurbiturils, and hydrophobic (or solvophobic) guests may also be used to direct assembly, Figure 1.4b. Guests such as ferrocene, stilbenes and
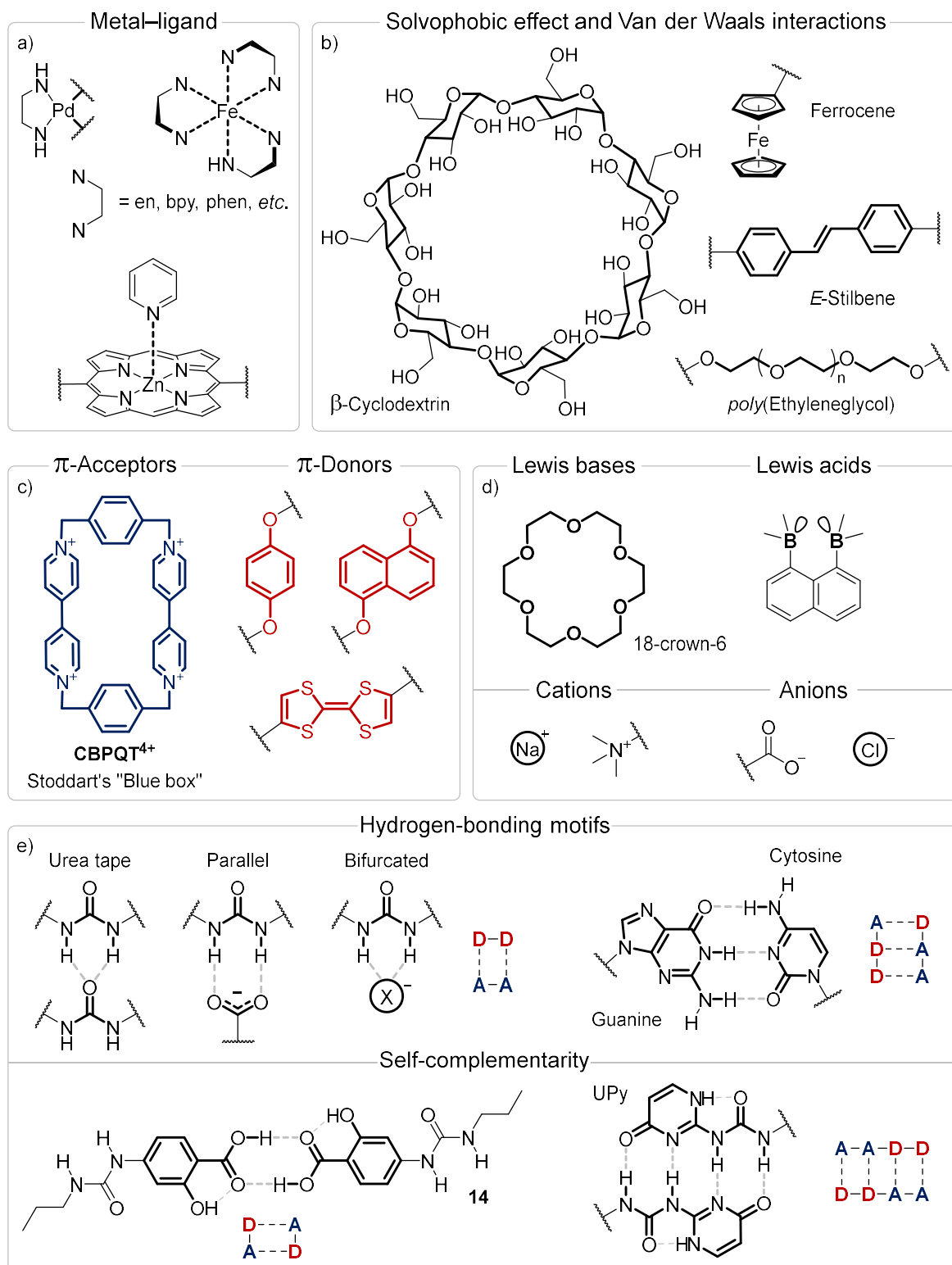
Figure 1.4. Selected supramolecular hosts and guests. a) Metal–ligand templates. b) Hosts and guests which interact through the Van der Waals interaction and solvophobic effects. c) π-Acceptors, π-donors (coloured blue and red, respectively, in the style of Stoddart), and d) Lewis bases and acids, cations, and anions, arranged into commonly interacting pairs. e) Complementary hydrogen-bonding motifs, and their representations as simple networks of hydrogen-bond donor (**D**) and acceptor (**A**) units. Solid lines denote a direct linkage (through covalent bonding or attachment to the same atom), and dashed lines denote primary hydrogen-bonding interactions. Other interactions have been omitted for clarity. X⁻ represents a generic anionic species.

azobenzenes can undergo triggered release upon redox-switching,[33,34] or conformational change of the double bond.[35–37] The binding of odorous compounds by β-CD is an important application to the consumer goods industry,[38] with in excess of \$1 billion in annual sales for the Febreze line of products from the Procter & Gamble Company.[39] The polyrotaxane slide-ring materials developed by Wang and coworkers (see Section 1.1.1) consist of PEG chains threaded through multiple connected β-CD rings. The nature of the solvophobic effect in different solvents has been quantified by Cockroft.[40]

The interaction between π-acceptors and π-donors has been extensively employed in templating molecular assemblies, Figure 1.4c, as the arrangement of the assembling π systems is predictably coplanar.[41] Examples include cyclobis(paraquat-*p*-phenylene) (CBPQT[4+]), commonly known as Stoddart's 'blue box', which interacts with hydroquinones and tetrathiafulvalenes.[42] A similar, but less directed interaction occurs between Lewis bases and cations, such as the crown ethers discovered by Pedersen[43] which bind alkali metal ions, ammonium ions and viologens, Figure 1.4d. As one of the earliest supramolecular hosts, crown ethers have been intensively utilised in interlocked systems. Lewis acids and anionic species interact in much the same way. Lewis acids that bear hydrogen-bond donors are particularly useful, see Section 1.2.1 and Section 1.3 below.

## 1.2.1 Hydrogen Bonding

Hydrogen-bonding interactions are particularly useful in creating supramolecular architectures, consisting of an association between a donor (D, a moiety containing a hydrogen atom covalently bound to an electronegative atom or electron-poor functional group), and an acceptor (A, a source of electron density). In terms of supramolecular interactions, the association between the donor and acceptor is highly directional (the D−H⋯A angle is usually greater than 130°), short (the D⋯A distance is usually ≤ 3.2 Å) and strong (for N/O donors and acceptors, $\Delta H_{bond}$ is usually 4–30 kJ mol$^{-1}$).[44]

Complementary hydrogen bonding arrays ensure rigid assemblies with predefined orientations. Hooper *et al.*, demonstrated that urea **14** formed dimers due to a self-complementary interaction between the carboxylic acids, Figure 1.4e. Such dimerisation was important in its gelation abilities.[45] Wang and coworkers exploited the ureidopyrimidine (UPy) motif, Figure 1.4e, to form dynamic self-assemblies that switch between macrocyclic and supramolecular polymeric forms, Figure 1.5. CBPQT[4+] stabilises the macrocyclic form of the dioxynaphthyl-containing molecule **15** through [2]catenane formation, Figure 1.5b.[46] At high concentrations, **16** forms 1D polymers. Bisparaquat threads crosslink the polymer through the formation of multiple pseudorotaxanes (similar to a rotaxane, but lacking
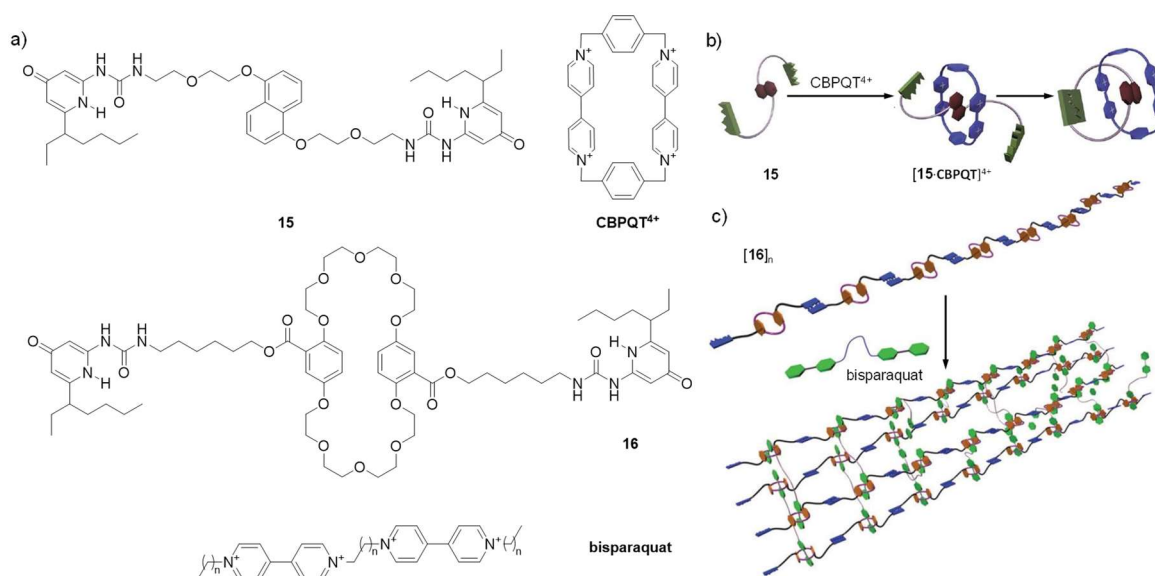
Figure 1.5. a) Structures of the macrocycles **15** and **16**, and threads used by Wang and coworkers. b) Formation of dynamic [2]catenanes. Image adapted from reference 46, copyright 2012 The Royal Society of Chemistry. c) Cross-linked sypramolecular polymer networks. Image adapted from reference 47, copyright 2011 the Royal Society of Chemistry.

stoppers to prevent slippage), increasing the solution viscosity, see Figure 1.5c.[47] The use of orthogonal hydrogen-bonding and π–π interactions to modulate the supramolecular assembly highlights how each new supramolecular synthon open up vast areas of chemical space.

While these self-complementary motifs display an array of exciting uses, complementary pairs of two different molecules allow the assembly to be broken into modular units each with specific functionality. The specificity of such pairs for each other is an essential part of the encoding of genetic information by DNA; the G–C pair is shown in Figure 1.4e. Simple two-donor systems, such as the urea functional group, bind well to molecules able to accept two hydrogen bonds. This occurs either through bifurcated binding from the one donor atom or parallel binding to a geometrically equivalent oxoanion, Figure 1.4e. Significant advances have been made by Beer and coworkers in using a central templating Cl⁻ anion to bring together two hydrogen-bonding components.[15,48–51] The direct templating interaction between two discrete components, in which one is a hydrogen-bonding donor and the other an anionic acceptor, is relatively undeveloped. As the urea–anion interaction is central to this work, and the following sections will discuss anion binding in the context of urea-based receptors.

## 1.3   Anion Binding

As introduced in Section 1.2, above, species with a negative charge may be stabilised through metal–ligand,[52] electrostatic/ion-pair, anion–π, halogen-bonding, or hydrogen-

bonding interactions. "Anion binding" is the term given to this broad field encompassing all anion–receptor interactions, and this field has been developed for a variety of purposes. This stems from the desire to recognise, transport or remove certain anions, or to perform catalysis on or with anionic species, amongst other applications.

Anions are interesting targets in supramolecular chemistry. They play a variety of roles in the natural and industrial worlds, being variously described as nutrients, substrates, contaminants and pollutants. They are larger than their isoelectronic cations, and so are more charge-diffuse, sometimes requiring high coordination numbers. Hofmeister and others established the trends in the "water absorbing effects of salts",[53,54] this later being formalised as energies of hydration. The placement of a particular anion within the Hofmeister series, which describes the relative solvation of various anions, also affects the strength of the binding by any given receptor. A list of ionic radii in the crystalline phase and in aqueous solutions, and Gibbs free energies of hydration of selected anions is presented in Table 1.1. This concept of hydration energy may be extended, and Farrokhpour and coworkers recently

Table 1.1. Ionic radii, Gibbs free energy of hydration, base dissociation constant, number of lone pairs, and observed hydrogen-bonded coordination numbers for a range of anions. Table reproduced in part from listed references.

| Ion | Radius (nm) | | | | $\lvert\Delta_{hyd}G\rvert$ [d] | $pK_b$ | No. | Obsv. | Geom. |
| | Crystal [a] | | Aq. [b] | $\Delta r_{hyd}$ [c] | (kJ mol$^{-1}$) | | lp [f] | CN [g] | [h] |
| Ref. | 55 | 56 | 55 | 56 | 56 | 57,58 | | 59–67 | |
| F$^-$ | 0.133 | 0.133 | 0.124 | 0.079 | 465 | 10.6 | 4 | 4,6,9 | Sph. |
| Cl$^-$ | 0.181 | 0.181 | 0.180 | 0.043 | 340 | n/a [e] | 4 | 4,6 | Sph. |
| Br$^-$ | 0.196 | 0.196 | 0.198 | 0.035 | 315 | n/a | 4 | 6 | Sph. |
| NO$_3^-$ | 0.179 | 0.179 | 0.177 | 0.044 | 300 | n/a | 8 | 3 | Trig. |
| H$_2$PO$_4^-$ | 0.238 | 0.200 | 0.238 | 0.033 | 465 | 3.7 | 8 | 5,6 | Tet. |
| PO$_4^{3-}$ | – | 0.238 | – | 0.054 | 2765 | 11.8 | 12 | 12 | Tet. |
| SO$_4^{2-}$ | 0.230 | 0.230 | 0.242 | 0.043 | 1080 | n/a | 12 | 5,8,9,12 | Tet. |
| AcO$^-$ | – | 0.162 | – | 0.055 | 365 | 9.2 | }5 | 2,4 | Trig. |
| BzO$^-$ | – | – | – | – | – | 9.8 | | | |

a) Pauling-type crystal ionic radii in nm. b) Calculated ionic radii in aqueous solution in nm. c) Thickness of the outer shell of the hydration sphere, assuming an inner ionic sphere, in nm. d) Absolute magnitude of the Gibbs free energy of hydration in kJ mol$^{-1}$. e) No $pK_b$, conjugate acid is strong. f) Number of lone pairs as estimated from Lewis structure. g) Some observed coordination numbers from hydrogen-bond donors in X-ray crystal structures, does not include coordination from hydrogen-bond acceptors. h) Approximate geometry, Sph. = Spherical Trig. = Trigonal planar, Tet. = Tetrahedral.

demonstrated a method for the estimation of solvation energies across various solvents.[68] Oxoanions, in particular, have complex geometries and are pH sensitive (Table 1.1 also contains the approximate geometries and p$K_b$ values for the anions listed). These properties, while often making anions challenging to bind, open up a range of possibilities in supramolecular chemistry. Structures templated by pH-sensitive anions, for example, may be dissembled or otherwise altered by pH change. Hydrogen bonding is a very attractive method for binding hard Lewis bases such as oxoanions and the smaller halide anions. This is due to the directional nature of the hydrogen bond, which means that receptors may be constructed such that they complement the shape and size of the anion. Naturally-occurring anion-binding sites in proteins such as proteases and dehydrogenases utilise amines, amides, guanidines, and the heterocyclic side chains of tryptophan and histidine.[69–71] In the following sections, the emphasis will be on hydrogen-bonding receptors.

While the above-mentioned functional groups are extensively used in synthetic receptors, the urea moiety is also highly popular in receptor design.[60,61,72–77] Due to the preference of the urea moiety for the *syn-syn* conformation, it tends to donate two codirectional hydrogen bonds and form rigid assemblies. The molecular dipole provided by the carbonyl functional group polarises the urea moiety. The electron-poor nature of the NH donors increases their binding affinity for hydrogen bond acceptors, over simple amines. For example the p$K_a$ of diphenylurea is 19.5, while that of diphenylamine is 25.0. This argument has been extended to produce receptors derived from the more acidic deltamides,[78,79] squaramides,[79–82] croconamides,[78,79] and thione analogues,[76,83] but these are outside the scope of this work. There are a large number of urea-based receptors in the literature, and these have been extensively reviewed.[60,75–77,84] One of the first to study the urea group and its affinity for hydrogen bond acceptors was Etter,[85] who analysed the crystalline adducts of various diphenylurea receptors – particularly di(3-nitrophenyl)urea – with a range of solvents. Wilcox, recognising the potential to bind complex organic molecules, then studied the binding of benzoate, sulfonates and phosphates in CDCl$_3$.[86] Hamilton soon moved the study of anion binding to the more competitive solvent DMSO-$d_6$.[87]

Several groups have focused on tying the interaction between the urea-based receptor and the anion to intrinsic properties related to the electronic structure of each molecule, Figure 1.6. Fabbrizzi and coworkers investigated the dramatic colour changes exhibited by the urea-derived receptors **17** and **18** upon the addition of F$^-$, ascribing it to a two-step mechanism of binding, followed by deprotonation to form the HF$_2^-$ anion, as had been suggested by Duke *et al.*[88] Extending their analysis to other anions, they concluded that the logarithmic 1:1 host–guest binding affinities (log$\beta_{1:1}$) expressed by simple, electron-poor,

urea-based anion receptors were entirely and linearly dependent on the negative charge present on the coordinating atoms of the anionic species, Figure 1.6a.[89,90] Hunter has recently reported parameters to describe the hydrogen-bond accepting properties of anions.[91] Bu *et al*. studied the *para*-substituent effect on the binding of electrochemically generated nitroarene radical anions (**19a–e**)$^{\cdot-}$ with diphenylurea. The difference in the binding affinities of the neutral and reduced nitro compounds were probed by cyclic voltammetry (CV). The binding affinities were related to the change in half-wave potential in the presence of diphenylurea, with the electron-donating *para*-amino moiety stabilising the interaction to the



| | 20a | 20b | 20c | 20d | 20e | 20f | 20g |
|---|---|---|---|---|---|---|---|
| R | NO$_2$ | Cl | F | H | $^t$Bu | OMe | NMe$_2$ |
| $\sigma_p$ | +0.78 | +0.23 | +0.06 | 0.00 | −0.20 | −0.27 | −0.83 |
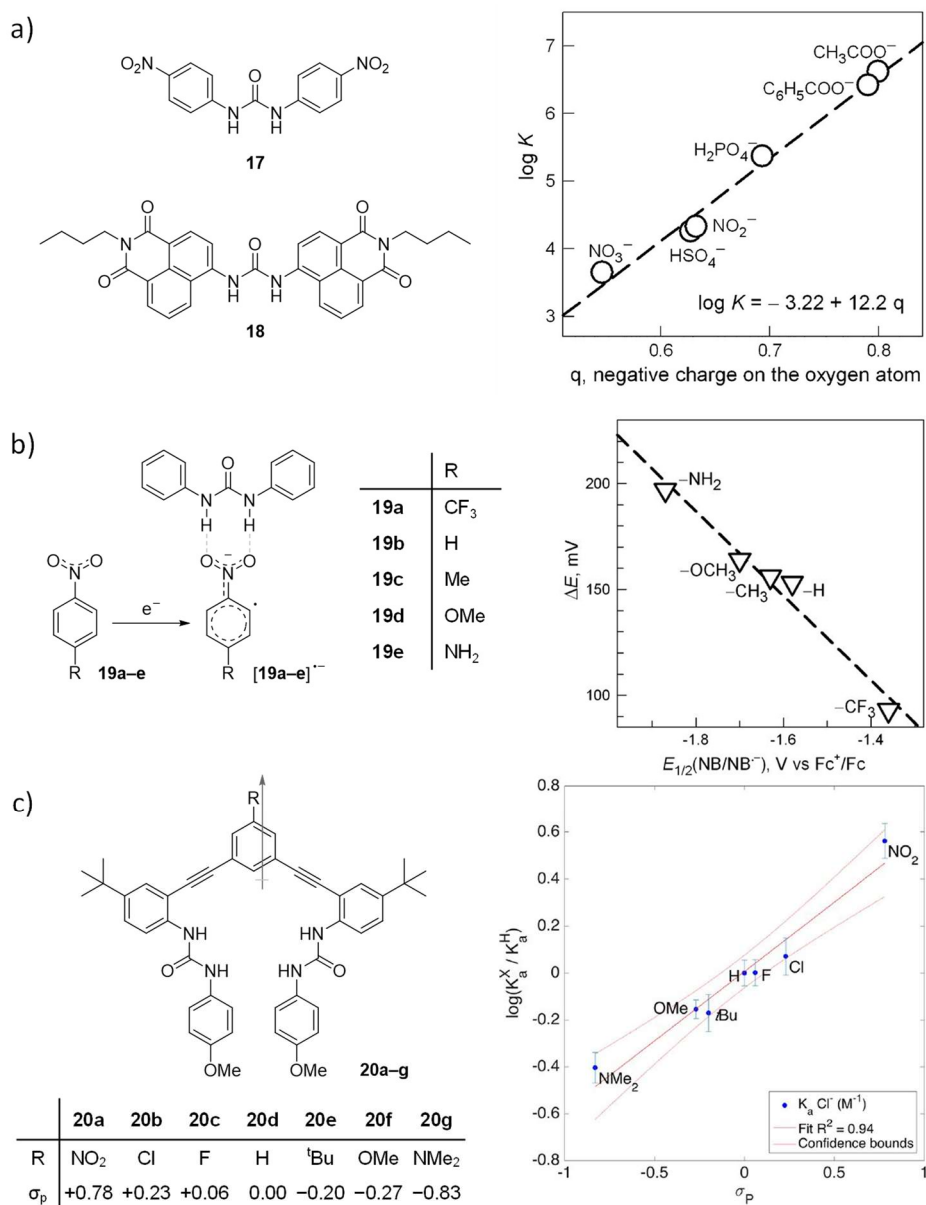
Figure 1.6. a) Binding affinities of various oxoanions for receptors **17** and **18** plotted against the calculated charge on the oxygen atoms. b) Interaction of the reduced (radical anion) form of nitrophenyl compounds of the type **19** with diphenylurea, and plot of the anodic shift of the reduction half-reaction upon addition of 50 eq. diphenylurea. Images reproduced from reference 84, copyright 2010 The Royal Society of Chemistry. c) Relative binding affinities for receptors of the type **20** with Cl⁻, plotted against Hammet *para*-substitution parameters. Image reproduced in part from reference 93, copyright 2015 American Chemical Society.

greatest extent, Figure 1.6b.[92] The estimated binding constants for the neutral and reduced forms of nitroaniline were $\log\beta_{1:1,\,0} = -2.6$ (**19e**) and $\log\beta_{1:1,\,-1} = +4.9$ (**19e$^{\cdot\,-}$**), respectively. The authors demonstrated that the interaction did not involve proton transfer, and was instead solely hydrogen bonding in nature. Expanding on these ideas, Johnson and coworkers determined that the bis(urea) receptors **20a–g** displayed *para*-substituent effects at the central aromatic ring when titrated with halide anions. The relative rate of binding, $\log(\beta_{1:1,R}\,/\,\beta_{1:1,H})$, displayed by these receptors formed a linear relationship with the *para* Hammet substituent parameter Figure 1.6c.[93] A pyridine-containing analogue also bound Cl$^-$ strongly, but only upon protonation of the pyridyl nitrogen atom.[94] These examples demonstrate that electron densities of the urea host and its anionic guest can play important roles in the binding event.

Another important aspect of binding is the preorganisation of the receptor towards its guest. The rotation around the diynyl linker in compound **21**, reported by Steed and coworkers, allows the two otherwise independent urea moieties to swivel into place upon binding of an anion of suitable size, Scheme 1.3.[95] The molecule planarises upon Cl$^-$ binding, leading to a switch ON fluorescence response. Other anions can still bind to the receptor, but do not induce a fluorescent response. This is possible because the co-planar form of **21** discriminates between anions on the basis of size, and so is preorganised towards the Cl$^-$ anion. The chemical input modulates the conformation and resulting molecular properties, also demonstrating a potential link to molecular machinery. Such a link was exploited by Feringa and coworkers with a series of bisurea-based anion receptors derived from the well-known tetrahydrobisindanylidene ("stiff-stilbene") molecular switch, which operates under
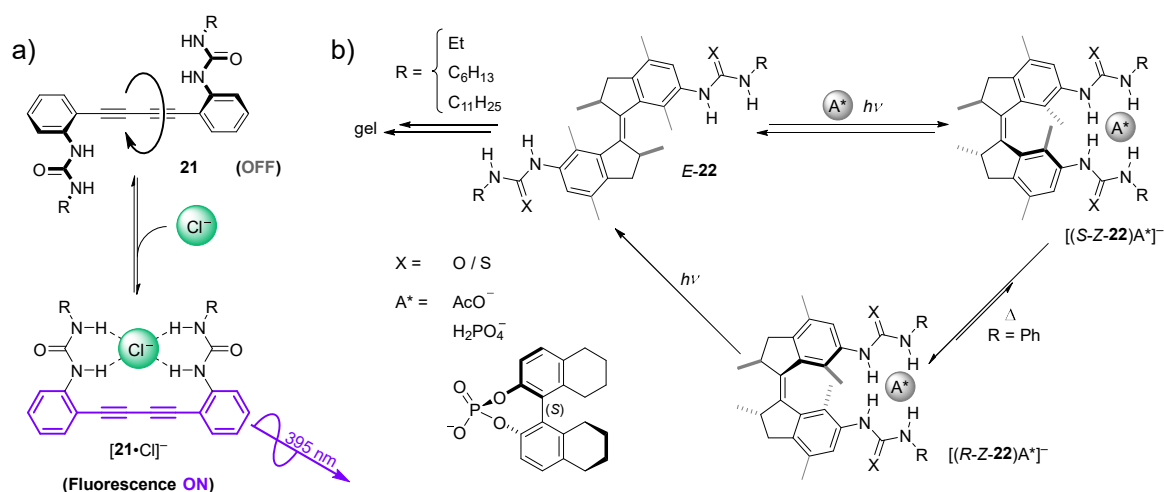


Scheme 1.3. Schematics of the behaviour of two classes of bisurea receptor. a) The diyne-containing receptor **21** planarises only upon binding of the Cl$^-$ anion, leading to a fluorescence output at 395 nm. b) The "stiff-stilbene" based receptors (**22**) reported by Feringa and coworkers switch conformation with light irradiation, heat, or in the presence of chiral anionic guests. The three-state system forms a simple molecular machine.

UV irradiation.[96–99] The *Z* form of **22** is preorganised to bind anions, while switching to the *E* form releases the anionic guest (and leads to gelation). In the case of especially hindered receptors or chiral guests, the *Z* form may occupy both stable and metastable states. It is the unidirectional manner of switching between these, and back to the open *E* state, that forms a simple molecular machine. The change of properties and binding of anions is modulated by a photo- or thermal impulse, and several applications exist for the controlled binding and release of anions.

## 1.3.1  Binding of Anionic Compounds for Removal and Transport

There currently exist several methods by which pollutant anions are removed from aqueous media on large scales, these centre on chemical precipitation, biological oxidation/reduction, anion-exchange resins and mineral adsorbents such as zeolites and clays.[100] Fluoride is currently removed by a number of means, for example, the exposed surfaces of the mineral hydroxyapatite convert to fluorapatite in the presence of $F^-$. Other species, however, are less easy to capture due to the diffuse charge and low reactivity of many anions. Moyer *et al.* have illustrated the pressing need for sulfate removal technologies in the treatment of nuclear waste prior to its vitrification.[101] Many of the approaches currently being developed utilise sophisticated macrocyclic hosts.

Systems which combine the specificity of supramolecular anion receptors with the bulk properties of solid and soft materials have garnered significant interest. Sessler and coworkers have reported the removal of anions from aqueous media using a water-soluble poly(vinylalcohol) (PVA) network containing covalently-linked tetra(imidazolium)
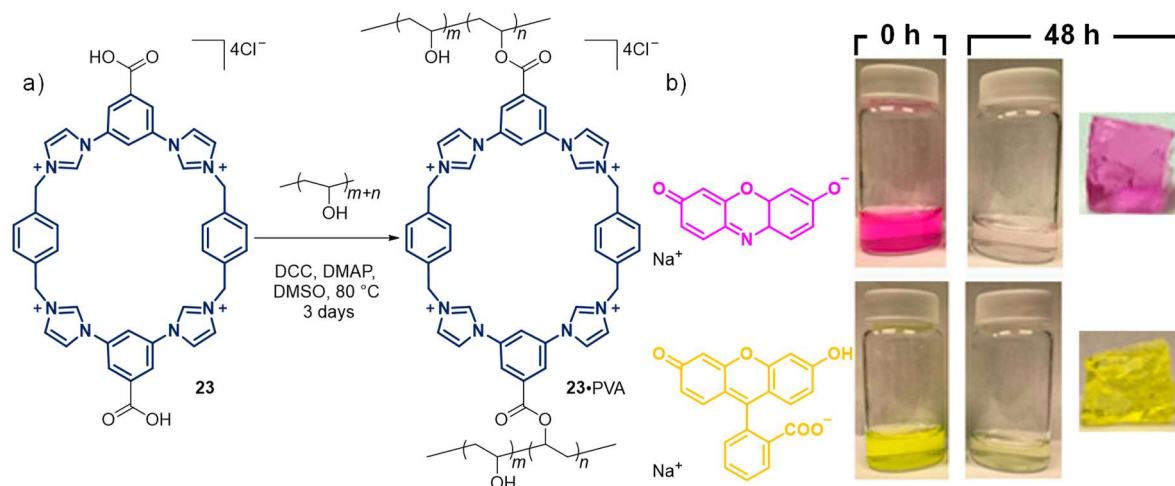


Figure 1.7. a) Chemical structures of the tetra(imidazolium) macrocycle **23** and the cross-linked poly(vinylalcohol) network **23·PVA**. b) Removal of coloured anionic dyes from aqueous solution by the hydrogel-forming polymeric network over 48 hours (gel samples pictured separately). Figure adapted from reference 102, copyright American Chemical Society 2018.

macrocyclic units, **23**·PVA in Figure 1.7a.[102] Upon addition of the PVA polymer to an aqueous solution it swells to form an anion-exchange hydrogel, releasing chloride anions upon binding of anionic species present in the solution. The uptake of several coloured anionic dyes (the sodium salts of resorufin and fluorescein, see Figure 1.7b) was monitored by changes in intensity of the UV-visible absorption spectra of the dyes, while the ability to absorb inorganic anions was demonstrated by a reduction in the conductivity of their solutions. Lifting out the hydrogel removes the anions from the aqueous phase, and the stored anions may then be released by regeneration of the chloride salt with the addition of dilute HCl. Similarly, Tian *et al*. have developed a cationic 3D supramolecular organic framework (SOF) which consists of self-assembling 4-(methoxyphenyl)pyridinium terminated units, stabilised by cucurbit[8]uril macrocycles. The polypseudorotaxane system was capable of absorbing /adsorbing a variety of anions, including various sulfonate dyes and sodium adefovir (a hepatitis B drug) from water.[103]

Zhang and coworkers developed a system for selective $ReO_4^-$ binding, as an analogue of the radioactive $^{99}TcO_4^-$ anion.[104] They synthesised resol oligomers **24** through the condensation of urea and phenol, Figure 1.8a. These were assembled around micelles, and mesoporous nanoparticles were formed from these oligomers through a hydrothermal process followed by calcination to remove the micellar template. The resulting spheres were highly-ordered mesoporous structures, see Figure 1.8b–c. At a loading of 1 g/L, these nanoparticles removed 88% of aqueous $ReO_4^-$ (0.25 mM) in 30 min, Figure 1.8d. The anion could be removed selectively in the presence of 1 eq. $CO_3^{2-}$, $SO_4^{2-}$, and $PO_4^{3-}$, while 43% of $ReO_4^-$ was removed in the presence of a hundredfold excess of $NO_3^-$.
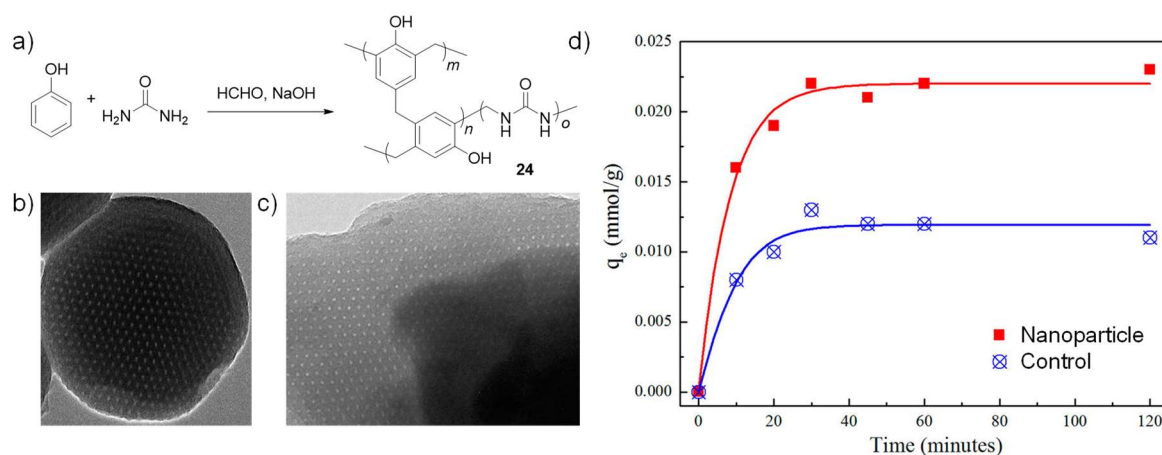


Figure 1.8. a) Synthesis of the urea-resol oligomers **24** from phenol, urea and formaldehyde under basic conditions. b–c) TEM images of a single nanoparticle and a portion of the control material, respectively, along the 111 axis of the body-centred cubic mesostructure. d) Adsorption of aqueous $ReO_4^-$ by the ordered nanoparticles (red squares) and the control (blue circles). Images reproduced in part from reference 104, copyright 2017 American Chemical Society.
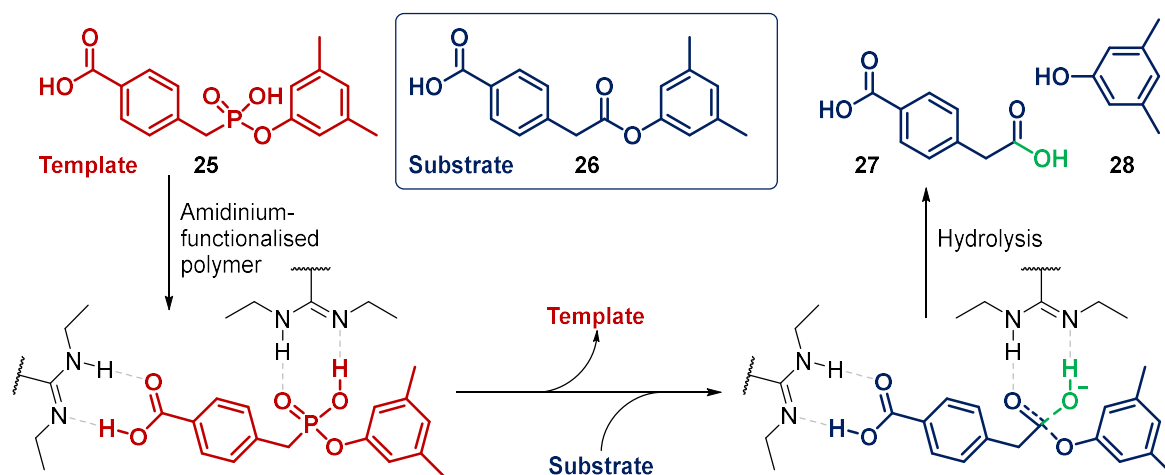
Scheme 1.4. The transition state analogue (**25**, **red**) of the dimethylphenyl ester substrate (**26**, **blue**) is used as a template, around which to form a molecularly imprinted polymer. The template **25** is washed out of the polymer, and the substrate binds to the same cavity along with a hydroxide ion (**green**), thus catalysing its hydrolysis to **27** and **28**.

Receptors may also be designed to bind a molecular analogue of a reaction transition state, in the expectation that the receptor will catalyse the specific change. Wulff *et al*. developed a molecularly imprinted polymer that stabilises the transition state analogue **25** of the dimethylphenyl ester **26**, catalysing hydrolysis of the latter in mixed aqueous pH 7.6 buffer/MeCN (1:1), Scheme 1.4.[105] While a modest increase ($\times$ 2.5) in reaction rate was observed in the presence of an analogous amidine organocatalyst, a hundredfold increase in reaction rate was observed with the phosphate-imprinted polymer (active site concentration estimated by quantity of washed-out template **25**). This rate was five times greater than with a polymer imprinted with benzoate, and 43 times greater than with the amidine organocatalyst alone. Such molecular imprinting systems demonstrate the utility of templation beyond the mere recognition of the original template molecule. The subsequent separation of the template and its host allows each molecule to bind complementary species.

Ghosh and coworkers demonstrated the use of a novel carbonate-containing dimeric capsule for the extraction of pollutant anions from aqueous media.[106] The dimeric adduct $[\mathbf{29}_2CO_3]^{2-}$ was dissolved in $CH_2Cl_2$ and stirred for 6 hours at room temperature with an aqueous solution of the potassium salt of the anionic pollutant (10 eq.), Figure 1.9a. Gravimetric analysis demonstrated that greater than 90% of the carbonate had been exchanged with each of the anions, which were sequestered by the receptor capsules. ^{1}H NMR experiments indicated that these capsules were stable in solution. Evaporation of the organic solvent yielded microcrystalline solids, which upon recrystallisation from DMSO, were identified as the capsular assemblies shown in Figure 1.9b–e. Receptor **30** was also
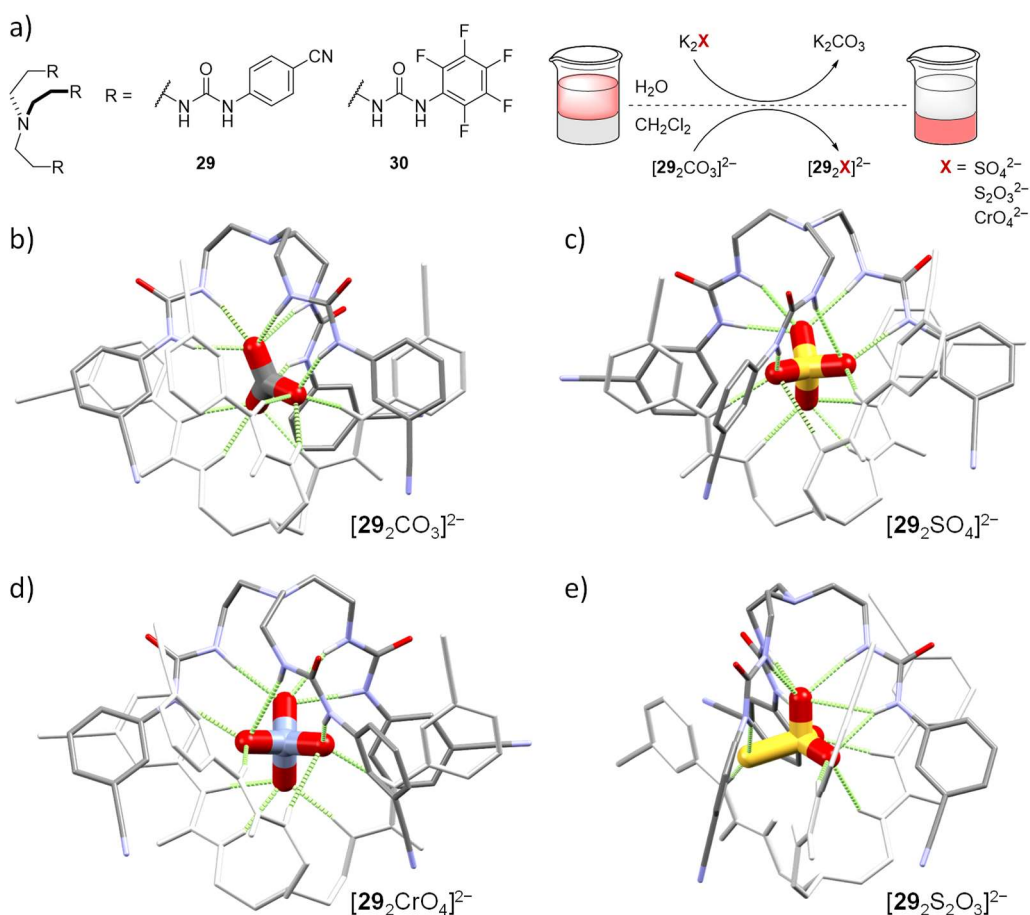
Figure 1.9. Structure of receptors **29** and **30**, and scheme describing the extraction of $SO_4^{2-}$, $S_2O_3^{2-}$ and $CrO_4^{2-}$ anions from water through anion exchange with carbonate adduct of **29**. a–d) Crystal structures of $[29_2CO_3]^{2-}$ (a), $[29_2SO_4]^{2-}$ (b), $[29_2CrO_4]^{2-}$ (c) and $[29_2S_2O_3]^{2-}$ (d). In each structure, one of the two receptor molecules has been coloured in light grey to illustrate the conformation of the receptor around the anion. Non-hydrogen bonding hydrogen atoms, solvent molecules and counterions are omitted for clarity.

able to sequester $SO_4^{2-}$, and had previously been observed to crystallise with an encapsulated $HAsO_4^{2-}$ anion.[107]

A variety of anion-binding molecules have been designed to encapsulate and chaperone molecules through cell membranes. Chloride transport is a goal of many research groups, with two distinct applications. In the first, rapid and uncontrolled ion exchange across a plasma membrane will lead to cell depolarisation and the triggering of apoptosis (programmed cell death), and this is attractive as a form of cancer chemotherapy.[108] In the second application, cystic fibrosis suffers possess a mutation in the gene for the chloride-transporting CTFR protein and benefit from anion transporter therapies.[109] A variety of urea-based anion transporters have been reported, and these may be arbitrarily broken into two classes based on structural similarities, Figure 1.10. First are those which utilise a carbon backbone, such as the decalin **31** and the sterol **32**, to orient the urea groups to form a molecular cavity.[109–111] The second class make use of rigid linkers such as the *ortho-*
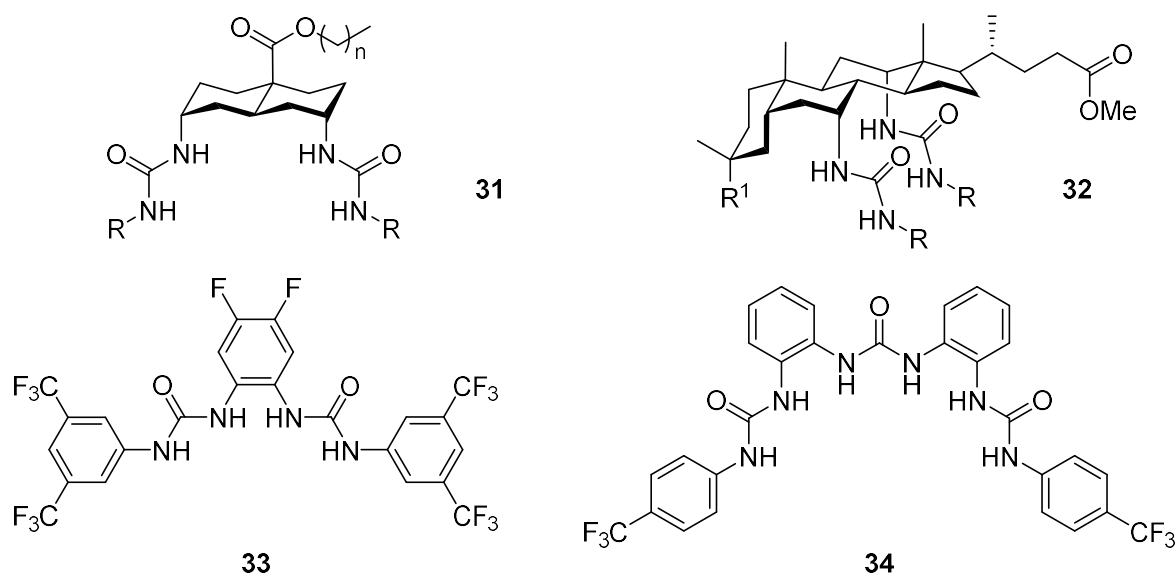
Figure 1.10. General structure of anion-transporting molecules **31**–**34**, previously reported by the Davis and Gale research groups.

phenylene group. Gale and coworkers have reported several bis- and tris-urea anion transporters of this type.[112,113] These $H_4$ and $H_6$ hydrogen-bond donor anion receptors **33** and **34** both contain the lipophilic and electron-withdrawing $CF_3$ group, which increases the binding affinity for anions and aids in the transport of these anions across membranes.

## 1.3.2 Anion–receptor Clusters

The efficiency of several processes involving anion removal and transport can be increased by designing receptors which bind to more than one anion at a time. To bind two or more anions in close proximity, the Coulombic repulsion between them must be overcome by the stabilisation energy that a receptor confers, Figure 1.11a.[61] This stabilisation energy is equal



$$\log K_i = -\frac{2.303}{RT}\Delta G_i$$

$$\alpha = \frac{4K_{1:2}}{(K_{1:1})^2}$$
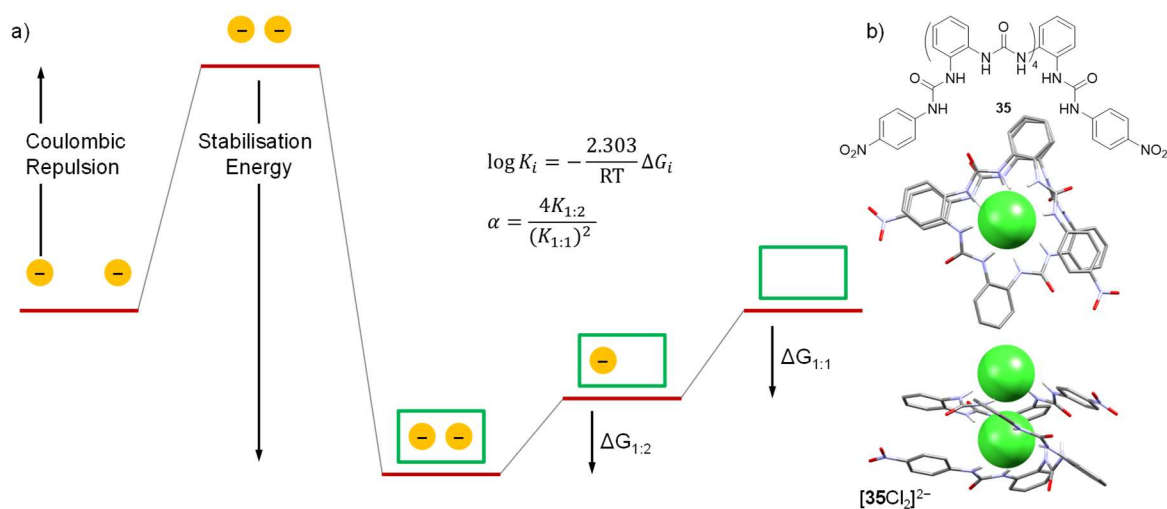
Figure 1.11. a) Illustrative energy diagram showing the relative energies of various arrangements of a receptor molecule (**green**) and anionic guests (**orange**). b) Structure of the hexaurea foldamer **35** reported by Wu *et al*. (top), with helical crystalline adduct [**35**·Cl$_2$]$^{2-}$ (views down and perpendicular to the Cl–Cl axis, centre and bottom respectively). Non-hydrogen bonding hydrogen atoms and TBA$^+$ cations are omitted for clarity.
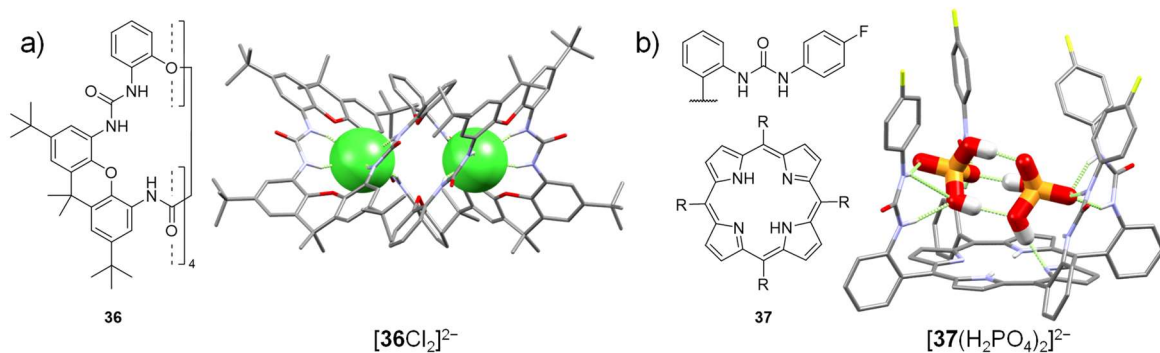
Figure 1.12. a) Structure of receptor **36** and solid-state structure of its di(chloride) adduct. One-quarter of the structure is drawn, dotted lines denote mirror symmetry. b) Structure of receptor **37** and solid-state structure of its adduct with the dimeric $H_4P_2O_8^{2-}$ anion. Non-hydrogen bonding hydrogen atoms, solvent molecules and counterions are omitted for clarity.

to the sum of the magnitudes of each binding energy and the Coulombic repulsion between the anions. The hexaurea foldamer receptor **35** reported by Wu *et al*. chelates two individual $Cl^-$ anions, holding them 4.025(1) Å apart, Figure 1.11b. The tri-, tetra- and penta-urea analogues were also observed to crystallise from $Et_2O/CHCl_3$/acetone with encapsulated chloride dimers.[114] However, NMR titrations with naphthyl and anthracenyl-terminated derivatives indicated that only 1:1 host–guest complexes were formed in DMSO-$d_6$ with low binding constants of $\log\beta_{1:1} \approx 2$.[115] With tetrahedral oxoanions, the triurea was instead observed to form 2:1 host–guest complexes in both solution and the solid phase.[116] It was only with the tetraurea receptor and the azide anion that 1:2 host–guest binding was observed in both phases.[117] The hexaurea macrocycle **36** developed by Meshcheryakov *et al*. folds to encapsulate two $Cl^-$ anions in a similar manner, see Figure 1.12a.[118]

In the case of some anions, such as phosphates, their Coulombic repulsion is mitigated by their tendency to form dimeric species in both organic and aqueous solution.[119–121]
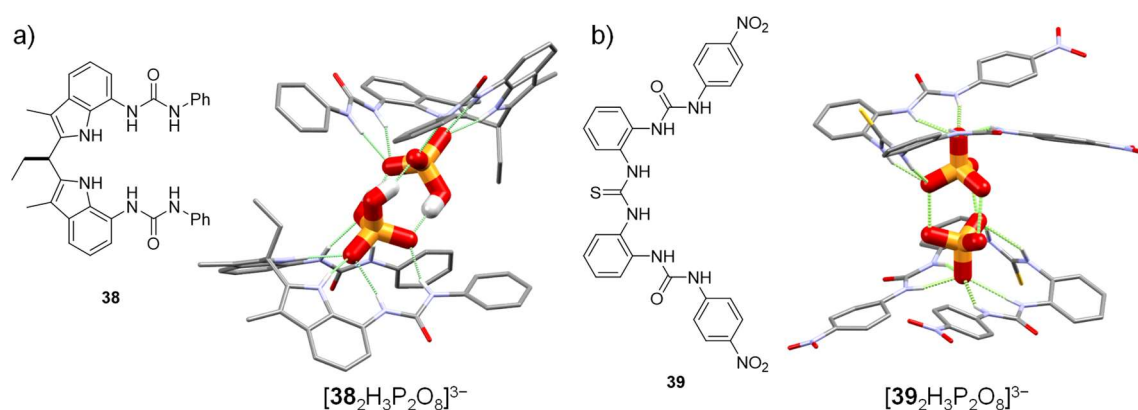


Figure 1.13. Structures of receptors a) **38** and b) **39**, and solid-state structures of their adducts with the dimeric $H_3P_2O_8^{3-}$ anion, respectively. Non-hydrogen bonding hydrogen atoms, solvent molecules and counterions are omitted for clarity. The hydrogen atoms present in the cluster are not shown in (b).
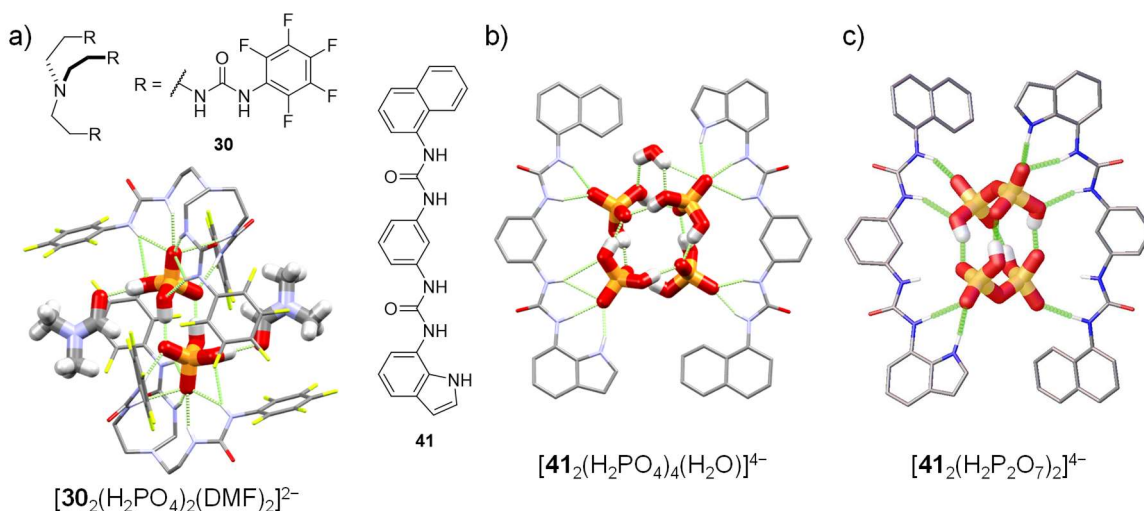
Figure 1.14. a) Structure of receptor **30** and crystal structure of the adduct $[30_2(H_2PO_4)_2(DMF)_2]^{2-}$. b–c) Structure of the receptor **41**, and crystal structures of the adducts $[41_2(H_2PO_4)_4(H_2O)]^{4-}$ and $[41_2(H_2P_2O_7)_2]^{4-}$. Non-hydrogen bonding hydrogen atoms, non-interacting solvent molecules and counterions are omitted for clarity.

Several forms of anion receptor take advantage of this effect to bind dimers, trimers and clusters of anions. Reports of phosphate clusters in the crystalline phase are particularly abundant in the literature.[67] For example, the simple dimer $H_4P_2O_8^{2-}$ was reported by Calderon-Kawasaki *et al.*, nestled within the cavity of the porphyrin-derived tetraurea **37**, Figure 1.12b.[122] The threefold symmetric $H_3P_2O_8^{3-}$ dimeric anion has been reported in crystal structures of adducts with both the indole containing diurea **38**[123] and the mixed thiourea/urea receptor **39**, Figure 1.13.[124]

Two molecules of the tris(aminoethyl) amine (tren) based receptor **30** also encapsulate a phosphate dimer, although there are only two hydrogen bonds between the $H_2PO_4^-$ units



Figure 1.15. Structures of the adamantine bisurea receptors **42** (a), **43** (b) and **44** (c), and solid-state structures of their adducts with the tetra(phosphate) anionic clusters. Non-hydrogen bonding hydrogen atoms, non-interacting solvent molecules and counterions are omitted for clarity.

in this case, two others being to DMF solvent molecules (Figure 1.14a).[125] The asymmetric indolyl/naphthyl-substituted *meta*-phenylene bisurea receptor **41** reported by Casula *et al*. was found to crystallise from Et$_2$O/MeCN/MeNO$_2$ with two receptor molecules flanking a phosphate tetramer (Figure 1.14b).[126] The crystal structure of **41** with the dibasic pyrophosphate anion (H$_2$P$_2$O$_7{}^{2-}$, PPi) is remarkably similar, with the pyrophosphate anions sharing four hydrogen bonds (Figure 1.14c). The anion binding properties of **41** and its isomers were investigated through $^1$H NMR and fluorescence titration experiments in DMSO. Despite the clusters of bound anions reported in the crystalline phase, the *meta* isomer **41** bound AcO$^-$, HCO$_3{}^-$ and H$_2$PO$_4{}^-$ less strongly than either the *para* or *ortho* isomers. While the addition of pyrophosphate led to the formation of a strong fluorescence emission at 476 nm in the case of both **41** and the *ortho* isomer, the emission of the latter was much stronger. The authors then incorporated this receptor into cetyltrimethylammonium bromide (CTAB) micelles to sense pyrophosphate in pure water.

Similarly, Blažek *et al*. reported tetrameric phosphate adducts of the adamantane bisureas **42**, **43** and **44**, Figure 1.15. The anionic cluster present in the adduct with the adamantyl di(phenylurea) **42** contained six water molecules and was flanked by two molecules of **42**, whereas the naphthyl analogues **43** and **44** each encapsulated the (H$_2$PO$_4$)$_4{}^{4-}$ cluster with four receptor molecules.[127]

Rajbanshi *et al*. reported large water–phosphate clusters with the bis(*ortho*-phenylene diurea) receptors **45** and **46**, as well as a linear tetraphosphate cluster with **45**, Figure 1.16.[67] The structure of the [(H$_2$PO$_4$)$_6$(H$_2$O)$_4$]$^{6-}$ anionic cluster is similar between receptors **45** and **46**, being unaffected by the modest increase in steric bulk from the longer *n*-butyl chain.



Figure 1.16. Structure of receptors **45** and **46**, and solid state structures of the adducts of **45** (a,b) and **46** (c) with phosphate anionic clusters. The hexameric water–phosphate clusters with **45** (b) and **46** (c) are similar in structure. Non-hydrogen bonding hydrogen atoms, non-interacting solvent molecules and counterions are omitted for clarity.

Figure 1.17. Structure of the tren-derived triurea receptor **47**, and crystal structures of two solid state adducts containing an anionic $(H_2PO_4)_4^{4-}$ core. a) $[\mathbf{47}_4(H_2PO_4)_4]^{4-}$. b) $[(\mathbf{H47})_4(H_2PO_4)_4(H_2O)_2(DMSO)_2]$, in which the central nitrogen atom of **47** is protonated. In each case, only one of the molecules of **47** is shown in colour to illustrate the conformation of each receptor. Non-hydrogen bonding hydrogen atoms (except for the ammonium proton), non-interacting solvent molecules and counterions are omitted for clarity.

Das and coworkers reported two clusters of phosphate anions with the tren-derived receptor **47**, Figure 1.17.[128] In the presence of TBAH$_2$PO$_4$, an adduct crystallised with four molecules of **47** surrounding a tetrahedral cluster of H$_2$PO$_4^-$ anions, Figure 1.17a. In the presence of phosphoric acid, however, the central nitrogen atom is protonated, and crystals
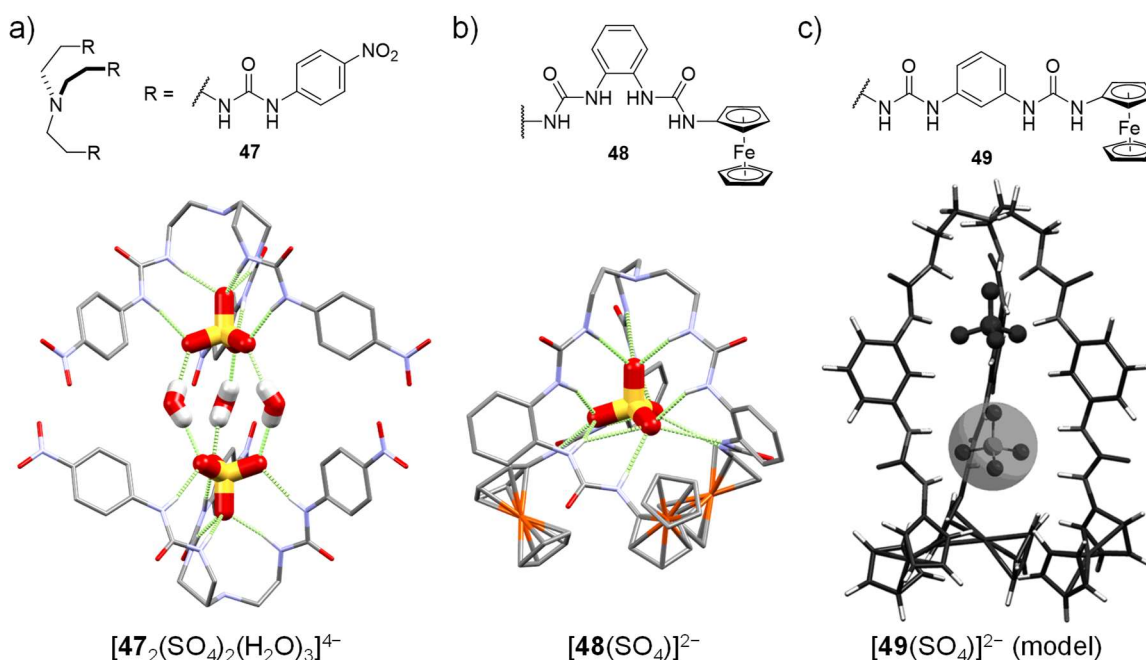


Figure 1.18. Structures of receptors **47** (a), **48** (b) and **49** (c), alongside the crystal structures of the adducts of **47** and **48** with the SO$_4^{2-}$ anion (a, b), and MMFF94 modelled structure of $[\mathbf{49}(SO_4)]^{2-}$ showing vacancy suitable for a second SO$_4^{2-}$ anion (c). Non-hydrogen bonding hydrogen atoms, non-interacting solvent molecules and counterions are omitted for clarity. Image reproduced from reference 63, copyright 2013 Wiley-VCH Verlag GmbH&Co. KGaA, Weinheim.

were formed in which four molecules of the [H**47**]$^+$ cation surround a square arrangement of H$_2$PO$_4^-$ anions, using only two of the three arms, Figure 1.17b.

Jose *et al*. had previously noted the crystallisation of **47** from MeCN/H$_2$O to form dimeric capsules with the SO$_4^{2-}$ anion and three bridging water molecules, Figure 1.18a.[129] Wu and coworkers reported the sulfate binding abilities of the ferrocenyl-terminated receptors **48** and **49** in solution, and MMFF94 (Merck Molecular Force Field) modelled structures of the sulfate complexes of these.[63] A crystal structure of [**48**(SO$_4$)]$^{2-}$ (Figure 1.18b) closely resembled the model, as well as a nitrophenyl-terminated analogue reported by Portis *et al*.[130] A calculated model of the sulfate adduct of the *meta*-substituted receptor **49**, however, showed that binding of a second sulfate anion within the molecular cavity was possible, Figure 1.18c. The anion binding properties of **48**, **49** and the *para*-phenylene isomer were investigated through $^1$H NMR titrations and cyclic voltammetry experiments in DMSO, which supported the respective models of 1:1 and 1:2 host–guest binding for **48** and **49** with SO$_4^{2-}$.[63]

## 1.3.2.1 Anion-centred Barrels, Mesocates, Helicates and Tetrahedra

The molecular modelling experiments with receptor **49** provide an insight into the possibilities for arranging anion receptors around anions. Barrels, mesocates and helicates form a different class of assembly to the capsules mentioned so far. Generally, a barrel is a tubular composition of receptors around a core axis, while a helicate possesses a helical
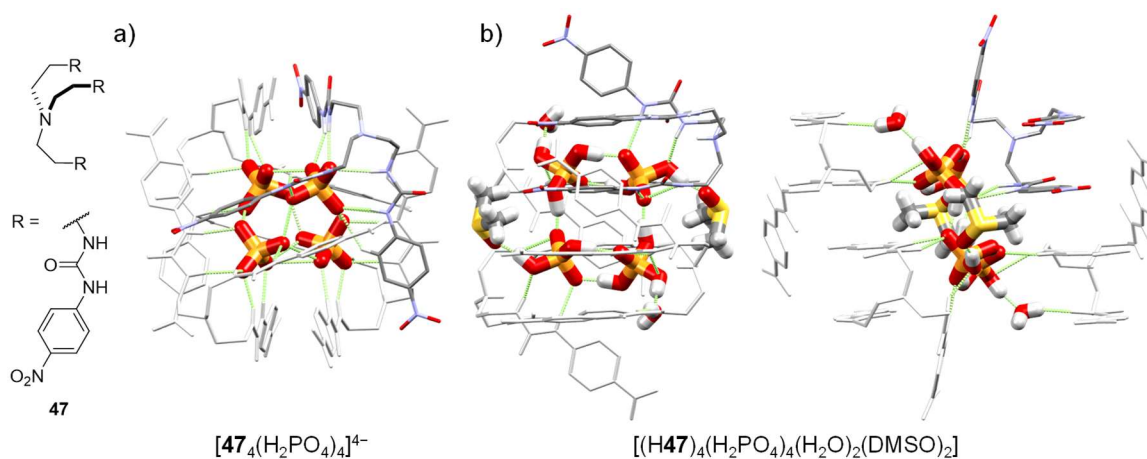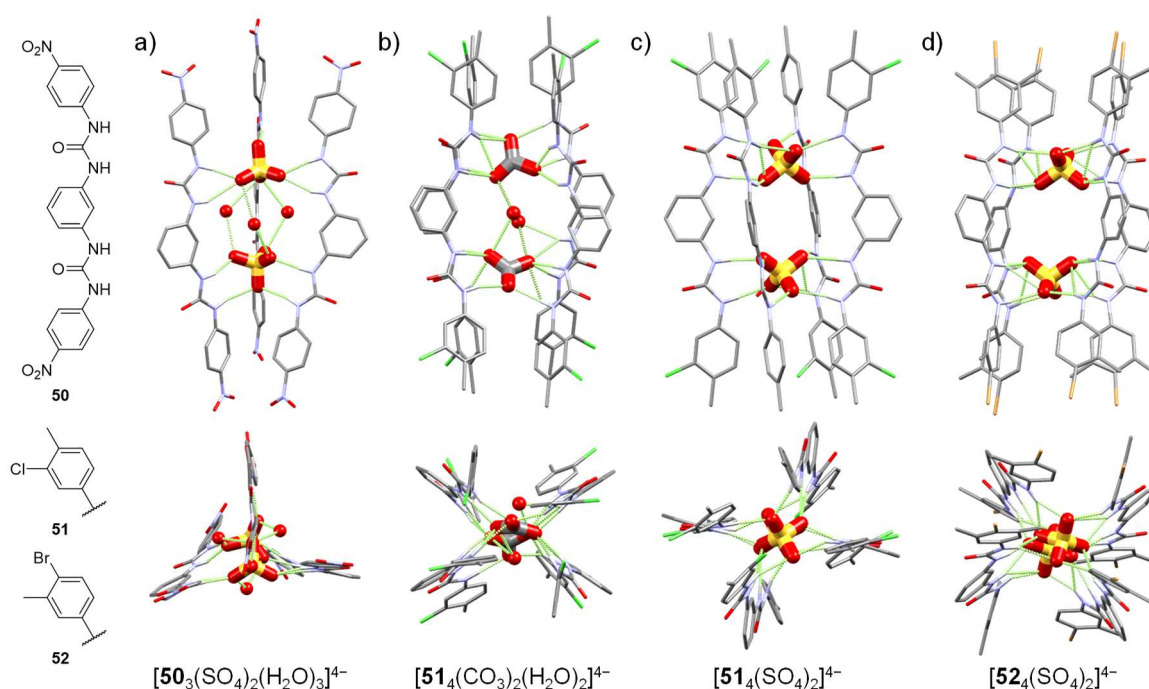


Figure 1.19. Structure of the meta-phenylene bis(phenylurea) receptors **50**, **51** and **52**, and crystal structures of their adducts with sulfate and carbonate (a–d). Non-hydrogen bonding hydrogen atoms, non-interacting solvent molecules and counterions are omitted for clarity.

sense to this arrangement. The mesocate is similar to the helicate, but contains a plane of symmetry perpendicular to the longitudinal axis of the assembly. A variety of barrels have been reported by Das and coworkers, Figure 1.9. The *meta*-phenylene bis(phenylurea) derivatives **52**–**50** were observed to crystallise from DMSO/DMF with carbonate and sulfate salts as three- and four-stranded barrel-shaped adducts.[64,131] Three molecules of **50** bound two $SO_4^{2-}$ anions, and four molecules of **52** were shown to hold two $CO_3^{2-}$ anions; with three, and two bridging water molecules respectively, Figure 1.9a–b. Conversely, the receptors **52** and **51** supported two discrete $SO_4^{2-}$ anions with no bridging or hydrogen-bonding interactions between them, Figure 1.9c–d. Noting the commonalities between the crystal structures of these adducts, the authors concluded that the electronic effect at the terminal rings had little effect on recognition of anions, and that these were properties dictated by the anions themselves.[131] However, meaningful binding constants were not calculated for the solution-state studies, and this behaviour remains unquantified. Das and coworkers also reported a similar system in which three molecules of the *ortho*-phenylene analogue of **52** each bound a $Cl^-$ anion, and were arranged around a central DMSO molecule.[132]

The first reports of anion templated helicates were by Sánchez-Quesada *et al.*[133] Unusually for anion-templated helicates, the data used to determine their existence came entirely from solution-state measurements, Figure 1.20. Receptors **53**–**55**, each containing two or four chiral guanidinium units, were observed to form helical structures in the presence of $SO_4^{2-}$ in organic solution. This was determined by the increase in CD signal intensity upon exchange of the chloride salt with sulfate, Figure 1.20iii. No such change was observed
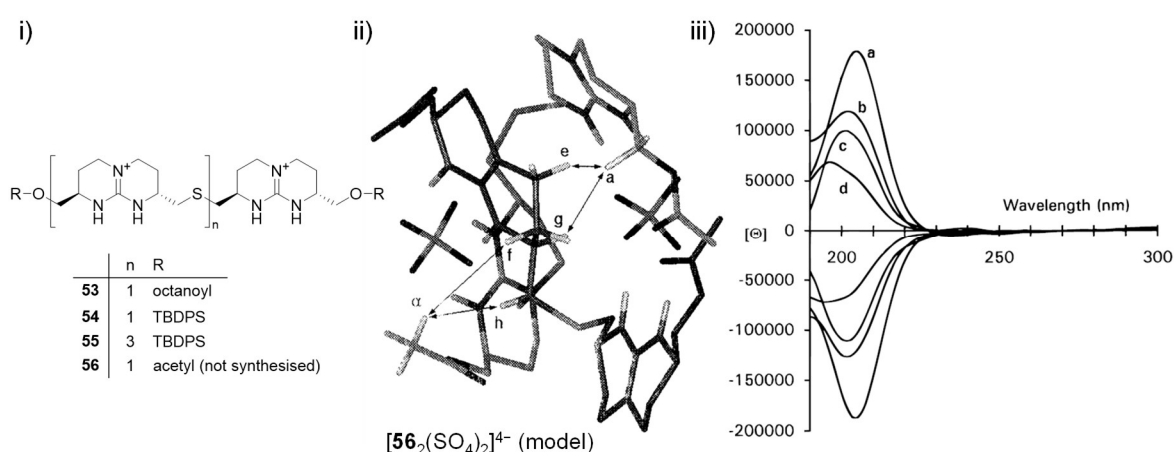


Figure 1.20. i) Structures of the chiral guanidinium compounds **53**–**56**. ii) Image of a molecular mechanics energy-minimised structure (AMBER force field) of the acetyl analogue **56**, with arrows indicating the through-space interactions observed in 2D ROESY spectra of **53** and **55**. iii) CD spectra of the sulfate and chloride salts of **55** (a, b) and **54** (c, d), and their enantiomers in MeCN. Images reproduced from reference 133, copyright 2012 The Royal Society of Chemistry.

with a simple receptor containing one guanidinium moiety. 2D ROESY experiments also suggested that the guanidinium units were arranged in such a way that two receptors were bound in close proximity, see molecular mechanics simulation in Figure 1.20ii.

Gale and coworkers reported a fluoride-templated helicate consisting of two molecules of the isophthalic diamide **57** and two fluoride anions, Figure 1.21a.[134] Keegan *et al.*,[135] and later Selvakumar *et al.*[136] used the tetraprotonated form of the dipyridyl receptor **58** to form the chloride- and bromide-templated helicates $[(H_4\mathbf{58})_2Cl_2]^{2+}$ and $[(H_4\mathbf{58})_2Br_2]^{2+}$, Figure 1.21b. A more recent example of a chloride-templated helicate from Yohei *et al.*, $[\mathbf{59}_2Cl_2]^{2-}$, incorporates two foldamer molecules which fully encapsulate two chloride anions, Figure 1.21c.[65] The manner in which the molecules of **59** wrap around the Cl⁻ anions bears close similarity to the earlier-mentioned chloride–foldamer adduct $[\mathbf{35}Cl_2]^{2-}$ reported by Wu and coworkers, compare Figure 1.11b. The sole example of an iodide-templated helicate, reported by Massena *et al.*, consisted of two iodopyridinium foldamer molecules around two iodide ions, and utilised halogen-bonding interactions.[137]
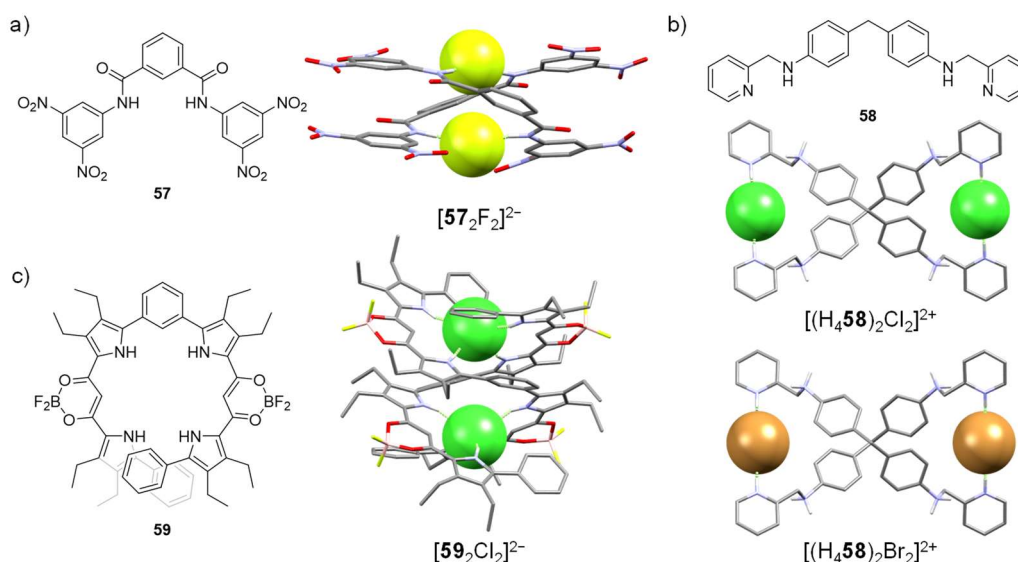


Figure 1.21. Structures of the receptors **57**, **58** and **59**, and the crystal structures of their halide-templated helicates $[\mathbf{57}_2F_2]^{2-}$ (a), $[(H_4\mathbf{58})_2Cl_2]^{2+}$ and $[(H_4\mathbf{58})_2Br_2]^{2+}$ (b), and $[\mathbf{59}_2Cl_2]^{2-}$ (c). Non-hydrogen bonding hydrogen atoms, solvent molecules and other ions are omitted for clarity.

All examples of phosphate-templated helicates to date have come from Wu and coworkers, and have utilised a nitrophenyl-terminated *ortho*-phenylene bisurea motif as the phosphate-binding unit. By varying the geometry of the linker, the assembly can be directed to form different shapes, see Figure 1.22 and Figure 1.23. The propyl- and *m*-xylyl-linked compounds **60** and **61** formed the mono-bridged dinuclear complex $[\mathbf{60}_3(PO_4)_2]^{6-}$, and the mesocate $[\mathbf{61}_3(PO_4)_2]^{6-}$, respectively (Figure 1.22a,b).[138] Meanwhile, the tripodal receptor **62** formed a tetrahedral inclusion complex with a tetramethylammoium (TMA⁺) cation
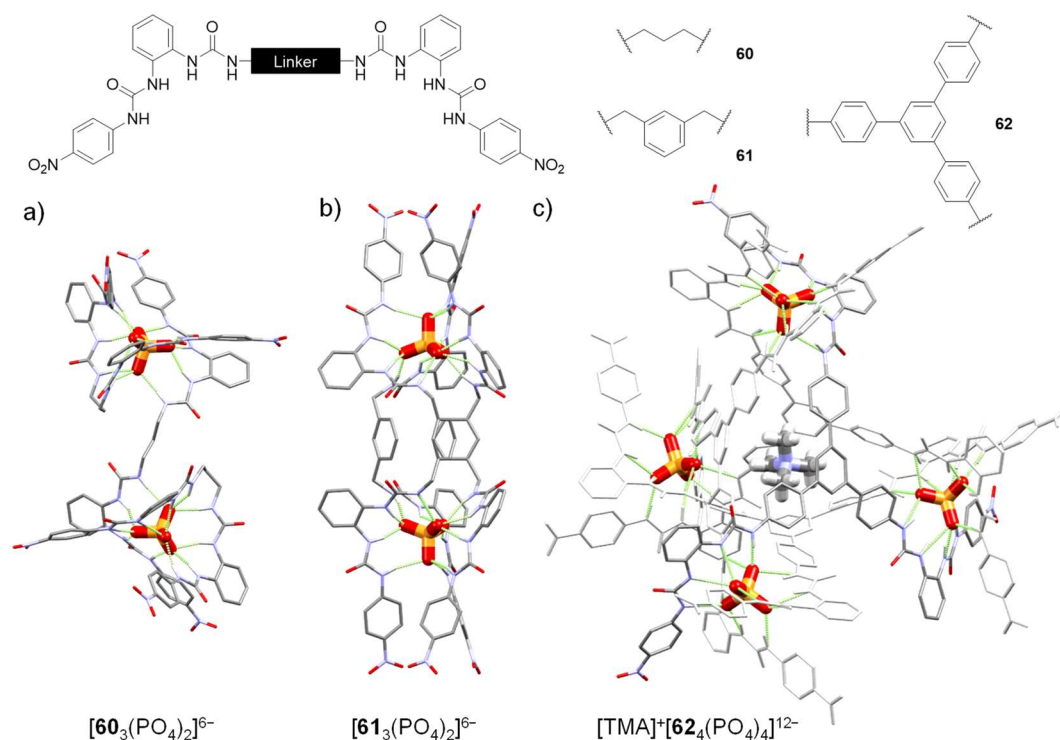
Figure 1.22. General structure of the receptors **60**, **61** and **62**, containing two or more *ortho*-phenylene bisurea motifs. a–c) Crystal structures of higher-order assemblies formed between phosphate anions and these receptors. a) Dinuclear bridged, or "ansa" complex [**60**$_3$(PO$_4$)$_2$]$^{6-}$, b) mesocate [**61**$_3$(PO$_4$)$_2$]$^{6-}$, c) Tetrahedral inclusion complex [TMA]$^+$[**62**$_4$(PO$_4$)$_4$]$^{12-}$. Only one molecule of **62** is shown in colour to illustrate the conformation of the receptor. Non-hydrogen bonding hydrogen atoms, solvent molecules and non-encapsulated ions are omitted for clarity.

(Figure 1.22c); the same tetrahedral structure was also found to form with various haloforms in place of TMA$^+$.[139]

As shown in Figure 1.23, helicates are formed when the linker used is a 1,2-ethyl (**63**),[62] 1,4-phenylene (**64**),[140] *para*-xylyl (**65**),[138] or 4,4′-diphenylmethylene group (**66**).[141] The crystal structure of the latter includes a trimethylammonium counterion within an open six-sided "aromatic box", which resembles the binding site of the choline-binding protein ChoX, Figure 1.23c–e. The binding of choline by the helical assembly [**66**$_3$(PO$_4$)$_2$]$^{6-}$ was monitored in solution through the marked shielding of the TMA$^+$ protons in $^1$H NMR experiments, and by displacement studies of a styrylpyridinium switch OFF fluorescent host–guest complex. Modelling of the interaction using DFT calculations demonstrated a potential hydrogen-bonding interaction with one of the urea moieties, Figure 1.23d–e. The selectivity of the assembly for choline binding was illustrated through competition experiments with acetylcholine, L-carnitine, and glycine betaine.[141] Further work demonstrated that the normally CD-silent racemate [**66**$_3$(PO$_4$)$_2$]$^{6-}$ could be induced to form

either the *P* or *M* helix upon binding of chiral ammonium guests, as monitored though the induction of a CD signal in MeCN.[142]

Similarly, the 1,4-phenylene linked receptor **64** was found to form both a triple-stranded helicate and a tetrahedral complex in acetone solution. More dilute concentrations (0.06 mM) or competitive solvent (DMSO) favoured the formation of the helicate, and only the tetrahedral TMA$^+$ inclusion complex could be crystallised, through ether diffusion in acetone, Figure 1.23f. The assembly could also be switched from the helical to the tetrahedral form by the addition of TMA$^+$, due to a templating effect of the TMA$^+$ cations on the edges
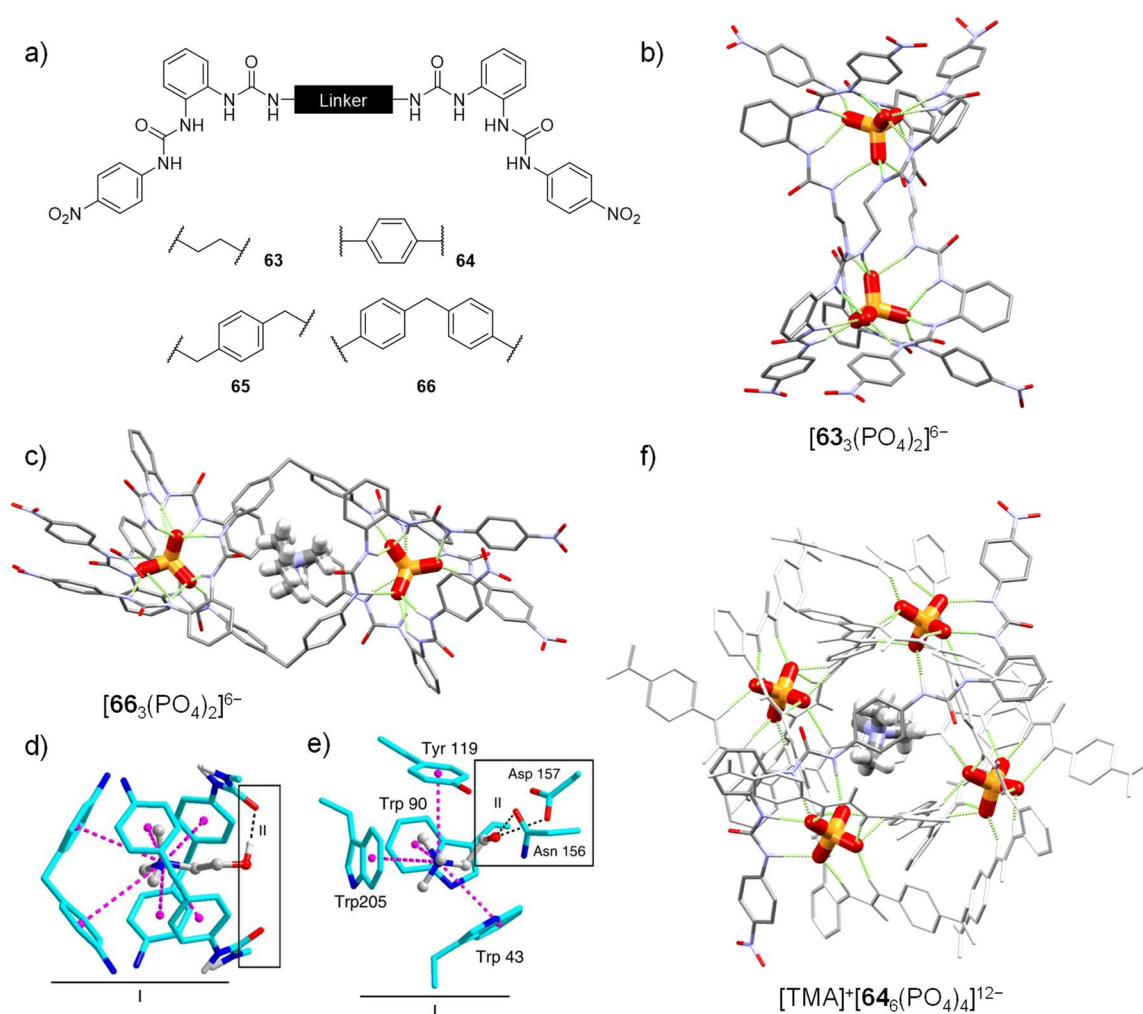


Figure 1.23. a) Chemical structures of the receptors **63**–**66**. Crystal structures of the phosphate templated helicate [**63**$_3$(PO$_4$)$_2$]$^{6-}$ (b), and the helicate inclusion complex [TMA]$^+$[**66**$_3$(PO$_4$)$_2$]$^{6-}$ (c). DFT optimised structure of the adduct between [**66**$_3$(PO$_4$)$_2$]$^{6-}$ and choline (d), and crystal structure of the binding site of ChoX with bound choline molecule (e). Region I is the "aromatic box" of each receptor, while region II is where the hydrogen bonding interactions between choline and the receptor occur. Figure adapted from reference 141, copyright Chuandong Jia *et al.*, under a Creative Commons Attribution 4.0 International License. f) Tetrahedral inclusion complex [TMA]$^+$[**64**$_6$(PO$_4$)$_4$]$^{12-}$. Only one molecule of **64** is shown in colour to illustrate the conformation of the receptor. Non-hydrogen bonding hydrogen atoms, solvent molecules, non-encapsulated ions and coordinated K[18]-crown-6 are omitted for clarity.

of the tetrahedron. Selective use of certain ammonium salts could therefore be used to generate tetrahedra with vacant guest sites.[140]

The previous sections have illustrated the use of hydrogen-bonding donor molecules to create novel anion-directed assemblies, with some degree of control over the structural behaviour of these assemblies. The variety of applications of anion binding chemistry in pollutant removal, transmembrane anion transport, and catalysis has also been described. The next sections focus on relevant work from the Gunnlaugsson research group, as well as the specific contribution of this work to the field.

## 1.4  Prior Work by Gunnlaugsson and Coworkers

The Gunnlaugsson group has had a long-standing interest in designing new interlocked and entangled systems. The past ten years have seen several examples of enantiopure Ln(III)-centred helicates from the Gunnlaugsson group, using a variety of linkers, Figure 1.24a. Early work by Stomeo, Comby and Lincheneau demonstrated that the chiral environment adjacent to the naphthalene antenna influenced the chirality of the resulting helicates.[143–145] Assignment of the stereochemistry of these helicates is possible by comparing the circular dichroism (CD) and circularly polarised luminescence (CPL) spectra of these assemblies to relevant complexes for which a crystal structure had previously been obtained.[146] Most recently, Kotova *et al*. have studied the effect of linker size on helicate formation, noting that the ligand centred emission of the *meta*-phenylene linked **67** increased upon addition of up to 0.67 eq. Eu(OTf)$_3$, suggesting interactions between the ligands and an increasing rigidity upon complexation. This was not the case when using the bulky cyclohexyl-bridged ligand **71**. The 2:3 metal–ligand binding constant was lower for **71** than that for **67**, perhaps due to steric interactions between neighbouring ligands in the assembly [Eu$_2$**71**$_3$]$^{6+}$.[147] The formation of these enantiopure systems were followed by CPL and CD titrations, providing an additional level of insight, *e.g.* the CD titration of (*S,S*)-**71** in Figure 1.24b.
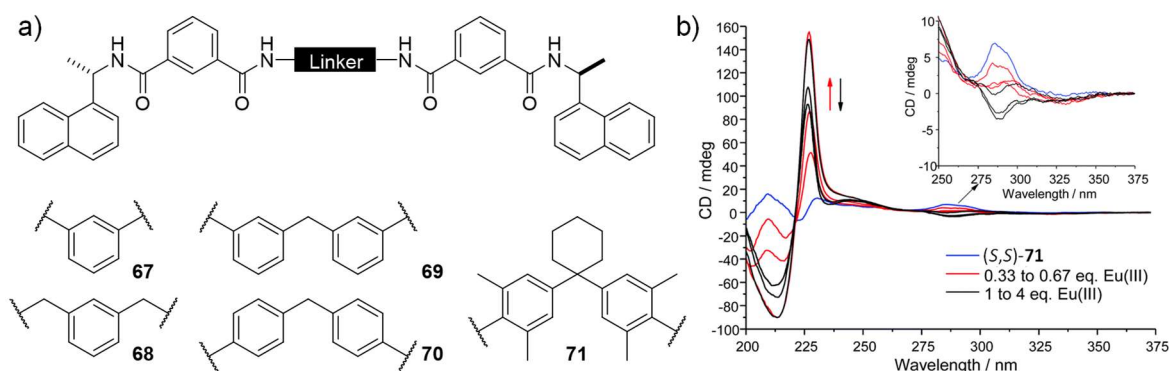


Figure 1.24. a) Structures of some of the Ln(III)-centred helicates published in recent years by Gunnlaugsson and coworkers. b) CD titration of (*S,S*)-**71** with Eu(OTf)$_3$ in CH$_3$CN ($1.34 \times 10^{-5}$ M, 0→4 eq.). Image reproduced in part from reference 147. Copyright 2018 The Royal Society of Chemistry.
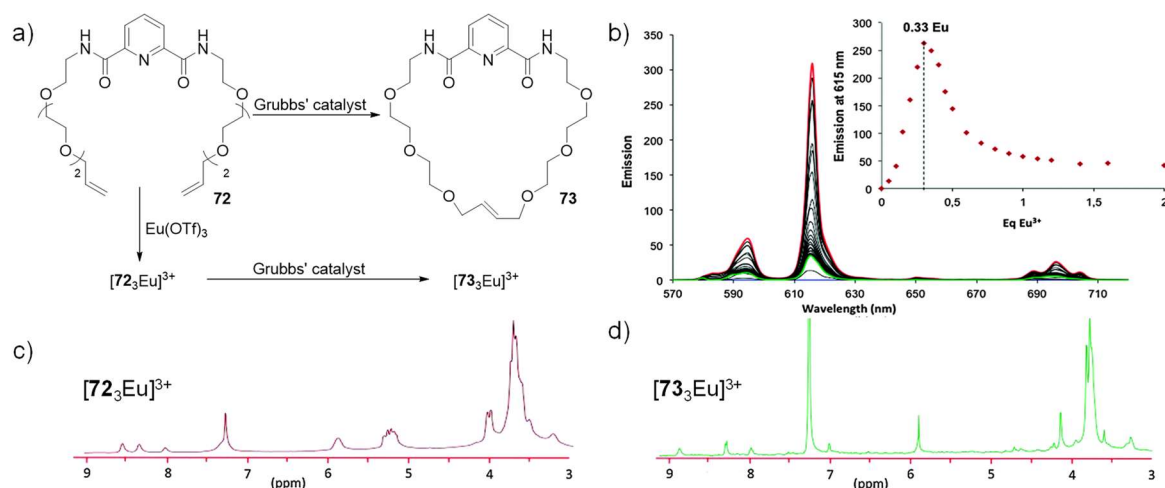
Figure 1.25 a) Synthesis of the macrocyclic ligand **73** and the Eu(III) complexes [**72**$_3$Eu]$^{3+}$ and [**73**$_3$Eu]$^{3+}$. b) Luminescence titrations of precursor **72** with Eu(OTf)$_3$ in MeCN ($\lambda_{ex}$ = 281 nm). c–d) $^1$H NMR spectra of the Eu(III) complexes [**72**$_3$Eu]$^{3+}$ and [**73**$_3$Eu]$^{3+}$. Images reproduced in part from reference 148. Copyright 2014 The Royal Society of Chemistry.

In 2014, Lincheneau *et al*. reported the formation of a Eu(III)-templated [3]catenane *via* the ring-closing metathesis of the corresponding 1:3 metal-ligand complex, Figure 1.25.[148] In this case, Eu(OTf)$_3$ was used to template the assembly of three molecules of the alkene-terminated dipicolylamide (dpa) ligand **72**. UV-visible titrations demonstrated that
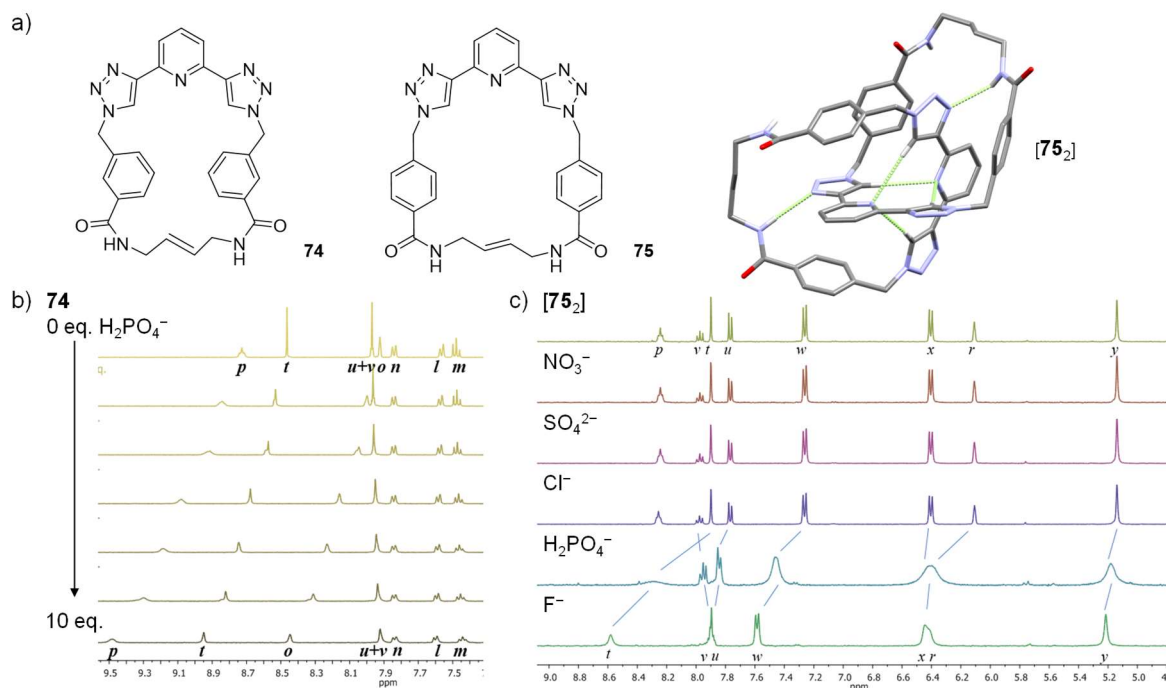


Figure 1.26. a) Structure of the macrocycles **75** and **74** and crystal structure of the self-assembled [2]catenane [**75**$_2$], showing C−H···N hydrogen-bonding interactions between the triazolyl protons and the pyridyl nitrogen atoms, and secondary interactions between the amido protons and the triazolyl nitrogen atoms. b) End-points of the titrations of [**75**$_2$] with various anions (10 eq.). c) Titration of the macrocyclic receptor **74** with H$_2$PO$_4^-$. Titrations performed in DMSO-$d_6$ with the TBA$^+$ salts, at 25 °C. Images adapted from reference 151.

the 1:3 metal-ligand complex [Eu.$72_3$] was very stable with a value of $\log\beta_{1:3} = 18.7 \pm 0.8$. Subsequent reaction of this complex under RCM conditions produced a mixture of products, appearing to contain the [3]catenane [$73_3$], along with the [2] and [3]catenates [Eu.$73_2$] and [Eu.$73_3$], as evidenced by MALDI-TOF mass spectrometry.

Meanwhile, Byrne, McCarney and Aletti have produced fully organic [2]catenanes from the bis(triazole)pyridine (btp) motif, Figure 1.26.[149–152] While originally designed as an $N_3$-terdentate ligand for metal ions, rotation around the pyridine–triazole bond allows these molecules to self-associate using a set of four C−H···N hydrogen bonds Figure 1.26a. The hydrogen bonding donors form a tetrahedral cavity into which anions such as phosphate may bind.[152] Work by Aletti demonstrated that the *meta*-substituted macrocycle **74** bound phosphate more strongly ($\log\beta_{1:1} = 2.14$) than [2]catenanes with *para*-substituted phenylene rings (for [$75_2$], $\log\beta_{1:1} = 2.05$). The binding constants of *para*-substituted macrocycles such as **75** for $H_2PO_4^-$ were lowest, $\log\beta_{1:1} = 1.2$–1.5. This was understood to be because an amido group at the *meta* position may take part in a chelating hydrogen-bonding interaction. Such an interaction is also possible with the four C−H hydrogen-bond donors in the [2]catenane [$75_2$], but this is ultimately less strong.[151] The chiral methyl-substituted receptor **76** and the corresponding [2]catenane [$76_2$] (structures in Figure 1.27) displayed no interaction with $H_2PO_4^-$, presumably due to steric hindrance of the binding site by the nearby methyl groups.

McCarney explored the self-assembly of btp molecules, through experiments on the threading of single macrocycles with linear btp molecules, and thereafter closing through RCM to form the desired [2]catenanes. Pseudorotaxane formation was evident after mixing **76** and **77** for 120 h in CDCl$_3$ (Figure 1.27), and the [2]catenane was observed to have formed within 24 h of addition of the catalyst to the solution. No such assembly was



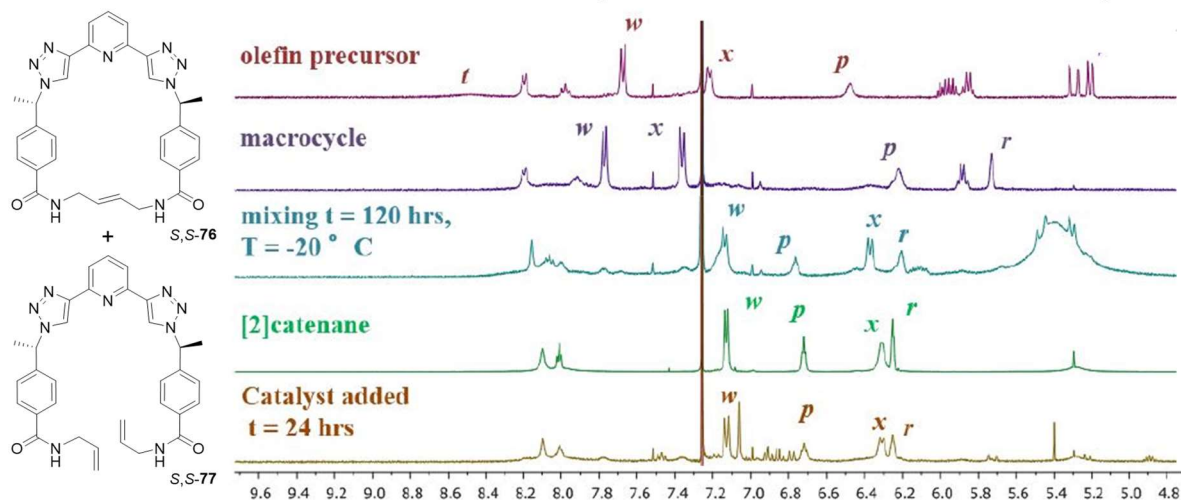Figure 1.27. Structures of the chiral macrocycle (*S,S*)-**76** and its precursor (*S,S*)-**77**, along with $^1$H NMR experiment showing formation of the pseudorotaxane [(*S,S*)-**76**·(*S,S*)-**77**], and formation of the [2]catenane [(*S,S*)-**76**$_2$] upon addition of Grubbs' catalyst. Image adapted from reference 150 under the Creative Commons Attribution-NonCommercial-ShareAlike 1.0 Generic Licence (CC BY-NC-SA 1.0).

observed in the more competitive solvent DMSO. The [2]catenane also failed to form when the benzylamide arms were replaced with an alkyl chain, demonstrating the importance of the secondary interactions between the amide moieties and the btp core in directing [2]catenane formation.[150]

In collaboration with Amendola and coworkers, Aletti has also explored the halide-binding abilities of a tri(imidazolium) cage [78]$^{3+}$, see Figure 1.28. Through ^{1}H NMR and UV-visible titrations, the binding affinities for F$^-$, Cl$^-$, Br$^-$ and I$^-$ were interrogated. The binding affinity for Cl$^-$ could not be obtained through NMR experiments as it appeared to be too strong to quantify. Analysis of crystal structures, 2D NOESY and DOSY NMR experiments, demonstrated that [78]$^{3+}$ changed from an oblate to a prolate conformation (with respect to the N–N axis) upon binding of a Cl$^-$ anion within the cavity, Figure 1.28.[151]

Complementing the complexity of the latter two examples, much work has been done on fundamental anion binding with simple receptors. In early work, the urea moiety was appended with aromatic fluorophores to monitor and quantify the binding through UV-visible absorption and fluorescence spectroscopy.[153–157] The anthracene-containing receptor **79** selectively senses AcO$^-$, H$_2$PO$_4^-$ and F$^-$ over Cl$^-$ and Br$^-$ by quenching the fluorescence of the anthracene group through photoinduced electron transfer (PET), see Figure 1.29a for structure.[158] This strategy has been employed across a range of anion receptors by the Gunnlaugsson group.[155,159,160] Other receptors were designed to take advantage of internal charge transfer (ICT), such as the naphthalimide-derived thiosemicarbazide receptor **80** (Figure 1.29a), which undergoes dramatic colour changes from yellow to deep purple upon addition of AcO$^-$ in pH-buffered DMSO.[156] Pyridyl thiosemicarbazides (**81**), on the other
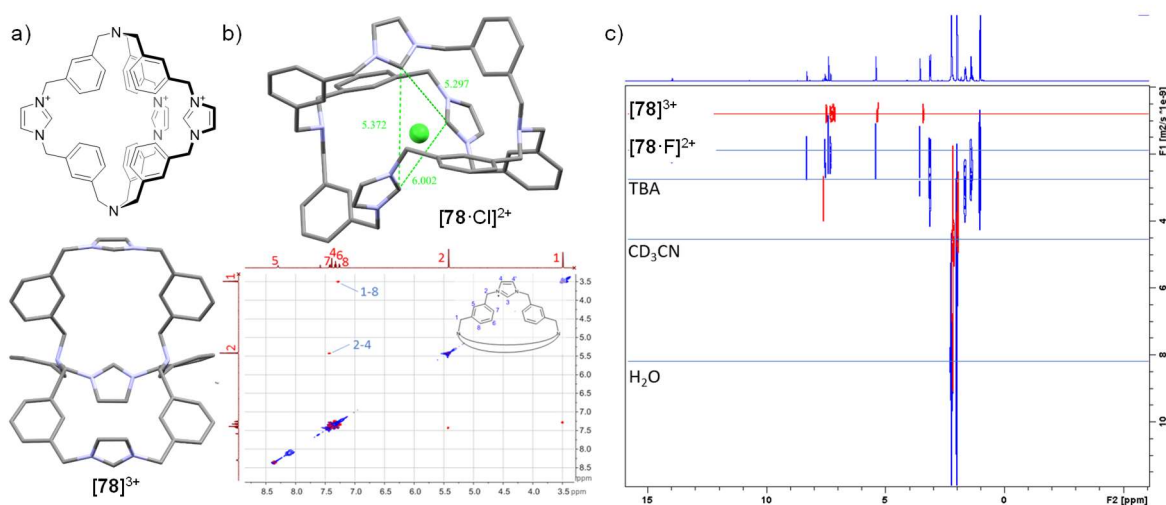


Figure 1.28. a) Chemical and crystal state structures of the tri(imidazolium) cage [78]$^{3+}$. b) Crystal structure of the chloride adduct [78Cl]$^{2+}$, and 2D NOESY spectrum showing that the cage adopts the same conformation in solution. c) DOSY experiment showing the different diffusion rates of [78]$^{3+}$ and [78F]$^{2+}$. Images reproduced in part from reference 151.
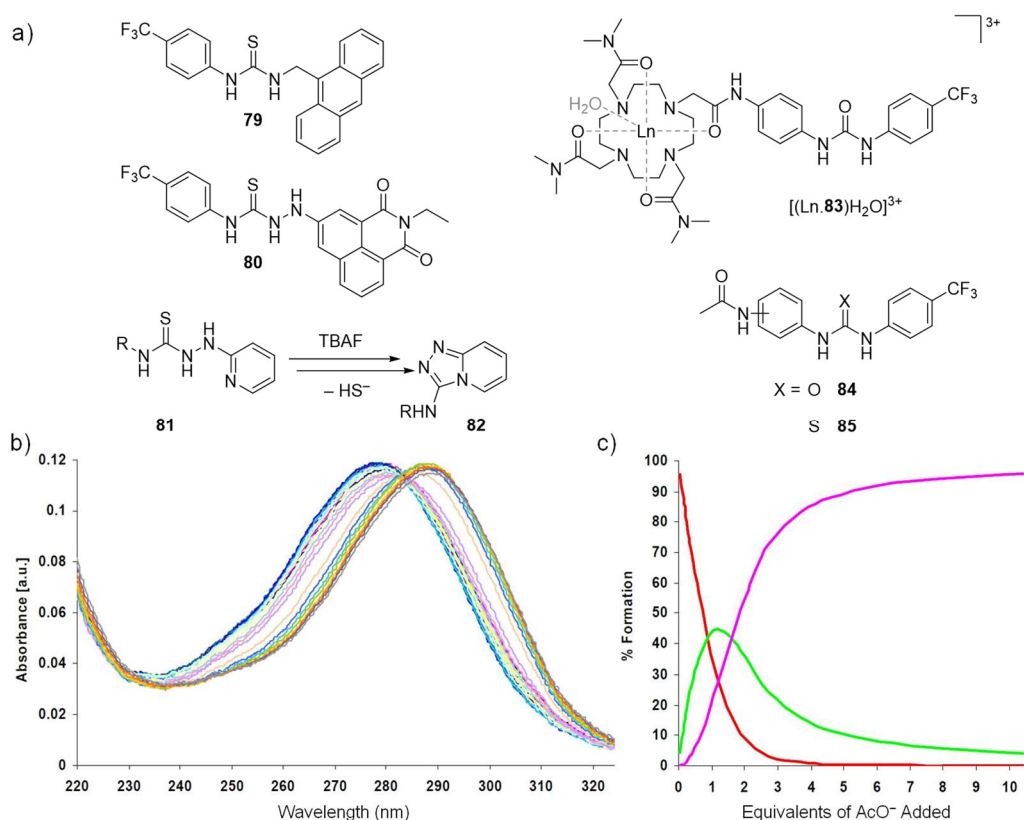
Figure 1.29 a) Structure of a selection of urea and thiourea derived receptors **79–85** reported by Gunnlaugsson and coworkers. b) UV-visible titration of the urea-appended Ln(III)-cyclen complex $[(Ln.\textbf{83})(H_2O)]^{3+}$ showing changes occurring upon addition of TBAH$_2$PO$_4$ to the Tb(III) complex. c) Corresponding speciation distribution diagram for the titration showing the existence of 1:1 and 1:2 host–guest binding equilibria. Images adapted from reference 167. Copyright 2007 The Royal Society of Chemistry.

hand, were found to undergo an elimination and a concomitant intramolecular cyclisation to form 3-amino-[1,2,4]-triazolopyridines (**82**) on the addition of F$^-$, see Figure 1.29a.[161,162]

Several systematic studies have been undertaken to elucidate the behaviour of anion receptors. Ali reported that a series of 36 simple diarylurea receptors exhibited several behaviours that seemed "counter-intuitive", with no clear trends in binding affinities,[163] demonstrating that much work is still needed to fully understand the behaviour of arylurea receptors. Thiourea-based receptors, for instance, bound dihydrogen phosphate less strongly than their urea analogues. It is now understood that disubstituted thiourea molecules have a preference for the poorly-binding *syn-anti* conformation.[164–166] Dos Santos *et al*. discovered an unexpected second binding equilibrium in the Ln(III)-cyclen/urea receptor $[(Ln.\textbf{83})(H_2O)]^{3+}$, see Figure 1.29b.[167] The reported allosteric binding of the Eu(III) and Tb(III) complexes of **83** led to further studies on acetamidophenyl urea receptors by dos Santos *et al*. and the thiourea analogues by Boyle *et al*. (**84** and **85**, see Figure 1.29).[168,169] These studies demonstrated the existence of a positional isomer effect, in which the binding affinities were most pronounced in the 3-acetamido isomers.

Another extension of this amidourea system was studied by Pandurangan, dos Santos, Boyle and Aletti, in which the benzenetricarboxamide (BTA) motif was appended with three urea or thiourea moieties.[151,170–172] The *para*-substituted tripodal receptor **86** was observed to bind $H_2PO_4^-$ and $SO_4^{2-}$ strongly in a 1:1 host–guest binding stoichiometry ($\log\beta_{1:1} = 4.2$ and 3.7, respectively). The *meta* isomer **87** bound $SO_4^{2-}$ less strongly, but possessed a slightly stronger affinity for $Cl^-$. MM2 force field calculations of the 1:1 binding modes of **86** and **87** with $Cl^-$ demonstrated that in each case the binding occurred solely through the urea moieties, and that the amide protons were directed outward from the assembly, Figure 1.30b. Comparison of the two calculated structures shows that **87** encapsulated the $Cl^-$ anion more effectively.[170] Noting the lack of interaction of the amido protons with the bound anion, the tris(*N*-methyl) receptor **88** was developed. A crystal structure was obtained in which two molecules of **88** were observed to bind a dimeric $[(H_2PO_4)_2(H_2O)]^{2-}$ phosphate cluster in a loose capsular assembly, Figure 1.30c.[171]

The dipodal hexyloxyphenyl urea compound **89** had been observed to form as a byproduct of the synthesis of its tripodal analogue.[171] Crystallisation experiments of the mixture of these compounds with $TBA_2SO_4$ led to the "self-sorting" of the $[(\mathbf{89})_4(SO_4)_4]^{8-}$
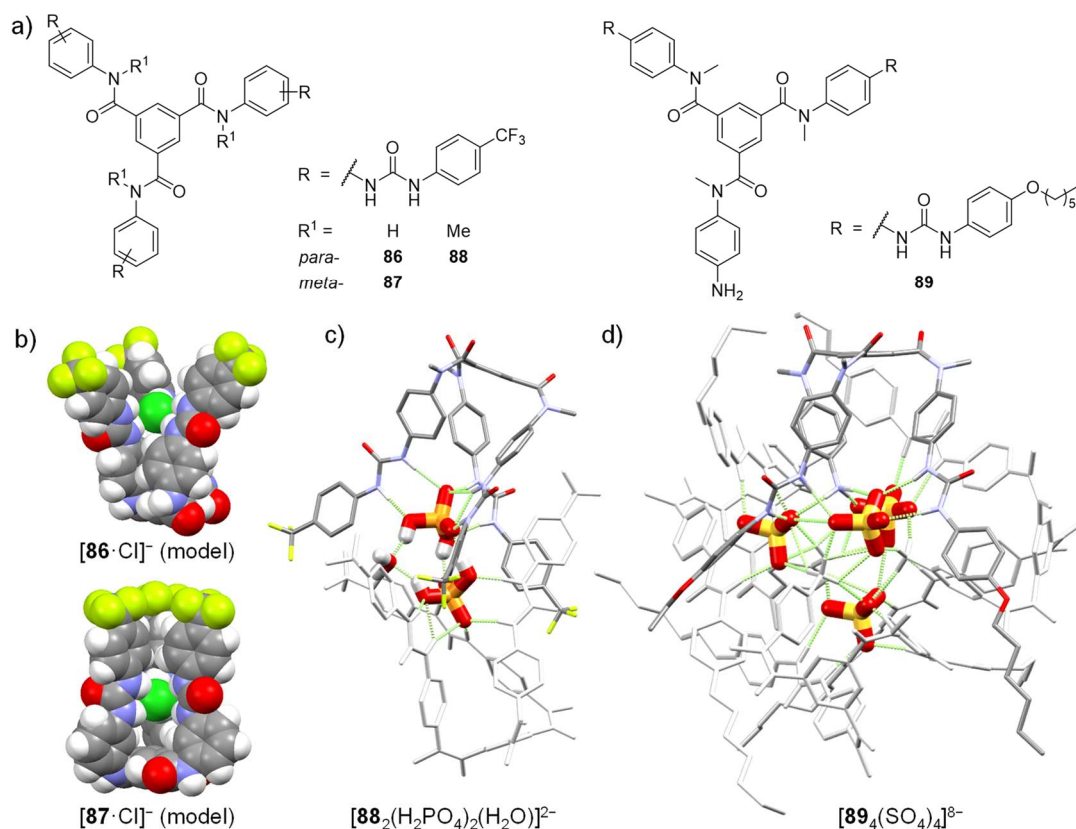


Figure 1.30. a) Chemical structures of the tripodal receptors **86**, **87** and **88**, and the dipodal receptor **89**. b) MM2 force field calculations of the adducts $[\mathbf{86}Cl]^-$ and $[\mathbf{87}Cl]^-$. Images adapted from reference 170. Copyright 2011 The Royal Society of Chemistry. c–d) Crystal structures of the anionic adducts $[\mathbf{88}_2(H_2PO_4)_2(H_2O)]^{2-}$ and $[\mathbf{89}_4(SO_4)_4]^{8-}$, respectively. All but one molecule of each receptor has been coloured
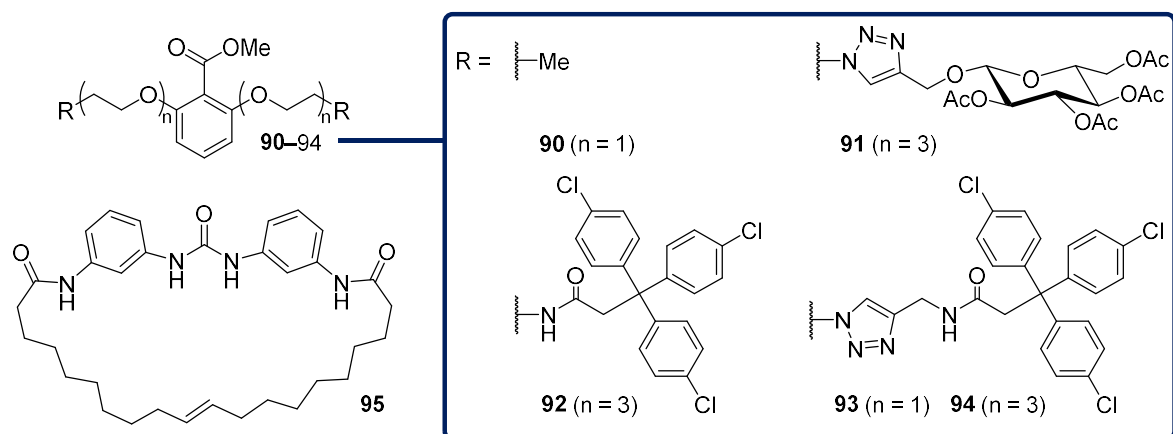
Figure 1.31. Macrocyclic di(amidophenyl)urea receptor **95** and methyl ester axle precursors **90–94** used by Boyle in the attempted synthesis of interlocked molecules.

adduct from the mixture. The tetrasulfate cluster within this assembly is stabilised by several N−H···O bonds from the amino moieties, which were positioned to the centre of the cluster, Figure 1.30d. The corresponding trifluoromethylphenyl thiourea receptor, being more readily synthesised than **89**, was studied through $^1$H NMR titrations. This was found to possess a high binding affinity for $SO_4^{2-}$, with a calculated value of $\log\beta_{2:1} > 6$ in CD$_3$CN/DMSO-$d_6$ (5:1), corresponding to a 2:1 host–guest capsular assembly.[151]

Boyle synthesised a series of vinyl-terminated di(amidophenyl)urea receptors along with the macrocyclic derivative **95**, Figure 1.31.[172] The anion-binding abilities of receptor **95** and its non-macrocyclic analogues towards $H_2PO_4^-$, BzO$^-$ and $SO_4^{2-}$ were studied, with strong binding affinities being reported for all three. A series of benzoic acid derived axles (**90–94**) were also synthesised as part of attempts to form rotaxanes, catenanes and pseudorotaxanes with **95**. This work will be discussed further in Chapter 3.

Having discussed the relevance of the fields of anion binding and interlocked systems through their applications across a wide variety of fields, as well as the structural requirements for such systems, the next section introduces the aims, scope and achievements of this work in brief.

## 1.5  Work Described in this Thesis

This work investigates urea- and amide-based hydrogen-binding systems as candidate components in assemblies of interlocked molecules, as well as small-molecule anion-binding systems in their own right. Specifically, it is envisaged that interlocked systems can be created in which both components are neutral, non-interacting molecules, but which form a strong and reversible association upon modulation of solution pH. In this regard, the urea-carboxylate interaction is seen as ideal, due to the apparent geometric complementarity of the hydrogen bond donor and acceptor, and the strength of their interaction. Equally
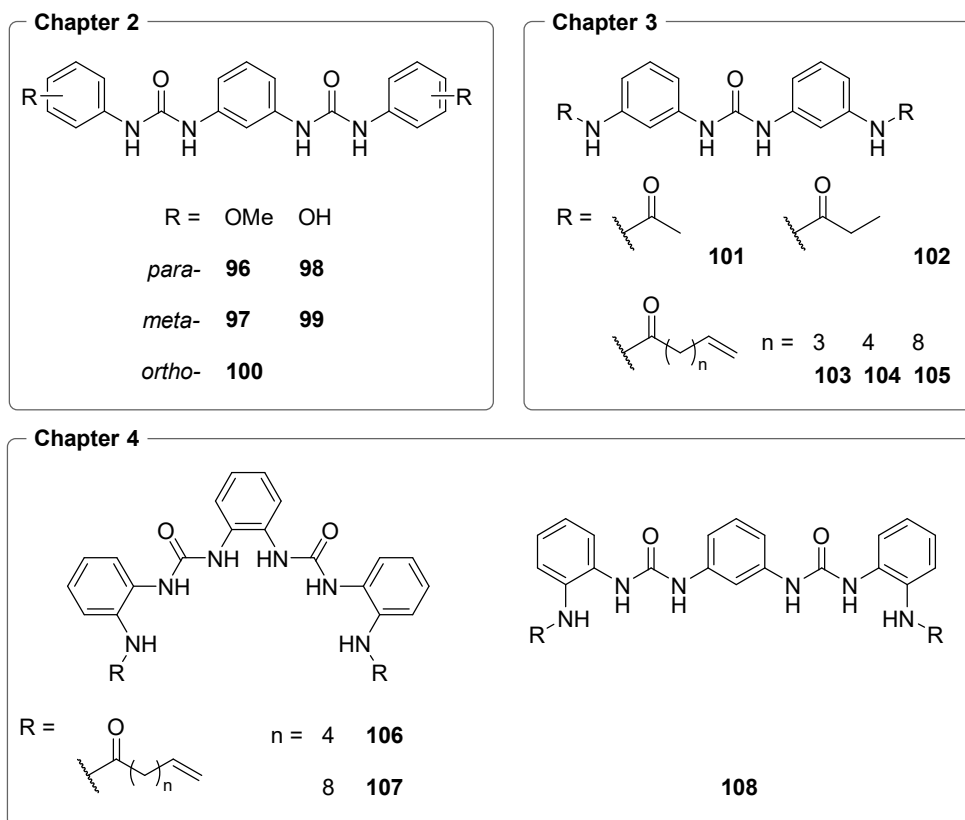
Figure 1.32 Structures of the 13 urea-based anion receptors **96**–**108** synthesised as part of this work.

important is the low affinity of urea-based receptors for the corresponding carboxylic acids. Nevertheless, the hydrogen-bonding receptors presented in this work have been studied with other classes of anion in order to fully capture their anion-binding behaviour, and screen for other possible uses. Interlocked molecules are an exciting class of chemical systems for various reasons including their capacity for novel catalytic and material properties, as well as their applicability in the burgeoning field of molecular machinery. An interlocked molecular system such as described above is expected to be able to switch between predesigned chemical and mechanical behaviours, with a simple change in pH.

In Chapter 2, a series of electron-rich *meta*-phenylene bis(phenylurea) derivatives will be presented, **96**–**100** in Figure 1.32, and their anion binding behaviour analysed in detail through ¹H NMR titrations with the tetrabutylammonium salts of several anions. The association between the receptor geometry and binding stoichiometry will be discussed. Additionally, the crystalline-phase adducts of these receptors with phosphate and acetate anions will be discussed, and an example of a triple stranded phosphate-templated helicate presented. From this work, a detailed picture of the binding behaviour of this motif with various classes of anions will be understood.

The work presented in Chapter 3 investigates the change in binding behaviour of the simple di(3-amidophenyl)urea motif with varying aliphatic chain length (**101**–**105** in Figure

1.32), building upon preliminary results reported by Boyle.[172] The synthesis of two new receptors will be presented, and their use as negative controls explained. The titrations of the $C_3$, $C_6$ and $C_{11}$ chain receptors with $H_2PO_4^-$, $BzO^-$ and $SO_4^{2-}$ will be discussed in detail. In this chapter, comparison will be made between the two sets of results, and attempts made to suggest a mechanism for the observed differences.

In Chapter 4, the synthesis of three classes of $H_6$–hexadentate receptor molecules will be presented, **106**–**108** in Figure 1.32, thus combining the properties of the receptors studied in Chapters 2 and 3. The attempted syntheses of their macrocyclic derivatives will also be discussed. The binding affinities of these molecules will be compared with respect to the dihydrogenphosphate and benzoate anions.

The overall conclusions for each chapter will be presented in Chapter 5. Chapter 6 will describe the experimental details of the work presented in Chapters 2–4, including synthesis and spectroscopic methods. The bibliography is provided in Chapter 7, while additional spectroscopic data, characterisation and some details on data analysis will be included within the appendices.

# Chapter 2

## Anion Recognition of Electron-Rich *meta*-Phenylene bis(Phenylurea) Receptors

## 2.1 Introduction and Rationale

The interest in electron-poor anion receptors has historically been strong, due to the anticipated increase in anion-binding affinity to the relatively acidic hydrogen-bond donor moieties, *e.g.* nitro- and trifluoromethyl-functionalised hosts.[82,85,157,173] However, electron-donating substituents are commonly used as synthetic handles (*i.e.* hydroxy, amino, thiol) and solubilising groups (*i.e.* alkyl, polyether), and the effects of these groups on the binding affinity of the receptor as a whole must be considered. Additionally, biasing receptors towards highly acidic NH moieties has been reported to lead to their deprotonation in the presence of more basic anions, leading to an interaction between anion and receptor that is dominated by the latter's acidity, and is often observed in both urea and thiourea based systems.[161,174,175] In some cases, where the receptor is highly acidic, the affinity for anions is less than its electron-rich counterparts,[83,160,176,177] in part due to proton transfer from the receptor to the anion, and subsequent dissociation of the host–guest complex in solution. Hunter[91] and Fabbrizzi[90] have described general trends in hydrogen bonding affinity of various anions for simple hydrogen-bonding receptors. As much as it is known that electron-poor receptors obey such trends on the basis of their acidic character, the effects of electron-rich substituents are not as well understood. As the acidity of the hydrogen bond donors is reduced, it is expected that the intrinsic affinity of the anions for such donors will play a less significant role, and the relative importance of the shape of the receptor will increase. This interest in electron-rich receptors is thus relevant to the wider study of anion-binding supramolecular systems, with the desire for creating functional and selective systems, where both electronic and geometric effects play a role.

Table 2.1. Selected Hammet[178] and steric (adjusted Taft) parameters[179] for various substituents.

| Substituent | Hammet Parameter [a] | | Steric Parameter [b] |
|---|---|---|---|
| $-R$ | $\sigma_m$ | $\sigma_p$ | Es* |
| $-H$ | 0.00 | 0.00 | 0.00 |
| $-OH$ | +0.12 | $-0.37$ | +0.55 |
| $-OMe$ | +0.12 | $-0.27$ | +0.55 |
| $-NO_2$ | +0.71 | +0.78 | $-2.52$ |
| $-CF_3$ | +0.43 | +0.54 | $-2.40$ |

a) $\sigma_m$ and $\sigma_p$ are the *meta* and *para* substituent parameters, respectively, as reported by Hansch *et al.*[178] b) Es* is the Taft steric parameter adjusted so that R = H is the datum (Es* = Es − 1.24), as reported by Unger *et al.*[179]

As noted in the introduction, dos Santos *et al.* reported an allosteric interaction between the urea and amide moieties of a series of amidophenyl urea receptors.[168] A similar effect should, therefore, be observed in the various phenylene bis(urea) isomers, Figure 2.1. While the highly convergent *ortho*-phenylene bis(urea) motif has been studied extensively by Gale and coworkers,[66,113,180–182] and Wu and coworkers,[62,63,138–141,183] among others, the *meta* isomer is less studied. Das and coworkers have developed several electron-poor *meta*-phenylene bis(phenylurea) receptors, and studied their crystalline adducts with anions.[64,131,184] These have shown the binding site to be adept at binding anionic clusters. The aromatic moieties of this framework have been extended by Ghosh *et al.*, with coumarin end-groups,[185] and by Caltagirone with asymmetric naphthalene and indole ring functionality.[126]
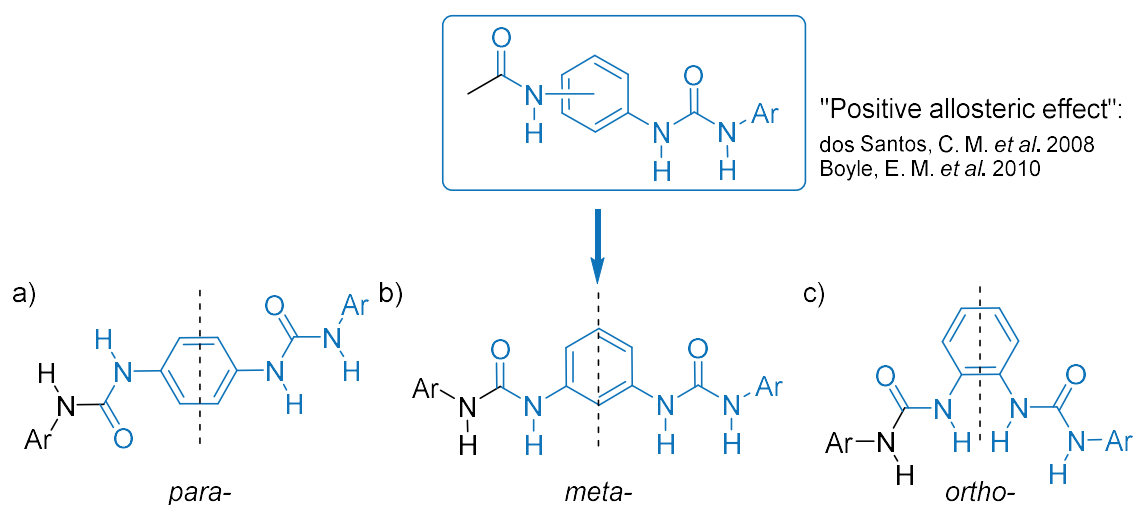


Figure 2.1. Three symmetric motifs may be produced by extending the amidourea motifs studied by dos Santos, and Boyle. The divergent nature of the *para* isomer, a) limits its utility to this work. This chapter considers electron-rich derivatives of the *meta* isomer b). The *ortho* isomer, c) is a well-studied carboxylate host.

The *meta*-phenylene bis(phenylurea) receptors **96–100** were designed for the investigation of the anticipated synergistic effect of two urea binding sites; with the intention of incorporating the bisurea motif into large multicomponent systems. Receptors **96–100** possess methoxy and hydroxy groups at the *ortho*, *meta* and *para* positions of the distal rings (Figure 2.1), the electronic and steric effects of these substitution patterns is outlined in Table 2.1, with comparison to the electron-withdrawing nitro and trifluoromethyl groups, as well as with no substitution (R = H). At the *meta* position, the slightly electron-donating nature of the methoxy and hydroxy groups are equivalent, while at the *para* position, the hydroxy group is lightly less electron-donating than the methoxy group. As such, the inclusion of hydroxy-substituted compounds in this work allows for the separation of the substituent effects. The possibility of further hydrogen bonding interactions in the *meta*-hydroxy substituted receptor **99** allows for any additional allosteric effects to be noted.

This chapter describes the synthesis and characterisation of *meta*-phenylene bis(phenylurea) receptors **96–100**, the $^1$H NMR titrations of **96–99** with the tetra-*N*-butylammonium (TBA$^+$) salts of $H_2PO_4^-$, AcO$^-$, BzO$^-$, Cl$^-$, $HSO_4^-$ and $SO_4^{2-}$, and the calculation of cumulative logarithmic binding constants (logβ). In this chapter, there is an emphasis on elucidating any cooperativity in the anion binding by these receptors, as probed through the cooperativity parameter logα. The use of these receptors in the formation of anion directed self-assembled structures is also discussed, through the analysis of their adducts in the solid-state. A novel supramolecular self-assembly helicate, consisting of a mixed-phosphate anionic core is presented. Part of the work presented in this chapter has been published in *The Journal of Organic Chemistry* (**2018**, *83*, 10398–10408).[186]

## 2.2   Synthesis and Characterisation of Receptors **96–100**

Receptors **96–100** were initially synthesised *via* reaction of 1,3-phenylene diisocyanate with the corresponding aniline. Upon analysis, 1,3-phenylene diisocyanate was considered to be unsatisfactory as a starting material. Firstly, it tends to form unpredictable mixtures of degradation products, oligomers, *etc.* upon dissolution in DMSO, the titration solvent (see Appendix A1.1.3). Secondly, its low solubility in other solvents meant that its complete removal from the host samples could not be assured. Thus, by this method it is possible that an array of impurities would be present in quantities in the titration solution. For this reason, an alternate synthesis of **96–97** was performed by grinding *m*-phenylene diamine with the corresponding commercially available methoxyphenyl isocyanate at room temperature for 2
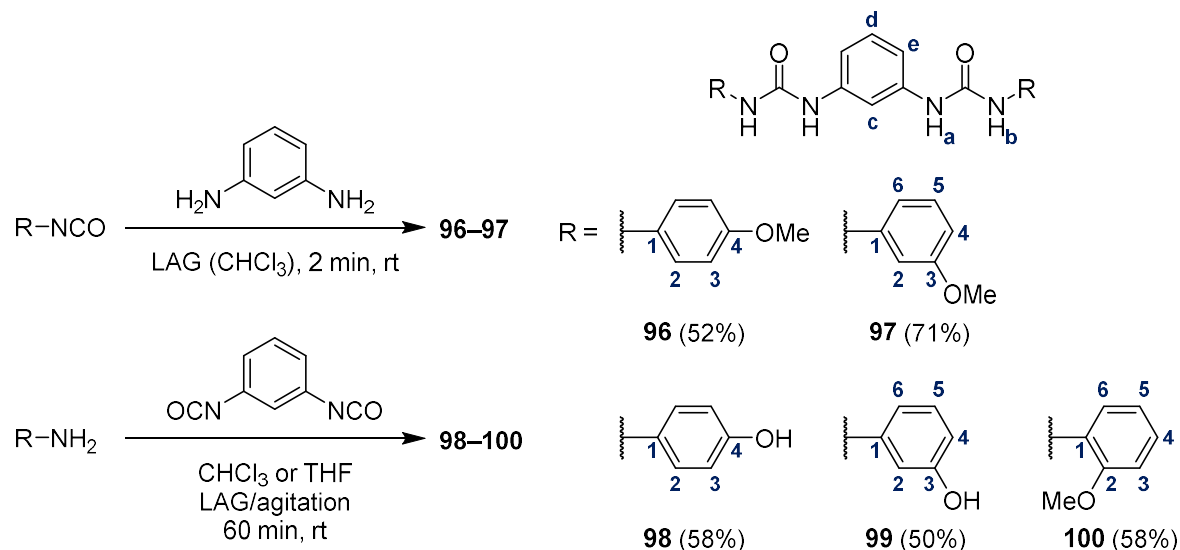


Scheme 2.1. Synthesis of compounds **96–100**, which are studied in this chapter, and with atom labelling used in NMR-related discussions (**blue**).

minutes, Scheme 2.1, forming a white paste. The ureas were isolated from this paste by successive trituration with methanol, acetonitrile and diethyl ether, with the solids being
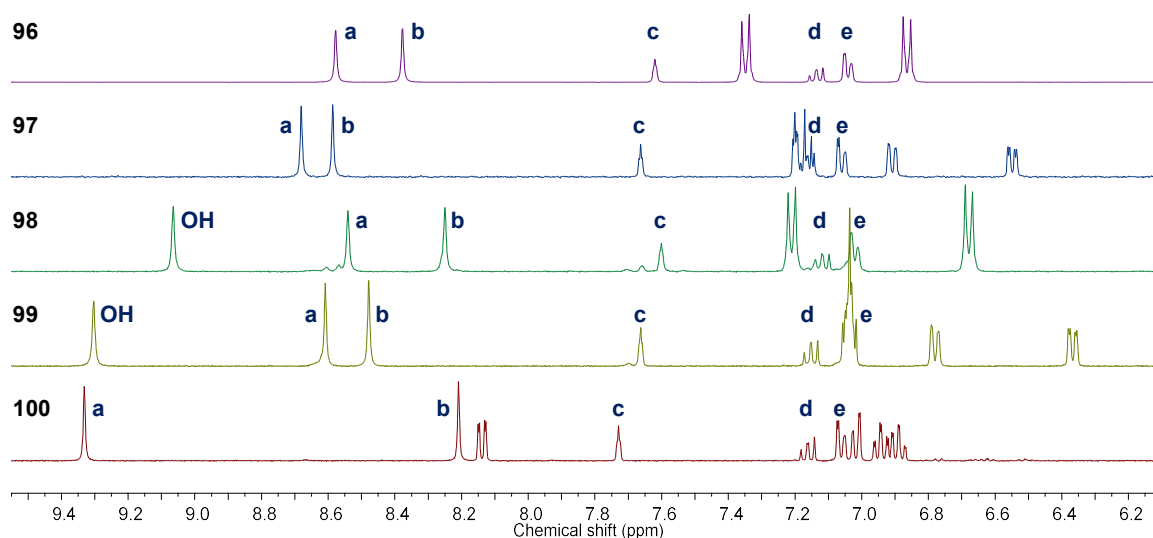
Figure 2.2. $^{1}$H NMR spectra (400 MHz, DMSO-$d_6$, 6.1–9.5 ppm) of compounds of compounds **96** (purple), **97** (blue), **98** (green), **99** (yellow) and **100** (red), with resonances Ha–e and the OH resonance labelled according to the system used in Scheme 2.1.

separated from the solvent each time upon centrifugation, followed by drying *in vacuo*. This yielded receptors **96** and **97** as white solids in 52% and 71% yields, respectively, and sufficiently high purity to be suitable for spectroscopic titration.

As noted, compounds **98**–**100** were produced with the commercially available 1,3-phenylene diisocyanate and an excess of the corresponding aniline derivative in organic solvent (CHCl$_3$ or THF) at room temperature by grinding or agitating for 2 minutes or 2 hours, respectively. The precipitated ureas were filtered under suction and washed with CHCl$_3$ and MeOH and dried *in vacuo*. Receptors **98**–**99** were obtained as pale solids in moderate yields (58% and 50%, respectively), and were soluble in DMF and DMSO. Receptor **100** was obtained as a white solid in 58% yield, with some of the product being recouped from the filtrate upon crystallisation. See Section 2.2.1 below for discussion of the solid state structure of **100**. The successful synthesis of compounds **96**–**100** was demonstrated by the presence of two proton resonances on the 8.2–8.7 ppm region of their $^{1}$H NMR spectra, corresponding to each NH moiety of the urea group, Figure 2.2. The Ha resonance of compound **100** was instead found at 9.33 ppm, most likely due to hydrogen bonding between the urea moiety and the adjacent methoxy ether. These resonances, along with the OH resonances at 9.06 ppm and 9.30 ppm for **98** and **99**, respectively, were observed to disappear upon addition of D$_2$O to the samples as they are in show chemical exchange with the water/D$_2$O resonance, see Appendix A1.1.1.

Similarly, the FTIR spectra of compounds **96**–**100** possess both N−H and C=O stretching frequencies, at *ca*. 3300 cm$^{-1}$ and 1640 cm$^{-1}$, corresponding to the vibrational modes of the urea group, Figure 2.3. Each receptor was analysed by ESI$^{+}$ high-resolution

mass spectrometry, giving either the protonated molecular ion (at $m/z$ = 407.17 for compounds **96**, **97** and **100**, and 379.14 for receptor **98**) or the sodium ion adduct (at $m/z$ = 401.12 for receptor **99**). The samples of receptors **96** and **97** were also proven to be analytically pure by elemental analysis.
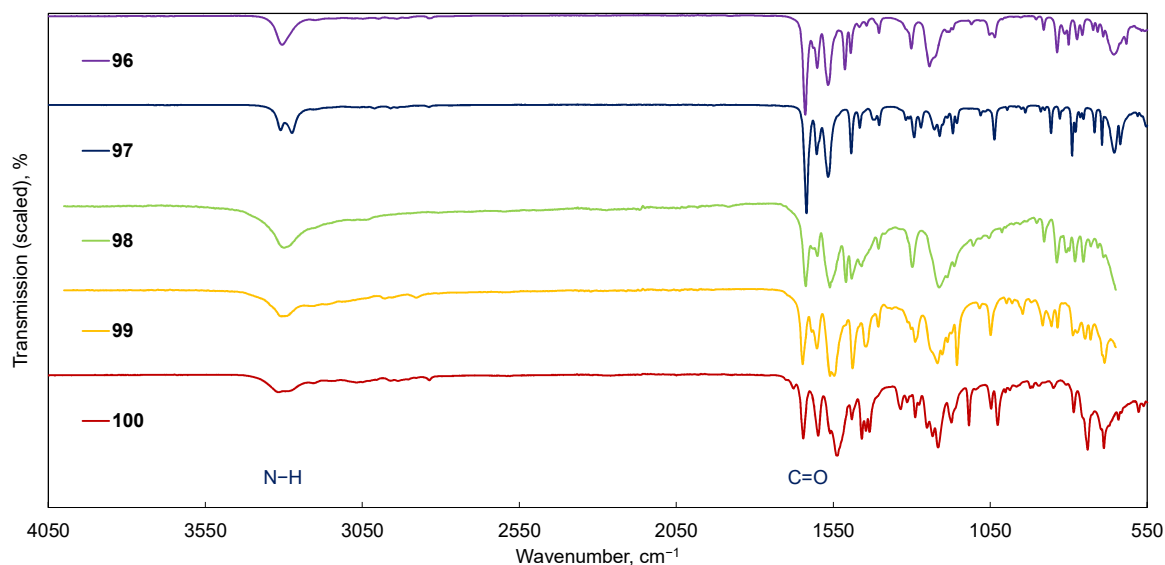


Figure 2.3. FTIR spectra (550–4050 cm$^{-1}$) of compounds **96** (purple), **97** (blue), **98** (green), **99** (yellow) and **100** (red), showing N−H stretching mode(s) at *ca*. 3300 cm$^{-1}$ and C=O stretching mode at *ca*. 1640 cm$^{-1}$.

## 2.2.1   X-ray Crystallographic Analysis and Powder Diffraction of **100**

As mentioned above, the *ortho*-substituted derivative **100** was obtained in crystalline form from the reaction filtrate. The crystal structure of **100** was obtained by single crystal X-ray diffraction, and the data solved in the orthorhombic space group *Pbcn* (measurement, solution and refinement by Dr Salvador Blasco, Table 2.7). The crystal structure is presented in Figure 2.4. In this structure the classical 'urea tape' hydrogen bonding network is observed between adjacent molecules. The C−N bonds between the urea and phenylene groups in the solid state are twisted, and the dihedral angles between the central and the two distal phenylene rings are calculated to be approximately 55° and 64°, Table 2.2.

Table 2.2. Torsion angles around the bonds between phenylene and urea groups, and dihedral angles between the central and the corresponding distal phenylene rings, in the crystal structure of **100**.

| Torsion angle around C−N bonds | | | | Dihedral angle between |
|---|---|---|---|---|
| Inner | | Outer | | phenylene rings |
| C6−C5−N2−C4 | 59.8(2)° | C19−C3−N1−C4 | 8.7(2)° | 55° |
| C6−C7−N3−C8 | 37.3(2)° | C15−C9−N4−C8 | 17.8(2)° | 64° |

See Figure 2.4 for atom labels. No uncertainties were calculated for the dihedral angles.
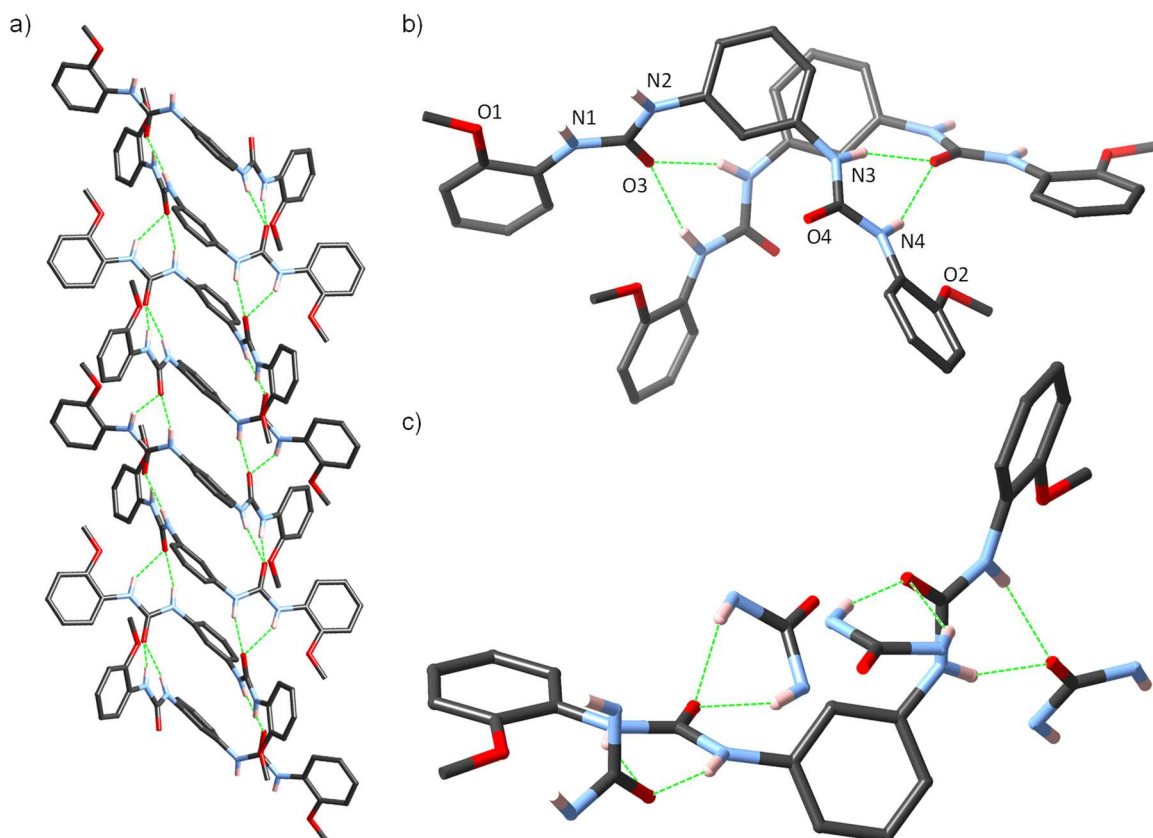
Figure 2.4. Solid-state structure of compound **100** (stick view), a) View down the b-axis, showing the extended structure with antiparallel urea tape motifs along the c-axis. b) View into the plane of the central phenylene ring of one molecule of **100**, showing how the adjacent molecule is 'offset'. c) Hydrogen bonding environment around a single molecule of **100**, showing the manner in which it hydrogen bonds to two others. Hydrogen atoms not engaged in hydrogen bonding interactions omitted for clarity.

The urea moieties are oriented in opposing directions within the crystal such that each urea is providing two hydrogen bond donors (N−H) and an acceptor (C=O) to the adjacent urea in the network, and the two urea tape motifs are antiparallel with respect to each other. The torsion angles around the C−N bonds between the distal rings and the urea moiety are smaller, this may be due to an intramolecular hydrogen-bonding interaction between the methyl ether and the adjacent urea proton. While the N−H···O angles of 111° and 107° are quite small, the N···O and H···O distances both fall within the range of hydrogen bonding interactions, Table 2.3.

Table 2.3. Bond angles and atom-to-atom distances in the crystal structure of **100**.

|  | Bond angle | N···O Distance |
|---|---|---|
| N1−H1···O1 | 111° | 2.608(2) Å |
| N4−H4···O2 | 107° | 2.591(2) Å |

See Figure 2.4 for atom labels. Angles involving H atoms are only approximate, and their uncertainties have been omitted.

A powder diffraction pattern was obtained of the bulk sample of compound **100** (collection by Dr Chris Hawes) and compared to the pattern calculated from the crystal structure, Figure 2.5. The two patterns are similar, but the angles and intensities of the peaks naturally differ for several reasons. The dimensions of the unit cell are smaller when calculated at 100 K during the single crystal X-ray diffraction, than during the room temperature powder diffraction experiment. The experimental peak intensities reflect a non-random distribution of orientations of the individual crystallites of the powder on the flat sample holder, and may differ from those simulated from the single crystal data. The small particle size and poor crystal quality of the precipitate led to a broad experimental linewidth, and the red trace in Figure 2.5 has been simulated with a FWHM of 0.25° to match this. With the notable exception of two extra peaks at 7.9° and 9.7°, denoted in Figure 2.5 by asterisks, the patterns match showing that the majority of the crystalline material within the precipitate is formed in the same phase as the crystal discussed above. Having fully characterised **96**–**100**, including the X-ray analysis of **100**, the binding abilities of the *para* and *meta* ureas **96**–**99** were next evaluated by ¹H NMR titrations. Titration with **100** was not pursued, due to the severe distortion of the planarity of the receptor in the solid phase, and the apparent interaction between Hb and the methyl ether. However, titrations with **100** are worthy of consideration in the future as the relative strengths of the interactions between the anion and the methoxy group with Hb could then be probed.
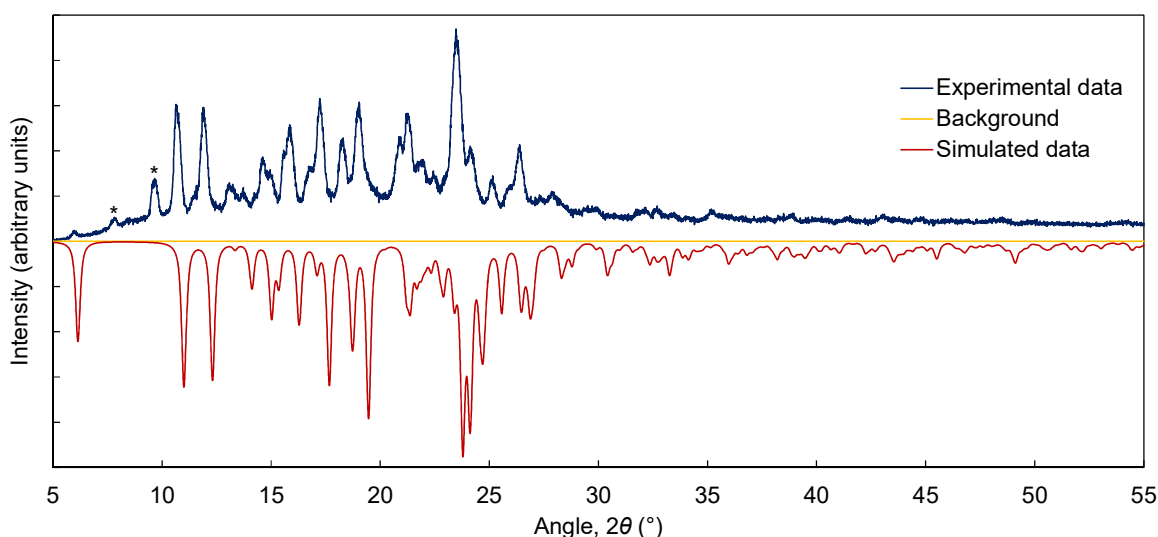


Figure 2.5. Comparison of the measured powder X-ray diffraction pattern for the bulk precipitate of compound **100** (**blue**) and the powder diffraction pattern simulated from the above crystal structure of **100** (**red**). The latter has been inverted for ease of comparison. The peaks marked with an asterisk (*) cannot be assigned to any of the simulated peaks.

## 2.3    Solution-State Anion Binding Studies

Anion titrations were performed with receptors **96–99** to gain insight into the anion recognition process for this family of structures. The binding constants for each titration were determined using the non-linear regression analysis programme HypNMR2008,[187] and where the titrations were repeated, these values are reported as the sample means with 95% confidence intervals. Whilst compounds **98** and **99** could not be produced to the same degree of purity as **96** and **97** (as noted above), preliminary anion titrations were performed to complete the picture. In these cases, the constants are reported as the result of a single fit, with the corresponding "standard deviation" statistical parameter as outputted by HypNMR2008. Notes on calculations and on fitting with HypNMR2008 are contained in Appendix A2.1. The resulting values were largely in agreement with those obtained with hosts **96** and **97**, with an exception in the case of the titration of compound **99** with phosphate. This titration did not fit to the same 1:1, 1:2 host–guest stoichiometric model expected for this kind of design, and consequently, the anion binding was not investigated further due to the aforementioned concerns. The following discussions will focus on the titrations of receptor **96**, with occasional reference to receptors **97–99**.

### 2.3.1    $^1$H NMR Titration of Receptors **96–99** with $H_2PO_4^-$

To investigate the anion binding of **96–99**, NMR titrations were carried out in the competitive aprotic polar solvent DMSO-$d_6$. It was anticipated that a variety of anions could be accommodated by the four hydrogen-bond donors, either through simple 1:1 host–guest binding stoichiometry, or through the higher order 1:2 stoichiometry. To investigate this, titrations were carried out using $TBAH_2PO_4$. Upon titration with $H_2PO_4^-$, large increases in chemical shift were noted for the protons of the urea moiety (8.6→9.8 ppm and 8.4→10.5 ppm for Ha and Hb, respectively) and proton He of the central phenylene ring (7.0→7.6 ppm) over the addition of the first equivalent of anion (see titration of receptor **96** in Figure 2.6). The aromatic resonance Hc was observed to move in a similar and opposite manner (7.6→7.0 ppm). More moderate and gradual changes were observed to occur with the remainder of the resonances, including those of the distal phenylene rings, with Hd shielding slightly (7.1→7.0 ppm) over the course of the titration.

An inflection in the trends in chemical shift of Ha–c and He was observed between the addition of 1→2 equivalents of anion, as they began to plateau. The chemical shifts of resonances Ha, Hc and He (9.82→9.75 ppm, 6.98→6.96 ppm and 7.61→7.64 ppm, respectively, in the case of **96**) changed by less than 0.1 ppm in the range of 2→5 eq.
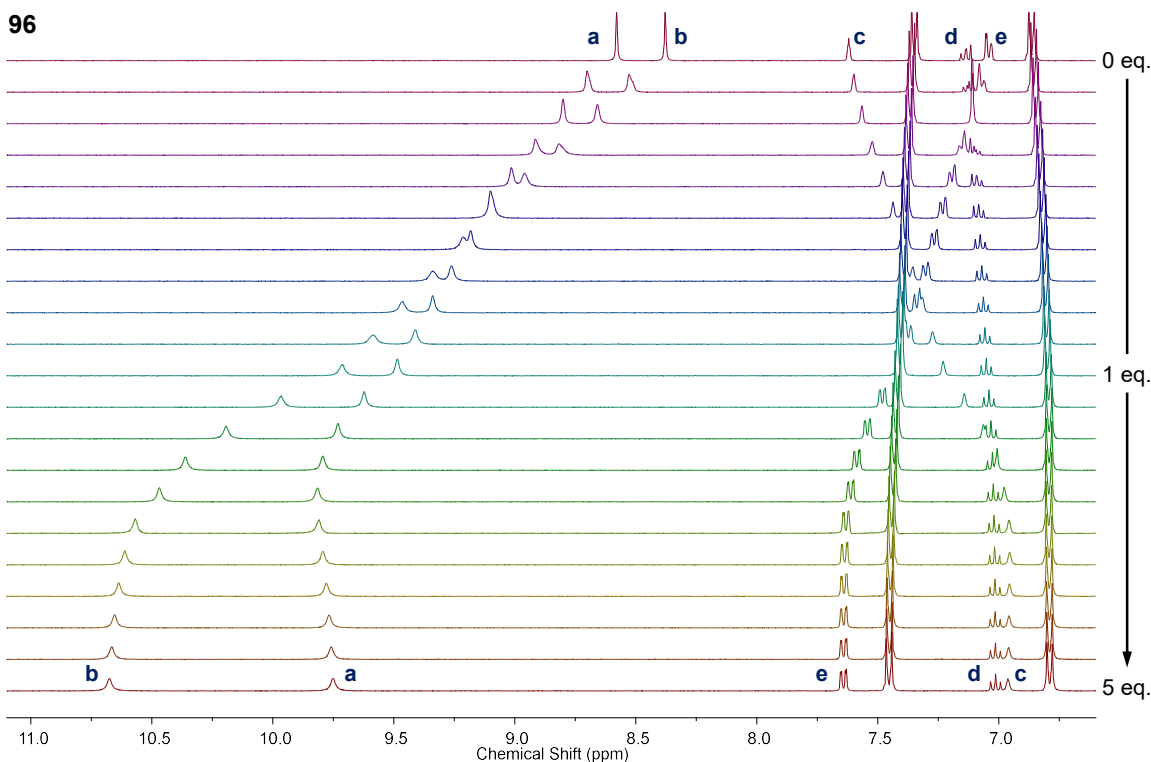
Figure 2.6. Stack plot of the individual $^1$H NMR spectra (400 MHz, DMSO-$d_6$, 6.6–11.1 ppm) from the titration of receptor **96** (7 mM) with 0→5 eq. $H_2PO_4^-$.

TBAH$_2$PO$_4$. Resonance Hb continued its deshielding trend in this range, 10.5→10.7 ppm, an effect that was replicated with receptors **97** and **98**. In the case of receptor **99**, the chemical shift of resonance Hb decreased after the addition of 2 eq. $H_2PO_4^-$, 10.2→10.0 ppm. This consistent change in gradient at 2 eq. for both resonances in all titrations was ascribed to the likely presence of a second binding equilibrium in solution. As such, each titration was fitted to a 1:1, 1:2 host–guest model, resulting in cumulative binding constants in the ranges log$\beta_{1:1}$ = 3.6–3.8 and log$\beta_{1:2}$ = 7.1–7.3 for receptors **96–97** (see Figure 2.7a and Table 2.4).
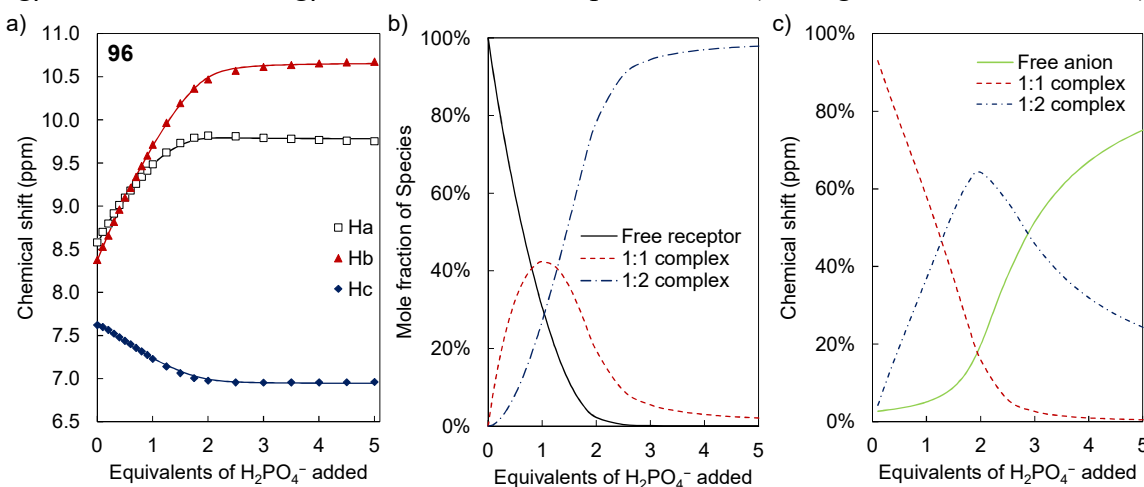


Figure 2.7. Titration of **96** with $H_2PO_4^-$. a) Experimentally measured chemical shifts (points) and calculated 1:1, 1:2 fit (lines) of resonances Ha–c of receptor **96**. b–c) Speciation distribution diagrams generated from the fitting of the experimental data. The concentrations are presented as mole-percentage values of each species relative to the sum of their concentrations.

49

The values of these constants for receptor **98** fell within the same range. It was not possible to fit the data from the titration of receptor **99** to a combined 1:1, 1:2 host–guest binding model. Fitting to a combined 1:1, 1:2, 1:3 host–guest binding model succeeded, but the logarithmic binding constants obtained, $\log\beta$ = 4.4, 8.1, and 10.6, were too high to be realistically determined through titrations at a concentration of 7 mM.

Table 2.4. Cumulative logarithmic binding constants, $\log\beta_{1:1}$ and $\log\beta_{1:2}$, assuming both 1:1 and 1:2 binding modes as determined from the analysis of $^1$H NMR titrations in DMSO-$d_6$ at 25.0 °C.

| Host | Binding mode, H:G | $H_2PO_4^-$ $\log\beta_{H:G}$ | $AcO^-$ $\log\beta_{H:G}$ | $BzO^-$ $\log\beta_{H:G}$ |
|---|---|---|---|---|
| **96** [a] | 1:1 | 3.74 ± 0.11 | 3.54 ± 0.23 | 3.18 ± 0.12 |
| | 1:2 | 7.14 ± 0.24 | 5.45 ± 0.33 | 4.75 ± 0.40 |
| **97** [a] | 1:1 | 3.63 ± 0.07 | 3.66 ± 0.28 | 3.13 ± 0.09 |
| | 1:2 | 7.24 ± 0.07 | 5.86 ± 0.49 | 4.88 ± 0.13 |
| **98** [b] | 1:1 | 3.77 ± 0.29 | 3.43 ± 0.06 | 3.37 ± 0.06 |
| | 1:2 | 7.13 ± 0.29 | 5.29 ± 0.08 | 5.08 ± 0.08 |
| **99** [b] | 1:1 | [c] | 3.40 ± 0.07 | 3.00 ± 0.10 |
| | 1:2 | | 5.44 ± 0.09 | 4.48 ± 0.20 |

Initial host concentration = 7 mM. Anions added as their TBA salts. a) Association constants shown are averaged values, the associated errors correspond to the 95% confidence interval (n = 3–4, see Apprendix A2 for details). b) Data from a single titration, associated error is the "standard deviation" parameter as reported by HypNMR2008. c) This titration could not be fit to a 1:1, 1:2 host–guest model.

The relative magnitudes of the 1:1 and 1:2 host–guest binding constants imply a strongly cooperative process, perhaps aided by hydrogen-bonding interactions between the phosphate anions. Such phosphate dimerisation has been described in MeCN and DMSO, and in aqueous solution,[119,120] and clusters of $H_2PO_4^-$ are commonly observed in solid-state structures.[67] The cooperativity of a 1:2 host–guest system may be quantified by the interaction parameter $\alpha = 4K_{1:2}/K_{1:1}$.[188] Cooperative, non-cooperative and anti-cooperative behaviours are described by values of $\alpha$ being greater than, equal to or less than unity, respectively. As HypNMR2008 reports cumulative logarithmic binding constants, $\log\beta$, the logarithm of the parameter $\alpha$ will be used. This is to avoid the introduction of additional sources of error. Thus, $\log\alpha$ is positive in the case of positive cooperativity, and negative in the case of negative cooperativity. In this system, the value of $\log\alpha$ was found to be in the range 0.2–0.6 for receptors **96**–**98** (see Table 2.6, and Appendix A2.3.8). In a similar 1,2-*trans*-cyclohexyl derived system reported by Amendola *et al.*, binding constants of

$\log\beta_{1:1} = 2.95$ and $\log\beta_{1:2} = 6.39$ were reported (values averaged over both enantiomers). While the binding was weaker overall, it was strongly cooperative, $\log\alpha = 1.1$. This was explained as a result of phosphate–phosphate hydrogen bonding, as had been observed in the crystalline phase.[189]

## 2.3.2  ^{1}H NMR Titration of Receptors **96**–**99** with AcO⁻

Similarly to the titrations of receptors **96**–**99** with $H_2PO_4^-$, above, large changes in the chemical shifts of the resonances Ha and Hb were observed upon titration with AcO⁻, Figure 2.8. More moderate changes were noted in the aromatic region, 6.5–8.0 ppm corresponding to Hc–e and H1–6 of the distal rings. In contrast to the behaviour shown towards $H_2PO_4^-$, the changes in Ha and Hb were monotonic 8.6→11.1 ppm and 8.4→11.2 ppm, respectively, on titration of **96**; with no inflection or other evidence from these trends of a second equilibrium species such as a 1:2 host–guest complex (Figure 2.9a). Resonance Hd was also observed to shift in a monotonic manner, Figure 2.8.
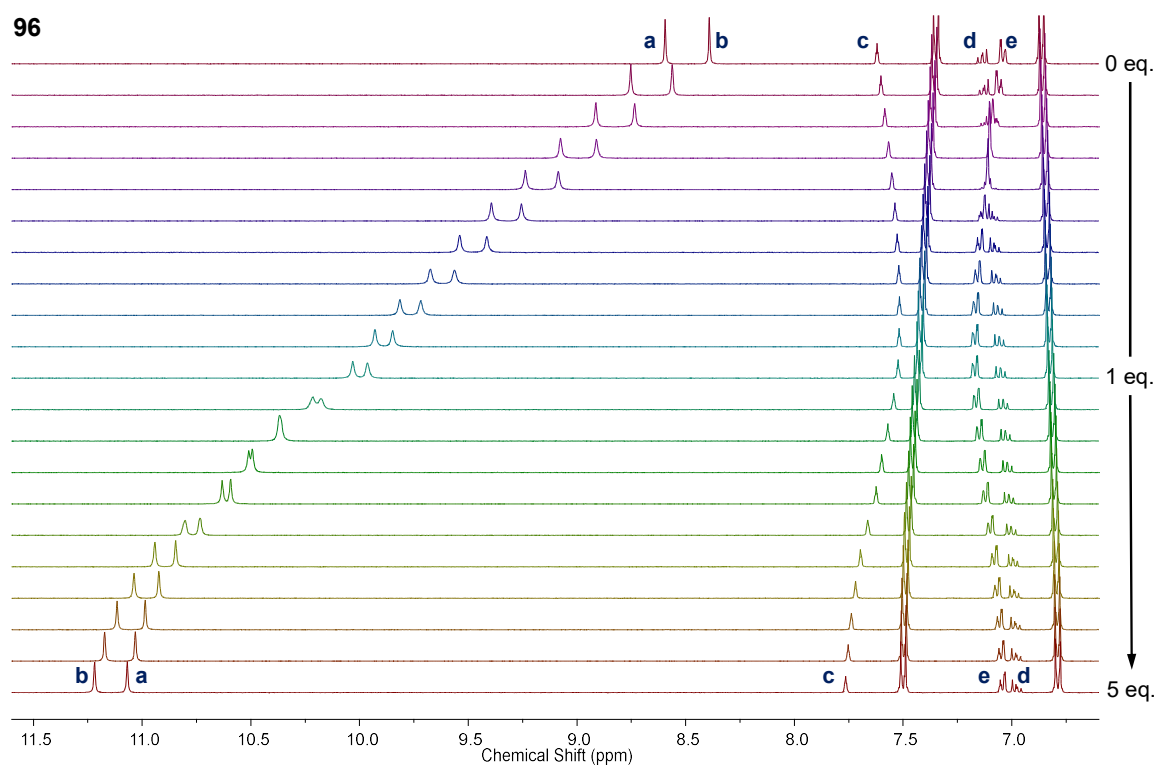


Figure 2.8. Stack plot of the individual ^{1}H NMR spectra (400 MHz, DMSO-$d_6$, 6.6–11.6 ppm) from the titration of receptor **96** (7 mM) with 0→5 eq. AcO⁻.

Such a difference in binding behaviour between the AcO⁻ and $H_2PO_4^-$ anions is not surprising, as the anions have quite different geometries. These data for Ha–b were fitted though non-linear regression analysis with a 1:1 host–guest binding model (Figure 2.9), affording a value of $\log\beta_{1:1} = 2.43 \pm 0.06$ for receptor **96**, and values of approximately 2.4 for **96**–**98**, Table 2.5. The value of $\log\beta_{1:1}$ for receptor **99** was slightly higher at *ca.* 2.5. These

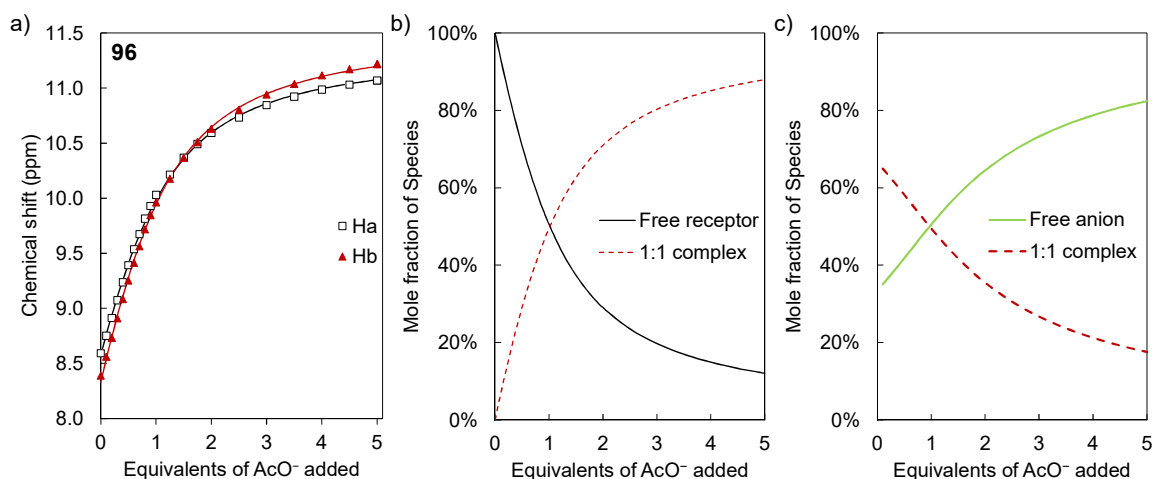Figure 2.9. Titration of **96** with AcO⁻. a) Experimentally measured chemical shifts (points) and calculated 1:1 fit (lines) of resonances Ha–b of receptor **96**. b–c) Speciation distribution diagrams generated from the fitting of the experimental data. The concentrations are presented as mole-percentage values of each species relative to the sum of their concentrations.

constants are low for urea-based receptors, as illustrated by Kadam *et al.*, who determined a value of $\log\beta_{1:1} = 3.3$ for diphenylurea in DMSO-$d_6$/water (99.5:0.5), with $\log\beta_{1:1}$ being in the range 2.5–4.9 for other aryl-substituted ureas.[182] Casula *et al.* reported binding constants in the range $\log\beta = 3.1$–3.9 for asymmetric phenylene bis(arylureas), with the corresponding *meta* isomer having the lowest binding affinity for acetate.[126] From that study, and other works, the *ortho*-phenylene bis(phenylurea) receptor displayed especially strong binding, whereby one carboxylate anion forms hydrogen bonds to all four NH donors.[66] A similar saturation of all hydrogen bonding donors in the *meta* system by a single carboxylate ion is improbable, as the receptor binding site is not concave in shape and the outermost nitrogen atoms are more distant from each other. This would leave part of the receptor available for binding to a second anion.

Table 2.5. Cumulative logarithmic binding constants, $\log\beta_{1:1}$, assuming a 1:1 binding mode only as determined from the analysis of ¹H NMR titrations in DMSO-$d_6$ at 25.0 °C.

| Host | AcO⁻ $\log\beta_{1:1}$ | BzO⁻ $\log\beta_{1:1}$ | Cl⁻ $\log\beta_{1:1}$ | SO$_4^{2-}$ $\log\beta_{1:1}$ | HSO$_4^-$ [b] $\log\beta_{1:1}$ |
|---|---|---|---|---|---|
| **96** [a] | $2.43 \pm 0.06$ | $2.33 \pm 0.06$ | $1.67 \pm 0.08$ | $1.06 \pm 0.62$ | $0.52 \pm 0.05$ |
| **97** [a] | $2.44 \pm 0.14$ | $2.36 \pm 0.03$ | $1.67 \pm 0.10$ | $0.92 \pm 0.19$ | $1.43 \pm 0.03$ |
| **98** [b] | $2.39 \pm 0.01$ | $2.31 \pm 0.01$ | $1.64 \pm 0.02$ | $1.15 \pm 0.03$ | $0.39 \pm 0.06$ |
| **99** [b] | $2.49 \pm 0.01$ | $2.38 \pm 0.01$ | n.d. [c] | n.d. [c] | n.d. [c] |

Initial host concentration = 7 mM. Anions added as their TBA salts. a) Association constants shown are averaged values, the associated errors correspond to the 95% confidence interval (n = 2–4, see Appendix A2 for details). b) Data from a single titration, associated error is the "standard deviation" parameter as reported by HypNMR2008. c) Not determined: this titration was not performed.
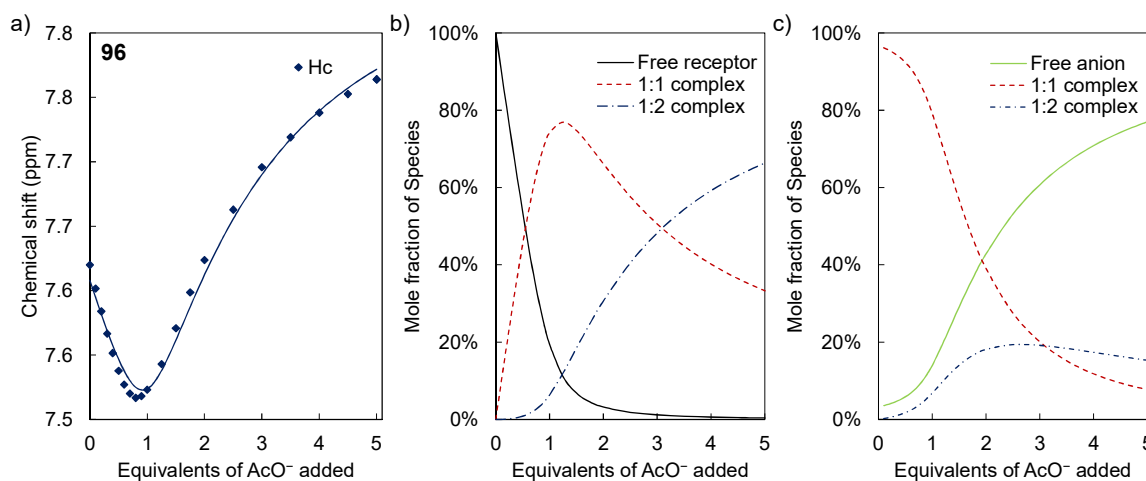
Figure 2.10. Titration of **96** with AcO⁻. a) Experimentally measured chemical shifts (points) and calculated 1:1, 1:2 fit (lines) of resonance Hc of receptor **96**. Ha–b were included in the fit, but are omitted here for clarity. b–c) Speciation distribution diagrams generated from the fitting of the experimental data. The concentrations are presented as mole-percentage values of each species relative to the sum of their concentrations.

While the trends in resonances Ha–b and Hd did not display any evidence of a second equilibrium, the resonances Hc and He both showed 'U-shaped' trends in their chemical shift, Figure 2.8. The chemical shift of Hc decreased up to the addition of 1 eq. AcO⁻, 7.62→7.52 ppm for receptor **96**, at which point an upward inflection followed by a gentle plateau was observed (7.5→7.8 ppm, see Figure 2.10a). This is indicative of an intermediate species, which can be seen by comparing the molar fractions of the 1:1 species in Figure 2.9b–c and Figure 2.10b–c. Fitting the data from all three resonances afforded binding constants of $\log\beta_{1:1} = 3.5$–3.7 and $\log\beta_{1:2} = 5.4$–5.9 (Table 2.4). This fit also appears to suggest a strongly negatively cooperative interaction, with $\log\alpha$ being −1.03 and −0.85 for receptors **96** and **97**. Similar values were determined for the phenolic receptors **98** and **99**, Table 3.

## 2.3.3  ¹H NMR Titration of Receptors **96**–**99** with BzO⁻

The urea resonances of **96**–**99** behaved similarly upon titration with BzO⁻, as with AcO⁻, above. In the titration of receptor **96**, Ha and Hb were observed to increase from 8.6→10.9 ppm and 8.4→11.0 ppm, respectively. The aromatic resonance Hc, meanwhile, followed a sigmoidal trend with positive curvature up to the addition of 1.5 eq. of anion, and a negative curvature thereafter, Figure 2.11.

Fitting the trends in Ha–c demonstrated that BzO⁻ interacted in a similar manner to the AcO⁻ anions. As above, both the simple 1:1, and mixed 1:1, 1:2 binding models were applied to the data from each titration. The values of $\log\beta_{1:1}$ obtained from the 1:1 fits are 2.33 ± 0.06 for receptor **96**, and in the range 2.3–2.4 for receptors **96**–**99** overall, Table 2.5. Once again, the $\log\beta_{1:1}$ values may be compared to the series of aryl-substituted urea receptors
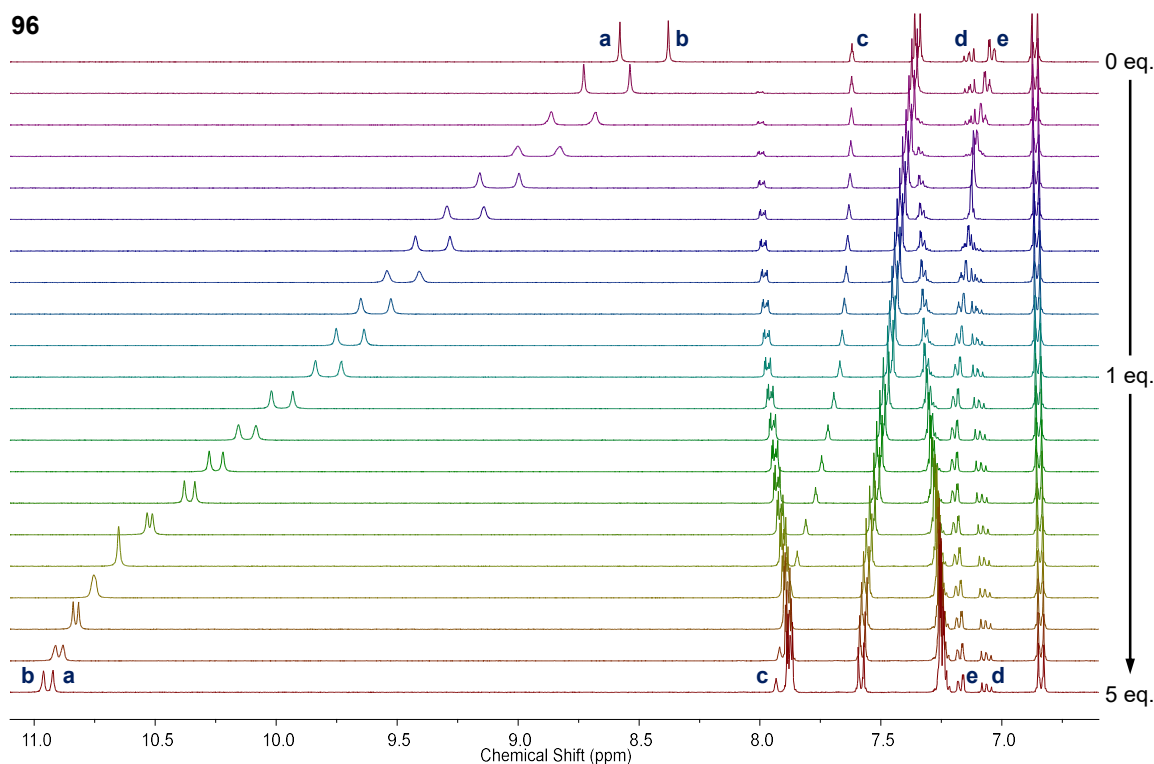
**Figure 2.11.** Stack plot of the individual $^1$H NMR spectra (400 MHz, DMSO-$d_6$, 6.6–11.1 ppm) from the titration of receptor **96** (7 mM) with 0→5 eq. BzO$^-$.

reported by Kadam *et al.*, where log$\beta_{1:1}$ is in the range 2.1–4.1.[182] The binding affinities of compounds **96**–**99** for the BzO$^-$ anion on the basis of the 1:1 fits are at the lower end of this scale. While in that work the binding for the benzoate anion is weaker than for the acetate anion by 0.3 log units or more, the 1:1 binding constants for **96**–**99** are more similar across the two anions. The difference can only be confirmed to be significant at the 5% level in the case of receptor **96**.

The chemical shift of Hc follows a sigmoidal trend as shown in Figure 2.13a, increasing slightly over the addition of the first equivalent of BzO$^-$ 7.62→7.67 ppm, and



**Figure 2.12.** Titration of **96** with BzO$^-$. a) Experimentally measured chemical shifts (points) and calculated 1:1 fit (lines) of resonances Ha–b of receptor **96**. b–c) Speciation distribution diagrams generated from the fitting of the experimental data. The concentrations are presented as mole-percentage values of each species relative to the sum of their concentrations.

much more significantly thereafter, finishing at 7.93 ppm. As with AcO⁻, inclusion of the data from Hc, along with the aforementioned Ha and Hb, allowed for the calculation of binding constants for a combined 1:1 and 1:2 host–guest binding equilibrium. In the case of receptor **96** these are $\log\beta_{1:1} = 3.2 \pm 0.1$ and $\log\beta_{1:2} = 4.8 \pm 0.4$, respectively, see Table 2.4. While the new fit describes the data from Ha and Hb just as well as the simple 1:1 fit, the speciation diagrams for the 1:1, 1:2 fit to Ha–c show a significant proportion of the 1:2 species in solution, compare Figure 2.12b–c and Figure 2.13b–c. Overall, the calculated ranges of $\log\beta_{1:1}$ and $\log\beta_{1:2}$ are 3.1–3.2 and 4.7–4.9, respectively, Table 2.4. The logarithmic cooperativity parameters indicated a similar degree of anticooperativity to the above acetate titrations, with $\log\alpha = -1.0 \pm 0.3$ for receptor **96**, and between −1.1 and −0.7 for receptors **96**–**99** overall, see Table 2.6.
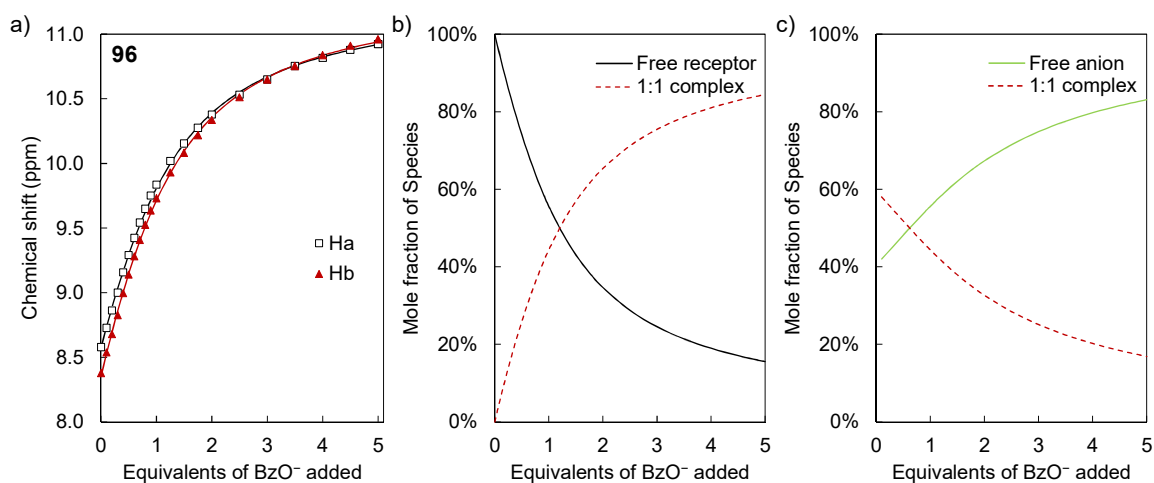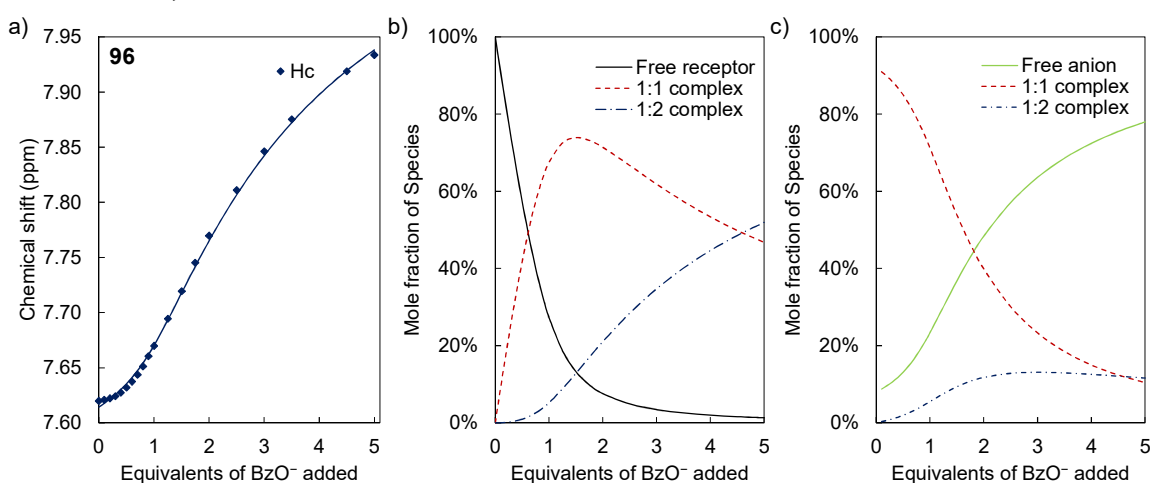


Figure 2.13. Titration of **96** with BzO⁻. a) Experimentally measured chemical shifts (points) and calculated 1:1, 1:2 fit (lines) of resonance Hc of receptor **96**. Ha–b were included in the fit, but are omitted here for clarity. b–c) Speciation distribution diagrams generated from the fitting of the experimental data. The concentrations are presented as mole-percentage values of each species relative to the sum of their concentrations.

Table 2.6. Logarithmic cooperativity parameters, $\log\alpha$, assuming both 1:1 and 1:2 binding modes as determined from the analysis of ¹H NMR titrations in DMSO-$d_6$ at 25.0 °C.

| Host | $H_2PO_4^-$ $\log\alpha$ | $AcO^-$ $\log\alpha$ | $BzO^-$ $\log\alpha$ |
|---|---|---|---|
| **96** [a] | $0.27 \pm 0.17$ | $-1.03 \pm 0.25$ | $-1.01 \pm 0.30$ |
| **97** [a] | $0.59 \pm 0.13$ | $-0.85 \pm 0.36$ | $-0.78 \pm 0.10$ |
| **98** [b] | $0.21 \pm 0.31$ | $-0.97 \pm 0.05$ | $-1.06 \pm 0.04$ |
| **99** [b] | [c] | $-0.75 \pm 0.06$ | $-0.91 \pm 0.05$ |

Initial host concentration = 7 mM. Anions added as their TBA salts. a) Cooperativity constants shown are averaged values, the associated errors correspond to the 95% confidence interval (n = 3–4, see Appendix A2 for details). b) Cooperativity constants are as calculated from a single fit, the associated errors are as propagated from the "standard deviation" parameter and covariance reported by HypNMR2008. c) This titration could not be fit to a 1:1, 1:2 host–guest model.

### 2.3.4 $^1$H NMR Titration of Receptors **96**–**97** with Cl$^-$

Small monotonic changes in chemical shift of less than 0.50 ppm were observed for each proton resonance over the addition of 5 equivalents of TBACl, see titration of receptor **96** in Figure 2.14a. Resonances Ha and Hb deshielded over the course of the titration, 8.6→9.0 ppm and 8.4→8.9 ppm, respectively, upon titration of **96**, while Hc showed a very slight increase in chemical shift (7.63→7.56 ppm). Resonances Hd and He converged over the course of the titration, 7.14→7.12 ppm and 7.05→7.08 ppm, respectively. There was no evidence for multiple equilibria in the titration solution, and these titrations were fitted to 1:1 host–guest models alone, Figure 2.14b, c. The results obtained by non-linear regression analysis of Ha–c for receptors **96** and **97** are equivalent, with log$\beta_{1:1}$ = 1.67 for both receptors, see Table 2.5. This is comparable to similar *ortho*-phenylene receptors, which have log$\beta_{1:1}$ values in the range 1.1–1.6,[181] but recent electron-poor Cl$^-$ transporters based on that motif possess higher log$\beta_{1:1}$ values at *ca.* 2.2.[113]
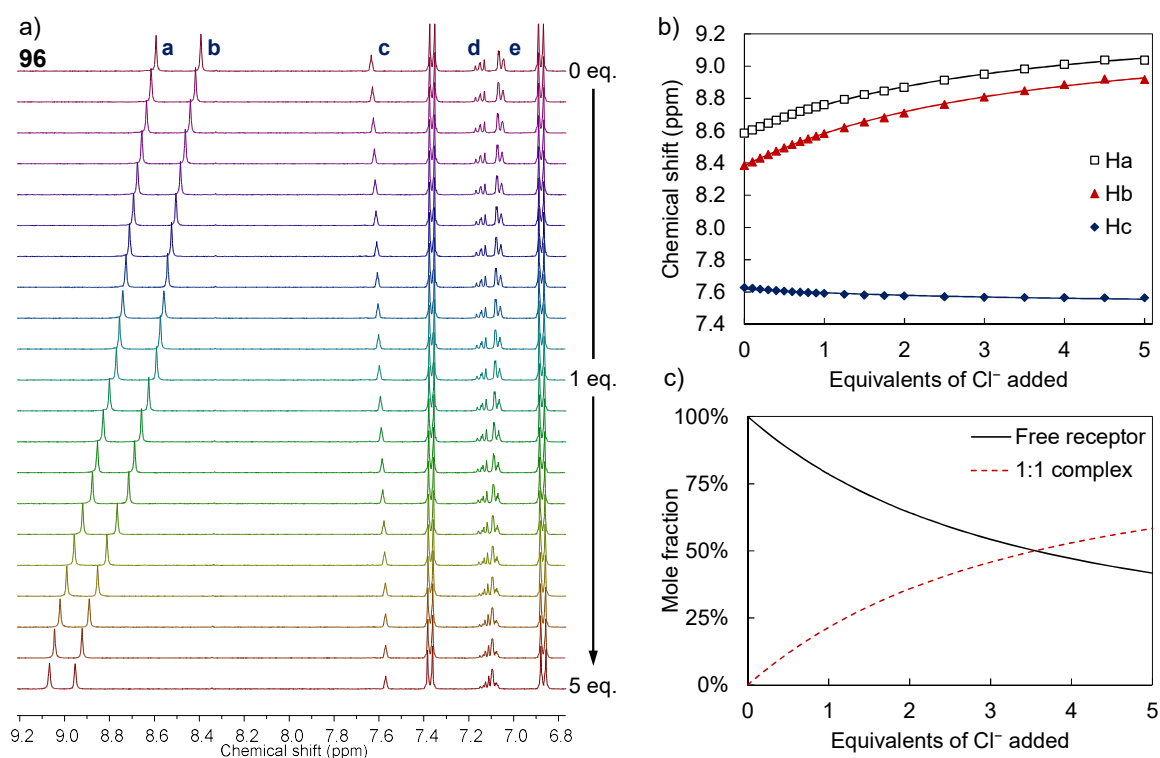


Figure 2.14. a) Stack plot of the individual $^1$H NMR spectra (400 MHz, DMSO-$d_6$, 6.8–9.2 ppm) from the titration of receptor **96** (7 mM) with 0→5 eq. Cl$^-$. b) Experimentally measured chemical shifts (points) and calculated fit (lines) of resonances Ha–c of receptor **96**. c) Speciation distribution diagram generated from the fitting of the experimental data. The concentrations are presented as mole-percentage values of each species relative to the sum of their concentrations.

### 2.3.5 $^1$H NMR Titration of Receptors **96**–**97** with SO$_4^{2-}$ and HSO$_4^-$

Titrations with TBA$^+$ SO$_4^{2-}$ and HSO$_4^-$ both showed small monotonic changes in chemical shift of less than 0.25 ppm for the urea resonances up to the addition of 5 eq. of anion, with

little to no curvature observed in this trend, as observed from the titrations of receptor **96** in Figure 2.15a and Figure 2.16a, respectively. In the case of $SO_4^{2-}$, these slight increases in chemical shift of resonances Ha and Hb were 8.6→9.2 ppm and 8.4→9.0 ppm, respectively, in the titration of **96**. Hc and Hd shielded very slightly over the titration, 7.62→7.57 ppm and 7.14→7.05 ppm, respectively. Meanwhile, resonance He deshielded slightly 7.04→7.16 ppm, crossing Hd after the addition of 1 eq. $TBA_2SO_4$. Fitting the data for Ha–c by non-linear regression analysis produced values of $\log\beta_{1:1}$ in the range 0.9–1.2, see Table 2.5.
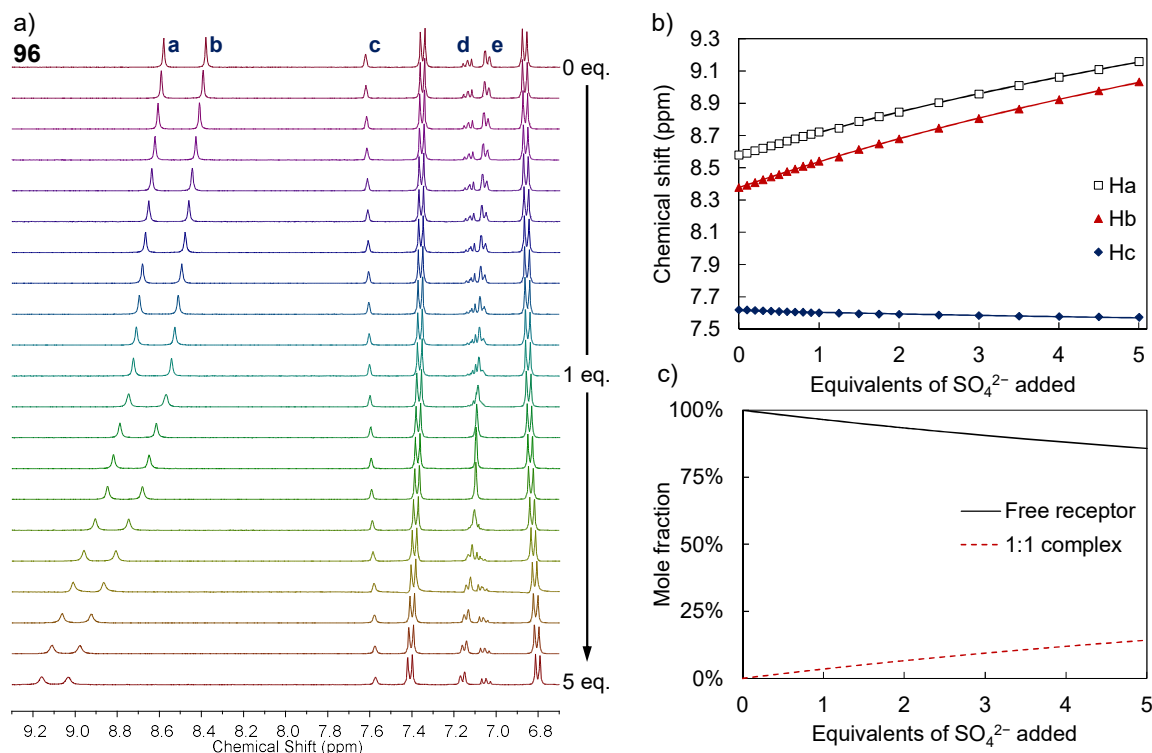


Figure 2.15. a) Stack plot of the individual $^1$H NMR spectra (400 MHz, DMSO-$d_6$, 6.7–9.3 ppm) from the titration of receptor **96** (7 mM) with 0→5 eq. $SO_4^{2-}$. b) Experimentally measured chemical shifts (points) and calculated fit (lines) of resonances Ha–c of receptor **96**. c) Speciation distribution diagram generated from the fitting of the experimental data. The concentrations are presented as mole-percentage values of each species relative to the sum of their concentrations.

As noted, the titrations with $HSO_4^-$ produced similar trends to $SO_4^{2-}$; however the changes in chemical shift were less significant. Ha and Hb deshielded slightly, 8.6→8.8 ppm and 8.4→8.6 ppm, respectively, on titration of **96** (Figure 2.16). The chemical shift of resonance Hc decreased very slightly, 7.62→7.59 ppm. Resonances Hd and He behaved similarly, converging at 7.09 ppm at the end of the titration. Fitting the data from the changes in Ha–c produced values of $\log\beta_{1:1}$ in the range 0.5–1.4, see Table 2.5.

The values of $\log\beta_{1:1}$ reported for the $SO_4^{2-}$ and $HSO_4^-$ anions should be viewed with some caution, and this is reflected in the rather large distributions of binding constants obtained upon repetition of the $SO_4^{2-}$ titrations with receptors **96** and **97**. In all cases, the
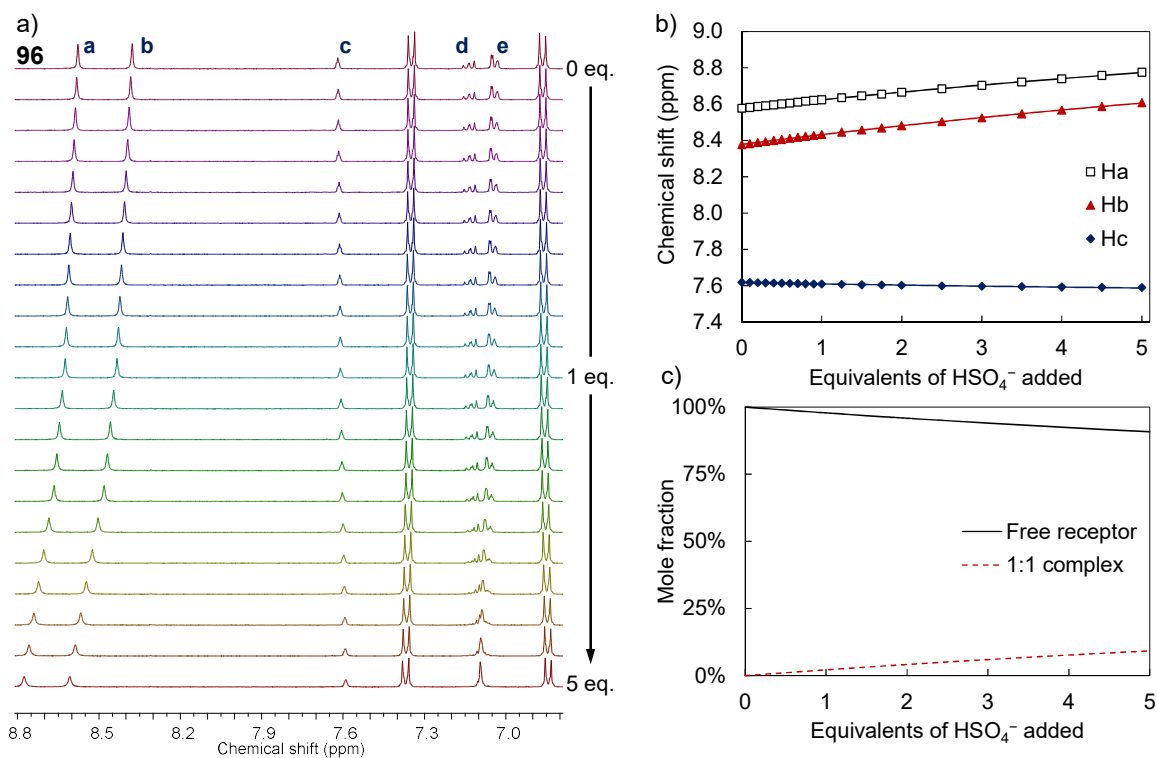
Figure 2.16. a) Stack plot of the individual $^1$H NMR spectra (400 MHz, DMSO-$d_6$, 6.8–8.8 ppm) from the titration of receptor **96** (7 mM) with 0→5 eq. HSO$_4^-$. b) Experimentally measured chemical shifts (points) and calculated fit (lines) of resonances Ha–c of receptor **96**. c) Speciation distribution diagram generated from the fitting of the experimental data. The concentrations are presented as mole-percentage values of each species relative to the sum of their concentrations.

trends followed by the urea resonances have a very small curvature and there is a small overall change in chemical shift, making the fits less reliable. Resonance Hc is also poorly described by these fits. It must also be noted that only preliminary titrations were performed with the HSO$_4^-$ salt. These values would indicate that **96–97** show a much lesser affinity for the strongly solvated sulfates compared to H$_2$PO$_4^-$, BzO$^-$ and AcO$^-$. This is unsurprising as hydrogen bond based receptors are generally expected to bind the HSO$_4^-$ anion least strongly of the anions studied herein.[90,91] In a similar study, the value of logβ$_{1:1}$ < 1 was determined for HSO$_4^-$ binding by *ortho*-phenylene bis(phenylurea).[181] However, more preorganised motifs, which bear three urea,[170,171,190] or *ortho*-phenylene diurea arms have been shown to bind the SO$_4^{2-}$ anion much more strongly, with logβ$_{1:1}$ = 5.5–5.9 for the latter.[130]

## 2.3.6   Studies into the Exchange of the Phenol Resonances of Receptors **98** and **99**

It was noted that during some of the titrations that the phenol resonance of receptors **98** and **99**, at 9.1 ppm and 9.3 ppm respectively, broadened over the course of the titration, while exhibiting little to no change in chemical shift. This broadening was especially apparent upon titration with H$_2$PO$_4^-$, whereupon the resonance vanished upon addition of 0.1 eq. TBAH$_2$PO$_4$, and to a lesser extent with AcO$^-$, where the broadening was complete after the

addition of 1 eq. of the salt, see Appendix A2. In the above calculations of binding constants, the behaviour of the phenol resonance was thus omitted from the fit. The origin of this behaviour was nonetheless investigated to rule out any secondary interactions between receptors **98** and **99** and the anions, which would affect the calculation of binding constants.

As noted in Section 2.2 above, the urea and phenol resonances of each receptor are in slow chemical exchange with the water resonance (for deuterium exchange experiments, see Appendix A1). The exchange of the phenol resonances of receptors **98** or **99** is catalysed by the addition of an acid such as TFA, as indicated by the coalescence of the TFA, $H_2O$ and phenol resonances (Figure 2.17 and Appendix A1)
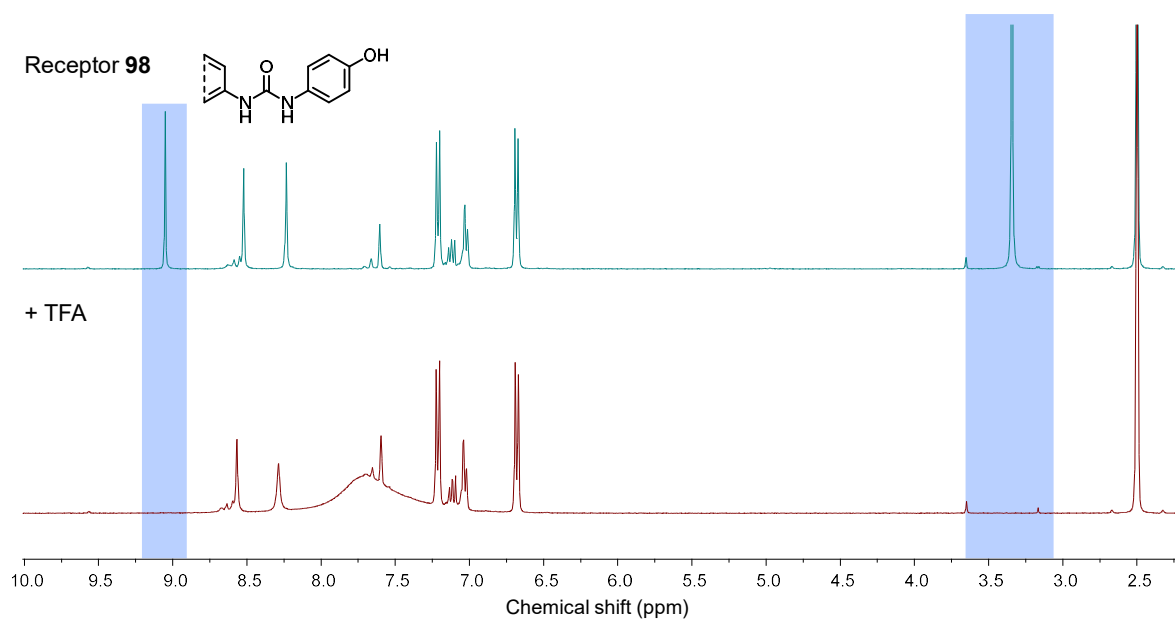


Figure 2.17. Addition of neat TFA to a solution of receptor **98**in DMSO-*$d_6$* leads to the coalescence of the $H_2O$, phenol and TFA resonances, as seen by the broad resonance at *ca.* 7.7 ppm.

The $H_2PO_4^-$ anion is a very poor base, with $pK_{b3} = 11.9$ in water, but it is also a weak acid, $pK_{a2} = 7.2$. Similarly, the $TBA^+$ cation itself is a weak Brønsted–Lowry acid with TBAOH being the conjugate base. These acidic tendencies can explain the disappearance of the phenol resonance as acid-catalysed proton exchange. If the mechanism for this was deprotonation, then a stoichiometric quantity of $TBAH_2PO_4$ would be required for complete disappearance of the phenol resonance, unlike the 0.10 eq. observed. Any anion binding behaviour would be expected to occur in a similarly stoichiometric manner. On the other hand, the broadening of the phenol resonance upon titration with acetate ($pK_b = 9.2$) and benzoate ($pK_b = 9.8$) may be due to base-catalysed proton exchange. On this basis it may be assumed that the broadening and disappearance of the phenolic resonance of receptors **98** and **99** in some titrations is entirely due to chemical exchange and therefore not of concern in terms of determining the binding constants of these receptors. The solution-state titration

experiments of receptors **96–99** being complete, analysis of their adducts in the solid state was undertaken.

## 2.4 Structural Studies of Crystalline Adducts of **96** and **97**

As the $^1$H NMR titrations of **96–99** showed stronger interactions with AcO$^-$ and H$_2$PO$_4^-$, co-crystallisations with these anions were considered. While the urea hosts **96** and **97** are poorly soluble in suitable crystallisation solvents, they may be solubilised in CHCl$_3$, MeCN and EtOAc by the addition of an excess of AcO$^-$ anion. Therefore, it must be noted that both the crystals of **96**(TBAOAc)$_2$·3H$_2$O and **97**$_3$(TBA$_3$H$_3$P$_2$O$_8$)·0.5CHCl$_3$ discussed in the following sections could only be prepared very sporadically as a product from a large excess of the mixed TBA salts, given the multitude of complex equilibria at play in such mixtures. As such, these crystalline adducts are presented as experimentally determined "snapshots" of two of the available binding modes, taking the additional driving force of crystallisation into account. As they are produced under different conditions, these adducts cannot prove any aspect of the solution-state behaviour, but are nevertheless informative of the possibilities of these systems.

### 2.4.1 X-ray Crystallographic Analysis of **96**(TBAOAc)$_2$·3H$_2$O

The *para*-methoxy substituted compound **96** was dissolved in a boiling mix of CHCl$_3$ and EtOAc in the presence of an excess of AcO$^-$ and H$_2$PO$_4^-$ as their TBA$^+$ salts. The solution was filtered whilst still hot and small thin colourless crystals of **96**(TBAOAc)$_2$·3H$_2$O were obtained by slow evaporation of the solvent. In some instances, various TBAOAc salts, hydrates and adducts crystallised from the solution instead.

A crystal of **96**(TBAOAc)$_2$·3H$_2$O was analysed by single crystal X-ray diffraction, the diffraction data were solved and the model refined in the monoclinic space group *Cc* (measurement, solution and refinement by Dr Chris Hawes, see Table 2.7). Searches were made for higher symmetry space groups, particularly *C*2/*c*. Although approximate two-fold symmetry is present when considering the TBA$^+$ cations and molecules of **96**, the non-symmetric arrangement of the acetate and water species prohibits a precise *C*2/*c* setting. The asymmetric unit of **96**(TBAOAc)$_2$·3H$_2$O contains one molecule of **96** in an acentric planar conformation, two acetate anions and associated TBA$^+$ cations, two full-occupancy water molecules, and one disordered water molecule split across three sites. One of the two acetate moieties displayed minor rotational disorder and was modelled over two related orientations. The hydrogen bonding interactions in **96**(TBAOAc)$_2$·3H$_2$O are largely centred on the interaction of one molecule of **96** with two acetate anions, bridged by a water molecule. One
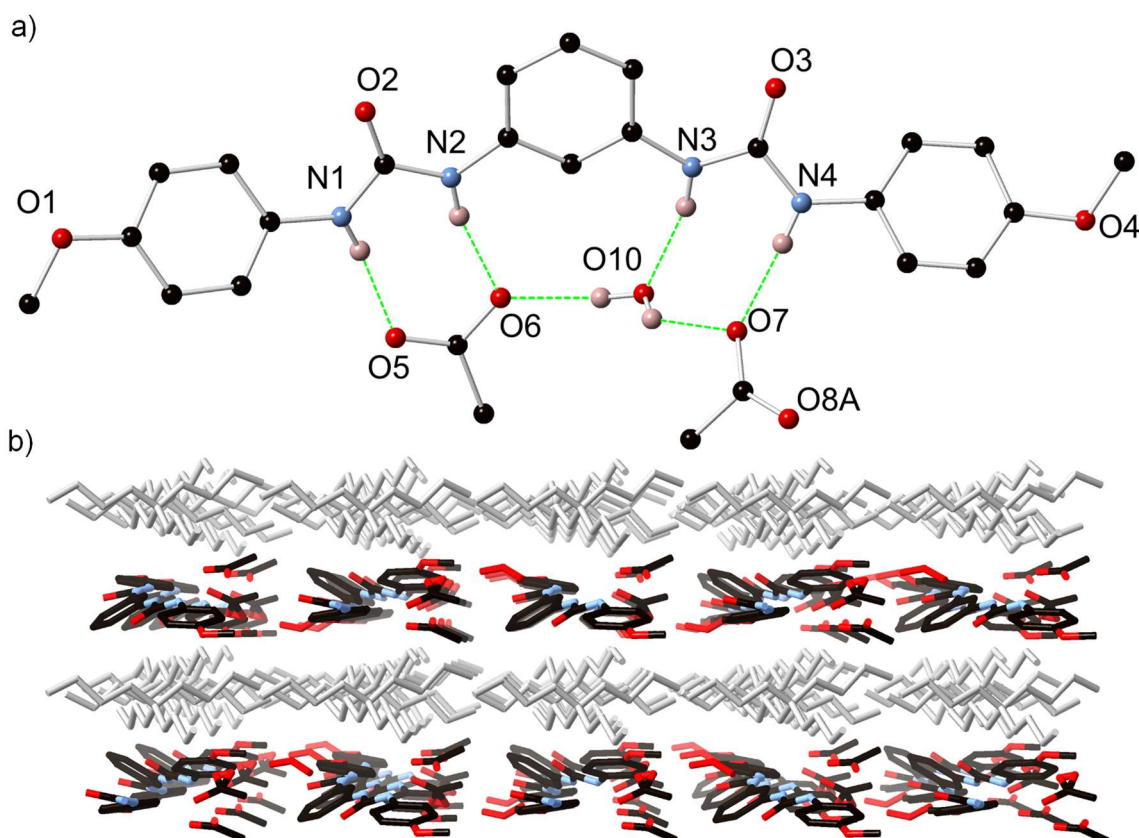
Figure 2.18. a) Hydrogen bonding environment of the host species within the structure of **96**(TBAOAc)$_2$·3H$_2$O with heteroatom labelling scheme. Hydrogen atoms not involved in hydrogen bonding, TBA$^+$ cations and disordered solvent molecules omitted for clarity; b) Extended structure of **96**(TBAOAc)$_2$·3H$_2$O showing alternating layers of TBA$^+$ cations (gray) and anionic host-anion layers (coloured).

acetate anion is bound in the well-known R$_2^2$(8) hydrogen bonding motif with a urea group,[191] with N···O distances 2.795(8) Å and 2.842(9) Å and N−H···O angles 166.6(4)° and 166.0(4)° for N1−H1···O5 and N2−H2···O6, respectively. The second acetate anion interacts with the remaining urea group *via* a single hydrogen bond, with the second potential interaction interrupted by the presence of a lattice water molecule O10, which donates a hydrogen bond to the acetate group and accepts a hydrogen bond from the inner urea N−H group, forming a cyclic assembly described by the R$_2^3$(8) graph set. The two distinct hydrogen bonding environments involving the urea groups are further linked by hydrogen bonding from the lattice water molecule O10 to acetate oxygen atom O6, defining a further cyclic R$_2^3$(10) motif edge-sharing with the two urea environments. Additional hydrogen bonding in the structure of **96**(TBAOAc)$_2$·3H$_2$O involves the remaining lattice water molecules; the well-defined water molecule O9 bridges adjacent **96**-acetate adducts through interactions with the acetate oxygen atom O5 and the urea oxygen atom O3 from an adjacent molecule of **96**. Although individual hydrogen atoms could not be assigned to the disordered water sites, their proximity to the disordered acetate anion suggests additional hydrogen bonding interactions

are likely. The extended structure of **96**$(TBAOAc)_2 \cdot 3H_2O$ consists of alternating anionic $[\mathbf{96} \cdot 2OAc \cdot 3H_2O]^{2-}$ layers and cationic $TBA^+$ layers, each extended in the *ac* plane. No significant discrete interactions are visible between the cationic and anionic groups, and no π-π interactions were evident between molecules of **96**.

Noting the incorporation of the bridging water molecule in the solid-state structure of this crystalline adduct, the effect of water on the binding interaction of receptors **96** and **97** was determined by adding deionised water to a mixture of each receptor and *ca.* 5 eq. TBAOAc, see Appendix A2. The urea and aromatic peaks moved such that the spectrum resembled that taken at approx. 1 eq. TBAOAc, suggesting that the addition of water diminished the proportion of bound receptor as expected through competitive hydrogen-bonding interactions.

## 2.4.2 X-ray Crystallographic Analysis of the Triple Stranded Helicate $\mathbf{97}_3(TBA_3H_3P_2O_8) \cdot 0.5CHCl_3$

The 3-methoxy substituted derivative **97** was dissolved in a boiling mixture of $CHCl_3$ and EtOAc in the presence of an excess of $AcO^-$ and $H_2PO_4^-$ as their $TBA^+$ salts. The orange solution was filtered whilst hot and crystals of $\mathbf{97}_3(TBA_3H_3P_2O_8) \cdot 0.5CHCl_3$ were obtained by slow evaporation of the solvent. Despite exhaustive efforts, and owing to the practical difficulties described above, it was not possible to optimise or repeat this crystallisation process for larger-scale preparations.

A crystal of $\mathbf{97}_3(TBA_3H_3P_2O_8) \cdot 0.5CHCl_3$ was analysed by single crystal X-ray diffraction, the data were solved and the model refined in the rhombohedral space group $R3c$ (measurement, solution and refinement by Dr Chris Hawes, see Table 2.7). The asymmetric unit contains one complete molecule of **97** in a planar acentric conformation, one tetrabutylammonium cation, a chloroform molecule overlapping the threefold axis with chemical occupancy of ½, and fragments of two phosphate-derived anionic species. Expansion of the structure through crystallographic symmetry elements reveals a complete assembly containing three equivalent molecules of **97** encapsulating two anions, with three accompanying tetrabutylammonium cations. Charge balance considerations require a total charge of −3 for the dimeric anionic species, implying the presence of three protons per $(PO_4)_2^{3-}$ moiety. The two phosphate groups share three crystallographically equivalent sites of hydrogen bonding, defined by a short $O \cdots O$ distance of 2.579(3) Å. Commensurate with the overall crystallographic symmetry and expected chemical formula of $[(H_2PO_4)(HPO_4)]^{3-}$, both oxygen atoms O6 and O7 were assigned riding hydrogen atoms at half occupancy, as a representation of the averaged configuration throughout the entire
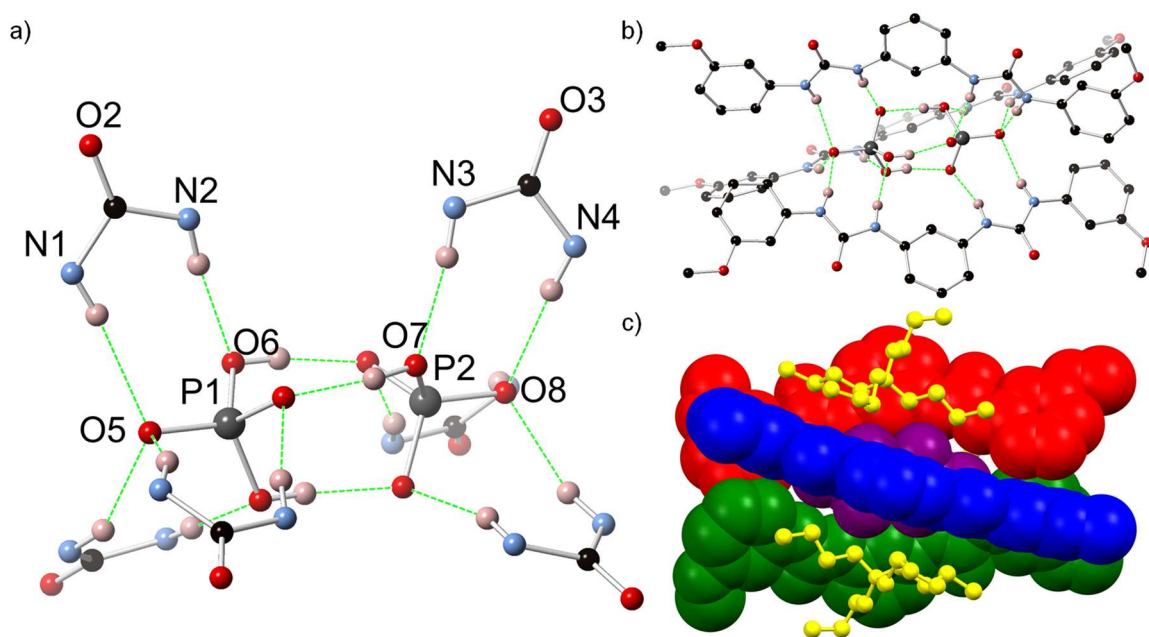
Figure 2.19. a) Hydrogen-bonding environment within the structure of $\mathbf{97}_3(TBA_3H_3P_2O_8)\cdot0.5CHCl_3$ with heteroatom labelling scheme, showing the encapsulation of the $(HPO_4)(H_2PO_4)$ moiety by six urea groups. Phosphate hydrogen atoms shown in representative positions; b) Complete structure of the anionic assembly in the structure of $\mathbf{97}_3(TBA_3H_3P_2O_8)\cdot0.5CHCl_3$. Selected hydrogen atoms are omitted for clarity, and phosphate hydrogen atoms are shown in representative positions. c) Interaction of $TBA^+$ cations (yellow) with the external grooves of the anionic assembly in the structure of $\mathbf{97}_3(TBA_3H_3P_2O_8)\cdot0.5CHCl_3$. Individual host molecules and central anionic moiety coloured separately.

structure. As noted in the Introduction, anion-centred helicates are relatively rare.[62,65,133–136,138,139,141,192] The phosphate adduct closely resembles that observed by Burns and coworkers in a related system, in which a $(H_2PO_4)_2^{2-}$ dimer lies encapsulated within the cavity of a tetra(urea)-substituted porphyrin, receiving seven hydrogen bonds from the surrounding urea groups.[122] The $[(H_2PO_4)(HPO_4)]^{3-}$ moiety presented is found in two structures reported by Didio *et al.*[123] and Zhang *et al.*[124] respectively. In each a bis- or tris(urea) molecule hydrogen bonds to the ends of the dimer, but neither of these associated organic molecules encapsulate the anions. The structure also bears a strong resemblance to several adducts reported by Das and coworkers: those barrels consist of three or four molecules of a similar *meta*-phenylene bis(phenylurea) receptor around anionic carbonate and sulfate clusters, although these lack the helical sense described above.[64,131]

The three molecules of **97** are arranged around each $H_3P_2O_8^{3-}$ group in a triple-stranded helical fashion, with the helical axis aligned with the crystallographic threefold axis in the [0,0,1] direction. The encapsulated anions are supported by a series of hydrogen-bonding interactions originating from the urea groups of **97**. The terminal oxygen atoms of each phosphate residue O5 and O8 each accept three symmetry-equivalent hydrogen bonds
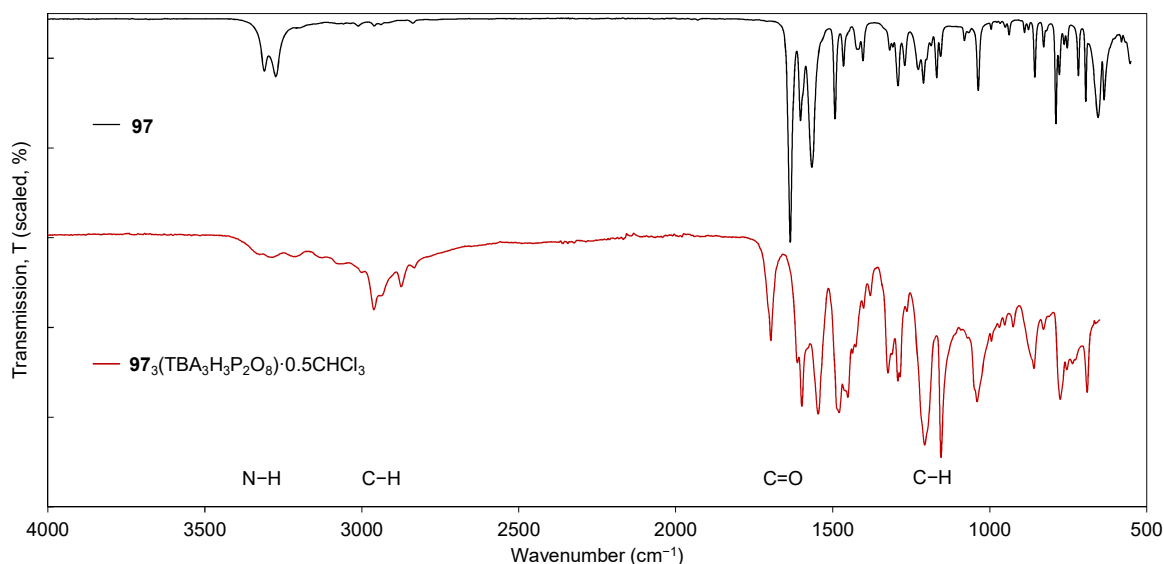
Figure 2.20. FTIR spectra of receptor **97** (top, black) and a crushed crystalline sample of **97**$_3$(TBA$_3$H$_2$P$_2$O$_8$)·0.5CHCl$_3$ (bottom, red).

from the outermost urea nitrogen atoms N1 and N4, respectively, with N···O distances 3.117(4) Å and 3.030(5) Å, and N−H···O angles 153.8(2)° and 164.2(2)°, respectively. In addition to the O−H···O interactions supporting the two phosphate groups, each of the six central oxygen atoms accepts one hydrogen bond from the inner urea N−H groups, with N···O distances 2.892(4) Å and 2.896(5) Å and N−H···O angles 173.2(2)° and 161.9(2)° for N3−H3···O7 and N2−H2···O6, respectively. The TBA$^+$ cations associate with the outer grooves of the adduct, with two of the four butyl groups on each cation aligned parallel to the long axis of each molecule of **97** and interacting with the adduct *via* a series of C−H···π interactions. With the TBA$^+$ cations occupying the interstitial regions, no substantial intermolecular interactions are observed between adjacent helicates in the structure of **97**$_3$(TBA$_3$H$_3$P$_2$O$_8$)·0.5CHCl$_3$, and no void space or additional guest molecules were detected.

The crystalline product **97**$_3$(TBA$_3$H$_3$P$_2$O$_8$)·0.5CHCl$_3$ was produced in sufficient quantities to perform analysis *via* powder FTIR and $^1$H NMR spectroscopy. In comparison to the solid host (**97**), the FTIR spectrum of the above crystalline material shows suppression and broadening of the N−H stretching bands (3400–3150 cm$^{-1}$), and a shift in the C=O stretching frequency from 1635 cm$^{-1}$ to 1698 cm$^{-1}$, Figure 2.20, indicative of the binding of an acceptor by the urea moiety in the solid state.[85]

The helicate assembly was observed by $^1$H NMR to degrade upon contact with CDCl$_3$ due to the slow leaching of the phosphate salts into solution in a greater proportion to receptor **97**, which remained as a white powder. The molar ratio of receptor **97** to TBA$^+$ in
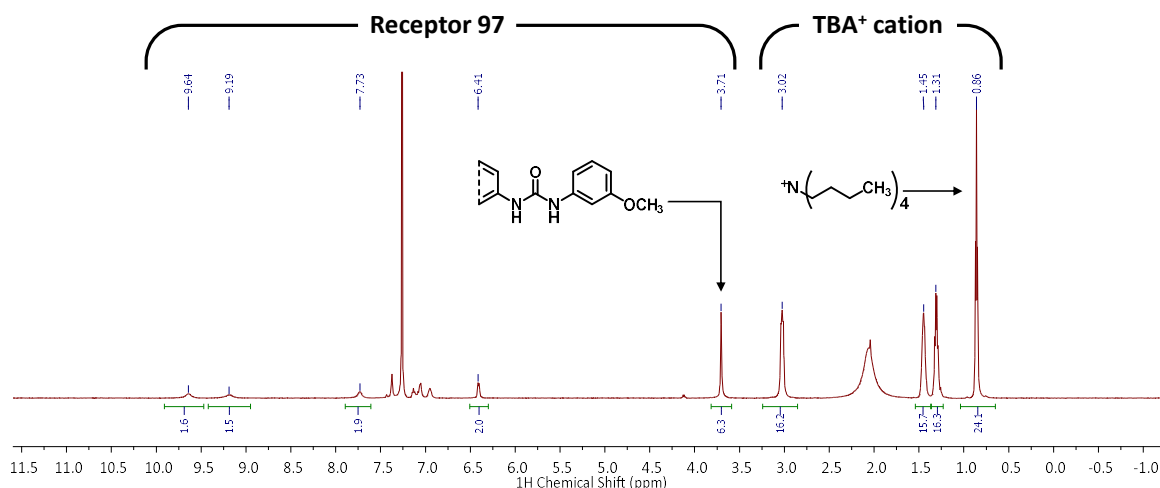
Figure 2.21. $^1$H NMR spectrum (400 MHz, −1.0 to 11.5 ppm) obtained after adding a crystal of **97**$_3$(TBA$_3$H$_2$P$_2$O$_8$)·0.5CHCl$_3$ to CDCl$_3$. The regions corresponding to the resonances of the receptor and TBA cation are highlighted. The integration has been normalised with respect to receptor **97**, demonstrating a receptor-cation ratio of 1:2, rather than the ratio of 1:1 present in the crystalline sample.

solution was observed to be 1:2 by integration, Figure 2.21, while these are present in a 1:1 ratio in the crystalline sample.

A similar $^1$H NMR experiment in DMSO-$d_6$ showed the urea resonances Ha and Hb to be shifted significantly more ($\Delta\delta \leq 2.5$ ppm) with regards to the host (**97**) than at 0.7 eq. H$_2$PO$_4^-$ in the corresponding titration, Figure 2.22, possibly due to a stronger interaction with the HPO$_4^{2-}$ ions present in the anionic assembly over the H$_2$PO$_4^-$ ions used in the corresponding titration. Thus, while the H$_2$PO$_4^-$ anion is known to form dimers in a 'monodentate' and a less abundant 'bidentate' form in solution,[120] discrete helicates of the type described above are unlikely to assemble spontaneously within solutions containing salts of the H$_2$PO$_4^-$ ion alone.
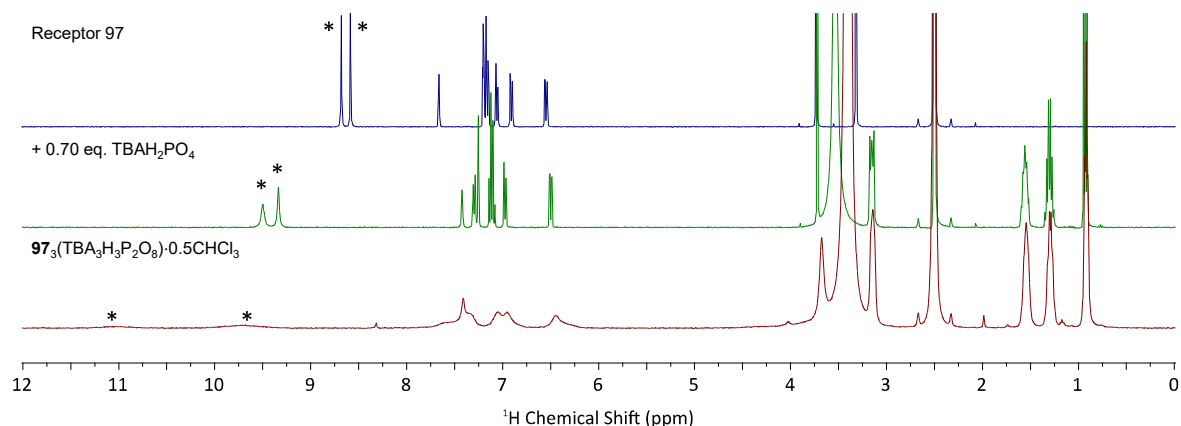


Figure 2.22. Stack plot comparing the $^1$H NMR spectra (400 MHz, DMSO-$d_6$, 0–12 ppm) of receptor **97** (top, blue), the same solution after the addition of 0.70 eq. of TBAH$_2$PO$_4$ (middle, green), and a dissolved sample of crystalline **97**$_3$(TBA$_3$H$_2$P$_2$O$_8$)·0.5CHCl$_3$ (bottom, red). The resonances corresponding to Ha and Hb are denoted by asterisks.

Table 2.7. Crystal and refinement data.

| Compound | **96**(TBAAcO)$_2$·3H$_2$O | **97**$_3$(TBA$_3$H$_3$P$_2$O$_8$) ·0.5CHCl$_3$ | **100** |
|---|---|---|---|
| Empirical formula | C$_{58}$H$_{106}$N$_6$O$_{11}$ | C$_{229}$H$_{355}$Cl$_3$N$_{30}$O$_{40}$P$_4$ | C$_{22}$H$_{22}$N$_4$O$_4$ |
| Formula weight | 1063.48 | 4398.64 | 406.43 |
| Temperature / K | 99.98 | 100 | 100(2) |
| Crystal system | Monoclinic | Trigonal | Orthorhombic |
| Space group | *Cc* | *R3c* | *Pbcn* |
| a / Å | 18.782(2) | 22.0110(7) | 28.768(2) |
| b / Å | 17.2873(18) | 22.0110(7) | 8.3744(6) |
| c / Å | 19.209(2) | 42.9761(14) | 16.5547(12) |
| α / ° | 90 | 90 | 90 |
| β / ° | 90.113(2) | 90 | 90 |
| γ / ° | 90 | 120 | 90 |
| Volume / Å$^3$ | 6236.9(12) | 18031.7(13) | 3988.3(5) |
| Z | 4 | 3 | 8 |
| $\rho_{calc}$ / g cm$^{-3}$ | 1.133 | 1.215 | 1.354 |
| μ / mm$^{-1}$ | 0.077 | 0.14 | 0.095 |
| F(000) | 2336 | 7110 | 1712 |
| Crystal size / mm$^3$ | 0.19 × 0.12 × 0.07 | 0.33 × 0.28 × 0.18 | 0.344 × 0.153 × 0.074 |
| Radiation | MoKα (λ = 0.71073 Å) | MoKα (λ = 0.71073 Å) | MoKα (λ = 0.71073 Å) |
| 2θ range / ° | 3.202 to 50.996 | 3.7 to 56.66 | 4.922 to 55.07 |
| Index ranges | −20 ≤ h ≤ 22, −20 ≤ k ≤ 20, −23 ≤ l ≤ 23 | −29 ≤ h ≤ 29, −28 ≤ k ≤ 21, −57 ≤ l ≤ 57 | −37 ≤ h ≤ 37, −10 ≤ k ≤ 10, −21 ≤ l ≤ 21 |
| Reflections collected | 35902 | 70836 | 48980 |
| Independent reflections | 10699 [R$_{int}$ = 0.0682, R$_{sigma}$ = 0.0867] | 9954 [R$_{int}$ = 0.0611, R$_{sigma}$ = 0.0412] | 4591 [R$_{int}$ = 0.0475, R$_{sigma}$ = 0.0232] |
| Data/restraints/ parameters | 10699/64/721 | 9954/3/474 | 4591/0/285 |
| Goodness-of-fit on F$^2$ | 1.015 | 1.043 | 1.096 |
| Final R indexes [I>=2σ (I)] | R$_1$ = 0.0720, wR$_2$ = 0.1718 | R$_1$ = 0.0550, wR$_2$ = 0.1422 | R$_1$ = 0.0441, wR$_2$ = 0.0943 |
| Final R indexes [all data] | R$_1$ = 0.1363, wR$_2$ = 0.2018 | R$_1$ = 0.0792, wR$_2$ = 0.1612 | R$_1$ = 0.0612, wR$_2$ = 0.1015 |
| Largest diff. peak/hole / e Å$^{-3}$ | 0.57/−0.27 | 0.43/−0.49 | 0.26/−0.22 |
| Flack parameter | 0.0(6) | 0.11(3) | n/a |
| CCDC | 1840843 | 1840844 | n/a |

The similar values of cooperativity constants in the cases of $AcO^-$ and $BzO^-$ binding suggest that the manner of binding of these ions is not dependent on their steric bulk. As these are anti-cooperative processes, it is postulated that there is either a non-steric interaction (*i.e.* electrostatic) between the binding anions, or that host–guest complex can adopt an alternate, less favoured, conformer to which the second anionic guest molecule may bind. In comparison, the positive cooperativity observed with $H_2PO_4^-$ leads to a binding, which is stronger than with $AcO^-$. This contrasts with a series previously derived for mono-urea based anion receptors, in which phosphate was bound less strongly than the carboxylates ($AcO^- > BzO^- > H_2PO_4^- > HSO_4^-$).[89,91,161,193,194] These positive cooperativity constants imply that phosphate–phosphate hydrogen may occur at the binding site, allowing for two anions to be simultaneously bound by the receptor more easily. As noted above, such phosphate–phosphate binding is well known to occur in solution.[119,120] Noting this binding behaviour, receptor **97** was also titrated with pyrophosphate ($HP_2O_7^{3-}$). Unfortunately, while sharp changes in chemical shift were noted at *ca*. 0.4 eq., 0.6 eq. and 1.3 eq. $HP_2O_7^{3-}$, no useful binding information could be obtained from this titration, see Appendix A2.3.7.

While it appears that the *meta* isomers **97** and **99** show differing binding strengths and cooperativities for $H_2PO_4^-$, $BzO^-$ and $AcO^-$, the associated errors are too large to draw any conclusions. Indeed, no meaningful correlation between the calculated binding affinities and the relevant Hammet values can be observed (see Appendix A2.3.9). While the values of $\log\beta_{1:1}$ and $\log\beta_{1:2}$ appear to be lower for receptors **97** and **99**, it must also be noted that the values calculated for the 1:1 fits are equivalent to or slightly higher than the values for the corresponding *para*-substituted receptors.

## 2.5   Conclusions and Future Work

Receptors **96**–**100** were synthesised to explore the *meta*-phenylene bis(urea) motif, and to probe the effectiveness of this geometry on anion binding. These compounds were fully characterised, and the solid-state structure of **100** was investigated, showing significant torsion of the urea groups, accommodating the formation of urea tapes. The logarithmic binding affinities, $\log\beta$ of receptors **96**–**99** to a variety of common anions have been determined through non-linear regression analysis of $^1H$ NMR titration data in DMSO-$d_6$. Evidence of both 1:1 and 1:2 host–guest complexes was observed with the $TBA^+$ salts of the $H_2PO_4^-$, $AcO^-$ and $BzO^-$ anions. From these data, cooperativity parameters, $\log\alpha$, were derived to elucidate the processes occurring at the binding site. The binding of the acetate and benzoate anions were found to be anti-cooperative. In comparison to similar urea-based receptors in the literature, the binding affinity for acetate appears relatively weak.[182] The

affinity for $H_2PO_4^-$ is strongest of the anions studied. The binding process is cooperative, and may be due to phosphate–phosphate hydrogen bonding at the receptor. A much lower affinity for $Cl^-$, $HSO_4^-$ and $SO_4^{2-}$ anions was observed. These studies complement research performed on electron-poor urea receptors by Das and coworkers.[64,131,184]

While there are strong indications that the *meta*-phenylene bis(phenylurea) motif interacted with carboxylate anions in a 1:2 host–guest binding mode, this was only evident by considering the central aromatic proton Hc in the analyses. Considering the behaviour of all protons in the vicinity of the binding site thus provides a much more convincing probe for studying the solution-state association processes of these systems, as well as giving a spectroscopic handle which is less sensitive to pH. Nevertheless, to ensure comparability to the 1:1 binding constants reported for similar receptors in the literature it was necessary to analyse **96**–**99** in the context of purely 1:1 host–guest binding models as well.

Attempts at producing solid state adducts of **96** and **97** with phosphate and acetate anions led to the discovery of a new helicate centred on a mixed-phosphate core. This adds to a somewhat limited set of anion-based helicates present in the literature.[65,133–136,141,192] The relative simplicity of this helical structure and the possibility of utilising phosphate dimerisation for cooperative binding makes this structure an interesting candidate for future studies. The three molecules of **97** forming each strand of the triple-stranded adduct $[\mathbf{97}_3(H_3P_2O_8)]^{3-}$ may conceivably be replaced by a single-molecule tripodal host, containing the required six urea moieties. Three such hexaurea receptors are outlined in Figure 2.23.
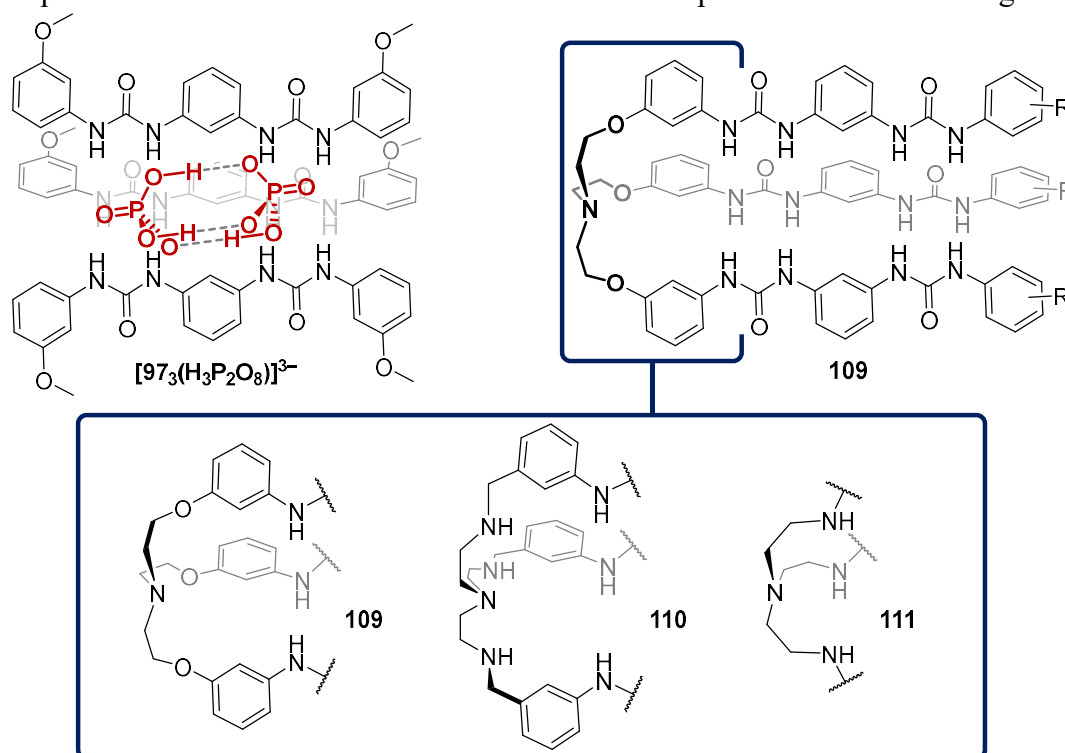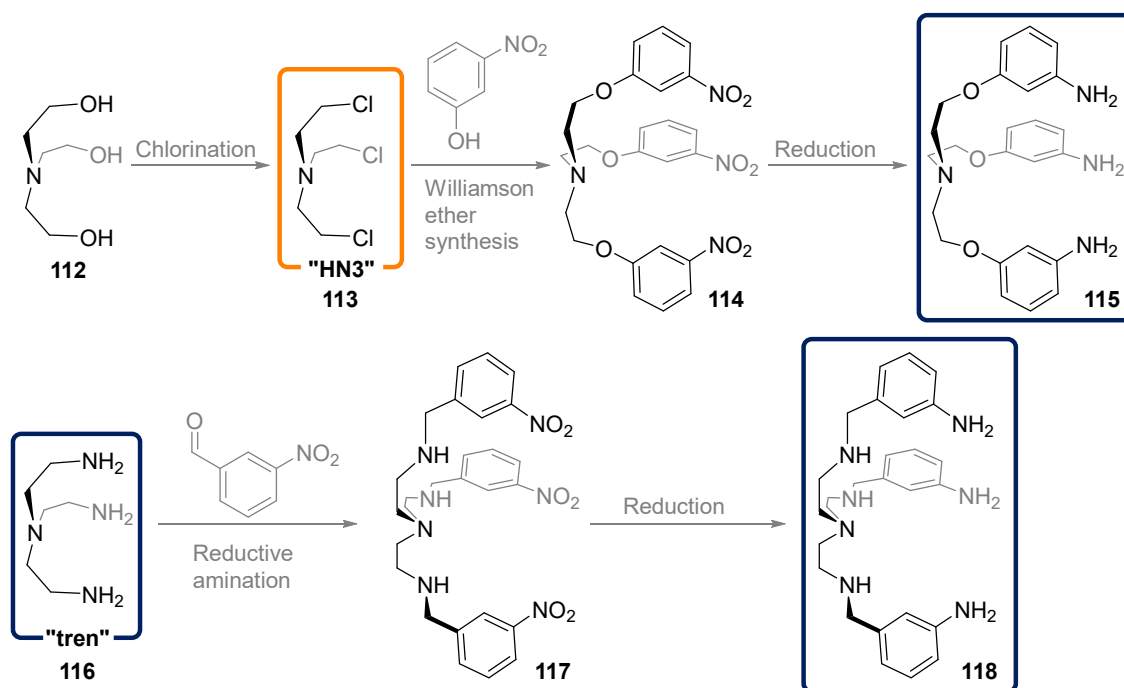


Figure 2.23. The three receptor molecules making up the anionic adduct $[\mathbf{97}_3(H_3P_2O_8)]^{3-}$ are replaced by a single hexaurea molecule. Receptors **109**–**111** are variants of this concept, each containing a different core.

Scheme 2.2. Possible synthetic routes to the triamine precursors **115** and **118**, from triethanolamine (**112**) and tris(2-aminoethyl)amine ("tren", **116**), respectively. The intermediate **113**("HN3") is of concern due to its extremely hazardous nature.

Receptors **109** and **111** may be thought of as extended structures of the tripodal hosts **29**, **30** and **47**, in the introduction,[106,107,125,128,129] and are similar to the bisurea receptors **48** and **49** reported by Wu and coworkers.[63] These molecules also bear a resemblance to a quinoline-containing ATP sensor reported by Butler,[195] however the latter utilises a zinc ion to bind phosphate residues.

The core of **109**, triamine **115**, is accessible through the synthetic procedure reported by Basu *et al.*, Scheme 2.2. However, the intermediate **113** (known as "HN3") is of concern, being an extremely hazardous nitrogen mustard and a Schedule I substance under the Chemical Weapons Convention. In order to avoid these risks, receptor **110** is also proposed, whereby the ether linkage is replaced by a secondary amine formed through the reductive amination of 3-nitrobenzaldehyde with tris(2-aminoethyl)amine ("tren", **116**, see Scheme 2.2). Tren/**116** is itself the precursor for hexaurea **111**, through alternating urea formation and reduction steps, Scheme 2.3. Triamines **115** and **118** would lead to receptors **109** and
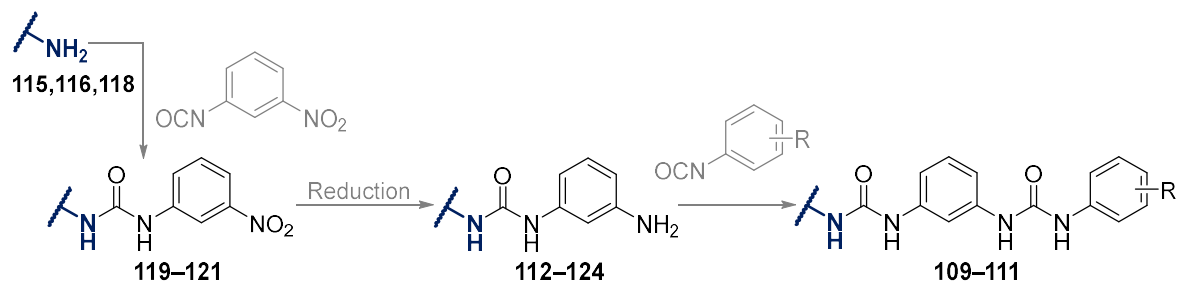


Scheme 2.3. Proposed synthesis of the tripodal hexaureas **109**–**111** from the triamine starting materials **115**, **118** and **116**, respectively.

**110** through an identical synthetic path. This synthetic pathway is preferred for **109**–**111** as the urea moieties are formed last, avoiding the inherent solubility issues of phenylene bisureas; and the synthesis radiates from the triamine core, allowing for synthetic flexibility at the periphery of the tripodal structure.

It is hoped that the knowledge gained from the work presented in this chapter will help drive further research in designed urea-based receptors. There is yet more that can be done to promote 1:2 binding based on phosphate dimerisation. Further exploration of such receptors may lead to the strong and selective binding of phosphate anions, as well as of oligophosphates such as pyrophosphate, ADP and ATP. The understanding, that protons which are not directly involved in the binding event can provide further insights, is capitalised on in the following chapters. Diamide derivatives of the *ortho*- and *meta*-phenylene bis(phenylurea) motifs are further explored in Chapter 4.

# Chapter 3

Investigation of Aliphatic Chain Length on Anion Binding in di(3-Amidophenyl)urea Receptors

## 3.1 Introduction and Rationale

As discussed in the Introduction, macrocyclic receptors offer a route towards interlocked molecules, by using complementary anionic components. Flood and coworkers have exemplified this approach; the cyanostar motif has a strong affinity for the $H_2PO_4^-$ anion, and its replacement with a phosphate diester axle allowed access to a [3]rotaxane.[196] If a macrocyclic receptor is to bear a single anion-binding site in a discrete location along its ring, then a relatively straightforward strategy towards macrocyclisation is to perform ring-closing metathesis (RCM) on long vinylic chains appended to the binding site. This approach has been used by many, for example Beer and coworkers,[49,197] and within this group.[152] Long-chain receptors themselves have potentially exciting applications in anion binding chemistry. There is currently much interest in anion-responsive soft materials and gels,[103,198] as well as the preconcentration effect that may occur upon supramolecular aggregation of receptor molecules or incorporation of the binding motif into materials.[102]

To address the challenge of creating macrocyclic receptors for anions as part of a series of interlocked molecules, Boyle designed and synthesised a series of linear di(3-amidophenyl) urea receptors (**103**–**105**, see Figure 3.1) bearing aliphatic chains of various lengths.[172] Receptors **103**–**105** possessed terminal alkene moieties to provide access to the corresponding macrocyclic analogues *via* RCM. The macrocyclic receptor **125**, bearing a 20-atom carbon chain, was successfully formed and analysed, whereas the syntheses of the smaller macrocyclic derivatives of **103** and **104** were not successful. The potential of receptors **103**–**105** for anion recognition were investigated through preliminary ${}^1$H NMR titrations in DMSO-$d_6$; while all had strong affinities for benzoate and phosphate, they also demonstrated an unexpectedly high binding ability for sulfate. In the case of the $C_6$-chain



Figure 3.1. Structures of receptors **101**–**105**, which are discussed in this chapter, and with atom labelling used in NMR-related discussions (**blue**). Receptors **103**–**105**, and the macrocyclic derivative **125**, were first reported by Boyle.

receptor **103**, its affinity for $SO_4^{2-}$ was estimated to be as strong as for $H_2PO_4^-$, see Table 3.1; titrations were also performed with $Cl^-$ and $NO_3^-$ but these small changes in chemical shift were not fitted. Anion titrations of **125** demonstrated a much weaker binding for the sulfate anion, which was assumed to be due to the restricted geometry of the macrocycle.

Table 3.1. Cumulative logarithmic binding constants, $\log\beta_{1:1}$ and $\log\beta_{1:2}$, reported by Boyle for diamidourea based receptors **103–125**, from the analysis of preliminary $^1H$ NMR titrations in DMSO-$d_6$ at 20.0 °C.[172]

| Receptor | Chain length | H:G [b)] | $\log\beta_{H:G}$ | | |
| --- | --- | --- | --- | --- | --- |
| | | | $BzO^-$ | $H_2PO_4^-$ | $SO_4^{2-}$ |
| **103** | 6 | 1:1 | 2.32 | 2.59 | 2.57 |
| | | 1:2 | 5.63 | 5.86 | 5.82 |
| **104** | 7 | 1:1 | 2.47 | 2.52 | 2.15 |
| | | 1:2 | 6.09 | 6.30 | 4.57 |
| **105** | 11 | 1:1 | 2.39 | 2.32 | 3.90 |
| | | 1:2 | 6.09 | 6.07 | – |
| **125** | n/a [a)] | 1:1 | 3.04 | – [c)] | – [d)] |

Initital host concentration = 7 mM. Anions added as their TBA salts. a) Macrocyclic derivative of receptor **105**. b) Stoichiometry of the host-guest binding equilibrium. c) Fitting not performed, as NH resonances were observed to split. d) Fitting not performed on titrations with these anions, as $\Delta\delta$ was small.

These results are of significant interest, as sulfate and bisulfate often have high coordination requirements,[59] and this requires a receptor (or receptors) with multiple hydrogen bond donor moieties.[63,64,131,199–205] Additionally, sulfates are highly solvated, appearing at the top of the Hofmeister series.[53] This leads to an overall low binding affinity of most receptors for sulfates, as the anion must be partially or completely desolvated in order to be bound by the receptor. There is some evidence of a 'dendritic effect' on anion binding by ferrocenyl dendrimers,[206,207] and it would be useful to be able to access such effects with a synthetically simple small-molecule receptor. While sulfates have limited applications in biological contexts, they are industrially important – and are especially prevalent as pollutants and impurities. In particular, the removal of sulfate from spent nuclear fuel is a challenging task necessary to ensure the waste may be properly vitrified and stored safely.[101]

Of the results reported by Boyle, also notable was the strongly sigmoidal behaviour of the trend in the chemical shift of the urea proton, Hb, in many of the titrations with $H_2PO_4^-$, $BzO^-$ and $SO_4^{2-}$ (see Figure 3.2). Fitting these resulted in the calculation of the 1:1 and 1:2 binding constants noted above. However, sigmoidal responses may occur for many reasons
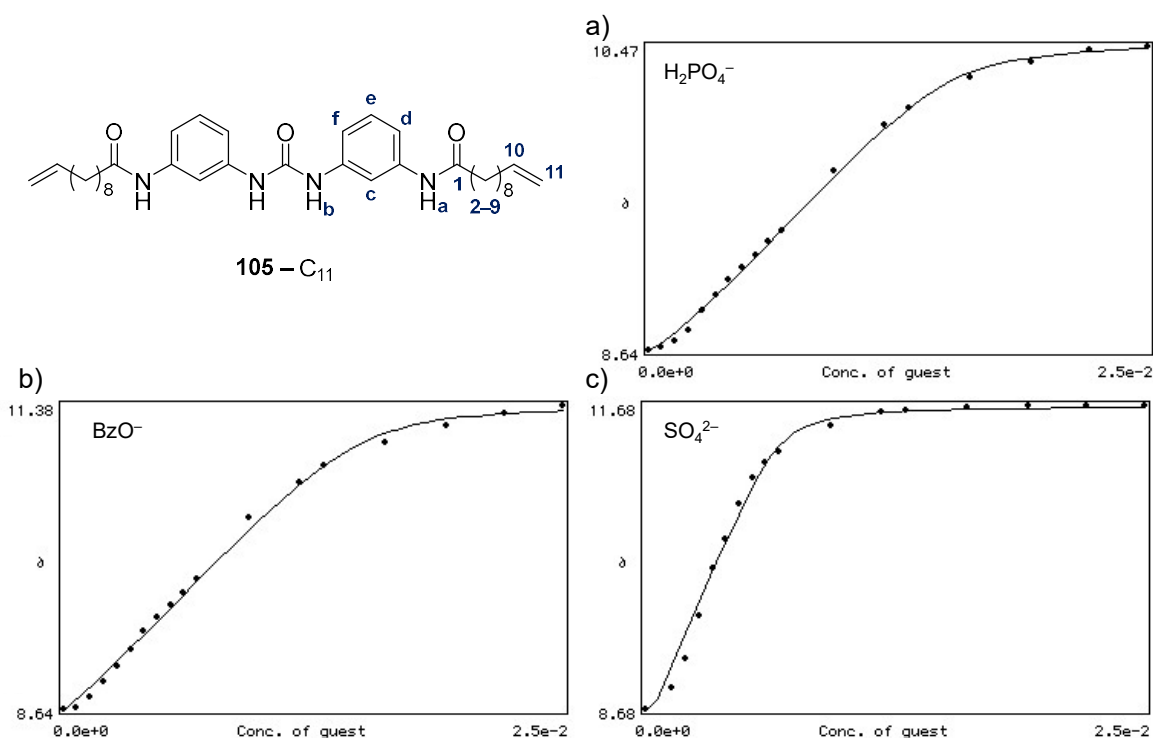
Figure 3.2. Binding isotherms and fits (NMRTit HG) for resonance Hb in preliminary titrations of receptor **105** with a) $H_2PO_4^-$, b) $BzO^-$ and c) $SO_4^{2-}$, as reported by Boyle. Images reproduced from reference 172.

including simple 1:2 host-guest binding,[168] but also more complex cooperative behaviour (such as described by the Hill plot and Langmuir isotherm), acid-base equilibria (as encountered in $pK_a$ determination),[187] and intermediate exchange in NMR experiments.[208] It is important to be able to distinguish between these cases so that the binding behaviour is not misrepresented.[208]

As the length of the aliphatic chains was the only independent variable in these experiments, the binding behaviour was seen as a combination of both the innate properties of the receptor core, and an effect due to the increasing length of the aliphatic chains. The work presented in this chapter has been pursued with the aim of investigating this fully. An understanding of the processes by which the observed binding behaviour was achieved would inform the future design of other receptors of high affinity for the sulfate anion.

## 3.2 Synthesis and Characterisation of Receptors **101**–**105**

In order to analyse the behaviour of the receptor core in the absence of aliphatic moieties, the $C_2$ receptor **101** was designed as a control, being structurally similar to the $C_{6-11}$ receptors **103**–**105**. Diamine **127** was synthesised by reaction of 3-nitroaniline with 3-nitrophenyl isocyanate at 100 °C to generate di(nitrophenyl)urea **126** in 83% yield, and subsequent reduction with hydrazine over palladium on carbon in methanol solution (90% yield, see
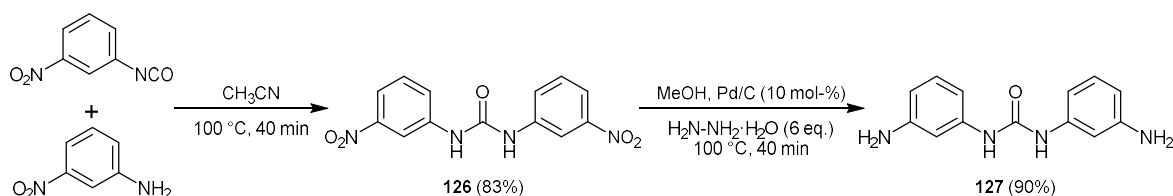
Scheme 3.1. Synthesis of the common diamine precursor **127**.

Scheme 3.1). The successful synthesis of **127** was demonstrated by the appearance of a singlet at 4.99 ppm in the $^1$H NMR spectrum, corresponding to the $NH_2$ resonance.

The $C_2$ derivative **101** was synthesised by stirring diamine **127** in neat acetic anhydride with a catalytic quantity of pyridine (1 mol%), for 24 hours under an argon atmosphere, Scheme 3.2. The resulting suspension was filtered under suction, and washed with water giving the desired product as a grey powder in 93% yield. $^1$H NMR spectroscopy confirmed the absence of the $NH_2$ moiety and the presence of the acetamide group with singlets at 9.9 ppm and 2.0 ppm, corresponding to the amide and the terminal $CH_3$ moieties, respectively. The solubility of compound **101** in DMSO was found to be less than 7 mM, the concentration at which previous titrations had been performed. This made it unsuitable for the purposes of this work, as the titrations could not be carried out using the same standard procedure used by Boyle.
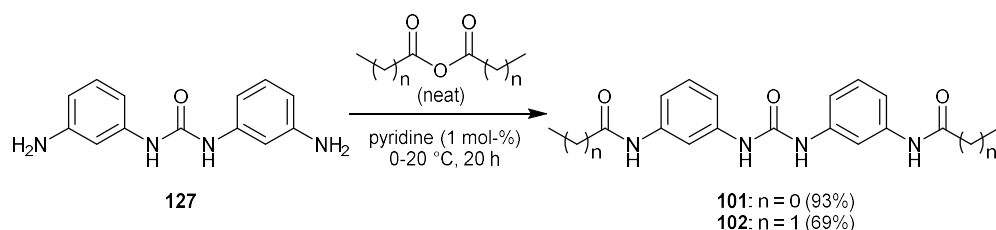


Scheme 3.2. Synthesis of receptors **101** and **102**, from diamine **127**.

The $C_3$ derivative **102** was synthesised and isolated in a similar manner, employing neat propionic anhydride and catalytic pyridine (1 mol%) and being isolated by filtration in 69% yield as a white solid after washing with water. $^1$H NMR spectroscopy again confirmed the presence of the amide (9.8 ppm) and the terminal $CH_2$ (2.3 ppm) and $CH_3$ (1.1 ppm) moieties. In the case of each receptor, the identity of the amide resonance was further confirmed by deuterium exchange (see Appendix A1), while $^{13}$C NMR spectroscopy showed the presence of a new quaternary carbon corresponding to the amide moiety, at 168.3 ppm and 172.1 ppm for receptors **101** and **102**, respectively. IR spectroscopy showed the sharpening of the peak around ca. 3300 cm$^{-1}$ due to the loss of the broad underlying $NH_2$ stretching mode; the appearance of additional C=O stretching modes in the 1630–1670 cm$^{-1}$ region; and the loss of the band at 1211 cm$^{-1}$, likely corresponding to a C−N stretch, Figure
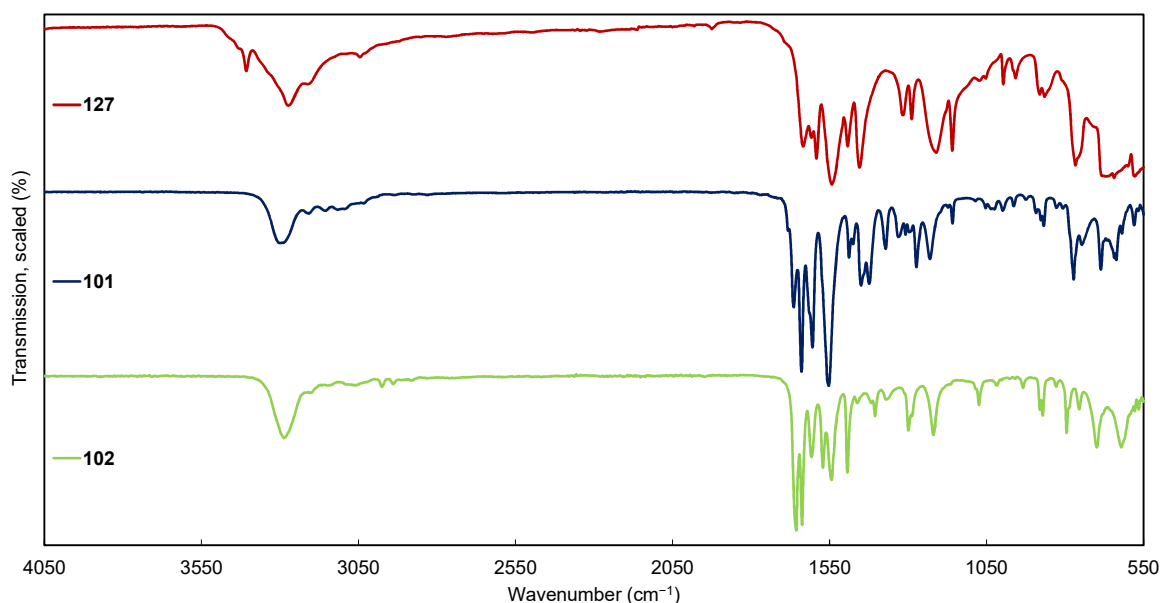
Figure 3.3. FTIR spectra (550–4050 cm$^{-1}$) of compounds **127** (red), **101** (blue) and **102** (green), showing sharpening at *ca.* 3300 cm$^{-1}$ and the appearance of a new C=O stretching mode (1630–1670 cm$^{-1}$) in each case.

3.3. In addition, analysis by mass spectrometry found the [M + H]$^+$ adducts of compounds **101** and **102** at $m/z$ = 327.1454 and 355.1763, respectively.

Receptors **103**–**105** were synthesised *via* a coupling reaction between common synthetic intermediate **127** and the corresponding ω-alkenoic acid, using EDC·HCl as a coupling reagent and DMAP as base in dry CH$_2$Cl$_2$, Scheme 3.3.
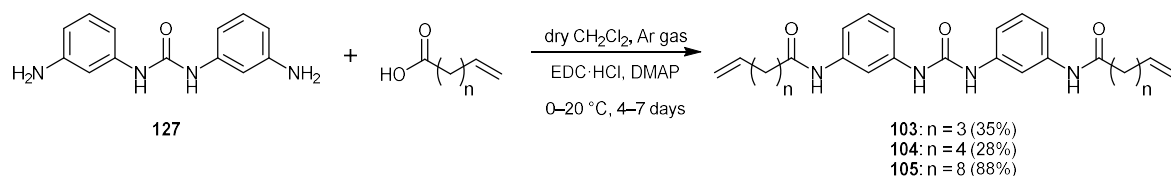


Scheme 3.3. Synthesis of the receptors **103**–**105** from diamine **127**.

Each receptor was isolated by evaporation of the solvent under reduced pressure, redissolution of the resulting oil with a small quantity of acetonitrile, precipitation with water, and separation by centrifugation. The product was purified by successive sonication of the solid in MeCN and MeOH, and separation from the supernatant by centrifugation, giving **103**–**105** in 35%, 28% and 88% yields, respectively. The lower yields of receptors **103** and **104** are likely due to a slight solubility in the MeCN and MeOH supernatant. The dissolved products were not recovered from the supernatant as the purity of the isolated compound would be unacceptably low for use in titrations. The $^1$H NMR spectra of compounds **103**–**105** (shown in Figure 3.4) matched those previously reported.[172]
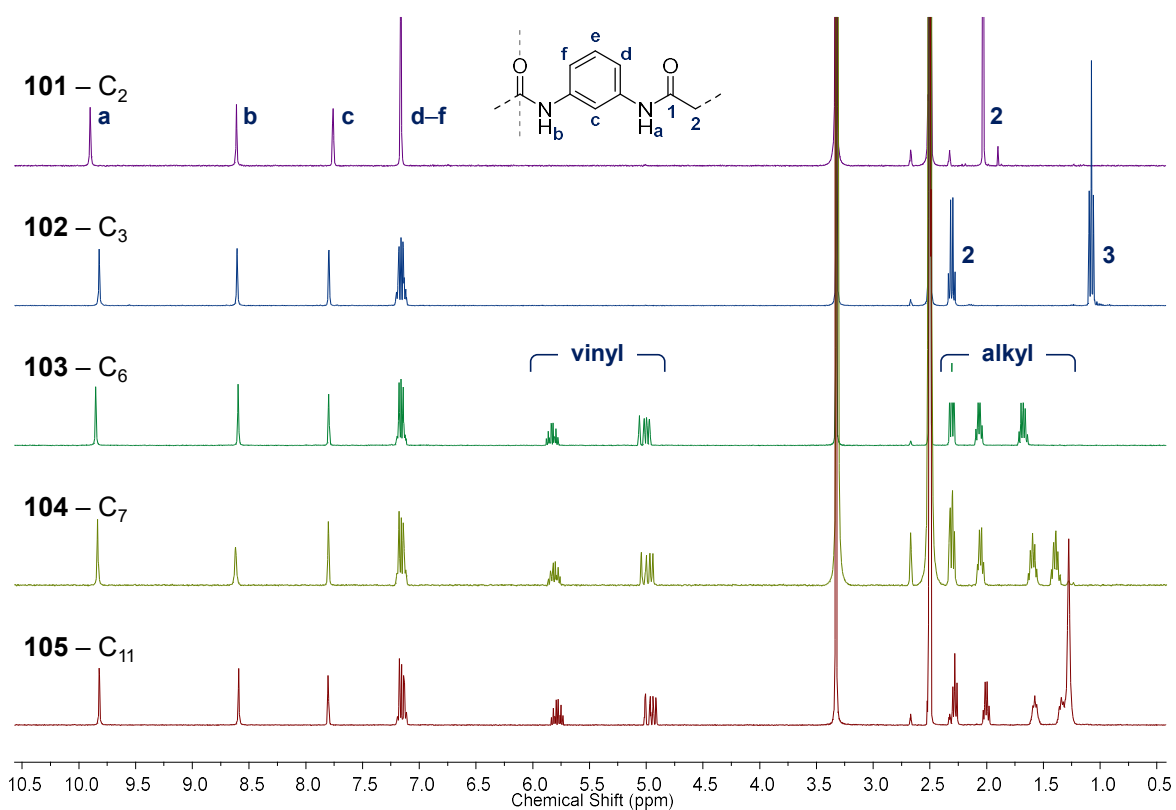
Figure 3.4. $^1$H NMR spectra (400 MHz, DMSO-$d_6$, 0.5–10.5 ppm) of receptors **101** (purple), **102** (blue), **103** (green), **104** (mustard green) and **105** (red), with resonances labelled according to the numbering system in Figure 3.1.

## 3.3  $^1$H NMR Studies with Receptor **102**

As noted above, the $C_2$ receptor **101** had a solubility in DMSO of less than 7 mM. In order to test whether the lower solubility of receptor **101** would translate into an aggregation effect observable in the remaining compounds, an aggregation study (0.04→20 mM) was undertaken on the $C_3$ receptor **102** in DMSO-$d_6$. This showed no significant changes in the $^1$H NMR spectrum of **102**: resonance Hb increased in chemical shift by less than 0.05 ppm,
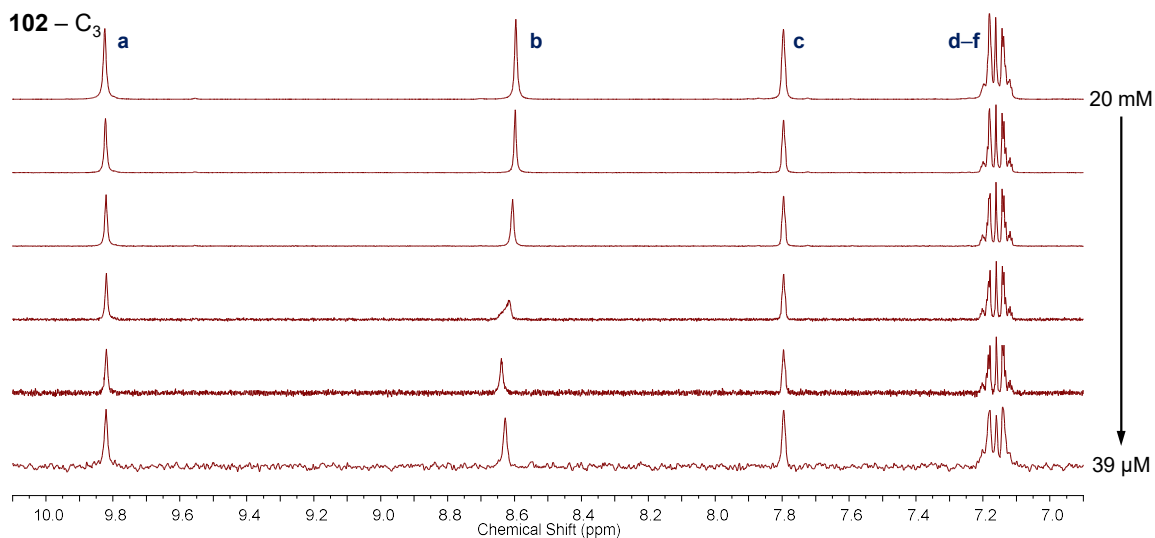


Figure 3.5. Stack plot of the individual $^1$H NMR spectra (400 MHz, DMSO-$d_6$, 6.5–10.5 ppm) of receptor **102** at concentrations of 20, 10, 2.5, 0.63, 0.16 and 0.039 mM.

and no changes in chemical shifts of the other resonances were observed (see Figure 3.5). On this basis, it was assumed that the concentration of the host solution would not affect the binding affinity, and the titrations were subsequently all performed at an initial receptor concentration of 7 mM (as in the original titrations of receptors **103**–**125**, in previous work[172]).

### 3.3.1  Titration of Receptor **102** with $SO_4^{2-}$

The $C_3$ receptor **102** was titrated with the tetra-*N*-butylammonium (TBA$^+$) salts of sulfate, benzoate, dihydrogenphosphate, chloride, and nitrate in order to compare its anion-binding ability to the longer-chain receptors studied in previous work.[172] Upon titration with $TBA_2SO_4$, the urea resonance Hb was noted to shift from 8.6 ppm to 9.6 ppm, Figure 3.6. The profile of this change is non-sigmoidal, with a very small negative curvature, Figure 3.7.

Moderate changes in chemical shift were noted in the amide (Ha; 9.82→9.80 ppm) and aromatic (Hc–f) resonances, with Hc deshielding over the course of the titration (7.80→7.83 ppm). The aromatic resonances within the peak envelope at 7.2 ppm diverged to the extent where they could be individually resolved. The chemical shift of the doublets corresponding to resonances Hd and Hf increased; 7.19→7.25 ppm and 7.13→7.15 ppm, respectively, while He shielded slightly over the course of the titration; 7.16→7.08 ppm. Fitting the data from resonances Ha–c to a 1:1 host-guest binding model gave an average value of $\log\beta_{1:1} = 0.57 \pm 0.54$.
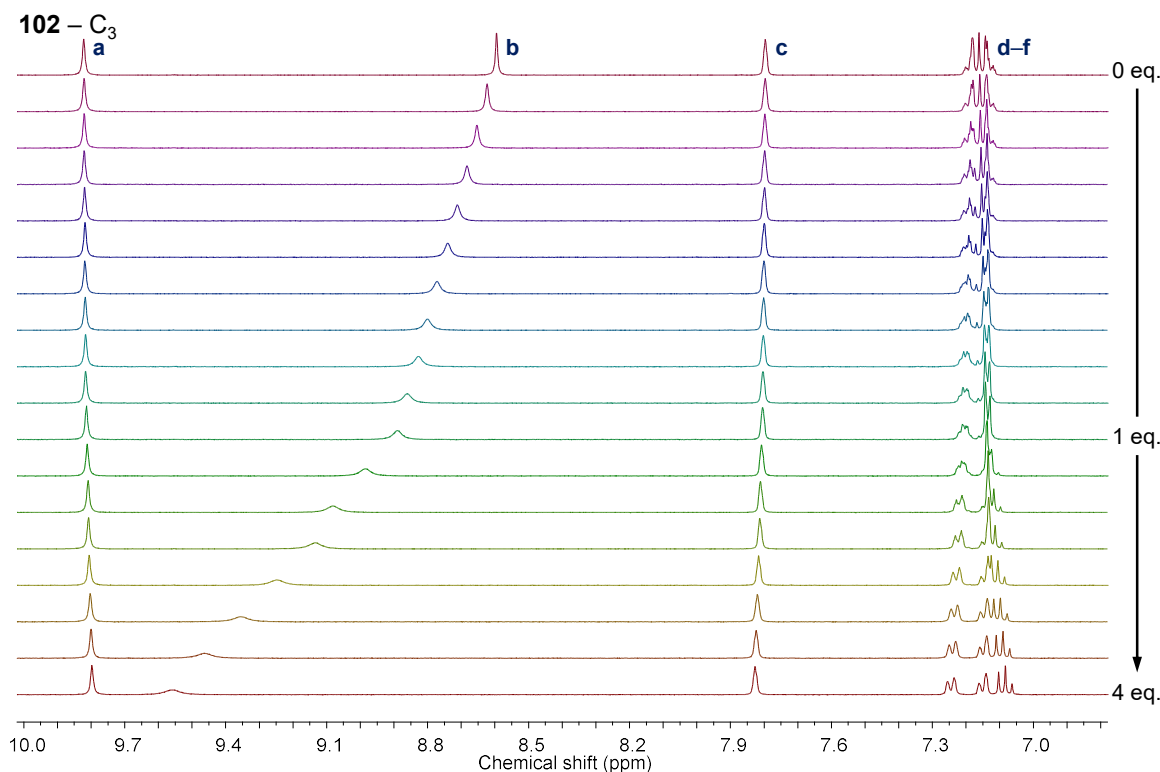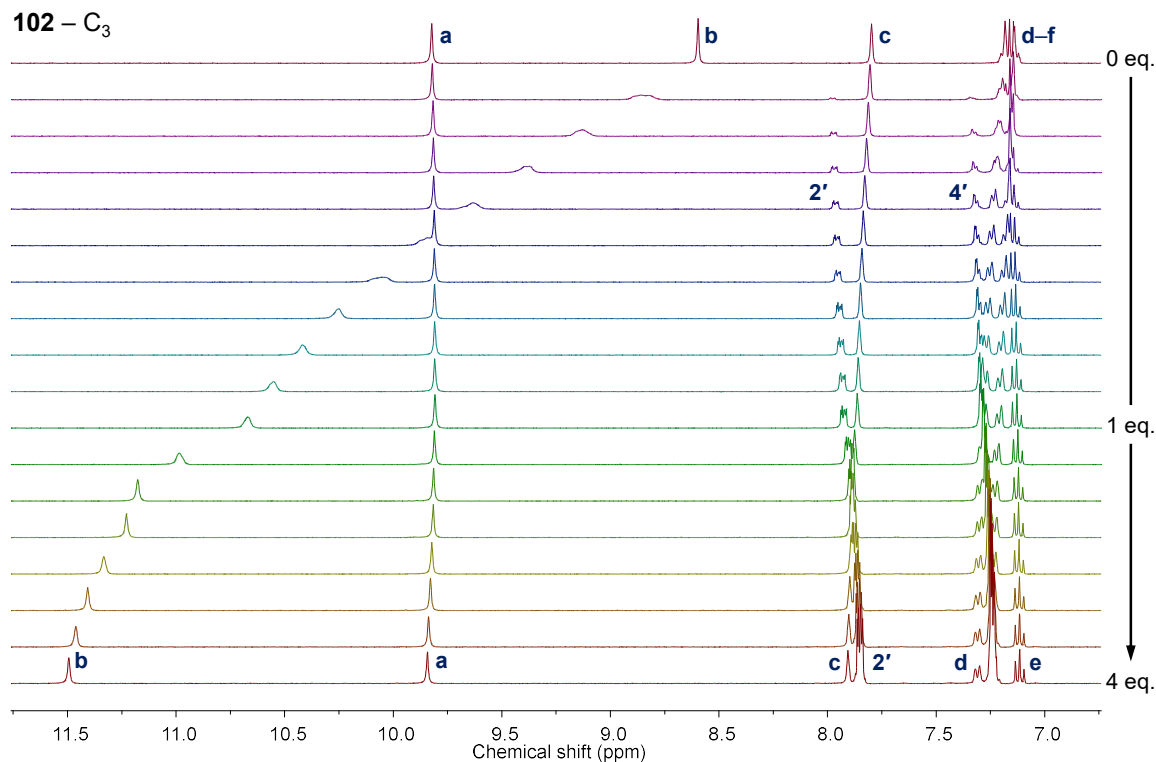


Figure 3.6. Stack plot of the individual ¹H NMR spectra (400 MHz, DMSO-$d_6$, 6.8–10.0 ppm) from the titration of receptor **102** (7 mM) with $SO_4^{2-}$ (0→4 eq.).
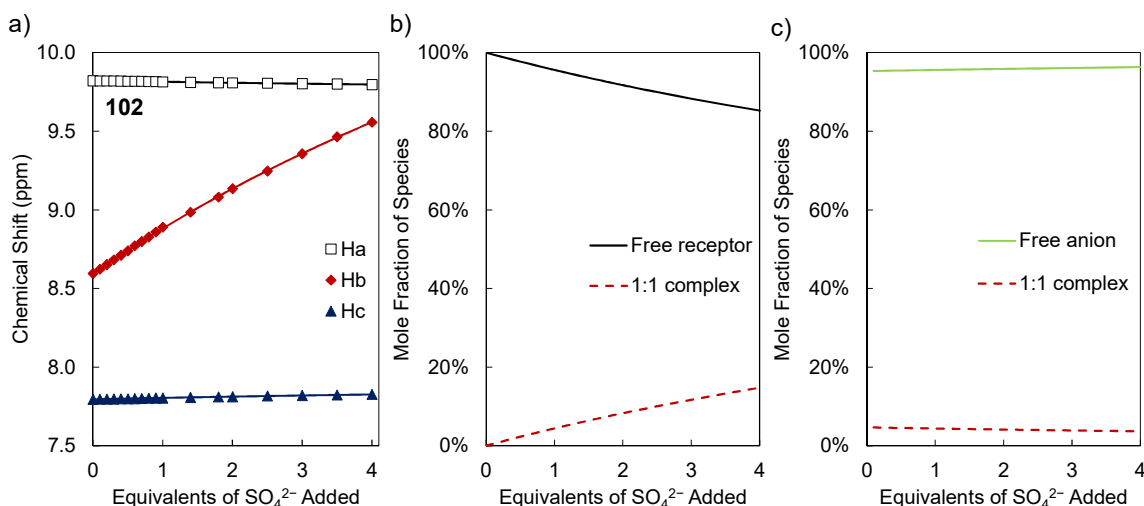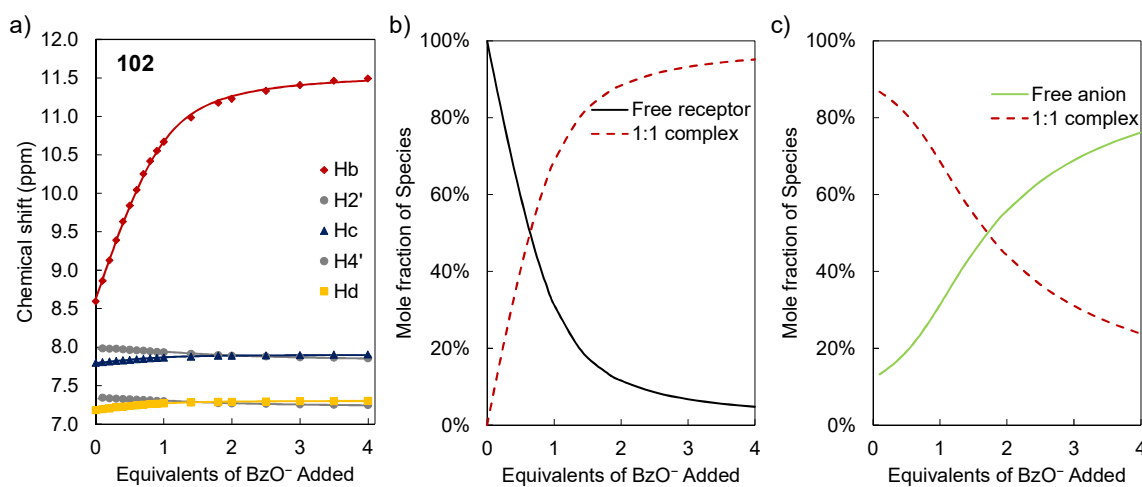
Figure 3.7. Titration of **102** with $SO_4{}^{2-}$. a) Experimentally measured chemical shifts, (points) and calculated fit (lines) of resonances Ha–f of receptor **102**. b–c) Speciation distribution diagrams generated from the fitting of the experimental data. The concentrations are presented as mole-percentage values of each species relative to the sum of their concentrations.

The titration data for receptor **102** cannot be compared to the preliminary work on receptors **103**–**125** in the absence of error estimates, which the fitting programme NMRTit HG does not provide. Therefore, the data from the titration of receptors **103**–**125** with $SO_4{}^{2-}$ were re-fitted with HypNMR2008, see Appendix A2.4.7. Similar results were obtained with each programme, but the statistical parameter which describes the magnitude of the residuals ($SE_y$) was an order of magnitude greater for **103**–**105** than for **102**. This implied that the fits were not accurately describing the trends followed by the proton resonances, especially in the case of **105** where a 1:1 fit was applied to sigmoidal data.

Noting the apparent increase in binding of sulfate with chain length when considering the above results in the contexts of the preliminary work on receptors **103**–**105**, three hypotheses were formed. Firstly, that the presence of the aliphatic chains was causing an increase in binding affinity through some solvophobic or solvation effect. Secondly, that this effect was diminished either by the 'tying-up' of the aliphatic chains upon macrocyclisation or, by the disruption of the binding site (perhaps leading to a change in its conformation) due the structural constraints of being part of such a macrocycle. Thirdly, that the sigmoidal shape of the binding isotherms of receptors **103** and **104** with $SO_4{}^{2-}$ was indicative of intermediate exchange on the NMR timescale, thereby obscuring the true binding isotherms and association constants.

### 3.3.2   Titration of Receptor **102** with $BzO^-$

In the titration of **102** with benzoate, a large increase in the chemical shift of the urea resonance (Hb: 8.6→11.5 ppm) was noted, along with more moderate changes in other

Figure 3.9. Stack plot of the individual $^1$H NMR spectra (400 MHz, DMSO-$d_6$, 6.5–12.0 ppm) from the titration of receptor **102** (7 mM) with BzO$^-$ (0→4 eq.).

resonances, Figure 3.9. This change in resonance Hb was monotonic and non-sigmoidal, Figure 3.8. The chemical shift of resonance Hc increased monotonically (7.80→7.91 ppm). Meanwhile, the resonances associated with the 2- and 4-positions of the benzoate anion itself were observed to shield as the titration progressed; 8.0→7.9 ppm and 7.3→7.2 ppm, respectively. A slight divergence of the peak envelope around 7.2 ppm (Hd–f) occurred, with



Figure 3.8. Titration of **102** with BzO$^-$. a) Experimentally measured chemical shifts (points) and calculated fit (lines) of resonances Hb–d of receptor **102**, and H2′ and H4′ of the benzoate anion. b–c) Speciation distribution diagrams generated from the fitting of the experimental data. The concentrations are presented as mole-percentage values of each species relative to the sum of their concentrations.

resonances Hd and Hf deshielding slightly; 7.18→7.31 ppm and 7.14→7.24 ppm, respectively. The chemical shift of He decreased slightly over the course of the titration, 7.16→7.11 ppm. Fitting of the data from the resonances Hb–d, and the H2′ and H4′ protons of the anion using HypNMR2008 afforded a value of $\log\beta_{1:1} = 2.92 \pm 0.18$.

The amide resonance Ha was observed to follow a small 'U-shaped' trend: starting at 9.82 ppm, the chemical shift decreased slightly to 9.81 ppm, until 1.00 eq. of $BzO^-$ had been added, and increased (9.81→9.84 ppm) thereafter. While the overall change was small, this inflection is indicative of there being more than one equilibrium species, or a subtle change in conformation. This may perhaps be explained by the anion first binding to the urea moiety, and later bridging the urea and amide groups (and so affecting the environment around Hc in between them), or *vice versa*. Fitting the 'U-shaped' trend of Ha, alone, to a 1:1, 1:2 host-guest binding model yielded average values for $\log\beta_{1:1}$ and $\log\beta_{1:2}$ of $2.3 \pm 0.2$ and $3.7 \pm 0.5$, respectively. On calculating of the fits for the two repetitions of this titration, values of the correlation coefficient, $\rho = -0.53$ and $+0.36$ respectively, were obtained suggesting an average $\rho$ around zero. The binding constant $\log\beta_{1:2}$ is cumulative: it increases linearly with $\log\beta_{1:1}$. As $\log\beta_{1:1}$ is an embedded variable in $\log\beta_{1:2}$, the value of $\rho$ is expected to be positive. These fits using only Ha were thus viewed with suspicion. In an attempt to reasonably describe the 'U-shaped' character of the trend in the amide resonance, fitting of the combined data from resonances Ha–c was attempted. Several initial conditions were tried: however these fits were not stable enough to allow for refinement of both binding constants, and an iterative approach towards finding the local minimum would fail if the value of $\log\beta_{1:1}$ were fixed and $\log\beta_{1:2}$ refined.

However, a series of fits could be obtained by fixing $\log\beta_{1:2}$ to values in the range 2.5–5.5, and fitting for $\log\beta_{1:1}$. These points are indicated by the black circles in Figure 3.10. As the magnitude of $\log\beta_{1:2}$ was decreased, $\log\beta_{1:1}$ converged to a value of 2.89 for the first titration ($2^{nd}$ titration: 3.19; average: 3.04). In order to illustrate this, and to understand the behaviour of the fit, a surface describing the quality of the fit (by residual parameter, or $SE_y$) was constructed from fixed values of $\log\beta_{1:1}$ and $\log\beta_{1:2}$. This is illustrated in Figure 3.10, with lower values of $SE_y$ being indicated by the colour blue. The shaded section of the graph is where $\log K_{1:2} < 0$. It can be seen from Figure 3.10 that, while $\log\beta_{1:1}$ converges, the value of $\log\beta_{1:2}$ is unstable and the surface does not contain a minimum in the window studied. This behaviour appears to suggest that if a second equilibrium exists for the interaction between **102** and $BzO^-$, then $\log K_{1:2}$ is negative (*i.e.* the formation of the 1:2 species is unfavourable). Considering the minute quantities of 1:2 host-guest complex that would be present, and the arbitrarily low association constant, this putative second equilibrium was
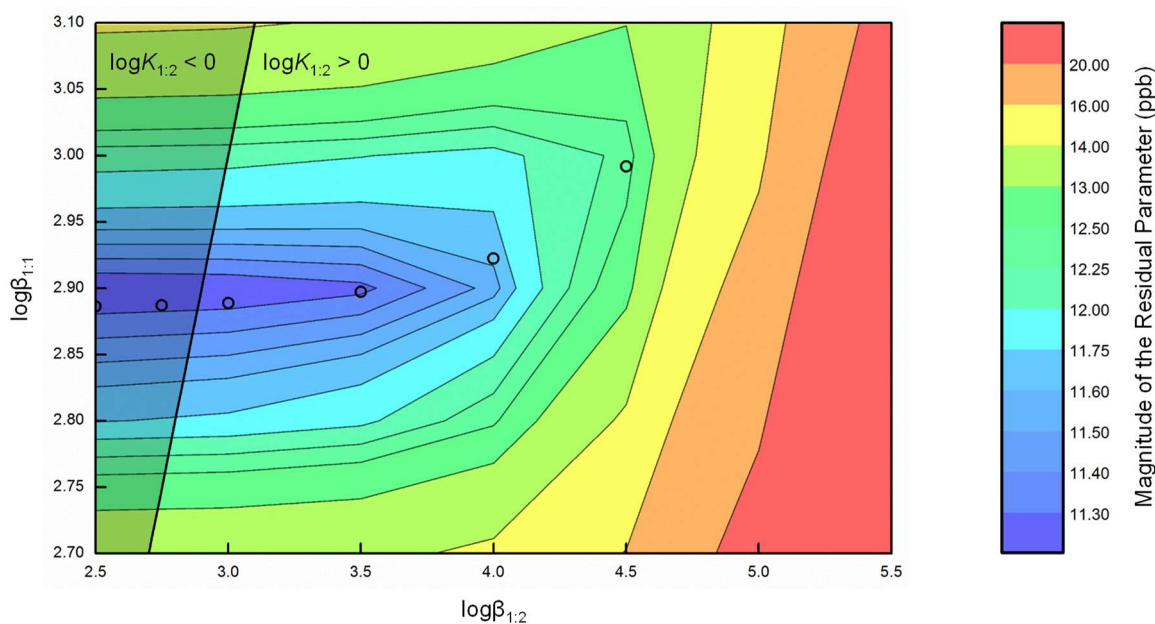
Figure 3.10. Contour map showing the magnitude of $SE_y$, the residual parameter (blue: below 11.3 ppb → red: above 20.0 ppb) of the 1:1, 1:2 fit, interpolated from an array of fixed values of $\log\beta_{1:1}$ (vertical axis) and $\log\beta_{1:2}$ (horizontal axis), in one repetition of the titration of receptor **102** with TBAOBz. Overlaid solid line shows the values at which $\log\beta_{1:1} = \log\beta_{1:2}$ (*i.e.* $\log K_{1:2} = 0$). Overlaid circles show the minimised values of $\log\beta_{1:1}$ for fixed values of $\log\beta_{1:2}$, demonstrating the convergence towards a value of $\log\beta_{1:1} = 2.89$, and the instability of $\log\beta_{1:2}$ towards small values.

disregarded for the purposes of quantifying the binding affinity. In Sections 3.4.2 and 3.5.2 below, no discussion is made on the fitting of resonance Ha, or of pure 1:1 host-guest binding models with BzO⁻.

### 3.3.3 Titration of Receptor **102** with $H_2PO_4^-$

Titrating receptor **102** with TBAH$_2$PO$_4$ led to significant movement of all resonances in the 7–10 ppm region, Figure 3.11. Unlike in the titration of receptor **102** with benzoate, above, while resonances Ha and Hb both became deshielded and approached each other, they did not cross. Ha exhibited moderate deshielding over the course of the titration, 9.8→10.9 ppm, with the changes being slightly sigmoidal in shape, Figure 3.12a. A large initial change was noted in the chemical shift of resonance Hb up to the addition of 1 eq. of the salt, 8.6→10.0 ppm, with a lesser change occurring thereafter, 10.0→10.5 ppm. Resonance Hc underwent moderate shielding over the course of the titration, 7.8→7.4 ppm. As with resonance Ha, the profile of this change was sigmoidal with respect to the number of equivalents of anion added.

The peak envelope corresponding to resonances Hd–f diverged, with the chemical shift of resonances Hd and Hf increasing (7.2→7.6 ppm and 7.1→7.5 ppm, respectively) and He shielding slightly over the course of the titration, 7.2→7.0 ppm. The changes in chemical
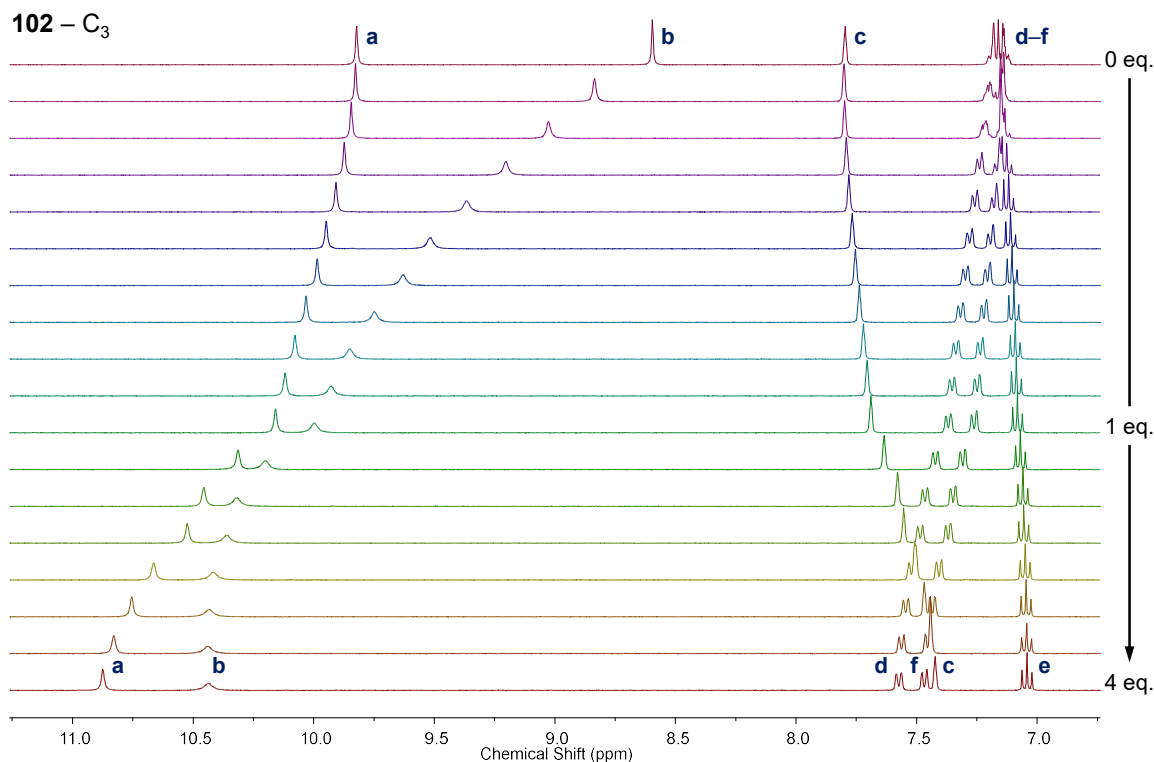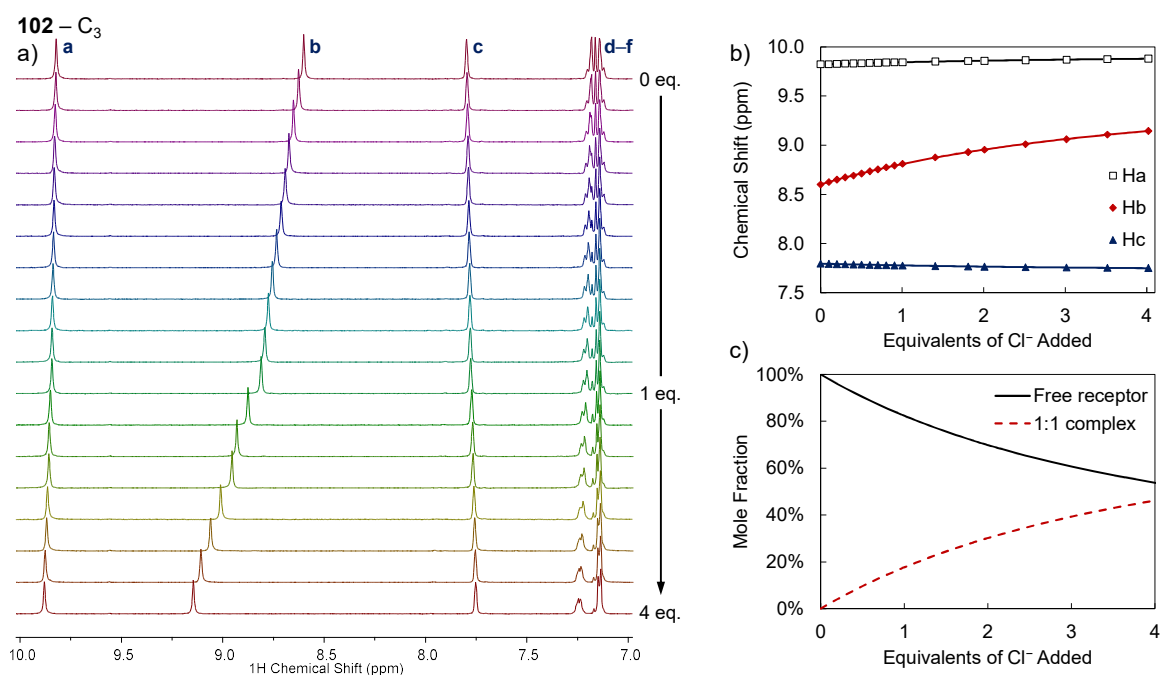
Figure 3.11. Stack plot of the individual $^1$H NMR spectra (400 MHz, DMSO-$d_6$, 6.5–11.5 ppm) from the titration of receptor **102** (7 mM) with $H_2PO_4^-$ (0→4 eq.).

shifts of resonances Ha–f were fitted to a combined 1:1, 1:2 host-guest binding model, Figure 3.12. Average values of $\log\beta_{1:1} = 2.8 \pm 0.4$ and $\log\beta_{1:2} = 5.0 \pm 0.5$ were obtained from these fits, with an associated logarithmic cooperativity constant of $\log\alpha = 0.1 \pm 0.4$. As the value of $\log\alpha$ is near zero, this suggests non-cooperative binding, in which the net interaction between the two binding sites is zero.
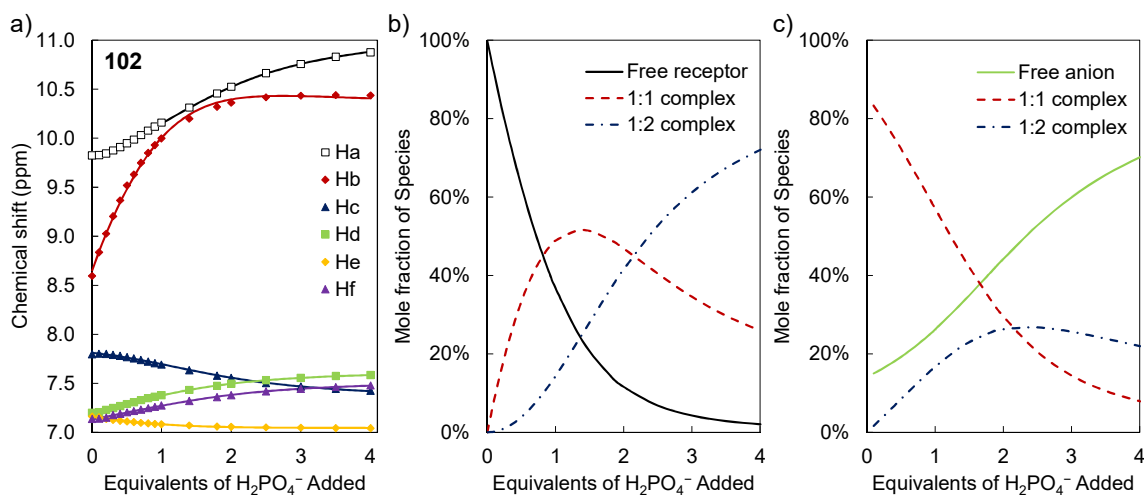


Figure 3.12. Titration of **102** with $H_2PO_4^-$. a) Experimentally measured chemical shifts, (points) and calculated fit (lines) of resonances Ha–c of receptor **102**. b–c) Speciation distribution diagrams generated from the fitting of the experimental data. The concentrations are presented as mole-percentage values of each species relative to the sum of their concentrations.

### 3.3.4 Titration of Receptor **102** with Cl⁻ and NO₃⁻

The titration with Cl⁻ followed similar trends to that found with BzO⁻ in Section 3.3.2 above, but the changes in chemical shift of the resonances were much smaller, Figure 3.13. Small changes were noted in the chemical shift of resonances Ha and Hc, with resonance Ha increasing slightly (9.82→9.88 ppm), and resonance Hc decreasing slightly (7.80→7.75 ppm) in chemical shift. A moderate deshielding (8.6→9.1 ppm) was noted in the urea resonance, Hb, over the course of the titration. Fitting these data (Ha–c) to a 1:1 host-guest binding model afforded a binding constant of $\log\beta_{1:1} = 1.582 \pm 0.009$.
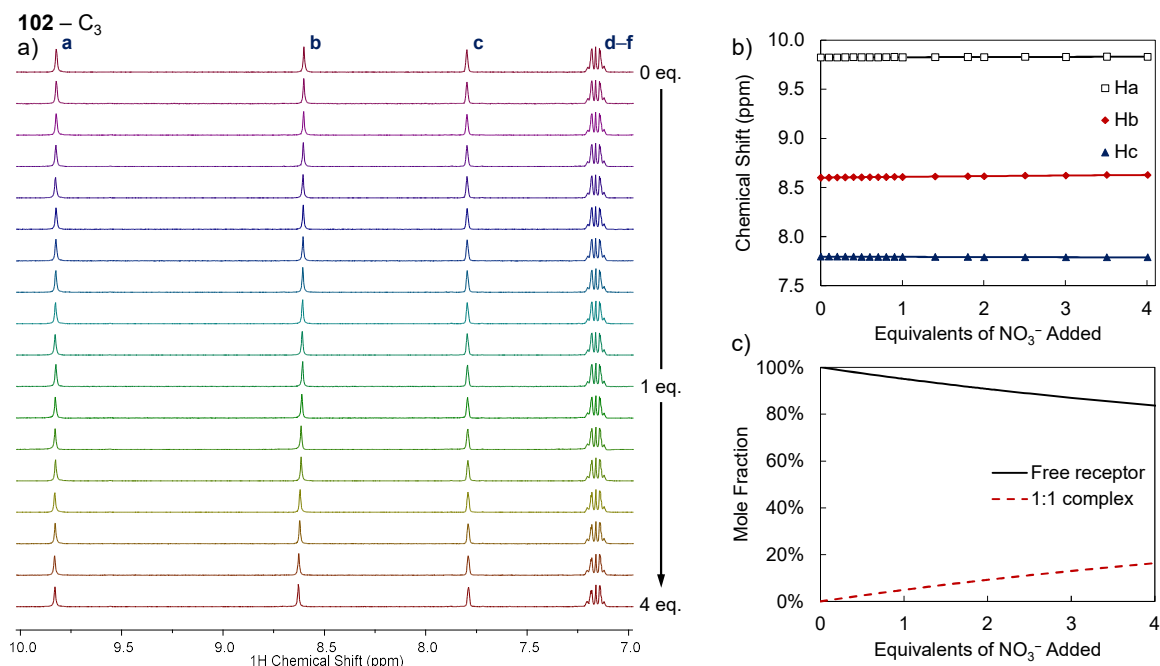


Figure 3.13. a) Stack plot of the individual $^1$H NMR spectra (400 MHz, DMSO-$d_6$, 7.0–10.0 ppm) from the titration of receptor **102** (7 mM) with Cl⁻ (0→4 eq.). b) Experimentally measured chemical shifts, (points) and calculated fit (lines) of resonances Ha–c of receptor **102**. c) Speciation distribution diagram generated from the fitting of the experimental data. The concentrations are presented as mole-percentage values of each species relative to the sum of their concentrations.

Very minor changes were observed upon titration with the nitrate salt, with Δδ < 0.03 ppm for all resonances, Figure 3.14. Resonances Ha (9.82→9.83 ppm) and Hb (8.60→8.63 ppm) were very slightly deshielded, while resonance Hc was slightly shielded (7.80→7.79 ppm). As these changes in chemical shift are only slightly larger than the anticipated experimental variation, the calculated value of $\log\beta_{1:1} = 0.9 \pm 0.3$ is both small and has a high percentage error of 32%.

The next two sections detail the titrations of receptors **103** and **105** with SO₄²⁻, BzO⁻ and H₂PO₄⁻. Comparative analysis of the medium- and long-chain receptors, along with the short-chain receptor **102**, should capture any solvophobic effect that occurs with this system.

Due to the poor quality of the 1:1 fit for the preliminary titration of **105** with $SO_4^{2-}$ and the sigmoidal nature of the binding isotherm for that titration, as noted in Section 3.3.1, this begins with an investigation into whether the difference in shape of the binding profiles is a kinetic or thermodynamic effect. These sections finish with a full summary of the results obtained. Finally, in Section 3.6 these results are briefly compared to the preliminary data reported by Boyle, and a possible explanation provided for the behaviour formerly observed.
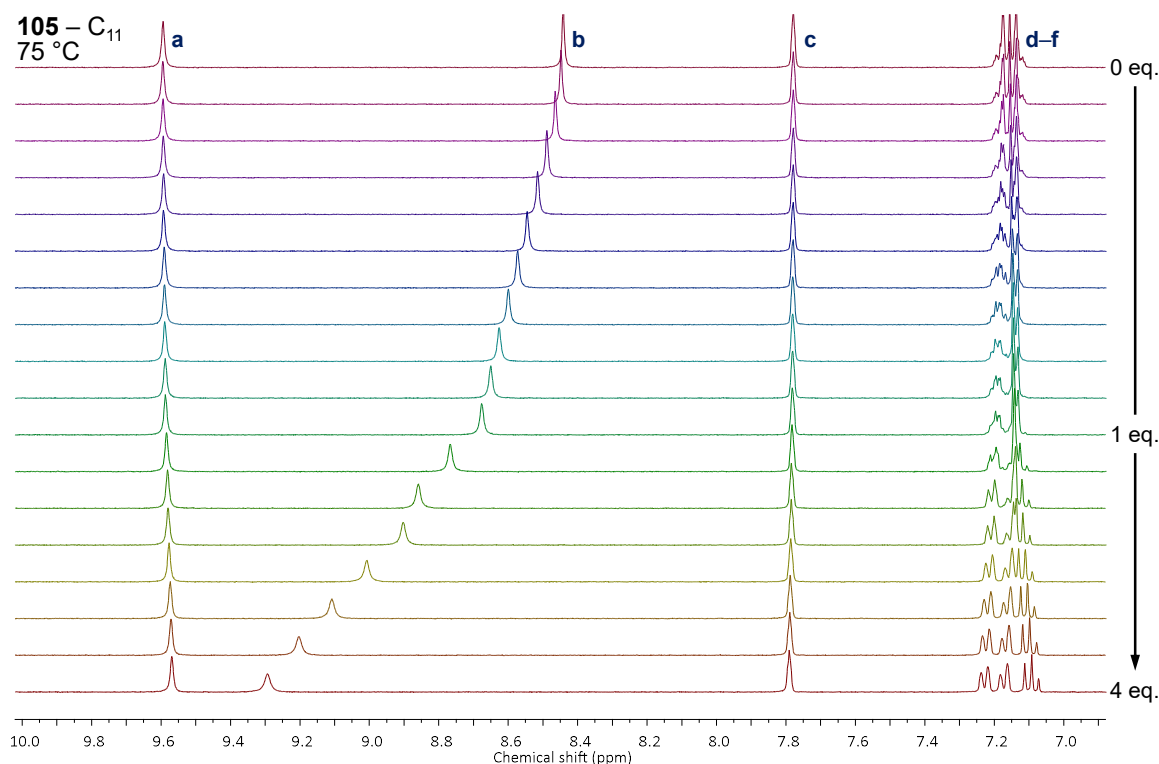


Figure 3.14. a) Stack plot of the individual $^1H$ NMR spectra (400 MHz, DMSO-$d_6$, 7.0–10.0 ppm) from the titration of receptor **102** (7 mM) with $NO_3^-$ (0→4 eq.). b) Experimentally measured chemical shifts (points) and calculated fit (lines) of resonances Ha–c of receptor **102**. c) Speciation distribution diagram generated from the fitting of the experimental data. The concentrations are presented as mole-percentage values of each species relative to the sum of their concentrations.

## 3.4  $^1H$ NMR Studies with Receptor **105**

Having investigated the anion-binding behaviour of the $C_3$ receptor **102** with several anions, the $C_{11}$ receptor **105** was studied next. Firstly, the working temperature of the spectrometer used in this work, 25 °C, was different to that used in the preliminary titrations of receptors **103**–**125** by Boyle; 20 °C.[172] It was felt that an accurate comparison could only be made at a single temperature. Additionally, as noted in Section 3.1, the trend in chemical shift of a resonance can become sigmoidal in shape if the species in equilibrium are in between the slow and fast exchange regimes. As such a shape had been observed in the preliminary titration of receptor **105** with $SO_4^{2-}$, the exchange kinetics warranted investigation. Thus, it was necessary to account for the temperature difference between the two sets of data, and to check whether a higher titration temperature would lead to a smoother titration curve.
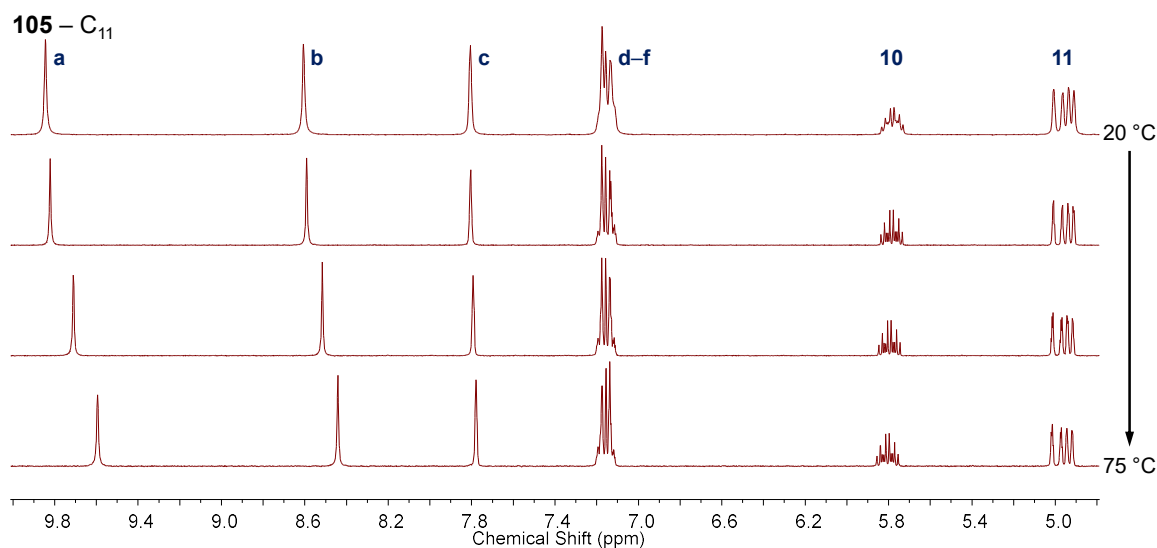
Figure 3.15. Stack plot of the individual $^1$H NMR spectra (400 MHz, DMSO-$d_6$, 4.0–10.0 ppm) from a variable temperature (VT; 20 °C, 25 °C, 50 °C and 75 °C) experiment performed on a sample of receptor **105** (7 mM), showing slight changes in chemical shift of the resonances in the 5–10 ppm region.

A variable temperature (VT) experiment was performed on a sample of **105** at a concentration of 7 mM. As a concentration-based aggregation experiment had earlier been performed with the C$_3$ chain receptor **102**, without showing any noticeable aggregation effects in the NMR spectrum, it was expected that aggregation would not be a confounding variable in the VT experiment. The chemical shifts of resonances Ha and Hb were observed to decrease moderately, 9.8→9.6 ppm and 8.6→8.4 ppm respectively, while a very slight change was noted for Hc ($\Delta\delta = 0.03$ ppm), see Figure 3.15.

### 3.4.1 Titrations of Receptor **105** with SO$_4^{2-}$ at Various Temperatures

A titration of the C$_{11}$ host **105** with sulfate was performed at 75 °C to reduce any possible effects due to slow exchange kinetics on the timescale of NMR spectroscopy. The NMR titration with sulfate at 75 °C displayed changes in chemical shift that were significantly different to that observed in previous work, Figure 3.16. Indeed, the isotherm more closely matched that for receptor **102**, above (*cf.* Figure 3.7). As with **102**, a slight decrease in the chemical shift of Ha (9.59→9.57 ppm) was observed, and an increase in Hc; 7.78→7.79 ppm. Hb deshielded over the course of the titration; 8.4→9.3 ppm.

Investigating this further, the titration was repeated at a temperature of 25 °C, Figure 3.18, with which revealed changes similar to those observed at 75 °C, Figure 3.16. This also reflected the changes noted with the C$_3$ chain receptor **102**, Figure 3.17. The changes in chemical shift of Ha and Hc were equally slight, 9.82→9.80 ppm and 7.80→7.83 ppm
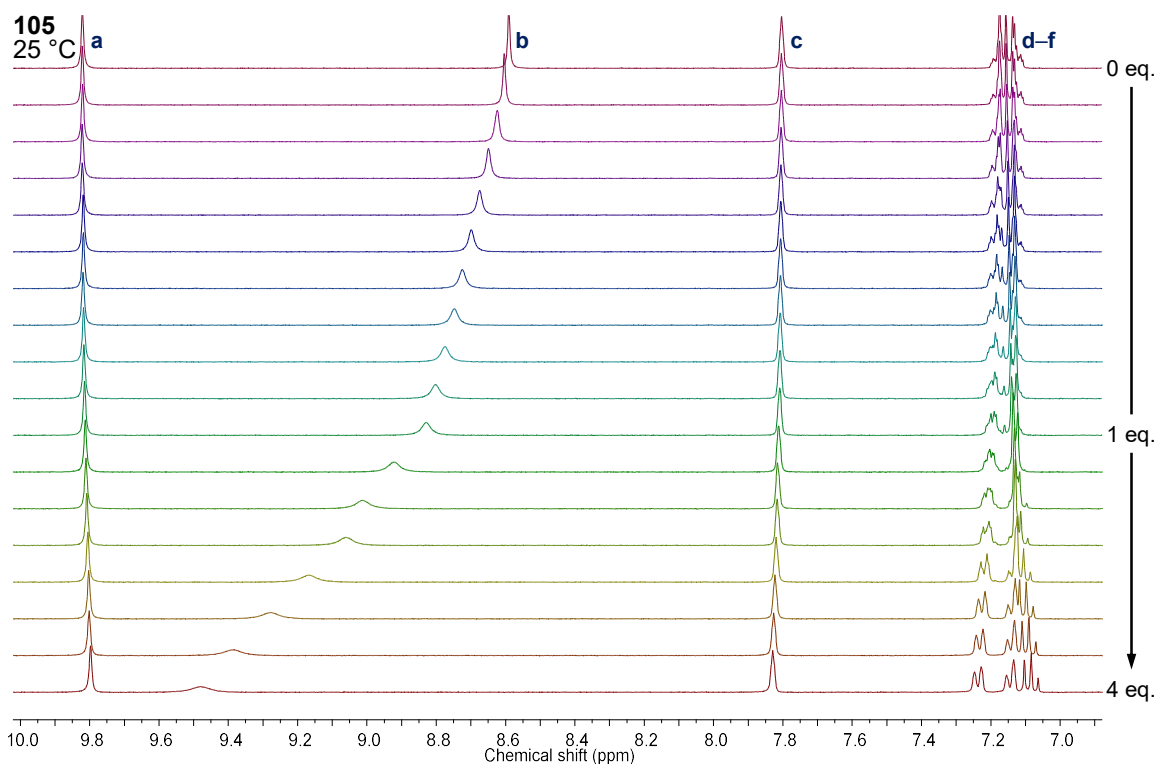
Figure 3.16. Stack plot of the individual $^1$H NMR spectra (400 MHz, DMSO-$d_6$, 6.8–10.0 ppm) from the titration of receptor **105** (7 mM) with $SO_4^{2-}$ (0→4 eq.) at 75 °C.

respectively. Resonance Hb was slightly broader at the lower temperature, but the deshielding was of the same magnitude, 8.6→9.5 ppm.

Finally, the spectra corresponding to the end points of the titration (free host and 5.00 eq. TBA$_2$SO$_4$) were re-acquired at 20 °C, the working temperature of the original titrations. This also deviated significantly from the previously obtained data, thus ruling out any significant thermodynamic or kinetic effects due to temperature, Figure 3.17a. Fitting the changes in chemical shift for resonances Ha–c from the NMR titrations at 25 °C and
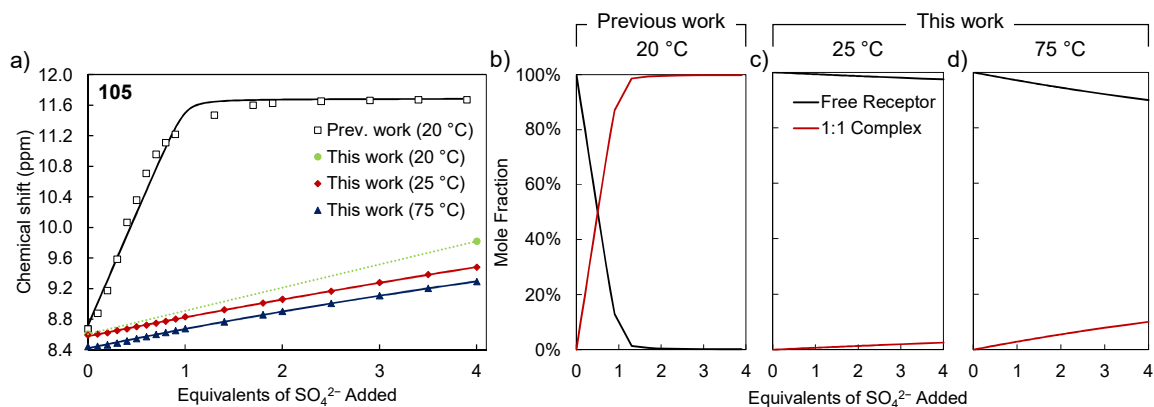


Figure 3.17. Titration of **105** with $SO_4^{2-}$. a) Comparison of the titration data (points) and binding isotherms (solid lines) following resonance Hb in the titration of receptor **105** with TBA sulfate under various conditions, in prior work at 20 °C (black), and in this work at 20 °C (green, titration end-points, the dotted line is to illustrate the overall change only), 25 °C (red), and 75 °C (blue). b–d) Speciation distribution diagrams from the fitting of the data: 20 °C (Boyle), 25 °C and 75 °C respectively.
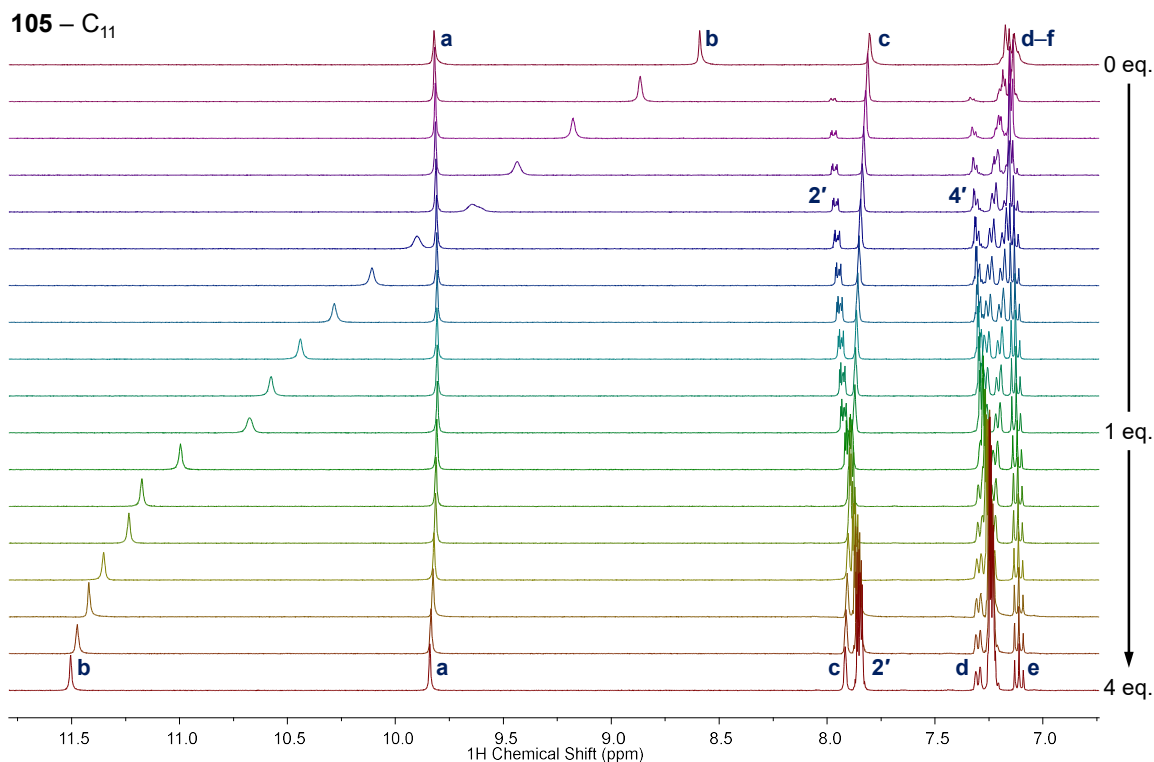
Figure 3.18. Stack plot of the individual $^1$H NMR spectra (400 MHz, DMSO-$d_6$, 6.9–10.0 ppm) from the titration of receptor **105** (7 mM) with $SO_4^{2-}$ (0→4 eq.) at 25 °C.

75 °C afforded values of $\log\beta_{1:1}$ of 0.01 ± 0.17 and 0.65 ± 0.07, respectively. Repetition of the titration at 25 °C gave consistent changes in chemical shift, and the difference between these data and the preliminary work will be further discussed in Section 3.6 below. As these data were reproducible, the remainder of the titrations were performed at 25 °C without regard to the preliminary work.

### 3.4.2  Titration of Receptor **105** with BzO$^-$

The changes observed in the $^1$H NMR spectrum of receptor **102** were characteristic to each anion being titrated. As in the previous section, these changes were fundamentally retained with receptors **105** and **103**. Upon titration of the C$_{11}$ host **105** with TBA benzoate at 25 °C, changes characteristic of interaction with the BzO$^-$ anion were observed. Resonances Hb–f became deshielded, while the remainder of the aromatic peaks, including those of the benzoate host itself, were observed to become more shielded as the titration progressed, Figure 3.19. Resonance Ha was observed to move slightly in a 'U-shaped' manner, decreasing in chemical shift up to the addition of 1 eq. of the salt (9.82→9.81 ppm), and increasing slightly thereafter (9.81→9.84 ppm).

The peak envelope corresponding to resonances Hd–f diverged slightly, with Hd and Hf deshielding slightly; 7.2→7.3 ppm, and 7.1→7.2 ppm, respectively. Resonance He decreased in chemical shift over the titration, 7.16→7.11 ppm. Meanwhile, the resonances
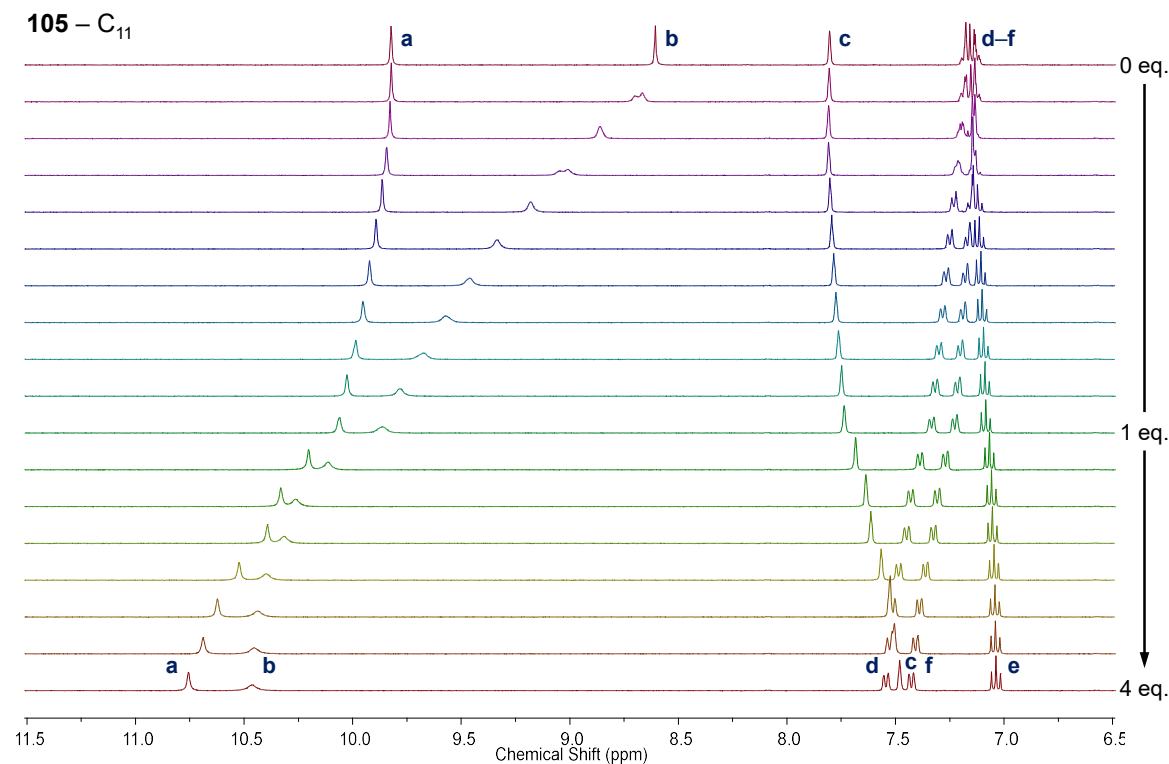
89

Figure 3.19. Stack plot of the individual $^1$H NMR spectra (400 MHz, DMSO-$d_6$, 6.7–11.8 ppm) from the titration of receptor **105** (7 mM) with BzO$^-$ (0→4 eq.).

corresponding to the 2- and 4-positions of the benzoate guest became more shielded over the course of the titration; 8.0→7.9 ppm and 7.3→7.2 ppm for H2′ and H4′, respectively. As with the C$_3$ chain receptor **102**, the trend in resonance Ha suggested the presence of a 1:2 species. Fitting the data from Ha was not possible for every repetition of the titration, and investigation into this equilibrium was not pursued on the basis of the arguments in Section 3.3.1, above (for the only successful fit, the correlation coefficient, ρ = +0.1). Noting the lack of significant evidence of a second equilibrium species a 1:1 host-guest binding model
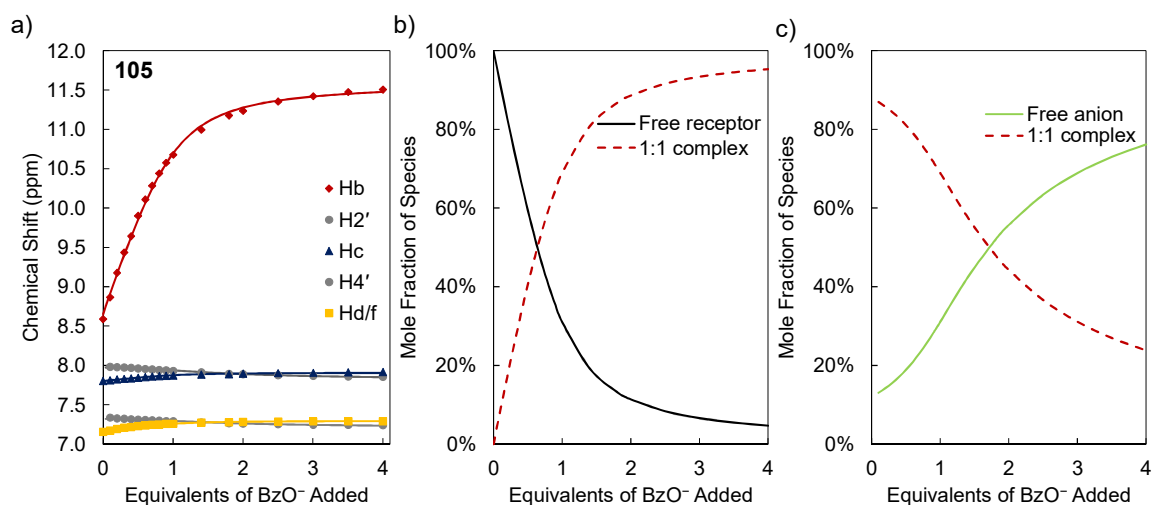


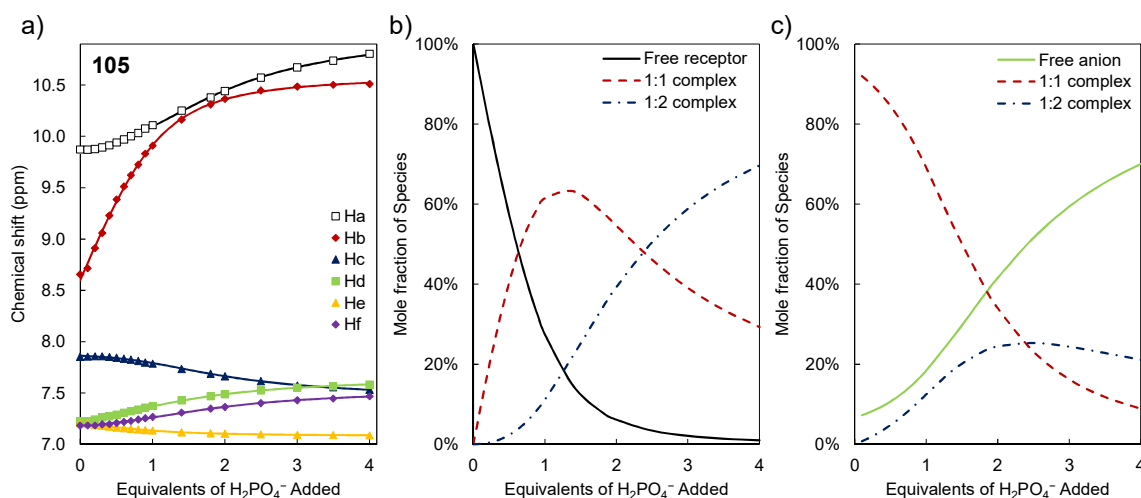Figure 3.20. Titration of **105** with BzO$^-$. a) Experimentally measured chemical shifts (points) and calculated fit (lines) of resonances Hb–d of receptor **105**, and H2′ and H4′ of the benzoate anion. b–c) Speciation distribution diagrams generated from the fitting of the experimental data. The concentrations are presented as mole-percentage values of each species relative to the sum of their concentrations.

was chosen to describe the data, Figure 3.20. Fitting the changes in chemical shift of resonances Hb–d from the aromatic ring of receptor **105**, along with the resonances at the 2- and 4-positions of the benzoate guest (H2′ and H4′), to such a model gave an average value of $\log\beta_{1:1} = 2.97 \pm 0.07$.

### 3.4.3  Titration of Receptor **105** with $H_2PO_4^-$

As with the $C_3$ receptor **102**, titrating **105** with TBAH$_2$PO$_4$ induced significant movement of all resonances in the 7–10 ppm region, Figure 3.21. The resonance at 10.8 ppm was identified as the amide proton, Ha, *via* a through-space response from resonance H2 at 2.3 ppm in a 1D ROE experiment, Figure 3.22. No interaction was observed with Hb. Resonances Hd and Hf, at 7.5 ppm and 7.4 ppm respectively, were distinguished from each other by the same experiment. Ha exhibited moderate deshielding over the course of the titration (9.8→10.8 ppm), with the changes being slightly sigmoidal in shape, Figure 3.23. A large initial change was noted in the chemical shift of resonance Hb up to the addition of 1 eq. of the salt (8.6→9.9 ppm), with a lesser change occurring thereafter (9.9→10.5 ppm). Resonance Hc underwent moderate shielding over the course of the titration (7.8→7.5 ppm), as with resonance Ha, the profile of this change was sigmoidal with respect to the number of equivalents of anion added.

The peak envelope corresponding to the protons Hd–f diverged, with Hd and Hf becoming slightly deshielded (7.2→7.5 ppm and 7.1→7.4 ppm, respectively) and proton He



Figure 3.21. Stack plot of the individual $^1$H NMR spectra (400 MHz, DMSO-$d_6$, 6.5–11.5 ppm) from the titration of receptor **105** (7 mM) with $H_2PO_4^-$ (0→4 eq.).
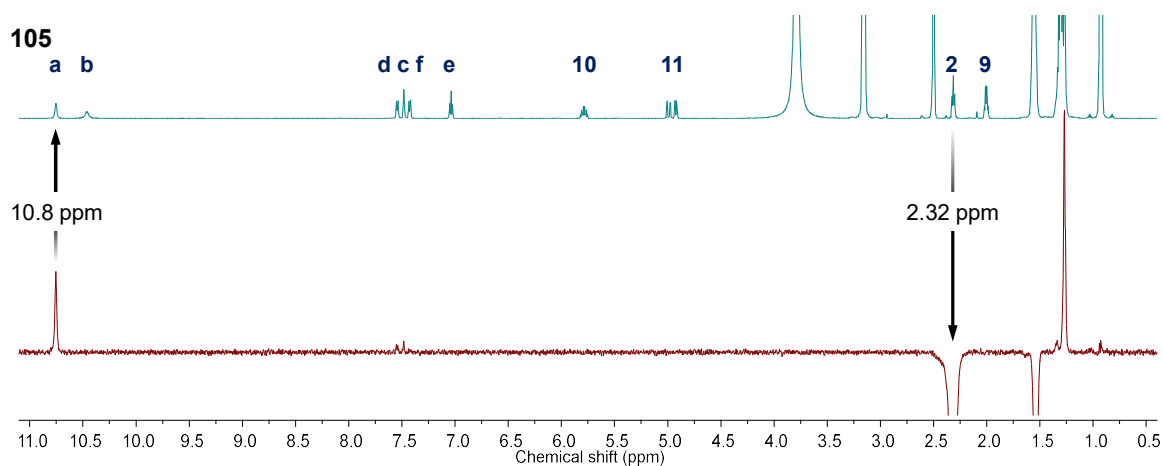
Figure 3.22. 1D Rotating-frame nuclear Overhauser effect (ROE, 400 MHz, DMSO-$d_6$, 0.5–11.0 ppm) experiment performed after the titration of receptor **105** (7 mM) with TBAH$_2$PO$_4$ (4 eq.). Irradiating the resonance at 2.32 ppm (H2) leads to a positive peak at 10.8 ppm (Ha). No interaction was observed with resonance Hb.

becoming more shielded (7.2→7.0 ppm) over the course of the titration. Fitting the chemical shift data from resonances Ha–f to a 1:1, 1:2 host-guest binding model afforded average values of logβ$_{1:1}$ = 3.3 ± 0.1 and logβ$_{1:2}$ = 5.5 ± 0.1. The system is slightly anticooperative or non-cooperative, with logα = −0.4 ± 0.1.



Figure 3.23. Titration of **105** with H$_2$PO$_4^-$. a) Experimentally measured chemical shifts (points) and calculated fit (lines) of resonances Ha–f of receptor **105**. b–c) Speciation distribution diagrams generated from the fitting of the experimental data. The concentrations are presented as mole-percentage values of each species relative to the sum of their concentrations.

## 3.5   $^1$H NMR Studies with Receptor **103**

Having investigated the binding affinity of receptor **105** for various anions, and not observing anomalous sulfate binding, or sigmoidal binding isotherms, the titrations of receptor **103** with SO$_4^{2-}$, BzO$^-$ and H$_2$PO$_4^-$ were repeated. The results obtained in this section will be compared to the preliminary data from Boyle in Section 3.6.

### 3.5.1 Titration of Receptor **103** with $SO_4^{2-}$

Titration of **103** with $TBA_2SO_4$ led to the same characteristic changes occurring, including a moderate increase in chemical shift of Hb (8.6→9.6 ppm), Figure 3.24. A slight shielding was noted for resonance Ha (9.85→9.83 ppm), and slight deshielding for resonance Hc (7.80→7.83 ppm). The peak envelope at 7.16 ppm, corresponding to resonances Hd–f was
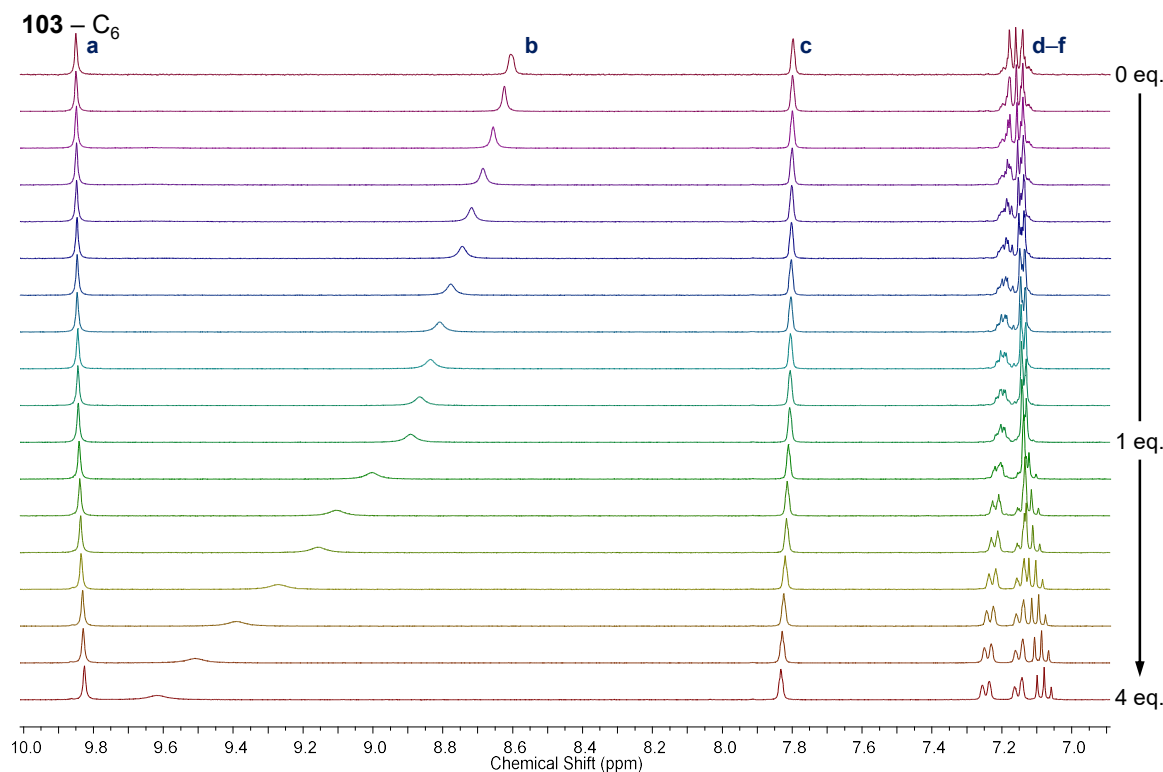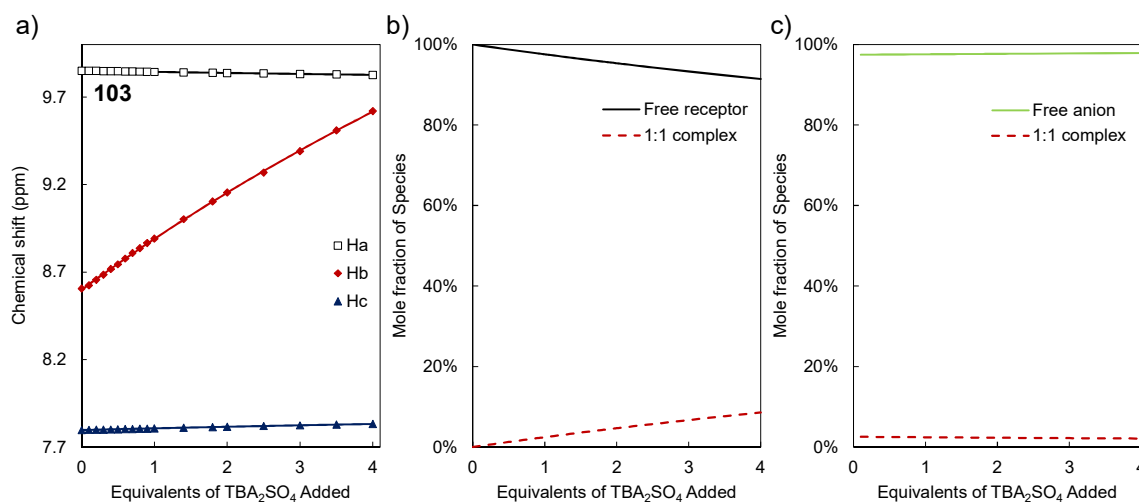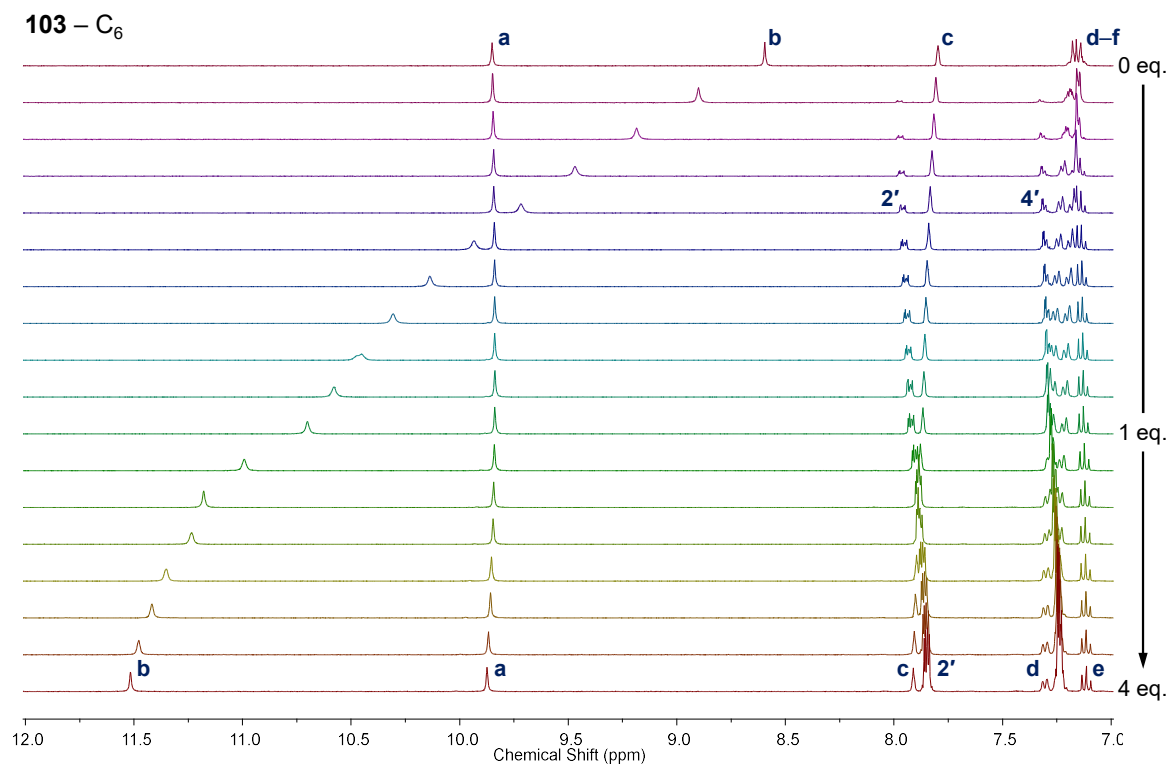


Figure 3.24. Stack plot of the individual $^1$H NMR spectra (400 MHz, DMSO-$d_6$, 6.9–10.0 ppm) from the titration of receptor **103** (7 mM) with $TBA_2SO_4$ (0→4 eq.).



Figure 3.25. Titration of **103** with $SO_4^{2-}$. a) Experimentally measured chemical shifts, (points) and calculated fit (lines) of resonances Ha–c of receptor **103**. b–c) Speciation distribution diagrams generated from the fitting of the experimental data. The concentrations are presented as mole-percentage values of each species relative to the sum of their concentrations.

observed to diverge slightly. Fitting the changes in resonances Ha–c to a 1:1 host-guest binding model (Figure 3.25) affords a value of $\log\beta_{1:1} = 0.58 \pm 0.04$. The residual parameter of this fit is 2.5 ppb. A comparison of this, and the remaining titrations of receptors **105** and **103** to the preliminary studies by Boyle is provided in Section 3.6.

### 3.5.2 Titration of Receptor **103** with BzO⁻

Upon addition of TBA benzoate to a solution of receptor **103**, resonance Ha followed the same 'U-shaped' trend described in Sections 3.3.2 and 3.4.2: with very slight shielding over the addition of the first equivalent of anion (9.85→9.84 ppm) and very slight deshielding thereafter, 9.84→9.87 ppm, Figure 3.26. Proton Hb displayed significant deshielding (8.6→11.5 ppm) over the course of the titration. The increase in chemical shift was much less significant for resonances Hc–e; 7.80→7.91 ppm, 7.17→7.30 ppm and 7.15→7.24 ppm, respectively.



Figure 3.26. Stack plot of the individual $^1$H NMR spectra (400 MHz, DMSO-$d_6$, 6.7–11.8 ppm) from the titration of receptor **103** (7 mM) with BzO⁻ (0→4 eq.).

A slight decrease in chemical shift was noted for resonance Hf, 7.16→7.11 ppm, while moderate shielding of the protons at the 2- and 4-positions of the benzoate guest were observed; 7.97→7.85 ppm and 7.32→7.24 ppm, respectively. The changes in the chemical shifts of resonances Hb–d of receptor **103** and resonances H2′ and H4′ of the benzoate guest were fitted to a 1:1 host-guest binding model, affording a value of $\log\beta_{1:1} = 3.04 \pm 0.03$, Figure 3.27.
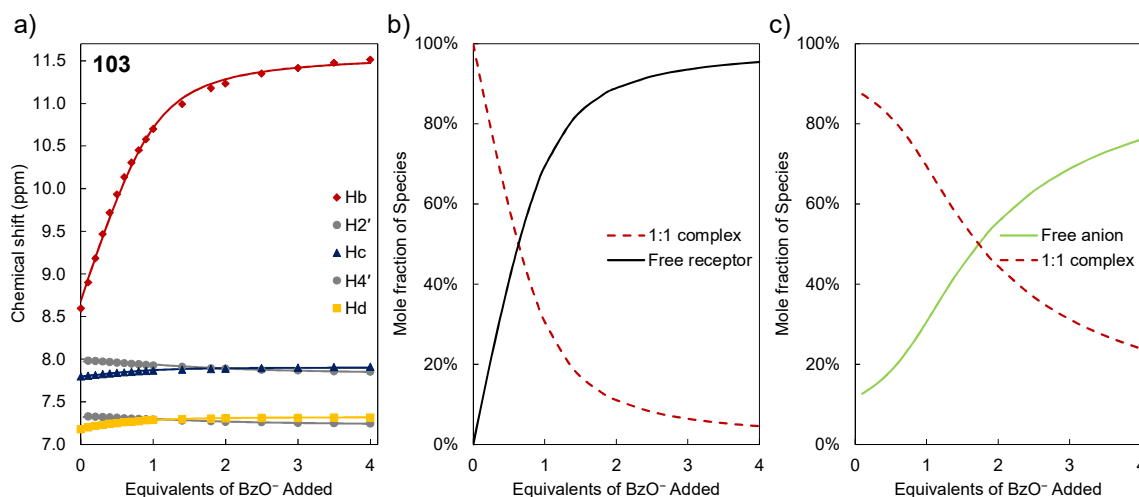
Figure 3.27. Titration of **103** with BzO⁻. a) Experimentally measured chemical shifts (points) and calculated fit (lines) of resonances Hb–d of receptor **103**, and H2′ and H4′ of the benzoate anion. b–c) Speciation distribution diagrams generated from the fitting of the experimental data. The concentrations are presented as mole-percentage values of each species relative to the sum of their concentrations.

### 3.5.3   Titration of Receptor **103** with H₂PO₄⁻

The chemical shifts of resonances Ha and Hb increased throughout the titration of receptor **103** with TBAH₂PO₄, following the same trend as described in Sections 3.3.3 and 3.4.3 above, see Figure 3.28. Proton Ha displayed moderate deshielding up to the addition of 1 eq. of salt (9.9→10.2 ppm), with a more significant increase in chemical shift occurring after this point (10.2→10.9 ppm). Conversely, the chemical shift of Hb increased significantly
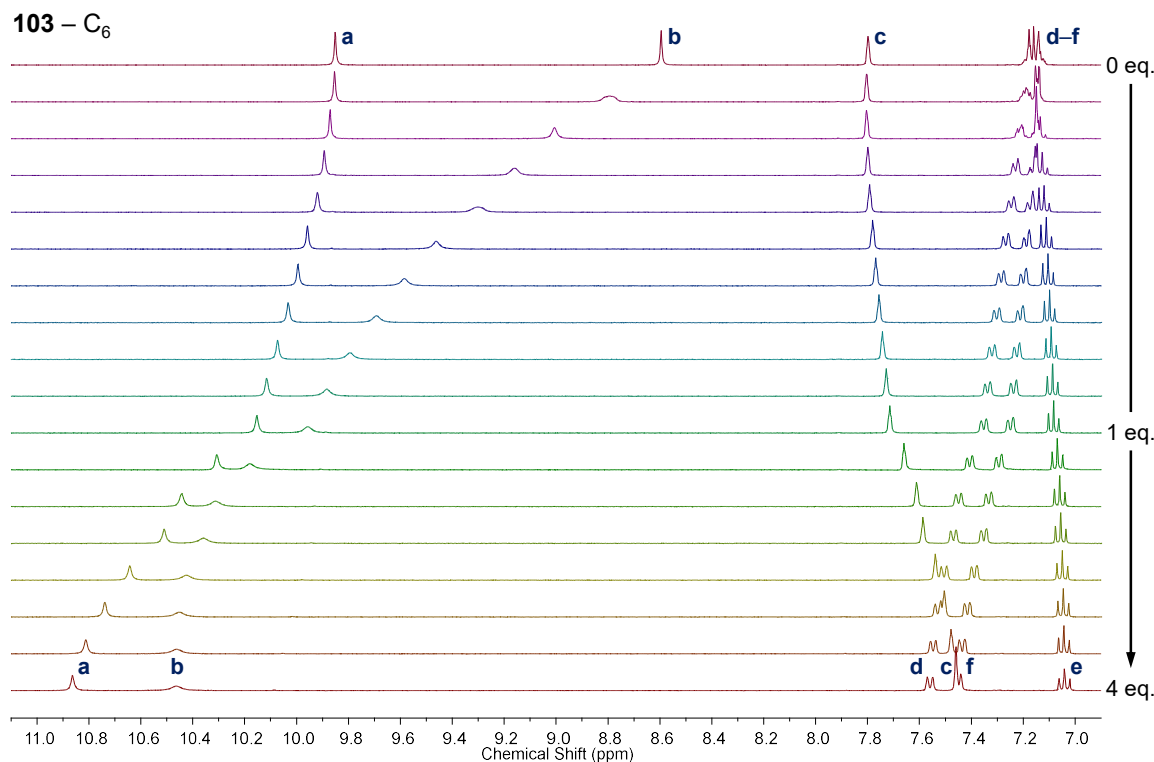


Figure 3.28. Stack plot of the individual ¹H NMR spectra (400 MHz, DMSO-$d_6$, 6.5–11.5 ppm) from the titration of receptor **103** (7 mM) with H₂PO₄⁻ (0→4 eq.).

95
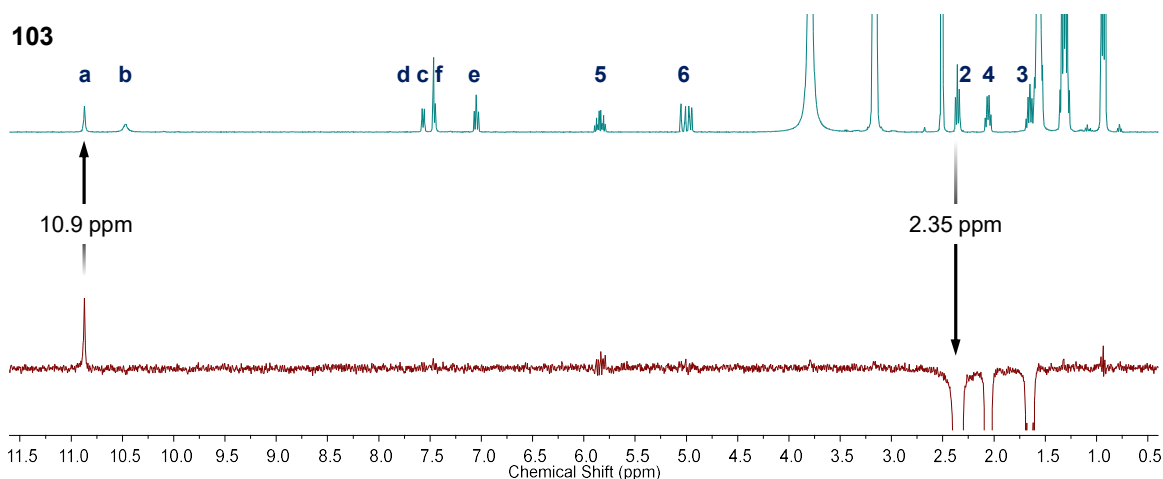
Figure 3.29. 1D Rotating-frame nuclear Overhauser effect (ROE, 400 MHz, DMSO-$d_6$, 0.5–11.0 ppm) experiment performed after the titration of receptor **103** (7 mM) with TBAH$_2$PO$_4$ (4 eq.). Irradiating the resonance at 2.35 ppm (H2) leads to a positive peak at 10.9 ppm (Ha). No interaction was observed with resonance Hb.

(8.6→10.0 ppm) over the first half of the titration, with a more moderate increase thereafter (10.0→10.5 ppm). As for the titration with receptor **105**, above, the identities of Ha and Hb were confirmed by a 1D ROE experiment, Figure 3.29. A moderate decrease in chemical shift was noted for resonance Hc (7.8→7.5 ppm), crossing over Hd and overlapping with Hf towards the end of the titration.

Lastly, the peak envelope at 7.2 ppm diverged, with Hd and Hf deshielding slightly (7.2→7.6 ppm and 7.2→7.5 ppm, respectively), and He shielding slightly (7.16→7.04 ppm) over the course of the titration. Fitting the changes in resonances Ha–f to a 1:1, 1:2 host-guest binding model gave average values of $\log\beta_{1:1} = 2.89 \pm 0.11$ and $\log\beta_{1:2} = 5.19 \pm 0.01$, Figure 3.30. Once again, the system is non-cooperative, with a value of $\log\alpha = 0.0 \pm 0.2$.
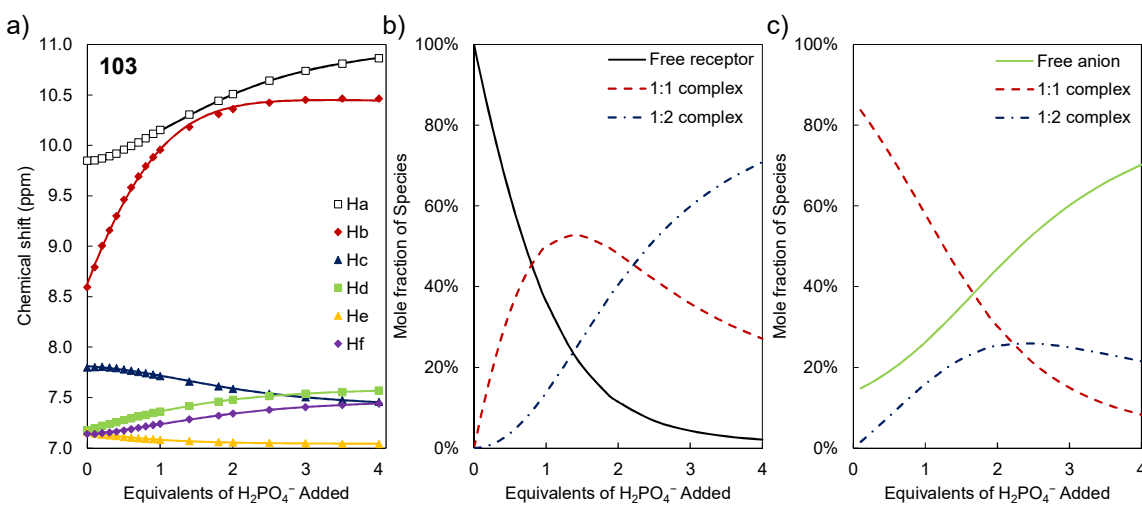


Figure 3.30. Titration of **103** with H$_2$PO$_4^-$. a) Experimentally measured chemical shifts (points) and calculated fit (lines) of resonances Ha–f of receptor **103**. b–c) Speciation distribution diagrams generated from the fitting of the experimental data. The concentrations are presented as mole-percentage values of each species relative to the sum of their concentrations.

Table 3.2. Cumulative logarithmic binding constants, $\log\beta_{1:1}$ and $\log\beta_{1:2}$, determined from the analysis of $^1$H NMR titrations in DMSO-$d_6$ at 25.0 °C.

| Receptor | Chain length | H:G [a)] | $\log\beta_{H:G}$ | | | | |
|---|---|---|---|---|---|---|---|
| | | | BzO$^-$ | H$_2$PO$_4^-$ | SO$_4^{2-}$ | Cl$^{-}$ [b)] | NO$_3^{-}$ [b)] |
| **102** | 3 | 1:1 | $2.92 \pm 0.18$ | $2.8 \pm 0.4$ | $0.57 \pm 0.54$ | $1.58 \pm 0.01$ | $0.90 \pm 0.29$ |
| | | 1:2 | | $5.0 \pm 0.5$ | | | |
| **103** | 6 | 1:1 | $3.04 \pm 0.01$ | $2.89 \pm 0.11$ | $0.64 \pm 0.13$ | $-$ [c)] | $-$ |
| | | 1:2 | | $5.19 \pm 0.01$ | | | |
| **105** | 11 | 1:1 | $2.97 \pm 0.07$ | $3.21 \pm 0.12$ | $0.01 \pm 0.17$ [b)] | $-$ | $-$ |
| | | 1:2 | | $5.38 \pm 0.17$ | | | |

Initital host concentration = 7 mM. Anions added as their TBA salts. Unless otherwise stated, all binding constants are averaged values, the associated errors correspond to the 95% confidence interval (n = 2, see Appendix A2 for details). a) Stoichiometry of the host-guest binding equilibrium. b) Data from a single titration, data for two repetitions of the titration of **105** with SO$_4^{2-}$ unable to be fit. Associated error is the "standard deviation" parameter as reported by HypNMR2008. c) Titration not performed.

It can be inferred from the data in Table 3.2 that the difference in binding affinities of the C$_3$ receptor **102** and the receptors **103** and **105**, for the anions BzO$^-$, H$_2$PO$_4^-$ and SO$_4^{2-}$, are not significant at the 5% probability level. The difference between **103** and **105** for H$_2$PO$_4^-$ binding does, however, appear to be significant at this level. There is insufficient data to make a claim regarding the significance of the difference in binding affinities of the C$_6$ and C$_{11}$ receptors in the case of SO$_4^{2-}$, due to an inability to fit two of the repetitions of this titration. Overall it may be concluded that anions bind to the di(amidophenyl)urea motif without any regard to chain length. That is, there does not appear to be a solvophobic effect on anion binding. Benzoate is bound in a 1:1 stoichiometry, with average binding constants of $\log\beta_{1:1} \approx 3.0$, any higher stoichiometries have vanishingly small association constants. In comparison to the 1:1 binding constants reported for receptors **96**–**99** in the previous chapter, those of **102**, **103** and **105** are relatively high. However, this value is lower than the 1:1 association constant of *ca.* 3.16 obtained when those receptors were fitted to a combined 1:1, 1:2 host-guest binding model. Comparing these binding constants to those reported by Kadam *et al.*, as in the previous chapter, it can be seen that while the binding for BzO$^-$ is stronger than for diphenylurea, it is weaker than that for all crescent-shaped, convergent hydrogen-bond donor receptors they reported.[182] The binding affinity for SO$_4^{2-}$ is lower than that reported for receptors **96**–**99** in Chapter 2, but comparison is difficult due to the large errors on these values.

The binding of $H_2PO_4^-$ by **102**, **103** and **105** occurs with clear 1:1 and 1:2 host-guest stoichiometries, and binding constants in the range of 2.8–3.2 for $\log\beta_{1:1}$, and 5.0–5.4 for $\log\beta_{1:2}$. The logarithmic cooperativity parameters, α, calculated for each receptor are 0.1 ± 0.4, 0.0 ± 0.2, and −0.4 ± 0.1, respectively. Once again, there is no evidence that the figure corresponding to receptor **102** is different from the others due to a large error on the value associated with this receptor. There does appear to be a small anti-cooperative effect that with receptor **105** that is not observed with the others. Thus, in comparison to receptors **96**–**99**, studied in Chapter 2, cooperative phosphate binding is not observed, and the much lower binding constants reflect this.

## 3.6   Comparison to Preliminary Studies

The data obtained in Sections 3.3–3.5 above may be compared to preliminary reports by Boyle.[172] Comparison of the trends in chemical shifts demonstrate that there is a fundamental difference between the sets of titrations. This cannot be fully explained by the difference in instrument temperature of 5 °C, or by the use of a different spectrometer to perform the
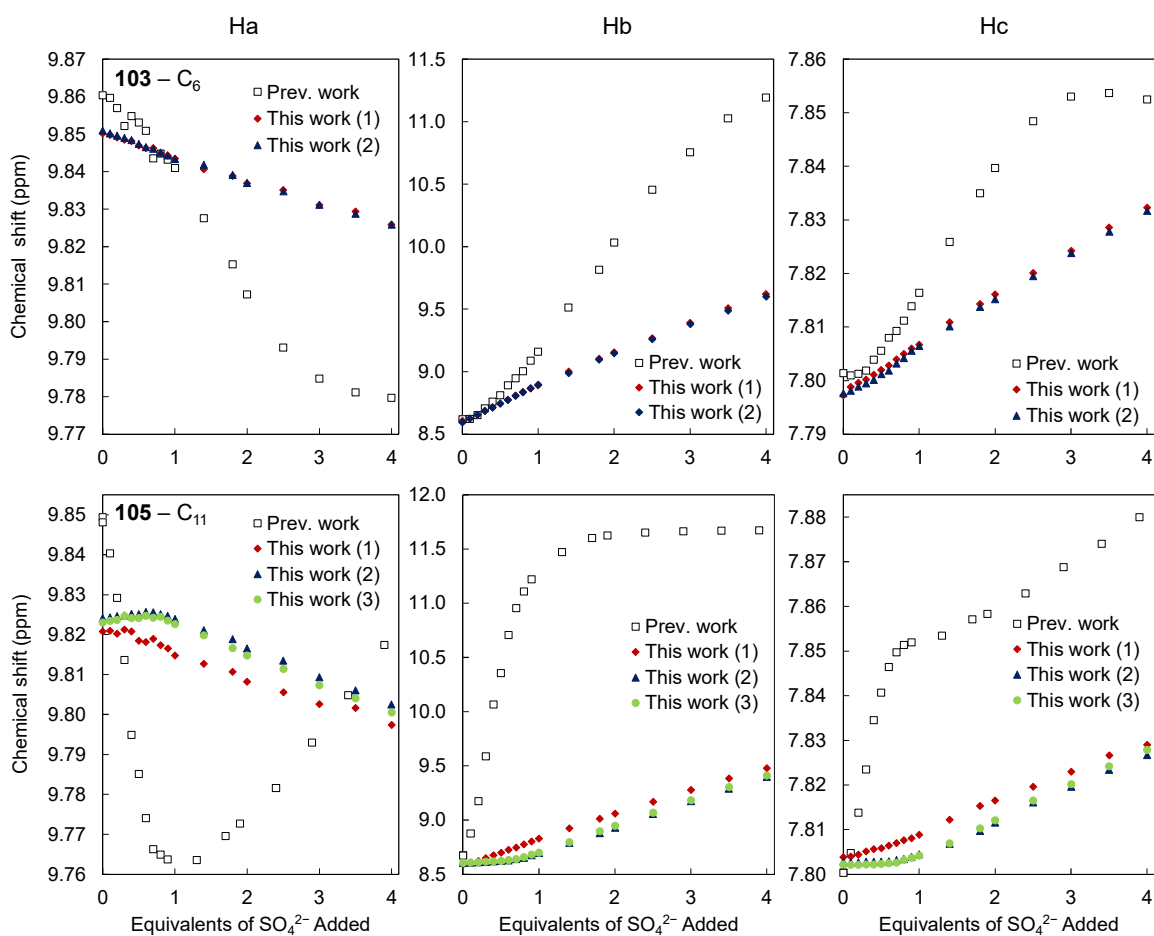


Figure 3.31. Comparison of the titration data following resonances Ha, Hb and Hc, in the titrations of receptors **103** (top) and **105** (bottom) with TBA$_2$SO$_4$, as reported by Boyle (white squares) and this work (First titration: red; Second titration: blue; Third titration: green). Note the less significant (and almost linear) changes in chemical shift in this work.
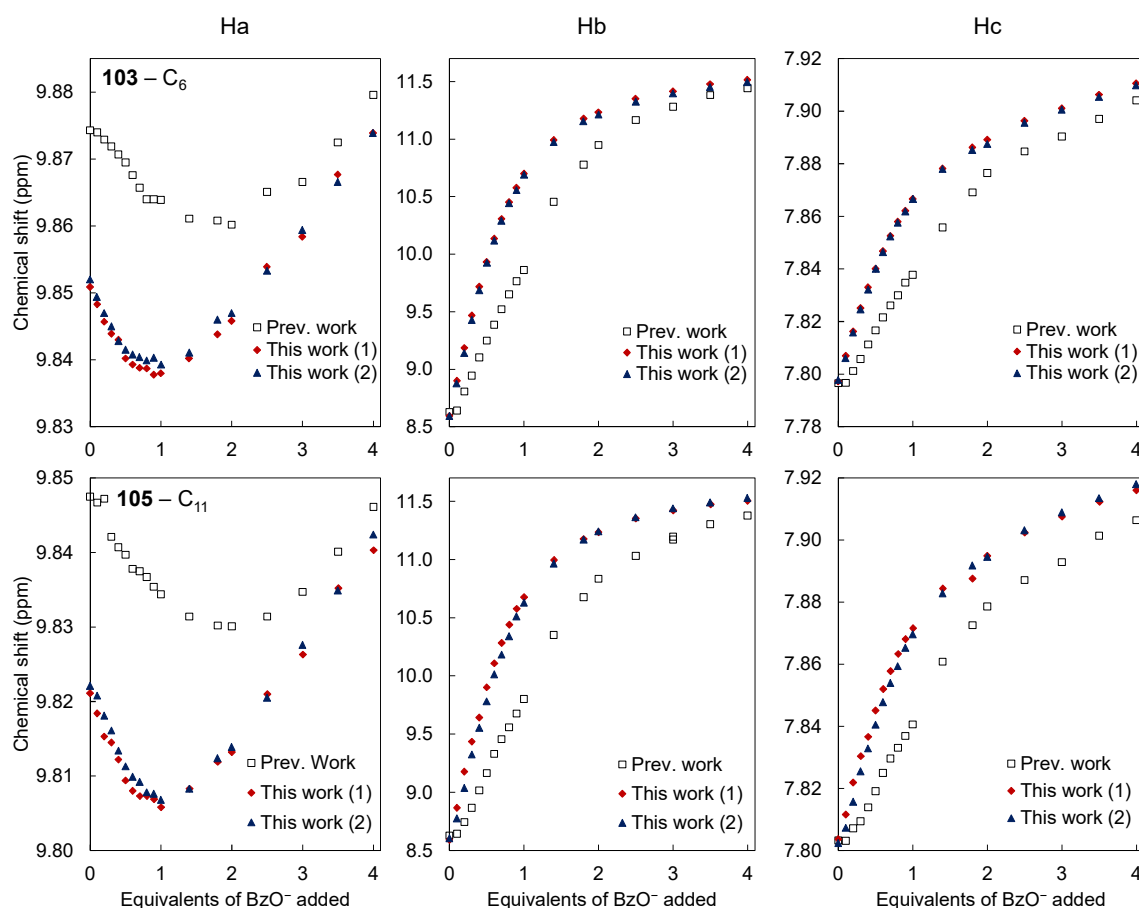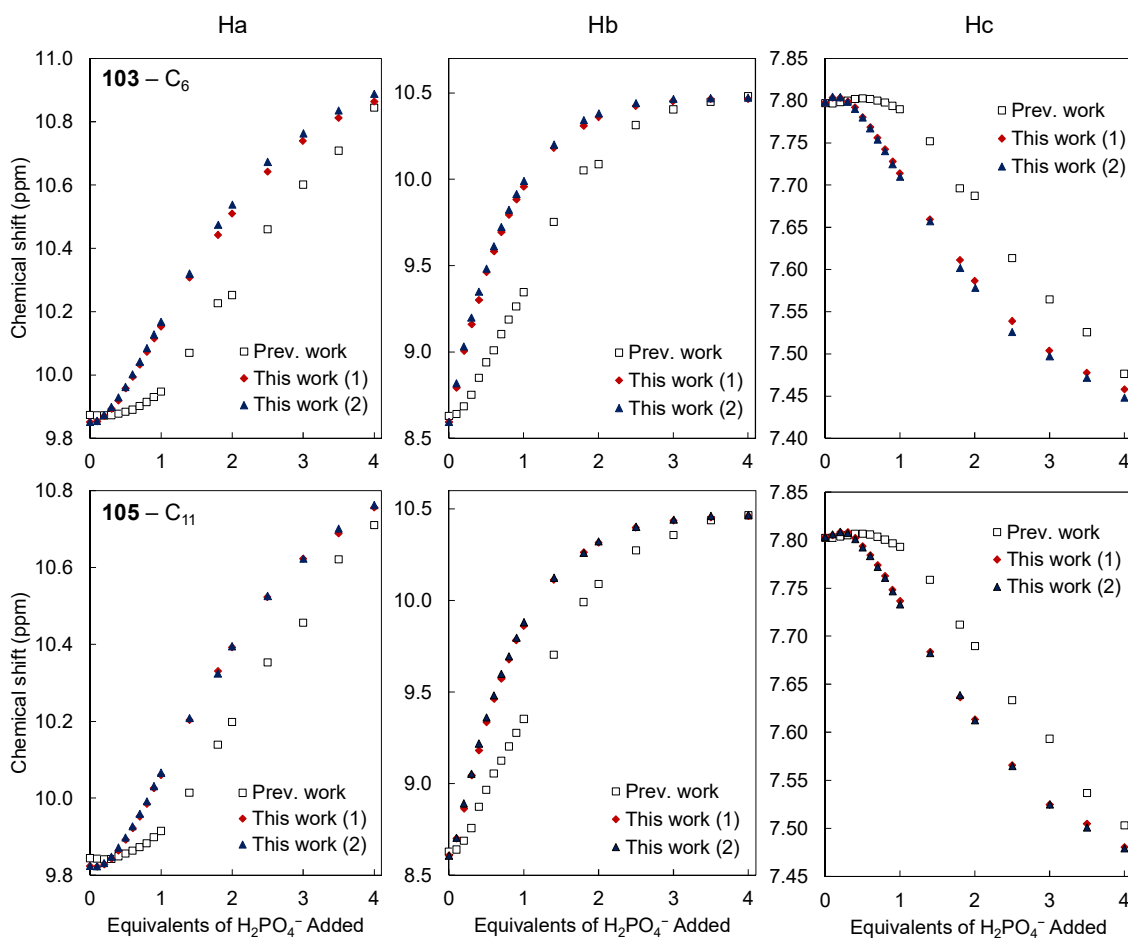
Figure 3.32. Comparison of the titration data following resonances Ha, Hb and Hc, in the titrations of receptors **103** (top) and **105** (bottom) with TBAOBz, as reported by Boyle (white squares) and this work (First titration: red; Second titration: blue). Note the earlier changes in chemical shift in this work.

experiment. In this work, the changes in chemical shift of resonances Ha–c upon titration with the $SO_4^{2-}$ anion are much less significant, and the trends are almost linear in shape as shown in Figure 3.31. Independent titrations with freshly dried $TBA_2SO_4$, and separately synthesised **105** gave coherent results. The difference in the initial chemical shifts of resonances Ha–c is, however, due to the 5 °C temperature difference, see Figure 3.15 in Section 3.4, above.

The general trends of each resonance upon titration with the benzoate salt are similar, Figure 3.32. However, the changes in chemical shift observed occurred earlier in each titration in this work, with the minimum chemical shift of resonance Ha being both lower (9.84 ppm *vs.* 9.86 ppm and 9.81 ppm *vs.* 9.83 ppm for receptors **103** and **105**, respectively), and occurring at 1 eq. (not 2 eq.) of added anion. Once again, repetition of these titrations with new solutions of TBA benzoate and separately synthesised batches of receptor produced coherent results (compare red and blue data points in Figure 3.32).

Figure 3.33. Comparison of the titration data following resonances Ha, Hb and Hc, in the titrations of receptors **103** (top) and **105** (bottom) with TBAH$_2$PO$_4$, as reported by Boyle (white squares) and this work (First titration: red; Second titration: blue). Note the earlier changes in chemical shift, and the absence of a sigmoidal trend in resonances Hb and Hc in the titrations in this work.

As above, the phosphate titrations reported in this work displayed similar overall changes in the chemical shift of resonances Ha–c after the addition of 4 eq. of anion. Again, these changes occurred earlier in the titration (Figure 3.33), while Hb did not change in a sigmoidal manner as had previously been reported.

From the above comparisons two observations can be made about the previously reported preliminary results.[172] Firstly, the changes in chemical shift which had previously been noted on titration with the BzO$^-$ and H$_2$PO$_4$$^-$ salts appear to be moderated or delayed. This may be explained by the presence of impurities in the samples of receptors **103** and **105** reported in the previous work that are, in effect 'NMR-silent'. Neither most inorganic anions, nor small quantities (*ca.* <5%) of residual starting material(s) or reaction byproducts may be observed *via* $^1$H NMR spectroscopy. Residual carboxylic acid would buffer the titrations with BzO$^-$ and H$_2$PO$_4$$^-$, likely leading to the sigmoidal shapes previously reported. Receptor

**105** was titrated with benzoic acid to probe the effect, if any, of the presence of a carboxylic acid impurity. No change in the spectrum of the host was observed (see Appendix A2).

The second observation is that the reported changes in chemical shift in the preliminary titrations with TBA$_2$SO$_4$ are not retained in this work, and those formerly observed changes more closely match the characteristic behaviour observed upon titration with the BzO$^-$ salt. This discrepancy is much more significant than that observed with the other anions, and its explanation would require a different mechanism. The impurity is postulated to be a carboxylate-containing moiety or a carbonate anion which interacted strongly with the receptor upon addition of TBA$_2$SO$_4$. Such an obscure mechanism would, however, require much more detailed investigation.

## 3.7    Conclusions and Future Work

Compounds **101**–**105**, bearing 2–11 carbon chains were synthesised and characterised to investigate a previously reported connection between alkyl chain length and anion-binding ability. Receptors **103**–**105** had been previously reported as part of preliminary studies by Boyle, in which strong 1:2 host-guest binding of the SO$_4^{2-}$ anion had been noted.[172] Novel compounds **101**–**102** were designed and synthesised as negative controls for this solvophobic effect, their alkyl chains being very short. Titration of receptors **102**, **103** and **105** with a range of anions revealed characteristic changes in chemical shift of the protons of the di(amidophenyl)urea core for H$_2$PO$_4^-$ and BzO$^-$. All receptors studied showed binding affinities of log$\beta_{1:1} \approx 3.0$ for BzO$^-$; non-cooperative binding for H$_2$PO$_4^-$, with ranges of log$\beta_{1:1} = 2.8$–3.2 and log$\beta_{1:2} = 5.0$–5.4; and small 1:1 binding constants for SO$_4^{2-}$.

When compared to preliminary reports, both the binding constants and assumed host-guest stoichiometries differ due to the proton resonances changing chemical shift in different ways. The difference in binding of the BzO$^-$ and H$_2$PO$_4^-$ anions may be due to a "buffering" effect from residual carboxylic acid, while the differences in magnitude of the change in chemical shift upon titration with SO$_4^{2-}$ remains unexplained. Thus it may be concluded that 6–11 carbon chains have little to no effect on the binding of the anions tested, and may instead be used to help solubilise the receptor or to tether additional functionality.

Two prospective uses arise from the linearity of compounds **103**–**105** and their terminal vinylic groups, respectively. Firstly, if the creation of an interlocked system is to remain a goal, a linear urea axle may instead be surrounded by a macrocycle containing a moiety known to bind to the urea, for example the dipicolylamide–crown ether macrocycle reported by Huang.[209] The bistriazolyl pyridine macrocycle reported by this group,[152] and the charge-assisted equivalents of both types of receptor reported by Beer,[49,197] are also

candidate urea-binding macrocycles. Secondly, the molecules could be incorporated into a polymer, being cross-linked *via* the alkene moieties. These uses notwithstanding, the main advantage of the di(3-amidophneyl)urea motif is its ease of synthesis; geometric constraints limit the intended use of these compounds as convergent macrocyclic receptors. That is a role which is better suited to the 2-amidophenyl isomers, see Section 4.5.

Chapter 4

*H$_6$* Hydrogen-bond Donor Receptors and their Macrocyclic
Derivatives

## 4.1   Introduction

The work presented in the previous two chapters covered two classes of *H₄* hydrogen-bond donors, in which the cores of each molecule are linear in shape. Therefore, despite the opportunity for multiple hydrogen-bonding interactions between the host and guest, these receptors were observed to bind anions such as $H_2PO_4^-$ in 1:2 host–guest stoichiometries, rather than with strong and selective 1:1 binding affinities. Additionally, the observed linear nature of these receptors causes a geometric difficulty in forming derived macrocycles – this is exemplified by the known synthetic issues faced in forming the macrocyclic derivatives of the compounds **103** and **104**,[172] which are also discussed in Chapter 3.

Having first studied the properties of the electron-donating and -withdrawing substituents on the distal phenylene rings and secondly, the effect of long-chain hydrocarbons appended to the receptor core, three new classes of receptors combining the structures studied in the previous chapters were designed, Figure 4.1. Each receptor bears six hydrogen-bond donor atoms, and at least one of the substitution patterns around the phenylene rings is *ortho*. The crescent-shaped *ortho*-phenylene bis(2-amidophenylurea) motif (receptors **106**, **107**, and **129**–**131**) has previously been studied in detail by the Gale and Leito groups, and is known to bind carboxylate anions a 1:1 host–guest stoichiometry.[182,210]  This is a specific case of the *ortho*-phenylene bis(phenylurea) class of
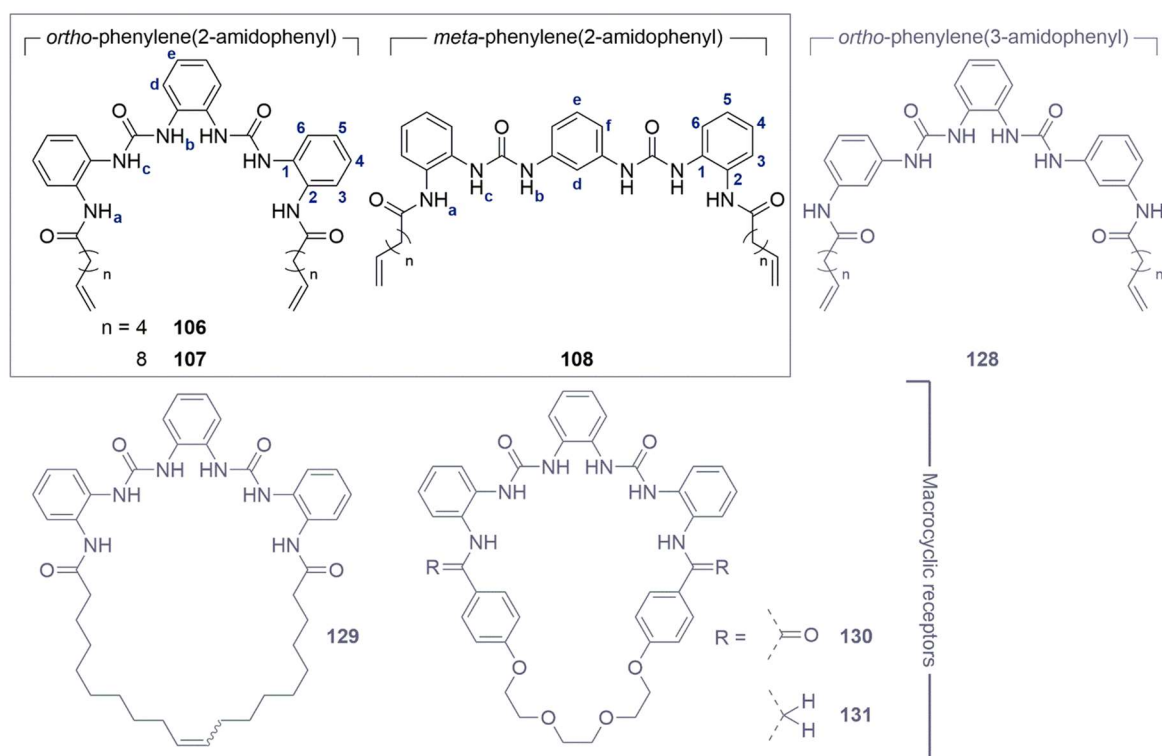


Figure 4.1. Chemical structures of compounds **106**–**131**, which are discussed in this chapter. Not all receptors were successfully synthesised.

receptors, which have been used extensively by Gale and coworkers as a carboxylate-binding "supramolecular synthon".[66,180,181]

## 4.2   Synthesis and Characterisation

The $H_6$ donor precursors **132**, **133**, and **134** were each synthesised from *ortho-* or *meta-* phenylene diamine and 2- or 3-nitrophenyl isocyanate (2.3 eq., see Scheme 4.1). The diamine and isocyanate were ground together in a mortar and pestle with CHCl₃, and the resulting thick yellow suspension filtered and washed with both CHCl₃ and Et₂O to yield the desired phenylene bis(nitrophenylurea) as a bright yellow solid. Compounds **132** and **133** were obtained in 70% and 81% yield, respectively. The successful formation of the urea moiety was demonstrated by the presence of two peaks in the 9–10 ppm region of the ¹H NMR spectrum of each compound, corresponding to the urea NH resonances, Figure 4.2. The FTIR spectrum of each compound contained both C=O and N−H stretching modes in the regions of *ca.* 1650 cm⁻¹ and 3300 cm⁻¹, respectively (Figure 4.3). Compound **134** was found to be a minor product of the synthesis, with a selectivity towards its production of *ca.* 17%. The mono-urea intermediate (*ca.* 68%) and the side-product di(3-nitrophenyl)urea (*ca.* 15%) were isolated and identified after trituration and either crystallisation or column chromatography. Compound **134** could not be isolated in its pure form, and the synthesis of **128** was not pursued as a result.
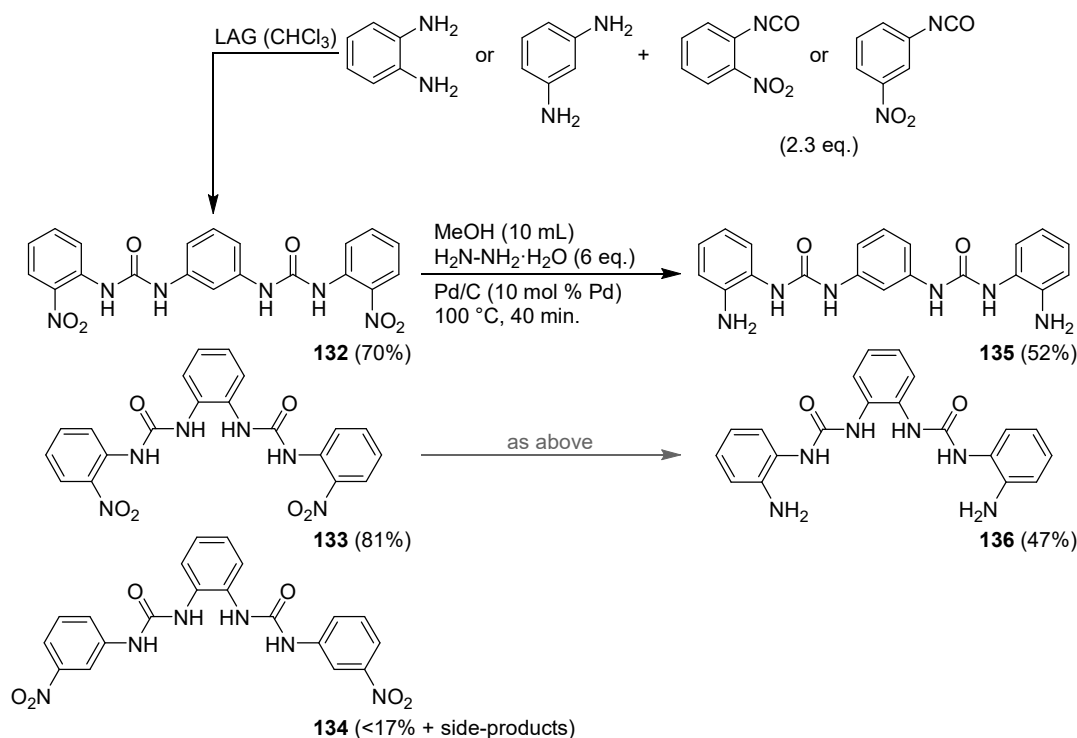


Scheme 4.1. Synthesis of the diamino precursor molecules **135** and **136**, via the reduction of dinitro intermediates **132** and **133**. Compound **134** was formed as the minor product of its reaction, and could not be isolated.
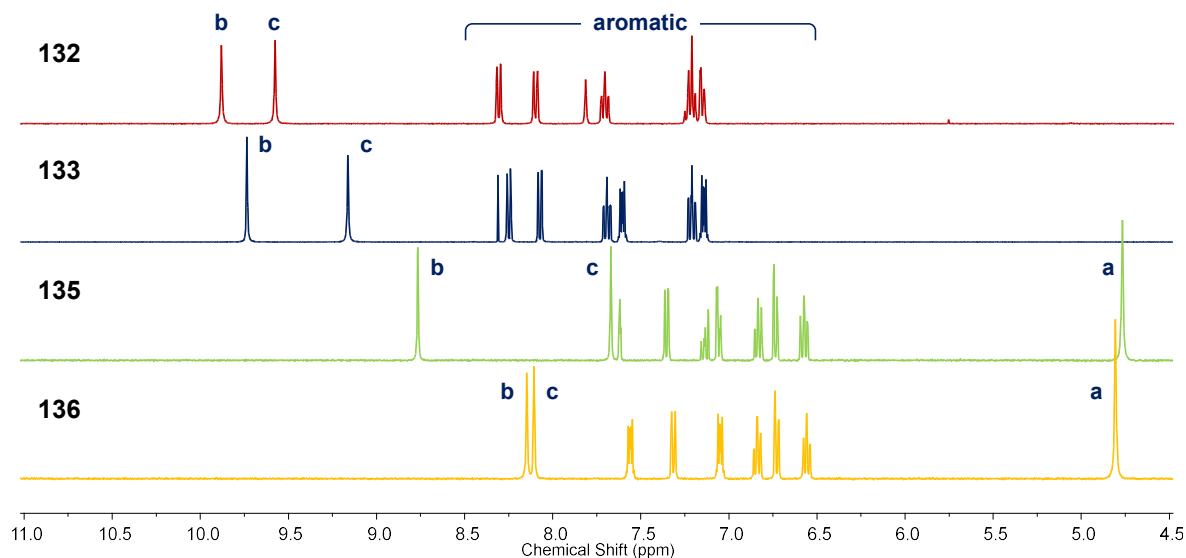
Figure 4.2. ¹H NMR spectra (400 MHz, 4.5–11.0 ppm, DMSO-$d_6$) of dinitro intermediates **132** and **133** and diamine intermediates **135** and **136**.

The dinitro compounds **132** and **133** were then reduced with hydrazine monohydrate (*ca.* 6 eq.) and palladium on carbon (*ca.* 10 mol %) under microwave irradiation to yield the diamino products **135** and **136**, Scheme 4.1. Filtering the reaction mixture through celite, removing the product-containing layer from the funnel, stirring it in DMF and filtering again through celite afforded a light yellow solution of the desired product. The product was then precipitated slowly from the filtrate by adding water and leaving to sit overnight, after which the flocculate was diluted with more water and filtered under suction to yield the product as
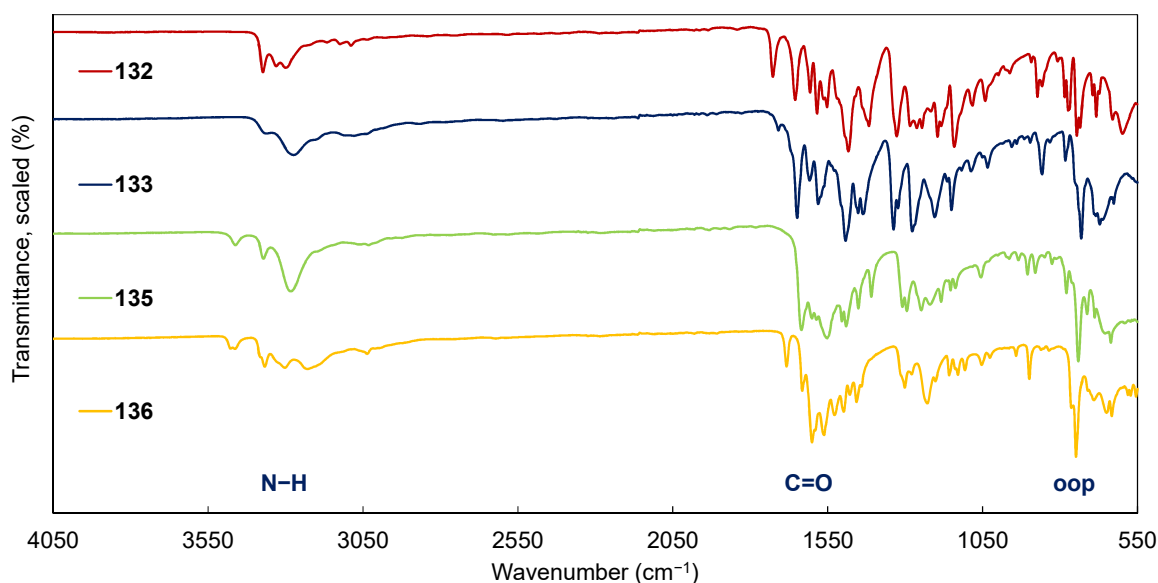


Figure 4.3. FTIR spectra (550–4050 cm⁻¹) of dinitro intermediates **132** (red) and **133** (blue) and diamine intermediates **135** (green) and **136** (yellow).

a white fibrous solid. Compounds **135** and **136** were obtained in 52% and 47% yield, respectively.

The successful reduction of the nitro group to an amine was demonstrated by $^1$H NMR spectroscopy, with the appearance of a new resonance at 4.8 ppm, along with the marked shielding of the urea resonances and the protons of the distal aromatic ring, Figure 4.2. Additional NH stretching modes at *ca*. 3500 cm$^{-1}$ were visible in the FTIR spectra of the products, Figure 4.3. This was accompanied by an increase in the frequency of the out-of-plane bending modes at *ca*. 870 cm$^{-1}$ and 760 cm$^{-1}$ (**135**) and *ca*. 730 cm$^{-1}$ (**136**), and the movement of bands within the 1400–1600 cm$^{-1}$ region.
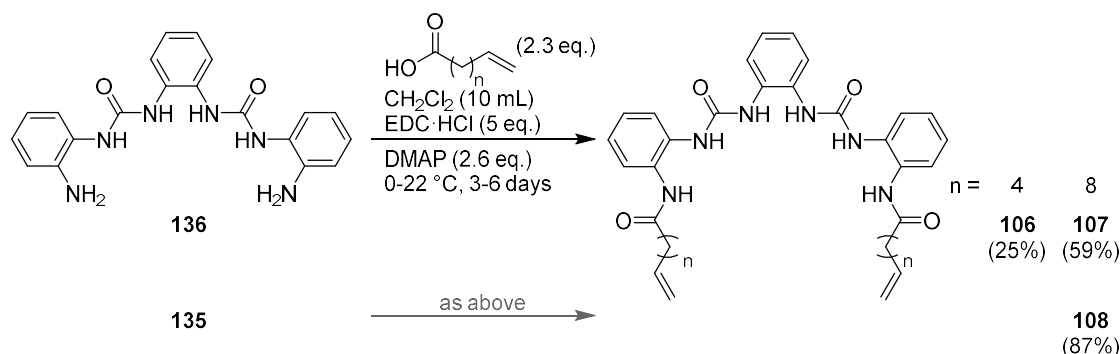


Scheme 4.2. Synthesis of the C$_7$ and C$_{11}$ receptors **106–108** *via* coupling reactions of **136** and **135** with 6-heptenoic or 10-undecenoic acid.

The C$_7$ and C$_{11}$-chain receptors **106–108** were synthesised by reaction of diamine intermediates **136** and **135** with 6-heptenoic acid or 10-undecenoic acid in dry CH$_2$Cl$_2$, Scheme 4.2. EDC·HCl and DMAP were used as coupling reagent and base. After 3–6 days, the reaction mixture was concentrated under reduced pressure, and dried *in vacuo*. The resulting oil was dissolved in a small amount of acetonitrile and the product precipitated with water and separated by centrifugation. In the case of receptor **106**, the reaction mixture was purified by sonication in Et$_2$O. The product was then washed with water, acetonitrile,
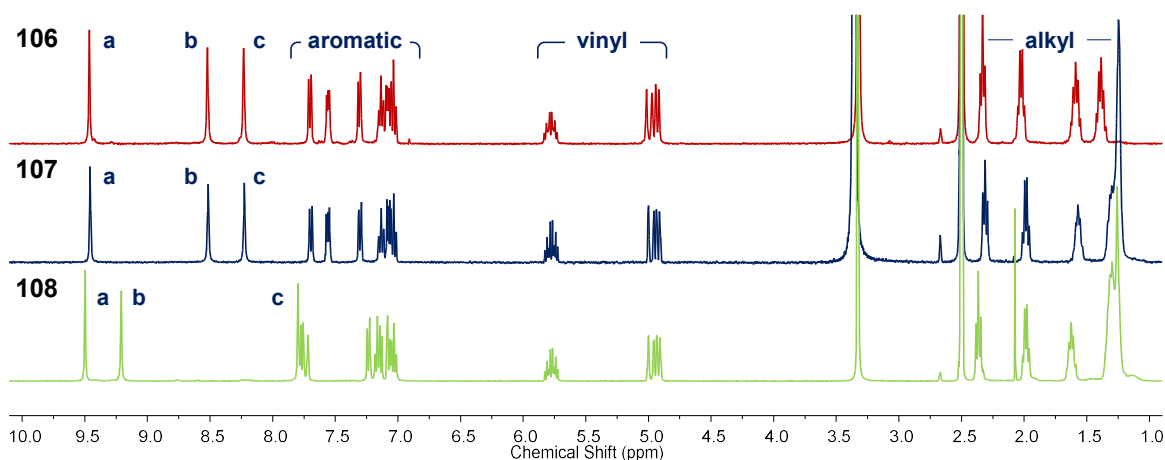


Figure 4.4. $^1$H NMR spectra (400 MHz, 0–10 ppm, DMSO-$d_6$) of receptors **106** (red), **107** (blue) and **108** (green).
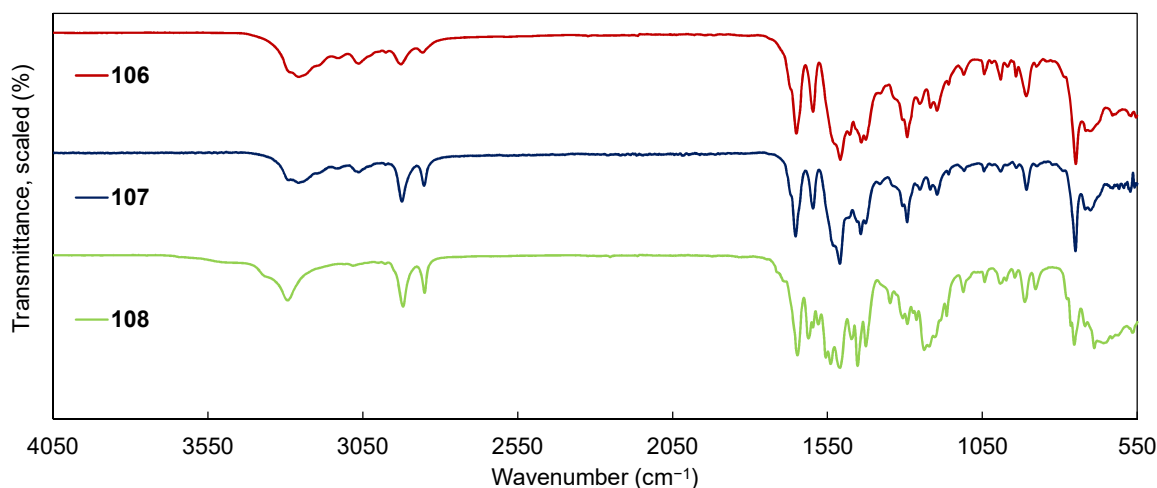
Figure 4.5. FTIR spectra (550–4050 cm$^{-1}$) of receptors **106** (red), **107** (blue) and **108** (green).

and methanol before being dried *in vacuo*. Receptors **106**–**108** were isolated as white solids in 25%, 59%, and 87% yields, respectively.

The synthesis of the amide group was indicated by the presence of a new NH resonance at *ca*. 9.5 ppm, Figure 4.4. A new carbon resonance corresponding to the amide carbonyl was also observed at 172 ppm. The FTIR spectra of **106**–**108** share several common features, Figure 4.5, including the two sharp C−H stretching modes around 2925 cm$^{-1}$ and 2850 cm$^{-1}$, and the simple structure of the C=O stretching bands in the 1600–1700 cm$^{-1}$ region. The absence of the NH stretch at *ca*. 3500 cm$^{-1}$ was also noted.

### 4.2.1  Attempted Synthesis of Macrocyclic Derivatives

Synthesis of the macrocyclic receptor **129** was attempted by means of ring-closing metathesis (RCM) of compound **107**, using the second generation Hoveyda–Grubbs catalyst, Scheme 4.3. The reaction was performed under an argon atmosphere in darkness, at a concentration of 1 mg mL$^{-1}$ in anhydrous CH$_2$Cl$_2$, and with a catalyst loading of 5 mol %. A conversion of 26% was observed by $^1$H NMR, however the exact identity of these mid-chain alkene product or products could not be determined. Compound **129** could not be isolated by available techniques, including column chromatography.
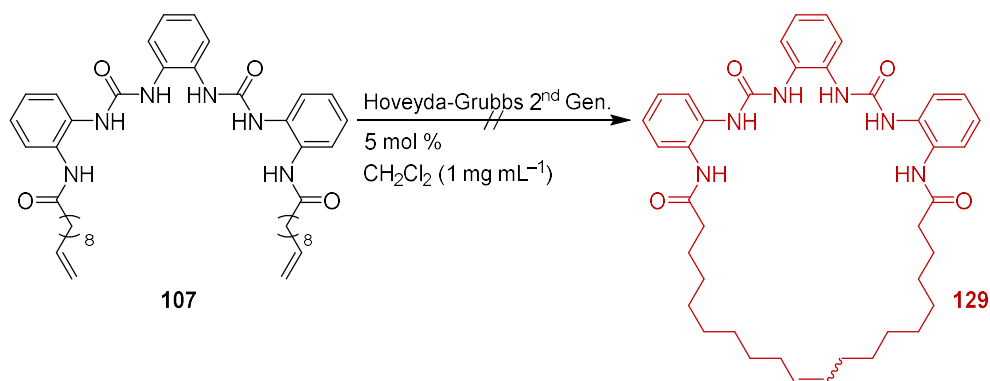


Scheme 4.3. Attempted ring closing metathesis (RCM) of compound **107**, to form macrocyclic receptor **129**.

Recognising the difficulties that were being encountered with RCM on a substrate that was not readily soluble in appropriate reaction solvents, an alternate macrocyclic receptor **130** was designed, containing a triethylene glycol (trigol) strap, Scheme 4.4. Two synthetic routes were envisaged. The first mirrored the approach taken to synthesise **136**, in which diol intermediate **137** is formed *via* amide coupling, and thereafter the ring closed by means of a double Williamson ether synthesis using trigol ditosylate. The second, convergent, route inverted the order of the reactions by first synthesising the trigol-containing diacid **138** and coupling this with the diamine **136**.
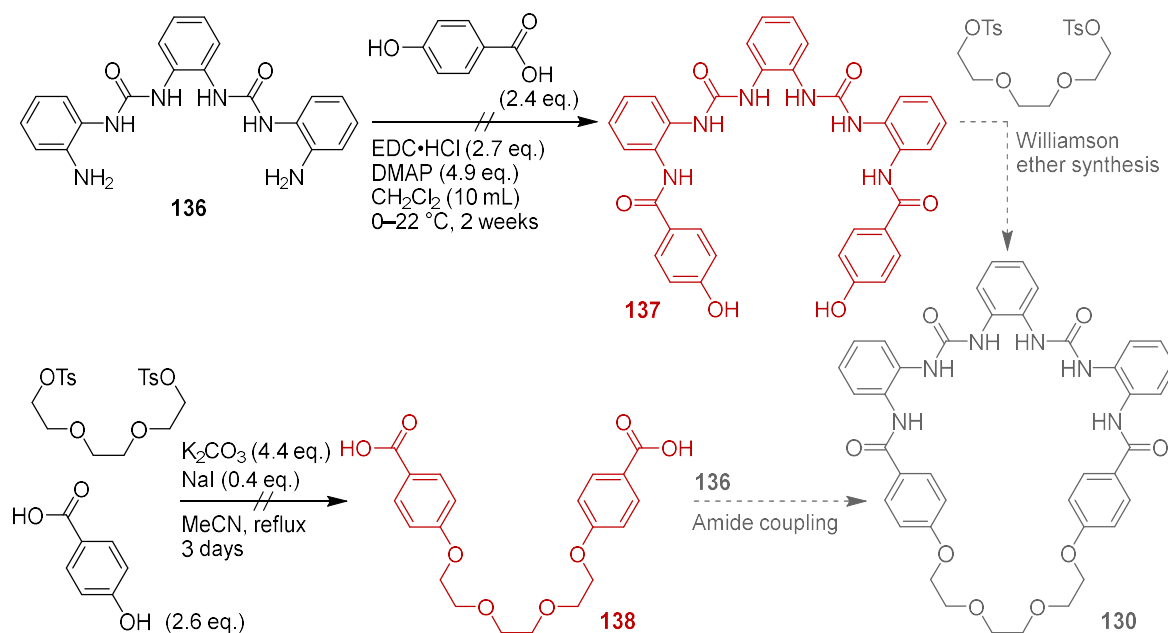


Scheme 4.4. Two attempted routes towards the synthesis of macrocyclic receptor **130** using amide coupling and Williamson ether synthesis, *via* the diol **137** (top) or the diacid **138** (bottom).

The amide coupling of **136** with 4-hydroxybenzoic acid to form **137** was attempted under the same conditions as for compounds **106–108**, above. After 3 days, an aliquot (1 mL) of the reaction mixture was removed *via* syringe, the solvent evaporated, and the residue washed and sonicated in a mixture of water and acetonitrile. This yielded a white solid, which ¹H NMR spectroscopy indicated was unreacted diamine **136**. To aid in the reactivity of the poorly soluble **136**, DMF was added to the reaction mixture *via* syringe (giving a 4:1 ratio of DCM/DMF) and the mixture stirred for a further 10 days. The reaction mixture was centrifuged to remove the suspended solid, which was confirmed by ¹H NMR spectroscopy to be almost entirely diamine **136**. A pale-coloured solid was precipitated from the dried supernatant using MeOH, and ¹H NMR spectroscopy identified this material as mostly diamine **136** also.

The synthesis of diacid **138** was attempted *via* a Williamson ether synthesis, starting from triethylene glycol ditosylate and 2.3 eq. of 4-hydroxybenzoic acid in MeCN, using a

large excess of $K_2CO_3$ as a base, and NaI as a Finkelstein reagent. The reaction was heated under reflux for 3 days, after which analysis by thin-layer chromatography showed the presence of several products, which could not be identified through staining. The $^1$H NMR spectrum of the crude product after extraction with EtOAc and washing with water showed the presence of a mixture of substituted aliphatic molecules, with the tosylate group forming the majority of the aromatic component. The presence of acid-substituted compounds could not be inferred due to the absence of a carboxylic acid resonance.

Noting that a) the transformation of **138** to macrocycle **130** might be easier if the macrocycle formation could be achieved under dynamic conditions, and b) the presence of the two amide groups was likely the main source of the solubility problems, reductive amination was considered as an alternative method to link the diphenyltriethyleneglycol moiety to **136**. Macrocycle **131** was designed as the corresponding product of these adapted routes, Scheme 4.5, *via* intermediate **139** or **140**.
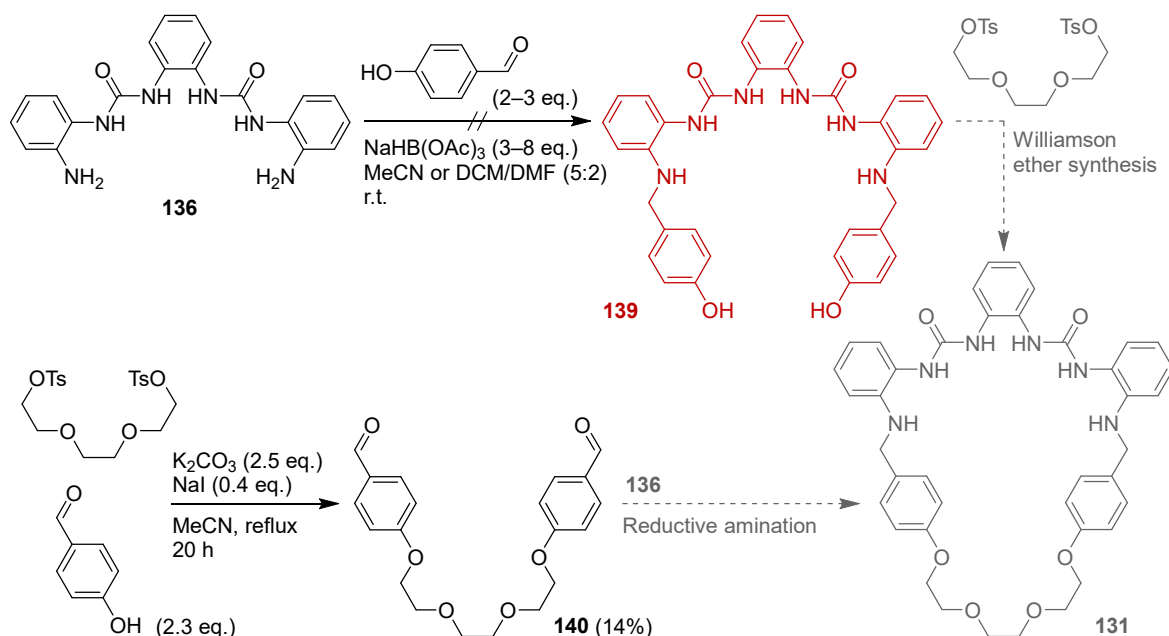


Scheme 4.5. Two attempted routes towards the synthesis of macrocyclic receptor **131** using reductive amination and Williamson ether synthesis, *via* the diol **139** (top) or the dialdehyde **140** (bottom).

Dialdehyde **140** was synthesised *via* a Williamson ether conditions, starting from triethylene glycol ditosylate and 2.3 eq. of 4-hydroxybenzaldehyde in acetonitrile, using $K_2CO_3$ as a base in slight excess, and NaI as a Finkelstein reagent. The reaction was heated under reflux for 20 h, at which point analysis by thin-layer chromatography showed the product ($R_f = 0.65$–0.70 in 100% EtOAc) to be the major component of the reaction mixture, alongside unreacted 4-hydroxy benzaldehyde ($R_f = 0.78$–0.84) and the mono-reacted intermediate ($R_f = 0.74$–0.78). After extraction into EtOAc and washing with water, column chromatography in EtOAc/hexane yielded the pure product as a white crystalline solid in

14% yield. Confirmation of the successful synthesis of **140** was obtained by $^1$H NMR spectroscopy; in particular, with the presence of two singlets at 9.82 ppm and 3.62 ppm corresponding to the aldehyde proton and the four equivalent protons of the central ethylene unit, respectively. The absence of any peaks corresponding to the tolyl- or hydroxyl-containing starting materials or intermediate was also noted. A resonance corresponding to the aldehyde group was found at 191.3 ppm in the $^{13}$C NMR spectrum. The remainder of the fractions were lost to a previously-reported intramolecular Cannizzaro reaction,[211] indicated by a colour change to bright pink and the presence of a carboxylic acid resonance in the $^1$H NMR spectrum.

Before proceeding with the attempted reductive amination with **136** and **140**, 4-hydroxybenzaldehyde was used both as a model for the dialdehyde, and to provide an alternative synthetic route as before. This synthesis of **139** was first attempted in MeCN, with 2.2 eq. 4-hydroxybenzaldehyde and 3.1 eq. NaHB(OAc)₃, while stirring at room temperature for 1 week. No reaction was observed. A mixture of anhydrous DCM/DMF (5:2) over molecular sieves was then employed as reaction solvent, with 3 eq. of aldehyde and 8 eq. of borohydride in an argon atmosphere. This was stirred at 0 °C, and warmed to room temperature, being stirred for 1 week. The mixture was filtered to remove the sieves, the solution concentrated under reduced pressure, and a solid precipitated from the solution by the addition of water. This was observed by $^1$H NMR spectroscopy to consist of a mixture of dozens of unidentifiable compounds, indicating degradation. No trace of **139** was found through mass spectrometry. Being unable to find a suitable synthetic procedure for the production of compound **139**, the synthesis of macrocycle **131** from diamine **136** and dialdehyde **140** was not pursued further.

## 4.3   Initial $^1$H NMR Titrations with Receptor **107**

The $C_{11}$ receptor **107** was chosen with which to perform preliminary $^1$H NMR titrations in order to optimise the titration set-up. These were first performed at an initial host concentration of 7 mM, with 0.28 M solutions of either TBA$^+$ benzoate or phosphate in DMSO-$d_6$ and at a temperature of 25.0 °C.

### 4.3.1   Titration of Receptor **107** with BzO$^-$ at 7.0 mM

The resonances associated with all three NH groups (Ha–c), and the aromatic resonances H3, Hd and H6 were observed to increase in chemical shift over the addition of 0→5 eq. of the TBA benzoate to the solution of **107**, see Figure 4.6. All other aromatic resonances, including those of the benzoate guest (H2′–4′), were observed to become more shielded as
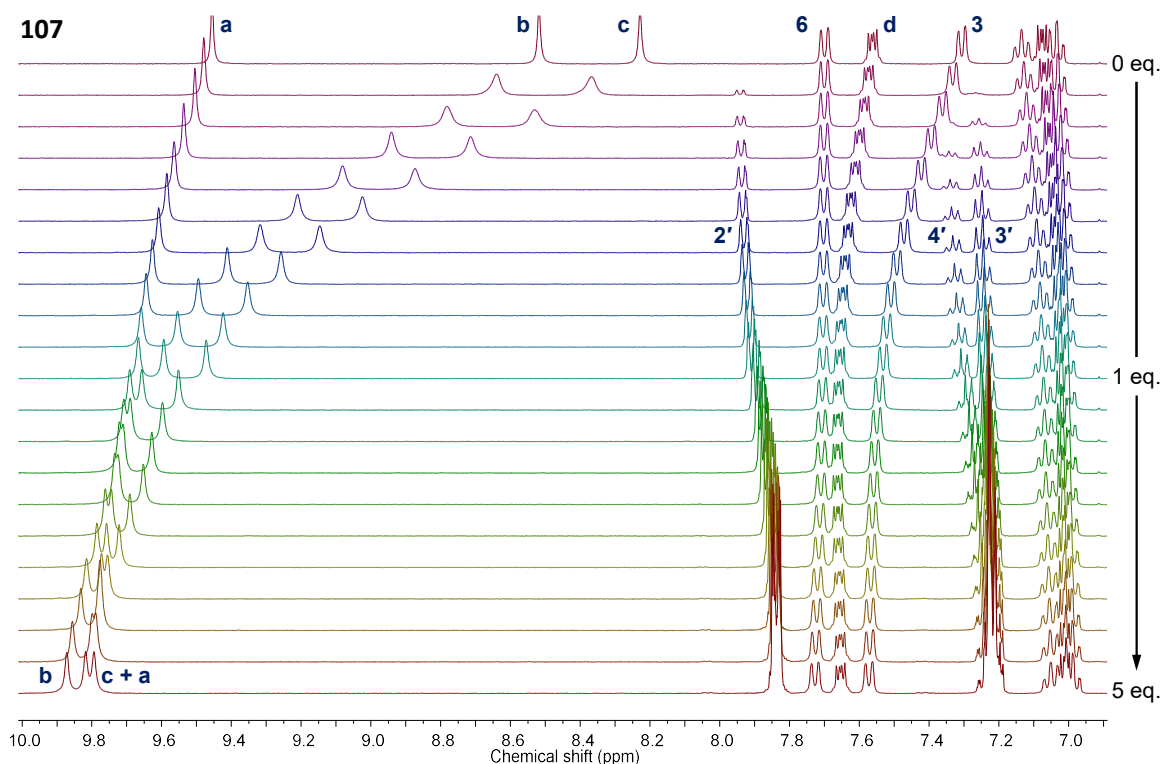
Figure 4.6. Stack plot of the individual ¹H NMR spectra (400 MHz, DMSO-$d_6$, 6.5–10.0 ppm) from the titration of receptor **107** (7 mM) with TBA benzoate (0→5 eq.).

the titration progressed. Most of the changes in the chemical shifts of the host molecule occurred over the addition of the first equivalent of TBA benzoate.

Moderate increases in chemical shift were displayed by the amide resonance Ha (9.5→9.8 ppm) and the aromatic resonance H3 (7.3→7.6 ppm) over the course of the titration, Figure 4.7. The urea protons also became more deshielded, with a sharp increase in chemical shift noted for Hb (8.5→9.6 ppm) and Hc (8.2→9.5 ppm) after the addition of
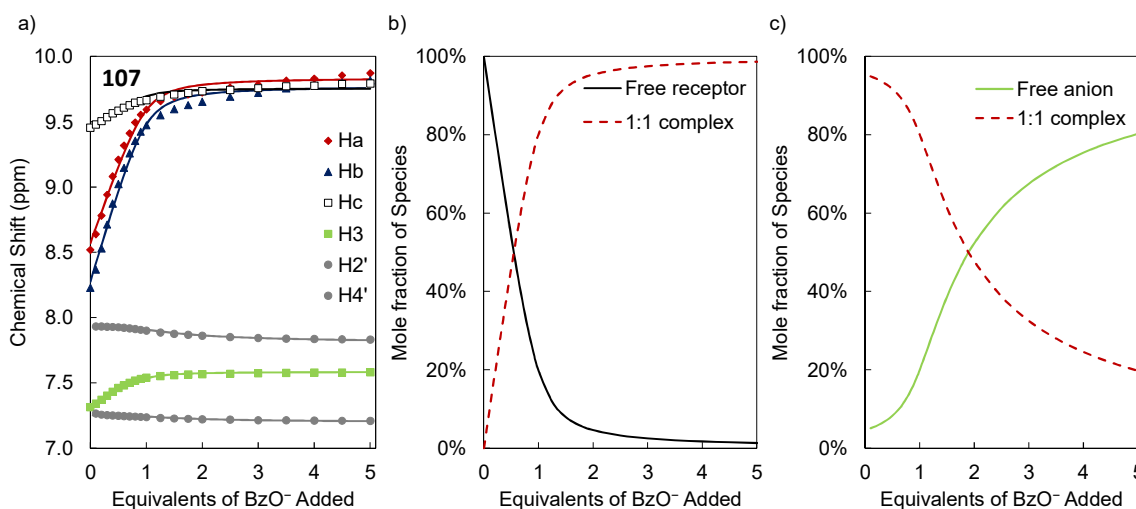


Figure 4.7. a) Binding fit for the titration of receptor **107** (7 mM) with TBA benzoate (0→5 eq.) in DMSO-$d_6$. Note the systematic differences between the data points and the fit in the region 1.0→2.5 eq. anion. b–c) Speciation distribution diagrams generated from the fitting of the experimental data. The concentrations are presented as mole-percentage values of each species relative to the sum of their concentrations.

1 eq. TBA benzoate, and a more moderate increase noted thereafter (9.6→9.9 ppm and 9.5→9.8 ppm, respectively). The protons at the 2 and 4 positions of the benzoate guest became more shielded, with slight decreases in chemical shift noted for H2′ (7.94→7.84 ppm) and H4′ (7.34→7.23 ppm). The shape of the change in chemical shift of these resonances was sigmoidal.

The data following the chemical shift of resonances Ha–c, H3, H2′ and H4′ were fit to a 1:1 host–guest binding model. A range of binding constants ($\log\beta_{1:1}$ = 3.47–3.81) were obtained from this fit, depending on whether the three NH resonances (Ha–c), the aromatic resonance H3, or all six were used in the fitting programme, see Table 4.1. The best quality fit was obtained from fitting the six resonances of interest simultaneously, see Figure 4.7. The binding constant derived from this fit was $\log\beta_{1:1}$ = 3.47 ± 0.05. It must be noted that the drop in $SE_y$ (from 38 ppb to 30 ppb and 26 ppb) upon fitting the extra resonances from the distal ring (H3) and benzoate anion (H2′, H4′) is likely because the overall change in chemical shift ($\Delta\delta$) for these resonances – and therefore each residual – is relatively small, skewing the calculated value. The value of $SE_y$ is included in Table 4.1 for the purposes of

Table 4.1. Comparison of the logarithmic binding constants, $\log\beta_{1:1}$, determined from the analysis of $^1$H NMR titrations of receptor **107** in DMSO-$d_6$ at 25.0 °C; according to the initial host concentration $[H]_0$, and the proton resonances used in the fitting of the data with HYPNMR2008. Also noted is the value of $SE_y$ from each fit, as well as the number of scans and receiver gain used in acquiring the spectra for each titration.

| Anion | $[H]_0$ (mM) | Resonances used [a] | $\log\beta_{1:1}$ | | | $SE_y$ [b] (ppb) | Scans | Gain |
|---|---|---|---|---|---|---|---|---|
| BzO⁻ | 7.0 | Ha–c | 3.46 | ± | 0.07 | 38.2 | 16 | 32 |
| | | Ha–c (deconvolution) | 3.46 | ± | 0.07 | 38.3 | | |
| | | H3 | 3.81 | ± | 0.11 | 7.4 | | |
| | | Ha–c, H3 | 3.47 | ± | 0.06 | 30.0 | | |
| | | Ha–c, H3, H2′, H4′ | 3.47 | ± | 0.05 | 25.6 | | |
| | 0.7 | Ha–c | 3.70 | ± | 0.02 | 12.0 | 32 | 456 |
| | | H3 | 3.71 | ± | 0.02 | 3.0 | | |
| | | Ha–c, H3 | 3.70 | ± | 0.01 | 9.4 | | |
| | | **Ha–c, H3, H2′, H4′** | **3.70** | **±** | **0.01** | **8.1** | | |
| H₂PO₄⁻ | 7.0 | Hd, H3 | 3.38 | ± | 0.10 | 12.3 | 16 | 23 |
| | 0.7 | **Hd, H3** | **4.24** | **±** | **0.05** | **10.4** | 32 | 456 |

Anions added as their TBA⁺ salts. Reported values are from a single titration, associated error is the "standard deviation" parameter reported by HYPNMR2008. [a] Resonance labelling as in Figure 4.1. H2′ and H4′ refer to the $^1$H resonances at the 2- and 4-positions of the benzoate guest, [b] Standard error of the *y*-estimate, measured in ppb.

comparing the residuals of corresponding entries at different concentrations, see also Sections 4.3.3 and 4.3.4 below. A better measure of the increasing quality between different types of fit is the reduction in the "standard deviation" parameter reported by the fitting programme, HYPNMR2008, as this is an estimate of the error on the binding constant itself.

When spectral resonances overlap, due to the addition of the signal intensities at each point, the peak maxima occur slightly closer together than they would if the resonances were narrow and did not overlap. The greater the overlap, the greater this inset. Noting the overlapping of Ha–c in the 1→5 eq. region of the titration, a deconvolution algorithm (using the MestReNova6 GSD package) was applied to these spectra, see Figure 4.8. Synthetic spectra were generated from these data, with narrow line widths (0.5 Hz) to ensure that there would be no peak overlap. The maxima of these deconvoluted peaks were fit to a 1:1 host–guest binding model, which afforded a value of $\log\beta_{1:1} = 3.46 \pm 0.07$, identical to the fit performed without deconvolution of the peaks. The residual parameter, $SE_y$, for the fit was similar (but slightly larger) at 38.3 ppb. Spectral deconvolution did not improve the fitting result in this case as the gain in resolution was only a small fraction of the total change in chemical shift; and that the poor fitting was due to the sharp curvature in the range of
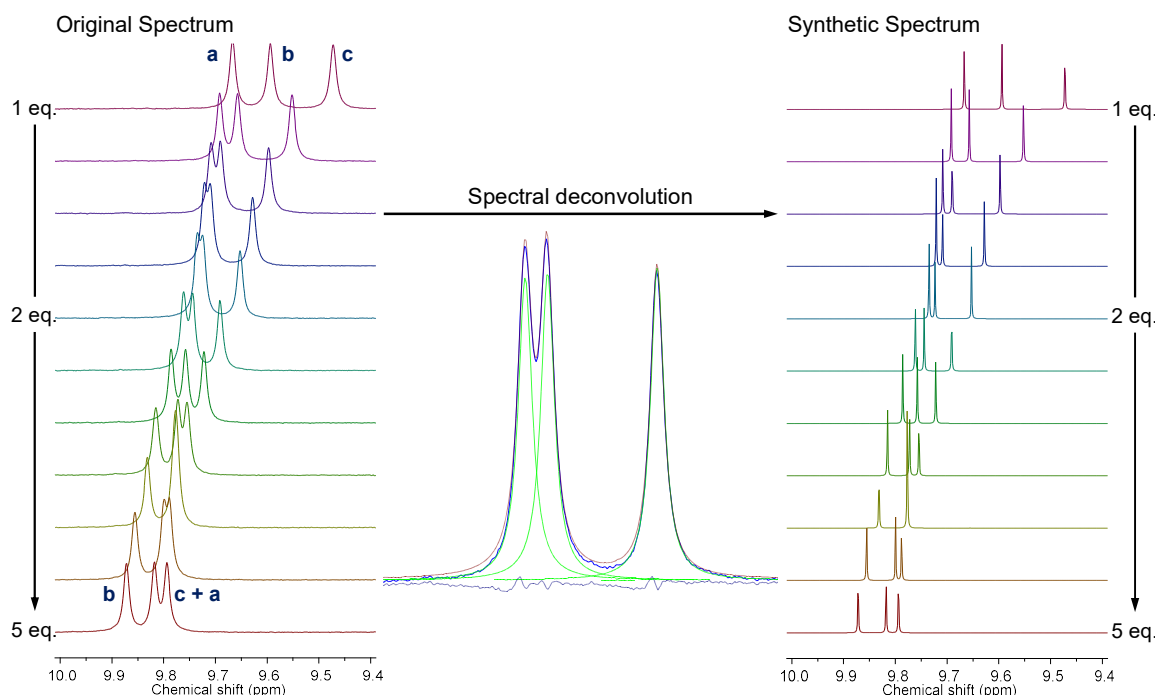


Figure 4.8. Application of spectral deconvolution to resonances Ha–c in in the range of 1→5 eq. TBA benzoate to create synthetic spectra with no peak overlap. In the centre, the result of the deconvolution can be seen, original spectrum in dark blue, fitted peaks in green, their sum in red, and the residual on the fit in grey. Synthetic spectra with linewidths of 0.5 Hz were then generated, from which peak maxima were measured.

0.70→1.25 eq. benzoate, immediately preceding the point in the titration where spectral overlap began, Figure 4.6a.

## 4.3.2   Titration of Receptor **107** with $H_2PO_4^-$ at 7.0 mM

Upon titration of receptor **107** with the $H_2PO_4^-$ salt, broadening of the urea and amide resonances (Ha–c) was observed, Figure 4.9. Resonance Ha increased significantly in chemical shift up to the addition of 1 eq. of $TBAH_2PO_4$ (9.5→10.0 ppm), after which it broadened such that the peak could not be resolved beyond the addition of 1.4 eq. anion. The urea resonances Hb (8.5 ppm) and Hc (8.2 ppm) were also observed to deshield significantly, but were difficult to resolve after the addition of 0.3 eq. of $TBAH_2PO_4$, and appeared as a single resonance at 9.6 ppm after the addition of 1 eq. of the salt. These resonances also broadened thereafter, with a single, very broad peak being observed at 11.6 ppm at the end of the titration. Moderate increases in chemical shift were noted over the first half of the titration (0→1 eq.) for the aromatic resonances Hd (7.6→7.8 ppm) and H3 (7.3→7.6 ppm). Less significant deshielding was noted for Hd (7.8→7.9 ppm) and H3 (7.6→7.7 ppm) over the remainder of the titration (1→5 eq.). A less significant increase in chemical shift was observed in resonance H6 of the distal ring. All other aromatic resonances became more shielded over the course of the titration.

As all NH resonances (Ha–c) broadened to the point where they could not be resolved from each other, or the baseline, the changes in the chemical shifts of the aromatic resonances Hd and H3 were used in the fit. Fitting these data to a 1:1 host–guest binding
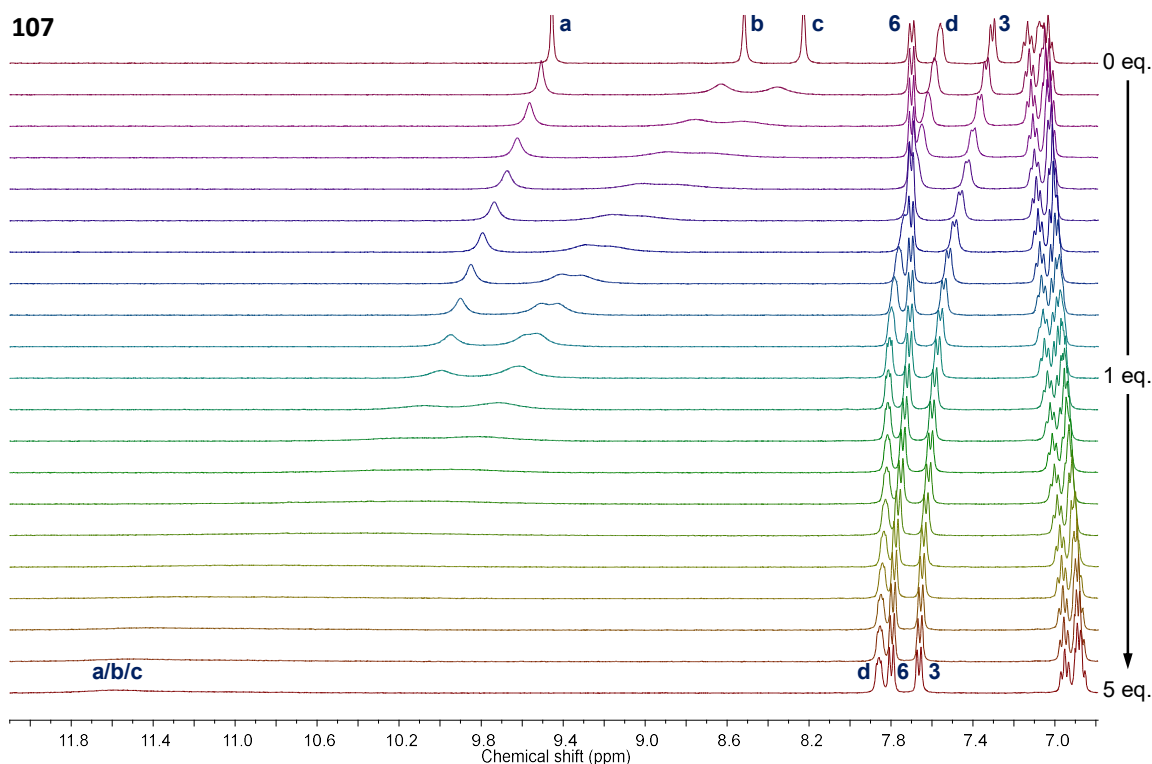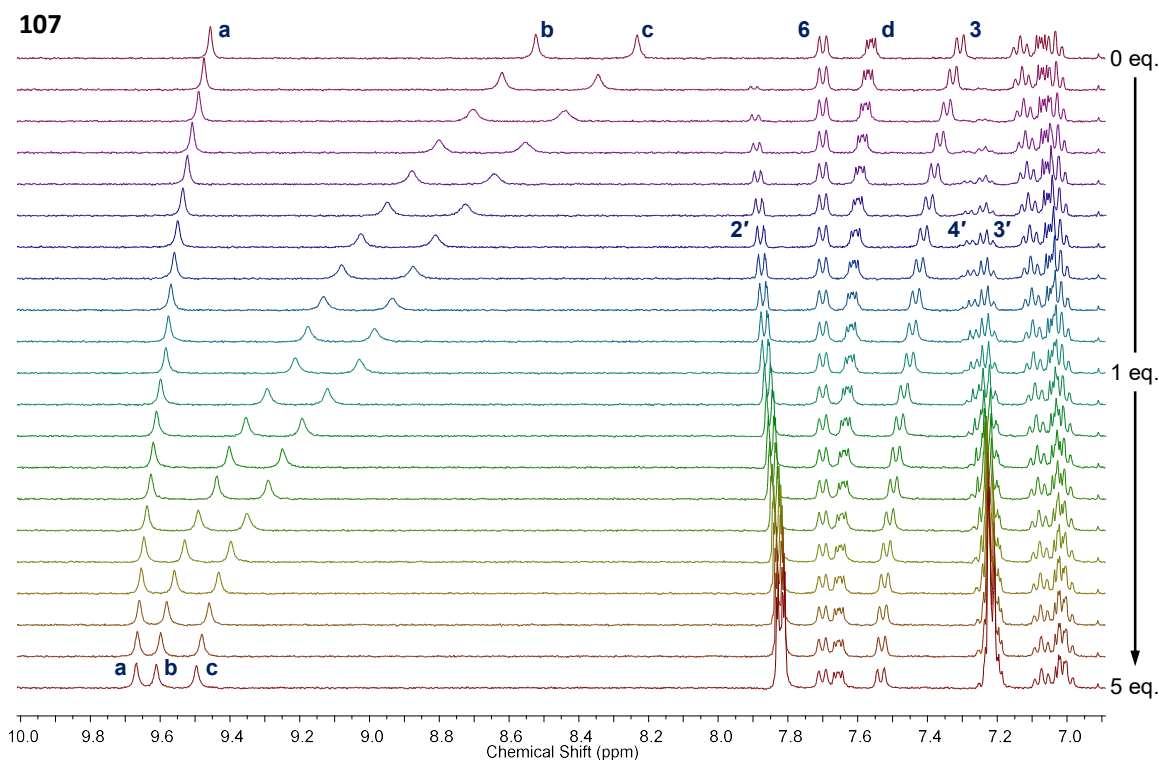


Figure 4.9. Stack plot of the individual ¹H NMR spectra (400 MHz, DMSO-$d_6$, 6.9–12.0 ppm) from the titration of receptor **107** (7 mM) with $TBAH_2PO_4$ (0→5 eq.).
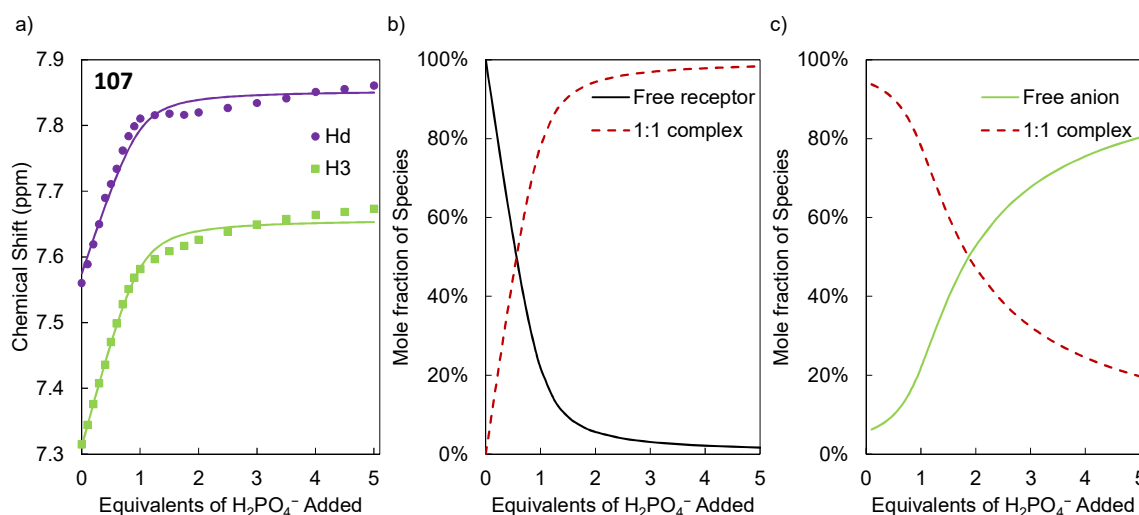
Figure 4.10. a) Binding fit for the titration of receptor **107** (7 mM) with TBAH$_2$PO$_4$ (0→5 eq.) in DMSO-$d_6$. Note the systematic differences between the data points and the fit in the region 1→5 eq. anion. b–c) Speciation distribution diagrams generated from the fitting of the experimental data. The concentrations are presented as mole-percentage values of each species relative to the sum of their concentrations.

model afforded a value of $\log\beta_{1:1}$ = 3.38 ± 0.10. The value of SE$_y$ for this fit is equal to 12.3 ppb, due to the relatively large systematic differences between the data points and the fit in the region of 1→5 eq. TBAH$_2$PO$_4$ (Figure 4.10).

Noting that a similar class of $H_6$ donor receptors reported by Wu and coworkers[212] bind PO$_4{}^{3-}$ and HPO$_4{}^{2-}$ anions in a 2:1 host–guest binding stoichiometry, attempts were also made to fit these data to such a model. Unrealistically large values of $\log\beta_{1:1}$ = 5 ± 3 and $\log\beta_{2:1}$ = 10 ± 5 were obtained from a fit of these same resonances (Hd and H3).

In the titration of a suspected 1:1 host–guest system, the preferred titration set-up is one in which the host concentration is roughly equal to the reciprocal of the anticipated value of β.[188,208] Above this concentration range, the increased curvature of the binding isotherm increases the error of the titration fit. Noting that fitting the changes in chemical shift in the titration of **107** with BzO$^-$ gave a range of binding constants depending on which resonance was fitted, and the relatively sharp curvature of the trend in the Hd and H3 resonances in the titration with H$_2$PO$_4{}^-$, this was investigated as a possible issue with the titration set-up. As the binding constants determined through the first titrations of **107** with both anions were in the range $\log\beta_{1:1}$ = 3–4, it was decided to repeat the titrations at an initial host concentration of 0.7 mM and a titrant concentration of 0.028 M. In order to obtain a useful signal-to-noise ratio, the number of scans in each spectrum was increased from 16 to 32, and the receiver gain was increased from 32 (or 23) to 456. All other parameters remained the same.

### 4.3.3   Titration of Receptor **107** with BzO⁻ at 0.7 mM

Upon repeating these titrations at this lower concentration, subtle but important differences were noted. In the titration with the benzoate salt, the overall trends were similar without the previously observed crossover of the urea (Hb–c) and amide (Ha) resonances. Resonance Ha displayed a moderate increase in chemical shift over the course of the titration (9.5→9.7 ppm), while larger increases were noted for Hb (8.5→9.6 ppm) and Hc (8.2→9.5 ppm). These changes were more gradual than had been observed in the titration at 7 mM. Proton H3 also became more deshielded (7.3→7.5 ppm) over the titration. The resonances of the benzoate guest, H2′ (7.90→7.82 ppm) and H4′ (7.29→7.23 ppm), became more shielded during the titration. These changes were also more gradual at this lower concentration, without the sigmoidal profile noted before (Figure 4.11, compare Figure 4.6 above).

Fitting the data from this titration (using resonances Ha–c, H3, H2′ and H4′ as before, see Figure 4.12a) gave a value of $\log\beta_{1:1} = 3.70 \pm 0.01$; no spread in the calculated values of $\log\beta_{1:1}$ was observed when these were determined from the data for different resonances (Table 4.1). The changes in chemical shift of resonances Hb and Hc were much smoother, allowing for a more accurate fit of the data. In the case of each fit, the value of $SE_y$ was approximately three times smaller than at a concentration of 7 mM.
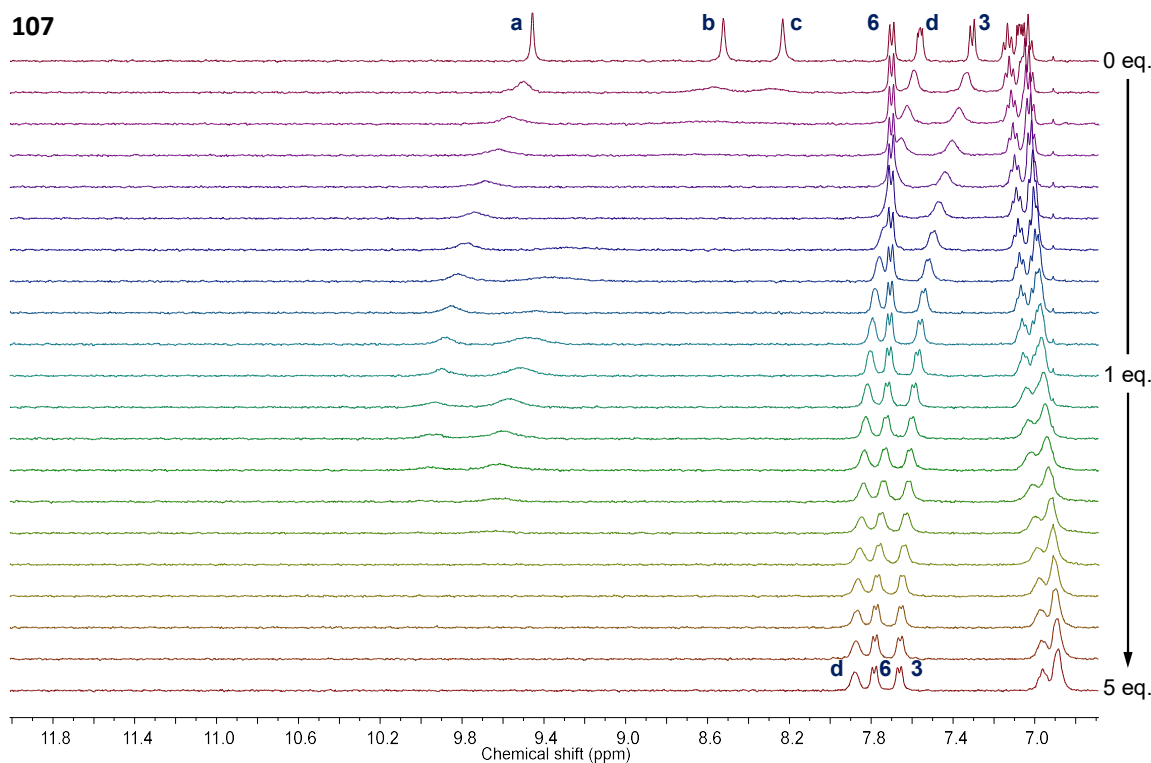


Figure 4.11. Stack plot of the individual ¹H NMR spectra (400 MHz, DMSO-$d_6$, 6.8–10.0 ppm) from the titration of receptor **107** (0.7 mM) with TBA benzoate (0→5 eq.) Note that the changes in chemical shift are more moderate than in Figure 4.6, and resonances Ha–c.
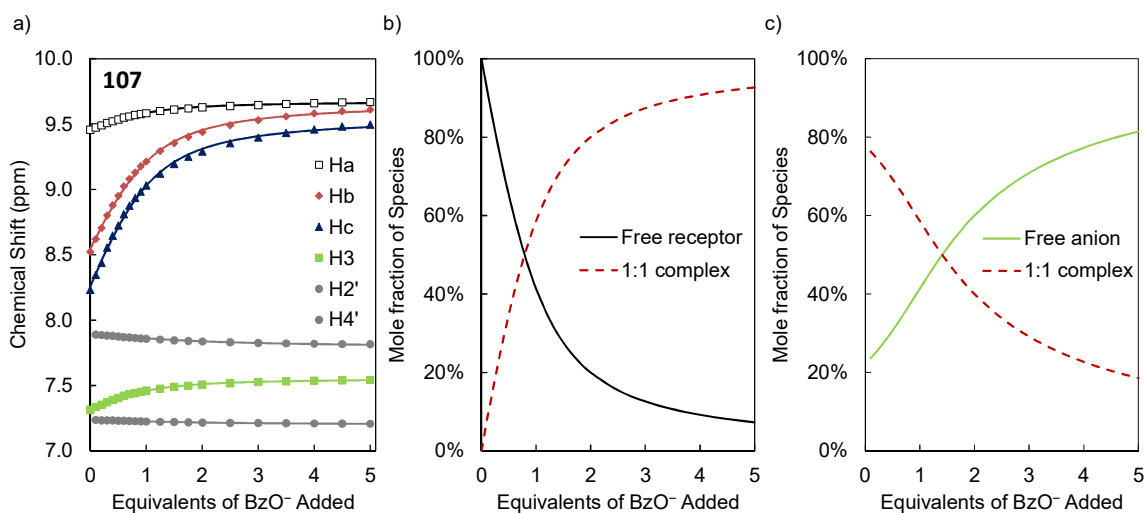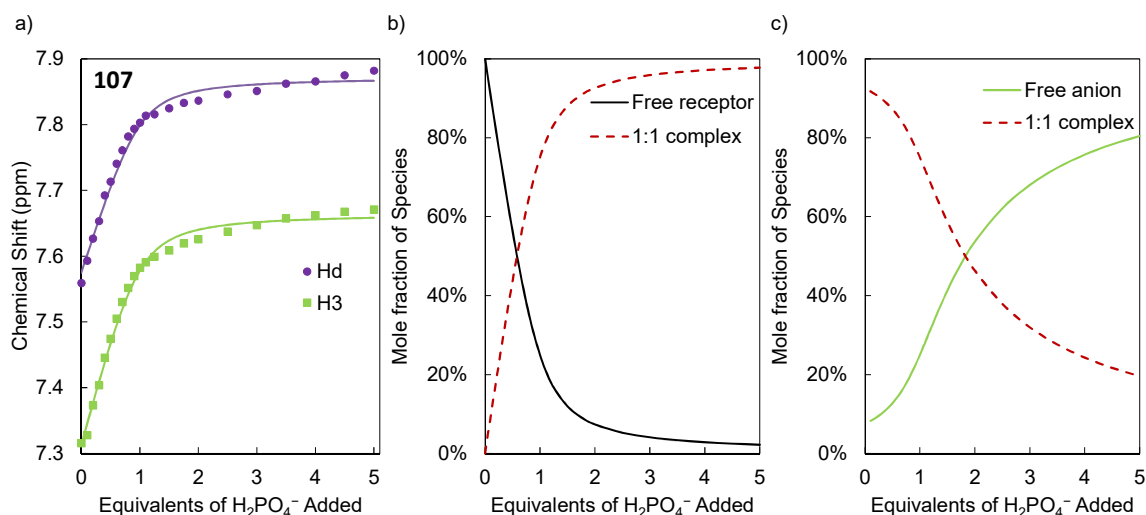
Figure 4.12. a) Binding fit for the titration of receptor **107** (0.7 mM) with TBA benzoate (0→5 eq.) in DMSO-$d_6$. b–c) Speciation distribution diagrams generated from the fitting of the experimental data. The concentrations are presented as mole-percentage values of each species relative to the sum of their concentrations.

### 4.3.4 Titration of Receptor **107** with $H_2PO_4^-$ at 0.7 mM

In the case of the titration with $H_2PO_4^-$, the broadening of the urea and amide resonances was more significant at the lower concentration of 0.7 mM. Over the addition of the first equivalent of anion, significant deshielding was noted for both Hb (8.5→9.5 ppm) and Hc (8.2→9.5 ppm), with a single resonance being observed (Figure 4.13). However, the extent of the broadening was such that the urea resonances could not be resolved after the addition
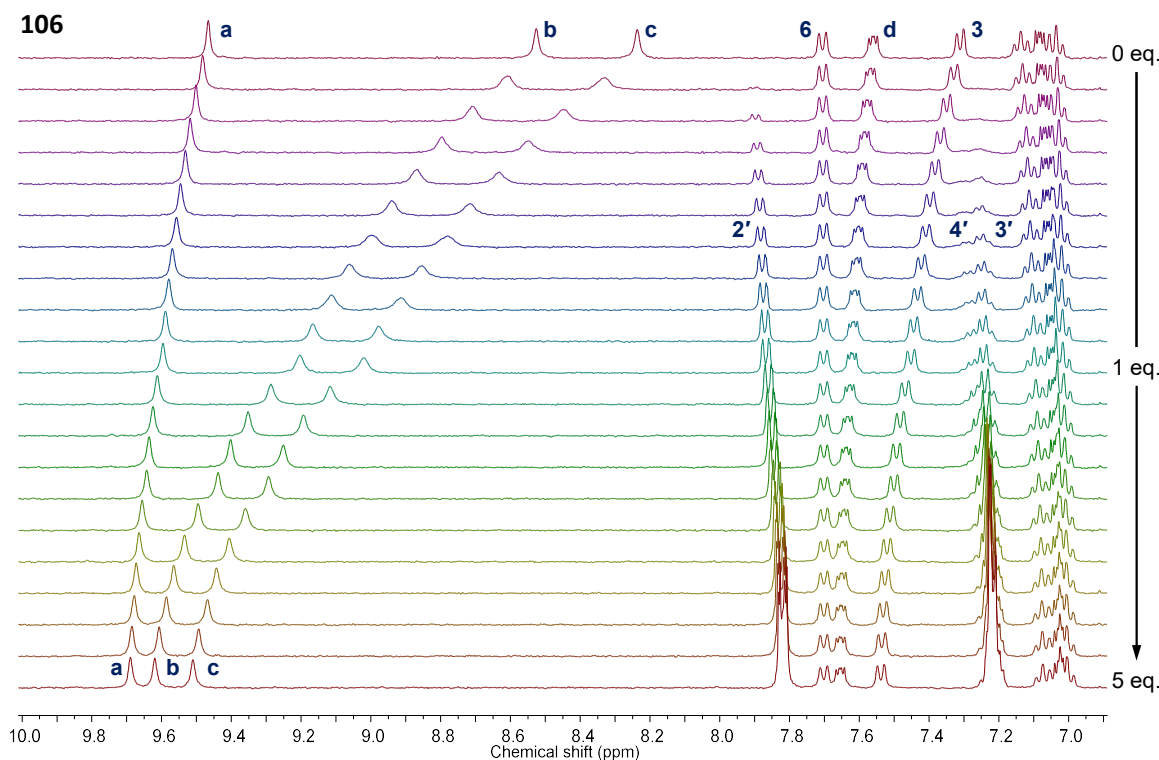


Figure 4.13. Stack plot of the individual ¹H NMR spectra (400 MHz, DMSO-$d_6$, 6.7–12.0 ppm) from the titration of receptor **107** (0.7 mM) with TBAH₂PO₄ (0→5 eq.).
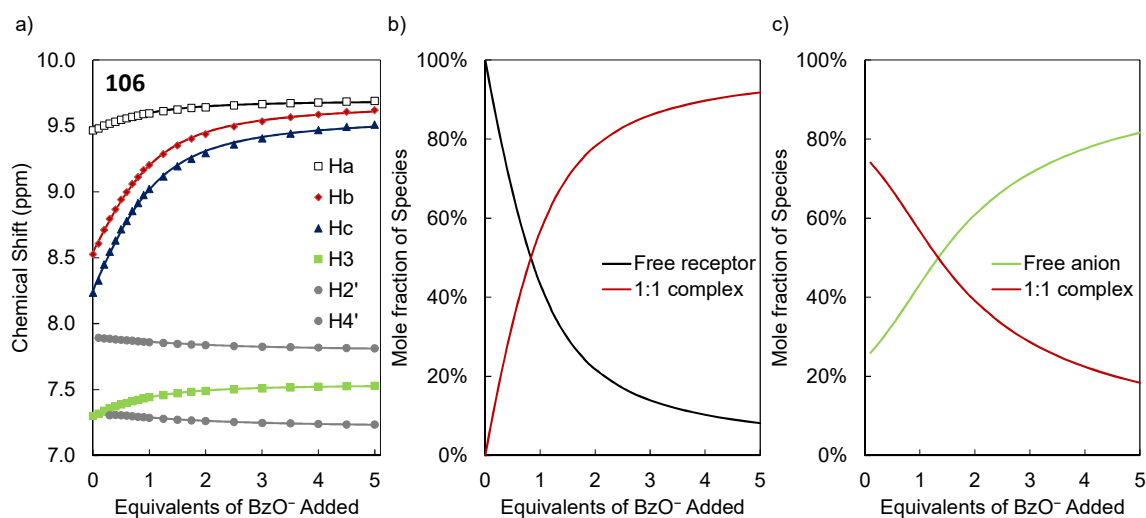
119

Figure 4.14. a) Binding fit for the titration of receptor **107** (0.7 mM) with TBAH₂PO₄ (0→5 eq.) in DMSO-$d_6$. b–c) Speciation distribution diagrams generated from the fitting of the experimental data. The concentrations are presented as mole-percentage values of each species relative to the sum of their concentrations.

of 0.3 eq. of phosphate anion, and the signal broadened into the baseline in the region of 0.3→0.7 eq. of phosphate. The chemical shift of the amide resonance Ha also increased (9.5→9.9 ppm) in this range, gradually broadening into the baseline. No NH resonances could be discerned after the addition of 3 eq. of anion. The behaviour of the aromatic resonances was much the same as had been observed in the titration performed at 7 mM, with moderate deshielding being observed for both Hd (7.6→7.8 ppm) and H3 (7.3→7.6 ppm) up to the addition of 1 eq. TBAH₂PO₄, and lesser increases in chemical shift thereafter (7.8→7.9 ppm and 7.6→7.7 ppm, respectively).

Fitting the changes in chemical shift of the Hd and H3 resonances to a 1:1 host guest binding model afforded a binding constant of $\log\beta_{1:1} = 4.25 \pm 0.05$. The trend in resonances Hd and H3 is much smoother (Figure 4.14), and better described by a 1:1 fit than at 7 mM, as demonstrated by a slightly lower residual parameter of 10.4 ppb (compared to 12.3 ppb at 7 mM, see Table 4.1). It is notable that the two logarithmic binding constants obtained by fitting the titration data at different concentrations differ by 0.86 log units, corresponding to a factor of 7.2 in terms of the association constants themselves.

As before, the titration data were also fitted to a combined 1:1, 2:1 host–guest binding model, giving values of $\log\beta_{1:1} = 4.7 \pm 0.2$ and $\log\beta_{2:1} = 8.9 \pm 0.5$, and a value of $\log\alpha = 0.2 \pm 0.1$ implying slight positive cooperativity. These values are lower than those calculated from the titrations at 7 mM, but the value of $\log\beta_{2:1}$ is still very large to be determined through NMR-based experiments. It is possible that a lower concentration, in the range of $10^{-5}$–$10^{-4}$ mM, would improve the smoothness of the data further. This could allow for a better description of the data by a 1:1 or 2:1 host–guest binding model. However, the trade-off of reducing concentration is either a significant escalation in experiment time, or a poorer

signal-to-noise ratio. The latter would lead to data of unacceptably low quality. Additionally, it is advantageous to have both the BzO⁻ and $H_2PO_4^-$ titrations recorded at the same concentration, in case of any unforeseen concentration effects.

## 4.4 Comparative ¹H NMR Titrations of Receptors **106** and **108** at 0.7 mM

Having optimised the titration concentration for the prototypical receptor **107**, all subsequent titrations were carried out at an initial host concentration of 0.7 mM.

### 4.4.1 Titrations of Receptor **106** with BzO⁻ and $H_2PO_4^-$

Upon addition of BzO⁻ to the 6-heptenamide receptor **106**, similar changes were observed as in the titration with the longer chain receptor **107**, above, Figure 4.15. With receptor **106**, the increases in chemical shift of Ha–c (9.5→9.7 ppm, 8.5→9.6 ppm and 8.2→9.5 ppm, respectively) were identical to those reported with **107** above, as was the extent of the deshielding of proton H3 (7.3→7.5 ppm) over the titration. Similarly, the H2′ and H4′ resonances of the benzoate guest behaved in the same manner (7.90→7.82 ppm and 7.29→7.23 ppm, respectively).

The shape of the changes in chemical shift were also maintained with receptor **106**, see Figure 4.15. Fitting these data from resonances Ha–c, H3, H2′ and H4′ to a 1:1 host–
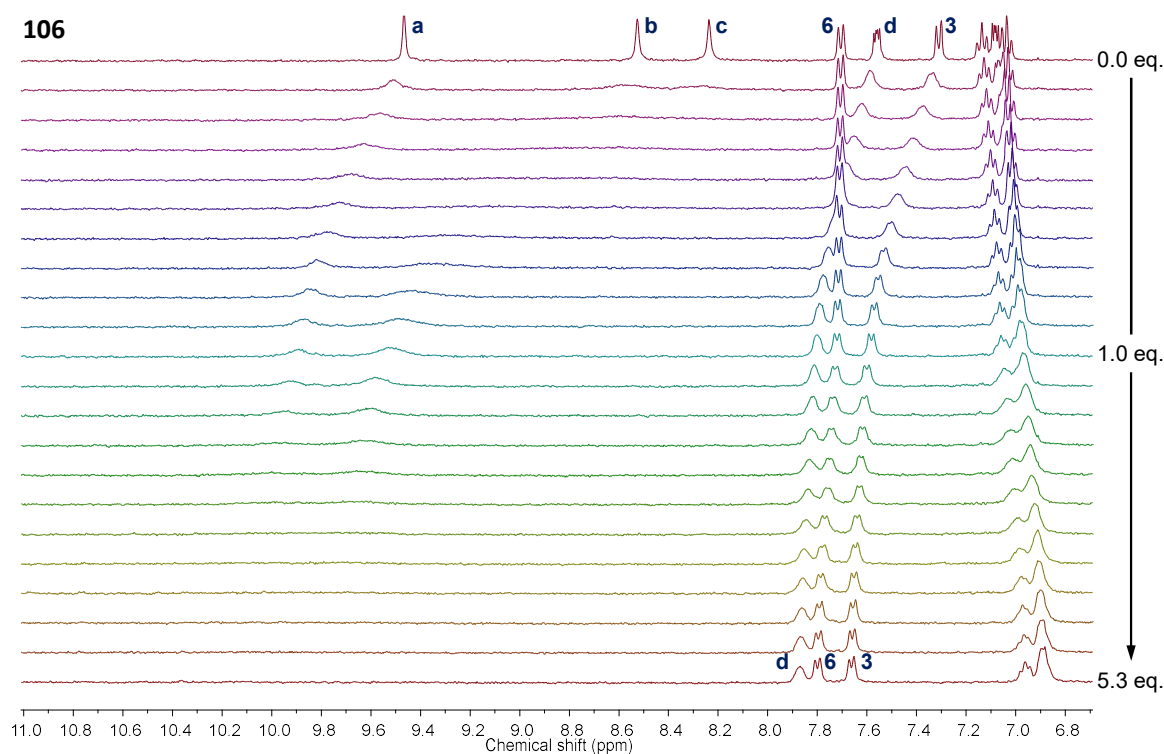


Figure 4.15. Stack plot of the individual ¹H NMR spectra (400 MHz, DMSO-*d₆*, 6.9–10.0 ppm) from the titration of receptor **106** (0.7 mM) with TBA benzoate (0→5 eq.) Note that the changes in chemical shift are indistinguishable from those in Figure 4.11.

Figure 4.16. a) Binding fit for the titration of receptor **106** (0.7 mM) with TBA benzoate (0→5 eq.) in DMSO-$d_6$. b–c) Speciation distribution diagrams generated from the fitting of the experimental data. The concentrations are presented as mole-percentage values of each species relative to the sum of their concentrations.

guest binding model (Figure 4.16) afforded a logarithmic binding constant of log$\beta_{1:1}$ = 3.64 ± 0.01. This is slightly lower than the value obtained with receptor **107**, above, see Table 4.2.

As with receptor **107**, above, the NH resonances of **106** broadened notably after the first addition of H$_2$PO$_4^-$ salt, with the urea resonances Hb and Hc difficult to distinguish after



Figure 4.17. Stack plot of the individual $^1$H NMR spectra (400 MHz, DMSO-$d_6$, 6.7–11.0 ppm) from the titration of receptor **106** (0.7 mM) with TBAH$_2$PO$_4$ (0→5.3 eq.).
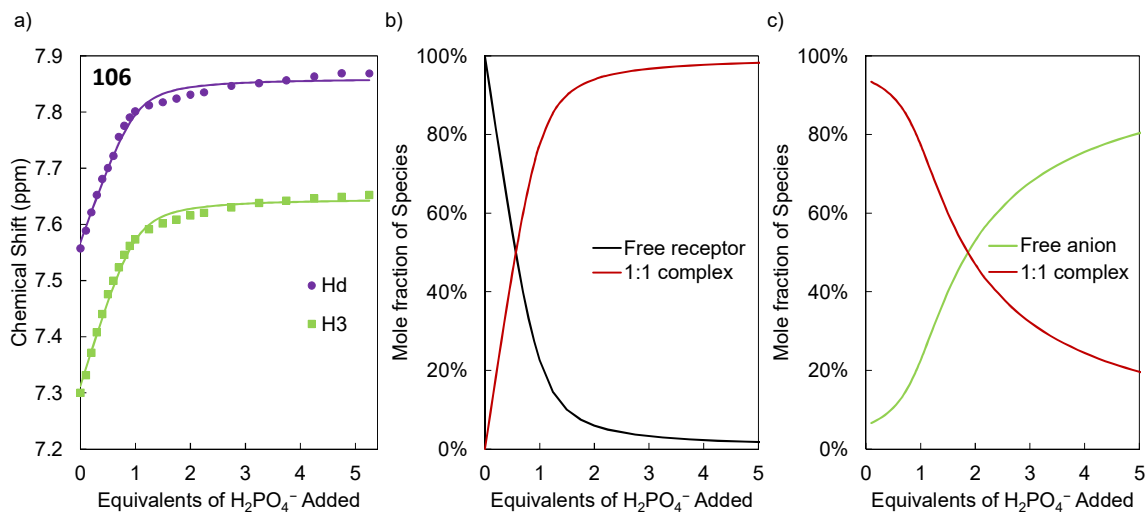
Figure 4.18. a) Binding fit for the titration of receptor **106** (0.7 mM) with TBAH₂PO₄ (0→5.3 eq.) in DMSO-$d_6$. b–c) Speciation distribution diagrams generated from the fitting of the experimental data. The concentrations are presented as mole-percentage values of each species relative to the sum of their concentrations.

the addition of 0.2 eq., and all three NH resonances broadening into the baseline after 2 eq. of the salt were added, Figure 4.17. This broadening is due to the proton experiencing a wider distribution of magnetic environments, possibly due to a wider distribution of binding orientations affecting the NH resonances more than others.

The characteristic changes in the chemical shift of the aromatic protons Hd and H3 which were previously noted with receptor **107** were also observed to occur here. A sharp increase in chemical shift up to 1 eq. $H_2PO_4^{2-}$ (7.6→7.8 ppm and 7.3→7.6 ppm, respectively), and a lesser increase thereafter (7.8→7.9 ppm and 7.6→7.7 ppm, respectively) were noted in this case with receptor **106**. Fitting the data from H3 and Hd to a 1:1 host–guest binding model (Figure 4.18) gave a value of $\log\beta_{1:1} = 4.35 \pm 0.07$. This is similar to the value reported above for receptor **107**, see Table 4.2.

### 4.4.2  Titrations of Receptor **108** with BzO⁻ and H₂PO₄⁻

Titrations were also performed with the *meta*-phenylene isomer **108**. As has been noted in Section 4.2 above, resonance Hc is significantly more shielded in receptor **108** than in receptors **107** and **106**. Upon addition of TBAOBz to a sample of **108** in DMSO-$d_6$, this resonance displayed a large increase in chemical shift, 7.8→9.6 ppm (Figure 4.19). Significant increases in chemical shift of the other NH resonances were also observed, with changes of 9.6→10.1 ppm and 9.2→10.4 ppm for Ha and Hb, respectively. These changes in the amide resonance (Ha) were much larger than those observed with the *ortho* receptors **107** and **106**, and may thus suggest a different mode of binding occurs with receptor **108**.
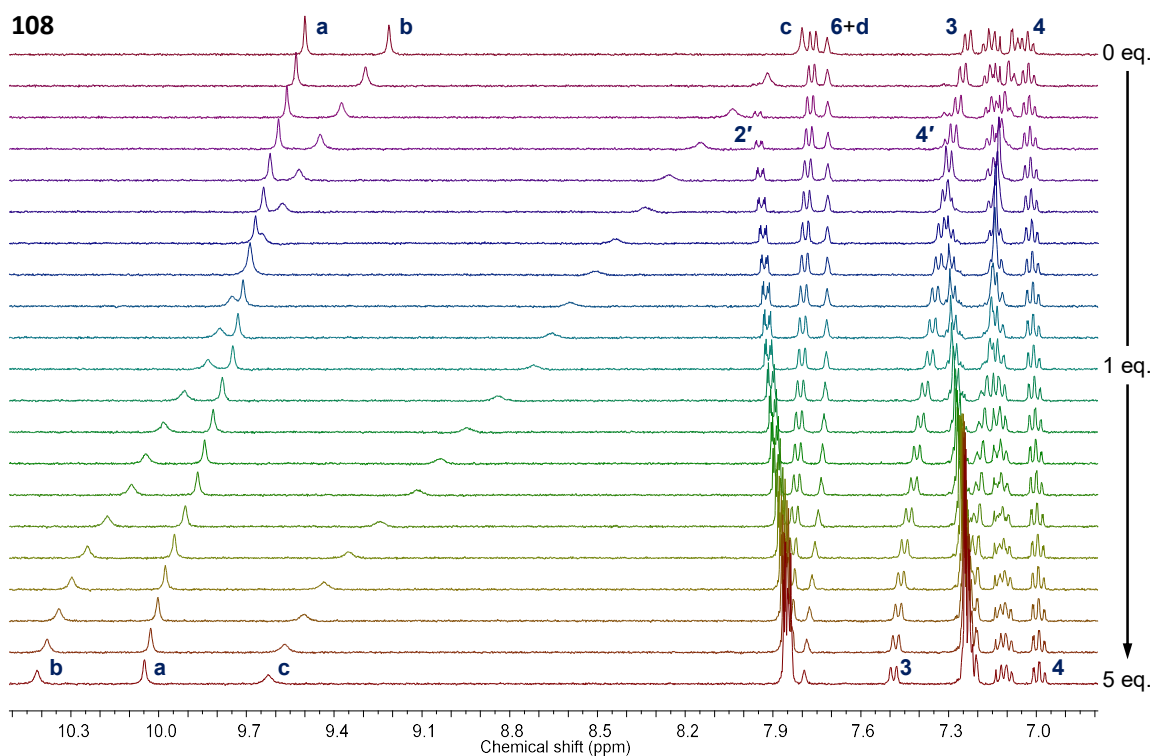
Figure 4.19. Stack plot of the individual $^1$H NMR spectra (400 MHz, DMSO-$d_6$, 6.8–10.5 ppm) from the titration of receptor **108** (0.7 mM) with TBAOBz (0→5 eq.).

The protons H2′ and H4′ became slightly more shielded over the course of the titration, with changes of 7.95→7.85 ppm and 7.32→7.24 ppm, respectively. The aromatic protons Hf, H3 and H6 all exhibited moderate deshielding over the course of the titration, Figure 4.20. Notably, these protons are all situated *ortho* to the urea and amide moieties, and this suggests a *syn* orientation of these protons relative to the magnetic anisotropy (deshielding)
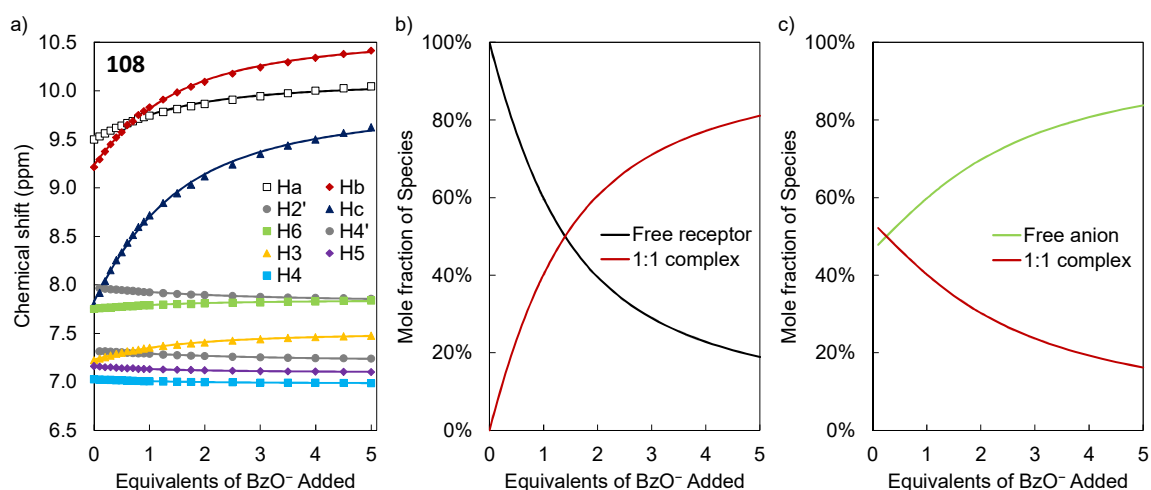


Figure 4.20. a) Binding fit for the titration of receptor **108** (0.7 mM) with TBA benzoate (0→5 eq.) in DMSO-$d_6$. b–c) Speciation distribution diagrams generated from the fitting of the experimental data. The concentrations are presented as mole-percentage values of each species relative to the sum of their concentrations.

cones of the carbonyl groups. The chemical shift of resonance Hd increased after the addition of approximately 1 eq. of BzO⁻. The remainder of the aromatic protons, He, H4 and H5 became more shielded. Resonances He and Hf overlapped significantly with other resonances for much of the titration, and were not fitted. Additionally, the changing shape of the peak envelopes due to the coupling behaviour made accurately following chemical shift of each resonance difficult. Fitting the data from all observed resonances except Hd–f afforded a value of $\log\beta_{1:1} = 3.22 \pm 0.01$, Table 4.2. The large changes in chemical shift of resonances Hb and Hc did not translate into a large 1:1 binding constant, as the curvatures of these changes are quite small, Figure 4.20a.[188] This binding constant is lower than that calculated for receptors **107** and **106**, see Table 4.2.

As **108** resembles receptors **96–99**, described in Chapter 2, fitting of the titration data to a combined 1:1, 1:2 host–guest binding model was attempted. This was also spurred by the observed inflection of the chemical shift of Hd after the addition of 1 eq. of anion. Unfortunately, no stable fit could be obtained by fitting the data to such a model, and all attempts at iteratively refining the individual binding constants failed.

Upon addition of 0→5 eq. of the $H_2PO_4^-$ salt to a solution of receptor **108**, significant changes in several resonances in the region 7–10 ppm were observed, with concomitant broadening and re-sharpening. Resonance Hc underwent significant deshielding
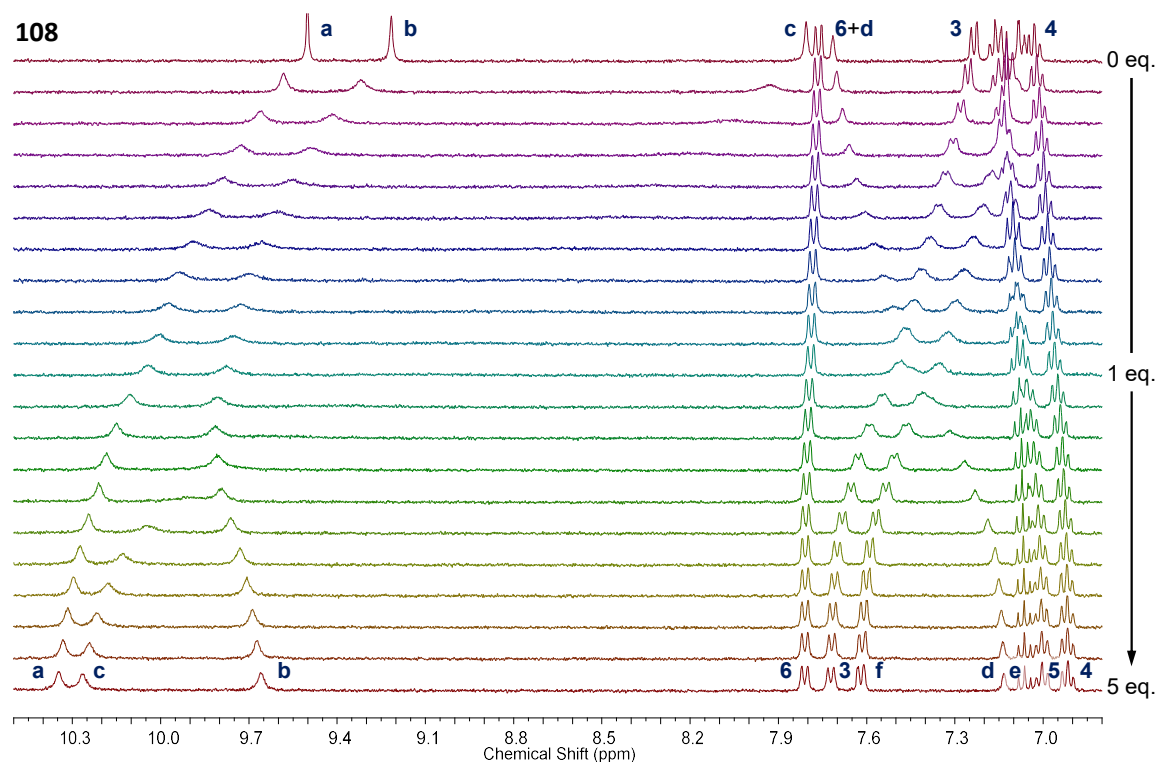


Figure 4.21. Stack plot of the individual ¹H NMR spectra (400 MHz, DMSO-*d₆*, 6.8–10.5 ppm) from the titration of receptor **108** (0.7 mM) with TBAH₂PO₄ (0→5 eq.).
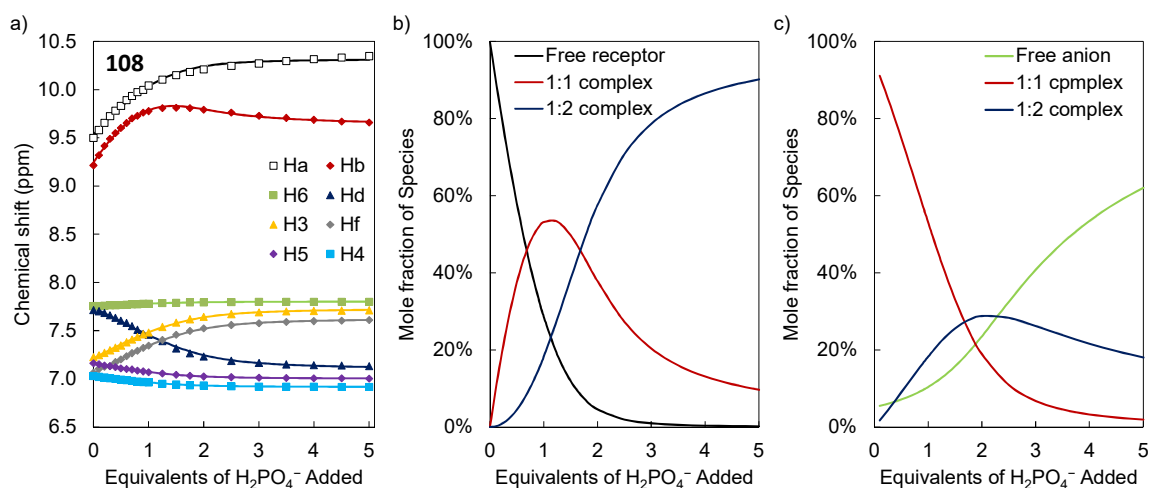
Figure 4.22. a) Binding fit for the titration of receptor **108** (0.7 mM) with TBAH$_2$PO$_4$ (0→5 eq.) in DMSO-$d_6$. b–c) Speciation distribution diagrams generated from the fitting of the experimental data. The concentrations are presented as mole-percentage values of each species relative to the sum of their concentrations.

(7.8→10.3 ppm), broadening into the baseline between 0.2 and 2.0 eq. of added anion. However, there is no evidence of slow or intermediate exchange kinetics in the changes in chemical shift. Resonances Hd, H3 and Hf each changed in chemical shift by ± 0.5 ppm, most likely due to a complexation-induced change in conformation.[204,213–215] A slight increase in chemical shift of H6, and a decrease for He, H4 and H5 were observed, Figure 4.21. The trends in chemical shift of resonances Ha and Hb are similar to those observed for the urea protons in Chapter 2, including the presence of a maximum at around 1 eq. These data, from all resonances except Hc, were fitted to a combined 1:1, 1:2 host–guest binding model, Figure 4.22. This afforded values of logβ$_{1:1}$ = 4.42 ± 0.12 and logβ$_{1:2}$ = 8.10 ± 0.07, Table 4.2. An approximate cooperativity constant of α = −0.1 ± 0.1 was calculated, which indicates non-cooperative or slightly anticooperative binding. This value of logβ$_{1:2}$ is quite large for NMR-based determination, and therefore further analysis will be required to confirm it.

Table 4.2. Cumulative logarithmic binding constants, logβ$_{1:1}$ and logβ$_{1:2}$, determined from the analysis of $^1$H NMR titrations in DMSO-$d_6$ at 25.0 °C.

| Receptor | Geometry | Chain length | H:G | logβ$_{H:G}$ BzO$^-$ | H$_2$PO$_4^-$ |
|----------|----------|--------------|-----|-----|-----|
| **106** | *ortho* | 7 | 1:1 | 3.70 ± 0.01 | 4.25 ± 0.05 |
| **107** | *ortho* | 11 | 1:1 | 3.64 ± 0.01 | 4.35 ± 0.07 |
| **108** | *meta* | 11 | 1:1 | 3.22 ± 0.01 | 4.42 ± 0.12 |
| | | | 1:2 | | 8.10 ± 0.07 |

Initial host concentration = 0.7 mM. Anions added as their TBA$^+$ salts. Reported values are from a single titration, associated error is the "standard deviation" parameter reported by HYPNMR2008.

The apparent complexation-induced shift of resonances Hd, H3 and Hf may provide valuable insights into the conformation of receptor **108** in the presence and absence of the $H_2PO_4^-$ anion. There are approximately $4 \times 10^3$ possible conformations (*syn/anti*) around the C−N bonds of **108**, but only some of them explain the observed differences in chemical shift upon binding. On the assumption that resonances Hd, H3 and Hf are in electronically equivalent positions on their respective phenylene rings, it is assumed that the initial orientation of Hd is *syn* to the anisotropy cone of the adjacent urea and the final orientation is *anti*, Figure 4.23. Conversely, resonances Hf and H3 are assumed to flip from *anti* to *syn* orientations relative to the urea and amide cones, respectively. By extension, resonance H6 is assumed to remain *syn* to the urea group. As a way to illustrate this, by representing *syn* as *0*, and *anti* as *1*, the conformation of the molecule as a whole can be written as a string of such binary values. This is merely to simplify the full description of the molecular
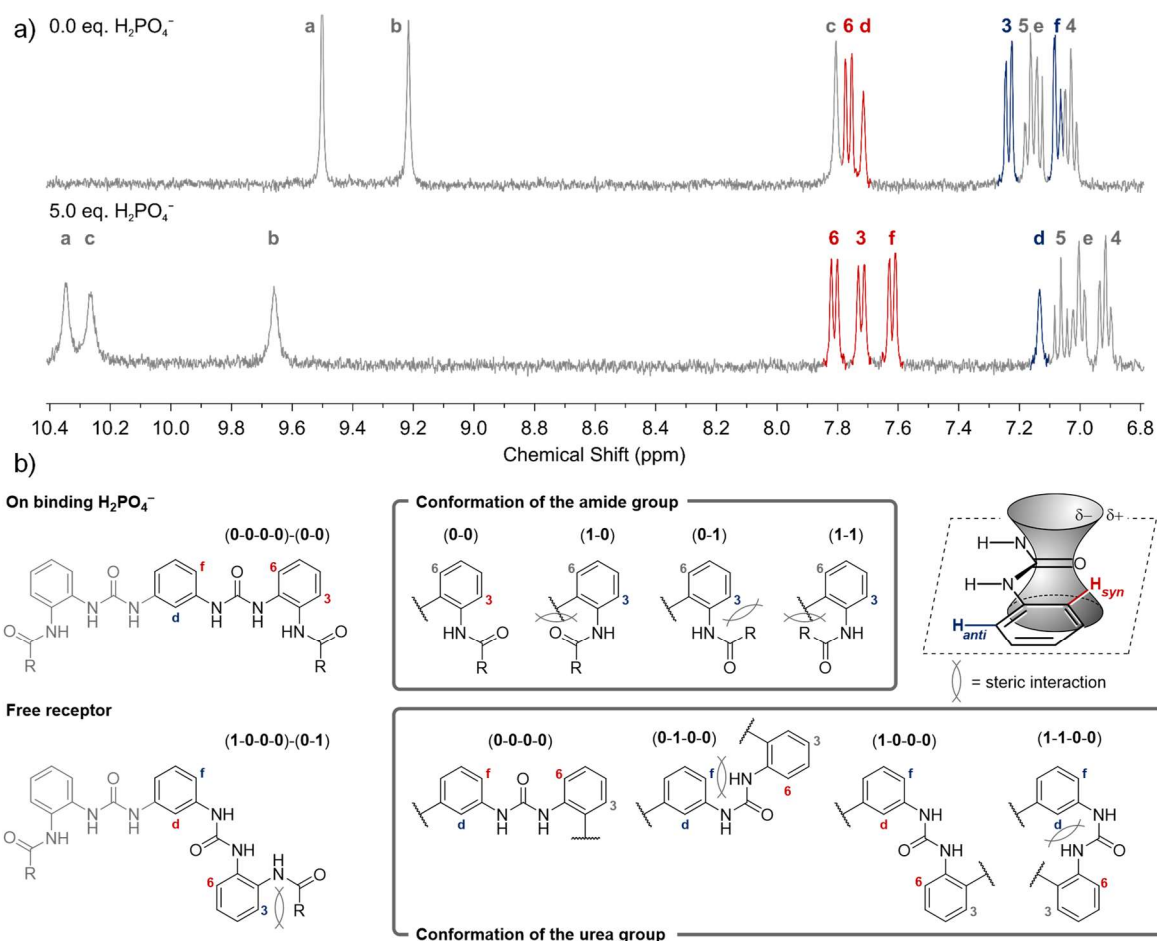


Figure 4.23. a) Endpoints of the 1H NMR titration (400 MHz, DMSO-d6, 6.8–10.4 ppm) of receptor **108** (7.0 mM) with TBAH₂PO₄ (0.0→5.0 eq.). Resonances Hd, Hf, H3 and H6 coloured red and blue according to whether they are above or below 7.4 ppm, respectively. b) Postulated changes in dominant conformation of receptor **108** in solution upon binding of the $H_2PO_4^-$ anion. Protons located within the anisotropy cone coloured red, protons not in the cone coloured blue. The numerical codes indicate which of the four bonds in the urea group, or which two in the amide group are rotated relative to the all-*syn* conformer.

conformation. For example, the all-*syn* conformer of **108** would be represented as (0-0-0-0)-(0-0), and matches the spectral information at 5.0 eq. $H_2PO_4^-$, Figure 4.23. An *anti* conformation at the centremost (first) and outermost (last) C−N bonds gives the conformer (1-0-0-0)-(0-1), which matches the observed spectral information for the free receptor. Note that there are other conformations of the amide group which would be expected to yield the same spectral data. Additionally, only one of the urea groups must adopt the *anti* conformation at the central C−N bond for Hd to become deshielded.

## 4.5   Conclusions and Future Work

The *H₆* hydrogen-bond donor molecules **106**–**108** were successfully synthesised, bearing $C_7$ and $C_{11}$ chains. Compounds **106** and **107** are members of the *ortho*-phenylene bis(2-amidophenylurea) class of receptors previously reported by the Gale and Leito groups.[182,210] Compound **108** is the *meta*-phenylene isomer of **107**, and is the first example of a new class of receptor. The synthesis of the *ortho*-phenylene bis(3-amidophenylurea) isomer **128** was hampered by the low-yielding, poorly selective synthesis of the dinitro precursor **134**. Various attempts to form macrocycles from the diamine **136** and the diamide **107** failed, most likely due to their low solubility in suitable solvents. The slightly more soluble $C_7$ chain compound **106** may be a more suitable substrate for RCM. Titrations of the $C_7$ and $C_{11}$ receptors **106**–**108** were performed in DMSO-$d_6$ with the $TBA^+$ salts of $H_2PO_4^-$ and $BzO^-$. Initial titrations with receptor **107** were performed at a host concentration of 7 mM, but a concentration of 0.7 mM was found to be more suitable for these hosts. As expected from the results obtained in Chapter 3, chain length had no observable effect on the anion binding properties of these receptors, and the 1:1 logarithmic binding affinities of **106** and **107** were equivalent. Values of $\log\beta_{1:1} \approx 3.7$ and 4.3 were obtained for $BzO^-$ and $H_2PO_4^-$, respectively, at a concentration of 0.7 mM (Table 4.2).

Titrations performed with the *meta*-phenylene isomer **108** showed a lower binding affinity ($\log\beta_{1:1} = 3.22 \pm 0.01$, Table 4.2) for $BzO^-$ on the basis of calculated 1:1 binding constants. Fitting of the data to a combined 1:1, 1:2 host–guest binding model was unsuccessful. Strong, non-cooperative 1:2 binding was observed with $H_2PO_4^-$, with values of $\log\beta_{1:1} = 4.42 \pm 0.12$ and $\log\beta_{1:2} = 8.10 \pm 0.07$ (Table 4.2). The binding affinities reported in Chapter 2 for the bisurea receptors **96**–**99** appear to be enhanced by the presence of the amide moieties *ortho* to the urea groups, but the cooperativity of the binding is lost. Further development of the *meta*-phenylene bis(phenylurea) motif to improve its phosphate-binding abilities and solubility could lead to high affinity phosphate and pyrophosphate transporters. This may be aided by a deeper understanding of the postulated complexation-induced shift
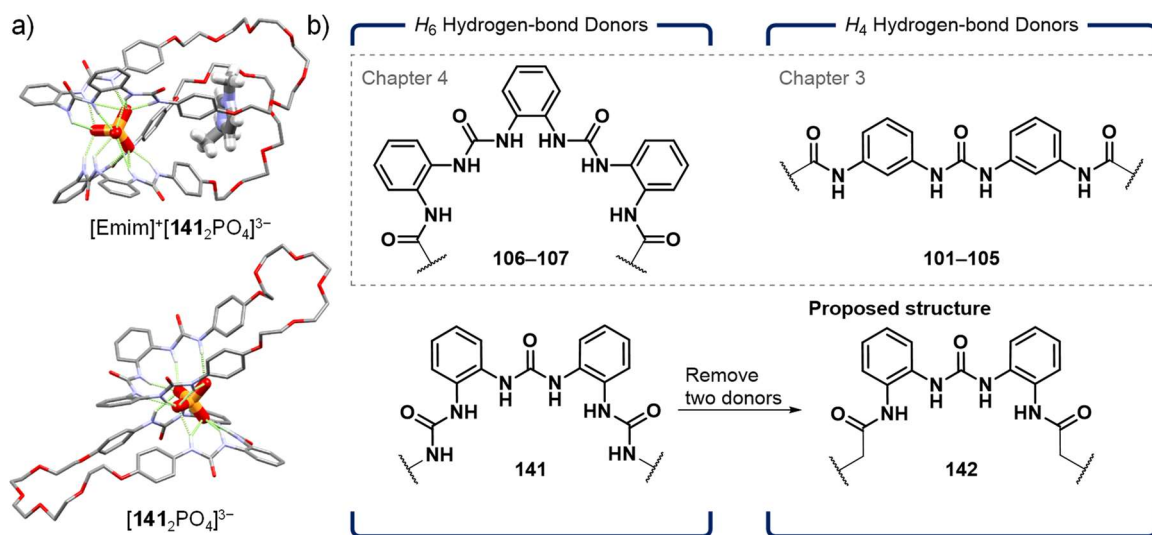
Figure 4.24. a) Crystal structures of 2:1 host–guest complexes of receptor **141** with PO₄³⁻, in the presence and absence of the Emim cation, showing the conical arrangement of the hydrogen-bond donors. b) The $H_6$ hydrogen-bond donors **106–108** presented in this chapter may also adopt such a conformation. The "overcrowding" may be mitigated by removing two of the NH moieties of **141** to create a di(amidophenyl)urea **142**. This is a geometric isomer of the core found in receptors **101–105** in the previous chapter.

of receptor **108** through more methodical studies. Computational modelling of the bound and free receptor, crystallisation studies, and UV-visible titrations may offer more insight. However, previous studies of simple urea-derived receptors in the group have shown that the changes in the UV-visible spectra are small, and not necessarily informative.

As mentioned elsewhere in this chapter, the $H_6$ hydrogen-bond donor receptor **141** reported by Ji *et al*. forms 2:1 host–guest sandwich complexes both in the solid state and in solution with phosphate anions.[212] The core of the receptor is puckered into a cone, and the anion sits 'over' the binding site, Figure 4.24a. It is entirely possible that the $H_6$ hydrogen-bond donor anion receptors **106–108** presented in this chapter behave in the same manner. Assuming that the anion adopts this binding conformation (instead of sitting within the macrocycle) due to the manner in which the puckered core forms a tight ring of hydrogen-bond donors, it is possible that removing two of the NH donors may 'open' the ring so as to allow the anion to sit within, Figure 4.24b. The resulting di(2-amidophenyl)urea receptors (**142**), as geometric isomers of receptors **101–105** in Chapter 3, would be readily synthesisable through amide coupling reactions. As these compounds are expected to be soluble in a broader range of solvents than the molecules presented in this chapter, RCM may be a simpler and more achievable task. Similarly, while [2]catenane systems may be accessible through the use of a PO₄³⁻ template to organise two molecules of **106** or **107** prior to RCM, the expected sandwich conformation (though not observed with H₂PO₄⁻ in this

work) of any 2:1 host–guest complex would not lead to a catenated product. Compound **142** may be able to arrange around the tetrahedral anion in a suitable manner.
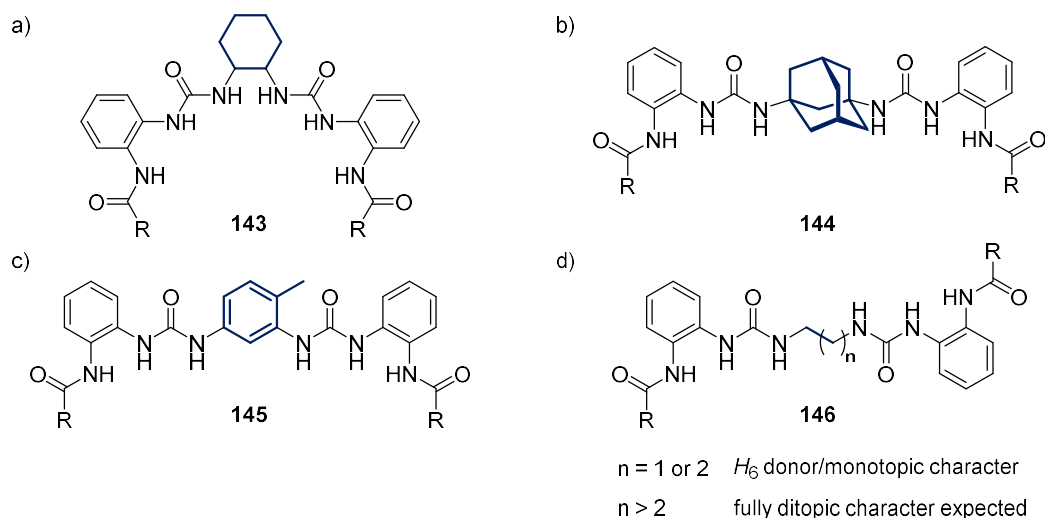


Figure 4.25. Compounds **143**–**146** were designed by replacing the central phenylene rings of receptors **106**–**108**with moieties intended to aid solubility and/or introduce molecular flexibility.

Another method of increasing solubility of these hydrogen-bond donors is to substitute the one of the aromatic rings for the cyclohexyl or adamantyl analogue, compounds **143** and **144** in Figure 4.25a,b. The (R,R) and (S,S) enantiomers of 1,2-cyclohexyl bis(4-nitrophenylurea) have been studied by Amendola *et al.*[189] The use of adamantane reflects the development of compounds **42**–**44** in the Introduction.[127] Alternatively, substitution of the central phenylene ring with a methyl group (compound **145** in Figure 4.25c) would induce deplanarisation of the molecule. Disrupting the structure of the binding site would lead to a lower affinity for anions, but the enhanced solubility would provide access to a greater variety of applications.[216] 2,4-Toluene diisocyanate is a widely used and readily available polyurethane feedstock, and thus its use would allow for more synthetic flexibility. Finally, replacement of the central ring by a two or three carbon chain would (**146**) allow a full range of molecular motion, while maintaining the close distance between the urea groups, Figure 4.25d. The similarity to Wu's bis(*ortho*-phenylene biurea) receptors (where R = NH−*p*-C₆H₅NO₂) suggests that such a molecule would instead bind a separate anionic species at each $H_3$ hydrogen-bond donor site.

# Chapter 5

# Conclusions

# Conclusions

In this work, four classes of urea- and amide-based hydrogen-binding receptors were studied. It is envisaged that interlocked systems can be created from such receptors in which both components are neutral, non-interacting molecules, but which form a strong and reversible association upon modulation of solution pH. The urea–carboxylate interaction is ideal for this purpose, but other forms of complementary anionic guests such as phosphate diesters exist. The hydrogen-bonding receptors presented in this work have thus been studied with a range of anions in order to understand their anion-binding behaviour more completely. The work presented in this thesis first studied the properties of the electron-donating and -withdrawing substituents on the distal phenylene rings in Chapter 2 and secondly, the effect of long chain hydrocarbons appended to the receptor core in Chapter 3, before combining this knowledge to design a new class of receptor in Chapter 4.

In Chapter 2, the anion binding affinities of the *meta*-phenylene bis(phenylurea) receptors **96**–**100** were quantified through $^1$H NMR titrations in DMSO-$d_6$. Cumulative logarithmic binding constants of approximately $\log\beta_{1:1} = 3.7$ and $\log\beta_{1:2} = 7.2$ for the $H_2PO_4^-$ anion were obtained through fitting of the titration data. Ranges of $\log\beta_{1:1} = 3.0$–$3.7$ and $\log\beta_{1:2} = 4.5$–$5.9$ were calculated for $AcO^-$ and $BzO^-$. The binding process for $H_2PO_4^-$ is cooperative, possibly as a result of phosphate-phosphate hydrogen bonding at the receptor. The 1:2 host–guest binding mode for $AcO^-$ and $BzO^-$ was found to be anticooperative, this was quantified using cooperativity constants, which are summarised in Table 2.6. As similar receptors have been reported in the literature with 1:1 host–guest binding constants, and as the presence of a 1:2 stoichiometry for the carboxylate guests was not immediately obvious, 1:1 binding constants were also calculated and reported. Values of $\log\beta_{1:1} = 2.3$–$2.4$ were calculated for the carboxylate anions, and lower constants were calculated for $Cl^-$, $HSO_4^-$ and $SO_4^{2-}$. These values are summarised in Table 2.5.

These titration studies were supplemented by two crystalline-phase adducts. In one of these adducts, compound **96** hydrogen-bonded to two $AcO^-$ anions, accompanied by a bridging water molecule. This is considered to be unrelated to the solution-state binding mode. A novel triple-stranded helicate was obtained with compound **97**, at the centre of which two phosphate anions form a $H_3P_2O_8^{3-}$ cluster. The relative simplicity of this helical structure and the possibility of utilising phosphate dimerization for cooperative binding makes this structure an interesting candidate for future studies.

In Chapter 3, two new di(3-aminophenyl)urea receptors **101** and **102** were synthesised as non-solvophobic controls for a study on the effect of aliphatic chain length. This was

prompted by preliminary data that suggested an associated increase in $SO_4^{2-}$ binding affinities with receptors **103**–**105**. Receptor **102** was titrated with $SO_4^{2-}$, $BzO^-$, $H_2PO_4^-$, $Cl^-$ and $NO_3^-$, while receptors **103** and **105** were titrated with $H_2PO_4^-$, $BzO^-$ and $SO_4^{2-}$. All receptors were titrated in DMSO-$d_6$, and the binding behaviour was compared to preliminary results reported by Boyle. All receptors studied showed binding affinities of $\log\beta_{1:1} \approx 3.0$ for $BzO^-$; non-cooperative binding for $H_2PO_4^-$, with ranges of $\log\beta_{1:1} = 2.8$–$3.2$ and $\log\beta_{1:2} = 5.0$–$5.4$; and small 1:1 binding constants for $SO_4^{2-}$. Thus it may be concluded that the presence or absence of 6–11 carbon chains has little to no effect on the binding of the anions tested to this motif, and may instead be used to help solubilise the receptor or to tether additional functionality.

In Chapter 4, the structural motifs studied in Chapters 2 and 3 were combined to create the *meta*-phenylene bis(2-amidophenylurea) receptor **108**. The *ortho* isomer of this motif has been partly studied by the Gale and Leito research groups. Two similar receptors from the latter class, **106** and **107**, were also studied. Attempts were made to synthesise macrocyclic derivatives of the latter motif, but these were not successful. Initial titrations on receptor **108** with $BzO^-$ and $H_2PO_4^-$ in DMSO-$d_6$ suggested that the receptor concentration of 7.0 mM was too high to yield accurate binding constants. Receptors **106**–**108** were thereafter titrated at a concentration of 0.7 mM. As expected, receptors **106** and **107** exhibited similar 1:1 host–guest binding constants of approximately $\log\beta_{1:1} = 3.7$ for $BzO^-$ and $\log\beta_{1:1} = 4.3$ for $H_2PO_4^-$.

Titrations performed with the *meta*-phenylene isomer **108** showed a lower binding affinity ($\log\beta_{1:1} = 3.22 \pm 0.01$) for $BzO^-$ on the basis of calculated 1:1 binding constants. Fitting of the data to a combined 1:1, 1:2 host–guest binding model was unsuccessful. Strong, but non-cooperative 1:2 binding was observed with $H_2PO_4^-$, with values of $\log\beta_{1:1} = 4.42 \pm 0.12$ and $\log\beta_{1:2} = 8.10 \pm 0.07$, accompanied by apparent complexation-induced shifts of several of the aromatic resonances. The binding affinity of the *meta*-phenylene bis(phenylurea) motif (Chapter 2) appeared to be enhanced by the presence of the amide moieties *ortho* to the urea groups, but the cooperativity of the binding observed with the simpler receptors is lost. Compound **108** is an interesting receptor for anions warranting further research.

# Chapter 6

# Experimental

## 6.1    General Experimental Methods

Water was purified to ISO3696 Type II specification using an Elga Veolia Purelab Option S7 water purifier. Tetra-*N*-butylammonium sulfate (TBA$_2$SO$_4$) was purchased as a 50% w/w aqueous solution and dried *in vacuo* while cycling between 77 K and room temperature. All other solvents and chemicals were purchased from commercial sources and used without further purification. Microwave-assisted reactions were carried out in a Biotage Initiator Eight EXP microwave reactor using sealed vials. Thin-layer chromatography (TLC) was carried out using MerckMillipore Kiesegel 60 F$_{254}$ silica plates and visualised under $\lambda_{ex}$ = 254 nm, by staining with an acidified solution of ninhydrinin in ethanol, or by staining in an iodine vapour chamber. Flash chromatography was carried out on a Teledyne Isco CombiFlash Rf 200 UV/Vis automated machine using pre-packed RediSep® cartridges.

Mass-spectrometry was carried out using HPLC grade solvents using electrospray mass spectrometry (ESI). High resolution ESI mass spectra were determined relative to a standard of leucine enkephalin. Infrared spectra were recorded on a Perkin Elmer Spectrum One FTIR spectrometer fitted with a universal ATR sampling accessory. Melting points were determined using an Electrothermal IA9100 digital melting point apparatus. Elemental analysis was either carried out by the UCD School of Chemistry Microanalytical Laboratory, University College Dublin, or by the Department of Chemistry, Maynooth University.

### 6.1.1   NMR spectroscopy

$^1$H NMR spectra were recorded at 400 MHz on a Bruker Avance III 400 NMR or Agilent 400-MR, or at 600 MHz on a Bruker Avance II 600 NMR. $^{13}$C NMR spectra were recorded at either 100.6 MHz or 150.9 MHz. All $^{13}$C NMR spectra were decoupled from $^1$H. Deuterated solvents used for NMR analysis (DMSO-$d_6$, D$_2$O, CDCl$_3$) were purchased from Apollo Scientific or Sigma Aldrich, and used as received. Chemical shifts are reported in ppm with the residual solvent as internal reference, while 2D spectra were graphically referenced. All NMR spectra were carried out at 25.0 °C unless otherwise stated.

#### 6.1.1.1    $^1$H NMR Titration Experiments

$^1$H NMR titration experiments were performed in DMSO-$d_6$ at 25.0 °C on a 400 MHz Bruker Avance III 400 NMR spectrometer. A Norrell 507-*HP* NMR tube was charged with 0.8 mL of a solution (7.0 mM or 0.7 mM) in DMSO-$d_6$ of the host being studied and the $^1$H NMR spectrum obtained (400 MHz). Sequential additions of a stock solution (0.28 M or 28 mM) in DMSO-$d_6$ of the appropriate TBA$^+$ salt were performed in 2–20 μL aliquots with a Gilson P20 pipette.

## 6.1.2 Single-crystal X-ray Crystallography

A summary of data collection and refinement parameters is presented in Table 2.7. All diffraction datasets were obtained using graphite-monochromated Mo Kα radiation (λ = 0.71073 Å) using a Bruker APEX-II DUO instrument with CCD detector, with samples mounted on Mitegen micromounts, coated in Paratone immersion oil and held at a temperature of 100K. The diffraction data were reduced and processed using the Bruker APEX suite of programs.[217] Multi-scan absorption corrections were applied using SADABS.[218] The data were solved using the Intrinsic Phasing routine in SHELXT and refined with full-matrix least squares procedures using SHELXL-2015 within the OLEX-2 GUI.[219–221] Non-hydrogen atoms were refined with anisotropic displacement parameters, while all hydrogen atoms were included in calculated positions with isotropic displacement parameters equal to 1.2 or 1.5 times the isotropic equivalent of their carrier atoms, unless involved in hydrogen bonding, in which case atoms were explicitly located from the Fourier residuals (where possible).

The crystallographic model obtained for compound **96**(TBAAcO)$_2$·3H$_2$O (CCDC 1840843) included significant disorder and was based on relatively poor quality diffraction data. The tetrabutylammonium cations and urea host molecule were modelled without restraints on position or anisotropic displacement parameters. Both of the two unique acetate anions were modelled at full occupancy, with isotropic approximations and/or rigid group approximations on the ADPs where necessary to prevent the emergence of non-positive definite U$_{ij}$ tensors. Slight positional disorder on one acetate anion was approximated by modelling one oxygen atom split over two nearby positions at 0.5:0.5 occupancy for each of the two parts O8 and O8A. Water molecules O9 and O10 were modelled at full occupancy with hydrogen atoms refined in riding positions. The remaining lattice water contribution was modelled split over three positions O11, O11A and O11B, with a total occupancy of one. No hydrogen atoms were modelled on these sites due to the low individual occupancies, however these atoms were included in the molecular formula to allow for correct calculation of absorption coefficient, density, etc., in the final refinement.

The asymmetric unit of compound **97**$_3$(TBA$_3$H$_3$P$_2$O$_8$)·0.5CHCl$_3$ (CCDC 1840844) contained minor disorder as described in the text which was modelled by fixing the lattice chloroform molecule to 0.5 occupancy, and modelling two orientations of the hydrogen atom attached to the central phosphate group, both refined as freely rotating groups (AFIX 147) with distance restraints between each hydrogen atom and corresponding hydrogen bond acceptor to maintain sensible geometries, and values of U$_{iso}$ fixed at 1.5 times that of the carrier atom.

### 6.1.3 X-Ray Powder Diffraction

X-ray powder diffraction patterns were recorded using a Bruker D2 Phaser instrument using Cu Kα radiation (1.54178 Å) and a Bruker LynxEye detector. Samples were finely ground and mounted on a silicon single crystal zero-background sample holder, and collected in the 2θ range 5–55° with constant rotation in φ of 1 revolution per minute at room temperature, and matched with simulated patterns calculated from the appropriate single-crystal data.
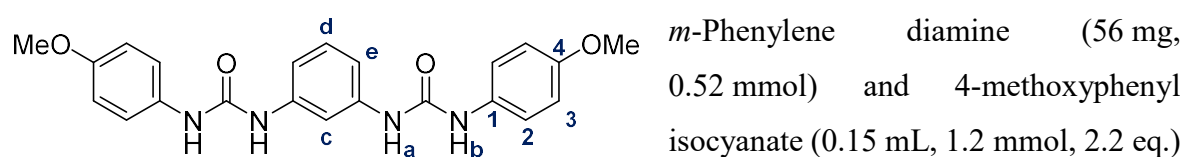
## 6.2 Synthesis of Compounds Presented in Chapter 2

Atoms are labelled according to the final/target compounds in their series, with the proton resonances of the core binding site in each receptor being labelled alphabetically (in order of decreasing chemical shift), and the remaining atoms labelled numerically. Thus, particular labels for atoms which are introduced through functional group interconversions may be missing from intermediates.

### 6.2.1 General synthetic procedure for ureas **96** and **97**

Compounds **96** and **97** were synthesised by grinding *m*-phenylene diamine with the corresponding commercially available methoxyphenyl isocyanate in a mortar and pestle at room temperature for 2 minutes. This resulted in the formation of a paste, from which the ureas were isolated by successive trituration with methanol, acetonitrile and diethyl ether, the products being separated from each solvent upon centrifugation, followed by drying *in vacuo*.

### 6.2.2 *meta*-Phenylene bis(4′-methoxyphenylurea) (**96**)



*m*-Phenylene diamine (56 mg, 0.52 mmol) and 4-methoxyphenyl isocyanate (0.15 mL, 1.2 mmol, 2.2 eq.) were ground together and CHCl$_3$ (5 mL) added as a solvent. The resulting white slurry was diluted with MeOH (10 mL), sonicated, separated by centrifugation and the process repeated with MeOH (5×10 mL) and MeCN (3×10 mL). Compound **96** was obtained as a white powder in 52% yield (110 mg, 2.7 mmol). mp 294 °C dec. HRMS–ESI (*m/z*): [M + H]$^+$ calcd for C$_{22}$H$_{23}$N$_4$O$_4$, 407.1714; found 407.1718. $^1$H NMR (600 MHz, DMSO-*d$_6$*, δ): 8.58 (s, 2H, NH, H**a**), 8.38 (s, 2H, NH, H**b**), 7.62 (t, *J* = 2.0 Hz, 1H, H**c**), 7.41–7.29 (m, 4H, H**2**), 7.14 (dd, *J* = 8.8, 7.2 Hz, 1H, H**d**), 7.04 (dd, *J* = 7.5, 2.0 Hz, 2H, H**e**), 6.93–6.80 (m, 4H, H**3**), 3.72 (s, 6H, CH$_3$). $^{13}$C NMR (151 MHz, DMSO-*d$_6$*, δ): 154.5 (quat., C**4**), 152.7 (quat., C=O), 140.3 (quat., C−N), 132.8 (quat., C−N, C**1**), 129.1 (C**d**), 120.0 (C**2**), 114.0 (C**3**), 111.5 (C**e**), 107.7 (C**c**), 55.2 (CH$_3$). FTIR (ATR, powder) v̄$_{max}$ (cm$^{-1}$): 3301 (m, N−H str.), 1638

(s, C=O str.), 1599 (m), 1560 (s, N−H vib.), 1510 (s), 1491 (s), 1403 (m), 1298 (m), 1218 (s, C−O str.), 1180 (m, N−C−N str.), 1108 (w), 1033 (m, C−O str.), 878 (w), 834 (m), 799 (m), 772 (m), 754 (m), 722 (m), 707 (m). Anal. calcd for $C_{22}H_{22}N_4O_4$: C, 65.01; H, 5.46; N, 13.78. Found: C, 64.96; H, 5.49; N, 13.83.

### 6.2.3 *meta*-Phenylene bis(3′-methoxyphenylurea) (**97**)
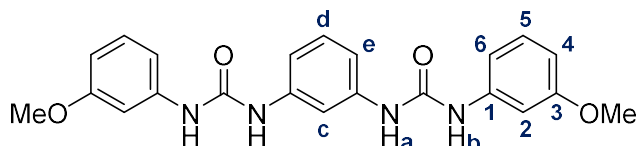


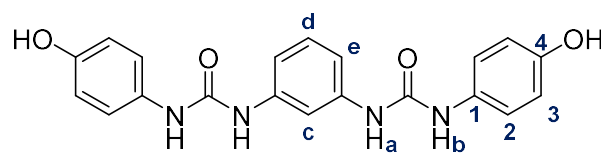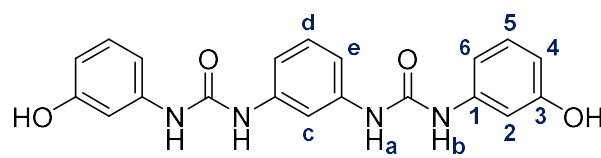An alternate synthesis and the complete characterization of compound **97** has been previously reported.[222] *m*-Phenylene diamine (53 mg, 0.49 mmol) and 3-methoxyphenyl isocyanate (0.15 mL, 1.1 mmol, 2.3 eq.) were ground together and CHCl$_3$ (5 mL) added as a solvent. The resulting white slurry was diluted with MeOH (10 mL), sonicated, separated by centrifugation and the process repeated with MeOH (5×10 mL) and MeCN (3×10 mL). Compound **97** was obtained as a white powder in 71% yield (141 mg, 0.35 mmol). mp 276 °C dec. (lit. 294–297 °C) HRMS–ESI (*m/z*): [M + H]$^+$ calcd for $C_{22}H_{23}N_4O_4$, 407.1714; found 407.1725. $^1$H NMR (400 MHz, DMSO-$d_6$, δ): 8.68 (s, 2H, NH, H**a**), 8.59 (s, 2H, NH, H**b**), 7.66 (t, $J$ = 1.8 Hz, 1H, H**c**), 7.23–7.12 (m, 5H, H**d**, H**5**, H**2**), 7.06 (dd, $J$ = 8.1, 1.5 Hz, 2H, H**e**), 6.91 (dd, $J$ = 8.0, 1.2 Hz, 2H, H**6**), 6.55 (dd, $J$ = 8.1, 2.2 Hz, 2H, H**4**), 3.73 (s, 6H, CH$_3$). $^{13}$C NMR (101 MHz, DMSO-$d_6$, δ): 159.8 (quat.), 152.4 (quat.), 141.0 (quat.), 140.1 (quat.), 129.6 (CH, C**5**), 129.2 (CH, C**d**), 111.8 (CH, C**e**), 110.5 (CH, C**6**), 107.9 (CH, C**c**), 107.3 (CH, C**4**), 103.9 (CH, C**2**), 55.0 (CH$_3$). FTIR (ATR, powder) $\bar{v}_{max}$ (cm$^{-1}$): 3274 (m, N−H str.), 1635 (s, C=O str.), 1600 (m), 1560 (s, N−H bend), 1490 (m), 1464 (m), 1402 (m), 1290 (m), 1269 (m), 1208 (m), 1167 (m, N−C−N str.), 1155 (m, N−C−N str.), 1080 (w), 1035 (m, C−O str.), 937 (w), 855 (m), 828 (w), 788 (m), 777 (m), 716 (m), 693 (m), 648 (s), 633 (s). Anal. Calcd for $C_{22}H_{22}N_4O_4$: C, 65.01; H, 5.46; N, 13.78. Found: C, 64.84; H, 5.33; N, 13.71.

### 6.2.4 General synthetic procedure for ureas **98**–**100**

Compounds **98**, **99** and **100** were produced by grinding or agitating commercially available 1,3-phenylene diisocyanate with an excess of the corresponding aminophenol in organic solvent (CHCl$_3$ or THF) at room temperature for 2 minutes (grinding) or 2 hours (agitation). The precipitated ureas were collected using vacuum filtration and washed with CHCl$_3$ and MeOH and dried *in vacuo*.

### 6.2.5   *meta*-Phenylene bis(4′-hydroxyphenylurea) (98)



1,3-Phenylene diisocyanate (501 mg, 3.13 mmol) and *p*-aminophenol (884 mg, 8.10 mg, 2.6 eq.) were added to $CHCl_3$ (8 mL) and agitated, the thick mixture was ground together, filtered, triturated in MeOH and filtered to obtain compound **98** as a brown solid in 58% yield (685 mg, 1.81 mmol). mp 240–250 °C dec. HRMS–ESI (*m/z*): $[M + H]^+$ Calcd for $C_{20}H_{19}N_4O_4$, 379.1406; found, 379.1404. $^1$H NMR (600 MHz, DMSO-*d₆*, δ): 9.06 (s, 2H, OH), 8.54 (s, 2H, NH, H**a**), 8.25 (s, 2H, NH, H**b**), 7.60 (s, 1H, H**c**), 7.21 (d, *J* = 8.8 Hz, 4H, H**2**), 7.17–7.09 (m, 1H, H**d**), 7.09–6.97 (m, 2H, H**e**), 6.68 (d, *J* = 8.8 Hz, 4H, H**3**). $^{13}$C NMR (101 MHz, DMSO-*d₆*, δ): 152.8 (quat.), 152.6 (quat.), 140.5 (quat., C−N), 131.2 (quat., C−N, C**1**), 129.1 (C**d**), 120.5 (C**2**), 115.3 (C**3**), 111.4 (C**e**), 107.6 (C**c**). FTIR (ATR, powder) $\bar{\nu}_{max}$ (cm$^{-1}$): 3300 (m, N−H str.), 1638 (s, C=O str.), 1601 (m), 1561 (s, NH), 1509 (s), 1492 (s), 1460 (m), 1406 (w), 1298 (m), 1213 (s, C−O str.), 878 (w), 838 (m), 808 (m), 780 (m), 754 (m), 730 (w).

### 6.2.6   *meta*-Phenylene bis(3′-hydroxyphenylurea) (99)



*m*-Aminophenol (712 mg, 6.53 mmol, 2.1 eq.) and 1,3-phenylene diisocyanate (501 mg, 3.13 mmol) were added to THF (15 mL) and agitated for 2 hours. The resulting suspension was filtered and the solid washed with THF. Compound **99** was obtained as an off-white solid and dried in air (587 mg, 1.55 mmol, 50% yield). mp *ca*. 250 °C dec. HRMS–ESI (*m/z*): $[M + Na]^+$ calcd for $C_{20}H_{18}N_4O_4Na$, 401.1226; found 401.1215. $^1$H NMR (400 MHz, DMSO-*d₆*, δ): 9.30 (s, 2H, OH), 8.61 (s, 2H, NH, H**a**), 8.48 (s, 2H, NH, H**b**), 7.66 (s, 1H, H**c**), 7.15 (t, *J* = 8.0 Hz, 1H, H**d**), 7.09–6.96 (m, 6H, H**e**, H**5**, H**2**), 6.78 (d, *J* = 8.1 Hz, 2H, H**6**), 6.36 (d, *J* = 8.1 Hz, 2H, H**4**). $^{13}$C NMR (101 MHz, DMSO-*d₆*, δ): 157.8 (quat.), 152.3 (quat.), 140.8 (quat.), 140.2 (quat.), 129.5 (C**5**), 129.1 (C**d**), 111.6 (C**e**), 109.0 (C**4**), 108.8 (C**6**), 107.7 (C**c**), 105.2 (C**2**). FTIR (ATR, powder) $\bar{\nu}_{max}$ (cm$^{-1}$): 3308 (m, N−H str.), 1647 (s, C=O str.), 1602 (m), 1560 (s, NH bend), 1489 (s), 1448 (m), 1407 (m), 1289 (m), 1218 (s, C−O str.), 1156 (s, N−C−N str.), 1049 (m, C−O str.), 947 (w), 883 (m), 855 (m), 836 (m), 787 (m), 748 (m), 731 (m), 686 (s).

### 6.2.7   *meta*-Phenylene bis(2′-methoxyphenylurea) (**100**)
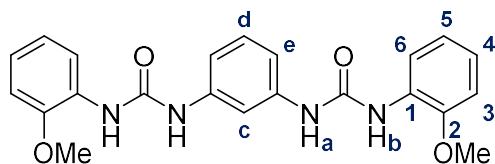


1,3-Phenylene diisocyanate (250 mg, 1.56 mmol) and *o*-anisidine (1.00 mL, 8.53 mmol, 5.5 eq.) were added to $CHCl_3$ (8 mL). A pale solid immediately formed and the resulting paste was stirred, filtered and washed with methanol to yield a white powder (308 mg, 0.757 mmol). The mother liquor was found to yield further product in crystalline form (66 mg, 0.16 mmol). Compound **100** was obtained in 58% yield overall (374 mg, 0.919 mmol). mp < 245 °C (powder) HRMS–ESI (*m/z*): $[M + H]^+$ calcd for $C_{22}H_{22}N_4O_4$, 407.1719; found 407.1721. $^1H$ NMR (400 MHz, DMSO-$d_6$, δ): 9.33 (s, 2H, NH**a**), 8.20 (s, 2H, NH**b**), 8.14 (dd, J = 7.8, 1.6 Hz, 2H, H**6**), 7.73 (t, J = 1.9 Hz, 1H, H**c**), 7.16 (t, J = 8.0 Hz, 1H, H**d**), 7.06 (dd, J = 8.0, 1.9 Hz, 2H, H**e**), 7.01 (dd, J = 8.0, 1.2 Hz, 2H, H**3**), 6.94 (ddd, J = 8.0, 7.7, 1.6 Hz, 2H, H**4**), 6.89 (ddd, J = 7.8, 7.7, 1.2 Hz, 2H, H**5**), 3.88 (s, 6H, $CH_3$). $^{13}C$ NMR (151 MHz, DMSO-$d_6$, δ): 152.3 (quat., C=O), 147.6 (quat., C**2**), 140.3 (quat., C−N), 129.2 (C**d**), 128.7 (quat., C**1**), 121.8 (C**4**), 120.6 (C**5**), 118.2 (C**6**), 111.4 (C**e**), 110.8 (C**3**), 107.4 (C**c**), 55.8 ($CH_3$). FTIR (ATR, powder) $\bar{v}_{max}$ ($cm^{-1}$): 3317 (m, N−H str.), 3036 (w), 2935 (w), 2836 (w), 1677 (w), 1646 (s, C=O str.), 1598 (s), 1560 (s, NH), 1540 (s), 1491 (m), 1459 (s), 1446 (m), 1435 (s), 1335 (m), 1315 (m), 1289 (m), 1251 (m), 1234 (s), 1216 (s, C−O str.), 1174 (m), 1118 (m, N−C−N str.), 1047 (m), 1026 (m, C−O), 1002 (w), 922 (w), 849 (w), 784 (m), 740 (s), 688 (s), 642 (m), 577 (m).

### 6.2.8   **96**(TBAOAc)$_2$·3H$_2$O

The 4′-methoxy substituted derivative **96** was dissolved in a boiling mix of $CHCl_3$ and EtOAc in the presence of excess $TBA^+$ $AcO^-$ and $H_2PO_4^-$. The solution was filtered while hot and small thin white crystals of **96**(TBAOAc)$_2$·3H$_2$O were obtained by slow evaporation of the solvent. This material was then recrystallized from MeCN to yield crystals of a higher quality.

### 6.2.9   **97**$_3$(TBA$_3$H$_3$P$_2$O$_8$)·0.5CHCl$_3$

The 3′-methoxy substituted derivative **97** was dissolved in a boiling mix of $CHCl_3$ and EtOAc in the presence of excess $TBA^+$ $AcO^-$ and $H_2PO_4^-$. The orange solution was filtered while hot and crystals of **97**$_3$(TBA$_3$H$_3$P$_2$O$_8$)·0.5CHCl$_3$ were obtained by slow evaporation of the solvent. FTIR (ATR, microcrystalline) $\bar{v}_{max}$ ($cm^{-1}$): 3286 (w), 3210 (w), 2961 (m), 2874 (w), 2065 (w), 1697 (m), 1612 (m), 1598 (s), 1546 (s), 1479 (s), 1451 (s), 1436 (m), 1401 (w), 1380 (w), 1324 (m), 1292 (s), 1285 (m), 1264 (w), 1207 (s), 1155 (s), 1040 (s), 994 (m), 969 (m), 952 (m), 925 (m), 859 (m), 828 (m), 775 (s), 754 (m), 736 (m), 689 (s), 663 (w).

## 6.3 Synthesis of Compounds Presented in Chapter 3

The syntheses of ureas **126** and **127**, and amides **103–105** has been previously reported by Boyle.[172] In some cases, minor changes have been made to these synthetic procedures.

### 6.3.1 Di(3-nitrophenyl)urea (**126**)
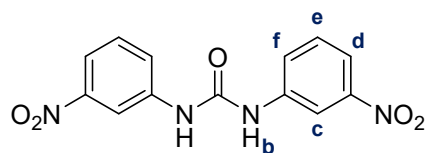
3-Nitrophenylisocyanate (253 mg, 1.54 mmol) 3-nitroaniline and (215 mg, 1.56 mmol, 1.0 eq.) were added to $CH_3CN$ (15 mL), and the reaction heated under microwave irradiation at 100 °C for 40 minutes. The solvent was removed under reduced pressure leaving a yellow solid. This was triturated with $CHCl_3$ and then filtered to give a light yellow solid in quantitative yield (464 mg, 1.54 mmol). mp 242–248 °C (lit.[172] 242–244 °C); HRMS–ESI (*m/z*): $[M + Na]^+$ calcd for $C_{13}H_{10}N_4NaO_5$, 325.0543; found 325.0548. $^1$H NMR (400 MHz, DMSO-*d*$_6$, δ): 9.41 (s, 2H, NH, H**b**), 8.56 (t, *J* = 2.2 Hz, 2H, H**c**), 7.86 (ddd, *J* = 8.2, 2.2, 0.9 Hz, 2H, H**d**), 7.78 (ddd, *J* = 8.2, 2.2, 0.9 Hz, 2H, H**f**), 7.59 (t, *J* = 8.2 Hz, 2H H**e**); $^{13}$C NMR (100 MHz, DMSO-*d*$_6$, δ) 152.4 (quat., C=O), 148.1 (quat., C−N), 140.6 (quat., C−N), 130.1 (CH), 124.7 (CH), 116.7 (CH), 112.5 (CH). FTIR (ATR) $\bar{v}_{max}$ (cm$^{-1}$): 3326 (w), 1659 (w), 1598 (w), 1553 (m), 1520 (m), 1433 (w), 1337 (s), 1284 (m), 1249 (m), 1222 (m), 1084 (w), 998 (w), 914 (w), 895 (m), 842 (w), 802 (s), 736 (s), 698 (s), 664 (m).

### 6.3.2 Di(3-aminophenyl)urea (**127**)
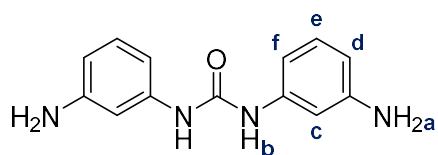
Compound **126** (108 mg, 0.357 mmol) was added to MeOH (10 mL each) across two batches. 10% w/w palladium on carbon (Pd/C, 45 mg, 0.043 mmol Pd, 12 mol% Pd) was added, followed by $N_2H_4·H_2O$ (0.10 μL, 2.0 mmol, 6 eq.) and the reaction heated under microwave irradiation at 100 °C for 40 mins. After filtering the reaction mixture through celite, removal of the solvent under reduced pressure, and further drying *in vacuo*, compound **127** was obtained as a white crystalline solid in 90% yield (78 mg, 0.32 mmol) (NB: compound is air-sensitive: solutions of this darken rapidly with exposure to air). mp 160 °C dec (lit.[172] 104–106 °C); HRMS–APCI (*m/z*): $[M + H]^+$ calcd for $C_{13}H_{15}N_4O$, 243.1240; found 243.1241. $^1$H NMR (600 MHz, DMSO-*d*$_6$, δ): 8.23 (s, 2H, NH, H**b**), 6.87 (t, *J* = 7.9 Hz, 2H, H**e**), 6.74 (t, *J* = 2.0 Hz, 2H, H**c**), 6.53 (ddd, *J* = 7.9, 2.0, 0.8 Hz, 2H, H**f**), 6.16 (ddd, *J* = 7.9, 2.0, 0.8 Hz, 2H, H**d**), 4.99 (s, 4H, NH$_2$, H**a**); FTIR (ATR) $\bar{v}_{max}$ (cm$^{-1}$): 3407 (w), 3273 (m), 3045 (w), 1925 (w), 1634 (s), 1608 (s), 1592 (s), 1543 (s),

1492 (s), 1455 (s), 1316 (m), 1288 (m), 1211 (s), 1159 (s), 1074 (m), 997 (m), 958 (w), 881 (m), 865 (m), 767 (s), 671 (s), 644 (s), 599 (s), 579 (s).

### 6.3.3 General synthetic procedure for amides **101** and **102**

The amides **101** and **102** were synthesised by stirring of diamine **127** in the neat carboxylic acid anhydride, with a catalytic quantity of pyridine (1 mol%) at room temperature for 20–24 hours.

### 6.3.4 Di(3-acetamidophenyl)urea (**101**)
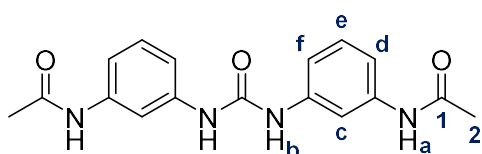


Compound **127** (43 mg, 0.18 mmol) was suspended in neat acetic anhydride (20 mL) at 0 °C. Pyridine (0.1 mL, 1 mol%) was added dropwise and the mixture warmed to room temperature with vigorous stirring over 24 h. Compound **101** was isolated as a grey powder by suction filtration in 93% yield (54 mg, 0.17 mmol). mp 280 °C dec; HRMS–APCI (*m/z*): [M + H]$^+$ calcd for $C_{17}H_{19}N_4O_3$, 327.1452; found 327.1454. $^1$H NMR (400 MHz, DMSO-$d_6$, δ): 9.90 (s, 2H, NH, H**a**), 8.61 (s, 2H, NH, H**b**), 7.76 (s, 2H, H**c**), 7.16 (m, 6H, H**d**–**f**), 2.03 (s, 6H, CH$_3$, H**a**). $^{13}$C NMR (151 MHz, DMSO-$d_6$, δ): 168.3 (C=O, C**1**), 152.3 (quat., C=O$_{urea}$), 140.0 (quat., C−N), 139.8 (quat., C−N), 128.9 (C**e**), 112.7 (C**f**), 112.6 (C**d**), 108.7 (C**c**), 24.0 (CH$_3$, C**2**). FTIR (ATR) $\bar{v}_{max}$ (cm$^{-1}$): 3299 (w), 1664 (m), 1639 (s), 1604 (s), 1553 (s), 1488 (w), 1450 (m), 1424 (m), 1371 (w), 1331 (w), 1308 (w), 1273 (w), 1230 (w), 1158 (w), 999 (w), 868 (w), 773 (m), 686 (m), 637 (w), 580 (w).

### 6.3.5 Di(3-propionamidophenyl)urea (**102**)
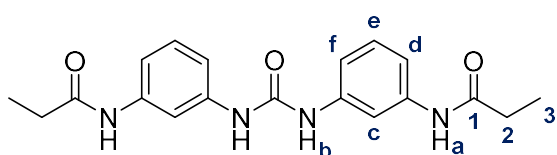


Compound **127** (34 mg, 0.14 mmol) was suspended in neat propionic anhydride (7 mL) at 0 °C. Pyridine (0.1 mL, 1 mol%) was added dropwise and the mixture warmed to room temperature with vigorous stirring over 20 h. Compound **102** was isolated as an off-white solid in 70% yield (41 mg, 0.12 mmol). mp 270 °C dec; HRMS–APCI (*m/z*): [M + H]$^+$ calcd for $C_{19}H_{23}N_4O_3$, 355.1765; found 355.1763. $^1$H NMR (400 MHz, DMSO-$d_6$, δ): 9.79 (s, 2H, NH, H**a**), 8.57 (s, 2H, NH, H**b**), 7.76 (s, 2H, H**c**), 7.21–7.04 (m, 6H, H**d**–**f**), 2.28 (q, *J* = 7.5 Hz, 4H, CH$_2$, H**2**), 1.04 (t, *J* = 7.5 Hz, 6H, CH$_3$, H**3**). $^{13}$C NMR (101 MHz, DMSO-$d_6$, δ): 172.1 (quat., C**1**), 152.3 (quat., C=O$_{urea}$), 140.0 (quat., C−N$_{urea}$), 139.8 (quat., C−N$_{amide}$), 129.0 (CH, C**e**), 112.8 (2 × CH, C**d** + C**f**), 108.9 (CH, C**c**), 29.6 (CH$_2$, C**2**), 9.8 (CH$_3$, C**3**). $^{15}$N (61 MHz, DMSO-$d_6$) 133 (N**a**), 108 (N**b**). FTIR (ATR) $\bar{v}_{max}$ (cm$^{-1}$): 3287 (w), 1655 (s), 1637 (s), 1608 (m), 1571 (m),

1543 (m), 1493 (m), 1405 (w), 1299 (w), 1219 (w), 1074 (w), 871 (w), 795 (w), 699 (m), 621 (m).

### 6.3.6 General synthetic procedure for amides **103**–**105**

Receptors **103**–**105** were synthesised *via* a coupling reaction between diamine **127** and the corresponding ω-alkenoic acid, using EDC·HCl as a coupling reagent and DMAP as base in dry $CH_2Cl_2$ cooled to 0 °C in an ice bath. Each receptor was isolated by evaporation of the solvent under reduced pressure, redissolution of the resulting oil with a small quantity of acetonitrile, precipitation with water, and separation by centrifugation. The product was purified by successive sonication of the solid in MeCN and MeOH, and separation from the supernatant by centrifugation

### 6.3.7 Di(3-(hex-5-enamido)phenyl)urea (**103**)
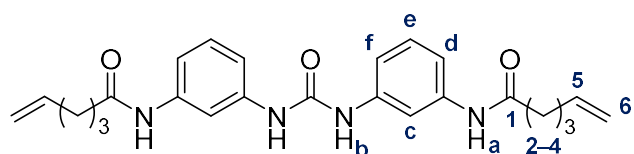


Dry $CH_2Cl_2$ (100 mL) was added to compound **127** (100 mg, 0.413 mmol) under an argon atmosphere and the mixture cooled to 0 °C in an ice bath. DMAP (143 mg, 1.17 mmol, 2.8 eq.), EDC·HCl (413 mg, 2.15 mmol, 5 eq.) and 5-hexenoic acid (0.12 mL, 1.0 mmol, 2.4 eq.) were added sequentially to the reaction mixture, flushing the flask with argon after each addition. The reaction mixture stirred at 0 °C for 1 hour, warmed to room temperature, and stirred for 4 days whereupon a white suspension had formed. The solvent was removed from the mixture under reduced pressure to form an orange oil, which was dissolved in MeCN (20 mL) and diluted with water (40 mL), which resulted in the formation of an off-white solid that was collected by centrifugation. Sonication in MeCN (2 × 20 mL) and centrifugation in afforded compound **103** as a white solid in 35% yield (62 mg, 0.14 mmol). mp 250–253 °C (lit.[172] 249–251 °C); HRMS–APCI (*m/z*): $[M + H]^+$ calcd for $C_{25}H_{31}N_4O_3$, 435.2391; found 435.2397. $^1H$ NMR (400 MHz, DMSO-$d_6$, δ): 9.85 (s, 2H, NH, H**a**), 8.60 (s, 2H, NH, H**b**), 7.80 (s, 2H, H**c**), 7.24–7.09 (m, 6H, H**d**–**f**), 5.83 (ddt, *J* = 16.9, 10.2, 6.6 Hz, 2H, H**5**), 5.04 (ddd, *J* = 17.1, 3.4, 1.6 Hz, 2H, H**6cis**), 4.98 (d, *J* = 10.2 Hz, 2H), 2.31 (t, *J* = 7.5 Hz, 4H, H**6trans**), 2.31 (t, *J* = 7.5 Hz, 4H, CH_2, H**2**), 2.07 (dt, *J* = 7.3 Hz, 4H, CH_2, H**4**), 1.74–1.61 (m, 4H, CH_2, H**3**); $^{13}C$ NMR (151 MHz, DMSO-$d_6$, δ): 171.0 (quat., C**1**), 152.2 (quat., C=O_urea), 139.9 (quat., C−N_urea), 139.8 (quat., C−N_amide), 138.3 (CH, C**5**), 128.9 (CH, C**e**), 115.2 (CH_2 , C**6**), 112.7 (2 × CH, C**d** + C**f**), 108.8 (CH, C**c**), 35.8 (CH_2, C**2**), 32.7 (CH_2, C**4**), 24.3 (CH_2, C**3**); $^{15}N$ NMR (61 MHz, DMSO-$d_6$, δ): 133.7 (NH, N**a**), 108.7 (NH, N**b**); FTIR (ATR) $\bar{v}_{max}$ (cm$^{-1}$): 3265 (w), 1653 (s), 1637 (s), 1607 (w), 1567 (m), 1542 (m), 1493 (w), 1403 (w), 1297 (w), 1205 (w), 911 (w), 884 (w), 796 (w), 694 (w), 607 (w).

## 6.3.8   Di(3-(hept-6-enamido)phenyl)urea (**104**)
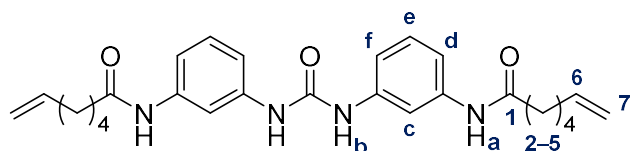


Compound **127** (36 mg, 0.062 mmol) was suspended in dry $CH_2Cl_2$ (30 mL) and cooled to 0 °C. DMAP (52 mg, 0.43 mmol, 3 eq.), EDC·HCl (157 mg, 0.82 mmol, 6 eq.) and 6-heptenoic acid (0.05 mL, 0.37 mmol, 2.5 eq.) were added and the reaction mixture stirred for 2 hrs, warmed to ambient temperature, and stirred for 5 days. The reaction mixture was concentrated to a yellow oil, dried in vacuo, and the product precipitated by the addition of MeOH (10 mL), followed by water (20 mL). The solids were separated by centrifugation and the remaining solvents removed by evaporation under reduced pressure. The impure product was then triturated twice with MeCN (2 × 10 mL) to yield the pure product as an off-white solid in 28% yield (19 mg, 0.041 mmol). (lit.[172] 239–241 °C); HRMS–APCI (*m/z*): $[M + H]^+$ calcd $C_{27}H_{35}N_4O_3$, 463.2704; found 463.2701. $^1H$ NMR (400 MHz, DMSO-$d_6$, δ): 9.83 (s, 2H, NH, H**a**), 8.62 (s, 2H, NH, H**b**), 7.80 (s, 2H, H**c**), 7.25–7.07 (m, 6H, H**d**–**f**), 5.81 (ddt, *J* = 17.0, 10.2, 6.8 Hz, 2H, H**6**), 5.02 (d, *J* = 17.0 Hz, 4H, H**7**$_{cis}$), 4.96 (d, *J* = 10.2 Hz, 2H, H**7**$_{trans}$), 2.30 (t, *J* = 7.6 Hz, 4H, CH$_2$, H**2**, *J* = 7.4 Hz), 2.05 (q, *J* = 7.1 Hz, 4H, CH$_2$, H**5**), 1.60 (app p, *J* = 7.5 Hz, 4H, CH$_2$, H**3**), 1.39 (app p, *J* = 7.5 Hz, 4H, CH$_2$, H**4**); FTIR (ATR) $\bar{v}_{max}$ (cm$^{-1}$): 3270 (w), 2932 (w), 1655 (s), 1638 (s), 1608 (w), 1566 (m), 1544 (m), 1494 (w), 1403 (w), 1297 (w), 1227 (w), 1201 (w), 991 (w), 912 (w), 884 (w), 797 (w), 714 (w), 603 (w).

## 6.3.9   Di(3-(undec-10-enamido)phenyl)urea (**105**)
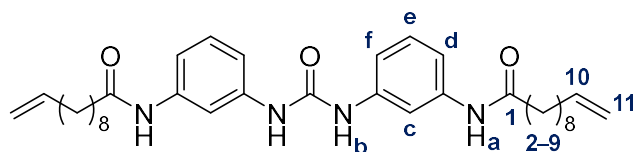


Compound **127** (85 mg, 0.35 mmol) was suspended in dry $CH_2Cl_2$ (10 mL) and cooled to 0 °C in an ice bath. EDC·HCl (336 mg, 1.75 mmol, 5 eq.), DMAP (107 mg, 0.876 mmol, 2.5 eq.) and 10-undecenoic acid (150 mg, 0.814 mmol, 2.3 eq.) were added and the reaction mixture stirred for 2 h, warmed to ambient temperature and stirred for 7 days. The reaction mixture was concentrated and redissolved in MeOH. A white precipitate was separated by centrifugation and filtration, and washed with water. Compound **105** was obtained as a white solid in 88% yield (178 mg, 0.310 mmol). mp 225–228 °C (lit.[172] 209–211 °C); HRMS–APCI (*m/z*): $[M + H]^+$ calcd for $C_{35}H_{51}N_4O_3$, 575.3956; found 575.3959. $^1H$ NMR (400 MHz, DMSO-$d_6$, δ): 9.82 (s, 2H, NH, H**a**), 8.59 (s, 2H, NH, H**b**), 7.80 (s, 2H, H**c**), 7.24–7.08 (m, 6H, H**d**–**f**), 5.78 (ddt, *J* = 16.9, 10.2, 6.7 Hz, 2H, H**10**), 4.99 (ddd, *J* = 17.2, 3.7, 1.6 Hz, 4H, H**11**$_{cis}$), 4.92 (ddt, *J* = 10.2, 2.2, 1.2 Hz, 2H, H**11**$_{trans}$), 2.28 (t, *J* = 7.4 Hz, 4H, CH$_2$, H**2**, *J* = 7.4 Hz),

2.00 (q, $J$ = 6.9 Hz, 4H, CH$_2$, H**9**), 1.65–1.50 (m, 4H, CH$_2$, H**3**), 1.41–1.18 (m, 20H, CH$_2$, H**4**–**8**); $^{13}$C NMR (151 MHz, DMSO-$d_6$, δ): 171.3 (quat., C**1**), 152.3 (quat., C=O$_{urea}$), 139.9 (quat., C−N), 139.8 quat., C−N), 138.8 (CH$_2$, C**10**), 128.9 (CH, C**e**), 114.6 (CH$_2$, C**11**), 112.7 (2×CH, C**d** + C**f**), 108.8 (CH, C**c**), 36.4 (CH$_2$, C**2**), 33.2 (CH$_2$, C**9**), 28.8 (CH$_2$, C**8**), 28.7 (2×CH$_2$), 28.5 (CH$_2$), 28.2 (CH$_2$), 25.2 (CH$_2$, C**3**); $^{15}$N (61 MHz, DMSO-$d_6$) 133 (N**a**), 108 (N**b**).; FTIR (ATR) $\bar{v}_{max}$ (cm$^{-1}$): 3278 (m), 2918 (m), 2849 (w), 1655 (s), 1636 (s), 1609 (m), 1572 (s), 1544 (s), 1494 (s), 1467 (w), 1406 (w), 1380 (w), 1300 (w), 1217 (w), 1194 (w), 1084 (w), 972 (w), 912 (w), 886 (w), 874 (w), 786 (w), 720 (w), 692 (m), 622 (m).

## 6.4 Synthesis of Compounds Presented in Chapter 4

### 6.4.1 General synthetic procedure for nitroaromatic compounds **132** and **133**

The H$_6$ donor precursors **132** and **133** were synthesised from *meta*- or *ortho*-phenylene diamine, respectively, and 2-nitrophenyl isocyanate (2.3 eq.). The diamine and isocyanate were ground together in a mortar to form a fine powder, with further grinding after the addition of chloroform (10 mL), the thick yellow suspensions were then filtered under suction, and washed with chloroform (20 mL) and diethyl ether (10 mL) to yield the desired phenylene bis(nitrophenylurea) as a bright yellow solid.

### 6.4.2 *meta*-Phenylene bis(2′-nitrophenylurea) (**132**)
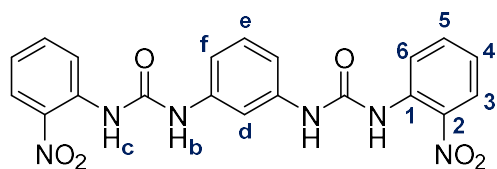


*m*-Phenylene diamine (176 mg, 1.63 mmol) and 2-nitrophenyl isocyanate (566 mg, 3.45 mmol, 2.1 eq.) were ground together in a mortar to give a fine powder. CH$_2$Cl$_2$ (5 mL) was added and the mixture ground for two minutes. The orange paste was filtered under suction, washed with CH$_2$Cl$_2$ (40 mL), and MeOH (10 mL), and the impure product sonicated in MeOH (30 mL) and triturated overnight. The suspension was filtered under suction and the residual solids sonicated in MeOH (50 mL total) and filtered. The collected solids were washed with Et$_2$O (20 mL) to yield compound **132** as a bright yellow solid in 88% (623 mg, 1.43 mmol) yield. mp 245 °C dec; HRMS–APCI (*m/z*): [M + H]$^+$ calcd for C$_{20}$H$_{17}$N$_6$O$_6$, 437.1204; found 437.1213. $^1$H NMR (600 MHz, DMSO-$d_6$, δ): 9.88 (s, 2H, H**b**), 9.58 (s, 2H**c**), 8.31 (d, $J$ = 8.4 Hz, 2H, H**6**), 8.10 (d, $J$ = 8.4 Hz, 2H, H**3**), 7.81 (s, 1H, H**d**), 7.70 (t, $J$ = 7.8 Hz, 2H, H**5**), 7.25–7.19 (m, 3H, H**e**+H**4**), 7.15 (d, $J$ = 8.4 Hz, 2H, H**f**). $^{13}$C NMR (151 MHz, DMSO-$d_6$, δ): 151.7 (quat., C=O), 139.7 (quat., C−N), 137.7 (quat., C**2**), 135.0 (CH, C**5**), 134.9 (quat., C**1**), 129.2 (CH, C**e**), 125.4 (CH, C**3**), 122.5 (CH, C**6**), 122.3 (CH, C**4**), 112.7 (CH, C**f**), 108.6 (CH, C**d**). FTIR (ATR) $\bar{v}_{max}$ (cm$^{-1}$): 3373 (w), 3330 (w), 3300 (w), 3089 (w), 1727

(w), 1655 (m), 1607 (m), 1584 (m), 1552 (m), 1483 (s), 1417 (s), 1327 (s), 1284 (s), 1263 (s), 1246 (s), 1218 (m), 1195 (s), 1142 (s), 1083 (m), 1042 (m), 999 (w), 963 (w), 893 (w), 873 (m), 858 (m), 808 (w), 773 (m), 746 (s), 683 (s), 630 (s), 599 (s).

### 6.4.3   *ortho*-Phenylene bis(2′-nitrophenylurea) (**133**)
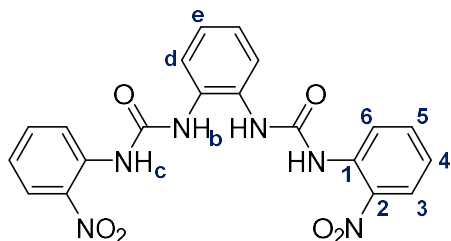


*o*-Phenylene diamine (200 mg, 1.9 mmol) and 2-nitrophenyl isocyanate (660 mg, 4.0 mmol, 2.2 eq.) were ground together to form a powder in a mortar. $CH_2Cl_2$ (10 mL) was added and the mixture ground for a further 5 minutes. The bright yellow paste was filtered under suction, washed with $CH_2Cl_2$ (40 mL) and $Et_2O$ (10 mL) to yield compound **133** as a pale yellow coloured solid in 81% (660 mg, 1.70 mmol) yield. mp 222–223 °C (lit.[182] 220.7 °C); HRMS–APCI (*m/z*): [M + H]$^+$ calcd for $C_{20}H_{17}N_6O_6$, 437.1204; found 437.1195. $^1$H NMR (400 MHz, DMSO-$d_6$, δ): 9.73 (s, 2H, NH), 9.16 (s, 2H, NH), 8.24 (dd, *J* = 8.5, 0.8 Hz, 2H), 8.07 (dd, *J* = 8.4, 1.5 Hz, 2H), 7.69 (ddd, *J* = 8.6, 7.4, 1.5 Hz, 2H), 7.65–7.55 (m, 2H), 7.26–7.18 (m, 2H), 7.18–7.09 (m, 2H). $^{13}$C NMR (101 MHz, DMSO-$d_6$, δ): 152.6 (quat.), 138.1 (quat.), 134.8 (quat.), 134.6 (quat.), 130.9 (CH), 125.3 (CH), 124.6 (CH), 124.5 (CH), 122.9 (CH), 122.4 (CH). FTIR (ATR) $\bar{\nu}_{max}$ (cm$^{-1}$): 3274 (w), 1709 (w), 1648 (s), 1608 (m), 1581 (m), 1492 (s), 1452 (s), 1437 (s), 1337 (s), 1323 (s), 1277 (s), 1205 (s), 1164 (m), 1151 (s), 1087 (m), 1034 (m), 956 (w), 896 (w), 858 (m), 783 (w), 732 (s), 685 (s), 672 (s), 627 (m).

### 6.4.4   General synthetic procedure for anilines **135** and **136**

The dinitro compounds **132** and **133** were then reduced with hydrazine monohydrate (6 eq.) and palladium on carbon (10 mol%) under microwave irradiation to yield the diamino products **135** and **136**. Purification was achieved by first filtering the reaction mixture through celite to remove unreacted starting material and hydrazine, leaving a mixture of the palladium catalyst and product atop the celite plug. This product-containing layer was removed, and the product dissolved in the minimum quantity of DMF. The DMF mixture was then filtered through the same celite plug and washed with small amounts of DMF to yield a pale yellow filtrate. The product was then precipitated slowly from the filtrate by the addition of water. Allowing the mixture to sit overnight, the compound precipitated as a flocculate or weak gel, which was diluted with more water and then filtered under suction to yield the product as a white fibrous solid

### 6.4.5   *meta*-Phenylene bis(2′-aminophenylurea) (**135**)
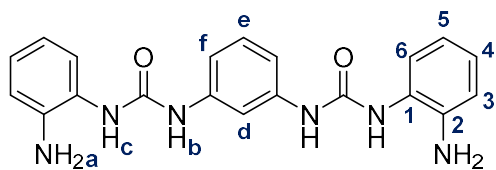
Compound **132** (406 mg, 0.93 mmol in total) and 10% w/w palladium on carbon (Pd/C, 62 mg, 0.06 mmol Pd, in total; 6 mol% Pd) were sonicated together in MeOH to give a fine suspension, across two batches. Hydrazine monohydrate (H₂NNH₂·H₂O, 0.20 mL, 4.2 mmol in total; 4.4 eq.) was added, along with methanol (total volume 10 mL, each), and the reaction mixture sealed and heated to 100 °C under microwave irradiation for 40 minutes. The ash-grey reaction mixture was vacuum filtered through a pad of celite and washed with MeOH (30 mL). The product containing layer was then redissolved in the minimum quantity of DMF (40 mL) and filtered through the celite to give a pale yellow solution. The solvent was removed by evaporation under reduced pressure, and the product precipitated by the addition of water (50 mL), and subsequent sonication. Compound **135** was collected by vacuum filtration and dried *in vacuo* to give a brittle white solid in 77% yield (270 mg, 0.717 mmol). mp 228 °C dec; HRMS–ESI (*m/z*): [M + Na]$^+$ calcd for $C_{20}H_{20}N_6NaO_2$, 399.1540; found 399.1550. $^1$H NMR (400 MHz, DMSO-$d_6$, δ): 8.77 (s, 2H, NH, H**b**), 7.67 (s, 2H, NH, H**c**), 7.62 (t, *J* = 1.9 Hz, 1H, H**d**), 7.35 (dd, *J* = 7.9, 1.4 Hz, 2H, H**6**), 7.14 (dd, *J* = 9.0, 6.9 Hz, 1H, H**e**), 7.09–7.02 (m, 2H, H**f**), 6.88–6.79 (m, 2H, H**4**), 6.74 (dd, *J* = 7.9, 1.5 Hz, 2H, H**3**), 6.57 (td, *J* = 7.8, 1.5 Hz, 2H, H**5**), 4.77 (s, 4H, NH₂, H**a**). $^{13}$C NMR (151 MHz, DMSO-$d_6$, δ): 153.0 (quat., C=O), 140.7 (quat., C**2**), 140.5 (quat., C−N), 129.0 (C**e**), 124.8 (quat., C**1**), 124.3 (C**4**), 123.5 (C**6**), 116.8 (C**5**), 115.9 (C**3**), 111.2 (C**f**), 107.3 (C**d**). FTIR (ATR) $\bar{v}_{max}$ (cm$^{-1}$): 3462 (w), 3371 (w), 3283 (m), 1635 (s), 1601 (m), 1586 (m), 1552 (s), 1504 (m), 1491 (s), 1451 (m), 1409 (m), 1309 (m), 1295 (m), 1248 (m), 1220 (m), 1184 (m), 1153 (m), 1138 (m), 1055 (w), 964 (w), 935 (w), 905 (w), 880 (w), 826 (w), 779 (m), 741 (s), 713 (m), 688 (m), 655 (s), 636 (s).

### 6.4.6   *ortho*-Phenylene bis(2′-aminophenylurea) (**136**)
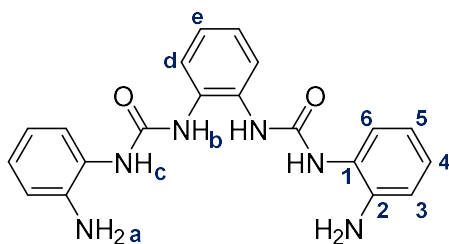
Compound **133** (416 mg, 0.953 mmol in total), 10% w/w palladium on carbon (Pd/C, 36 mg, 0.034 mmol Pd, in total; 4 mol% Pd) were added to methanol (total volume 10 mL, each) along with hydrazine monohydrate (H₂NNH₂·H₂O, 0.20 mL, 4.2 mmol, in total; 4 eq.), across two batches. The reaction vials were sealed and heated to 100 °C under microwave irradiation for 40 minutes. The green-grey reaction mixture was vacuum filtered through a pad of celite and washed with MeOH (20 mL). The product containing layer was

then redissolved in DMF (25 mL) and filtered through the celite to give a pale yellow solution. The product precipitated from this solution overnight after by the gradual addition of water (30 mL). This suspension was diluted with water (20 mL) and compound **136** was collected by vacuum filtration and dried *in vacuo* to give a white fibrous solid in 47% yield (169 mg, 0.449 mmol). mp 249 °C, 307 °C dec (lit.[182] 317.2 °C) HRMS–APCI (*m/z*): [M + H]$^+$ calcd for C$_{20}$H$_{21}$N$_6$O$_2$, 377.1721; found 377.1727. $^1$H NMR (400 MHz, DMSO-$d_6$, δ): 8.15 (s, 2H, NH), 8.11 (s, 2H, NH), 7.56 (dt, *J* = 9.6, 3.7 Hz, 2H), 7.32 (dd, *J* = 8.0, 1.0 Hz, 2H), 7.05 (dt, *J* = 9.6, 3.7 Hz, 2H), 6.84 (td, *J* = 7.9, 1.4 Hz, 1H), 6.73 (dd, *J* = 7.9, 1.3 Hz, 2H), 6.56 (td, *J* = 7.8, 1.3 Hz, 2H), 4.81 (s, 4H, NH$_2$). $^{13}$C NMR (101 MHz, DMSO-$d_6$, δ): 153.8 (quat.), 141.1 (quat.), 131.4 (quat.), 124.6 (2 × CH), 124.1 (CH), 123.9 (CH), 123.7 (CH), 116.7 (CH), 115.8 (CH). FTIR (ATR) $\bar{v}_{max}$ (cm$^{-1}$): 3463 (w, N−H str.), 3367 (w), 3302 (w), 3229 (w), 3037 (w), 1683 (w), 1632 (m), 1601 (s), 1562 (s), 1528 (m), 1498 (m), 1479 (m), 1457 (m), 1301 (m), 1228 (m), 1202 (w), 1158 (w), 1130 (w), 1107 (w), 1053 (w), 1027 (w), 942 (w), 899 (w), 836 (w), 749 (s), 691 (m), 650 (m), 633 (m), 581 (m), 572 (m), 555 (m).

## 6.4.7   General synthetic procedure for amides **106**–**108**

The C$_7$-chain receptor **106**, and the C$_{11}$-chain receptors **107** and **108** were synthesised *via* amide coupling reactions of 6-heptenoic acid and 10-undecenoic acid, respectively, with diamine intermediates **132** or **136**. EDC·HCl (5 eq.) and DMAP (2.6 eq.) were used as coupling reagent and base in dry CH$_2$Cl$_2$ (10 mL) at 0 °C. After 3–6 days, the reaction mixture was concentrated under reduced pressure, and dried *in vacuo*. The resulting oils were dissolved in a small amount of acetonitrile (< 5 mL) and the product precipitated with water (10 mL). The solids were separated by centrifugation and washed with water, acetonitrile, and methanol before being dried *in vacuo*.

## 6.4.8   *ortho*-Phenylene bis(2′-(hept-6-enamido)phenylurea) (**106**)
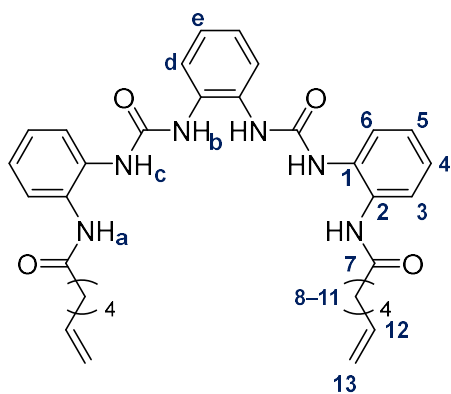


Compound **136** (99 mg, 0.26 mmol) was added to a solution of 10-undecenoic acid (0.08 mL, 0.59 mmol, 2.2 eq.), DMAP (129 mg, 1.06 mmol, 4 eq.) and EDC·HCl (155 mg, 0.809 mmol, 3.1 eq.) in dry CH$_2$Cl$_2$ (10 mL) at 0 °C under an argon atmosphere. The reaction mixture was sealed and stirred vigorously for 1 hour, warmed to room temperature and stirred for 4 days, after which the reaction mixture was concentrated under reduced pressure and dried *in vacuo*, giving an orange oil. This oil was

dissolved in MeCN (5 mL) and the product precipitated by the addition of water (50 mL). The solid was separated by centrifugation and washed with Et$_2$O (3 × 10 mL) before being dried *in vacuo*. Receptor **106** was isolated as a white solid in 25% (35 mg, 0.059 mmol) yield. mp 185–186 °C. HRMS–APCI (*m/z*): [M + H]$^+$ calcd for C$_{34}$H$_{41}$N$_6$O$_4$ 597.3184; found 597.3176. $^1$H NMR (400 MHz, DMSO-*d$_6$*, δ): d 9.46 (s, 2H, NH, H**a**), 8.52 (s, 2H, NH, H**b**), 8.23 (s, 2H, NH, H**c**), 7.70 (d, *J* = 8.0 Hz, 2H, H**6**), 7.60–7.50 (m, 2H, H**d**), 7.31 (d, *J* = 7.8 Hz, 2H, H**3**), 7.14 (t, *J* = 7.6 Hz, 2H, H**5**), 7.11–7.06 (m, 2H, H**e**), 7.04 (t, *J* = 7.6 Hz, 2H, H**4**), 5.78 (dq, *J* = 10.0, 6.7 Hz, 2H, H**12**), 4.99 (d, *J* = 17.2 Hz, 2H, H**13**$_{cis}$), 4.93 (d, *J* = 10.1 Hz, 2H, H**13**$_{trans}$), 2.33 (t, *J* = 7.3 Hz, 4H, CH$_2$, H**8**), 2.02 (dd, *J* = 13.9, 6.9 Hz, 4H, CH$_2$, H**11**), 1.59 (dt, *J* = 15.0, 7.4 Hz, 4H, CH$_2$, H**9**), 1.39 (dt, *J* = 14.4, 7.2 Hz, 4H, CH$_2$, H**10**). $^{13}$C NMR (151 MHz, DMSO-*d$_6$*, δ): 171.9 (quat., C=O, C**7**), 153.6 (quat., C=O$_{urea}$), 138.6 (CH, C**12**), 133.0 (quat., C−N, C**2**), 131.3 (quat., C−N$_{urea}$), 129.2 (quat., C−N, C**1**), 125.7 (CH, C**3**), 125.4 (CH, C**5**), 124.2 (CH, C**d**), 124.1 (CH, C**e**), 123.3 (CH, C**6**), 123.2 (CH, C**4**), 114.8 (CH$_2$, C**13**), 35.7 (CH$_2$, C**8**), 33.0 (CH$_2$, C**11**), 27.9 (CH$_2$, C**10**), 24.6 (CH$_2$, C**9**). FTIR (ATR) $\bar{v}_{max}$ (cm$^{-1}$): 3257 (w), 3063 (w), 2927 (w), 2857 (w), 1651 (s), 1597 (m), 1509 (s), 1478 (s), 1441 (s), 1426 (s), 1293 (s), 1252 (m), 1217 (m), 1197 (m), 1159 (w), 1110 (w), 1044 (w), 991 (w), 969 (w), 942 (w), 909 (m), 876 (w), 748 (s), 702 (s), 630 (m), 570 (m), 554 (m).

### 6.4.9  *ortho*-Phenylene bis(2′-(undec-10-enamido)phenylurea) (**107**)
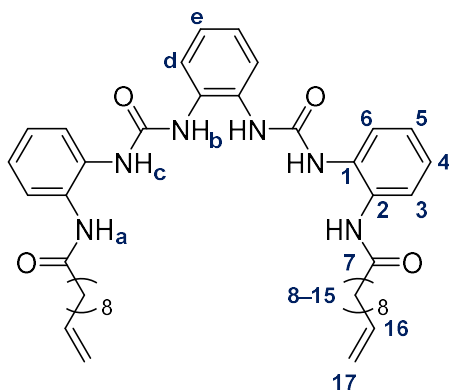


Compound **136** (103 mg, 0.274 mmol) was suspended in dry CH$_2$Cl$_2$ (10 mL) at 0 °C under an argon atmosphere. DMAP (87 mg, 0.71 mmol, 2.6 eq.), EDC·HCl (253 mg, 1.32 mmol, 5 eq.) and 10-undecenoic acid (117 mg, 0.635 mmol, 2.3 eq.) were added sequentially. The reaction mixture was sealed and stirred vigorously for 1 hour, warmed to room temperature and stirred for 6 days, after which the clear solution was concentrated under reduced pressure giving an oil which was further dried *in vacuo*,. The product was precipitated by the addition of water (100 mL) and sonication, and separated by centrifugation. The solid was separated by centrifugation and washed with water (10 mL), acetonitrile (2 × 10 mL), and methanol (10 mL) before being dried *in vacuo*. Receptor **107** was isolated as a white solid in 59% (115 mg, 0.162 mmol) yield. mp 176–180 °C; HRMS–APCI (*m/z*): [M + H]$^+$ calcd for C$_{42}$H$_{57}$N$_6$O$_4$, 709.4436; found 709.4459. $^1$H NMR (400 MHz, DMSO-*d$_6$*, δ): 9.46 (s, 2H, NH, H**a**), 8.52 (s, 2H, NH, H**b**), 8.23 (s, 2H,

NH, H**c**), 7.69 (d, $J$ = 8.0 Hz, 2H, H**6**), 7.56 (dd, $J$ = 5.8, 3.7 Hz, 2H, H**d**), 7.30 (d, $J$ = 7.7 Hz, 2H, H**3**), 7.13 (t, $J$ = 7.5 Hz, 2H, H**5**), 7.08 (dd, $J$ = 5.9, 3.6 Hz, 2H, H**e**), 7.03 (t, $J$ = 7.8 Hz, 2H, H**4**), 5.78 (ddt, $J$ = 17.0, 10.1, 6.8 Hz, 2H, H**16**), 4.98 (d, $J$ = 17.0 Hz, 2H, H**17**$_\text{cis}$), 4.92 (d, $J$ = 10.1 Hz, 2H, H**17**$_\text{trans}$), 2.31 (t, $J$ = 7.3 Hz, 4H, CH$_2$, H**8**), 1.99 (q, $J$ = 6.8 Hz, 4H, CH$_2$, H**15**), 1.67–1.46 (m, 4H, CH$_2$, H**9**), 1.42–1.10 (m, 20H, CH$_2$, H**10**–**14**). $^{13}$C NMR (151 MHz, DMSO-$d_6$, δ): 172.0 (quat., C=O, **7**), 153.6 (quat., C=O$_\text{urea}$), 138.8 (CH, **16**), 132.9 (quat., C−N, C**2**), 131.3 (quat., C−N), 129.2 (quat. C−N, C**1**), 125.7 (CH, C**3**), 125.4 (CH, C**5**), 124.1 (CH, C**d**), 124.0 (CH, C**e**), 123.3 (CH, C**6**), 123.2 (CH, C**4**), 114.6 (CH$_2$, C**17**), 35.9 (CH$_2$, C**8**), 33.2 (CH$_2$, C**15**), 28.8 (CH$_2$), 28.8 (CH$_2$), 28.7 (CH$_2$), 28.5 (CH$_2$), 28.3 (CH$_2$), 25.1 (CH$_2$, C**9**). $^{15}$N NMR (61 MHz, DMSO-$d_6$, δ): 127.4 (N**a**), 102.2 (N**c**), 100.8 (N**b**). FTIR (ATR) $\bar{v}_\text{max}$ (cm$^{-1}$): 3257 (NH), 2924 (CH), 2852 (CH), 1653, 1597, 1510, 1443, 1293, 1196, 908, 749, 701. Anal. calcd for C$_{42}$H$_{56}$N$_6$O$_4$: C, 71.15; H, 7.96; N, 11.86. Found: C, 71.37; H, 8.08; N, 12.10.

### 6.4.10 *meta*-Phenylene bis(2′-(undec-10-enamido)phenylurea) (**108**)
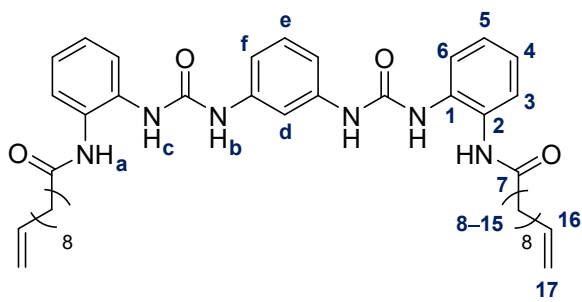


Compound **135** (199 mg, 0.529 mmol) was added to a solution of 10-undecenoic acid (230 mg, 1.25 mmol, 2.4 eq.), DMAP (179 mg, 1.47 mmol, 2.8 eq.) and EDC·HCl (545 mg, 2.84 mmol, 5 eq.) in dry CH$_2$Cl$_2$ (20 mL) at 0 °C under an argon atmosphere. The reaction mixture was sealed and stirred vigorously for 2 hours, let warm to room temperature and stirred for 3 days, after which the solution was concentrated under reduced pressure and dried *in vacuo*, giving an orange oil. This oil was dissolved in MeCN (5 mL) and the product precipitated by the addition of water (20 mL), sonicated, and separated by centrifugation. The solid was triturated with acetonitrile (3 × 5 mL), and methanol (2 × 5 mL) and diethyl ether (5 mL), each time being separated by centrifugation. Receptor **108** was isolated, after drying in air, as a white solid in 87% yield (325 mg, 0.458 mmol). mp 211–214 °C. HRMS–APCI (*m/z*): [M + H]$^+$ calcd for C$_{42}$H$_{57}$N$_6$O$_4$, 709.4436; found 709.4443. $^1$H NMR (400 MHz, DMSO-$d_6$, δ): 9.50 (s, 2H, NH, H**a**), 9.21 (s, 2H, NH, H**b**), 7.80 (s, 2H, NH, H**c**), 7.77 (d, $J$ = 8.1 Hz, 2H, H**6**), 7.72 (s, 1H, H**d**), 7.24 (d, $J$ = 7.8 Hz, 2H, H**3**), 7.15 (m, 3H, H**5** + H**e**), 7.11 (m, 4H, H**f**), 6.97 (m, 4H, H**4**), 5.78 (ddt, $J$ = 17.1, 10.2, 6.6 Hz, 2H, H**16**), 4.98 (dd, $J$ = 17.1, 1.4 Hz, 2H, H**17**$_\text{cis}$), 4.92 (d, $J$ = 10.2 Hz, 2H, H**17**$_\text{trans}$), 2.37 (t, $J$ = 7.4 Hz, 4H, CH$_2$, H**8**), 1.99 (dd, $J$ = 13.6, 6.8 Hz, 4H, CH$_2$, H**15**), 1.63 (dt, $J$ = 14.6, 7.2 Hz, 4H, CH$_2$, H**9**), 1.37–1.22 (m, 20H, CH$_2$, H**10**–**14**). $^{13}$C NMR (151 MHz,

DMSO-$d_6$, δ): 172.1 (quat., C**7**), 152.7 (quat., C=O$_{urea}$), 140.3 (quat., C−N$_{central}$), 138.8 (CH$_2$, C**16**), 133.6 (quat., C−N, C**1**), 129.0 (CH, C**e**), 128.7 (quat., C−N, C**2**), 126.1 (CH, C**3**), 125.7 (CH, C**5**), 122.9 (CH, C**4**), 122.8 (CH, C**6**), 114.6 (CH$_2$, C**17**), 111.6 (CH, C**f**), 107.8 (CH, C**d**), 35.8 (CH$_2$, C**8**), 33.2 (CH$_2$, C**15**), 28.8 (CH$_2$), 28.8 (CH$_2$), 28.7 (CH$_2$), 28.5 (CH$_2$), 28.3 (CH$_2$, C**14**), 25.1 (CH$_2$, C**9**). $^{15}$N (61 MHz, DMSO-$d_6$, δ) 125 (N**a**), 109 (N**b**), 102 (N**c**). FTIR (ATR) $\bar{v}_{max}$ (cm$^{-1}$): 3293 (w), 2920 (w), 2851 (w), 1647 (s), 1611 (s), 1597 (m), 1580 (m), 1555 (s), 1540 (s), 1509 (s), 1472 (s), 1453 (s), 1426 (s), 1348 (w), 1307 (m), 1292 (m), 1263 (m), 1238 (s), 1165 (m), 1112 (w), 1043 (w), 992 (w), 945 (w), 913 (w), 879 (w), 765 (m), 754 (s), 718 (m), 689 (s), 659 (s), 632 (s), 566 (m).

### 6.4.11 Di(4-oxytoluyl)tri(ethylene glycol) / 4,4′-(trigol)dibenzaldehyde (**140**)
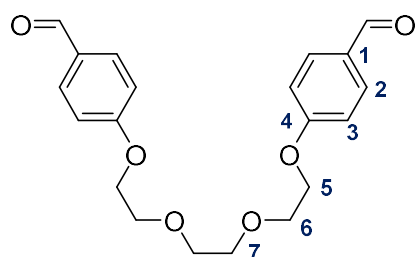


Triethylene glycol ditosylate (1.00 g, 2.18 mmol), 4-hydroxy benzaldehyde (607 mg, 4.97 mmol, 2.3 eq.), K$_2$CO$_3$ (749 mg, 5.4 mmol, 2.5 eq.) and NaI (134 mg, 0.89 mmol, 0.4 eq.) were heated to reflux in MeCN (200 mL) for 20 h. Analysis by thin-layer chromatography showed di-aldehyde **140** ($R_f$ = 0.65–0.70 in 100% EtOAc) to be the major component of the reaction mixture, alongside unreacted 4-hydroxy benzaldehyde ($R_f$ = 0.78–0.84) and the mono-reacted intermediate ($R_f$ = 0.74–0.78). The solvent was evaporated under reduced pressure and the mixture redissolved in water (250 mL) and EtOAc (150 mL). The aqueous layer was extracted with EtOAc (2 × 75 mL) and the combined organic layers washed with water (2 × 125 mL) and brine (120 mL). The solution was dried over MgSO$_4$ and the solvent removed under reduced pressure to give an orange oil (888 mg). Column chromatography in EtOAc/hexane yielded the pure product as a white crystalline solid in 14% yield (111 mg, 0.310 mmol). mp 72–75 °C (lit.[211] 72–74 °C) HRMS–APCI (*m/z*): [M + H]$^+$ calcd for C$_{20}$H$_{23}$O$_6$, 359.1489; found 359.1489. $^1$H NMR (400 MHz, DMSO-$d_6$, δ): 9.86 (s, 2H, CHO), 7.85 (d, *J* = 8.6 Hz, 4H, H**2**), 7.12 (d, *J* = 8.6 Hz, 4H, H**3**), 4.21 (t, *J* = 4.5 Hz, 4H, CH$_2$, H**5**), 3.78 (t, *J* = 4.5 Hz, 4H, CH$_2$, H**6**), 3.62 (s, 4H, CH$_2$, H**7**). $^{13}$C NMR (101 MHz, DMSO-$d_6$, δ): 191.3 (CHO), 163.5 (quat., C−O, C**4**), 131.8 (CH, C**2**), 129.6 (quat., C**1**), 114.9 (CH, C**3**), 69.9 (CH$_2$, C**7**), 68.7 (CH$_2$, C**6**), 67.7 (CH$_2$, C**5**). FTIR (ATR) $\bar{v}_{max}$ (cm$^{-1}$): 2884 (w), 1687 (s, C=O), 1593 (s), 1511 (m), 1479 (w), 1311 (m), 1269 (s, C−O−C), 1214 (m), 1159 (m), 1126 (s, C−O−C), 1037 (m), 988 (m), 857 (w), 828 (s), 811 (w), 792 (w), 638 (w), 619 (m).

# Chapter 7

# References

# References

1.      The 2016 Nobel Prize in Chemistry. *Nobel Media AB*, Nobelprize.org, 2016.

2.      Reuleaux, F. *The Kinematics of Machinery: Outlines of a Theory of Machines*; Macmillan and Co.: London, 1867.

3.      Bruns, C. J.; Stoddart, J. F. *The Nature of the Mechanical Bond*, 2016.

4.      Zhang, L.; Marcos, V.; Leigh, D. A. *Proc. Natl. Acad. Sci. U. S. A.* **2018**, *115*, 9397–9404.

5.      Kay, E. R.; Leigh, D. A.; Zerbetto, F. *Angew. Chem. Int. Ed.* **2007**, *46*, 72–191.

6.      Mitra, R.; Zhu, H.; Grimme, S.; Niemeyer, J. *Angew. Chem. Int. Ed.* **2017**, *56*, 11456–11459.

7.      van Dongen, S. F. M.; Cantekin, S.; Elemans, J. A. A. W.; Rowan, A. E.; Nolte, R. J. M. *Chem. Soc. Rev.* **2014**, *43*, 99–122.

8.      Wikoff, W. R.; Liljas, L.; Duda, R. L.; Tsuruta, H.; Hendrix, R. W.; Johnson, J. E. *Science* **2000**, *289*, 2129–2133.

9.      Champoux, J. J. *Annu. Rev. Biochem* **2001**, *70*, 369–413.

10.     Naughton, C.; Avlonitis, N.; Corless, S.; Prendergast, J. G.; Mati, I. K.; Eijk, P. P.; Cockroft, S. L.; Bradley, M.; Ylstra, B.; Gilbert, N. *Nat. Struct. Mol. Biol.* **2013**, *20*, 387–395.

11.     Gil-Ramirez, G.; Leigh, D. A.; Stephens, A. J. *Angew. Chem. Int. Ed.* **2015**, *54*, 6110–6150.

12.     Evans, N. H. *Chem. Eur. J.* **2018**, *24*, 3101–3112.

13.     De Bo, G.; Kuschel, S.; Leigh, D. A.; Lewandowski, B.; Papmeyer, M.; Ward, J. W. *J. Am. Chem. Soc.* **2014**, *136*, 5811–5814.

14.     Lewandowski, B.; De Bo, G.; Ward, J. W.; Papmeyer, M.; Kuschel, S.; Aldegunde, M. J.; Gramlich, P. M. E.; Heckmann, D.; Goldup, S. M.; D'Souza, D. M.; Fernandes, A. E.; Leigh, D. A. *Science* **2013**, *339*, 189–193.

15.     Caballero, A.; Swan, L.; Zapata, F.; Beer, P. D. *Angew. Chem. Int. Ed.* **2014**, *53*, 11854–11858.

16.     Xue, M.; Yang, Y.; Chi, X.; Yan, X.; Huang, F. *Chem. Rev.* **2015**, *115*, 7398–7501.

17.     Bin Imran, A.; Esaki, K.; Gotoh, H.; Seki, T.; Ito, K.; Sakai, Y.; Takeoka, Y. *Nat. Commun.* **2014**, *5*, 5124.

18.     Noda, Y.; Hayashi, Y.; Ito, K. *J. Appl. Polym. Sci.* **2014**, *131*, 40509.

19.     Benson, C. R.; Fatila, E. M.; Lee, S.; Marzo, M. G.; Pink, M.; Mills, M. B.; Preuss, K. E.; Flood, A. H. *J. Am. Chem. Soc.* **2016**, *138*, 15057–15065.

20.     Frampton, M. J.; Anderson, H. L. *Angew. Chem. Int. Ed.* **2007**, *46*, 1028–1064.

21.     Chiu, S.-H.; Tung, S.-T.; Cheng, H.-T.; Inthasot, A.; Hsueh, F.-C.; Yan, P.-C.; Gu, T.-J.; Lai, C.-C. *Chem. Eur. J.* **2017**, *24*, 1522–1527.

22.     Harrison, I. T.; Harrison, S. *J. Am. Chem. Soc.* **1967**, *89*, 5723–5724.

23.     Hasenknopf, B.; Lehn, J.-M.; Boumediene, N.; Dupont-Gervais, A.; Van Dorsselaer, A.; Kneisel, B.; Fenske, D. *J. Am. Chem. Soc.* **1997**, *119*, 10956–10962.

24. Hasenknopf, B.; Lehn, J.-M.; Kneisel, B. O.; Baum, G.; Fenske, D. *Angew. Chem. Int. Ed. Engl.* **1996**, *35*, 1838–1840.

25. Ayme, J.-F.; Beves, J. E.; Leigh, D. A.; McBurney, R. T.; Rissanen, K.; Schultz, D. *J. Am. Chem. Soc.* **2012**, *134*, 9488–9497.

26. Leigh, D. A.; Pritchard, R. G.; Stephens, A. J. *Nat. Chem.* **2014**, *6*, 978–982.

27. Marcos, V.; Stephens, A. J.; Jaramillo-Garcia, J.; Nussbaumer, A. L.; Woltering, S. L.; Valero, A.; Lemonnier, J.-F.; Vitorica-Yrezabal, I. J.; Leigh, D. A. *Science* **2016**, *352*, 1555–1559.

28. Forgan, R. S.; Sauvage, J.-P.; Stoddart, J. F. *Chem. Rev.* **2011**, *111*, 5434–5464.

29. Beves, J. E.; Blight, B. A.; Campbell, C. J.; Leigh, D. A.; McBurney, R. T. *Angew. Chem. Int. Ed.* **2011**, *50*, 9260–9327.

30. Inokuma, Y.; Arai, T.; Fujita, M. *Nat. Chem.* **2010**, *2*, 780.

31. Fujita, M.; Tominaga, M.; Hori, A.; Therrien, B. *Acc. Chem. Res.* **2005**, *38*, 369–378.

32. Wang, S.-P.; Shen, Y.-F.; Zhu, B.-Y.; Wu, J.; Li, S. *Chem. Commun.* **2016**, *52*, 10205–10216.

33. Jeon, W. S.; Moon, K.; Park, S. H.; Chun, H.; Ko, Y. H.; Lee, J. Y.; Lee, E. S.; Samal, S.; Selvapalam, N.; Rekharsky, M. V.; Sindelar, V.; Sobransingh, D.; Inoue, Y.; Kaifer, A. E.; Kim, K. *J. Am. Chem. Soc.* **2005**, *127*, 12984–12989.

34. Matsue, T.; Evans, D. H.; Osa, T.; Kobayashi, N. *J. Am. Chem. Soc.* **1985**, *107*, 3411–3417.

35. Ueno, A.; Takahashi, K.; Osa, T. *J. Chem. Soc., Chem. Commun.* **1980**, 837–838.

36. Herrmann, W.; Wehrle, S.; Wenz, G. *Chem. Commun.* **1997**, 1709–1710.

37. Yamauchi, K.; Takashima, Y.; Hashidzume, A.; Yamaguchi, H.; Harada, A. *J. Am. Chem. Soc.* **2008**, *130*, 5024–5025.

38. Trinh, T.; Cappel, J. P.; Geis, P. A.; Hollingshead, J. A.; McCarty, M. L.; Zwerdling, S. S. Composition for Reducing Malodor Impression on Inanimate Surfaces. U.S. Patent 5,783,544, 21 July 1998.

39. Byron, E. Febreze Joins P&G's $1 Billion Club. *The Wall Street Journal*, 9 March 2011.

40. Yang, L.; Adam, C.; Cockroft, S. L. *J. Am. Chem. Soc.* **2015**, *137*, 10084–10087.

41. Barin, G.; Coskun, A.; Fouda, M. M. G.; Stoddart, J. F. *ChemPlusChem* **2012**, *77*, 159–185.

42. Odell, B.; Reddington, M. V.; Slawin, A. M. Z.; Spencer, N.; Stoddart, J. F.; Williams, D. J. *Angew. Chem. Int. Ed. Engl.* **1988**, *27*, 1547–1550.

43. Pedersen, C. J. *Angew. Chem. Int. Ed. Engl.* **1988**, *27*, 1021–1027.

44. Steiner, T. *Angew. Chem. Int. Ed.* **2002**, *41*, 48–76.

45. Hooper, A. E.; Kennedy, S. R.; Jones, C. D.; Steed, J. W. *Chem. Commun.* **2015**, *52*, 198–201.

46. Xiao, T.; Li, S.-L.; Zhang, Y.; Lin, C.; Hu, B.; Guan, X.; Yu, Y.; Jiang, J.; Wang, L. *Chem. Sci.* **2012**, *3*, 1417–1421.

47. Li, S.-L.; Xiao, T.; Hu, B.; Zhang, Y.; Zhao, F.; Ji, Y.; Yu, Y.; Lin, C.; Wang, L. *Chem. Commun.* **2011**, *47*, 10755–10757.

48. Spence, G. T.; Beer, P. D. *Acc. Chem. Res.* **2013**, *46*, 571–586.

49. White, N. G.; Beer, P. D. *Chem. Commun.* **2012**, *48*, 8499–8501.

50. Evans, N. H.; Serpell, C. J.; Beer, P. D. *Angew. Chem. Int. Ed.* **2011**, *50,* 2507–2510.

51. Evans, N. H.; Beer, P. D. *Chem. Eur. J.* **2011**, *17*, 10542–10546.

52. Aletti, A. B.; Gillen, D. M.; Gunnlaugsson, T. *Coord. Chem. Rev.* **2018**, *354*, 98–120.

53. Hofmeister, F. *Arch. Exp. Pathol. Pharmakol.* **1888**, *24*, 247–260.

54. Kunz, W.; Henle, J.; Ninham, B. W. *Curr. Opin. Colloid Interface Sci.* **2004**, *9*, 19–37.

55. Marcus, Y. *Chem. Rev.* **1988**, *88*, 1475–1498.

56. Marcus, Y. *J. Chem. Soc., Faraday Trans.* **1991**, *87*, 2995–2999.

57. Armstrong, F.; Atkins, P.; Rourke, J.; Overton, T.; Weller, M. Acids and Bases. In *Inorganic Chemistry*; 4th Revised ed.; Oxford University Press: Oxford, UK, 2006, 111-140.

58. Wade, L. G., Jr. Carboxylic Acids. In *Organic Chemistry*; 4th ed.; Corey, P. F., Ed.; Prentice-Hall International Inc.: London, UK, 1999, 909–946.

59. Bowman-James, K. *Acc. Chem. Res.* **2005**, *38*, 671–678.

60. Zhao, J.; Yang, D.; Yang, X.-J.; Wu, B. *Coord. Chem. Rev.* **2019**, *378*, 415–444.

61. He, Q.; Tu, P.; Sessler, J. L. *Chem* **2018**, *4*, 46–93.

62. Li, S.; Jia, C.; Wu, B.; Luo, Q.; Huang, X.; Yang, Z.; Li, Q.-S.; Yang, X.-J. *Angew. Chem. Int. Ed.* **2011**, *50*, 5721–5724.

63. Huang, X.; Wu, B.; Jia, C.; Hay, B. P.; Li, M.; Yang, X.-J. *Chem. Eur. J.* **2013**, *19*, 9034–9041.

64. Manna, U.; Chutia, R.; Das, G. *Cryst. Growth Des.* **2016**, *16*, 2893–2903.

65. Yohei, H.; Hiromitsu, M. *Chem. Eur. J.* **2011**, *17*, 1485–1492.

66. Brooks, S. J.; Gale, P. A.; Light, M. E. *CrystEngComm* **2005**, *7*, 586–591.

67. Rajbanshi, A.; Wan, S.; Custelcean, R. *Cryst. Growth Des.* **2013**, *13*, 2233–2237.

68. Farrokhpour, H.; Manassir, M. *J. Phys. Chem. A* **2015**, *119*, 160–171.

69. Chakrabarti, P. *J. Mol. Biol.* **1993**, *234*, 463–482.

70. Hirsch, A. K. H.; Fischer, F. R.; Diederich, F. *Angew. Chem. Int. Ed.* **2007**, *46*, 338–352.

71. Copley, R. R.; Barton, G. J. *J. Mol. Biol.* **1994**, *242*, 321–329.

72. Alfonso, I. *Chem. Commun.* **2016**, *52*, 239–250.

73. Elmes, R. B.; Jolliffe, K. A. *Chem. Commun.* **2015**, *51*, 4951–4968.

74. Blondeau, P.; Segura, M.; Perez-Fernandez, R.; de Mendoza, J. *Chem. Soc. Rev.* **2007**, *36*, 198–210.

75. Gale, Philip A.; Howe, Ethan N. W.; Wu, X. *Chem* **2016**, *1*, 351–422.

76. Blažek Bregović, V.; Basarić, N.; Mlinarić-Majerski, K. *Coord. Chem. Rev.* **2015**, *295*, 80–124.

77. Jia, C.; Zuo, W.; Zhang, D.; Yang, X.-J.; Wu, B. *Chem. Commun.* **2016**, *52*, 9614–9627.

78.   Zwicker, V. E.; Yuen, K. K. Y.; Smith, D. G.; Ho, J.; Qin, L.; Turner, P.; Jolliffe, K. A. *Chem. Eur. J.* **2018**, *24*, 1140–1150.

79.   Ho, J.; Zwicker, V. E.; Yuen, K. K. Y.; Jolliffe, K. A. *J. Org. Chem.* **2017**, *82*, 10732–10736.

80.   Amendola, V.; Bergamaschi, G.; Boiocchi, M.; Fabbrizzi, L.; Milani, M. *Chem. Eur. J.* **2010**, *16*, 4368–4380.

81.   Rostami, A.; Colin, A.; Li, X. Y.; Chudzinski, M. G.; Lough, A. J.; Taylor, M. S. *J. Org. Chem.* **2010**, *75*, 3983–3992.

82.   Edwards, S. J.; Valkenier, H.; Busschaert, N.; Gale, P. A.; Davis, A. P. *Angew. Chem. Int. Ed.* **2015**, *54*, 4592–4596.

83.   Busschaert, N.; Elmes, R. B. P.; Czech, D. D.; Wu, X.; Kirby, I. L.; Peck, E. M.; Hendzel, K. D.; Shaw, S. K.; Chan, B.; Smith, B. D.; Jolliffe, K. A.; Gale, P. A. *Chem. Sci.* **2014**, *5*, 3617–3626.

84.   Amendola, V.; Fabbrizzi, L.; Mosca, L. *Chem. Soc. Rev.* **2010**, *39*, 3889–3915.

85.   Etter, M. C.; Panunto, T. W. *J. Am. Chem. Soc.* **1988**, *110*, 5896–5897.

86.   Smith, P. J.; Reddington, M. V.; Wilcox, C. S. *Tetrahedron Lett.* **1992**, *33*, 6085–6088.

87.   Fan, E.; Van Arman, S. A.; Kincaid, S.; Hamilton, A. D. *J. Am. Chem. Soc.* **1993**, *115*, 369–370.

88.   Duke, R. M.; Gunnlaugsson, T. *Tetrahedron Lett.* **2007**, *48*, 8043–8047.

89.   Esteban-Gomez, D.; Fabbrizzi, L.; Licchelli, M. *J. Org. Chem.* **2005**, *70*, 5717–5720.

90.   Boiocchi, M.; Del Boca, L.; Gomez, D. E.; Fabbrizzi, L.; Licchelli, M.; Monzani, E. *J. Am. Chem. Soc.* **2004**, *126*, 16507–16514.

91.   Pike, S. J.; Hutchinson, J. J.; Hunter, C. A. *J. Am. Chem. Soc.* **2017**, *139*, 6700–6706.

92.   Bu, J.; Lilienthal, N. D.; Woods, J. E.; Nohrden, C. E.; Hoang, K. T.; Truong, D.; Smith, D. K. *J. Am. Chem. Soc.* **2005**, *127*, 6423–6429.

93.   Tresca, B. W.; Hansen, R. J.; Chau, C. V.; Hay, B. P.; Zakharov, L. N.; Haley, M. M.; Johnson, D. W. *J. Am. Chem. Soc.* **2015**, *137*, 14959–14967.

94.   Carroll, C. N.; Berryman, O. B.; Johnson, C. A.; Zakharov, L. N.; Haley, M. M.; Johnson, D. W. *Chem. Commun.* **2009**, 2520–2522.

95.   Swinburne, A. N.; Paterson, M. J.; Beeby, A.; Steed, J. W. *Chem. Eur. J.* **2010**, *16*, 2714–2718.

96.   Wezenberg, S. J.; Feringa, B. L. *Nat. Commun.* **2018**, *9*, 1984.

97.   Wezenberg, S. J.; Feringa, B. L. *Org. Lett.* **2017**, *19*, 324–327.

98.   Wezenberg, S. J.; Croisetu, C. M.; Stuart, M. C. A.; Feringa, B. L. *Chem. Sci.* **2016**, *7*, 4341–4346.

99.   Wezenberg, S. J.; Vlatković, M.; Kistemaker, J. C. M.; Feringa, B. L. *J. Am. Chem. Soc.* **2014**, *136*, 16784–16787.

100. Lito, P. F.; Aniceto, J. P. S.; Silva, C. M. *Water, Air, Soil Pollut.* **2012**, *223*, 6133–6155.

101. Moyer, B. A.; Custelcean, R.; Hay, B. P.; Sessler, J. L.; Bowman-James, K.; Day, V. W.; Kang, S. O. *Inorg. Chem.* **2013**, *52*, 3473–3490.

102. Ji, X.; Wu, R.-T.; Long, L.; Guo, C.; Khashab, N. M.; Huang, F.; Sessler, J. L. *J. Am. Chem. Soc.* **2018**, *140*, 2777–2780.

103. Tian, J.; Zhou, T.-Y.; Zhang, S.-C.; Aloni, S.; Altoe, M. V.; Xie, S.-H.; Wang, H.; Zhang, D.-W.; Zhao, X.; Liu, Y.; Li, Z.-T. *Nat. Commun.* **2014**, *5*, 5574.

104. Shen, J.; Chai, W.; Wang, K.; Zhang, F. *ACS Appl. Mater. Interfaces* **2017**, *9*, 22440–22448.

105. Wulff, G.; Gross, T.; Schönfeld, R. *Angew. Chem. Int. Ed. Engl.* **1997**, *36*, 1962–1964.

106. Dutta, R.; Chakraborty, S.; Bose, P.; Ghosh, P. *Eur. J. Inorg. Chem.* **2014**, 4134–4143.

107. Dutta, R.; Bose, P.; Ghosh, P. *Dalton Trans.* **2013**, *42*, 11371–11374.

108. Ko, S.-K.; Kim, S. K.; Share, A.; Lynch, V. M.; Park, J.; Namkung, W.; Van Rossom, W.; Busschaert, N.; Gale, P. A.; Sessler, J. L.; Shin, I. *Nat. Chem.* **2014**, *6*, 885–892.

109. Wu, X.; Judd, Luke W.; Howe, Ethan N. W.; Withecombe, Anne M.; Soto-Cerrato, V.; Li, H.; Busschaert, N.; Valkenier, H.; Pérez-Tomás, R.; Sheppard, David N.; Jiang, Y.-B.; Davis, Anthony P.; Gale, Philip A. *Chem* **2016**, *1*, 127–146.

110. Li, H.; Valkenier, H.; Judd, L. W.; Brotherhood, P. R.; Hussain, S.; Cooper, J. A.; Jurček, O.; Sparkes, H. A.; Sheppard, D. N.; Davis, A. P. *Nat. Chem.* **2015**, *8*, 24–32.

111. Valkenier, H.; Dias, C. M.; Butts, C. P.; Davis, A. P. *Tetrahedron* **2017**, *73*, 4955–4962.

112. Caltagirone, C.; Gale, P. A.; Olivari, M.; Horton, P.; Coles, S.; Mapp, L. K.; Berry, S.; Karagiannidis, L. E.; Montis, R. *Dalton Trans.* **2016**, *45*, 11892–11897.

113. Dias, C. M.; Li, H.; Valkenier, H.; Karagiannidis, L. E.; Gale, P. A.; Sheppard, D. N.; Davis, A. P. *Org. Biomol. Chem.* **2018**, *16*, 1083–1087.

114. Wu, B.; Jia, C.; Wang, X.; Li, S.; Huang, X.; Yang, X.-J. *Org. Lett.* **2012**, *14*, 684–687.

115. Yang, P.; Wang, J.; Jia, C.; Yang, X.-J.; Wu, B. *Eur. J. Org. Chem.* **2013**, *2013*, 3446–3454.

116. Jia, C.; Wu, B.; Li, S.; Yang, Z.; Zhao, Q.; Liang, J.; Li, Q.-S.; Yang, X.-J. *Chem. Commun.* **2010**, *46*, 5376–5378.

117. Wang, X.; Jia, C.; Huang, X.; Wu, B. *Inorg. Chem. Commun.* **2011**, *14*, 1508–1510.

118. Meshcheryakov, D.; Böhmer, V.; Bolte, M.; Hubscher-Bruder, V.; Arnaud-Neu, F.; Herschbach, H.; Van Dorsselaer, A.; Thondorf, I.; Mögelin, W. *Angew. Chem. Int. Ed.* **2006**, *45*, 1648–1652.

119. Bregović, N.; Cindro, N.; Frkanec, L.; Užarević, K.; Tomišić, V. *Chem. Eur. J.* **2014**, *20*, 15863–15871.

120. Rull, F.; Del Valle, A.; Sobron, F.; Veintemillas, S. *J. Raman Spectrosc.* **1989**, *20*, 625–631.

121. Fatila, E. M.; Pink, M.; Twum, E. B.; Karty, J. A.; Flood, A. H. *Chem. Sci.* **2018**, *9*, 2863–2872.

122. Calderon-Kawasaki, K.; Kularatne, S.; Li, Y. H.; Noll, B. C.; Scheidt, W. R.; Burns, D. H. *J. Org. Chem.* **2007**, *72*, 9081–9087.

123. Dydio, P.; Zieliński, T.; Jurczak, J. *Org. Lett.* **2010**, *12*, 1076–1078.

124. Zhang, Y.; Zhang, R.; Zhao, Y.; Ji, L.; Jia, C.; Wu, B. *New J. Chem.* **2013**, *37*, 2266–2270.

125. Lakshminarayanan, P. S.; Ravikumar, I.; Suresh, E.; Ghosh, P. *Chem. Commun.* **2007**, 5214–5216.

126. Casula, A.; Bazzicalupi, C.; Bettoschi, A.; Cadoni, E.; Coles, S. J.; Horton, P. N.; Isaia, F.; Lippolis, V.; Mapp, L. K.; Marini, G. M.; Montis, R.; Scorciapino, M. A.; Caltagirone, C. *Dalton Trans.* **2016**, *45*, 3078–3085.

127. Blažek, V.; Molčanov, K.; Mlinarić-Majerski, K.; Kojić-Prodić, B.; Basarić, N. *Tetrahedron* **2013**, *69*, 517–526.

128. Chutia, R.; Dey, S. K.; Das, G. *Cryst. Growth Des.* **2015**, *15*, 4993–5001.

129. Jose, D. A.; Kumar, D. K.; Ganguly, B.; Das, A. *Inorg. Chem.* **2007**, *46*, 5817–5819.

130. Portis, B.; Mirchi, A.; Emami Khansari, M.; Pramanik, A.; Johnson, C. R.; Powell, D. R.; Leszczynski, J.; Hossain, M. A. *ACS Omega* **2017**, *2*, 5840–5849.

131. Manna, U.; Kayal, S.; Samanta, S.; Das, G. *Dalton Trans.* **2017**, *46*, 10374–10386.

132. Manna, U.; Nayak, B.; Das, G. *Cryst. Growth Des.* **2016**, *16*, 7163–7174.

133. Sánchez-Quesada, J.; Seel, C.; Prados, P.; de Mendoza, J.; Dalcol, I.; Giralt, E. *J. Am. Chem. Soc.* **1996**, *118*, 277–278.

134. Coles, S. J.; Frey, J. G.; Gale, P. A.; Hursthouse, M. B.; Light, M. E.; Navakhun, K.; Thomas, G. L. *Chem. Commun.* **2003**, 568–569.

135. Keegan, J.; Kruger, P. E.; Nieuwenhuyzen, M.; O'Brien, J.; Martin, N. *Chem. Commun.* **2001**, 2192–2193.

136. Selvakumar, P. M.; Jebaraj, P. Y.; Sahoo, J.; Suresh, E.; Prathap, K. J.; Kureshy, R. I.; Subramanian, P. S. *RSC Adv.* **2012**, *2*, 7689–7692.

137. Massena, C. J.; Wageling, N. B.; Decato, D. A.; Martin Rodriguez, E.; Rose, A. M.; Berryman, O. B. *Angew. Chem. Int. Ed.* **2016**, *55*, 12398–12402.

138. Wu, B.; Li, S.; Lei, Y.; Hu, H.; de Sousa Amadeu, N.; Janiak, C.; Mathieson, J. S.; Long, D.-L.; Cronin, L.; Yang, X.-J. *Chem. Eur. J.* **2015**, *21*, 2588–2593.

139. Yang, D.; Zhao, J.; Zhao, Y.; Lei, Y.; Cao, L.; Yang, X. J.; Davi, M.; Amadeu de Sousa, N.; Janiak, C.; Zhang, Z.; Wang, Y. Y.; Wu, B. *Angew. Chem. Int. Ed.* **2015**, *54*, 8658–8661.

140. Bai, X.; Jia, C.; Zhao, Y.; Yang, D.; Wang, S. C.; Li, A.; Chan, Y. T.; Wang, Y. Y.; Yang, X. J.; Wu, B. *Angew. Chem. Int. Ed.* **2018**, *57*, 1851–1855.

141. Jia, C.; Zuo, W.; Yang, D.; Chen, Y.; Cao, L.; Custelcean, R.; Hostaš, J.; Hobza, P.; Glaser, R.; Wang, Y.-Y.; Yang, X.-J.; Wu, B. *Nat. Commun.* **2017**, *8*, 938.

142. Zuo, W.; Huang, Z.; Zhao, Y.; Xu, W.; Liu, Z.; Yang, X.-J.; Jia, C.; Wu, B. *Chem. Commun.* **2018**, *54*, 7378–7381.

143. Stomeo, F.; Lincheneau, C.; Leonard, J. P.; O'Brien, J. E.; Peacock, R. D.; McCoy, C. P.; Gunnlaugsson, T. *J. Am. Chem. Soc.* **2009**, *131*, 9636–9637.

144. Comby, S.; Stomeo, F.; McCoy, C. P.; Gunnlaugsson, T. *Helv. Chim. Acta* **2009**, *92*, 2461–2473.

145. Lincheneau, C.; Peacock, R. D.; Gunnlaugsson, T. *Chem. Asian J.* **2010**, *5*, 500–504.

146. Leonard, J. P.; Jensen, P.; McCabe, T.; O'Brien, J. E.; Peacock, R. D.; Kruger, P. E.; Gunnlaugsson, T. *J. Am. Chem. Soc.* **2007**, *129*, 10986–10987.

147. Kotova, O.; Comby, S.; Pandurangan, K.; Stomeo, F.; O'Brien, J. E.; Feeney, M.; Peacock, R. D.; McCoy, C. P.; Gunnlaugsson, T. *Dalton Trans.* **2018**, *47*, 12308–12317.

148. Lincheneau, C.; Jean-Denis, B.; Gunnlaugsson, T. *Chem. Commun.* **2014**, *50*, 2857–2860.

149. Byrne, J. Novel btp [2,6]-bis(1,2,3-triazol-4-yl)pyridine] Systems: a Versatile Motif for the Formation of Supramolecular Self-assembly Structures. PhD Thesis, Trinity College Dublin, the University of Dublin, Dublin, 2014.

150. McCarney, E. P. Templated Synthesis of Novel Molecules and Materials using 1,4-Disubstituted-1,2,3-triazole Supramolecular Building Blocks. PhD Thesis, Trinity College Dublin, the University of Dublin, Dublin, 2017.

151. Aletti, A. Anion-Templated Self-Assembly – From Anion Complexes to the Formation of Supramolecular 2D Networks. PhD Thesis, Trinity College Dublin, the University of Dublin, Dublin, 2018.

152. Byrne, J. P.; Blasco, S.; Aletti, A. B.; Hessman, G.; Gunnlaugsson, T. *Angew. Chem. Int. Ed.* **2016**, *55*, 8938–8943.

153. Ali, H. D. P.; Quinn, S. J.; McCabe, T.; Kruger, P. E.; Gunnlaugsson, T. *New J. Chem.* **2009**, *33*, 793–800.

154. Ali, H. D. P.; Kruger, P. E.; Gunnlaugsson, T. *New J. Chem.* **2008**, *32*, 1153–1161.

155. Gunnlaugsson, T.; Ali, H. D. P.; Glynn, M.; Kruger, P. E.; Hussey, G. M.; Pfeffer, F. M.; dos Santos, C. M. G.; Tierney, J. *J. Fluoresc.* **2005**, *15*, 287–299.

156. Gunnlaugsson, T.; Kruger, P. E.; Jensen, P.; Tierney, J.; Ali, H. D. P.; Hussey, G. M. *J. Org. Chem.* **2005**, *70*, 10875–10878.

157. Duke, R. M.; Gunnlaugsson, T. *Tetrahedron Lett.* **2011**, *52*, 1503–1505.

158. Gunnlaugsson, T.; Davis, A. P.; Glynn, M. *Chem. Commun.* **2001**, 2556–2557.

159. Gunnlaugsson, T.; Kruger, P. E.; Lee, T. C.; Parkesh, R.; Pfeffer, F. M.; Hussey, G. M. *Tetrahedron Lett.* **2003**, *44*, 6575–6578.

160. Gunnlaugsson, T.; Glynn, M.; Tocci, G. M.; Kruger, P. E.; Pfeffer, F. M. *Coord. Chem. Rev.* **2006**, *250*, 3094–3117.

161. Pandurangan, K.; Kitchen, J. A.; Gunnlaugsson, T. *Tetrahedron Lett.* **2013**, *54*, 2770–2775.

162. Pandurangan, K.; Aletti, A. B.; Montroni, D.; Kitchen, J. A.; Martinez-Calvo, M.; Blasco, S.; Gunnlaugsson, T.; Scanlan, E. M. *Org. Lett.* **2017**, *19*, 1068–1071.

163. Ali, H. D. P. H. Synthesis and Physical Evaluation of Urea- and Thiourea-based Receptors and Sensors for Anions. PhD Thesis, Trinity College Dublin, the University of Dublin, Dublin, 2007.

164. Supady, A.; Hecht, S.; Baldauf, C. *Org. Lett.* **2017**, *19*, 4199–4202.

165. Custelcean, R.; Gorbunova, M. G.; Bonnesen, P. V. *Chem. Eur. J.* **2005**, *11*, 1459–1466.

166. Gosavi, R. K.; Agarwala, U.; Rao, C. N. R. *J. Am. Chem. Soc.* **1967**, *89*, 235–239.

167. dos Santos, C. M. G.; Fernández, P. B.; Plush, S. E.; Leonard, J. P.; Gunnlaugsson, T. *Chem. Commun.* **2007**, 3389–3391.

168. dos Santos, C. M. G.; McCabe, T.; Watson, G. W.; Kruger, P. E.; Gunnlaugsson, T. *J. Org. Chem.* **2008**, *73*, 9235–9244.

169. Boyle, E. M.; McCabe, T.; Gunnlaugsson, T. *Supramol. Chem.* **2010**, *22*, 586–597.

170. dos Santos, C. M.; Boyle, E. M.; De Solis, S.; Kruger, P. E.; Gunnlaugsson, T. *Chem. Commun.* **2011**, *47*, 12176–12178.

171. Pandurangan, K.; Kitchen, J. A.; Blasco, S.; Boyle, E. M.; Fitzpatrick, B.; Feeney, M.; Kruger, P. E.; Gunnlaugsson, T. *Angew. Chem. Int. Ed.* **2015**, *54*, 4566–4570.

172. Boyle, E. M. Thio(Urea) Derivatives – From Anion Sensing and Recognition Towards Supramolecular Assemblies. PhD Thesis, Trinity College Dublin, the University of Dublin, Dublin, 2012.

173. Gale, P. A.; Caltagirone, C. *Coord. Chem. Rev.* **2018**, *354*, 2–27.

174. Pfeffer, F. M.; Kruger, P. E.; Gunnlaugsson, T. *Org. Biomol. Chem.* **2007**, *5*, 1894–1902.

175. Esteban-Gomez, D.; Fabbrizzi, L.; Licchelli, M.; Monzani, E. *Org. Biomol. Chem.* **2005**, *3*, 1495–1500.

176. Li, A.-F.; Wang, J.-H.; Wang, F.; Jiang, Y.-B. *Chem. Soc. Rev.* **2010**, *39*, 3729–3745.

177. Veale, E. B.; Gunnlaugsson, T. *Annu. Rep. Prog. Chem., Sect. B: Org. Chem.* **2010**, *106*, 376–406.

178. Hansch, C.; Leo, A.; Taft, R. W. *Chem. Rev.* **1991**, *91*, 165–195.

179. Unger, S. H.; Hansch, C. In *Progress in Physical Organic Chemistry*; Taft, R. W., Ed.; John Wiley & Sons, Inc.: Hoboken, NJ, USA, 1976; Vol. 12, 91–118.

180. Brooks, S. J.; Edwards, P. R.; Gale, P. A.; Light, M. E. *New J. Chem.* **2006**, *30*, 65–70.

181. Brooks, S. J.; Gale, P. A.; Light, M. E. *Chem. Commun.* **2005**, 4696–4698.

182. Kadam, S. A.; Martin, K.; Haav, K.; Toom, L.; Mayeux, C.; Pung, A.; Gale, P. A.; Hiscock, J. R.; Brooks, S. J.; Kirby, I. L.; Busschaert, N.; Leito, I. *Chem. Eur. J.* **2015**, *21*, 5145–5160.

183. Li, R.; Zhao, Y.; Li, S.; Yang, P.; Huang, X.; Yang, X.-J.; Wu, B. *Inorg. Chem.* **2013**, *52*, 5851–5860.

184. Manna, U.; Das, G. *CrystEngComm* **2017**, *19*, 5622–5634.

185. Ghosh, K.; Adhikari, S.; Fröhlich, R.; Petsalakis, I. D.; Theodorakopoulos, G. *J. Mol. Struct.* **2011**, *1004*, 193–203.

186. Gillen, D. M.; Hawes, C. S.; Gunnlaugsson, T. *J. Org. Chem.* **2018**, *83*, 10398–10408.

187. Frassineti, C.; Ghelli, S.; Gans, P.; Sabatini, A.; Moruzzi, M. S.; Vacca, A. *Anal. Biochem.* **1995**, *231*, 374–382.

188. Thordarson, P. *Chem. Soc. Rev.* **2011**, *40*, 1305–1323.

189. Amendola, V.; Boiocchi, M.; Esteban-Gomez, D.; Fabbrizzi, L.; Monzani, E. *Org. Biomol. Chem.* **2005**, *3*, 2632–2639.

190. Brunetti, E.; Picron, J.-F.; Flidrova, K.; Bruylants, G.; Bartik, K.; Jabin, I. *J. Org. Chem.* **2014**, *79*, 6179–6188.

191. Etter, M. C. *Acc. Chem. Res.* **1990**, *23*, 120–126.

192. Custelcean, R.; Bonnesen, P. V.; Roach, B. D.; Duncan, N. C. *Chem. Commun.* **2012**, *48*, 7438–7440.

193. Evans, L. S.; Gale, P. A.; Light, M. E.; Quesada, R. *Chem. Commun.* **2006**, 965–967.

194. Gunnlaugsson, T.; Kruger, P. E.; Jensen, P.; Pfeffer, F. M.; Hussey, G. M. *Tetrahedron Lett.* **2003**, *44*, 8909–8913.

195. Butler, S. J. *Chem. Eur. J.* **2014**, *20*, 15768–15774.

196. Lee, S.; Chen, C.-H.; Flood, A. H. *Nat. Chem.* **2013**, *5*, 704–710.

197. Wisner, J. A.; Beer, P. D.; Drew, M. G.; Sambrook, M. R. *J. Am. Chem. Soc.* **2002**, *124*, 12469–12476.

198. Piepenbrock, M.-O. M.; Lloyd, G. O.; Clarke, N.; Steed, J. W. *Chem. Rev.* **2010**, *110*, 1960–2004.

199. Basu, A.; Das, G. *J. Org. Chem.* **2014**, *79*, 2647–2656.

200. Hoque, M. N.; Das, G. *Cryst. Growth. Des.* **2014**, *14*, 2962–2971.

201. Gogoi, A.; Das, G. *Supramol. Chem.* **2013**, *25*, 819–830.

202. Jia, C.; Wu, B.; Li, S.; Huang, X.; Yang, X.-J. *Org. Lett.* **2010**, *12*, 5612–5615.

203. Zhou, H.; Zhao, Y.; Gao, G.; Li, S.; Lan, J.; You, J. *J. Am. Chem. Soc.* **2013**, *135*, 14908–14911.

204. Gavette, J. V.; Evoniuk, C. J.; Zakharov, L. N.; Carnes, M. E.; Haley, M. M.; Johnson, D. W. *Chem. Sci.* **2014**, *5*, 2899–2905.

205. Katayev, E. A.; Pantos, G. D.; Reshetova, M. D.; Khrustalev, V. N.; Lynch, V. M.; Ustynyuk, Y. A.; Sessler, J. L. *Angew. Chem. Int. Ed.* **2005**, *44*, 7386–7390.

206. Ornelas, C.; Ruiz, J.; Astruc, D. *Organometallics* **2009**, *28*, 4431–4437.

207. Valério, C.; Fillaut, J.-L.; Ruiz, J.; Guittard, J.; Blais, J.-C.; Astruc, D. *J. Am. Chem. Soc.* **1997**, *119*, 2588–2589.

208. Williamson, M. P. *Prog. Nucl. Magn. Reson. Spectrosc.* **2013**, *73*, 1–16.

209. Huang, Y.-L.; Hung, W.-C.; Lai, C.-C.; Liu, Y.-H.; Peng, S.-M.; Chiu, S.-H. *Angew. Chem. Int. Ed.* **2007**, *46*, 6629–6633.

210. Martin, K.; Nõges, J.; Haav, K.; Kadam, S. A.; Pung, A.; Leito, I. *Eur. J. Org. Chem.* **2017**, *2017*, 5231–5237.

211. Ruiz-Sanchez, A. J.; Vida, Y.; Suau, R.; Perez-Inestrosa, E. *Tetrahedron* **2008**, *64*, 11661–11665.

212. Ji, L.; Yang, Z.; Zhao, Y.; Sun, M.; Cao, L.; Yang, X.-J.; Wang, Y.-Y.; Wu, B. *Chem. Commun.* **2016**, *52*, 7310–7313.

213. Ośmiałowski, B.; Mroczyńska, K.; Kolehmainen, E.; Kowalska, M.; Valkonen, A.; Pietrzak, M.; Rissanen, K. *J. Org. Chem.* **2013**, *78*, 7582–7593.

214. Ośmiałowski, B.; Kolehmainen, E. *New J. Chem.* **2014**, *38*, 2701–2703.

215. Kwiatkowski, A.; Grela, I.; Ośmiałowski, B. *New J. Chem.* **2017**, *41*, 1073–1081.

216. Isare, B.; Pembouong, G.; Boué, F.; Bouteiller, L. *Langmuir* **2012**, *28*, 7535–7541.

217. *Bruker APEX-3*; Bruker-AXS Inc.: Madison, WI, 2016.

218. *SADABS*; Bruker-AXS Inc.: Madison, WI, 2016.

219. Sheldrick, G. *Acta Crystallogr. Sect. A* **2015**, *71*, 3–8.

220. Sheldrick, G. *Acta Crystallogr. Sect. C* **2015**, *71*, 3–8.

221. Dolomanov, O. V.; Bourhis, L. J.; Gildea, R. J.; Howard, J. A. K.; Puschmann, H. *J. Appl. Cryst.* **2009**, *42*, 339–341.

222. Easton, A.; Gould, P.; Marsh, A. Use of DDX3X Inhibitors for the Treatment of Pneumovirus Infections. WO2015136292A1,

*NMR spectroscopy is like your mother; not as sensitive as you may sometimes like, but always telling you the truth. Mass spectrometry, on the other hand, is like your lover; always sensitive, but willing to say whatever you want to hear.*

—Various, including Anna Aletti, PhD

# Appendix 1.

## Additional Experimental Details and Characterisation

# A1.1 Appendices for Chapter 2

## A1.1.1 Characterisation of receptors **96–100**
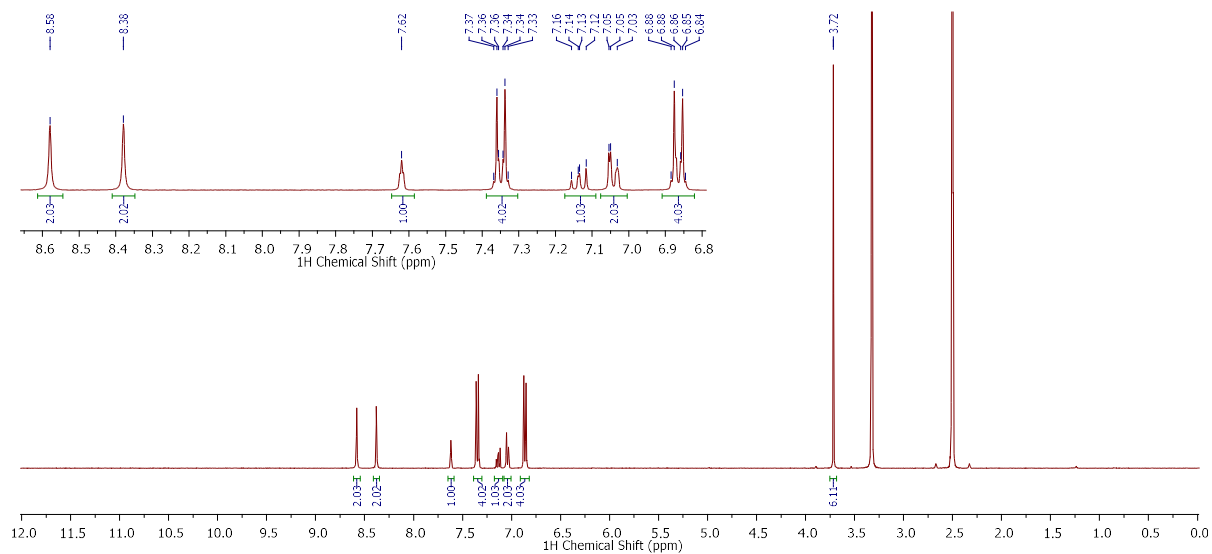
Figure A1.1. $^1$H NMR Spectrum of receptor **96**.
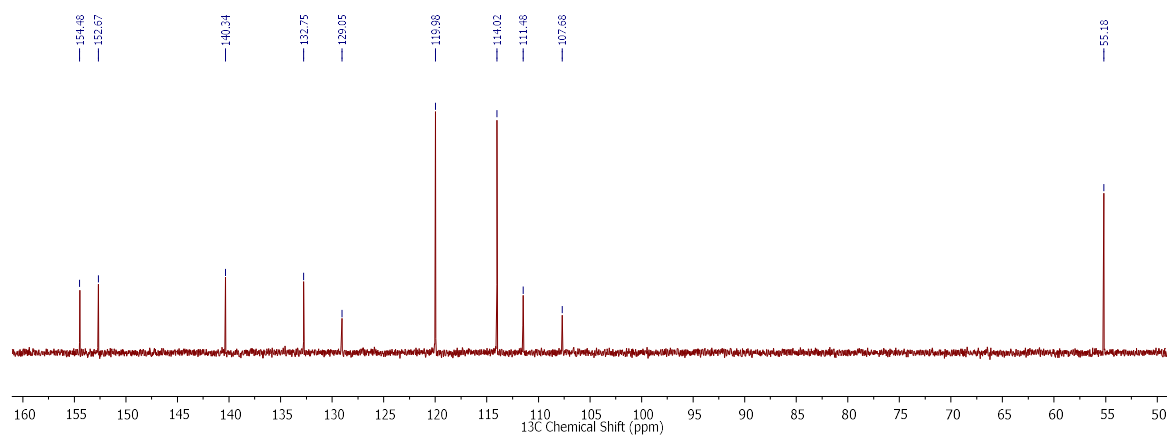
Figure A1.2. $^{13}$C NMR spectrum of receptor **96**.
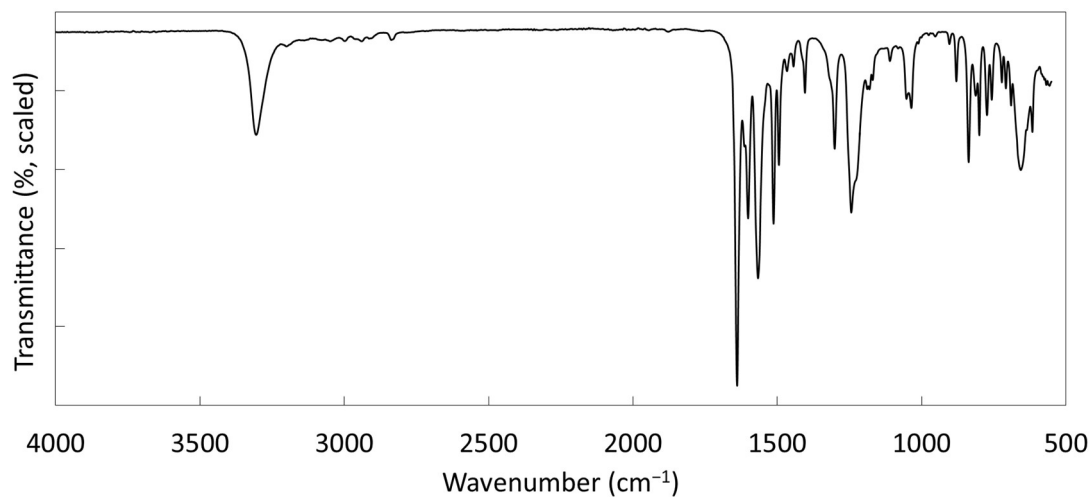
Figure A1.3. FTIR spectrum of receptor **96**.
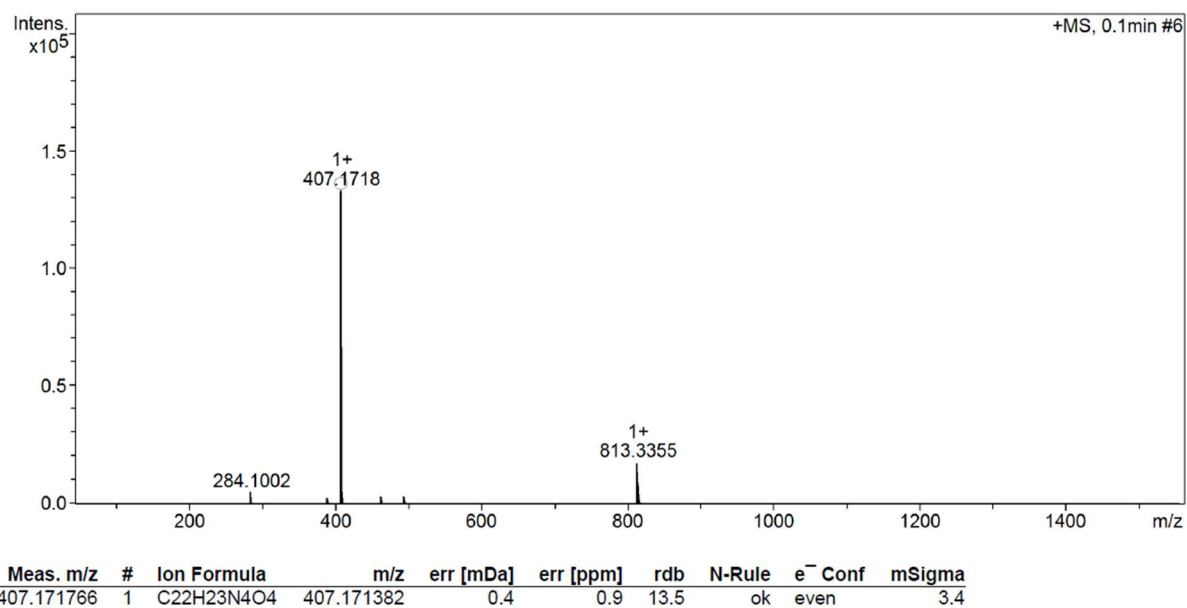
Figure A1.4. Mass spectrograph of receptor **96**.
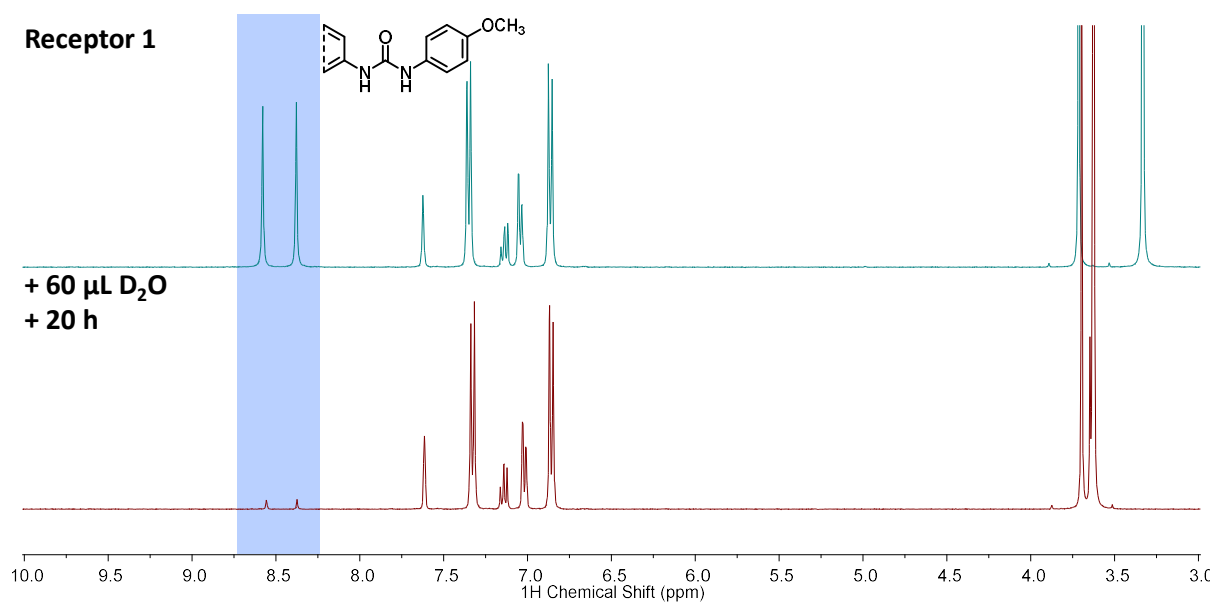


Figure A1.5. Deuterium exchange experiment, showing the change in the ${}^{1}$H NMR spectrum (exchanging urea resonances highlighted in blue) of a sample of receptor **96** after the addition of 60 µL D$_2$O.
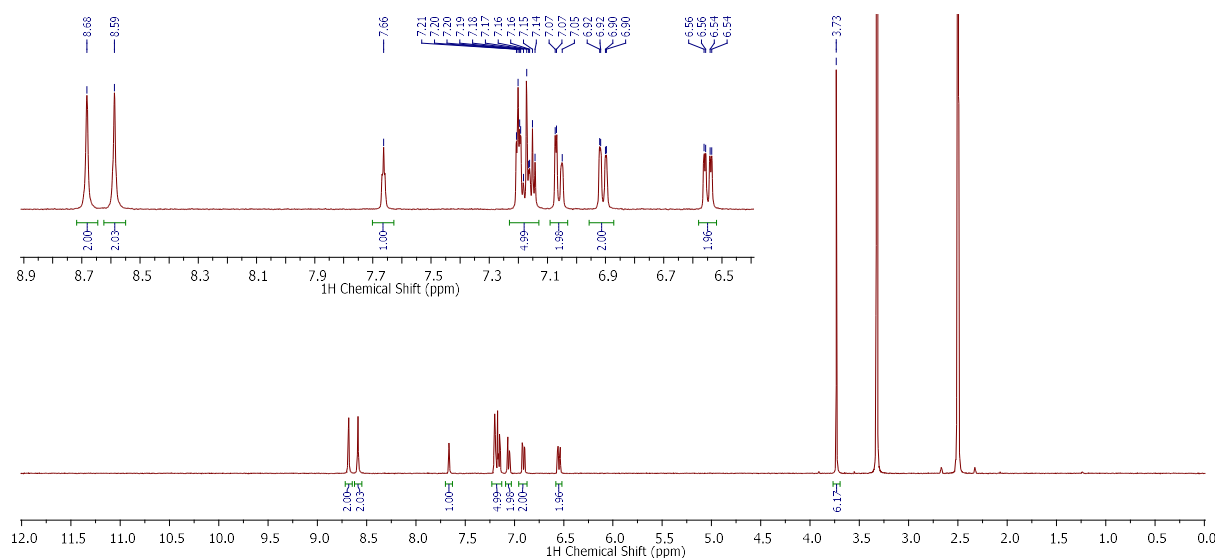
Figure A1.6. $^1$H NMR spectrum of receptor **97**.
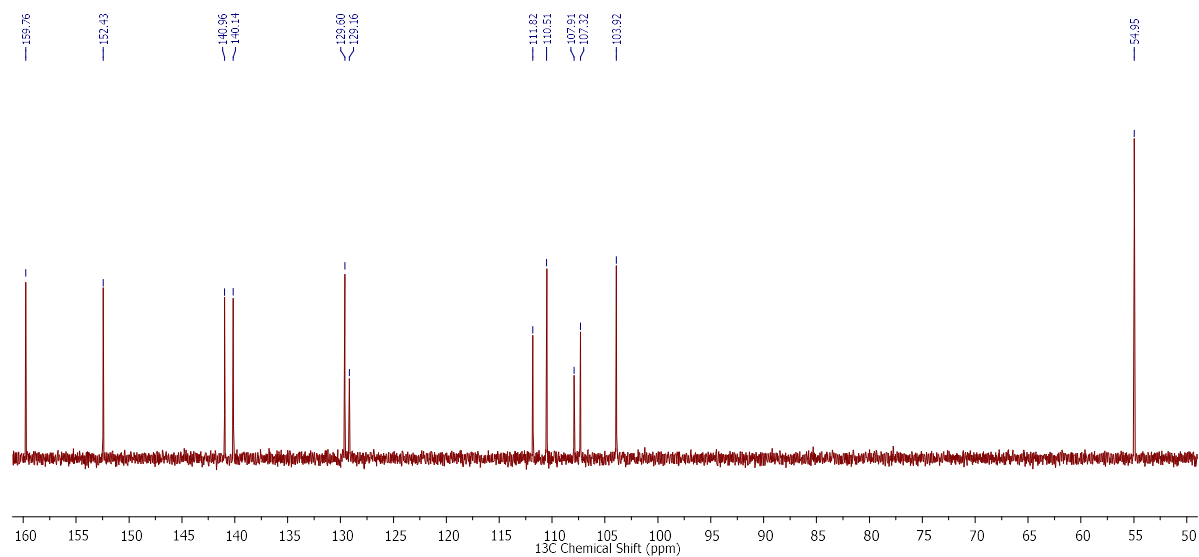
Figure A1.7. $^{13}$C NMR spectrum of receptor **97**.
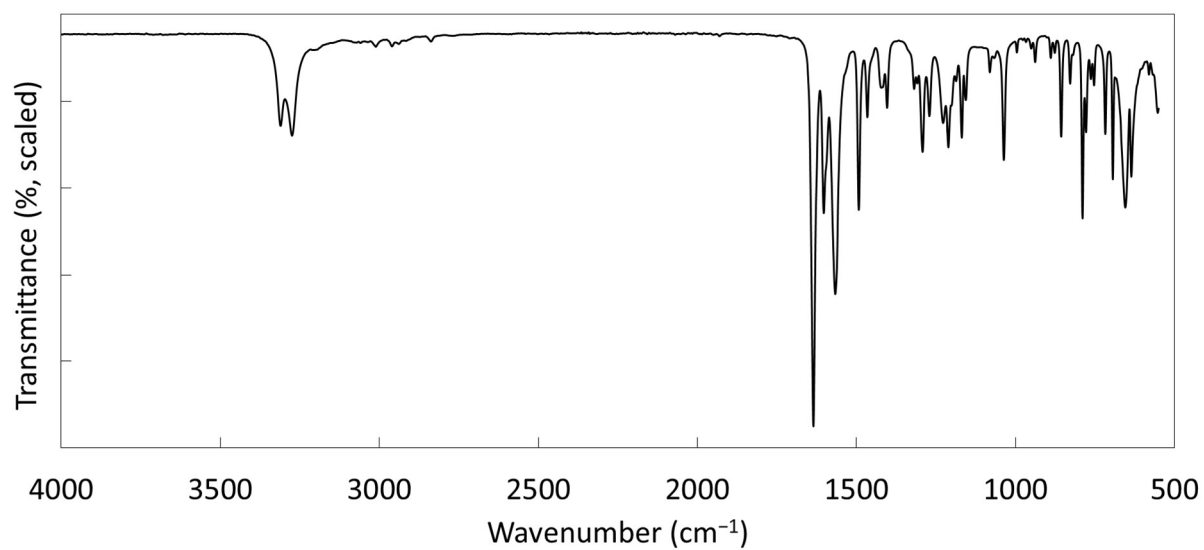
Figure A1.8. FTIR spectrum of receptor **97**.

| Meas. m/z | # | Ion Formula | m/z | err [mDa] | err [ppm] | rdb | N-Rule | e⁻ Conf | mSigma |
|---|---|---|---|---|---|---|---|---|---|
| 407.172460 | 1 | C22H23N4O4 | 407.171382 | 1.1 | 2.6 | 13.5 | ok | even | 46.9 |
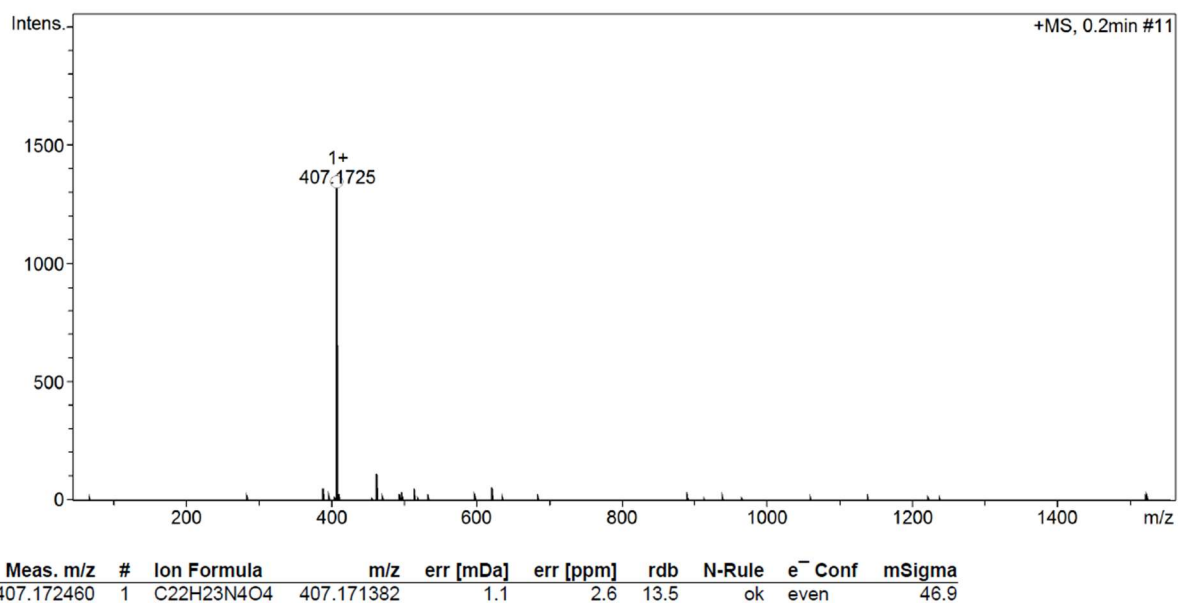
Figure A1.9. Mass spectrograph of receptor **97**.
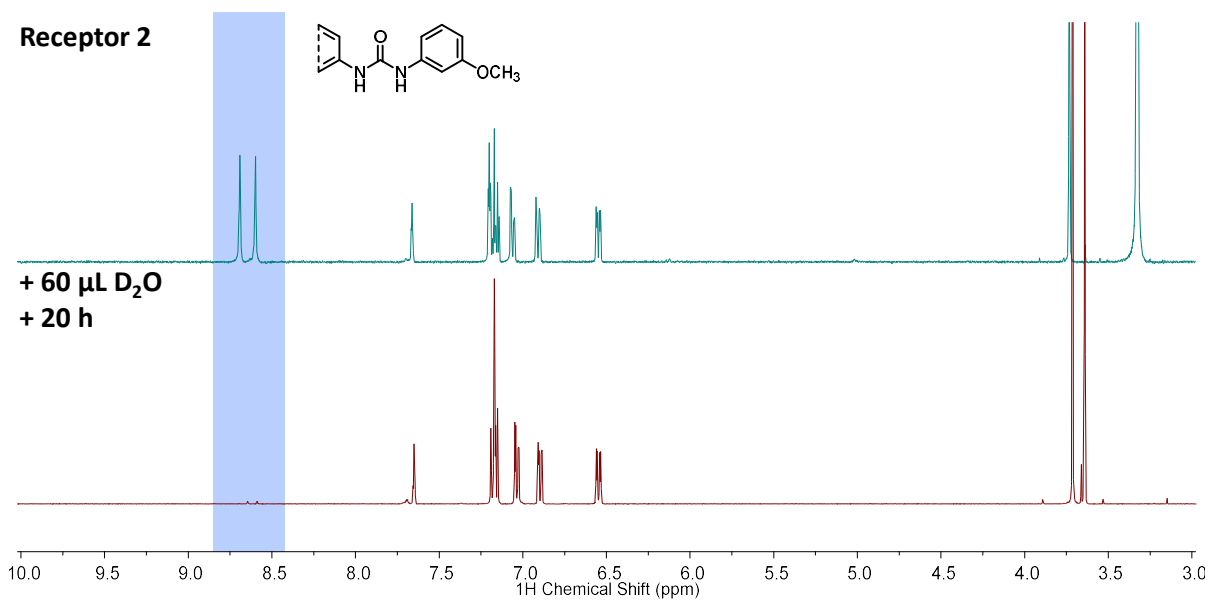


Figure A1.10. Deuterium exchange experiment, showing the change in the $^1$H NMR spectrum (exchanging urea resonances highlighted in blue) of a sample of receptor **97** after the addition of 60 μL D₂O.
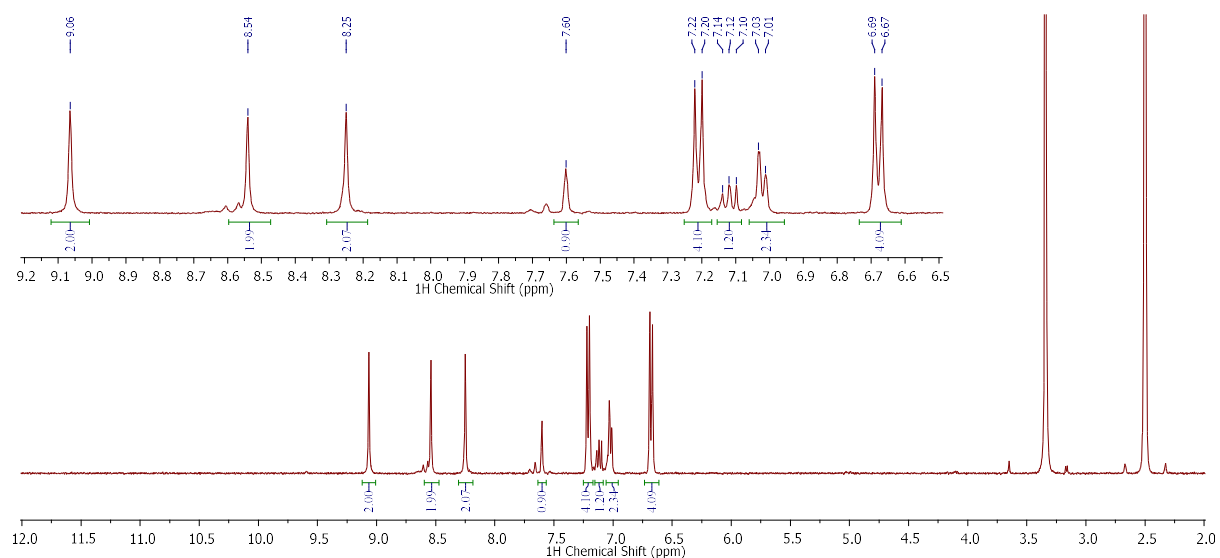
Figure A1.11. $^1$H NMR spectrum of receptor **98**.
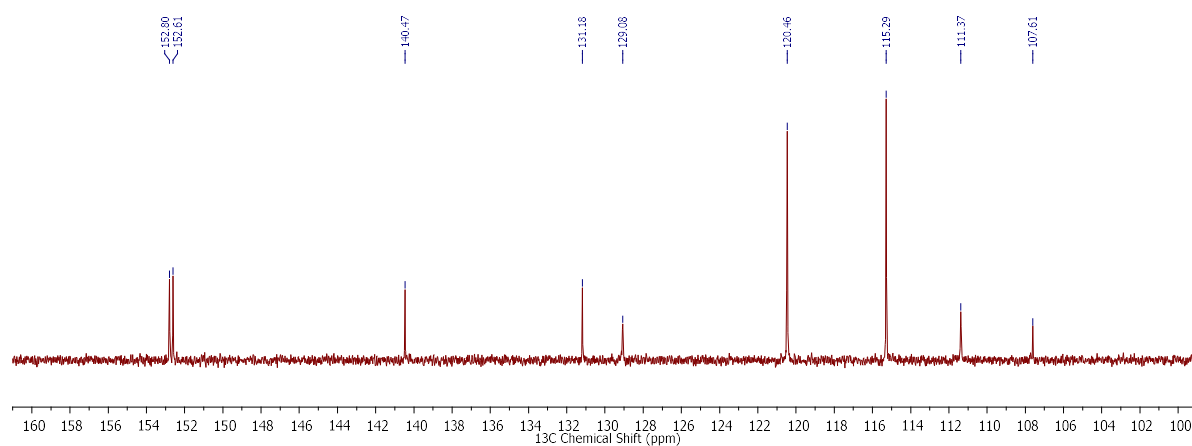


Figure A1.12. $^{13}$C NMR spectrum of receptor **98**.
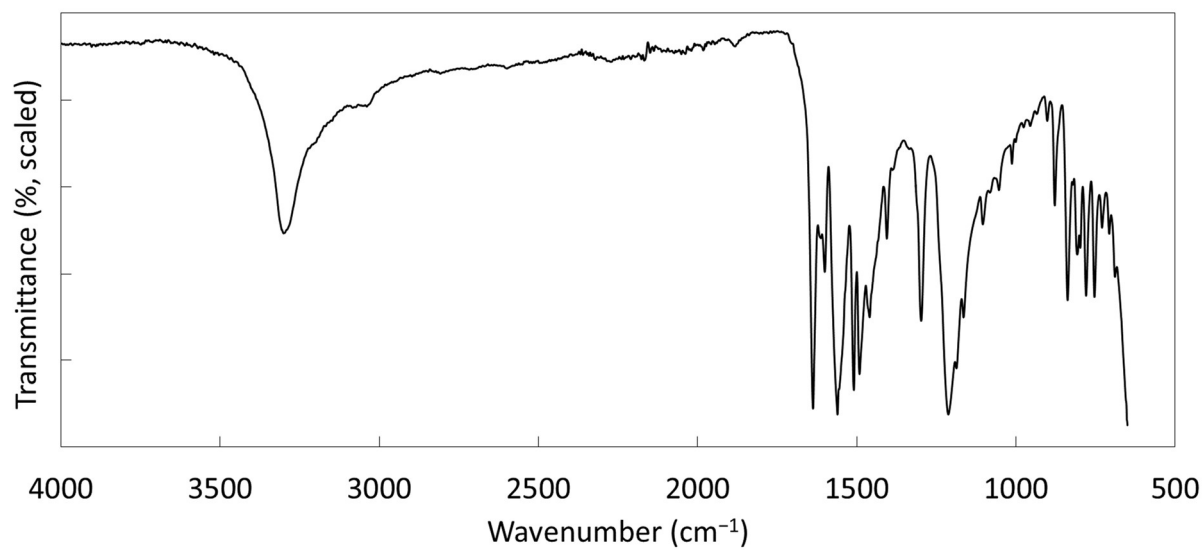


Figure A1.13. FTIR spectrum of receptor **98**.

Figure A1.14. Mass spectrograph of receptor **98**.
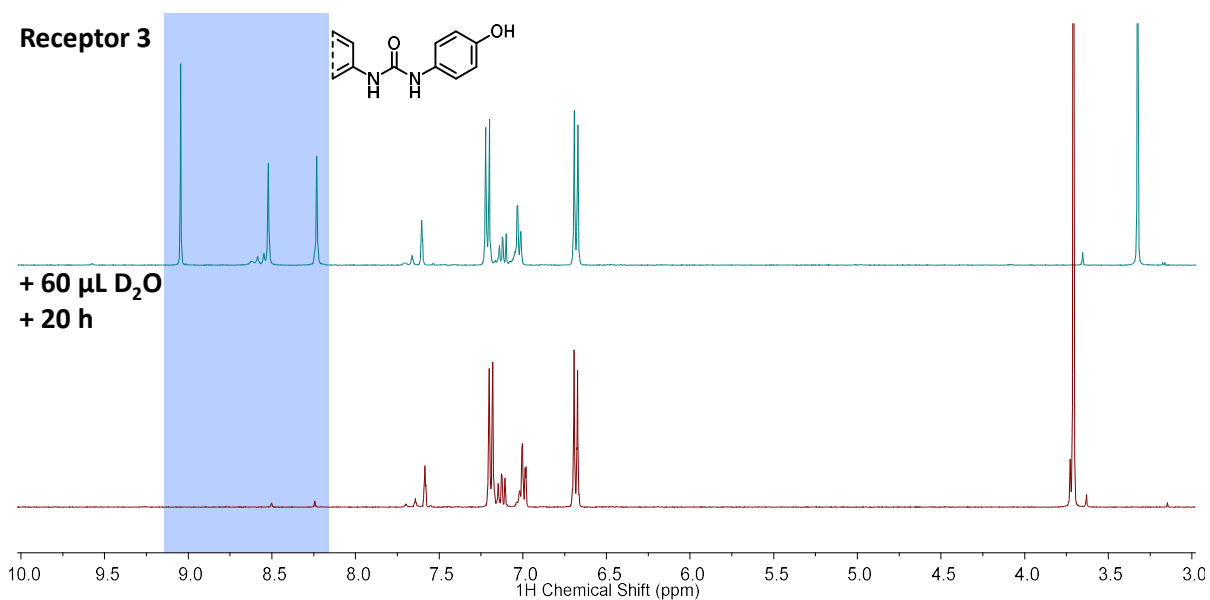


Figure A1.15. Deuterium exchange experiment, showing the change in the $^1$H NMR spectrum (exchanging phenol and urea resonances highlighted in blue) of a sample of receptor **98** after the addition of 60 μL D$_2$O.

**Receptor 3**

**+ TFA**
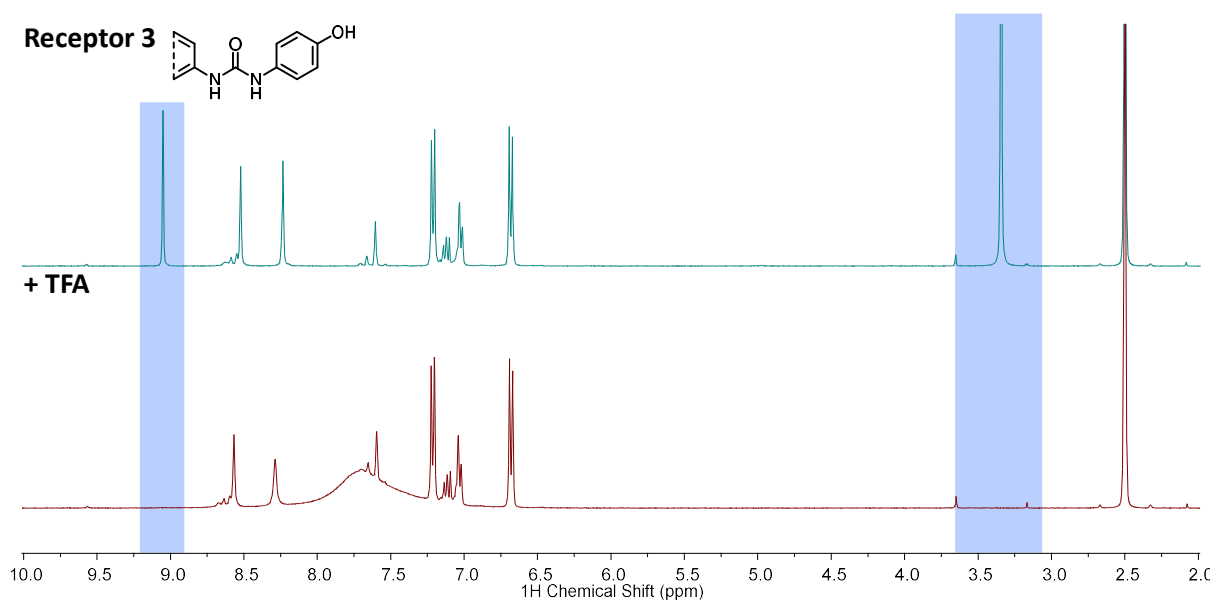
Figure A1.16. Change in the $^1H$ NMR spectrum (coalescing phenol and $H_2O$ resonances highlighted in blue) of a sample of receptor **98** after the addition of 3 drops of neat trifluoroacetic acid (TFA). This demonstrates that the exchange of the phenol and $H_2O$ resonances may be catalyzed by the presence of acids. In this case, the rate of exchange is in the fast regime on the NMR timescale, $k_{ex} \gg |\Delta v|$, as seen by the presence of a single broad resonance at 7.2–8.0 ppm.
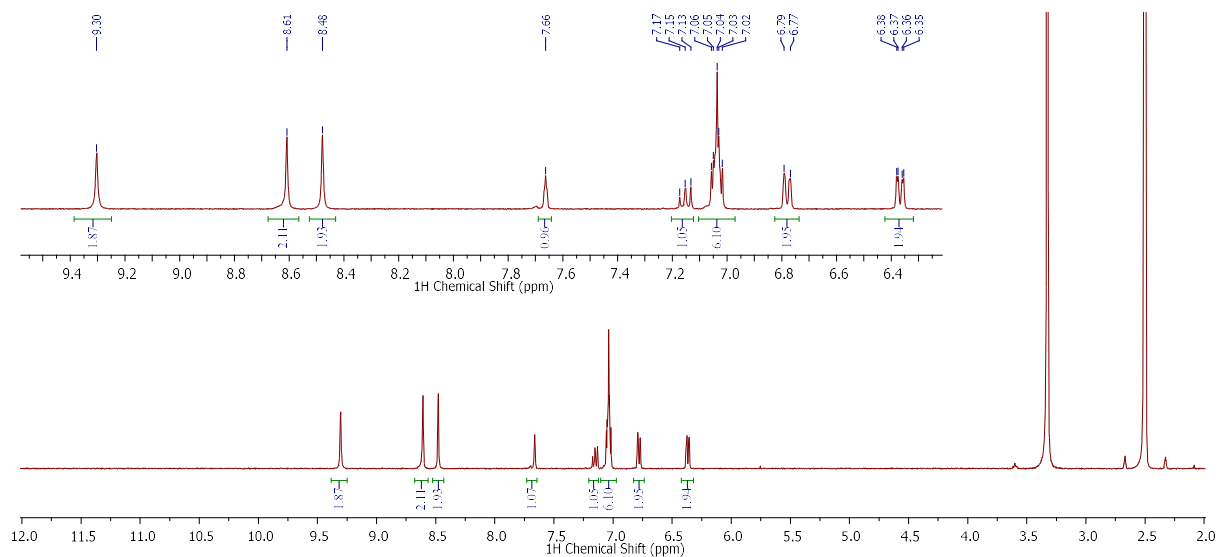


Figure A1.17. $^1H$ NMR spectrum of receptor **99**.
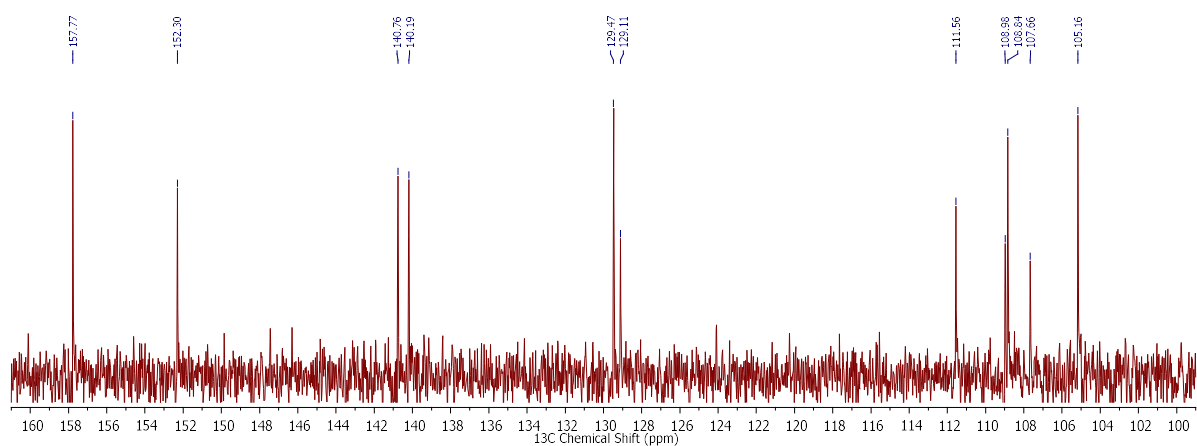
Figure A1.18. $^{13}$C NMR spectrum of receptor **99**.
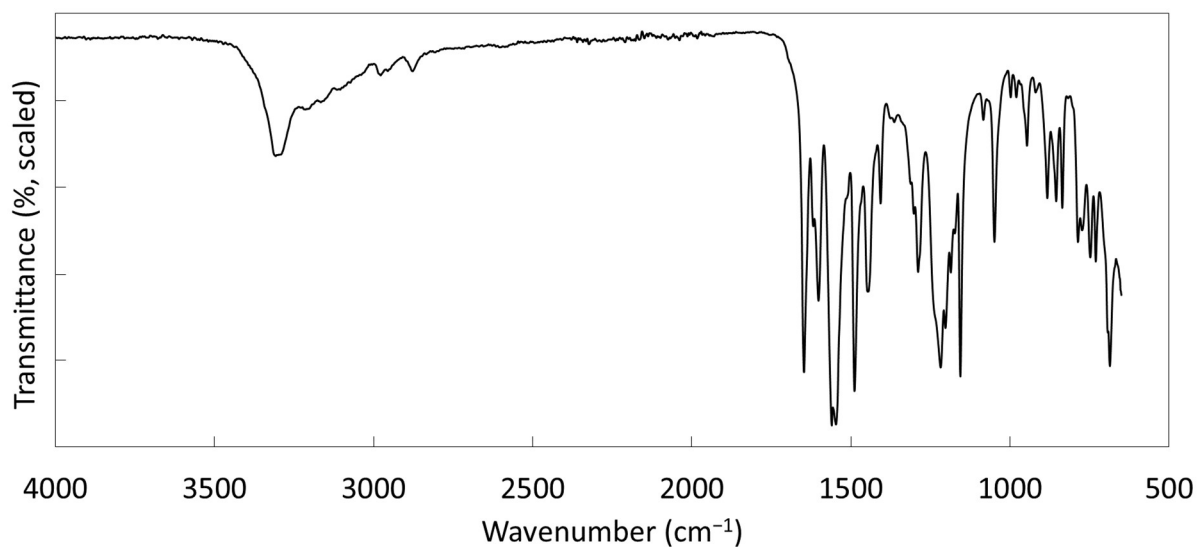


Figure A1.19. FTIR spectrum of receptor **99**.



LCT20141125MF010 17 (0.283)

TOF MS ES+
3.69e+003

| Minimum: | | | | -1.5 | | | | | | |
|----------|------|-----|-----|-------|-------|---------|------|----|----|-----|
| Maximum: | | 5.0 | 5.0 | 500.0 | | | | | | |
| | | | | | | | | | | |
| Mass | Calc. Mass | mDa | PPM | DBE | i-FIT | Formula | | | | |
| | | | | | | | | | | |
| 401.1215 | 401.1226 | -1.1 | -2.7 | 13.5 | 1.7 | C20 | H18 | N4 | O4 | Na |
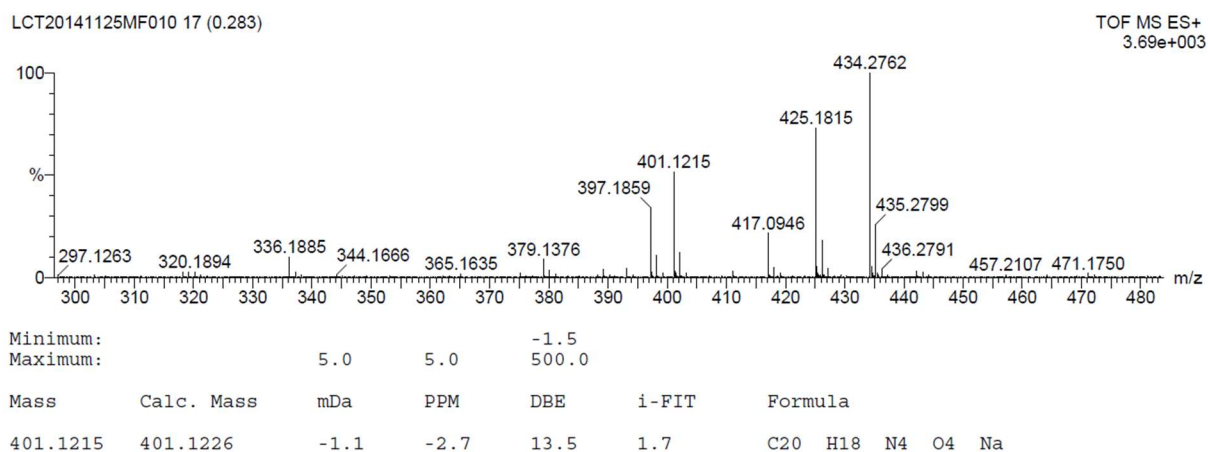
Figure A1.20. Mass spectrograph of receptor **99**.

178
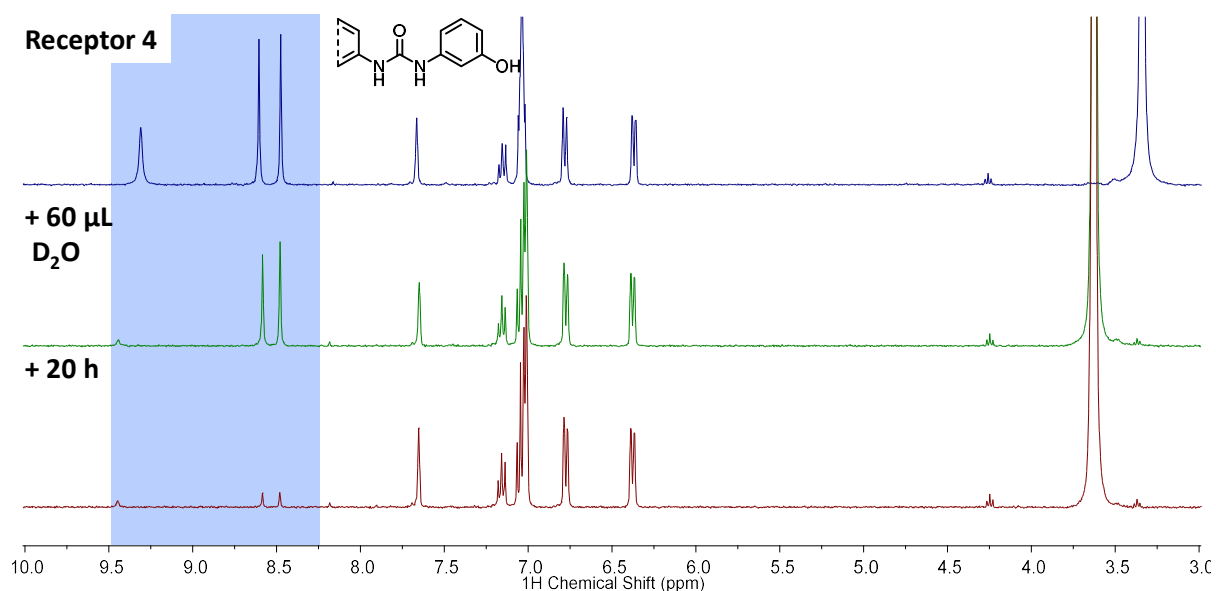
Figure A1.21. Deuterium exchange experiment, showing the change in the $^1$H NMR spectrum (exchanging phenol and urea resonances highlighted in blue) of a sample of receptor **99** after the addition of 60 μL D$_2$O.
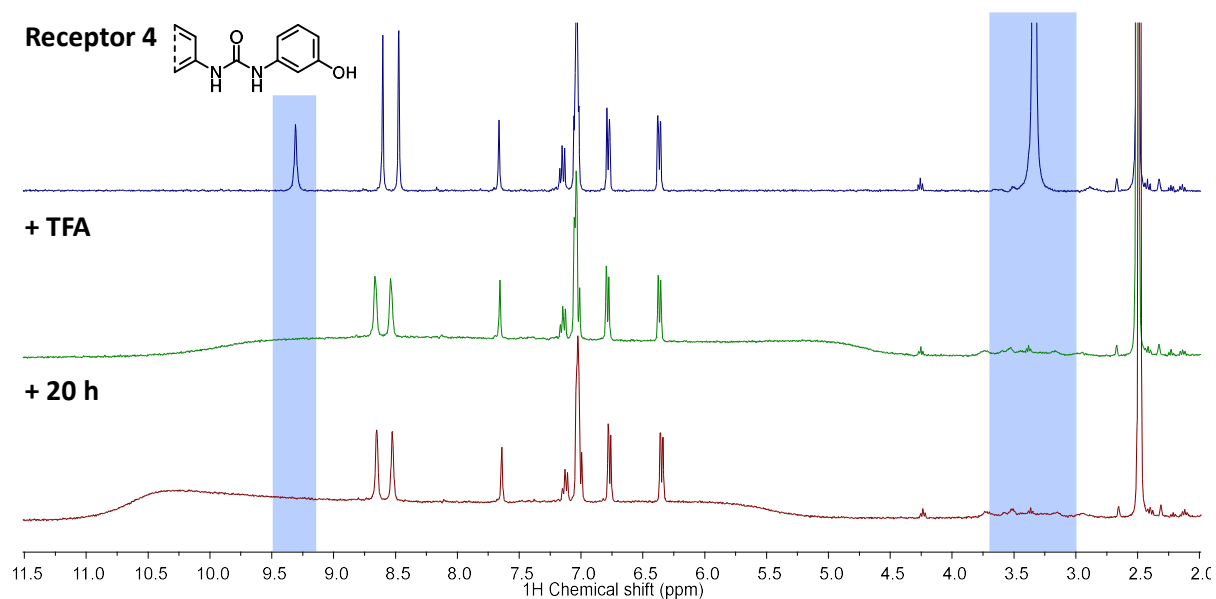


Figure A1.22. Change in the $^1$H NMR spectrum (coalescing phenol and H$_2$O resonances highlighted in blue) of a sample of receptor **4** after the addition of 3 drops of neat trifluoroacetic acid (TFA). This demonstrates that the exchange of the phenol and H$_2$O resonances may be catalyzed by the presence of acids. In this case, the rate of exchange is within the intermediate regime on the NMR timescale, $k_{ex} \approx |\Delta\nu|$, as seen by the presence of a wide, flat resonance over the region 4.5–11.0 ppm.
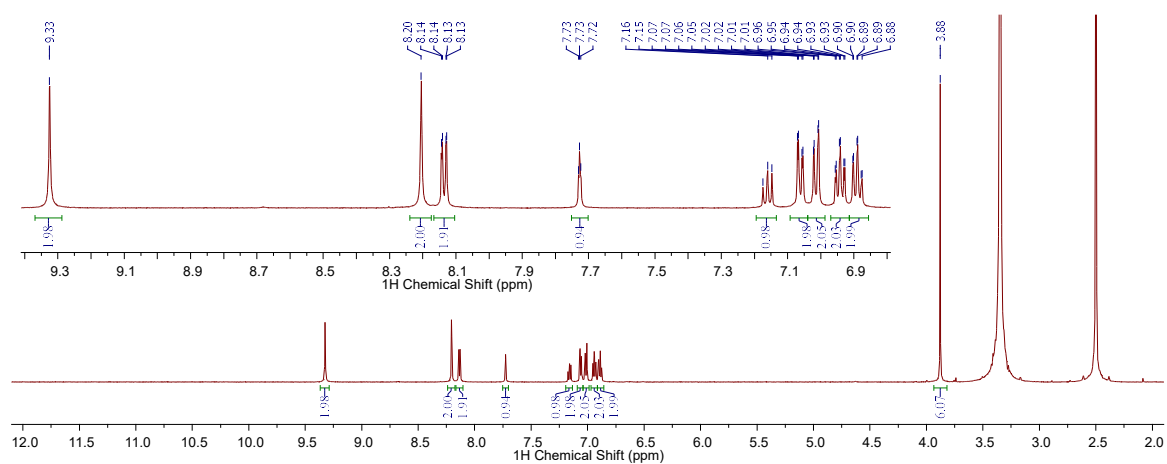
Figure A1.23. $^1$H NMR spectrum of receptor **100**.
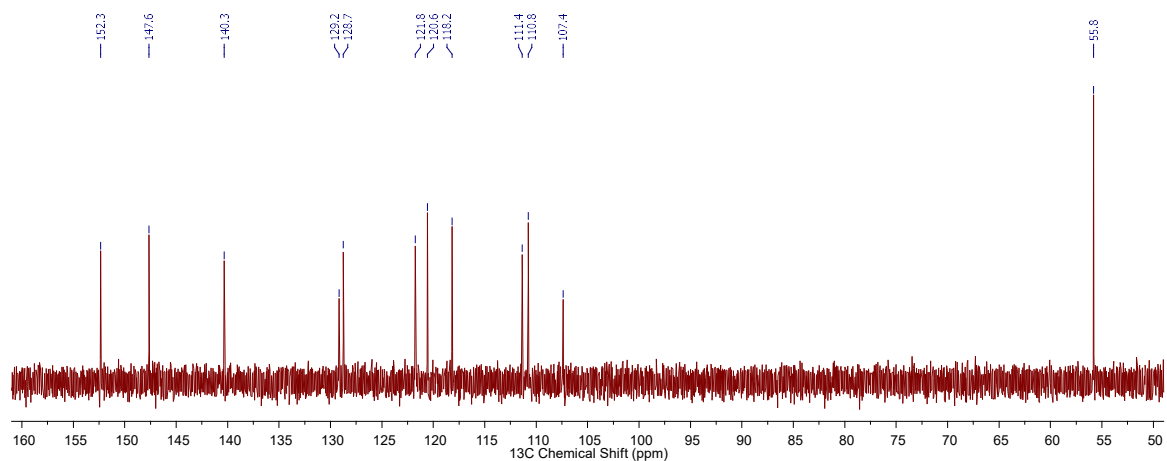
Figure A1.24. $^{13}$C NMR spectrum of receptor **100**.
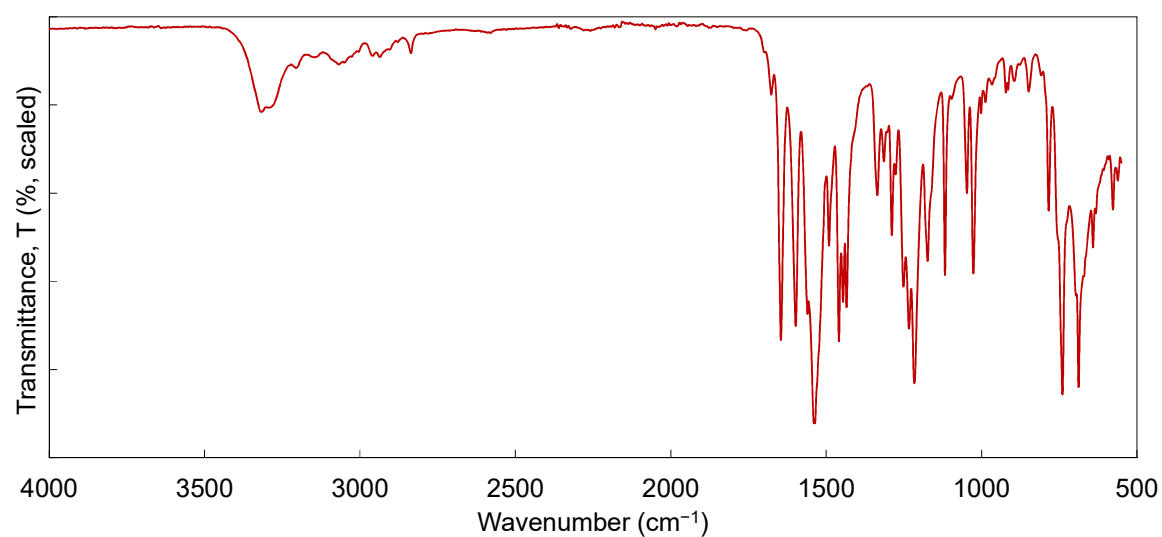
Figure A1.25. FTIR spectrum of receptor **100**.

Figure A1.26. Mass spectrograph of receptor **100**.

## A1.1.2 Crystalline adducts

### A1.1.2.1 X-ray: Ellipsoid plots
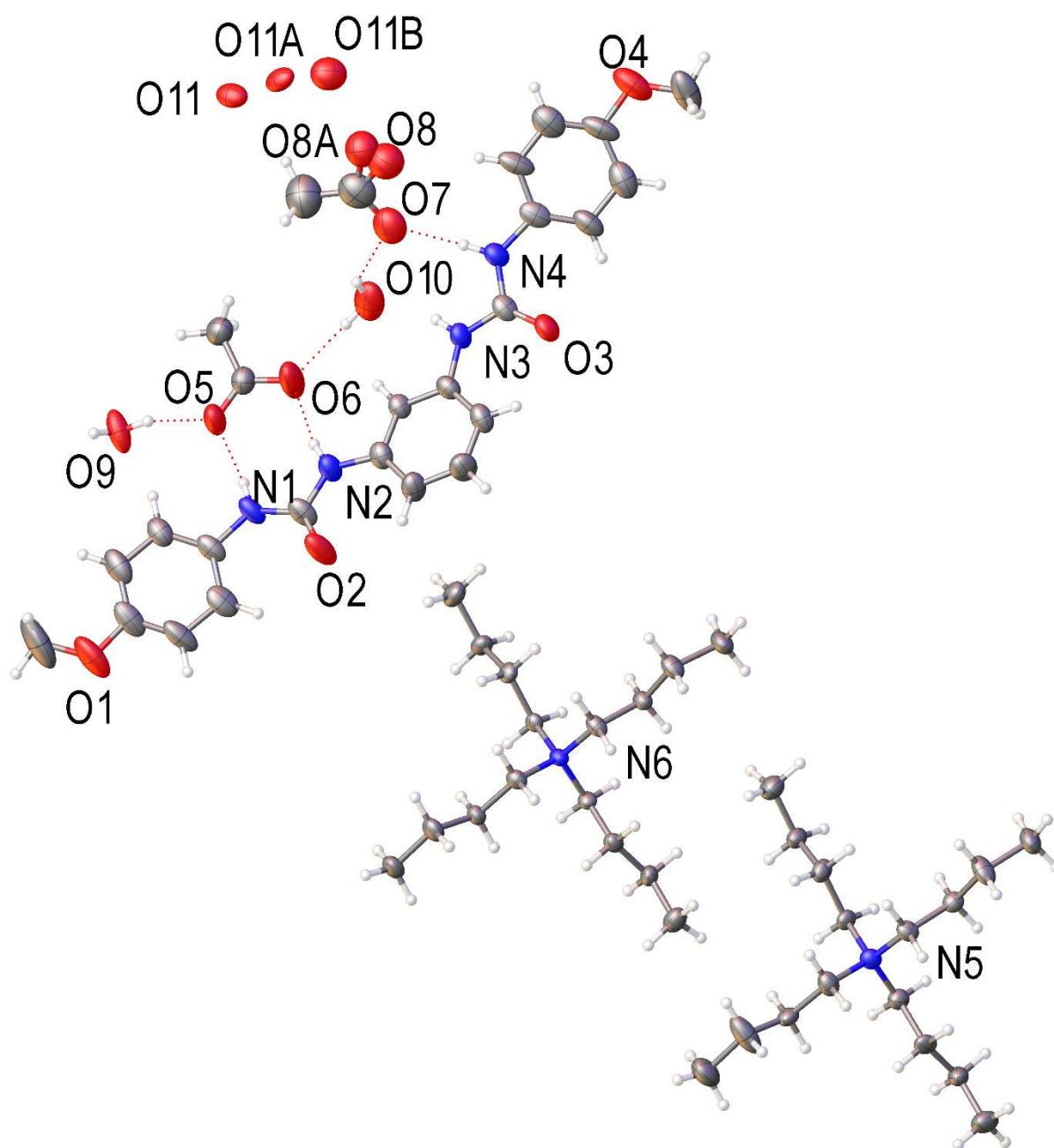


Figure A1.27. Asymmetric unit of **1**(TBAOAc)$_2$·3H$_2$O with heteroatom labelling scheme. Ellipsoids rendered at 50% probability level.
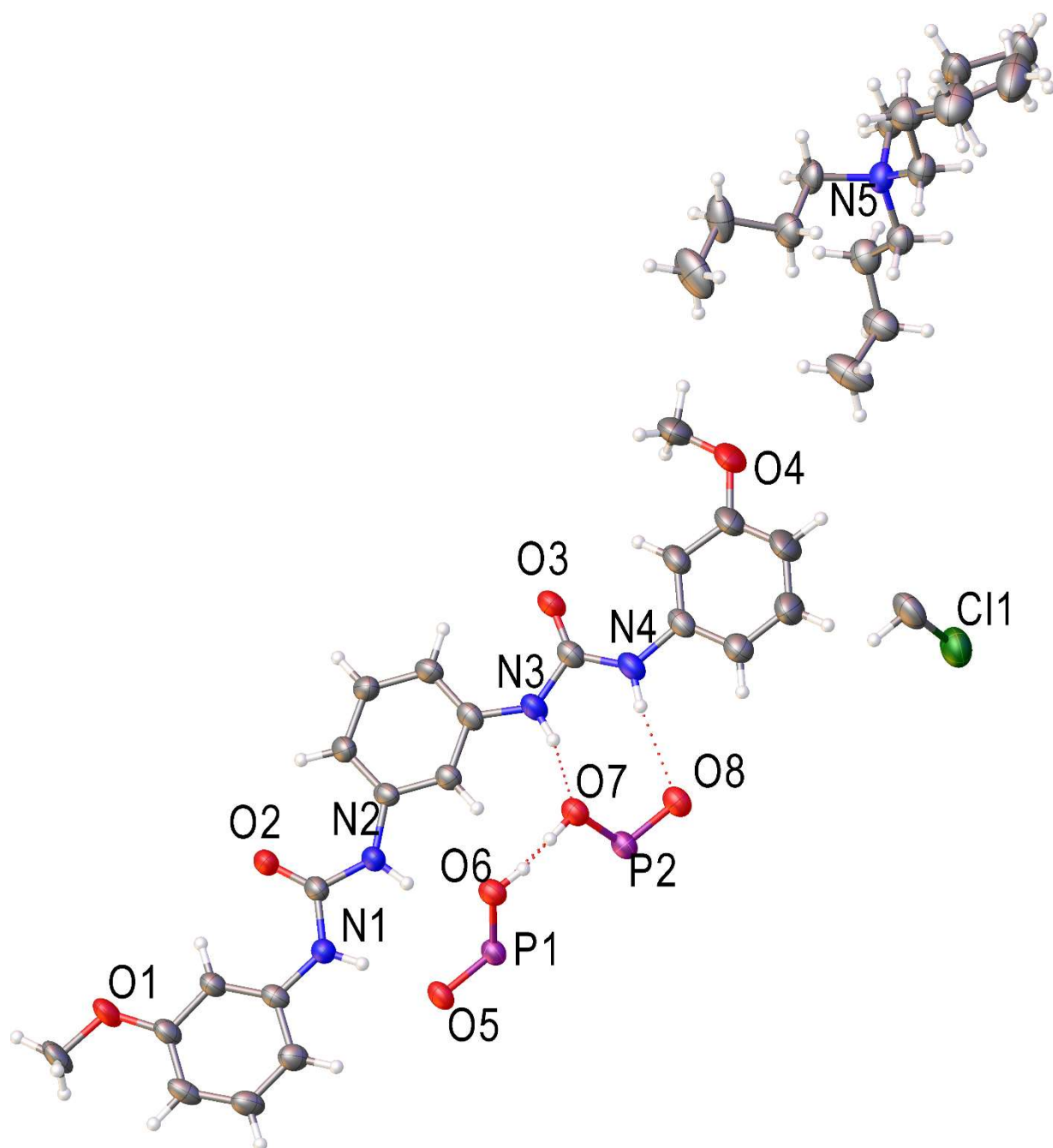
Figure A1.28. Asymmetric unit of $\mathbf{3}_3$(TBA$_3$H$_3$P$_2$O$_8$)·0.5CHCl$_3$ with heteroatom labelling scheme. Ellipsoids rendered at 50% probability level.

A1.1.2.2 Characterization of **2**₃(TBA₃H₂P₂O₈)·0.5CHCl₃

*1.1.2.2.1   ¹H NMR Experiments*
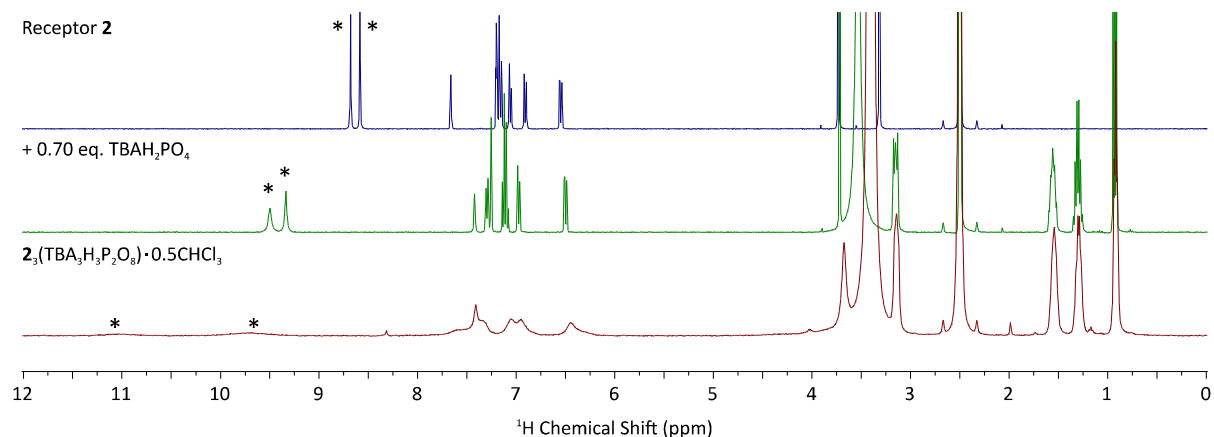


Figure A1.29. Stack plot comparing the ¹H NMR spectra (0–12 ppm) of receptor **2** (top, blue), the same solution after the addition of 0.70 equivalents of TBAH₂PO₄ (middle, green), and a dissolved sample of crystalline **2**₃(TBA₃H₂P₂O₈)·0.5CHCl₃ (bottom, red), all in DMSO-*d₆*.
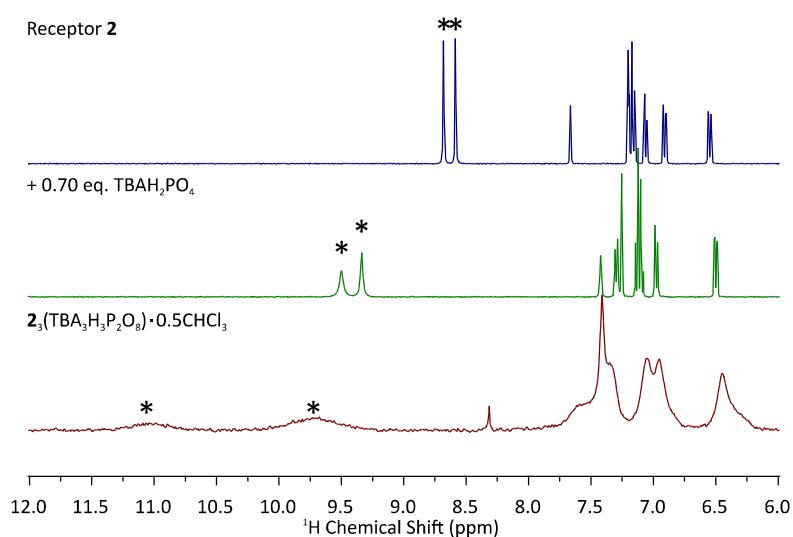


Figure A1.30. Expansion of the 6–12 ppm region, showing the location of the NH resonances (marked with asterisks). The resonance at 8.3 ppm in the bottom spectrum is due to the chloroform present within the crystal of **2**₃(TBA₃H₂P₂O₈)·0.5CHCl₃.
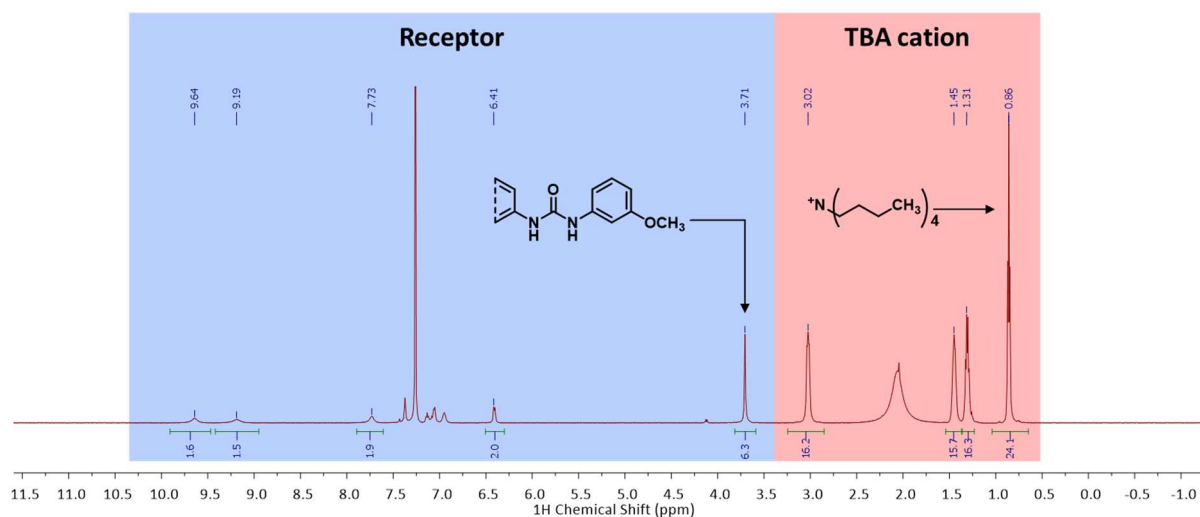
Figure A1.31. $^1$H NMR spectrum obtained after adding a crystal of $\mathbf{2}_3(TBA_3H_2P_2O_8)\cdot0.5CHCl_3$ to CDCl$_3$. The regions corresponding to the resonances of the receptor and TBA cation are highlighted in blue and red, respectively. The integration has been normalized with respect to receptor $\mathbf{2}$, demonstrating a receptor-cation ratio of 1:2, rather than the ratio of 1:1 present in the crystalline sample.

### 1.1.2.2.2  FTIR Spectra
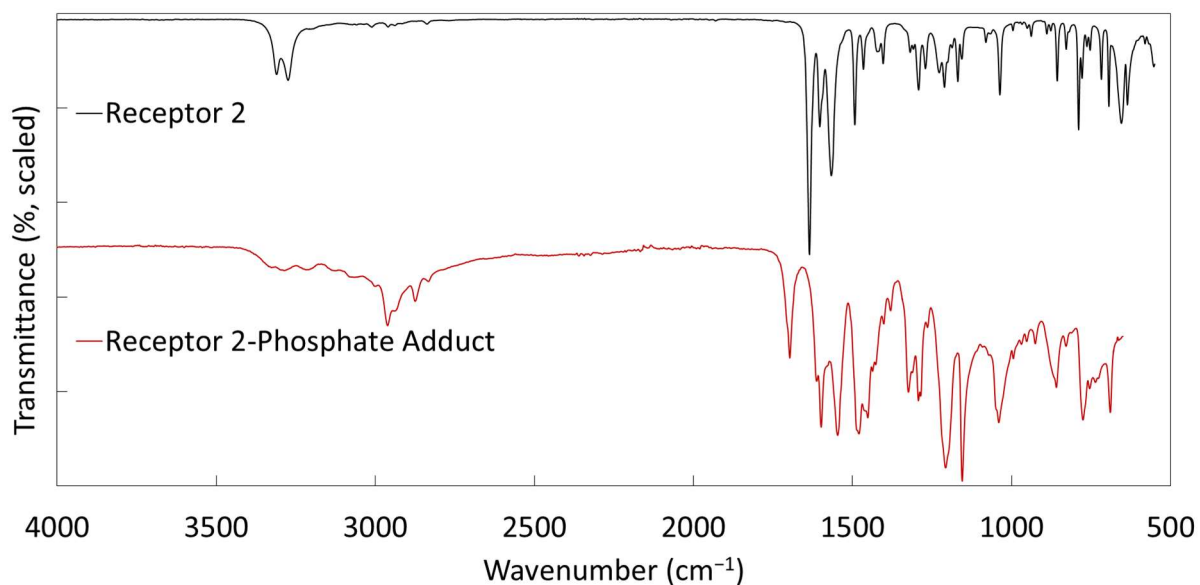


Figure A1.32. FTIR spectra of receptor $\mathbf{2}$ (top, black) and $\mathbf{2}_3(TBA_3H_2P_2O_8)\cdot0.5CHCl_3$ (bottom, red).

## A1.1.3 ^{1}H NMR spectra of 1,3-phenylene diisocyanate in DMSO-*d$_6$*
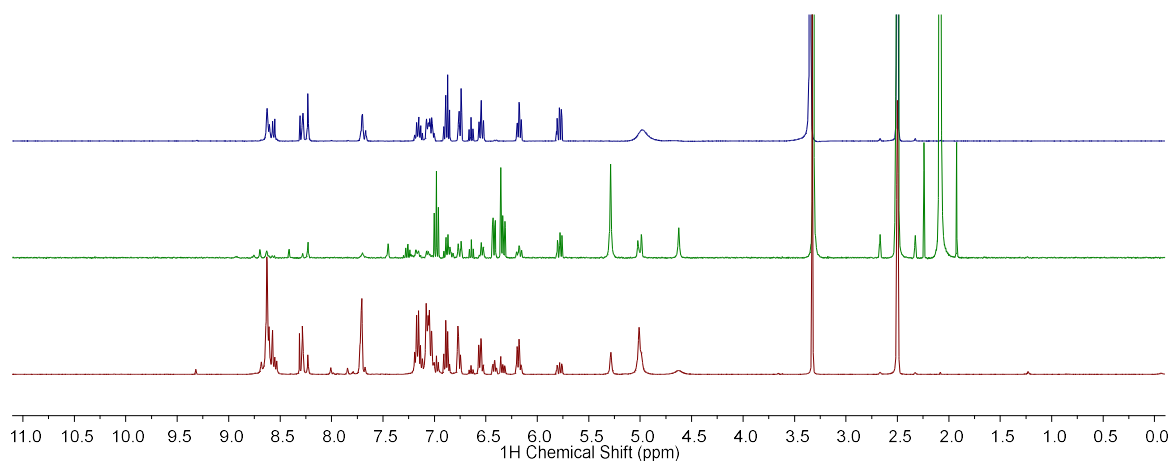


Figure A1.33. Three ^{1}H NMR spectra (400 MHz, 0–11 ppm, DMSO-*d$_6$*)showing the mix of degradation products formed when 1,3-phenylene diisocyanate is dissolved in DMSO-*d$_6$*.

# A1.2 Appendices for Chapter 3

## A1.2.1 Characterisation of Intermediates **126** and **127**
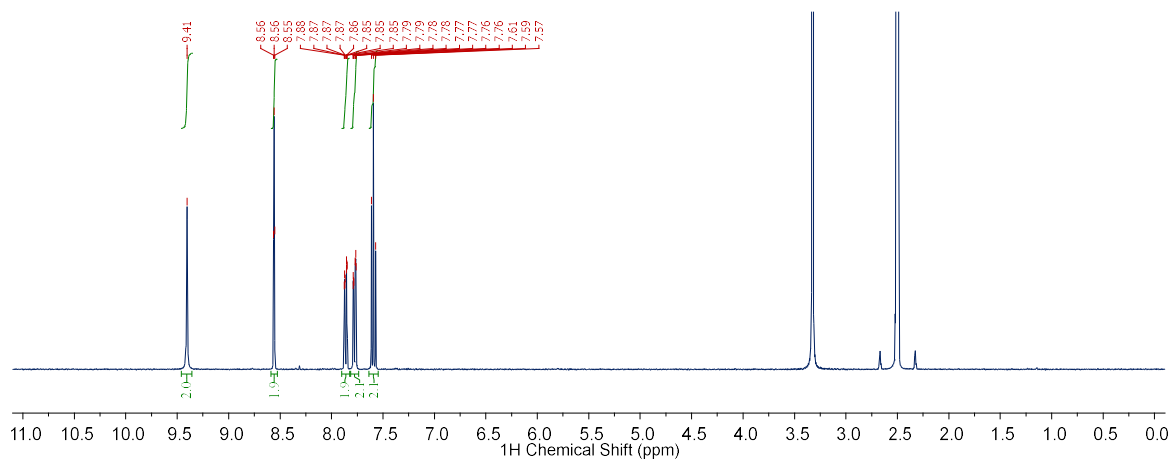


Figure A1.34. ^{1}H NMR spectrum of **126** (400 MHz, 0–11 ppm, DMSO-*d$_6$*)
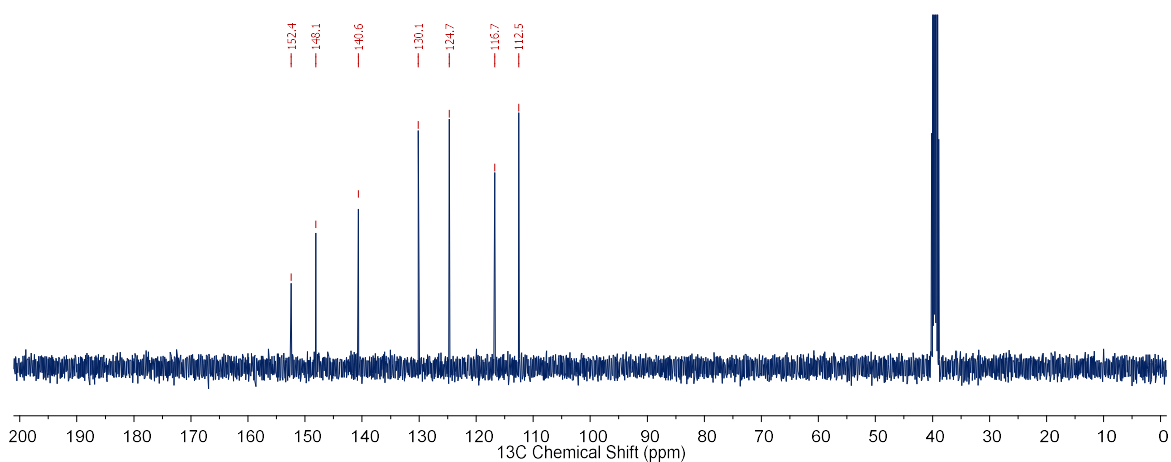
Figure A1.35. $^{13}$C NMR spectrum of **126** (101 MHz, 0–200 ppm, DMSO-$d_6$)
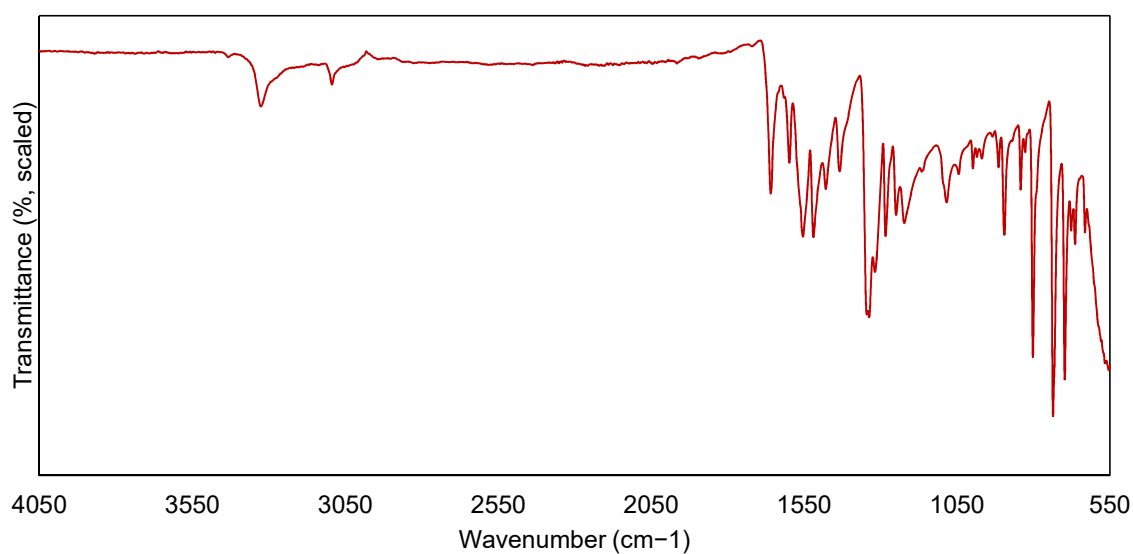


Figure A1.36. FTIR spectrum of **126** (550–4050 cm$^{-1}$).
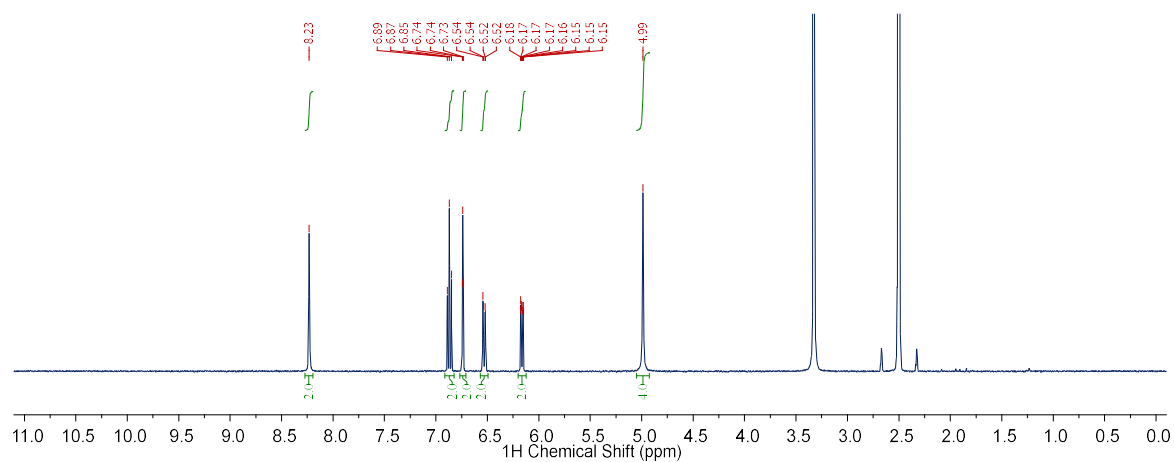


Figure A1.37. $^1$H NMR spectrum of **127** (400 MHz, 0–11 ppm, DMSO-$d_6$)
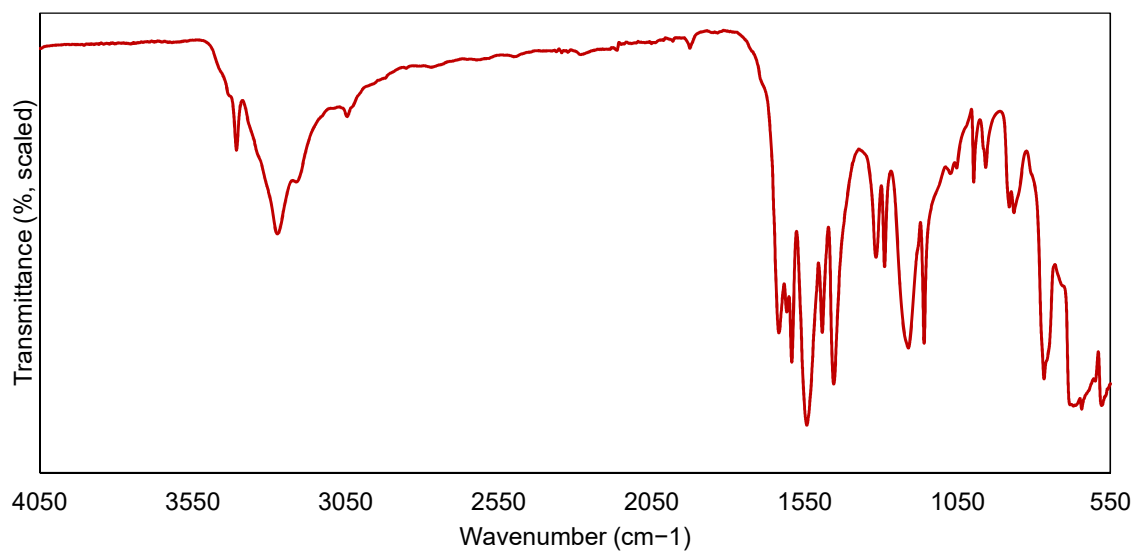
Figure A1.38. FTIR spectrum of **127** (550–4050 cm$^{-1}$).

## A1.2.2 Characterisation of Receptors **101**–**105**
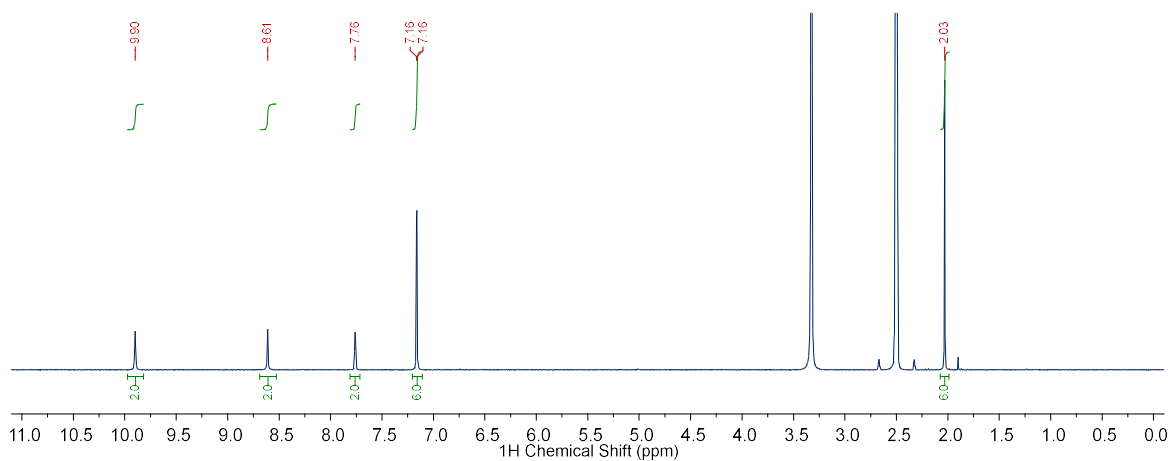


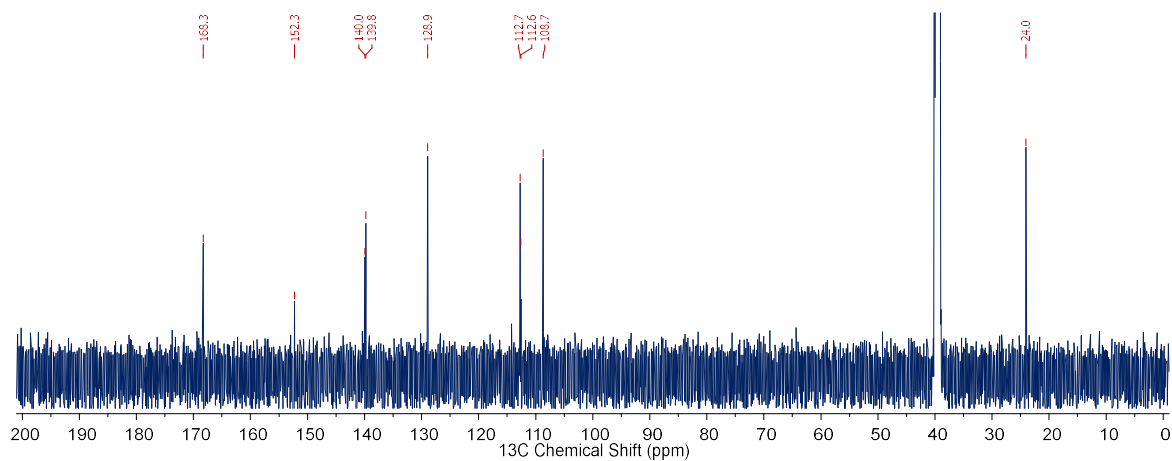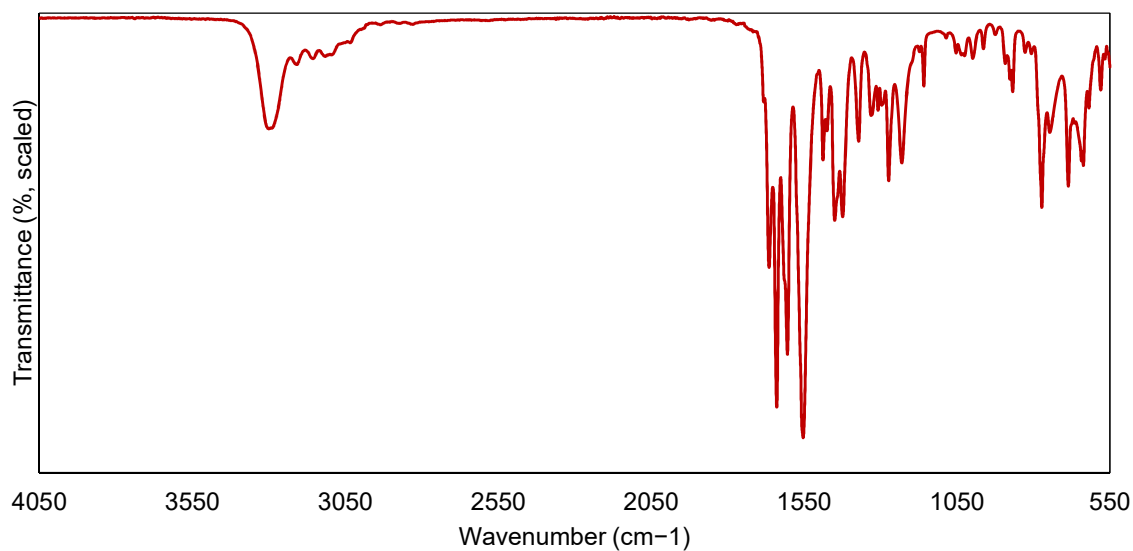Figure A1.39. $^1$H NMR spectrum of **101** (400 MHz, 0–11 ppm, DMSO-$d_6$)



Figure A1.40. $^{13}$C NMR spectrum of **101** (151 MHz, 0–200 ppm, DMSO-$d_6$)

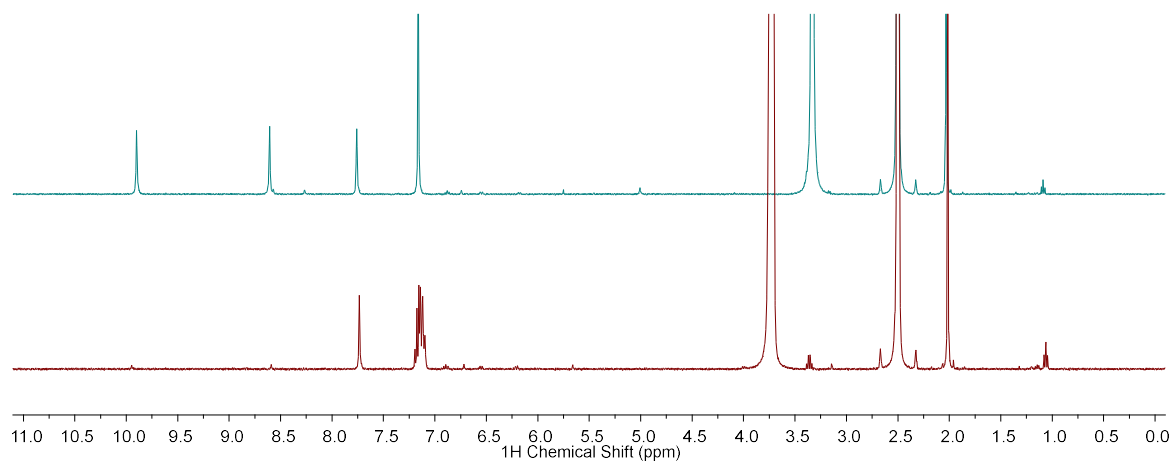Figure A1.41. FTIR spectrum of **101** (550–4050 cm$^{-1}$).



Figure A1.42. Deuterium exchange experiment, showing the change in the $^1$H NMR spectrum of a sample of receptor **101** after the addition of D$_2$O.
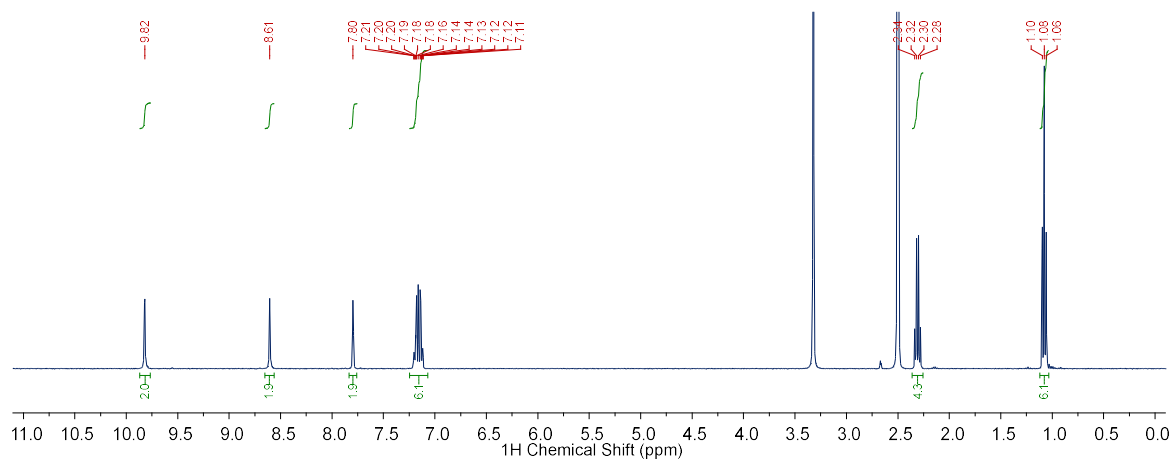


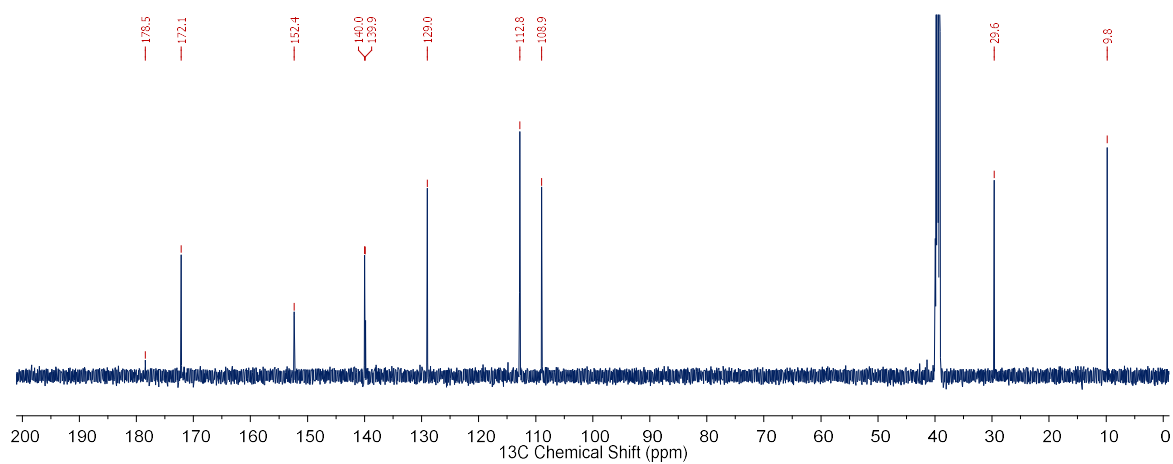Figure A1.43. $^1$H NMR spectrum of **102** (400 MHz, 0–11 ppm, DMSO-$d_6$)

189

Figure A1.44. $^{13}C$ NMR spectrum of **102** (151 MHz, 0–200 ppm, DMSO-$d_6$)

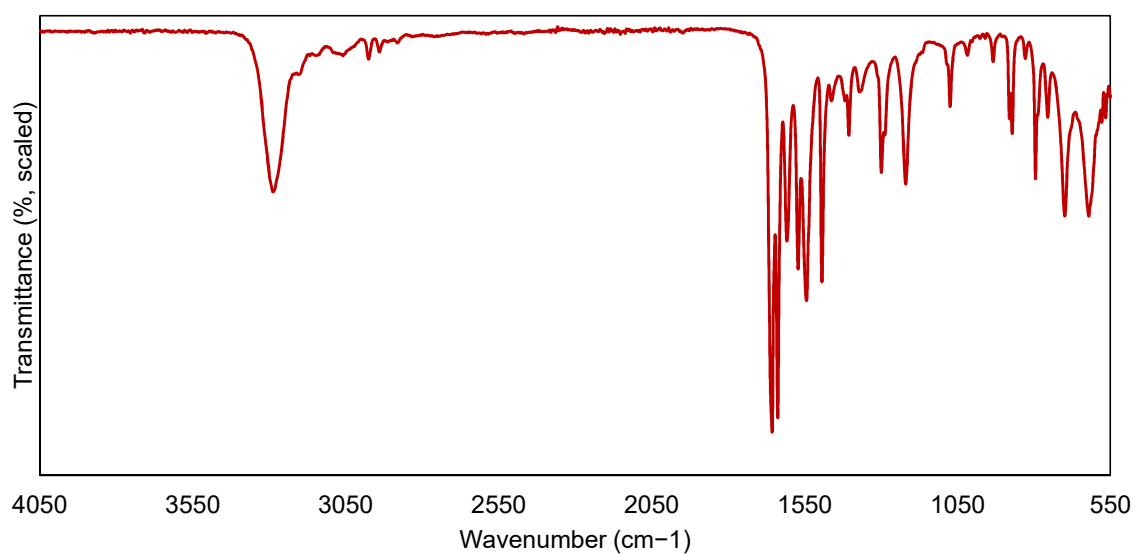

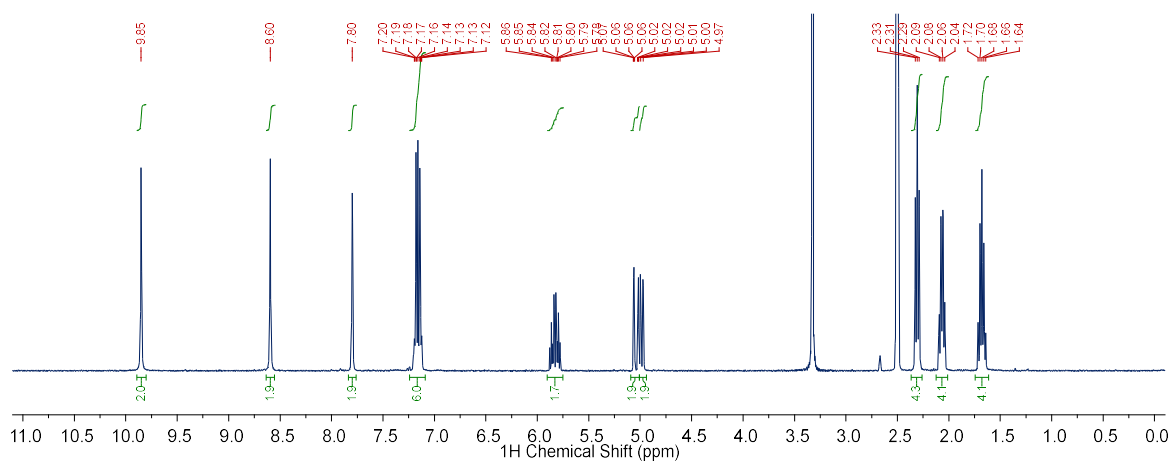Figure A1.45. FTIR spectrum of **102** (550–4050 cm$^{-1}$).



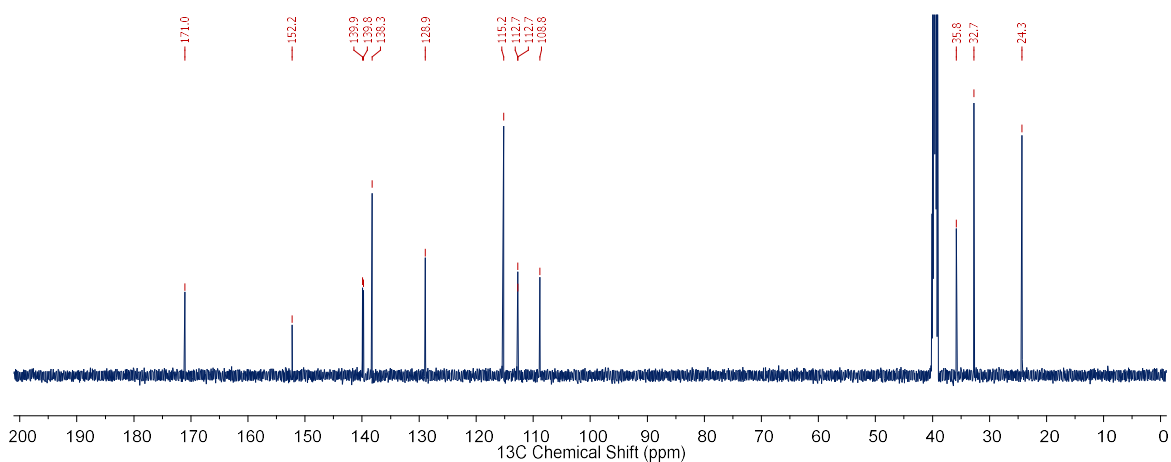Figure A1.46. $^1H$ NMR spectrum of **103** (400 MHz, 0–11 ppm, DMSO-$d_6$)

Figure A1.47. $^{13}$C NMR spectrum of **103** (151 MHz, 0–200 ppm, DMSO-*d₆*)
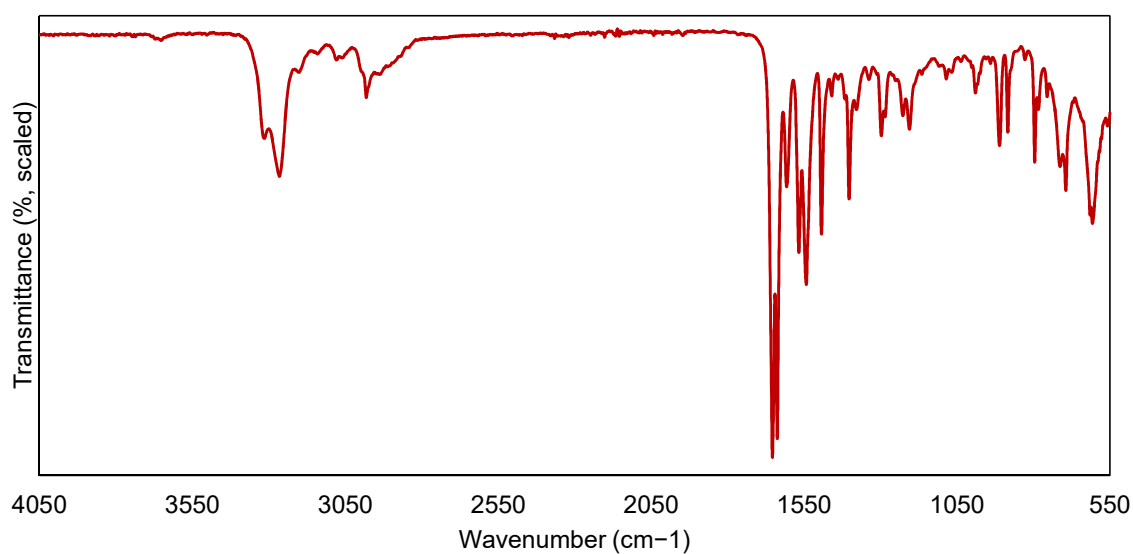


Figure A1.48. FTIR spectrum of **103** (550–4050 cm$^{-1}$).



Figure A1.49. $^1$H NMR spectrum of **104** (400 MHz, 0–11 ppm, DMSO-*d₆*)

Figure A1.50. FTIR spectrum of **104** (550–4050 cm$^{-1}$).



Figure A1.51. $^1$H NMR spectrum of **105** (400 MHz, 0–11 ppm, DMSO-*d₆*)



Figure A1.52. $^{13}$C spectrum NMR of **105** (151 MHz, 0–200 ppm, DMSO-*d₆*)
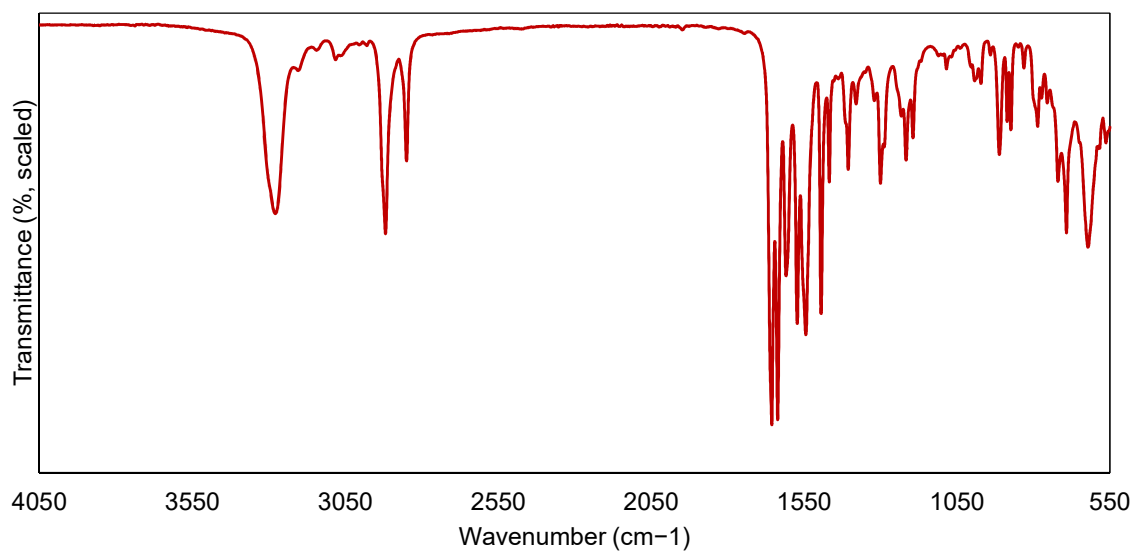
Figure A1.53. FTIR spectrum of **105** (550–4050 cm$^{-1}$).



Figure A1.54. Deuterium exchange experiment, showing the change in the $^{1}$H NMR spectrum of a sample of receptor **105** after the addition of D$_2$O.

# A1.3 Appendices for Chapter 4

## A1.3.1 Characterisation of Intermediates **132**–**136** and **140**



Figure A1.55. $^1$H spectrum NMR of **132** (600 MHz, 0–11 ppm, DMSO-$d_6$)



Figure A1.56. $^{13}$C spectrum NMR of **132** (151 MHz, 0–200 ppm, DMSO-$d_6$)
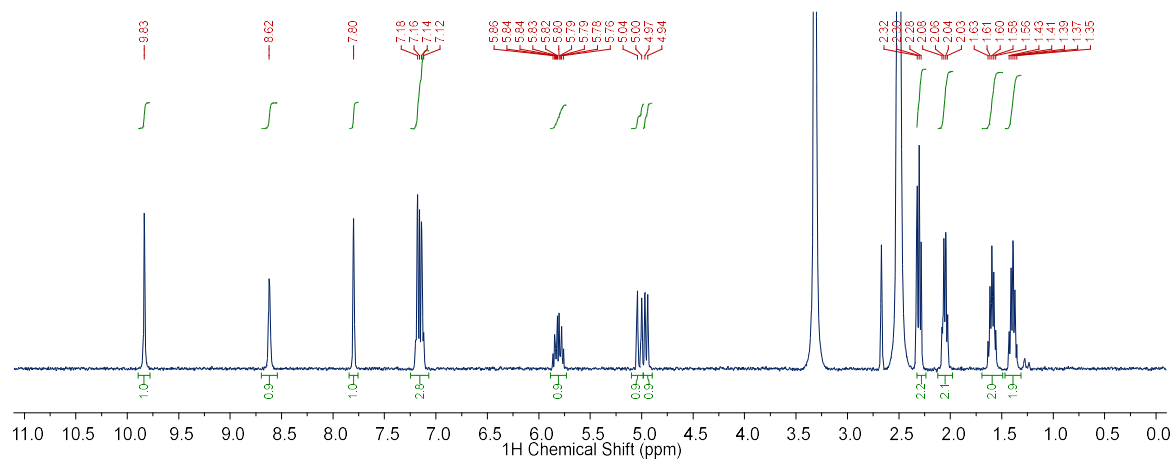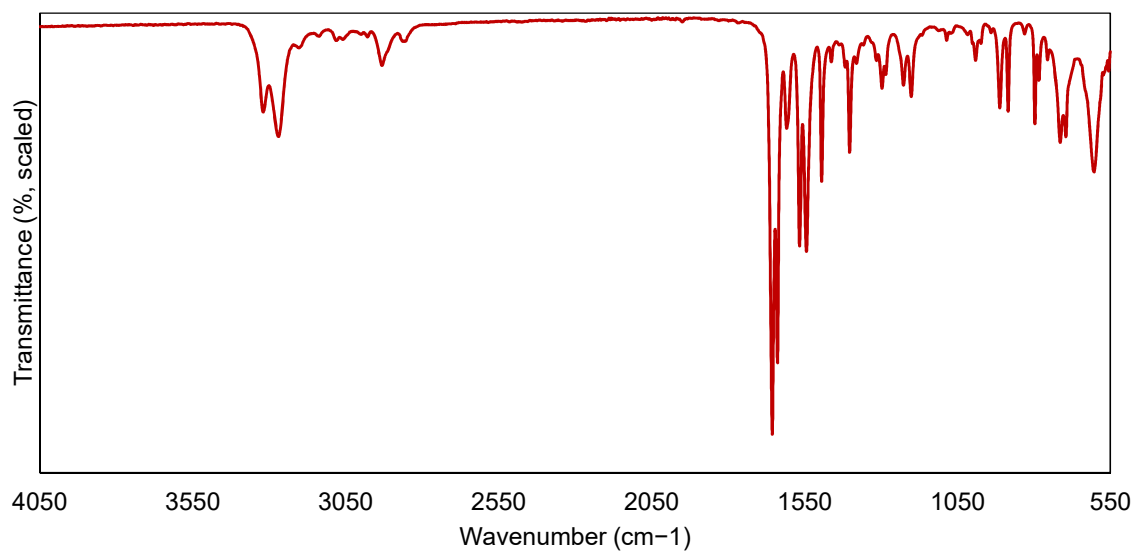
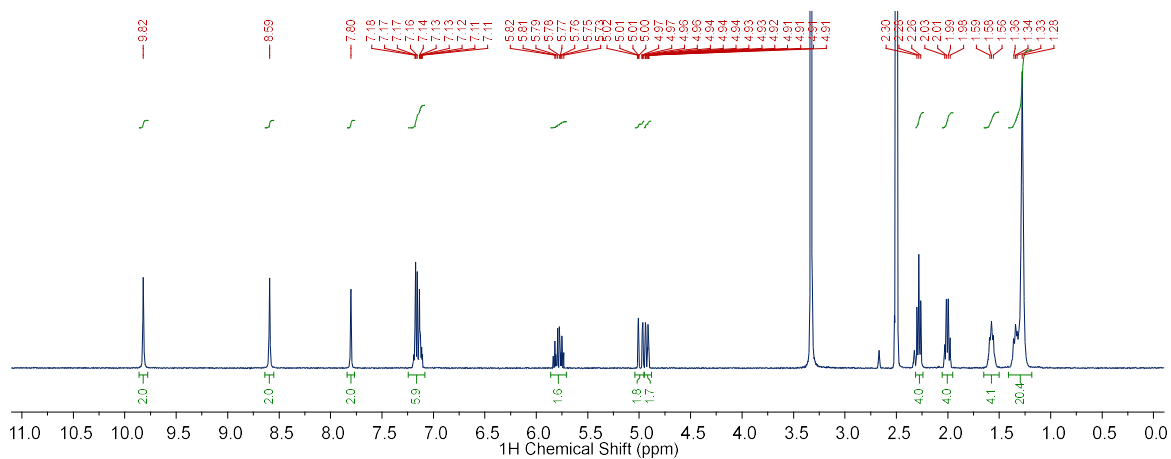Figure A1.57. FTIR spectrum of **132** (550–4050 cm⁻¹).

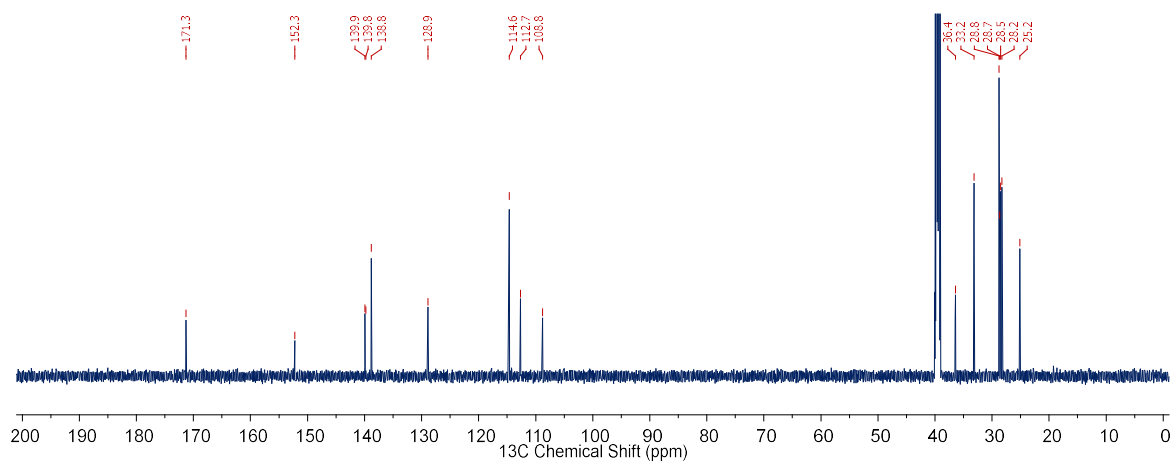Figure A1.58. ¹H spectrum NMR of **133** (400 MHz, 0–11 ppm, DMSO-*d₆*)
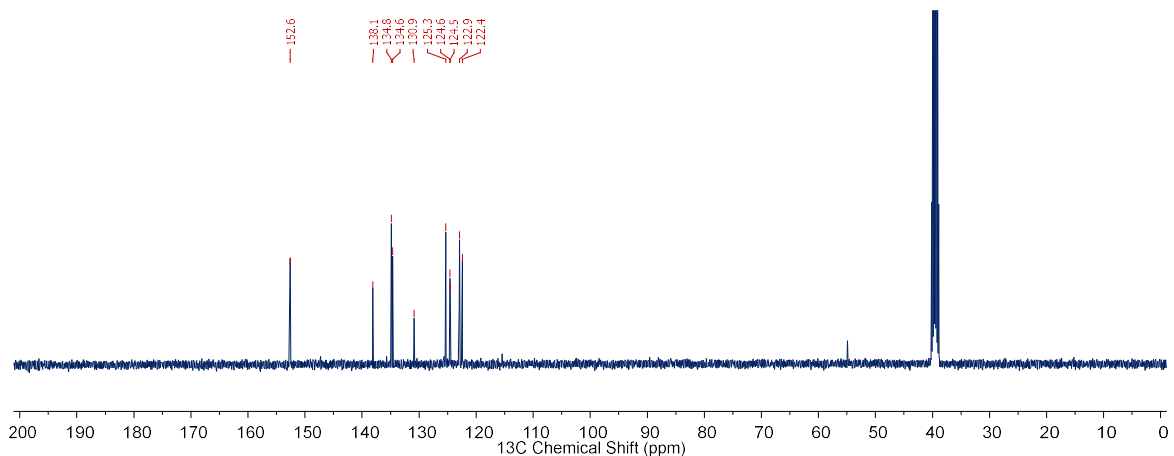
Figure A1.59. ¹³C spectrum NMR of **133** (101 MHz, 0–200 ppm, DMSO-*d₆*)
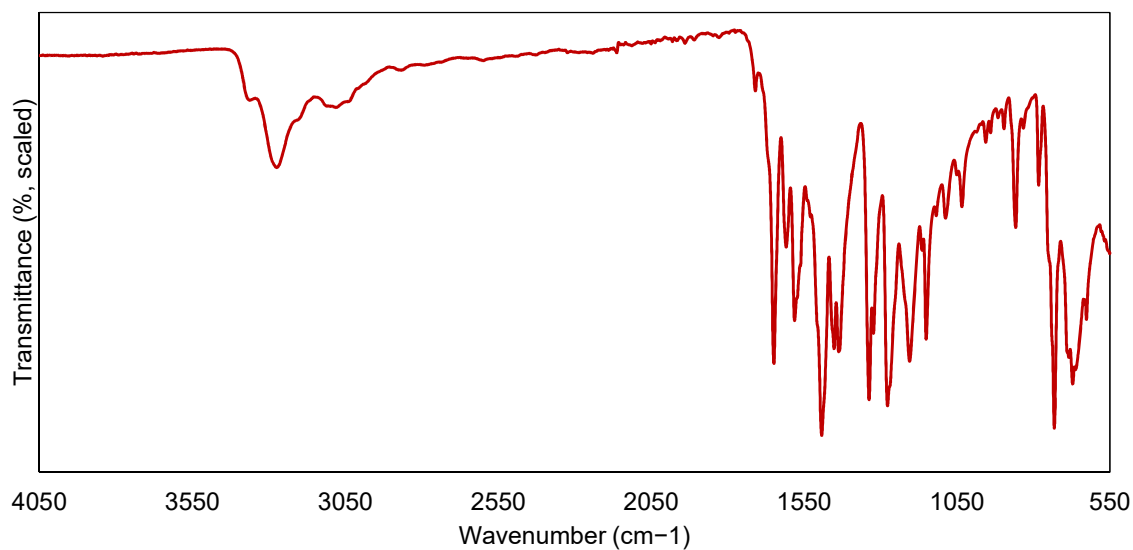
Figure A1.60. FTIR spectrum of **133** (550–4050 cm⁻¹).
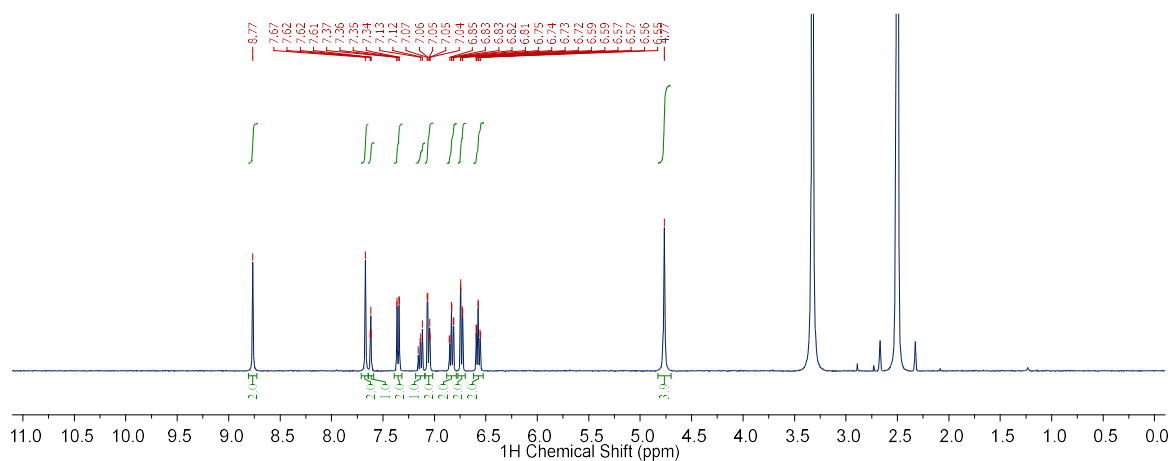
Figure A1.61. $^1$H spectrum NMR of **135** (400 MHz, 0–11 ppm, DMSO-$d_6$)
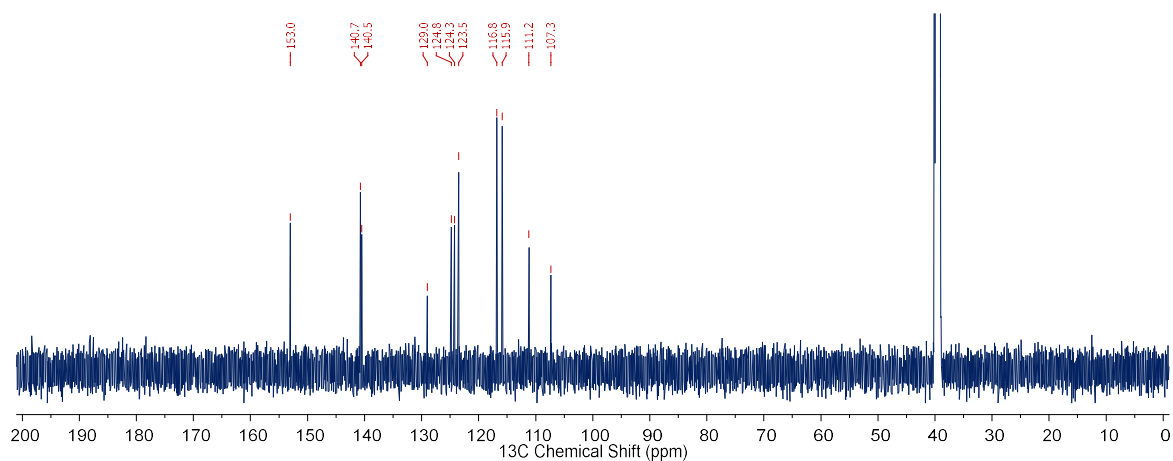


Figure A1.62. $^{13}$C spectrum NMR of **135** (151 MHz, 0–200 ppm, DMSO-$d_6$)



Figure A1.63. FTIR spectrum of **135** (550–4050 cm$^{-1}$).

196

Figure A1.64. $^1$H spectrum NMR of **136** (400 MHz, 0–11 ppm, DMSO-$d_6$)
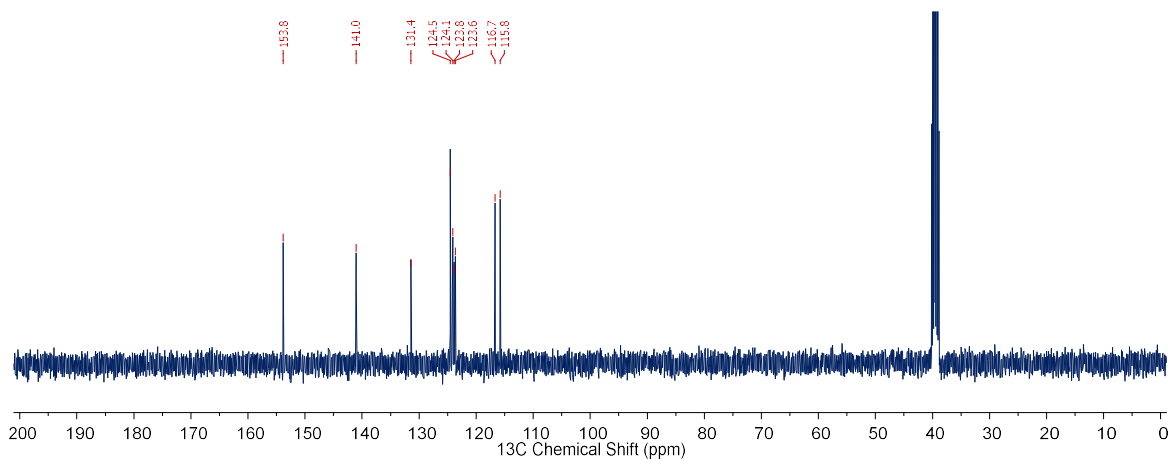


Figure A1.65. $^{13}$C spectrum NMR of **136** (101 MHz, 0–200 ppm, DMSO-$d_6$)



Figure A1.66. FTIR spectrum of **136** (550–4050 cm$^{-1}$).
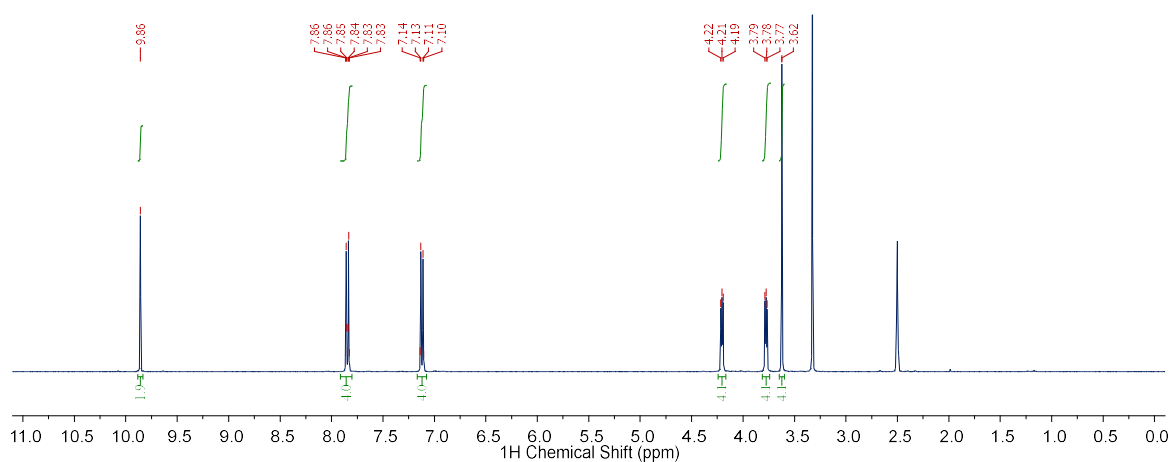
Figure A1.67. $^1$H spectrum NMR of **140** (400 MHz, 0–11 ppm, DMSO-$d_6$)
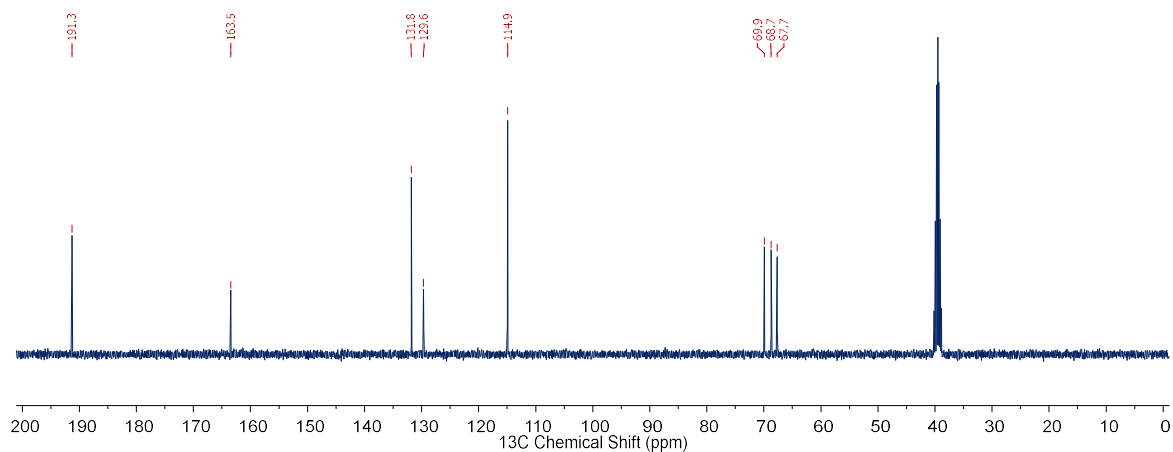


Figure A1.68. $^{13}$C spectrum NMR of **140** (101 MHz, 0–200 ppm, DMSO-$d_6$)
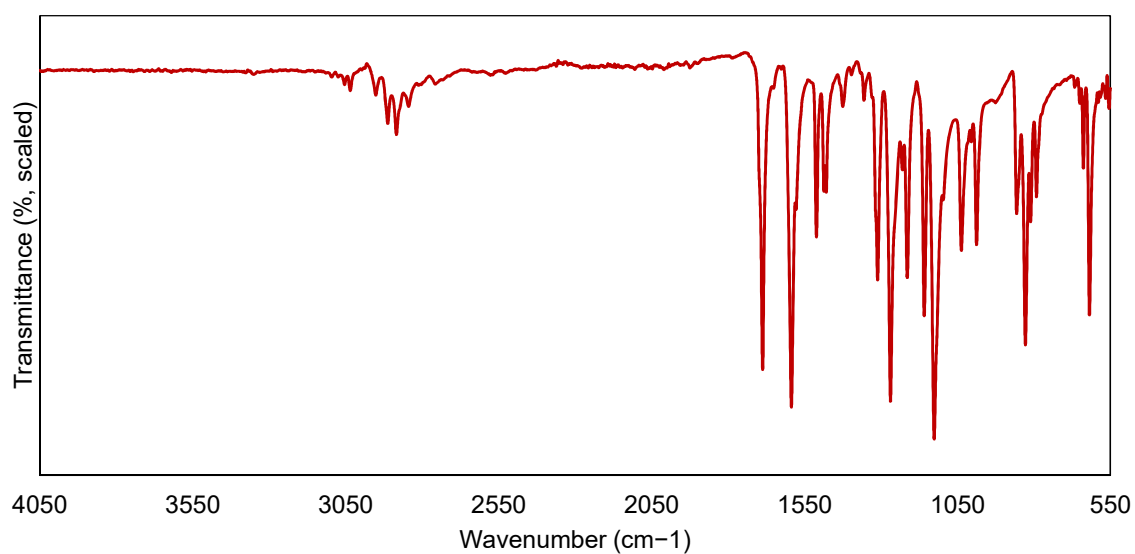


Figure A1.69. FTIR spectrum of **140** (550–4050 cm$^{-1}$).

## A1.3.2 Characterisation of Receptors **106–108**
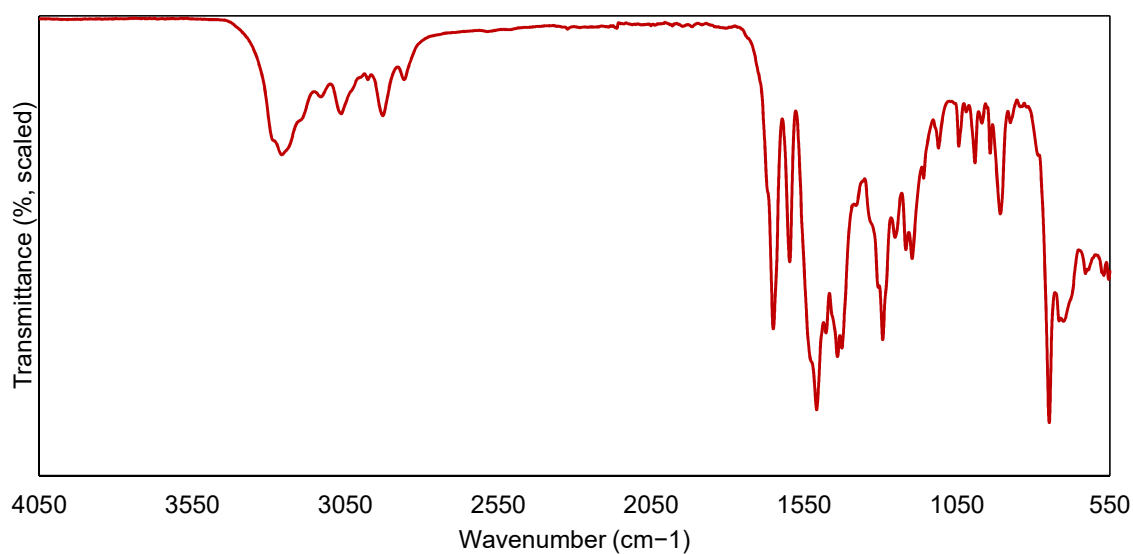


Figure A1.70. FTIR spectrum of **106** (550–4050 cm$^{-1}$).
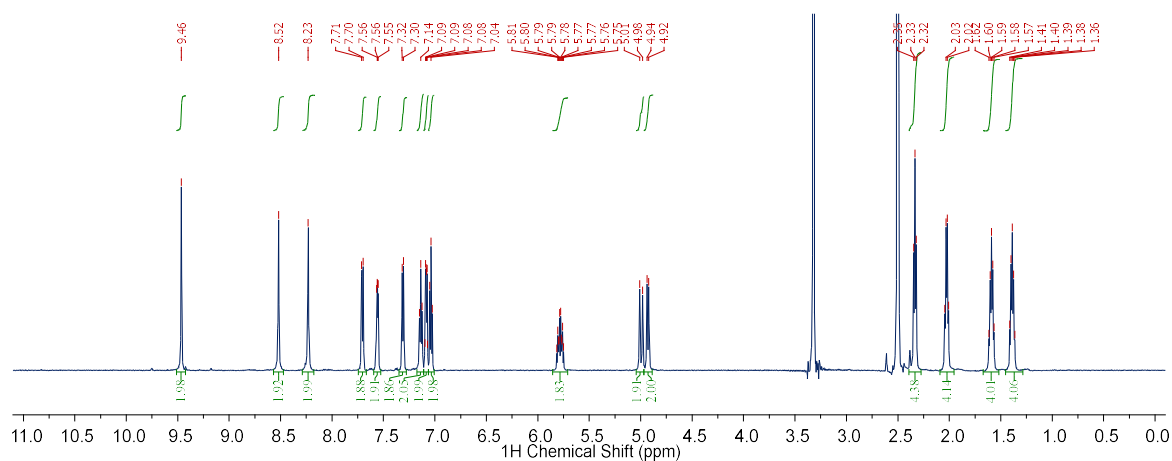


Figure A1.71. $^1$H spectrum NMR of **106** (600 MHz, 0–11 ppm, DMSO-$d_6$)
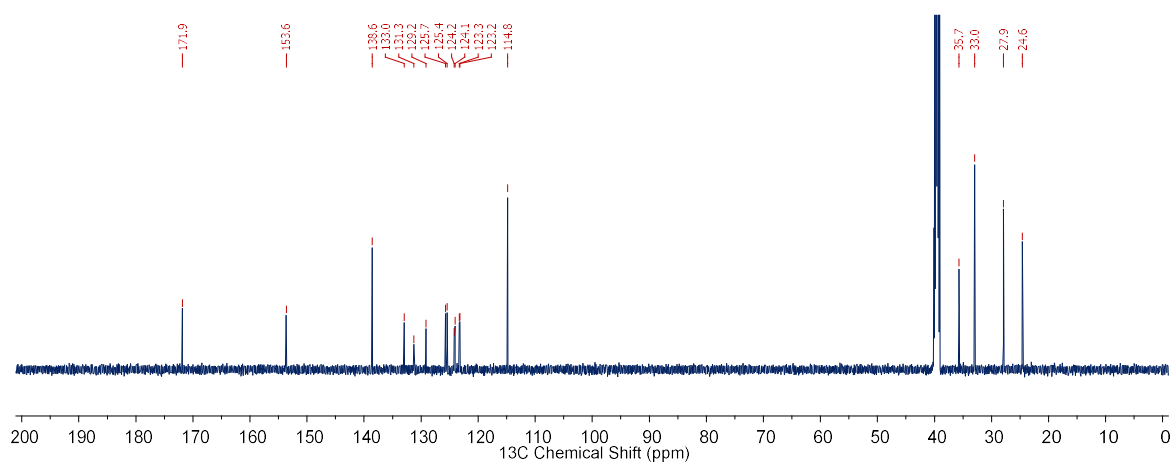


Figure A1.72. $^{13}$C spectrum NMR of **106** (151 MHz, 0–200 ppm, DMSO-$d_6$)
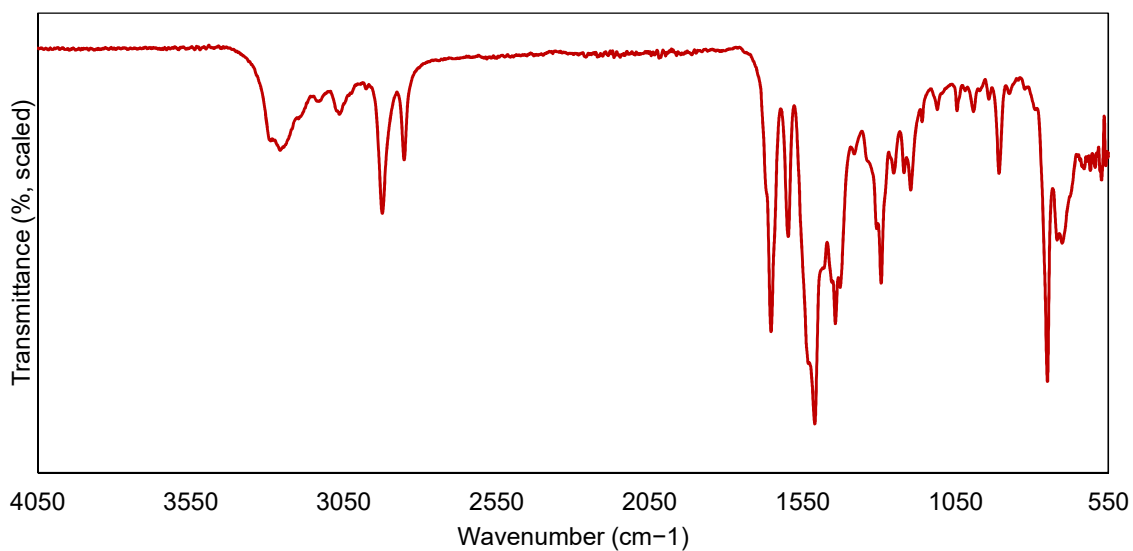
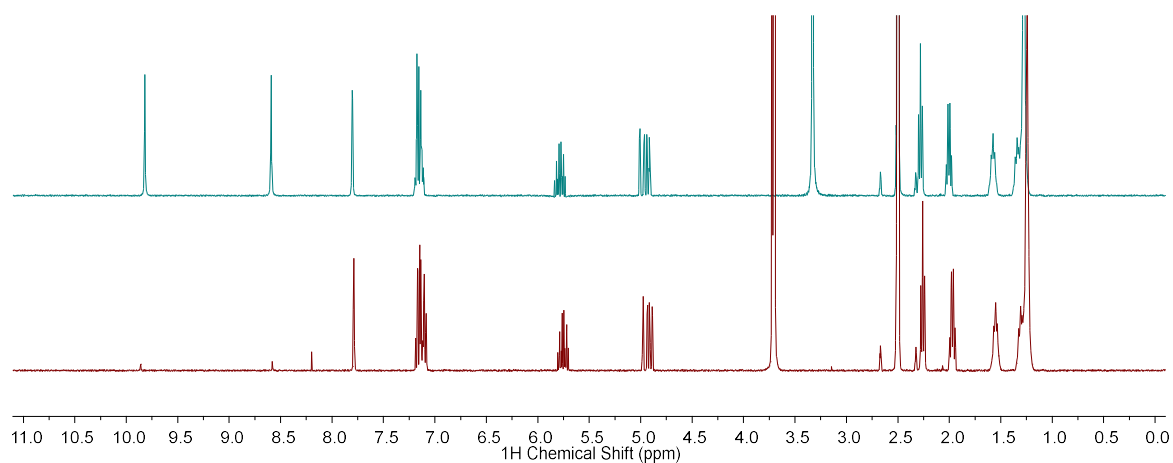Figure A1.73. FTIR spectrum of **107** (550–4050 cm$^{-1}$).
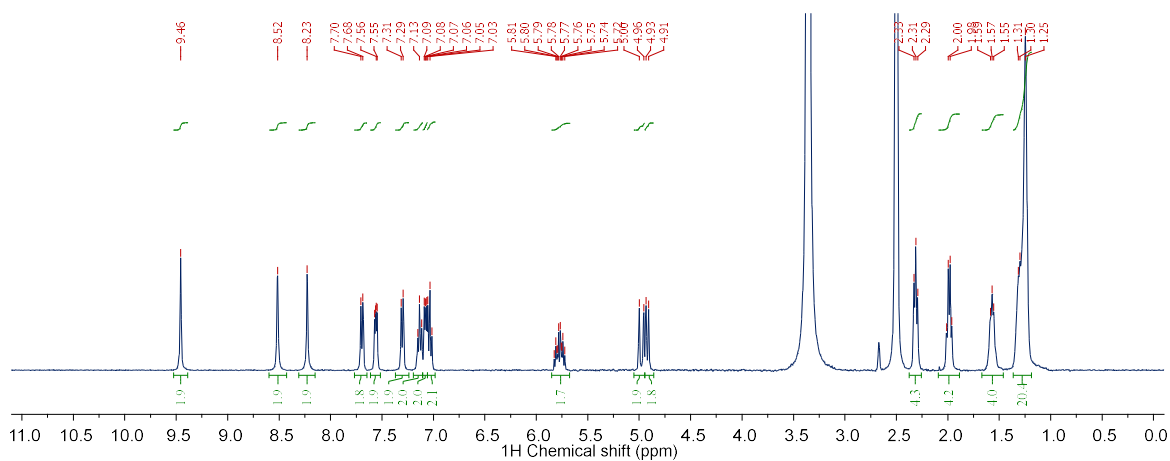


Figure A1.74. $^1$H spectrum NMR of **107** (400 MHz, 0–11 ppm, DMSO-$d_6$)
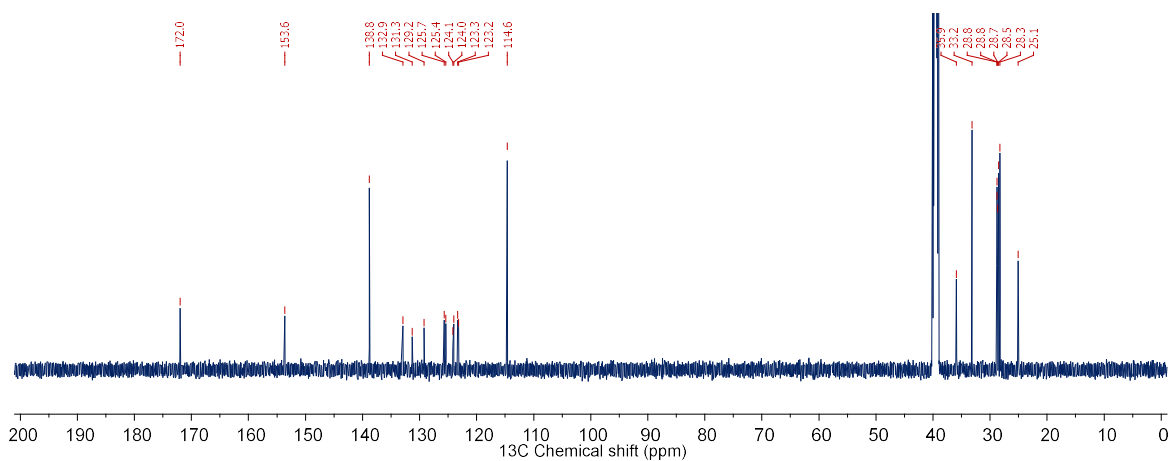


Figure A1.75. $^{13}$C spectrum NMR of **107** (151 MHz, 0–200 ppm, DMSO-$d_6$)

Figure A1.76. FTIR spectrum of **108**
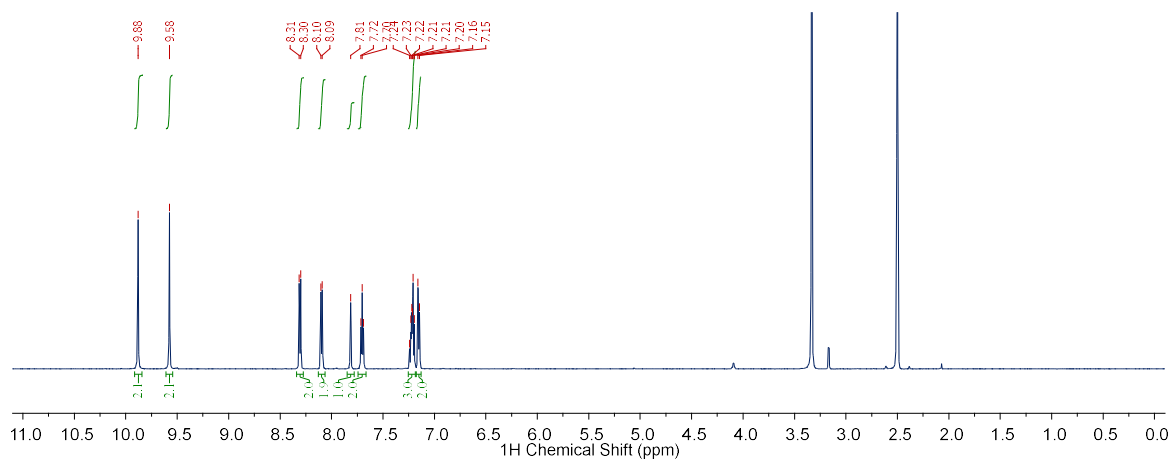


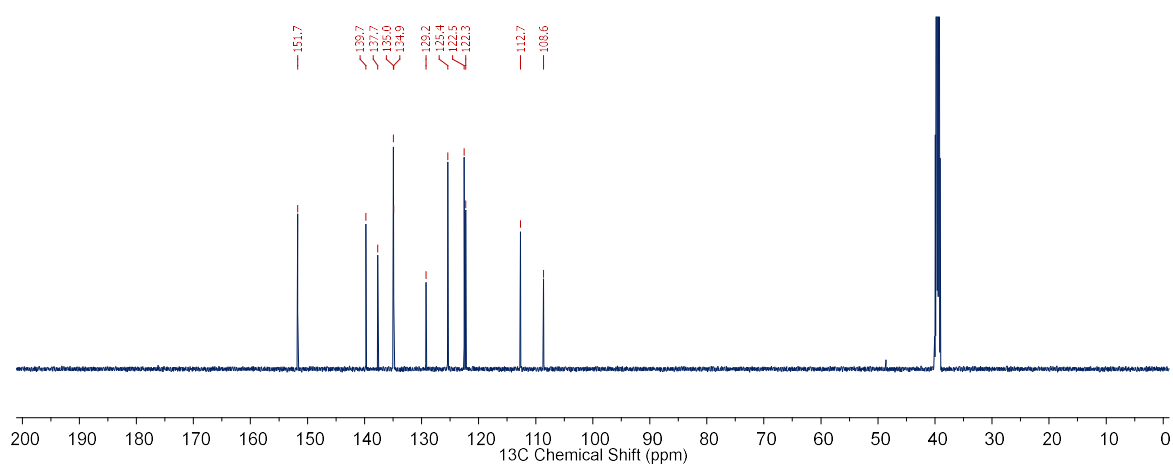Figure A1.77. $^1$H spectrum NMR of **108** (600 MHz, 0–11 ppm, DMSO-$d_6$)



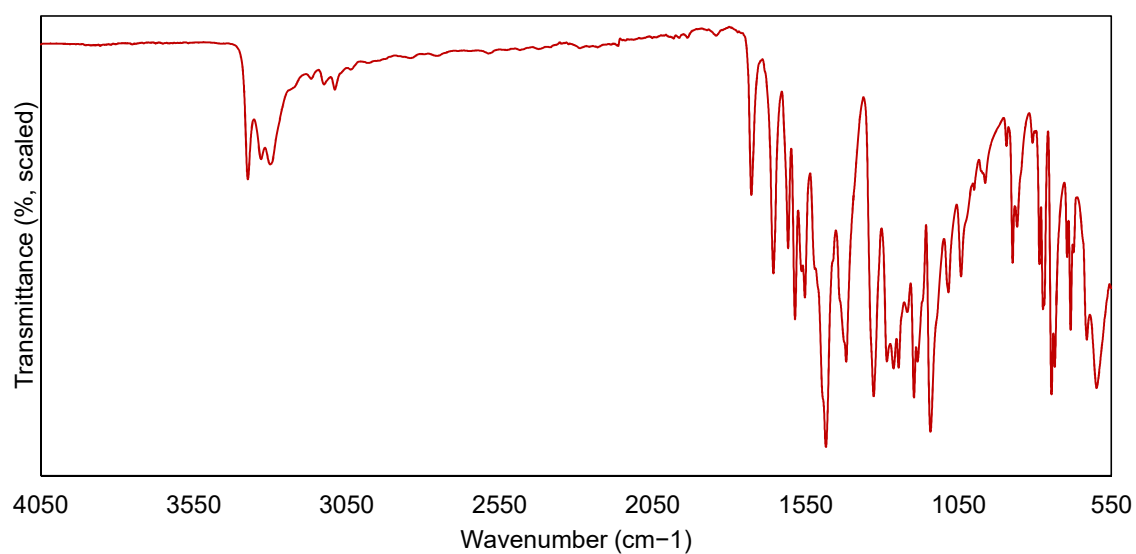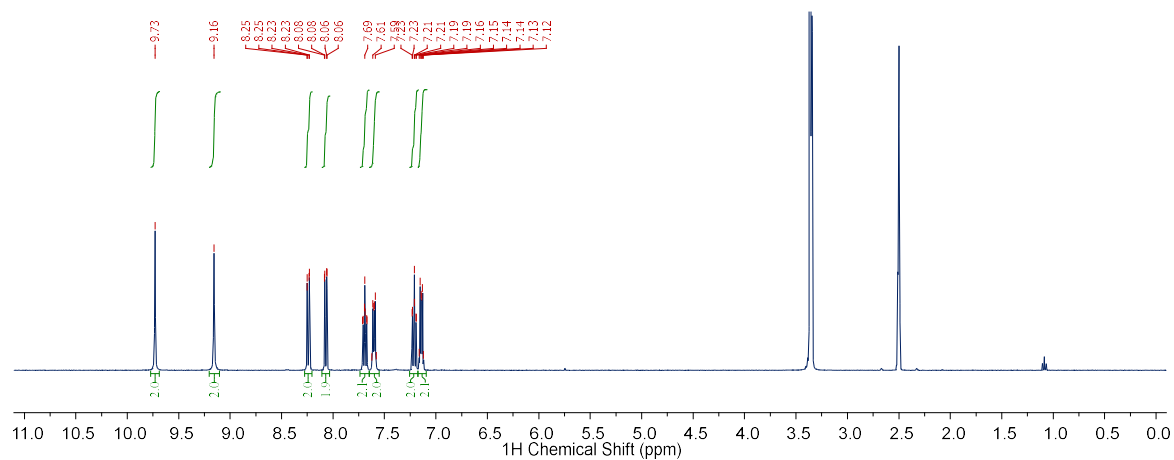Figure A1.78. $^{13}$C spectrum NMR of **108** (151 MHz, 0–200 ppm, DMSO-$d_6$)

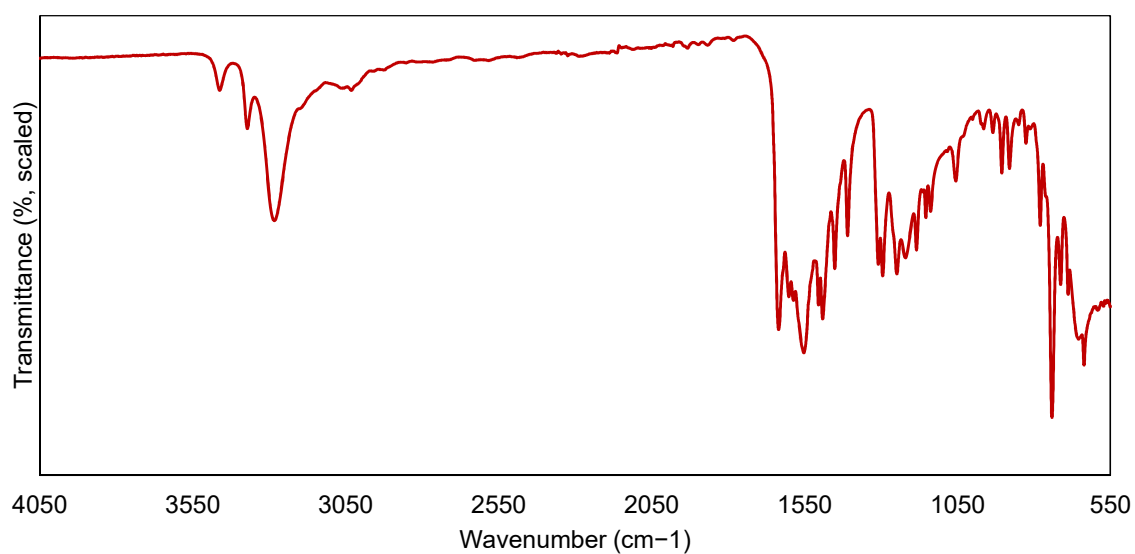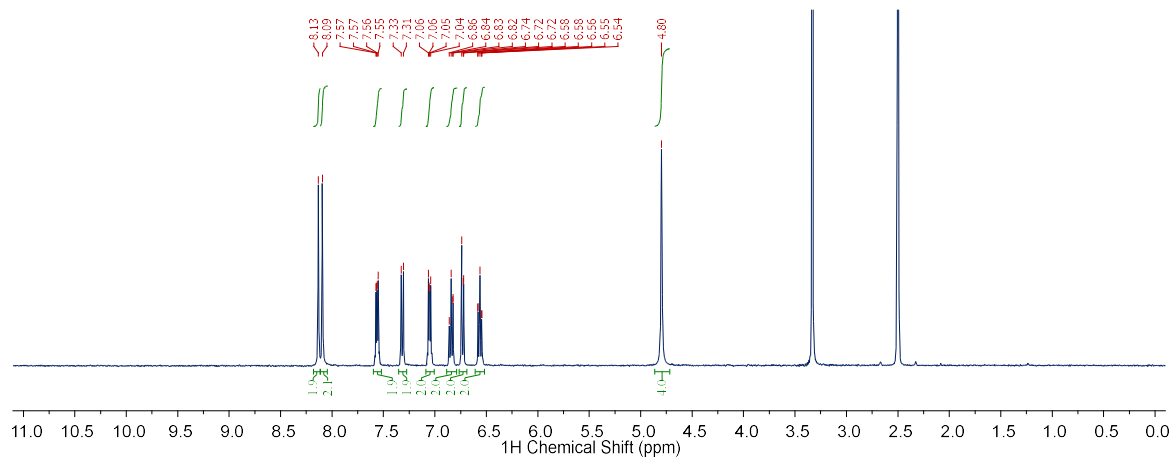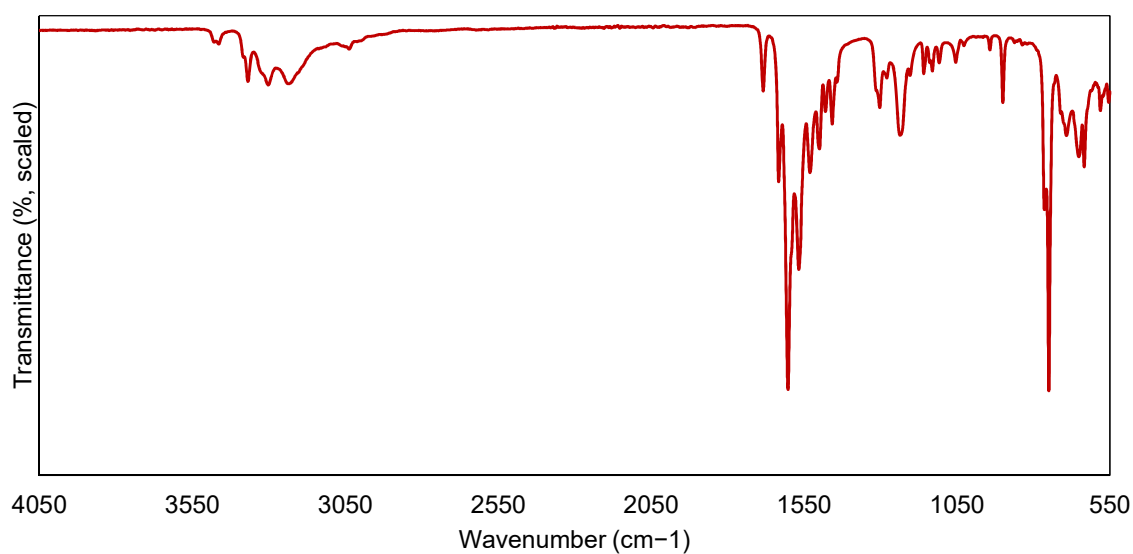Appendix 2.

$^1$H NMR Titration Experiments and Data Fitting

## A2.1 Fitting NMR Data with HypNMR2008

Fitting programmes such as HypNMR2008 assume that the host–guest equilibrium occurs under conditions of fast chemical exchange, and thus, that the observed chemical shift of a nucleus ($\delta_{obs}$) represents the population-weighted average of the chemical shifts of the nucleus over all species in solution, **Equation 1**.

$$\delta_{obs} = \left.\sum \delta_i n_i \middle/ \sum n_i\right.$$ 
(Equation 1)

Where $\delta_i$ and $n_i$ are the chemical shift and the molar quantity of that species, respectively.

The fitting programme HypNMR2008 minimises the deviation of the fit from the data through a damped version of the least-squares method known as the Levenberg–Marquardt algorithm. The minimised parameter is labelled as sigma ($\sigma$) by the programme, but is equivalent to the standard error on the *y*-estimate, SE$_y$, of the fit, **Equation 2**.

$$SE_y = \left.1\middle/_s\right. \sqrt{\left.\Sigma\left(\delta_{fit,j} - \delta_j\right)^2 \middle/ \nu\right.}$$ 
(Equation 2)

Where $\delta_{fit,j}$ and $\delta_j$ are the calculated and experimental chemical shifts at each point $j$, $\nu$ is the number of statistical degrees of freedom from the dataset, and $s$ is a scaling factor. In this work, $s$ has been chosen such that SE$_y$ is presented in units of ppb (s = $10^{-3}$). By analogy with the distribution of experimental data about the mean, SE$_y$ resembles the standard deviation, which is presumably the reasoning behind the choice of the letter sigma. In large datasets, where the difference between the number of degrees of freedom and the number of data points is small, SE$_y$ also approximates the root-mean-square residual. To avoid confusion with the true standard deviation, this parameter is referred to by the more correct term "SE$_y$", or as the "residual parameter".

The binding constants calculated by HypNMR2008 are accompanied by a "standard deviation" parameter. This is an estimate of the error of a single fit, and is often much smaller than the standard deviation of the values determined from several repetitions of the titration. A confidence interval may be constructed by multiplying this parameter by the relevant Student *t* statistic. The individual titrations in Chapter 2 have $\nu$ = 57 or 58 degrees of freedom, as there are 21 data points for each resonance, but two refined parameters for each resonance, plus the binding constant(s). For a 95% confidence interval, and $\nu$ = 58, the Student *t* statistic is $t_{0.975}$ = 2.00. For the remaining chapters, $\nu$ = 30–200, giving $t$ = 1.97–2.04, therefore in all cases the 95% confidence interval for a single fit would be twice the "standard deviation" parameter reported by HypNMR2008. A more in-depth overview of host–guest titrations, their fitting and interpretation is provided in a series of tutorial reviews

by Thordarson.[1,2] Further details on the fitting procedure used herein are reported by Gans,[3] as well as within the HypNMR2008 documentation.[4]

## A2.2 Reported Quantities

The error reported for individual measurements of $\log \beta$ is the "standard deviation" parameter as outputted by HypNMR2008, this is the case with the data for receptors **98**, **99** and **106**–**108** as these titrations were performed once. The values of $\log \beta$ reported in the text for receptors **96**, **97**, **102**, **104** and **105** are averaged values, with their associated 95% confidence intervals. Individual values of $\log K_{1:2}$ were calculated from the corresponding values of $\log \beta$, **Equation 3**. The error reported for each value of $\log K_{1:2}$ was determined by the method of propagation of uncertainty, **Equation 4**. Averaged values of $\log K_{1:2}$ are reported above alongside their 95% confidence intervals. If $K_{1:2} = \beta_{1:2}/\beta_{1:1}$, then:

$$\log K_{1:2} = \log \beta_{1:2} - \log \beta_{1:1} \tag{Equation 3}$$

$$\Delta \log K_2 = \sqrt{(\Delta \log \beta_2)^2 + (\Delta \log \beta_1)^2 - 2\rho_{12}\Delta \log \beta_1 \Delta \log \beta_2} \tag{Equation 4}$$

Where $\rho_{12}$ is the correlation coefficient between $\log \beta_{1:1}$ and $\log \beta_{1:2}$, and $\Delta x$ is the uncertainty on $x$.

The values of $\log \alpha$ reported in the text for receptors **96**, **97**, **102**, **104** and **105** were calculated using averaged values for $\log \beta_{1:1}$ and $\log K_{1:2}$, using **Equation 5**. The uncertainties on these values were estimated by the method of propagation of uncertainty, **Equation 6**. If $\alpha = 4K_{1:2}/K_{1:1} = 4K_{1:2}/\beta_{1:1}$, then:

$$\log \alpha = \log 4 + \log K_{1:2} - \log \beta_{1:1} \tag{Equation 5}$$

$$\Delta \log \alpha = \sqrt{(\Delta \log K_{1:2})^2 + (\Delta \log \beta_{1:1})^2} \tag{Equation 6}$$

Where $\Delta x$ is the uncertainty on $x$.

The values of $\log \alpha$ for receptors **98**, **99** and **108** were calculated directly from the values of $\log \beta$ outputted by HypNMR, **Equation 7**. The uncertainties on these values were estimated by the method of propagation of uncertainty, **Equation 8**. If $\alpha = 4K_{1:2}/K_{1:1} = 4\beta_{1:2}/(\beta_{1:1})^2$, then:

$$\log \alpha = \log 4 + \log \beta_{1:2} - 2 \log \beta_{1:1} \tag{7}$$

$$\Delta \log \alpha = \sqrt{(\Delta \log \beta_{1:2})^2 + 4(\Delta \log \beta_{1:1})^2 - 4\rho_{12}\Delta \log \beta_{1:1} \Delta \log \beta_{1:2}} \tag{8}$$

Where $\rho_{12}$ is the correlation coefficient between $\log \beta_{1:1}$ and $\log \beta_{1:2}$, and $\Delta x$ is the uncertainty on $x$.

# A2.3 Titration Data for Chapter 2

## A2.3.1 Titrations with H$_2$PO$_4^-$

### A2.3.1.1  Receptor **96** and H$_2$PO$_4^-$
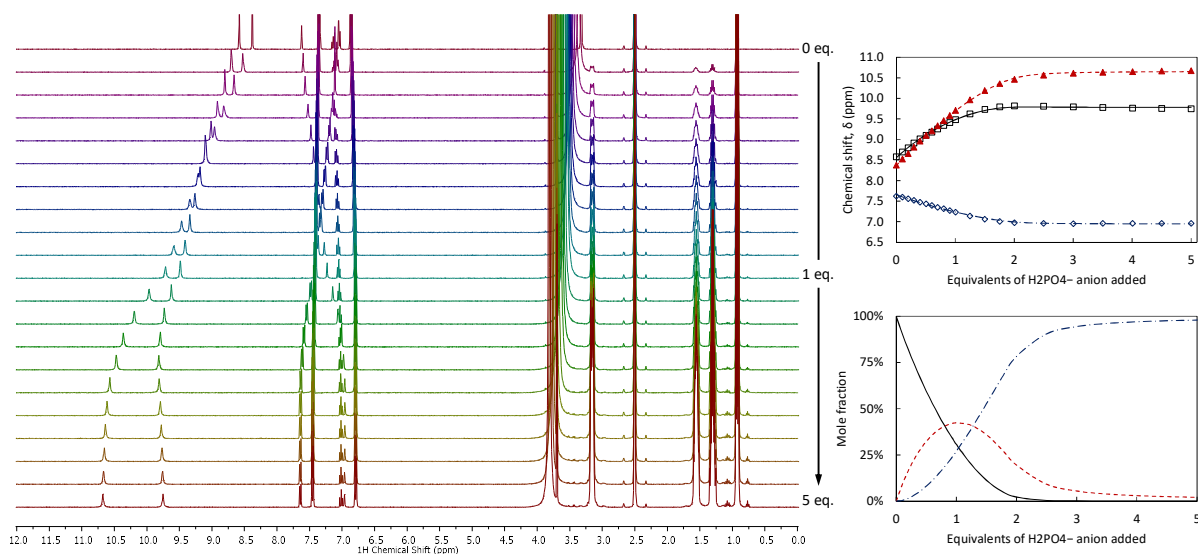


Figure A2.1. Titration of receptor **96** with H$_2$PO$_4^-$. Main: Stack plot (0–12 ppm) showing the change in resonances over 1 → 5 eq. Top right: Experimental data (points) and calculated fit (lines) for a 1:1, 1:2 host-guest binding model. Bottom right: Speciation distribution diagram from the fit.

Table A2.1. Data output from the fitting of the above titration data, and averaged values with associated 95% confidence intervals.

|  | logβ$_{1:1}$ | Standard deviation | Percentage error | logβ$_{1:2}$ | Standard deviation | Percentage error | SE$_y$ (ppb) |
|---|---|---|---|---|---|---|---|
| Titration 1 | 3.65 | 0.24 | 6% | 6.93 | 0.25 | 4% | 18.9 |
| Titration 2 | 3.83 | 0.27 | 7% | 7.35 | 0.31 | 4% | 18.9 |
| Titration 3 | 3.73 | 0.21 | 6% | 7.13 | 0.26 | 4% | 17.1 |
| **Average** | **3.74** | **0.11** | **3%** | **7.14** | **0.24** | **3%** | |

Table A2.2. Further data output from the fitting of the above titration data, derived stepwise binding constants with propagated uncertainty, averaged value with associated 95% confidence interval, and calculated cooperativity parameter with associated propagated uncertainty.

|  | Correlation coefficient | logK$_{1:2}$ | Standard deviation | Percentage error | logα | Error |
|---|---|---|---|---|---|---|
| Titration 1 | 95% | 3.29 | 0.08 | 2% | | |
| Titration 2 | 96% | 3.52 | 0.09 | 3% | | |
| Titration 3 | 95% | 3.40 | 0.09 | 3% | | |
| **Average** | | **3.40** | **0.13** | **4%** | **0.27** | **0.17** |

## A2.3.1.2   Receptor **97** and $H_2PO_4^-$



Figure A2.2. Titration of receptor **97** with $H_2PO_4^-$. Main: Stack plot (0–12 ppm) showing the change in resonances over 1 → 5 eq. Top right: Experimental data (points) and calculated fit (lines) for a 1:1, 1:2 host-guest binding model. Bottom right: Speciation distribution diagram from the fit.

Table A2.3. Data output from the fitting of the above titration data, and averaged values with associated 95% confidence intervals.

| | $log\beta_{1:1}$ | Standard deviation | Percentage error | $log\beta_{1:2}$ | Standard deviation | Percentage error | $SE_y$ (ppb) |
|---|---|---|---|---|---|---|---|
| Titration 1 | 3.67 | 0.27 | 7% | 7.18 | 0.29 | 4% | 19.7 |
| Titration 2 | 3.55 | 0.30 | 8% | 7.23 | 0.30 | 4% | 20.1 |
| Titration 3 | 3.65 | 0.27 | 7% | 7.31 | 0.29 | 4% | 18.9 |
| **Average** | **3.63** | **0.07** | **2%** | **7.24** | **0.07** | **1%** | |

Table A2.4. Further data output from the fitting of the above titration data, derived stepwise binding constants with propagated uncertainty, averaged value with associated 95% confidence interval, and calculated cooperativity parameter with associated propagated uncertainty.

| | Correlation coefficient | $logK_{1:2}$ | Standard deviation | Percentage error | $log\alpha$ | Error |
|---|---|---|---|---|---|---|
| Titration 1 | 95% | 3.51 | 0.09 | 3% | | |
| Titration 2 | 92% | 3.68 | 0.12 | 3% | | |
| Titration 3 | 94% | 3.66 | 0.10 | 3% | | |
| **Average** | | **3.62** | **0.11** | **3%** | **0.59** | **0.13** |

## A2.3.1.3 Receptor **98** and $H_2PO_4^-$



Figure A2.3. Titration of receptor **98** with $H_2PO_4^-$. Main: Stack plot (0–12 ppm) showing the change in resonances over $1 \rightarrow 5$ eq. Note the immediate broadening of the phenol resonance due to an increase in the rate of exchange. Top right: Experimental data (points) and calculated fit (lines) for a 1:1, 1:2 host-guest binding model. Bottom right: Speciation distribution diagram from the fit.

Table A2.5. Data output from the fitting of the above titration data.

|  | $\log\beta_{1:1}$ | Standard deviation | Percentage error | $\log\beta_{1:2}$ | Standard deviation | Percentage error | $SE_y$ (ppb) |
|---|---|---|---|---|---|---|---|
| Titration 1 | 3.77 | 0.29 | 8% | 7.13 | 0.29 | 4% | 17.7 |

Table A2.6. Further data output from the fitting of the above titration data, derived stepwise binding constant with propagated uncertainty, and calculated cooperativity parameter with associated propagated uncertainty.

|  | Correlation coefficient | $\log K_{1:2}$ | Standard deviation | Percentage error | $\log\alpha$ | Error |
|---|---|---|---|---|---|---|
| Titration 1 | 97% | 3.37 | 0.07 | 2% | 0.21 | 0.31 |

### A2.3.1.4  Receptor **99** and H$_2$PO$_4^-$



Figure A2.4. Titration of receptor **99** with H$_2$PO$_4^-$. Main: Stack plot (0–12 ppm) showing the change in resonances over 1 → 5 eq. Note the immediate broadening of the phenol resonance due to an increase in the rate of exchange. Right: Experimental data, could not be fit to a 1:1, 1:2 host-guest model. A 1:1, 1:2, 1:3 host-guest binding model gave unrealistic logarithmic binding constants (log$\beta_{1:1}$ = 4.4, log$\beta_{1:2}$ = 8.1, and log$\beta_{1:3}$ = 10.6), given the titration concentration (7 mM).

### A2.3.2 Titrations with AcO$^-$

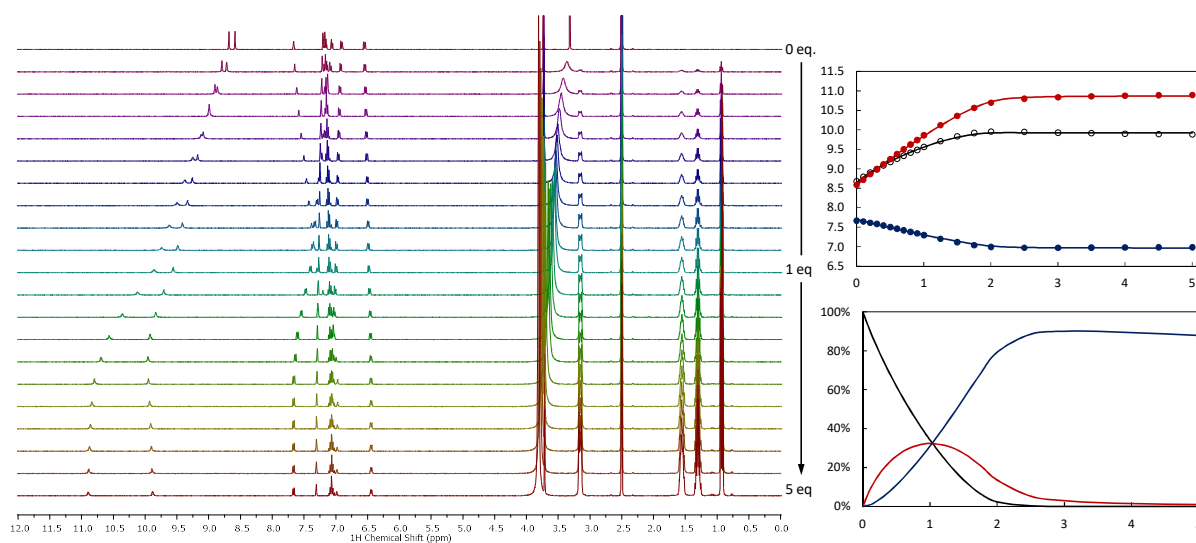### A2.3.2.1  Receptor **96** and AcO$^-$
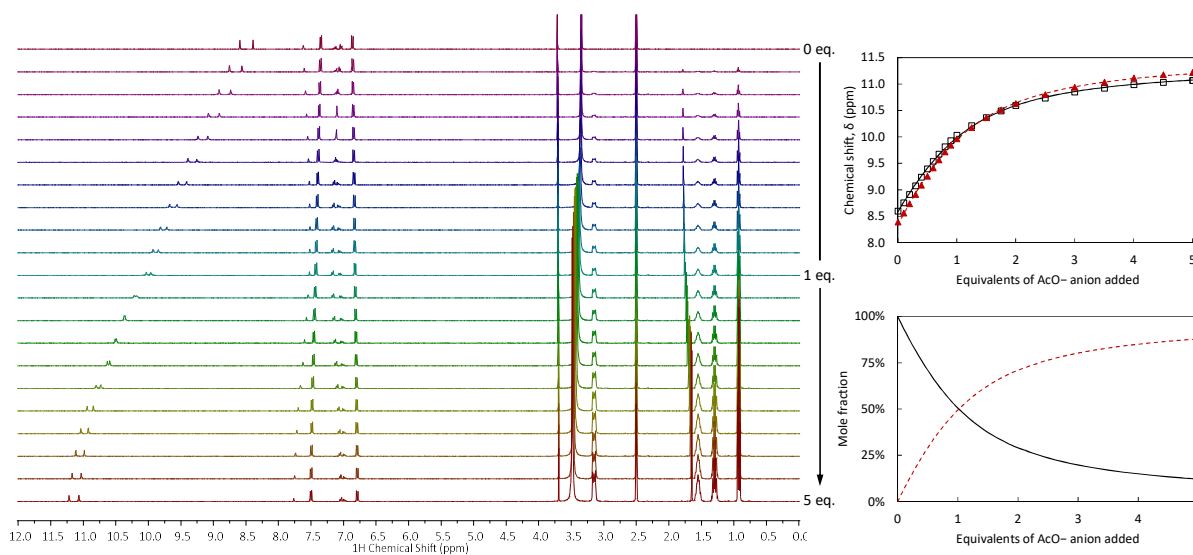


Figure A2.5. Titration of receptor **96** with AcO$^-$. Main: Stack plot (0–12 ppm) showing the change in resonances over 1 → 5 eq. Top right: Experimental data (points) and calculated fit (lines) for a 1:1 host-guest binding model. Bottom right: Speciation distribution diagram from the fit.

Table A2.7. Data output from the fitting of the above titration data, and averaged values with associated 95% confidence intervals.

|  | $\log\beta_{1:1}$ | Standard deviation | Percentage error | $SE_y$ (ppb) |
|---|---|---|---|---|
| Titration 1 | 2.33 | 0.01 | 0.6% | 25.5 |
| Titration 2 | 2.48 | 0.01 | 0.5% | 22.3 |
| Titration 3 | 2.45 | 0.01 | 0.4% | 19.1 |
| Titration 4 | 2.45 | 0.01 | 0.5% | 11.2 |
| **Average** | **2.43** | **0.06** | **3%** |  |
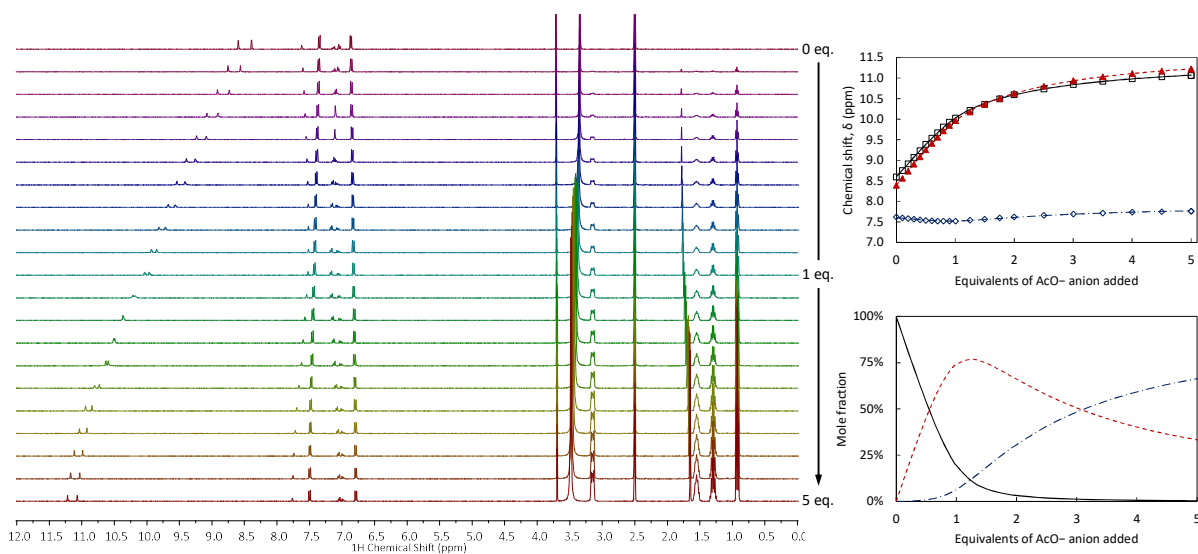


Figure A2.6. Titration of receptor **96** with AcO⁻. Main: Stack plot (0–12 ppm) showing the change in resonances over 1 → 5 eq. Top right: Experimental data (points) and calculated fit (lines) for a 1:1, 1:2 host-guest binding model. Bottom right: Speciation distribution diagram from the fit.

Table A2.8. Data output from the fitting of the above titration data, and averaged values with associated 95% confidence intervals.

|  | $\log\beta_{1:1}$ | Standard deviation | Percentage error | $\log\beta_{1:2}$ | Standard deviation | Percentage error | $SE_y$ (ppb) |
|---|---|---|---|---|---|---|---|
| Titration 1 | 3.83 | 0.07 | 2% | 5.85 | 0.08 | 1% | 6.0 |
| Titration 2 | 3.38 | 0.09 | 3% | 5.17 | 0.13 | 3% | 12.0 |
| Titration 3 | 3.32 | 0.08 | 3% | 5.19 | 0.12 | 2% | 11.2 |
| Titration 4 | 3.63 | 0.07 | 2% | 5.61 | 0.09 | 2% | 8.3 |
| **Average** | **3.54** | **0.23** | **7%** | **5.45** | **0.33** | **6%** |  |

Table A2.9. Further data output from the fitting of the above titration data, derived stepwise binding constants with propagated uncertainty, averaged value with associated 95% confidence interval, and calculated cooperativity parameter with associated propagated uncertainty.

| | Correlation coefficient | logK$_{1:2}$ | Standard deviation | Percentage Error | logα | Error |
|---|---|---|---|---|---|---|
| Titration 1 | 99% | 2.01 | 0.01 | 0.7% | | |
| Titration 2 | 96% | 1.79 | 0.05 | 3% | | |
| Titration 3 | 97% | 1.87 | 0.04 | 2% | | |
| Titration 4 | 98% | 1.98 | 0.02 | 1% | | |
| **Average** | | **1.91** | **0.10** | **5%** | **-1.03** | **0.25** |
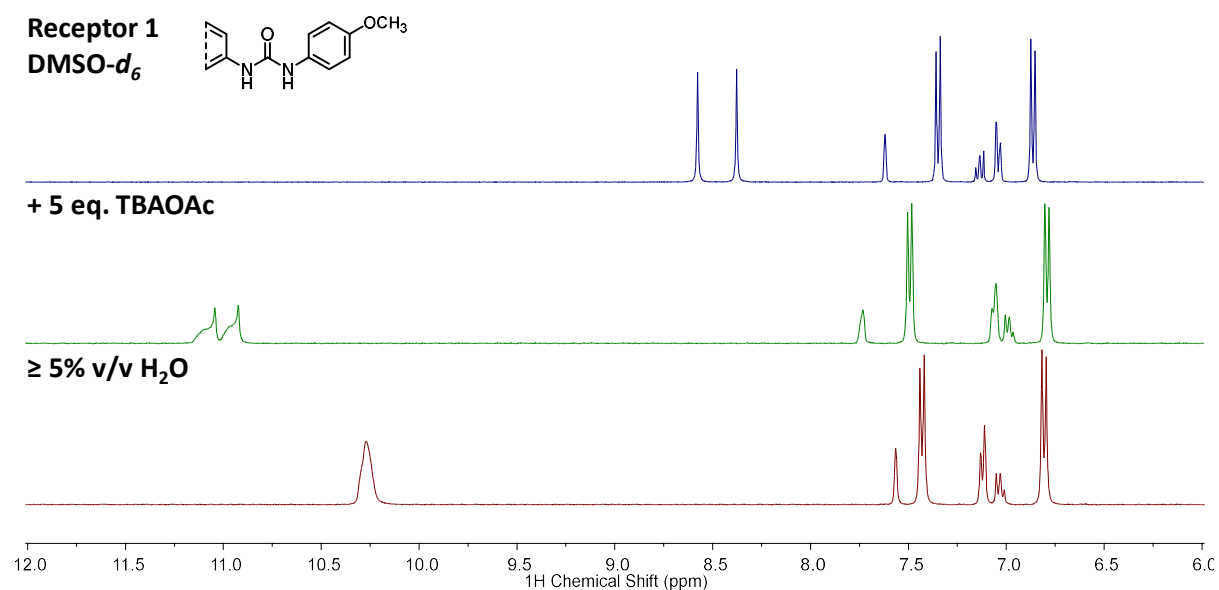


Figure A2.7. Addition of water to a mixture of receptor **96** and *ca.* 5 equivalents of TBAOAc in DMSO-*d₆*. This last spectrum resembles the midpoint of the titration (*ca.* 1 eq. TBAOAc), which suggests that the presence of water diminishes the proportion of bound receptor through competition for hydrogen bonding interactions.
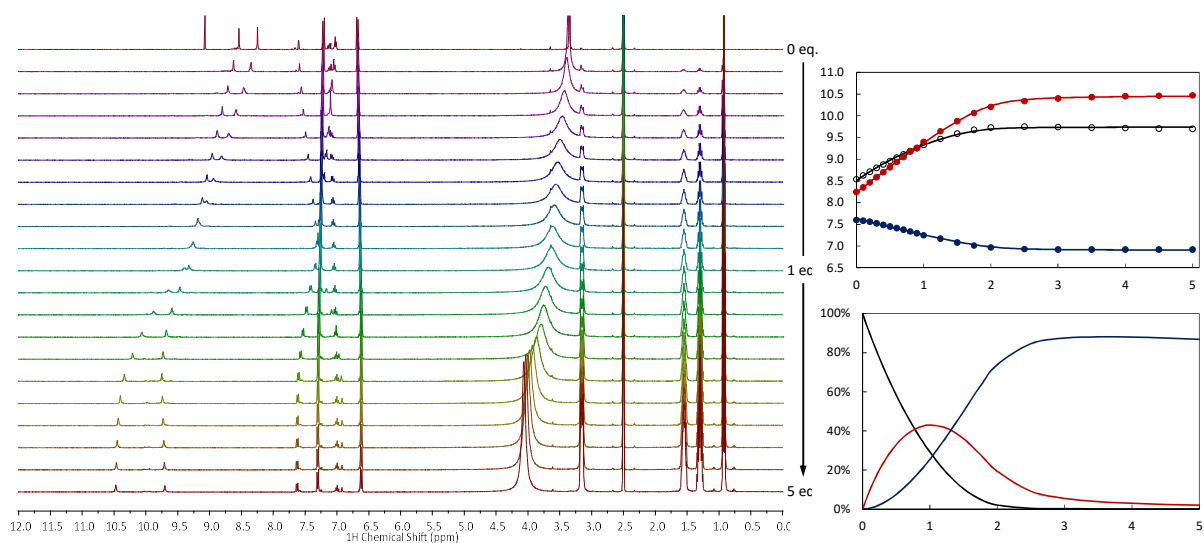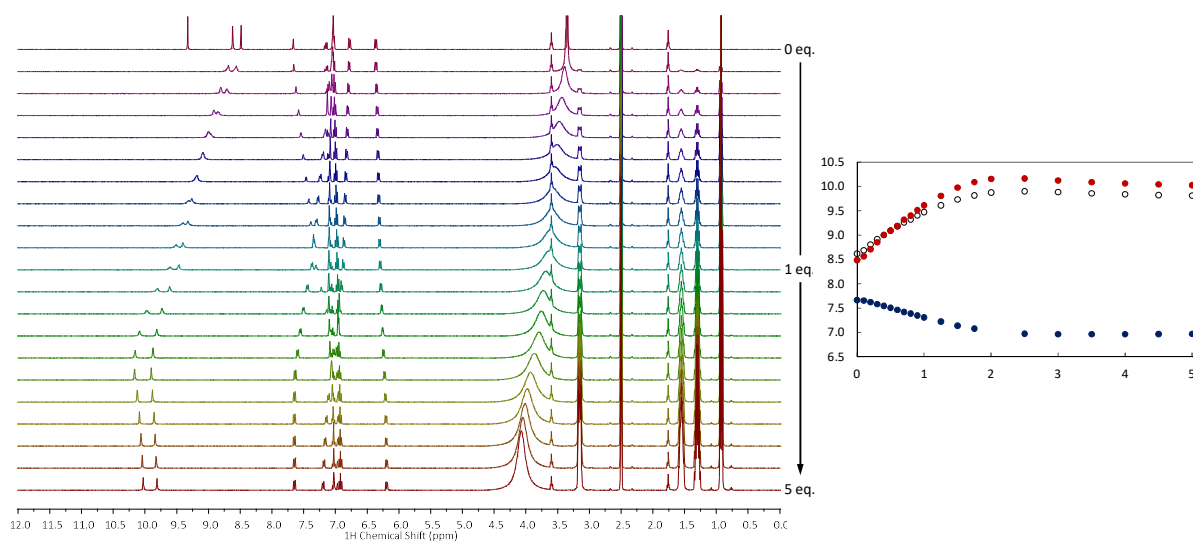
### A2.3.2.2 Receptor **97** and AcO⁻



Figure A2.8. Titration of receptor **97** with $H_2PO_4^-$. Main: Stack plot (0–12 ppm) showing the change in resonances over 1 → 5 eq. Top right: Experimental data (points) and calculated fit (lines) for a 1:1 host-guest binding model. Bottom right: Speciation distribution diagram from the fit.

Table A2.10. Data output from the fitting of the above titration data, and averaged values with associated 95% confidence intervals.

|  | $\log\beta_{1:1}$ | Standard deviation | Percentage error | $SE_y$ (ppb) |
|---|---|---|---|---|
| Titration 1 | 2.23 | 0.02 | 1% | 38.8 |
| Titration 2 | 2.49 | 0.01 | 0.5% | 23.2 |
| Titration 3 | 2.53 | 0.02 | 1% | 54.9 |
| Titration 4 | 2.51 | 0.01 | 0.4% | 17.3 |
| **Average** | **2.44** | **0.14** | **6%** | |



Figure A2.9. Titration of receptor **97** with AcO⁻. Main: Stack plot (0–12 ppm) showing the change in resonances over 1 → 5 eq. Top right: Experimental data (points) and calculated fit (lines) for a 1:1, 1:2 host-guest binding model. Bottom right: Speciation distribution diagram from the fit.

213

*Appendix A2: $^1H$ NMR Titration Experiments and Data Fitting*

Table A2.11. Data output from the fitting of the above titration data, and averaged values with associated 95% confidence intervals.

|  | $\log\beta_{1:1}$ | Standard deviation | Percentage error | $\log\beta_{1:2}$ | Standard deviation | Percentage error | $SE_y$ (ppb) |
|---|---|---|---|---|---|---|---|
| Titration 1 | 3.88 | 0.24 | 6% | 6.11 | 0.25 | 4% | 14.9 |
| Titration 2 | 3.54 | 0.11 | 3% | 5.62 | 0.14 | 2% | 13.8 |
| Titration 3 | 3.90 | 0.22 | 6% | 6.42 | 0.26 | 4% | 33.3 |
| Titration 4 | 3.31 | 0.09 | 3% | 5.30 | 0.13 | 2% | 13.0 |
| **Average** | **3.66** | **0.28** | **8%** | **5.86** | **0.49** | **8%** | |

Table A2.12. Further data output from the fitting of the above titration data, derived stepwise binding constants with propagated uncertainty, averaged value with associated 95% confidence interval, and calculated cooperativity parameter with associated propagated uncertainty.

|  | Correlation coefficient | $\log K_{1:2}$ | Standard deviation | Percentage error | $\log\alpha$ | Error |
|---|---|---|---|---|---|---|
| Titration 1 | 99% | 2.22 | 0.03 | 1% | | |
| Titration 2 | 97% | 2.08 | 0.04 | 2% | | |
| Titration 3 | 98% | 2.53 | 0.06 | 2% | | |
| Titration 4 | 96% | 1.98 | 0.05 | 2% | | |
| **Average** | | **2.20** | **0.23** | **10%** | **-0.85** | **0.36** |
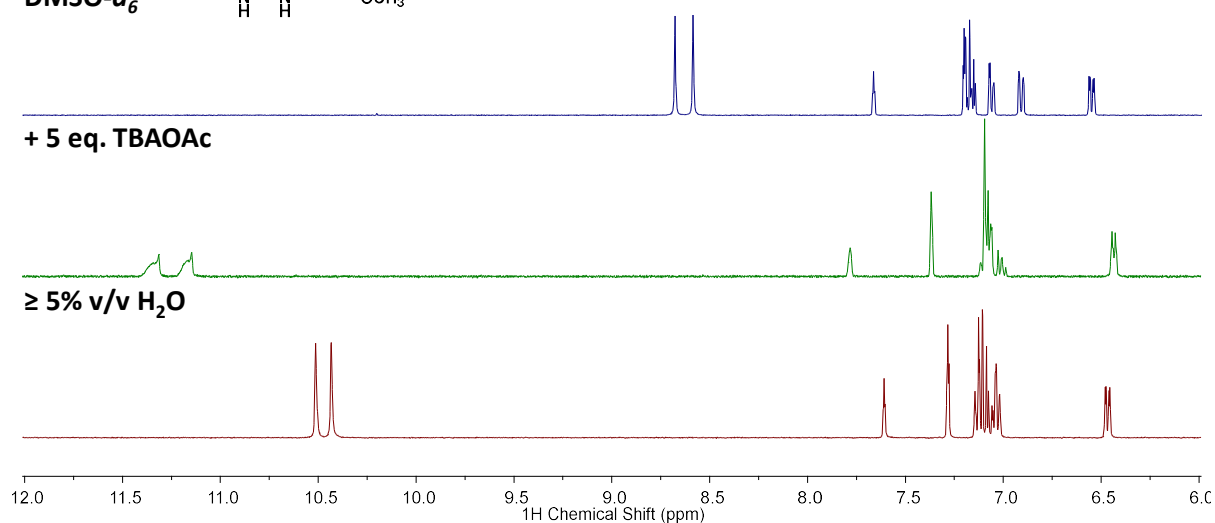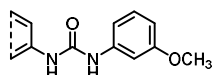


Figure A2.10. Addition of water to a mixture of receptor **97** and *ca.* 5 equivalents of TBAOAc in DMSO-$d_6$. This last spectrum resembles the midpoint of the titration (*ca.* 1 eq. TBAOAc), which suggests that the presence of water diminishes the proportion of bound receptor through competition for hydrogen bonding interactions.
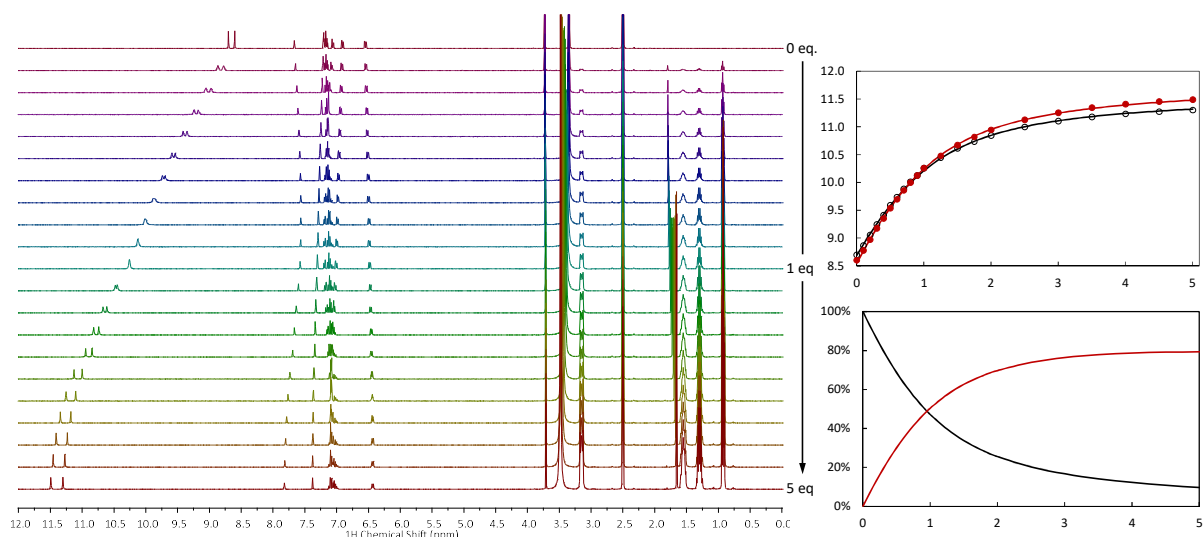
### A2.3.2.3 Receptor **98** and AcO⁻
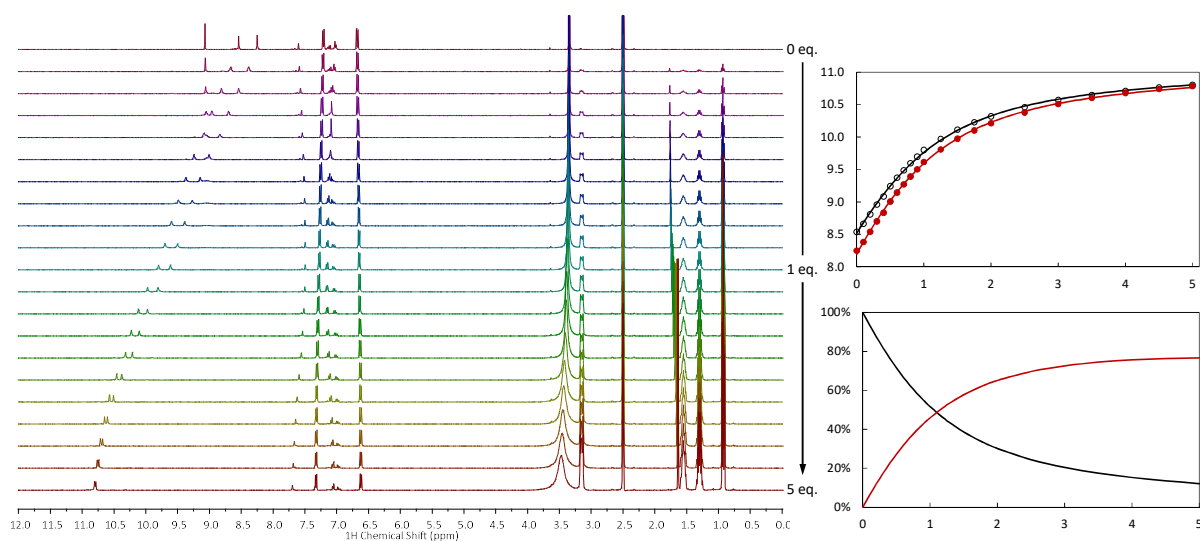


Figure A2.11. Titration of receptor **98** with $H_2PO_4^-$. Main: Stack plot (0–12 ppm) showing the change in resonances over 1 → 5 eq. Note the broadening of the phenol resonance due to an increase in the rate of exchange. Top right: Experimental data (points) and calculated fit (lines) for a 1:1 host-guest binding model. Bottom right: Speciation distribution diagram from the fit.

Table A2.13. Data output from the fitting of the above titration data

|  | $log\beta_{1:1}$ | Standard deviation | Percentage error | $SE_y$ (ppb) |
|---|---|---|---|---|
| Titration 1 | 2.39 | 0.01 | 0.5% | 19.0 |
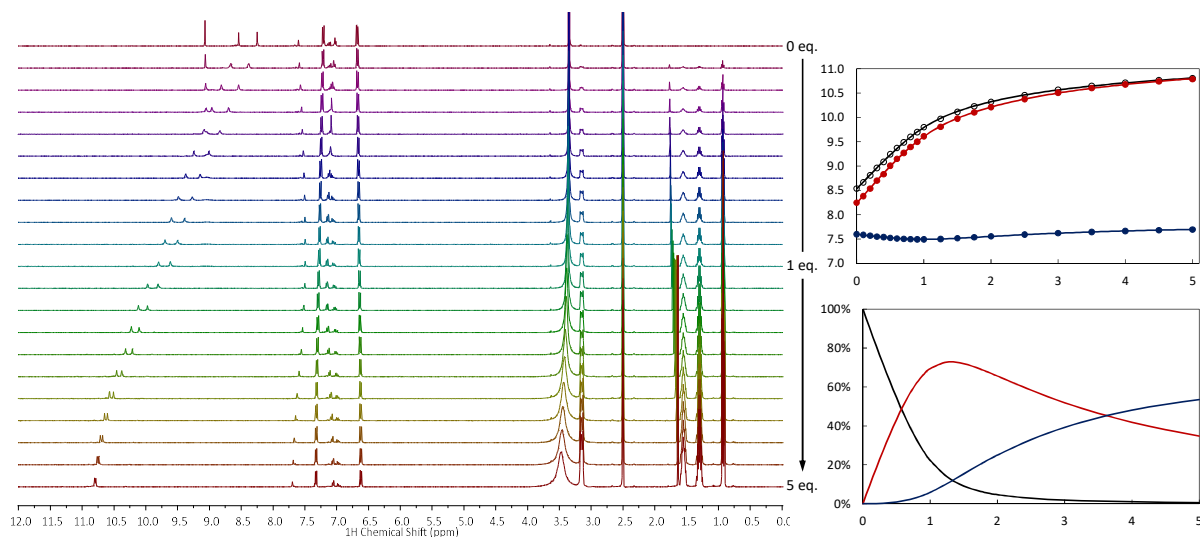


Figure A2.12. Titration of receptor **98** with AcO⁻. Main: Stack plot (0–12 ppm) showing the change in resonances over 1 → 5 eq. Note the broadening of the phenol resonance due to an increase in the rate of exchange. Top right: Experimental data (points) and calculated fit (lines) for a 1:1, 1:2 host-guest binding model. Bottom right: Speciation distribution diagram from the fit.

Table A2.14. Data output from the fitting of the above titration data

|  | $\log\beta_{1:1}$ | Standard deviation | Percentage error | $\log\beta_{1:2}$ | Standard deviation | Percentage error | $SE_y$ (ppb) |
|---|---|---|---|---|---|---|---|
| Titration 1 | 3.43 | 0.06 | 2% | 5.29 | 0.08 | 2% | 7.0 |

Table A2.15. Further data output from the fitting of the above titration data, derived stepwise binding constant with propagated uncertainty, and calculated cooperativity parameter with associated propagated uncertainty.

|  | Correlation coefficient | $\log K_{1:2}$ | Standard deviation | Percentage error | $\log\alpha$ | Error |
|---|---|---|---|---|---|---|
| Titration 1 | 97% | 1.86 | 0.03 | 1% | -0.97 | 0.05 |

## A2.3.2.4  Receptor **99** and AcO$^-$



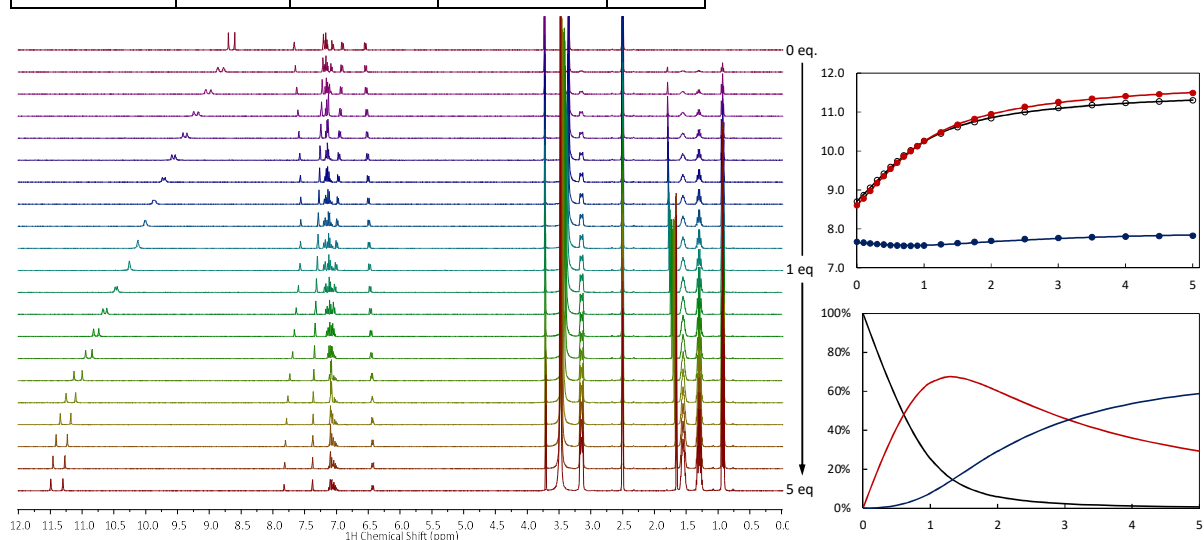Figure A2.13. Titration of receptor **99** with $H_2PO_4^-$. Main: Stack plot (0–12 ppm) showing the change in resonances over $1 \rightarrow 5$ eq. Note the broadening of the phenol resonance due to an increase in the rate of exchange. Top right: Experimental data (points) and calculated fit (lines) for a 1:1 host-guest binding model. Bottom right: Speciation distribution diagram from the fit.

Table A2.16. Data output from the fitting of the above titration data

|  | $\log\beta_{1:1}$ | Standard deviation | Percentage error | $SE_y$ (ppb) |
|---|---|---|---|---|
| Titration 1 | 2.487 | 0.009 | 0.3% | 14.6 |
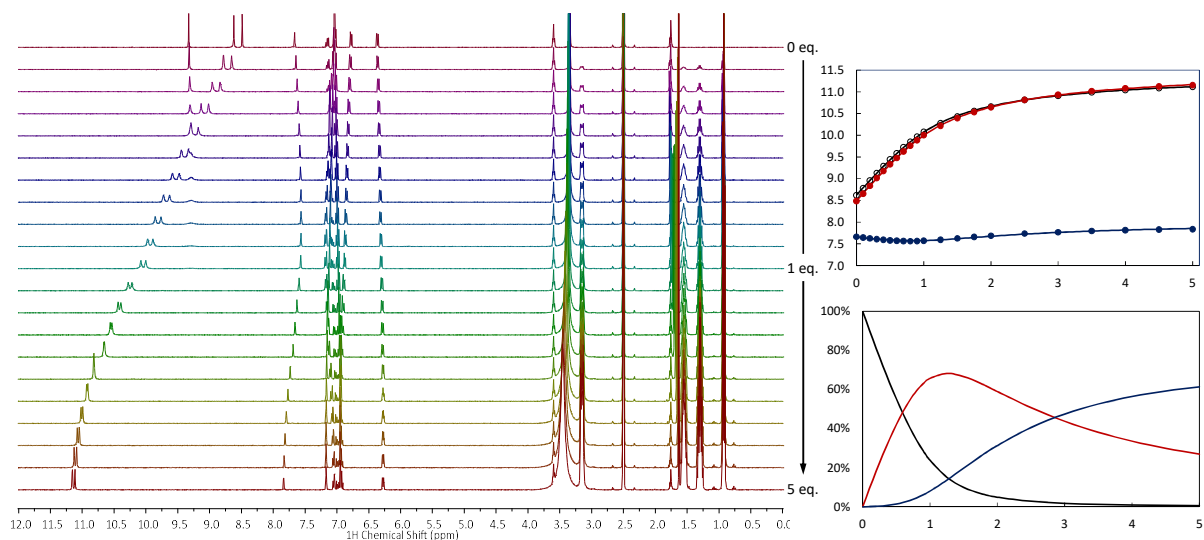
Figure A2.14. Titration of receptor **99** with AcO⁻. Main: Stack plot (0–12 ppm) showing the change in resonances over 1 → 5 eq. Note the broadening of the phenol resonance due to an increase in the rate of exchange. Top right: Experimental data (points) and calculated fit (lines) for a 1:1, 1:2 host-guest binding model. Bottom right: Speciation distribution diagram from the fit.

Table A2.17. Data output from the fitting of the above titration data

|  | $\log\beta_{1:1}$ | Standard deviation | Percentage error | $\log\beta_{1:2}$ | Standard deviation | Percentage error | $SE_y$ (ppb) |
|---|---|---|---|---|---|---|---|
| Titration 1 | 3.40 | 0.07 | 2% | 5.44 | 0.09 | 2% | 9.0 |

Table A2.18. Further data output from the fitting of the above titration data, derived stepwise binding constant with propagated uncertainty, and calculated cooperativity parameter with associated propagated uncertainty.

|  | Correlation coefficient | $\log K_{1:2}$ | Standard deviation | Percentage error | $\log\alpha$ | Error |
|---|---|---|---|---|---|---|
| Titration 1 | 97% | 2.04 | 0.03 | 1% | -0.75 | 0.06 |

## A2.3.3 Titrations with BzO⁻

### A2.3.3.1 Receptor **96** and BzO⁻



Figure A2.15. Titration of receptor **96** with BzO⁻. Main: Stack plot (0–12 ppm) showing the change in resonances over 1 → 5 eq. Top right: Experimental data (points) and calculated fit (lines) for a 1:1 host-guest binding model. Bottom right: Speciation distribution diagram from the fit.

Table A2.19. Data output from the fitting of the above titration data, and averaged values with associated 95% confidence intervals.

|  | $\log\beta_{1:1}$ | Standard deviation | Percentage error | $SE_y$ (ppb) |
|---|---|---|---|---|
| Titration 1 | 2.242 | 0.009 | 0.4% | 15.2 |
| Titration 2 | 2.48 | 0.01 | 0.5% | 22.3 |
| Titration 3 | 2.45 | 0.01 | 0.4% | 19.1 |
| Titration 4 | 2.32 | 0.01 | 0.4% | 17.6 |
| **Average** | **2.33** | **0.06** | **3%** | |

Figure A2.16. Titration of receptor **96** with BzO⁻. Main: Stack plot (0–12 ppm) showing the change in resonances over 1 → 5 eq. Top right: Experimental data (points) and calculated fit (lines) for a 1:1, 1:2 host-guest binding model. Bottom right: Speciation distribution diagram from the fit.

Table A2.20. Data output from the fitting of the above titration data, and averaged values with associated 95% confidence intervals.

| | $\log\beta_{1:1}$ | Standard deviation | Percentage error | $\log\beta_{1:2}$ | Standard deviation | Percentage error | $SE_y$ (ppb) |
|---|---|---|---|---|---|---|---|
| Titration 1 | 3.31 | 0.05 | 1% | 5.14 | 0.06 | 1% | 4.7 |
| Titration 2 | 3.38 | 0.09 | 3% | 5.17 | 0.13 | 3% | 12.0 |
| Titration 3 | 3.32 | 0.08 | 3% | 5.19 | 0.12 | 2% | 11.2 |
| Titration 4 | 3.21 | 0.08 | 2% | 4.92 | 0.11 | 2% | 8.0 |
| **Average** | **3.18** | **0.12** | **4%** | **4.75** | **0.40** | **8%** | |

Table A2.21. Further data output from the fitting of the above titration data, derived stepwise binding constants with propagated uncertainty, averaged value with associated 95% confidence interval, and calculated cooperativity parameter with associated propagated uncertainty.

| | Correlation coefficient | $\log K_{1:2}$ | Standard deviation | Percentage Error | $\log\alpha$ | Error |
|---|---|---|---|---|---|---|
| Titration 1 | 98% | 1.84 | 0.02 | 0.8% | | |
| Titration 2 | 95% | 1.18 | 0.20 | 17% | | |
| Titration 3 | 97% | 1.54 | 0.07 | 4% | | |
| Titration 4 | 97% | 1.71 | 0.04 | 2% | | |
| **Average** | | **1.57** | **0.28** | **18%** | **-1.01** | **0.30** |

### A2.3.3.2   Receptor **97** and BzO⁻
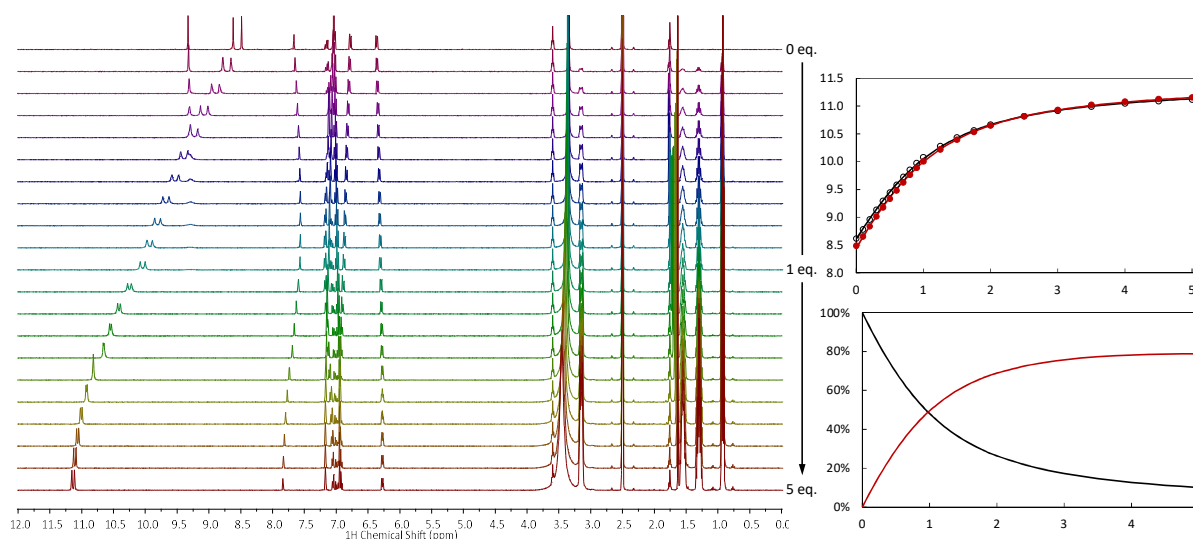


Figure A2.17. Titration of receptor **97** with BzO⁻. Main: Stack plot (0–12 ppm) showing the change in resonances over 1 → 5 eq. Top right: Experimental data (points) and calculated fit (lines) for a 1:1 host-guest binding model. Bottom right: Speciation distribution diagram from the fit.

Table A2.22. Data output from the fitting of the above titration data, and averaged values with associated 95% confidence intervals.

|  | $\log\beta_{1:1}$ | Standard deviation | Percentage error | $SE_y$ (ppb) |
|---|---|---|---|---|
| Titration 1 | 2.36 | 0.01 | 0.4% | 17.2 |
| Titration 2 | 2.34 | 0.01 | 0.4% | 15.1 |
| Titration 3 | 2.387 | 0.009 | 0.4% | 15.9 |
| **Average** | **2.36** | **0.03** | **1%** | |



Figure A2.18. Titration of receptor **97** with BzO⁻. Main: Stack plot (0–12 ppm) showing the change in resonances over 1 → 5 eq. Top right: Experimental data (points) and calculated fit (lines) for a 1:1, 1:2 host-guest binding model. Bottom right: Speciation distribution diagram from the fit.

Table A2.23. Data output from the fitting of the above titration data, and averaged values with associated 95% confidence intervals.

| | $\log\beta_{1:1}$ | Standard deviation | Percentage Error | $\log\beta_{1:2}$ | Standard deviation | Percentage error | $SE_y$ (ppb) |
|---|---|---|---|---|---|---|---|
| Titration 1 | 3.04 | 0.10 | 3% | 4.76 | 0.15 | 3% | 12.0 |
| Titration 2 | 3.18 | 0.07 | 2% | 4.98 | 0.10 | 2% | 8.1 |
| Titration 3 | 3.16 | 0.07 | 2% | 4.90 | 0.10 | 2% | 8.0 |
| **Average** | **3.13** | **0.09** | **3%** | **4.88** | **0.13** | **3%** | |

Table A2.24. Further data output from the fitting of the above titration data, derived stepwise binding constants with propagated uncertainty, averaged value with associated 95% confidence interval, and calculated cooperativity parameter with associated propagated uncertainty.

| | Correlation coefficient | $\log K_{1:2}$ | Standard deviation | Percentage error | $\log\alpha$ | Error |
|---|---|---|---|---|---|---|
| Titration 1 | 97% | 1.72 | 0.06 | 4% | | |
| Titration 2 | 97% | 1.80 | 0.03 | 2% | | |
| Titration 3 | 97% | 1.74 | 0.04 | 2% | | |
| **Average** | | **1.75** | **0.05** | **3%** | **-0.78** | **0.10** |

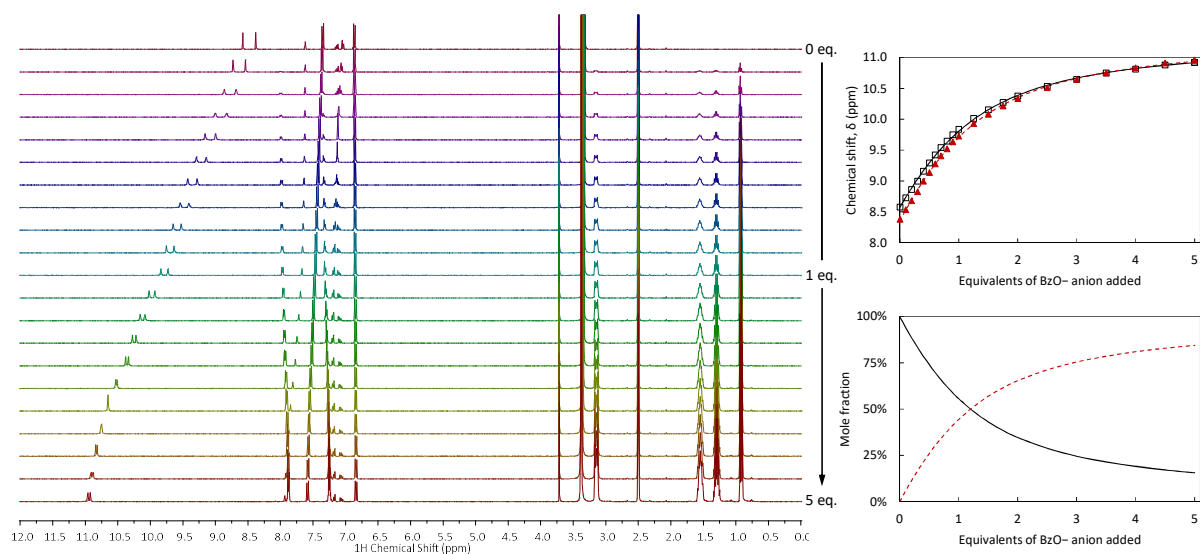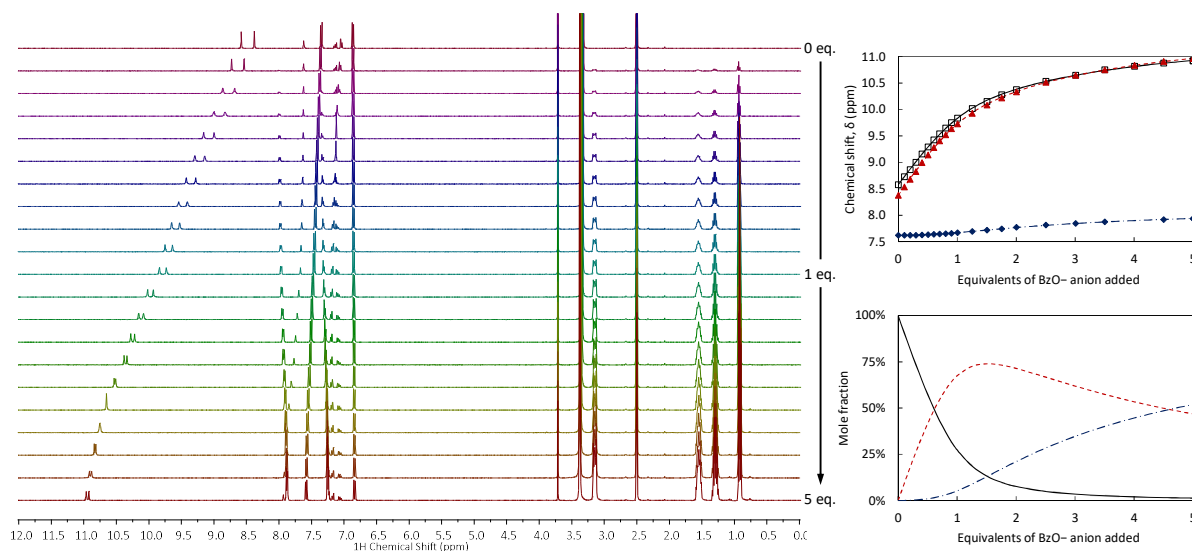### A2.3.3.3  Receptor **98** and BzO$^-$



Figure A2.19. Titration of receptor **98** with BzO$^-$. Main: Stack plot (0–12 ppm) showing the change in resonances over $1 \rightarrow 5$ eq. Note the broadening of the phenol resonance due to an increase in the rate of exchange. Top right: Experimental data (points) and calculated fit (lines) for a 1:1 host-guest binding model. Bottom right: Speciation distribution diagram from the fit.

*Appendix A2: ¹H NMR Titration Experiments and Data Fitting*

Table A2.25. Data output from the fitting of the above titration data.

|  | $\log\beta_{1:1}$ | Standard deviation | Percentage error | $SE_y$ (ppb) |
|---|---|---|---|---|
| Titration 1 | 2.31 | 0.01 | 0.5% | 17.9 |



Figure A2.20. Titration of receptor **98** with BzO⁻. Main: Stack plot (0–12 ppm) showing the change in resonances over 1 → 5 eq. Top right: Experimental data (points) and calculated fit (lines) for a 1:1, 1:2 host-guest binding model. Bottom right: Speciation distribution diagram from the fit.

Table A2.26. Data output from the fitting of the above titration data.

|  | $\log\beta_{1:1}$ | Standard deviation | Percentage error | $\log\beta_{1:2}$ | Standard deviation | Percentage error | $SE_y$ (ppb) |
|---|---|---|---|---|---|---|---|
| Titration 1 | 3.37 | 0.06 | 2% | 5.08 | 0.08 | 2% | 5.4 |

Table A2.27. Further data output from the fitting of the above titration data, derived stepwise binding constant with propagated uncertainty, and calculated cooperativity parameter with associated propagated uncertainty.

|  | Correlation coefficient | $\log K_{1:2}$ | Standard deviation | Percentage error | $\log\alpha$ | Error |
|---|---|---|---|---|---|---|
| Titration 1 | 97% | 1.71 | 0.03 | 2% | -1.06 | 0.04 |

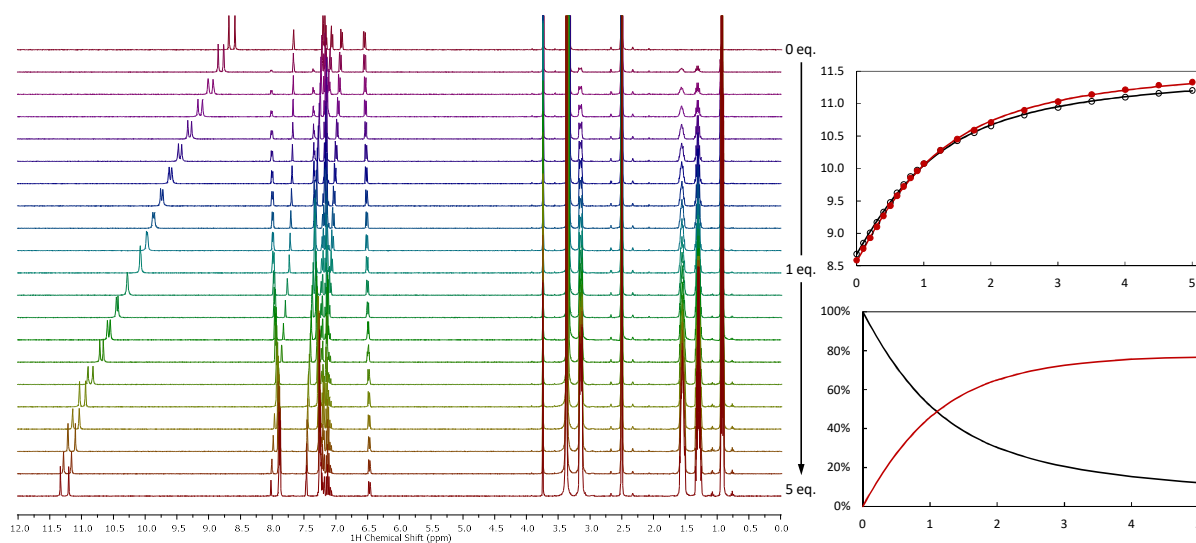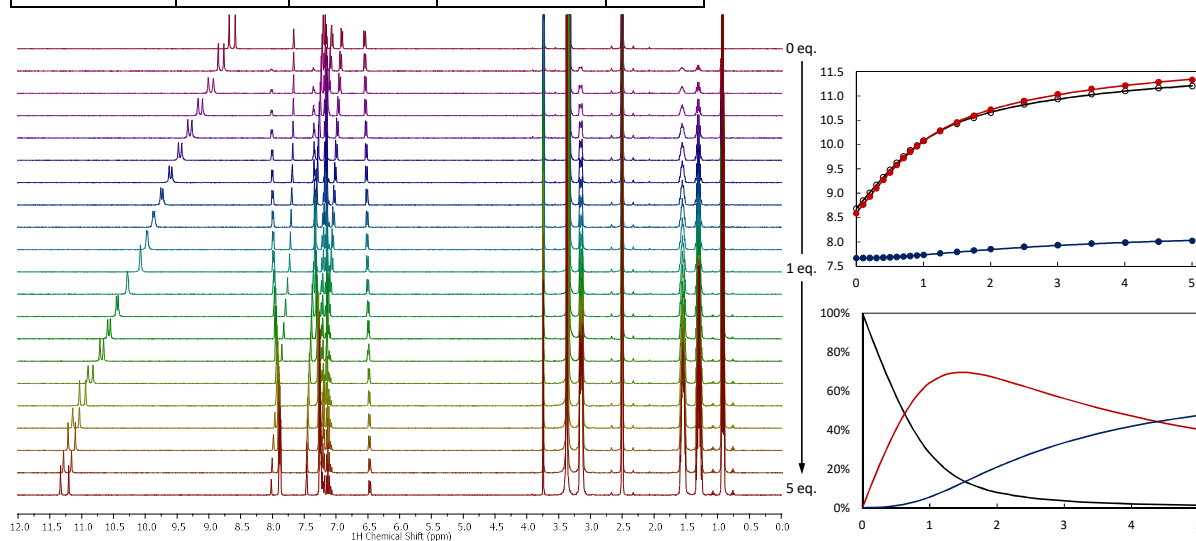### A2.3.3.4  Receptor **99** and BzO⁻



Figure A2.21. Titration of receptor **99** with BzO⁻. Main: Stack plot (0–12 ppm) showing the change in resonances over 1 → 5 eq. Note the broadening of the phenol resonance due to an increase in the rate of exchange. Top right: Experimental data (points) and calculated fit (lines) for a 1:1 host-guest binding model. Bottom right: Speciation distribution diagram from the fit.

Table A2.28. Data output from the fitting of the above titration data.

|            | $\log\beta_{1:1}$ | Standard deviation | Percentage error | $SE_y$ (ppb) |
|------------|-------------------|--------------------|------------------|--------------|
| Titration 1 | 2.38             | 0.01               | 0.5%             | 20.3         |



Figure A2.22. Titration of receptor **99** with BzO⁻. Main: Stack plot (0–12 ppm) showing the change in resonances over 1 → 5 eq. Top right: Experimental data (points) and calculated fit (lines) for a 1:1, 1:2 host-guest binding model. Bottom right: Speciation distribution diagram from the fit.
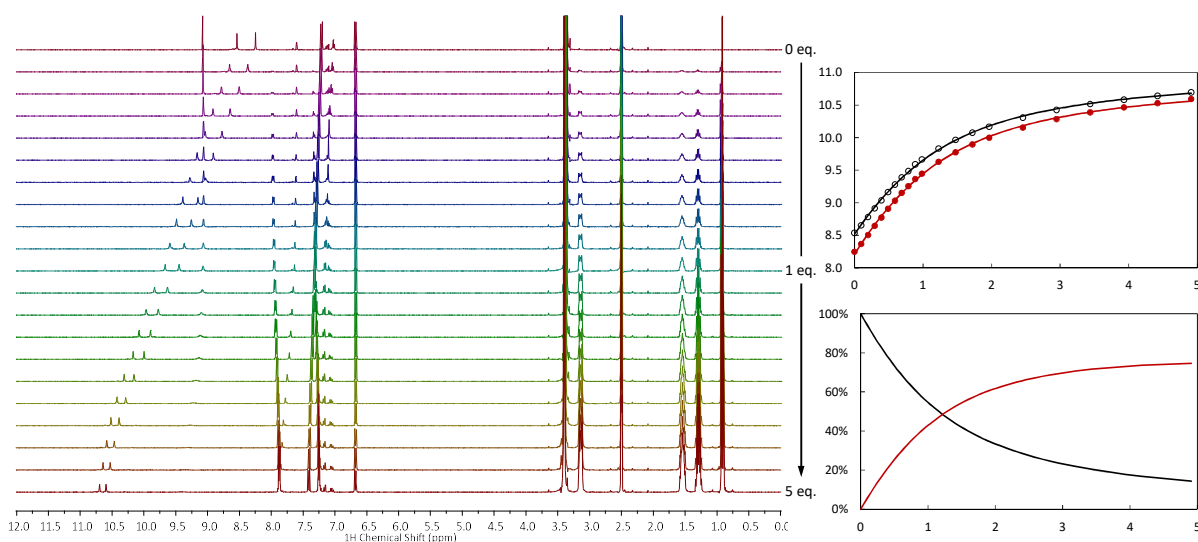
223

Table A2.29. Data output from the fitting of the above titration data.

| | $\log\beta_{1:1}$ | Standard deviation | Percentage error | $\log\beta_{1:2}$ | Standard deviation | Percentage error | $SE_y$ (ppb) |
|---|---|---|---|---|---|---|---|
| Titration 1 | 3.00 | 0.10 | 3% | 4.48 | 0.20 | 4% | 10.6 |

Table A2.30. Further data output from the fitting of the above titration data, derived stepwise binding constant with propagated uncertainty, and calculated cooperativity parameter with associated propagated uncertainty.

| | Correlation coefficient | $\log K_{1:2}$ | Standard deviation | Percentage error | $\log\alpha$ | Error |
|---|---|---|---|---|---|---|
| Titration 1 | 97% | 1.49 | 0.11 | 7% | -0.91 | 0.05 |

## A2.3.4 Titrations with Cl⁻

### A2.3.4.1 Receptor **96** and Cl⁻



Figure A2.23. Titration of receptor **96** with Cl⁻. Main: Stack plot (0–12 ppm) showing the change in resonances over 1 → 5 eq. Top right: Experimental data (points) and calculated fit (lines) for a 1:1 host-guest binding model. Bottom right: Speciation distribution diagram from the fit.

Table A2.31. Data output from the fitting of the above titration data, and averaged values with associated 95% confidence intervals.

| | $\log\beta_{1:1}$ | Standard deviation | Percentage error | $SE_y$ (ppb) |
|---|---|---|---|---|
| Titration 1 | 1.63 | 0.02 | 1% | 4.3 |
| Titration 2 | 1.71 | 0.02 | 1% | 5.1 |
| **Average** | **1.67** | **0.08** | **5%** | |

## A2.3.4.2 Receptor **97** and Cl⁻
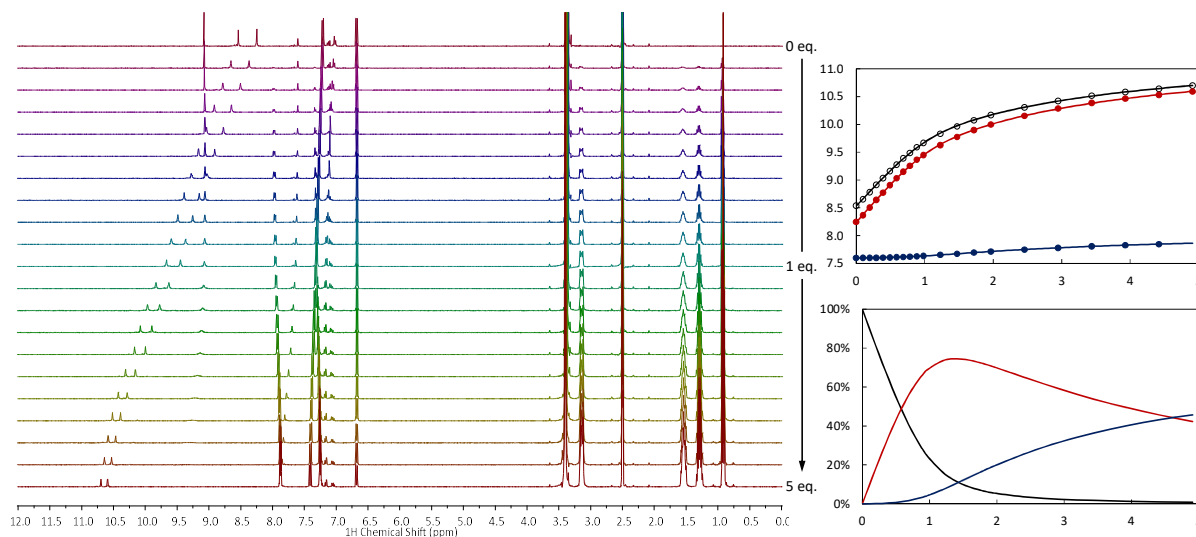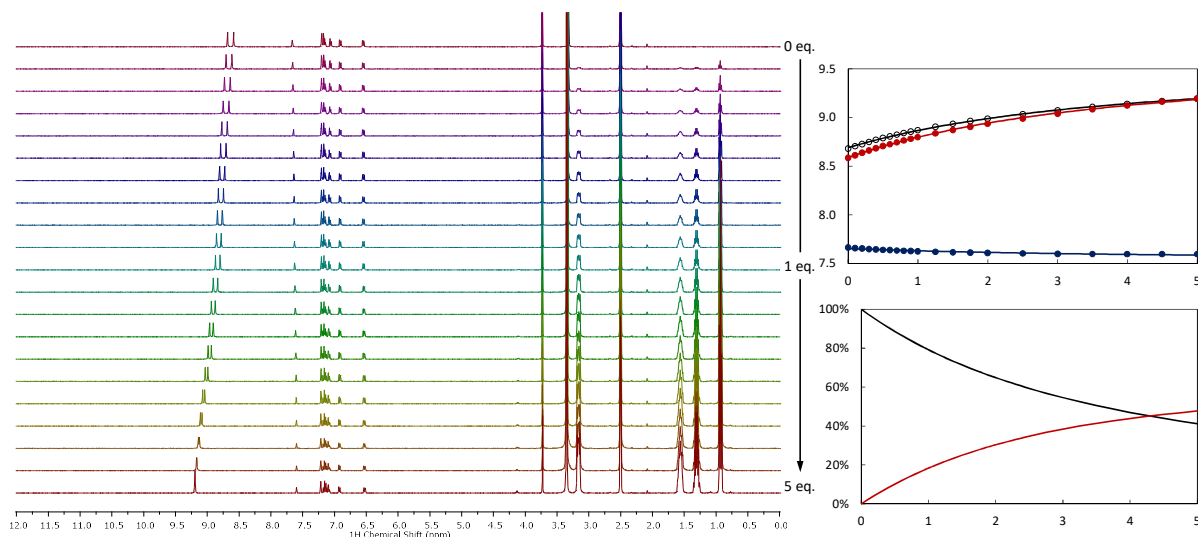


Figure A2.24. Titration of receptor **97** with Cl⁻. Main: Stack plot (0–12 ppm) showing the change in resonances over 1 → 5 eq. Top right: Experimental data (points) and calculated fit (lines) for a 1:1 host-guest binding model. Bottom right: Speciation distribution diagram from the fit.

Table A2.32. Data output from the fitting of the above titration data, and averaged values with associated 95% confidence intervals.

|  | $\log\beta_{1:1}$ | Standard deviation | Percentage error | $SE_y$ (ppb) |
|---|---|---|---|---|
| Titration 1 | 1.72 | 0.02 | 0.9% | 4.7 |
| Titration 2 | 1.62 | 0.02 | 1% | 4.8 |
| **Average** | **1.67** | **0.10** | **6%** | |

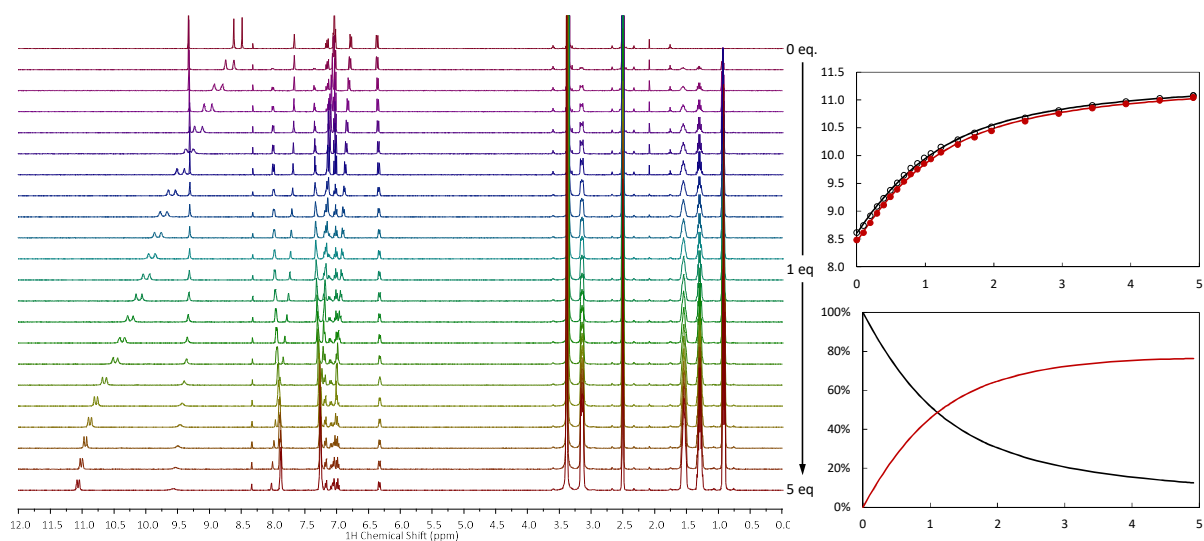## A2.3.4.3 Receptor **98** and Cl⁻



Figure A2.25. Titration of receptor **98** with Cl⁻. Main: Stack plot (0–12 ppm) showing the change in resonances over 1 → 5 eq. Top right: Experimental data (points) and calculated fit (lines) for a 1:1 host-guest binding model. Bottom right: Speciation distribution diagram from the fit.

Table A2.33. Data output from the fitting of the above titration data.

|  | $\log\beta_{1:1}$ | Standard deviation | Percentage error | $SE_y$ (ppb) |
|---|---|---|---|---|
| Titration 1 | 1.64 | 0.02 | 1% | 3.9 |

## A2.3.5 Titrations with $SO_4^{2-}$
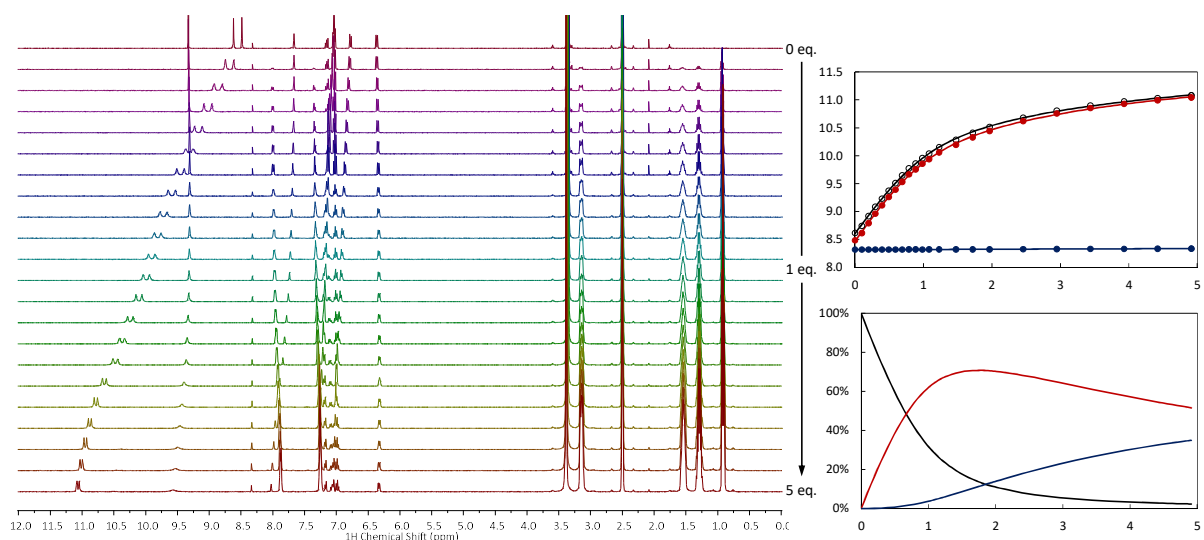
### A2.3.5.1 Receptor **96** and $SO_4^{2-}$



Figure A2.26. Titration of receptor **96** with $SO_4^{2-}$. Main: Stack plot (0–12 ppm) showing the change in resonances over 1 → 5 eq. Top right: Experimental data (points) and calculated fit (lines) for a 1:1 host-guest binding model. Bottom right: Speciation distribution diagram from the fit.

Table A2.34. Data output from the fitting of the above titration data, and averaged values with associated 95% confidence intervals.

|  | $\log\beta_{1:1}$ | Standard deviation | Percentage error | $SE_y$ (ppb) |
|---|---|---|---|---|
| Titration 1 | 1.37 | 0.03 | 2% | 1.3 |
| Titration 2 | 0.74 | 0.03 | 4% | 2.7 |
| **Average** | **1.06** | **0.62** | **58%** | |

## A2.3.5.2  Receptor **97** and $SO_4^{2-}$



Figure A2.27. Titration of receptor **97** with $SO_4^{2-}$. Main: Stack plot (0–12 ppm) showing the change in resonances over 1 → 5 eq. Top right: Experimental data (points) and calculated fit (lines) for a 1:1 host-guest binding model. Bottom right: Speciation distribution diagram from the fit.

Table A2.35. Data output from the fitting of the above titration data, and averaged values with associated 95% confidence intervals.

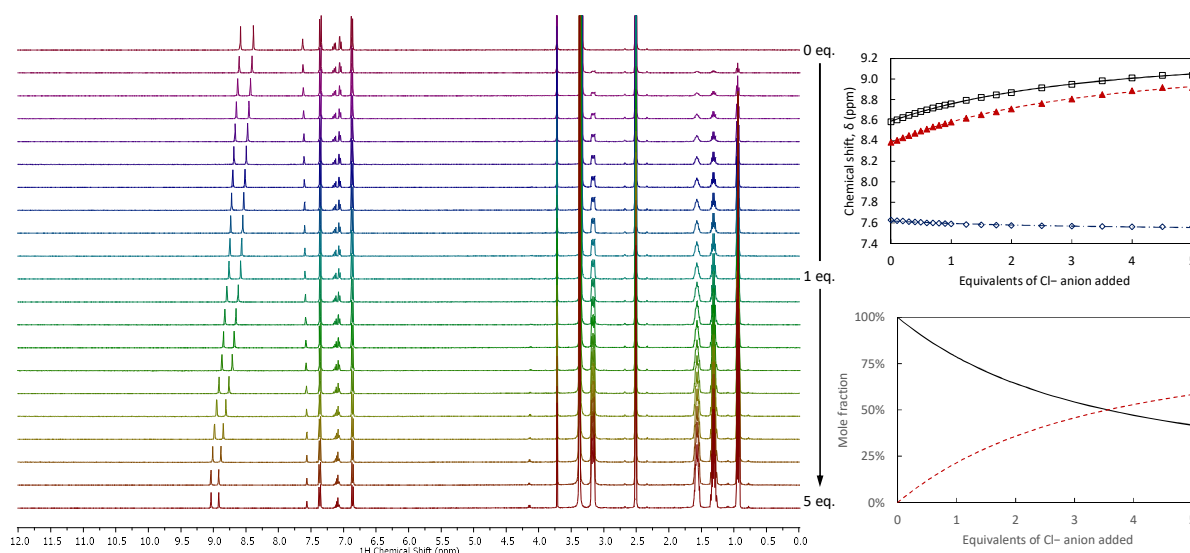|             | $\log\beta_{1:1}$ | Standard deviation | Percentage Error | $SE_y$ (ppb) |
|-------------|--------|--------|------|------|
| Titration 1 | 1.02   | 0.03   | 3%   | 3.8  |
| Titration 2 | 0.83   | 0.03   | 3%   | 2.7  |
| **Average** | **0.92** | **0.19** | **21%** |      |

## A2.3.5.3  Receptor **98** and $SO_4^{2-}$
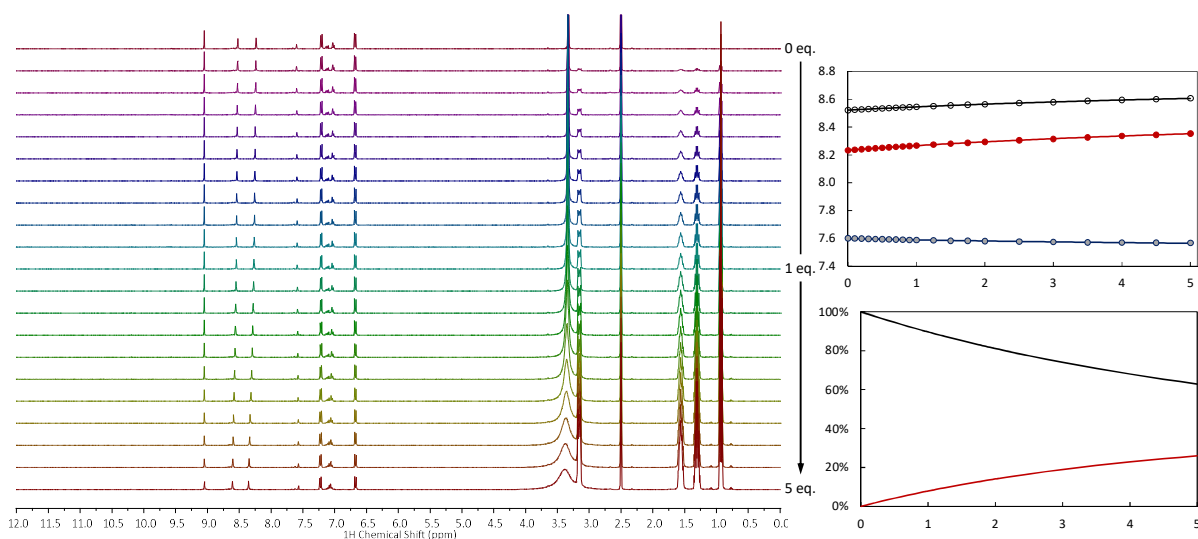


Figure A2.28. Titration of receptor **98** with $SO_4^{2-}$. Main: Stack plot (0–12 ppm) showing the change in resonances over 1 → 5 eq. Top right: Experimental data (points) and calculated fit (lines) for a 1:1 host-guest binding model. Bottom right: Speciation distribution diagram from the fit.

Table A2.36. Data output from the fitting of the above titration data.

|  | $\log\beta_{1:1}$ | Standard deviation | Percentage error | $SE_y$ (ppb) |
|---|---|---|---|---|
| Titration 1 | 1.15 | 0.03 | 3% | 9.4 |

## A2.3.6 Titrations with $HSO_4^-$

### A2.3.6.1 Receptor **96** and $HSO_4^-$



Figure A2.29. Titration of receptor **96** with $HSO_4^-$. Main: Stack plot (0–12 ppm) showing the change in resonances over $1 \rightarrow 5$ eq. Top right: Experimental data (points) and calculated fit (lines) for a 1:1 host-guest binding model. Bottom right: Speciation distribution diagram from the fit.

Table A2.37. Data output from the fitting of the above titration data.

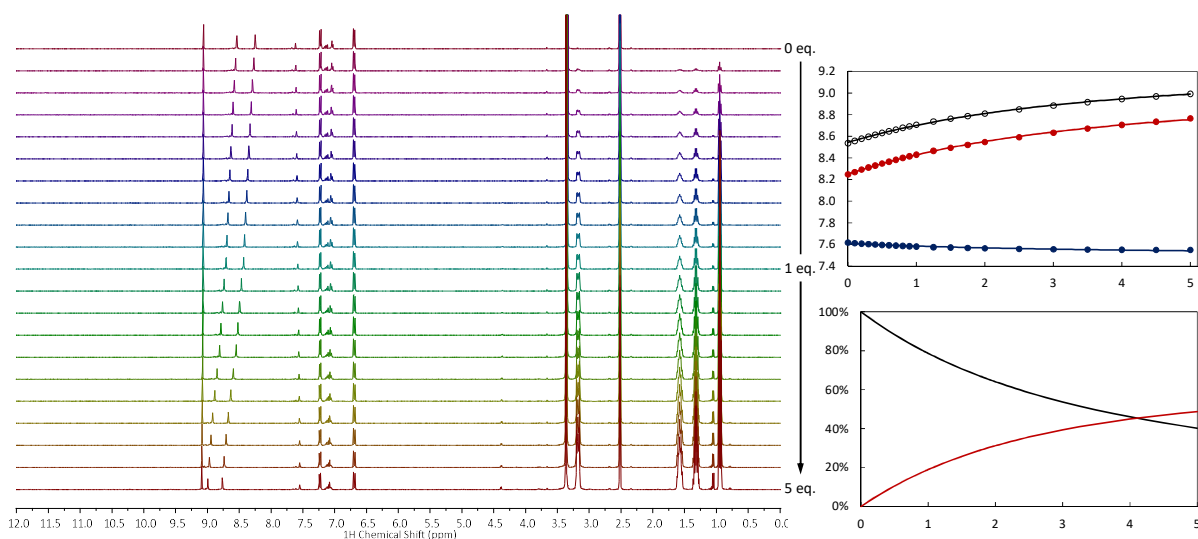|  | $\log\beta_{1:1}$ | Standard Deviation | Percentage error | $SE_y$ (ppb) |
|---|---|---|---|---|
| Titration 1 | 0.52 | 0.05 | 10% | 1.1 |

## A2.3.6.2 Receptor **97** and HSO$_4^-$



Figure A2.30. Titration of receptor **97** with HSO$_4^-$. Main: Stack plot (0–12 ppm) showing the change in resonances over 1 → 5 eq. Top right: Experimental data (points) and calculated fit (lines) for a 1:1 host-guest binding model. Bottom right: Speciation distribution diagram from the fit.

Table A2.38. Data output from the fitting of the above titration data.

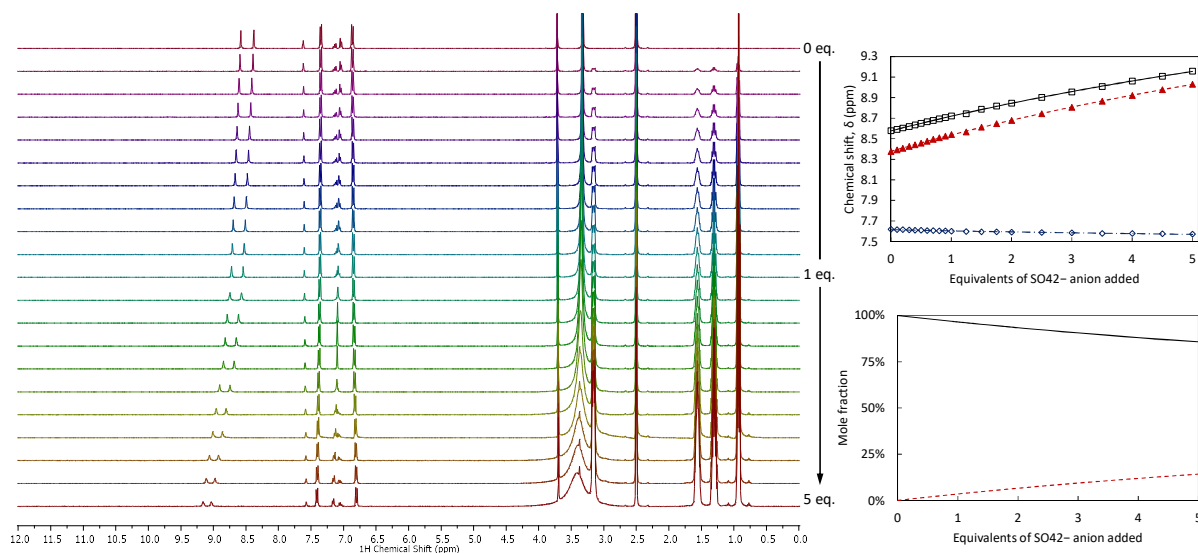|  | logβ$_{1:1}$ | Standard deviation | Percentage error | SE$_y$ (ppb) |
|---|---|---|---|---|
| Titration 1 | 1.43 | 0.03 | 2% | 1.2 |

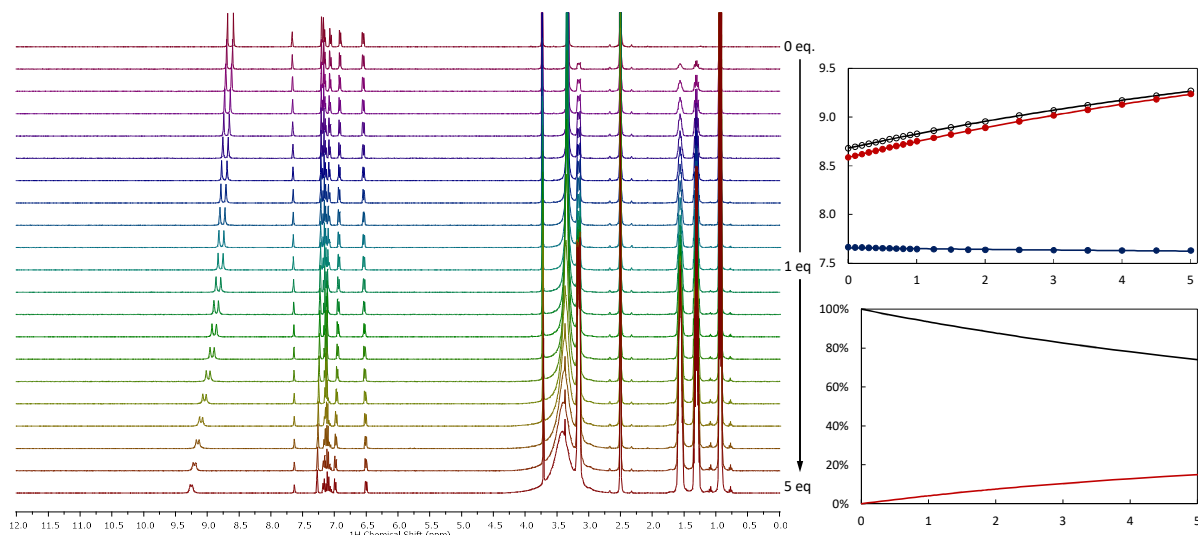## A2.3.6.3 Receptor **98** and HSO$_4^-$



Figure A2.31. Titration of receptor **98** with HSO$_4^-$. Main: Stack plot (0–12 ppm) showing the change in resonances over 1 → 5 eq. Top right: Experimental data (points) and calculated fit (lines) for a 1:1 host-guest binding model. Bottom right: Speciation distribution diagram from the fit.

*Appendix A2: $^1H$ NMR Titration Experiments and Data Fitting*

Table A2.39. Data output from the fitting of the above titration data.

| | $\log\beta_{1:1}$ | Standard deviation | Percentage error | $SE_y$ (ppb) |
|---|---|---|---|---|
| Titration 1 | 0.39 | 0.06 | 15% | 0.8 |

## A2.3.7 Titration of Receptor **97** with $HP_2O_7{}^{3-}$ (Pyrophosphate)
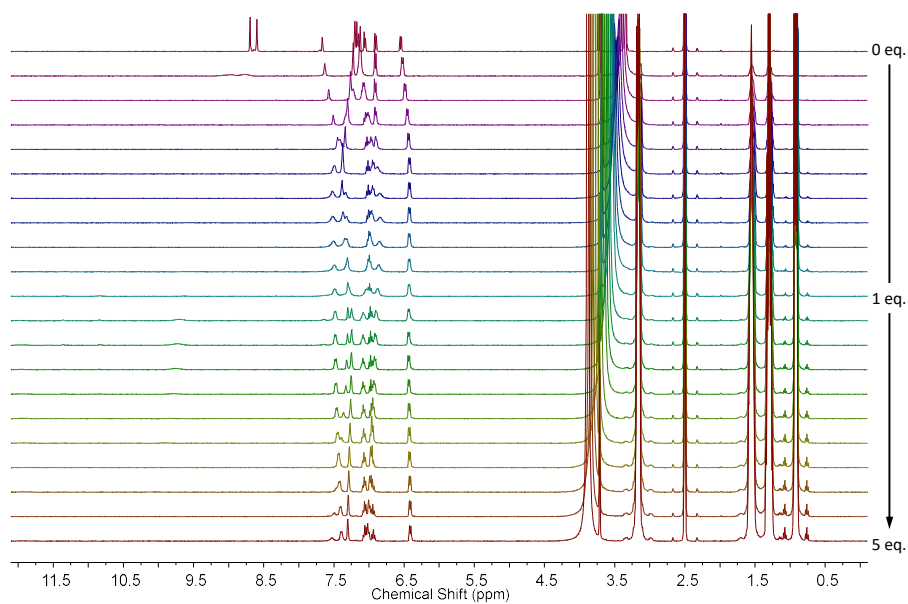


Figure A2.32. Stack plot (0–12 ppm) of the titration of receptor **97** with $HP_2O_7{}^{3-}$, showing the change in resonances over $1 \rightarrow 5$ eq.
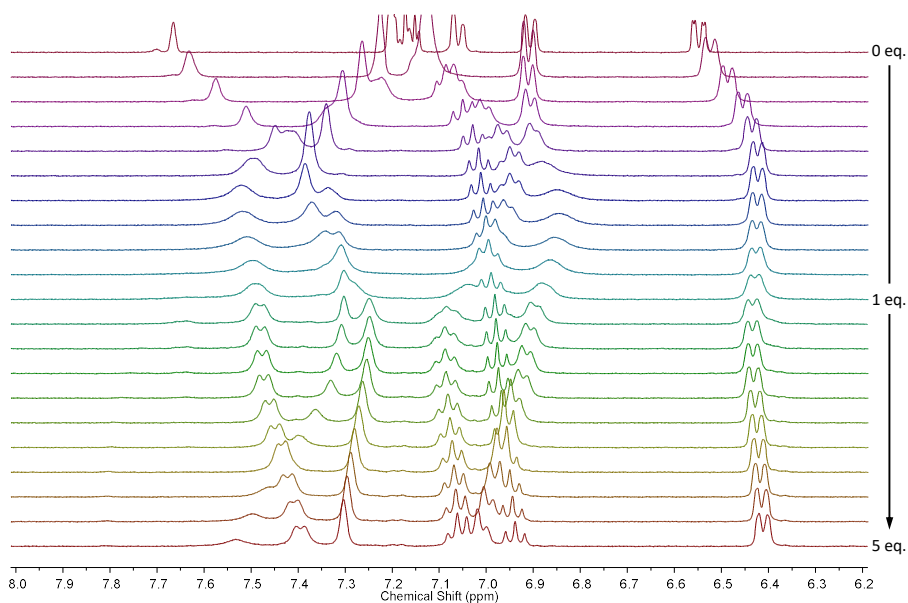


Figure A2.33. Stack plot (6.2–8 ppm) of the titration of receptor **97** with $HP_2O_7{}^{3-}$, showing the change in resonances over $1 \rightarrow 5$ eq.
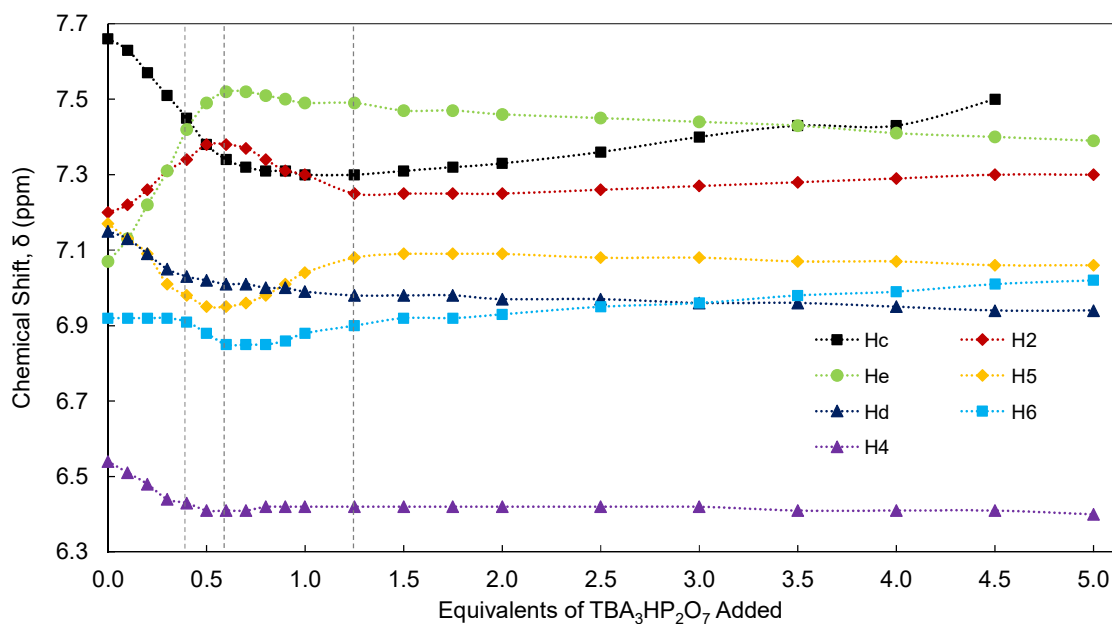
Figure A2.34. Experimental data for the titration of receptor **97** with $HP_2O_7^{3-}$ (1 → 5 eq.). Showing the sharp changes in resonances at *ca*. 0.4 eq., 0.6 eq. and 1.3 eq. $HP_2O_7^{3-}$.

## A2.3.8 Plot of Logarithmic Cooperativity Parameters
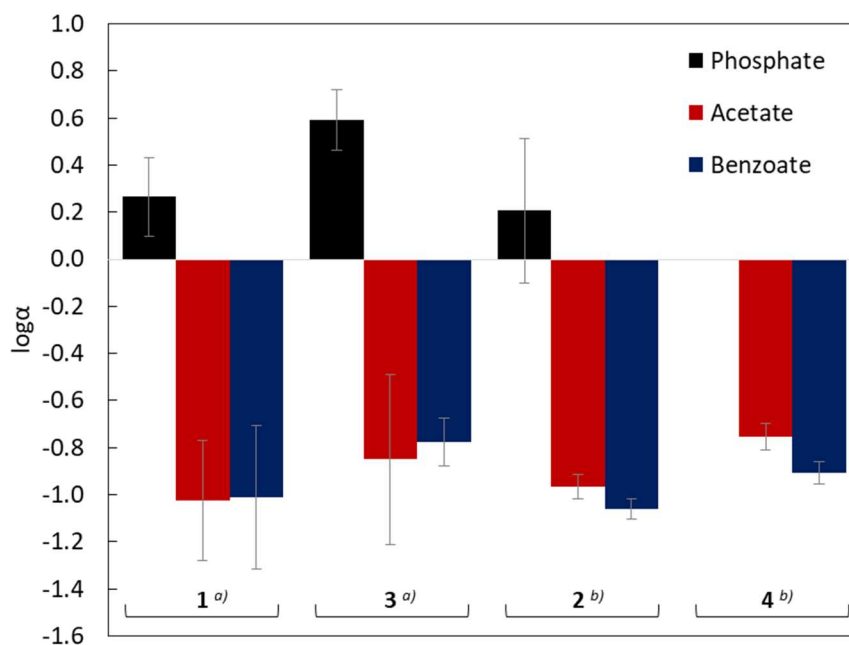


Figure A2.35. Logarithmic Cooperativity Parameters, logα, assuming both 1:1 and 1:2 Binding Modes as Determined from the Analysis of 1H NMR Titrations in DMSO-d6 at 298.2 K. [a] Cooperativity constants shown are averaged values, the errors shown are at the 95% confidence interval, [b] Cooperativity constants are as calculated from a single fit, the associated errors are as propagated from the "standard deviation" parameter and covariance reported by HypNMR.

## A2.3.9 Plot of the 1:1 Logarithmic Binding Constants against Hammet Parameter, σ
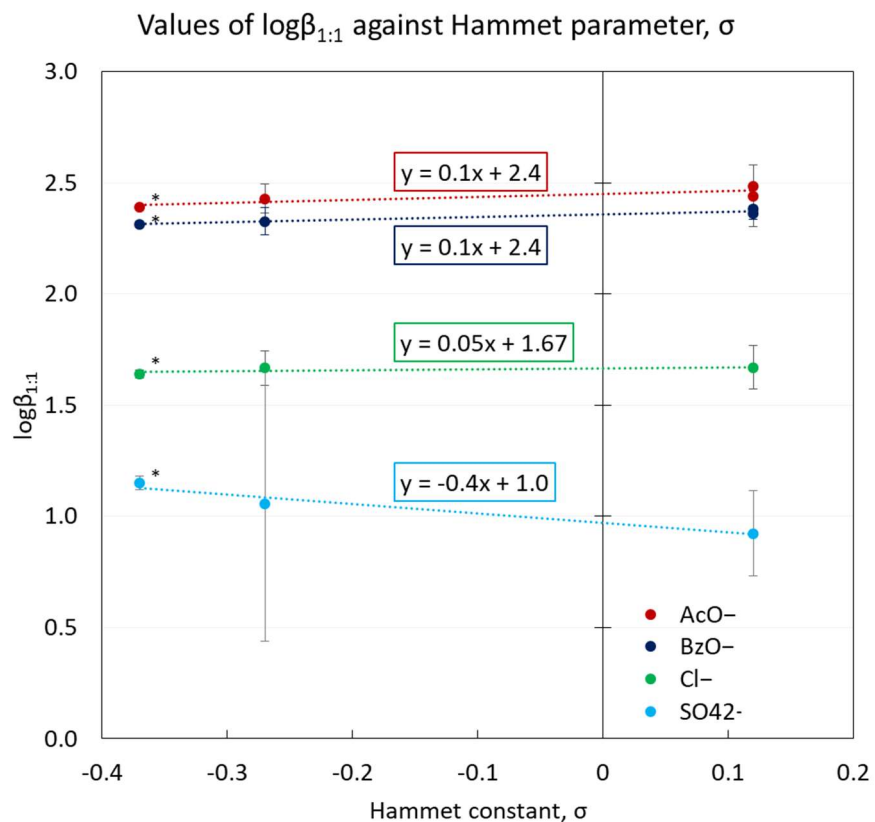


Figure A2.36. Plot of the values of $\log\beta_{1:1}$ against the relevant *meta* or *para* Hammet constant, σ. *Preliminary data from a single titration. Key: red: $AcO^-$; dark blue: $BzO^-$; green: $Cl^-$; light blue: $SO_4^{2-}$. The large spread in values associated with the repetitions in the $SO_4^{2-}$ titrations suggests that this trend may not be real.

# A2.4 Titration Data for Chapter 3

## A2.4.1 Titrations with $H_2PO_4^-$
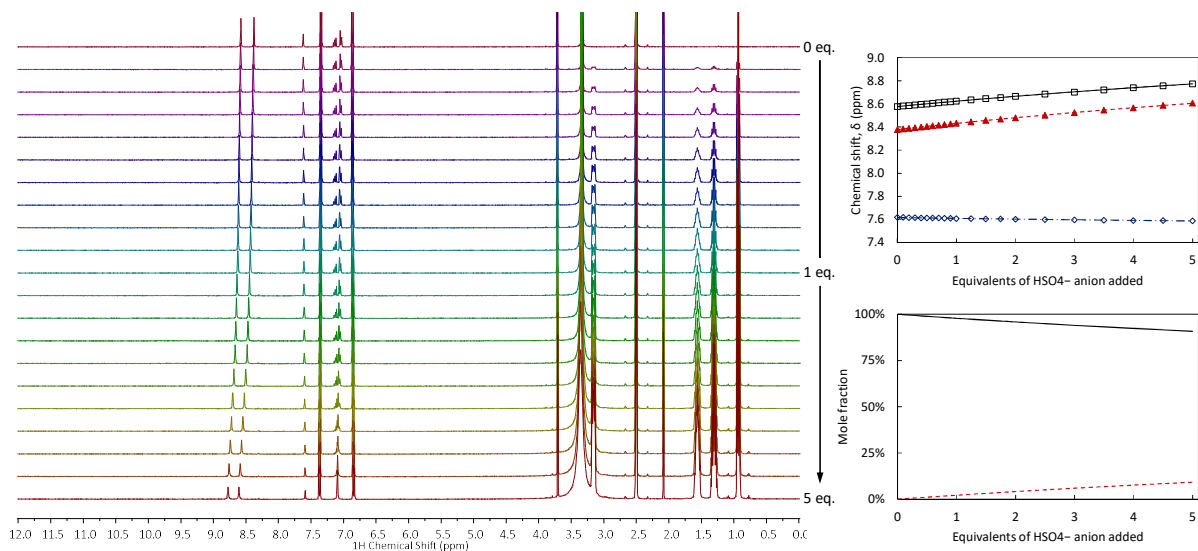
### A2.4.1.1 Receptor **102** and $H_2PO_4^-$
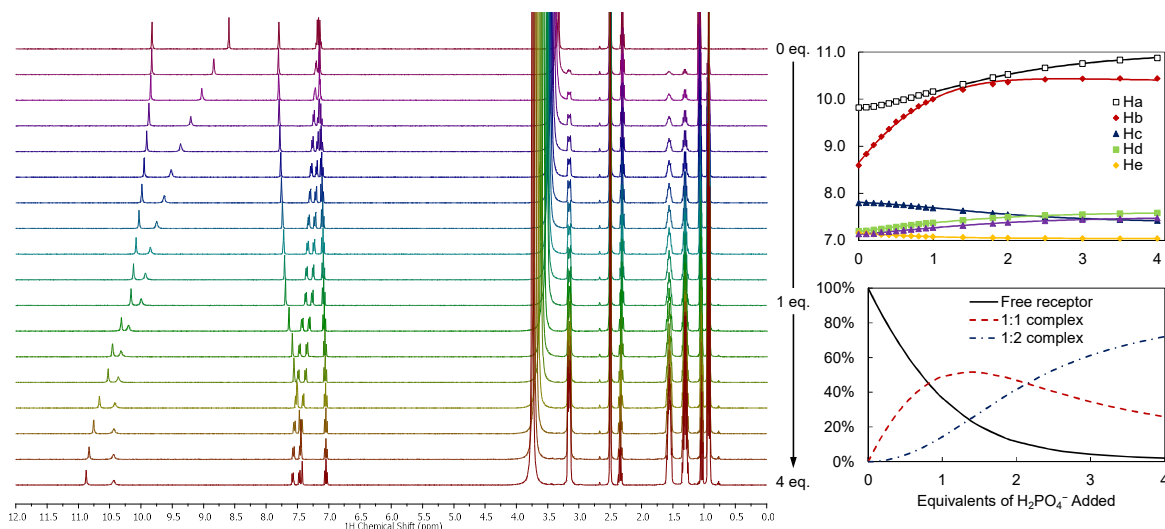


Figure A2.37. Titration of receptor **102** with $H_2PO_4^-$. Main: Stack plot (0–12 ppm) showing the change in resonances over 1 → 5 eq. Top right: Experimental data (points) and calculated fit (lines) for a 1:1 host-guest binding model. Bottom right: Speciation distribution diagram from the fit.

Table A2.40. Data output from the fitting of the above titration data.

|  | $\log\beta_{1:1}$ | Standard deviation | Percentage error | $\log\beta_{1:2}$ | Standard deviation | Percentage error | $SE_y$ (ppb) |
|---|---|---|---|---|---|---|---|
| Titration 1 | 2.57 | 0.08 | 3% | 4.71 | 0.08 | 2% | 7.7 |
| Titration 2 | 2.94 | 0.09 | 3% | 5.22 | 0.12 | 2% | 13.1 |
| **Average** | **2.75** | **0.36** | **13%** | **4.96** | **0.50** | **10%** | |

Table A2.41. Further data output from the fitting of the above titration data, derived stepwise binding constant with propagated uncertainty, and calculated cooperativity parameter with associated propagated uncertainty.

|  | Correlation coefficient | $\log K_{1:2}$ | Standard deviation | Percentage error | $\log\alpha$ | Error |
|---|---|---|---|---|---|---|
| Titration 1 | 74% | 2.14 | 0.06 | 3% | | |
| Titration 2 | 76% | 2.28 | 0.08 | 3% | | |
| **Average** | | **2.21** | **0.14** | **6%** | **0.1** | **0.4** |

*Appendix A2: $^1$H NMR Titration Experiments and Data Fitting*
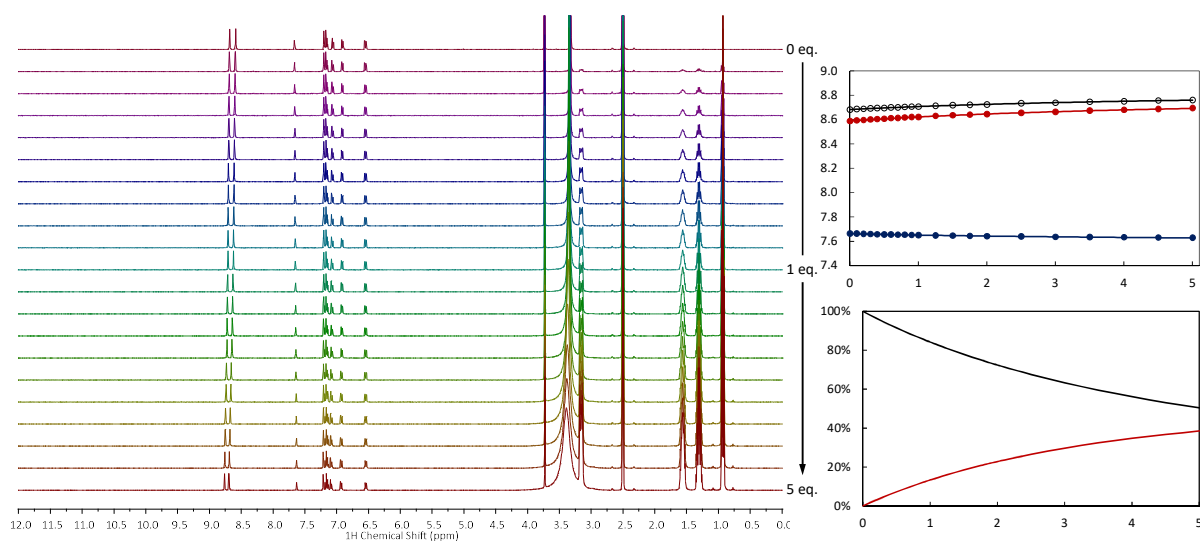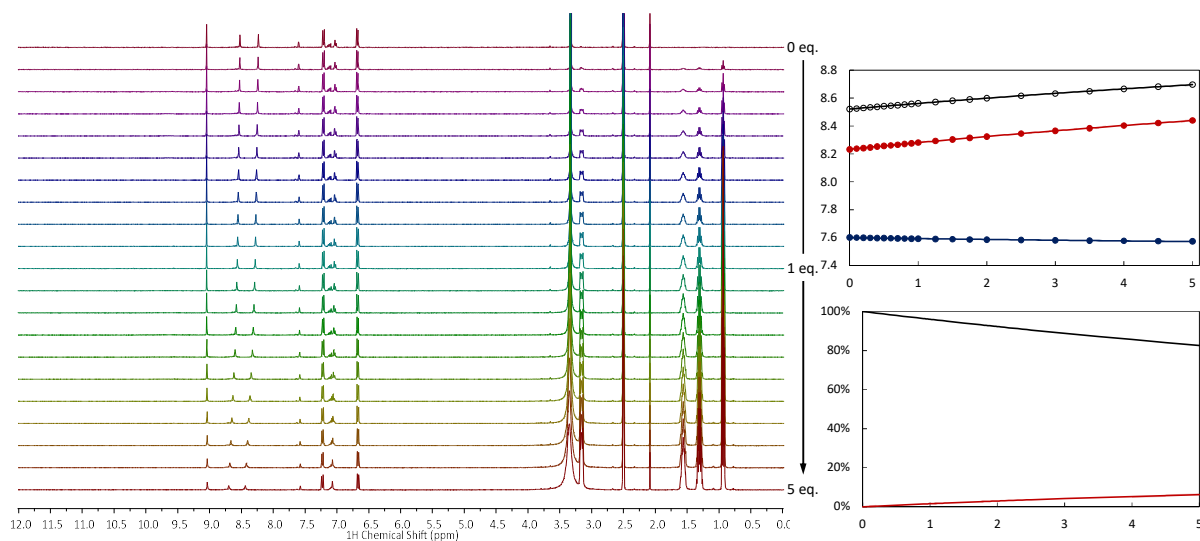
## A2.4.1.2   Receptor **103** and H$_2$PO$_4^-$



Figure A2.38. Titration of receptor **103** with H$_2$PO$_4^-$. Main: Stack plot (0–12 ppm) showing the change in resonances over 1 → 5 eq. Top right: Experimental data (points) and calculated fit (lines) for a 1:1 host-guest binding model. Bottom right: Speciation distribution diagram from the fit.

Table A2.42. Data output from the fitting of the above titration data.

|  | logβ$_{1:1}$ | Standard deviation | Percentage error | logβ$_{1:2}$ | Standard deviation | Percentage error | SE$_y$ (ppb) |
|---|---|---|---|---|---|---|---|
| Titration 1 | 2.95 | 0.07 | 2% | 5.20 | 0.09 | 2% | 9.6 |
| Titration 2 | 2.84 | 0.09 | 3% | 5.19 | 0.10 | 2% | 11.2 |
| **Average** | **2.89** | **0.11** | **4%** | **5.19** | **0.01** | **0.2%** | |

Table A2.43. Further data output from the fitting of the above titration data, derived stepwise binding constant with propagated uncertainty, and calculated cooperativity parameter with associated propagated uncertainty.

|  | Correlation coefficient | logK$_{1:2}$ | Standard deviation | Percentage error | logα | Error |
|---|---|---|---|---|---|---|
| Titration 1 | 78% | 2.25 | 0.06 | 3% | | |
| Titration 2 | 76% | 2.35 | 0.07 | 3% | | |
| **Average** | | **2.30** | **0.10** | **4%** | **0.0** | **0.2** |

## A2.4.1.3   Receptor **105** and $H_2PO_4^-$
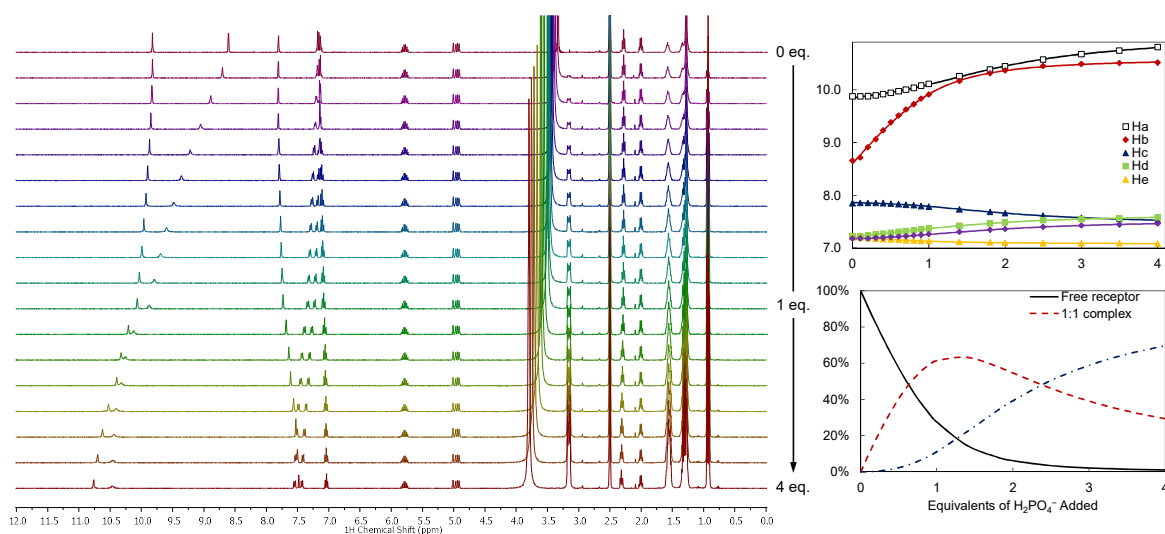


Figure A2.39. Titration of receptor **105** with $H_2PO_4^-$. Main: Stack plot (0–12 ppm) showing the change in resonances over 1 → 5 eq. Top right: Experimental data (points) and calculated fit (lines) for a 1:1 host-guest binding model. Bottom right: Speciation distribution diagram from the fit.

Table A2.44. Data output from the fitting of the above titration data.

|  | $\log\beta_{1:1}$ | Standard deviation | Percentage error | $\log\beta_{1:2}$ | Standard deviation | Percentage error | $SE_y$ (ppb) |
|---|---|---|---|---|---|---|---|
| Titration 1 | 3.30 | 0.09 | 3% | 5.51 | 0.11 | 2% | 10.8 |
| Titration 2 | 3.12 | 0.07 | 2% | 5.26 | 0.08 | 2% | 8.2 |
| **Average** | **3.21** | **0.12** | **4%** | **5.38** | **0.17** | **3%** | |

Table A2.45. Further data output from the fitting of the above titration data, derived stepwise binding constant with propagated uncertainty, and calculated cooperativity parameter with associated propagated uncertainty.

|  | Correlation coefficient | $\log K_{1:2}$ | Standard deviation | Percentage error | $\log\alpha$ | Error |
|---|---|---|---|---|---|---|
| Titration 1 | 87% | 2.21 | 0.05 | 2% | | |
| Titration 2 | 83% | 2.13 | 0.05 | 2% | | |
| **Average** | | **2.17** | **0.05** | **2%** | **−0.4** | **0.1** |

## A2.4.2 Titrations with BzO⁻

### A2.4.2.1 Receptor **102** and BzO⁻
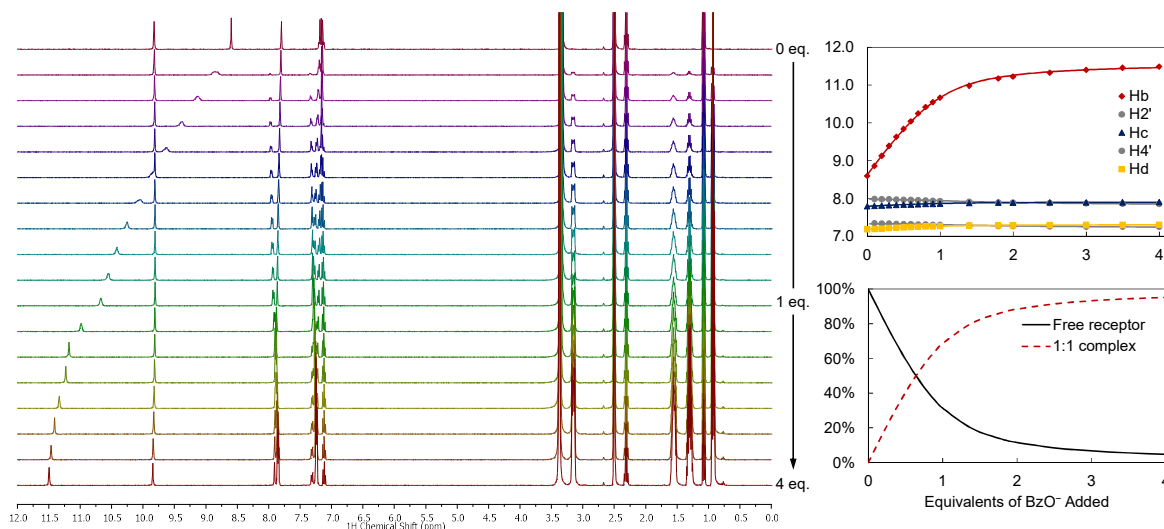


Figure A2.40. Titration of receptor **102** with BzO⁻. Main: Stack plot (0–12 ppm) showing the change in resonances over 1 → 5 eq. Top right: Experimental data (points) and calculated fit (lines) for a 1:1 host-guest binding model. Bottom right: Speciation distribution diagram from the fit.

Table A2.46. Data output from the fitting of the above titration data.

|  | $\log\beta_{1:1}$ | Standard deviation | Percentage error | $SE_y$ (ppb) |
|---|---|---|---|---|
| Titration 1 | 2.83 | 0.01 | 0.3% | 9.0 |
| Titration 2 | 3.01 | 0.01 | 0.4% | 11.5 |
| **Average** | **2.92** | **0.18** | **6%** |  |

### A2.4.2.2 Receptor **103** and BzO⁻



Figure A2.41. Titration of receptor **103** with BzO⁻. Main: Stack plot (0–12 ppm) showing the change in resonances over 1 → 5 eq. Top right: Experimental data (points) and calculated fit (lines) for a 1:1 host-guest binding model. Bottom right: Speciation distribution diagram from the fit.

Table A2.47. Data output from the fitting of the above titration data.

|  | logβ$_{1:1}$ | Standard deviation | Percentage error | SE$_y$ (ppb) |
|---|---|---|---|---|
| Titration 1 | 3.04 | 0.03 | 0.8% | 22.0 |
| Titration 2 | 3.05 | 0.02 | 0.8% | 20.6 |
| **Average** | **3.04** | **0.01** | **0.4%** | |

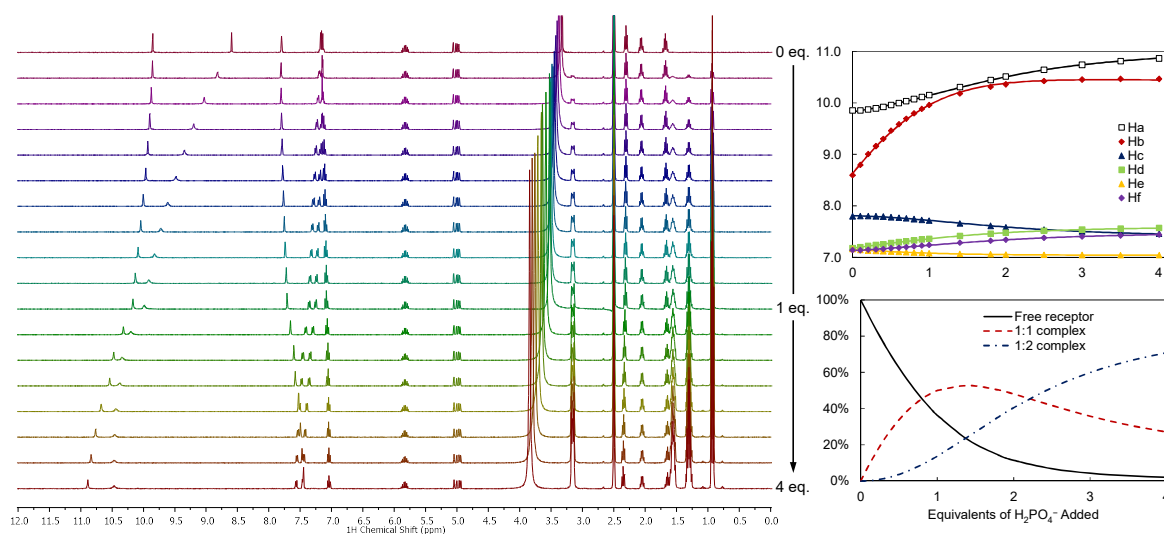### A2.4.2.3  Receptor **105** and BzO⁻



Figure A2.42. Titration of receptor **105** with BzO⁻. Main: Stack plot (0–12 ppm) showing the change in resonances over 1 → 5 eq. Top right: Experimental data (points) and calculated fit (lines) for a 1:1 host-guest binding model. Bottom right: Speciation distribution diagram from the fit.

Table A2.48. Data output from the fitting of the above titration data.

|  | logβ$_{1:1}$ | Standard deviation | Percentage error | SE$_y$ (ppb) |
|---|---|---|---|---|
| Titration 1 | 3.02 | 0.02 | 0.6% | 17.3 |
| Titration 2 | 2.92 | 0.02 | 0.5% | 15.8 |
| **Average** | **2.97** | **0.07** | **2%** | |

## A2.4.3 Titrations with $SO_4^{2-}$

### A2.4.3.1 Receptor **102** and $SO_4^{2-}$
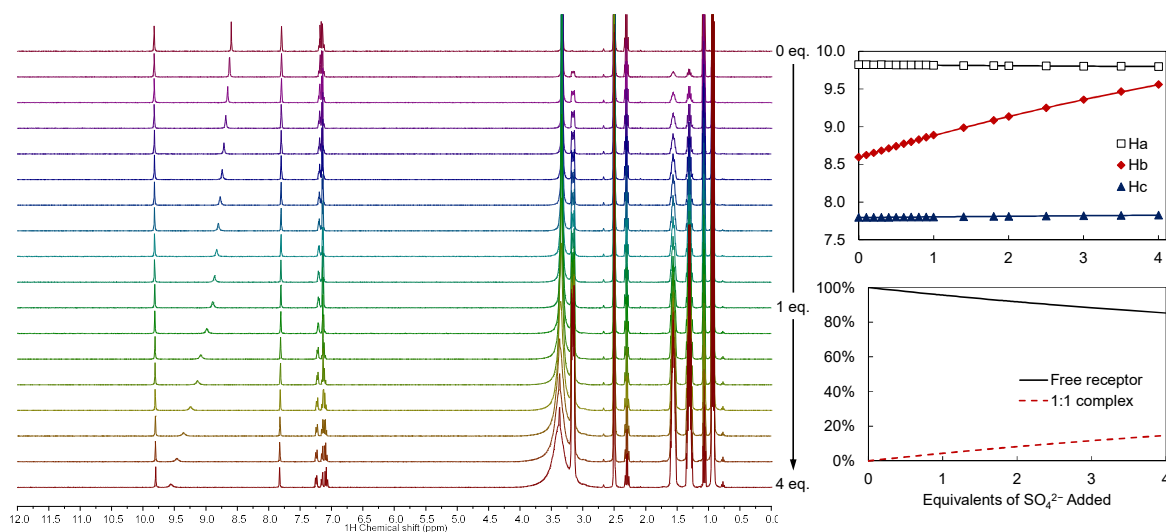


Figure A2.43. Titration of receptor **102** with $SO_4^{2-}$. Main: Stack plot (0–12 ppm) showing the change in resonances over 1 → 5 eq. Top right: Experimental data (points) and calculated fit (lines) for a 1:1 host-guest binding model. Bottom right: Speciation distribution diagram from the fit.

Table A2.49. Data output from the fitting of the above titration data.

|  | $\log\beta_{1:1}$ | Standard deviation | Percentage error | $SE_y$ (ppb) |
|---|---|---|---|---|
| Titration 1 | 0.30 | 0.04 | 12% | 1.1 |
| Titration 2 | 0.85 | 0.02 | 2% | 1.9 |
| **Average** | **0.57** | **0.54** | **95%** | |

### A2.4.3.2 Receptor **103** and $SO_4^{2-}$
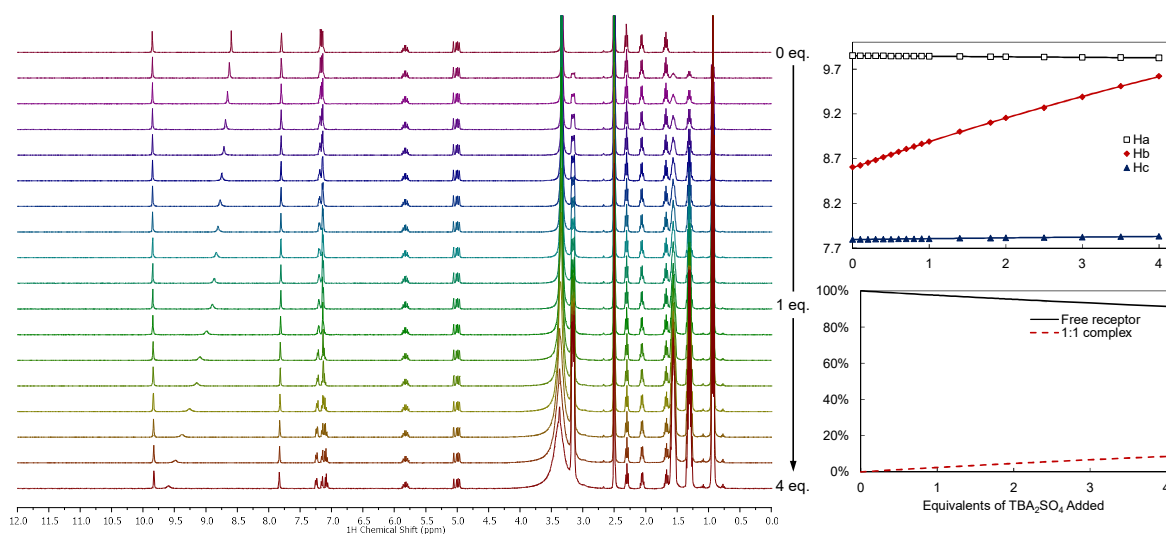


Figure A2.44. Titration of receptor **103** with $SO_4^{2-}$. Main: Stack plot (0–12 ppm) showing the change in resonances over 1 → 5 eq. Top right: Experimental data (points) and calculated fit (lines) for a 1:1 host-guest binding model. Bottom right: Speciation distribution diagram from the fit.

Table A2.50. Data output from the fitting of the above titration data.

|  | logβ$_{1:1}$ | Standard deviation | Percentage error | SE$_y$ (ppb) |
|---|---|---|---|---|
| Titration 1 | 0.58 | 0.04 | 7% | 0.25 |
| Titration 2 | 0.71 | 0.04 | 5% | 0.28 |
| **Average** | **0.64** | **0.13** | **20%** | |

## A2.4.3.3  Receptor **105** and SO$_4^{2-}$
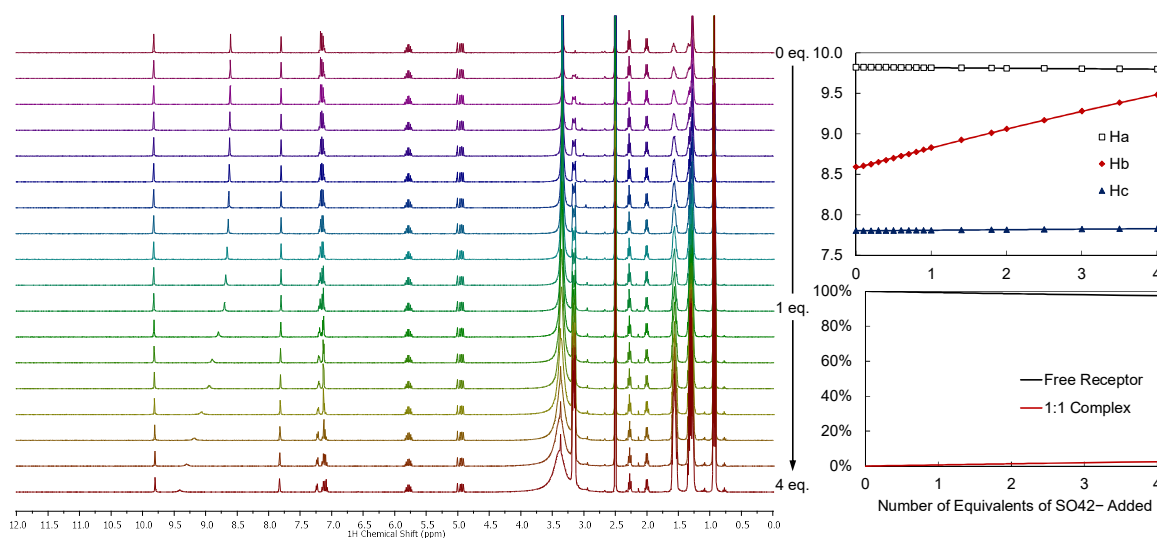


Figure A2.45. Titration of receptor **105** with SO$_4^{2-}$. Main: Stack plot (0–12 ppm) showing the change in resonances over 1 → 5 eq. Top right: Experimental data (points) and calculated fit (lines) for a 1:1 host-guest binding model. Bottom right: Speciation distribution diagram from the fit.

Table A2.51. Data output from the fitting of the above titration data.

|  | logβ$_{1:1}$ | Standard deviation | Percentage error | SE$_y$ (ppb) |
|---|---|---|---|---|
| Titration 1 | 0.01 | 0.17 | 1238% | 0.28 |
| Titration 2 | – $^{a)}$ | | | |
| Titration 3 | – $^{a)}$ | | | |

a) No fit could be obtained from the data.

## A2.4.4 Titration of Receptor **102** with Cl$^-$
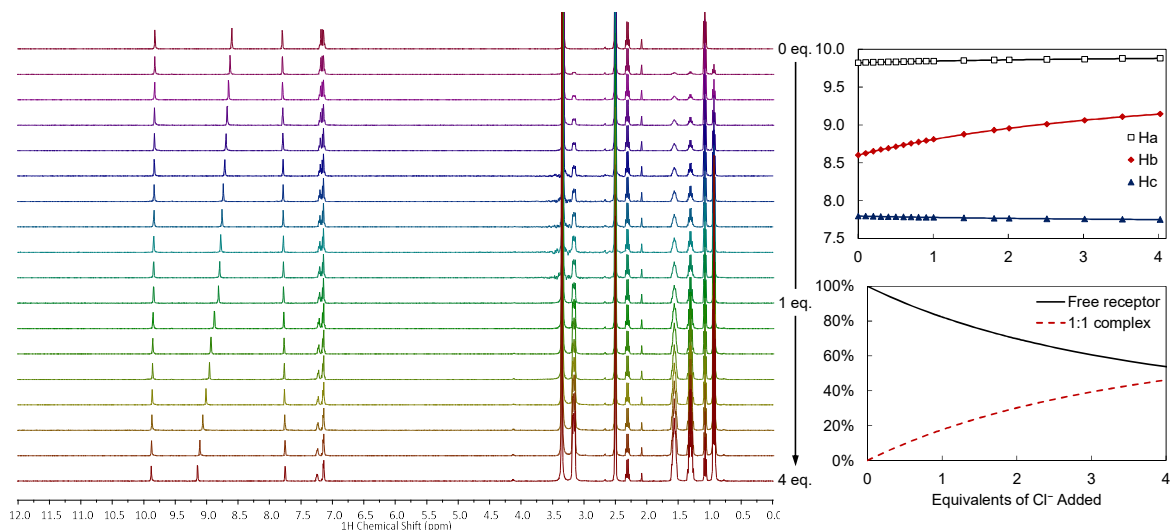


Figure A2.46. Titration of receptor **102** with Cl$^-$. Main: Stack plot (0–12 ppm) showing the change in resonances over 1 → 5 eq. Top right: Experimental data (points) and calculated fit (lines) for a 1:1 host-guest binding model. Bottom right: Speciation distribution diagram from the fit.

Table A2.52. Data output from the fitting of the above titration data.

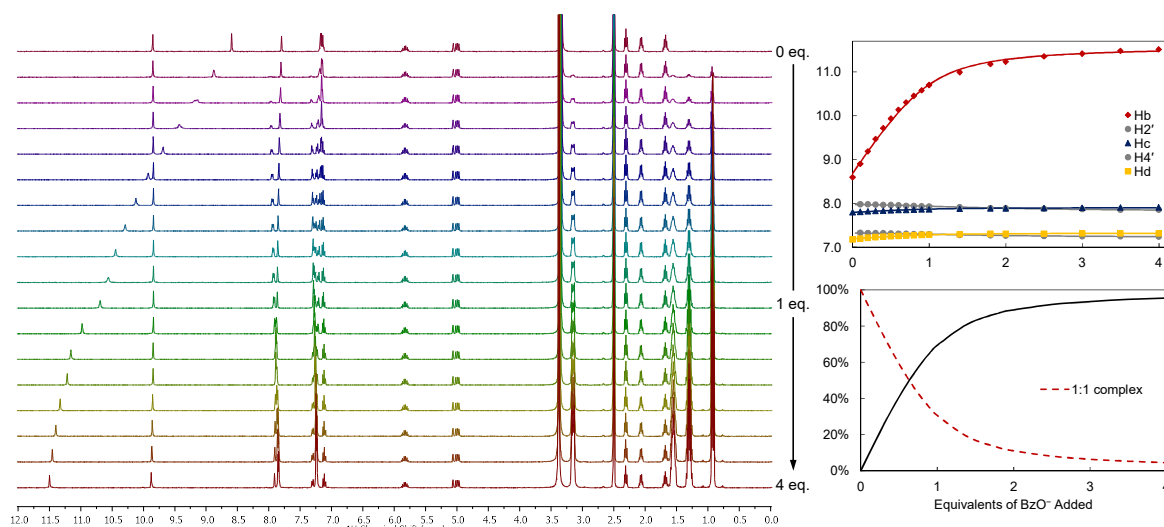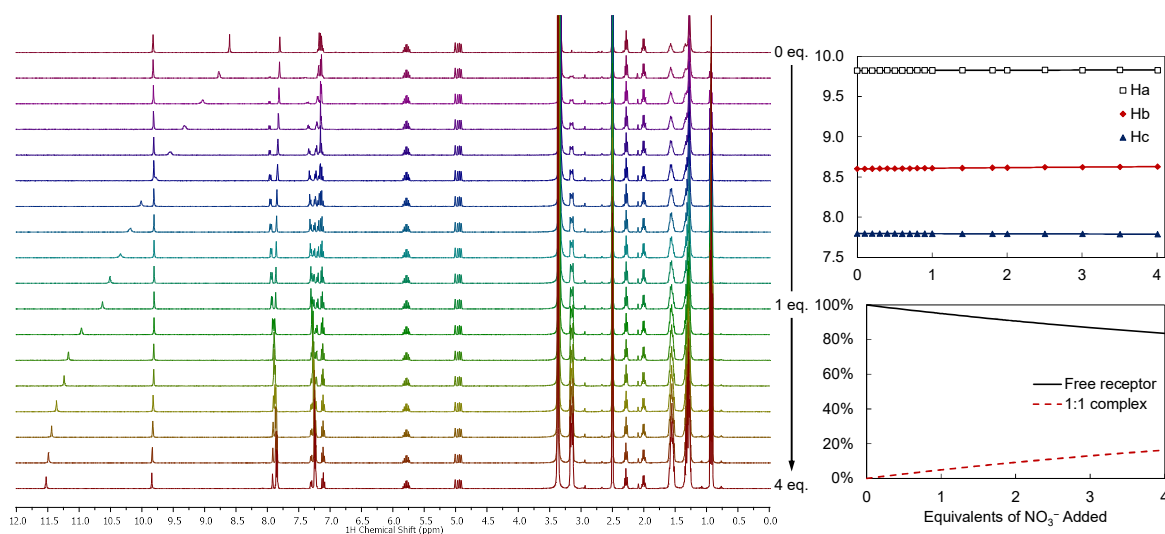|  | log$\beta_{1:1}$ | Standard Deviation | Percentage error | SE$_y$ (ppb) |
|---|---|---|---|---|
| Titration 1 | 1.58 | 0.01 | 0.6% | 0.13 |

## A2.4.5 Titration of Receptor **102** with NO$_3^-$
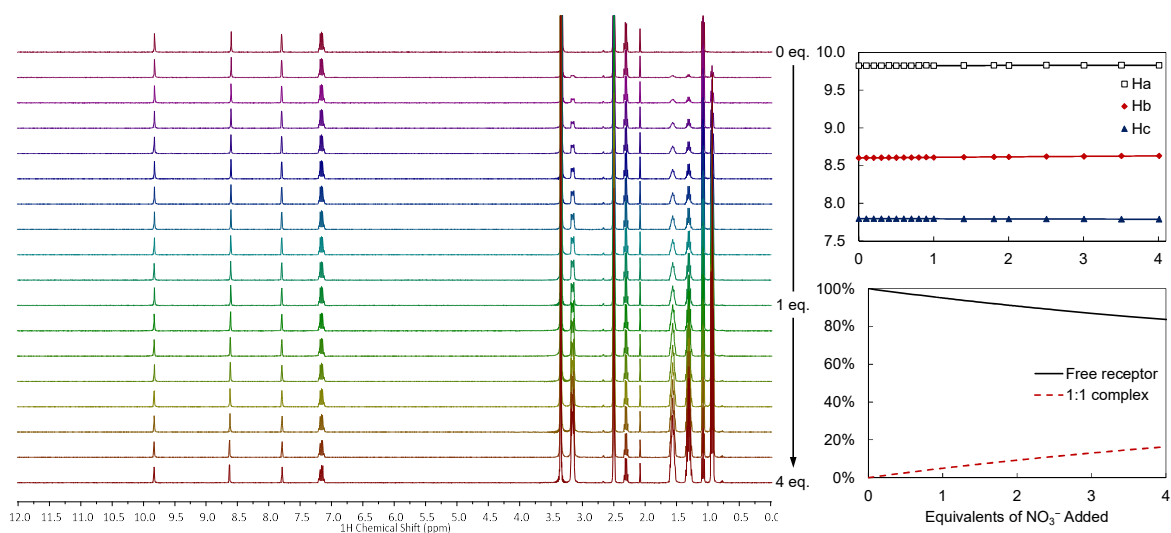


Figure A2.47. Titration of receptor **102** with NO$_3^-$. Main: Stack plot (0–12 ppm) showing the change in resonances over 1 → 5 eq. Top right: Experimental data (points) and calculated fit (lines) for a 1:1 host-guest binding model. Bottom right: Speciation distribution diagram from the fit.

Table A2.53. Data output from the fitting of the above titration data.

| | $\log\beta_{1:1}$ | Standard Deviation | Percentage error | $SE_y$ (ppb) |
|---|---|---|---|---|
| Titration 1 | 0.90 | 0.29 | 32% | 0.09 |

## A2.4.6 Titration of Receptor **105** with Benzoic Acid

Upon titration of the receptor with benzoic acid, no change in the chemical shifts of any of the species in solution during the titration of the C$_{11}$ host **105** with benzoic acid could be observed, Figure A2.48. Thus, any residual carboxylic acid remaining after incomplete purification would not be expected to affect the appearance of the NMR spectrum within the aromatic or NH regions (7–10 ppm).
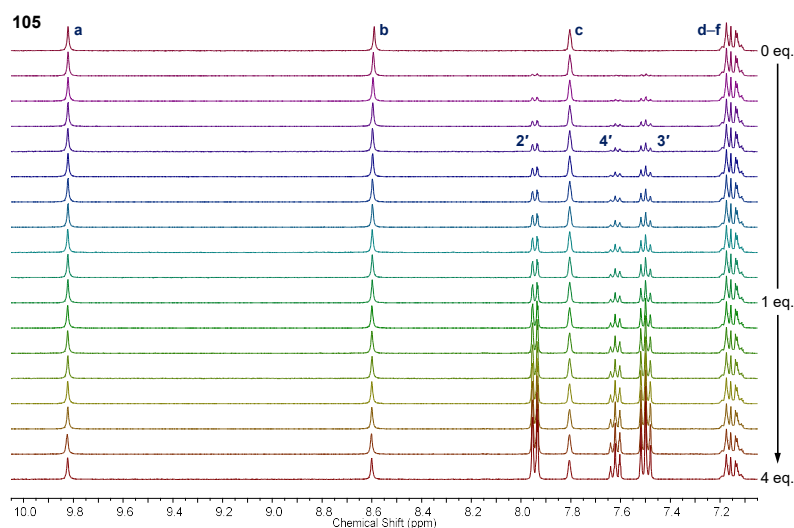


Figure A2.48. Stack plot of the individual $^1$H NMR spectra (400 MHz, DMSO-$d_6$, 7–10 ppm) from the titration of receptor **105** (7 mM) with benzoic acid (0→4 eq.).

*Appendix A2: ^{1}H NMR Titration Experiments and Data Fitting*

## A2.4.7 Comparative Tables of Binding Constants between this work and reference 5

Table A2.54. Comparison of the logarithmic binding constants for $SO_4^{2-}$ obtained using HypNMR and NMRTit (obtained by Boyle in previous work[5]) as fitting programmes.

| | Receptor | Chain length | HypNMR | | | NMRTit | |
|---|---|---|---|---|---|---|---|
| | | | $\log\beta_{1:1}$ | $\log\beta_{1:2}$ | $SE_y$ (ppb) [d] | $\log\beta_{1:1}$ | $\log\beta_{1:2}$ |
| This work | 101 | 3 | 0.6(5) | | 1.5 | n/a [e] | |
| | 103 | 6 | 0.6(1) | | 2.6 | | |
| | 105 | 11 | 0.0(2) [b] | | 2.8 | | |
| Reference 5 | 103 | 6 | 4.1(3) | 6.6(3) | 22.8 | 2.6 | 5.8 |
| | 104 | 7 | 2.5(2) | 4.6(1) | 12.4 | 2.2 | 4.6 |
| | 105 | 11 | 4.5(5) [c] | | 71.6 | 3.9 | |
| | 125 | n/a [a] | 1.2(1) | | 1.3 | – [f] | |

All titrations performed with $TBA_2SO_4$ at an initial host concentration of 7 mM. This work: Titrations performed at 25 °C, constants shown are their average values, associated errors represent the 95% confidence interval. Preliminary studies from reference 5: Titration performed at 20 °C, constants shown are from fitting a single titration, associated errors are the 'standard deviation' parameter as output by HypNMR2008. a) Macrocyclic derivative of receptor **105**, b) Only one titration could be fit. c) Data corrected for error in first addition, $\log\beta_{1:1} = 4.0 \pm 0.1$ otherwise. d) See Section A2.1 for definition, e) Data not analysed with NMRTit (this work), f) Fitting not performed (previous work), NH resonances were observed to split.

Table A2.55. Comparison of the logarithmic binding constants for $BzO^-$ obtained using HypNMR and NMRTit (obtained by Boyle in previous work[5]) as fitting programmes.

| | Receptor | Chain length | HypNMR | | | NMRTit | |
|---|---|---|---|---|---|---|---|
| | | | $\log\beta_{1:1}$ | $\log\beta_{1:2}$ | $SE_y$ (ppb)[b] | $\log\beta_{1:1}$ | $\log\beta_{1:2}$ |
| This work | 101 | 3 | 2.9(2) | | 10.2 | n/a [c] | |
| | 103 | 6 | 3.04(1) | | 21.3 | | |
| | 105 | 11 | 2.97(7) | | 17.5 | | |
| Reference 5 | 103 | 6 | 2.8(2) | 5.7(2) | 16.3 | 2.32 | 5.63 |
| | 104 | 7 | 2.08(6) | | 69.8 | 2.47 | 6.09 |
| | 105 | 11 | 2.01(7) | | 68.9 | 2.39 | 6.09 |
| | 125 | n/a [a] | 3.12(5) | | 47.7 | 3.04 | |

All titrations performed with TBABzO at an initial host concentration of 7 mM. This work: Titrations performed at 25 °C, constants shown are their average values, associated errors represent the 95% confidence interval. Preliminary studies from reference 5: Titration performed at 20 °C, constants shown are from fitting a single titration, associated errors are the 'standard deviation' parameter as output by HypNMR2008. a) Macrocyclic derivative of receptor **105**, b) See Section A2.1 for definition, c) Data not analysed with NMRTit (this work).

Table A2.56. Comparison of the logarithmic binding constants for $H_2PO_4^-$ obtained using HypNMR and NMRTit (obtained by Boyle in previous work[5]) as fitting programmes.

| | Receptor | Chain length | HypNMR | | | NMRTit | |
|---|---|---|---|---|---|---|---|
| | | | $\log\beta_{1:1}$ | $\log\beta_{1:2}$ | $SE_y$ (ppb) [c] | $\log\beta_{1:1}$ | $\log\beta_{1:2}$ |
| This work | **101** | 3 | 2.8(4) | 5.0(5) | 10.4 | n/a [d] | |
| | **103** | 6 | 2.9(1) | 5.19(1) | 10.4 | | |
| | **105** | 11 | 3.2(1) | 5.4(2) | 9.5 | | |
| Reference 5 | **103** | 6 | 3.4(2) | 5.3(1) | 6.8 | 2.59 | 5.86 |
| | **104** | 7 | 3.4(3) | 4.8(2) | 8.2 | 2.52 | 6.30 |
| | **105** | 11 | 2.4(6) | 5.2(2) | 32.4 | 2.32 | 6.07 |
| | **125** [a] | n/a [b] | 3.87(3) | 6.2(3) | 33.6 | – [e] | |

All titrations performed with TBAH$_2$PO$_4$ at an initial host concentration of 7 mM. This work: Titrations performed at 25 °C, constants shown are their average values, associated errors represent the 95% confidence interval. Preliminary studies from reference 5: Titration performed at 20 °C, constants shown are from fitting a single titration, associated errors are the 'standard deviation' parameter as output by HypNMR2008. a) Two titrations were performed, average values shown with their 95% confidence intervals, b) Macrocyclic derivative of receptor **105**, c) See Section A2.1 for definition, d) Data not analysed with NMRTit (this work), e) Fitting not performed (previous work), as Δδ was small.

## A2.5 Titration Data for Chapter 4

### A2.5.1 Titrations with BzO⁻

#### A2.5.1.1  Receptor **107** and BzO⁻ (7.0 mM)
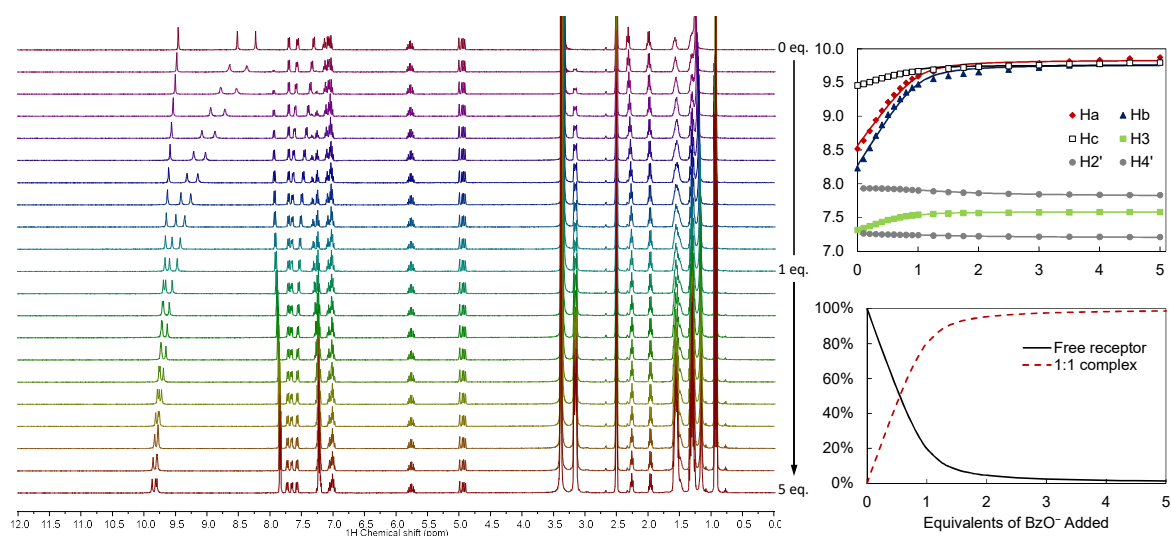


Figure A2.49. Titration of receptor **107** with BzO⁻. Main: Stack plot (0–12 ppm) showing the change in resonances over 1 → 5 eq. Top right: Experimental data (points) and calculated fit (lines) for a 1:1 host-guest binding model. Bottom right: Speciation distribution diagram from the fit.

Table A2.57. Data output from the fitting of the above titration data.

|  | $log\beta_{1:1}$ | Standard Deviation | Percentage error | $SE_y$ (ppb) |
| --- | --- | --- | --- | --- |
| Titration 1 | 3.47 | 0.05 | 1% | 27.5 |

#### A2.5.1.2  Receptor **107** and BzO⁻ (0.7 mM)



Figure A2.50. Titration of receptor **107** with BzO⁻. Main: Stack plot (0–12 ppm) showing the change in resonances over 1 → 5 eq. Top right: Experimental data (points) and calculated fit (lines) for a 1:1 host-guest binding model. Bottom right: Speciation distribution diagram from the fit.

Table A2.58. Data output from the fitting of the above titration data.

|  | logβ$_{1:1}$ | Standard Deviation | Percentage error | SE$_y$ (ppb) |
|---|---|---|---|---|
| Titration 1 | 3.70 | 0.01 | 0.3% | 8.7 |

## A2.5.1.3   Receptor **106** and BzO⁻ (0.7 mM)



Figure A2.51. Titration of receptor **106** with BzO⁻. Main: Stack plot (0–12 ppm) showing the change in resonances over 1 → 5 eq. Top right: Experimental data (points) and calculated fit (lines) for a 1:1 host-guest binding model. Bottom right: Speciation distribution diagram from the fit.

Table A2.59. Data output from the fitting of the above titration data.

|  | logβ$_{1:1}$ | Standard Deviation | Percentage error | SE$_y$ (ppb) |
|---|---|---|---|---|
| Titration 1 | 3.64 | 0.01 | 0.2% | 6.7 |

## A2.5.1.4   Receptor **108** and BzO⁻ (0.7 mM)



Figure A2.52. Titration of receptor **108** with BzO⁻. Main: Stack plot (0–12 ppm) showing the change in resonances over 1 → 5 eq. Top right: Experimental data (points) and calculated fit (lines) for a 1:1 host-guest binding model. Bottom right: Speciation distribution diagram from the fit.

Table A2.60. Data output from the fitting of the above titration data.

| | $\log\beta_{1:1}$ | Standard Deviation | Percentage error | $SE_y$ (ppb) |
|---|---|---|---|---|
| Titration 1 | 3.22 | 0.01 | 0.3% | 9.3 |

## A2.5.2 Titrations with $H_2PO_4^-$

### A2.5.2.1 Receptor **107** and $H_2PO_4^-$ (7.0 mM)
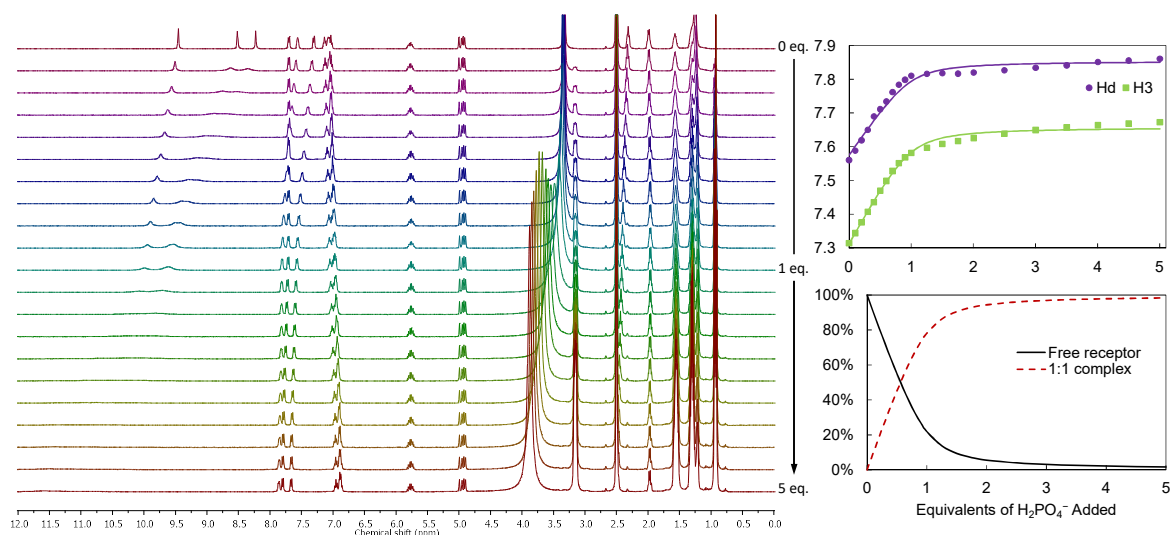


Figure A2.53. Titration of receptor **107** with $H_2PO_4^-$. Main: Stack plot (0–12 ppm) showing the change in resonances over $1 \rightarrow 5$ eq. Top right: Experimental data (points) and calculated fit (lines) for a 1:1 host-guest binding model. Bottom right: Speciation distribution diagram from the fit.

Table A2.61. Data output from the fitting of the above titration data.

| | $\log\beta_{1:1}$ | Standard Deviation | Percentage error | $SE_y$ (ppb) |
|---|---|---|---|---|
| Titration 1 | 3.38 | 0.10 | 3% | 12.3 |

### A2.5.2.2 Receptor **107** and $H_2PO_4^-$ (0.7 mM)
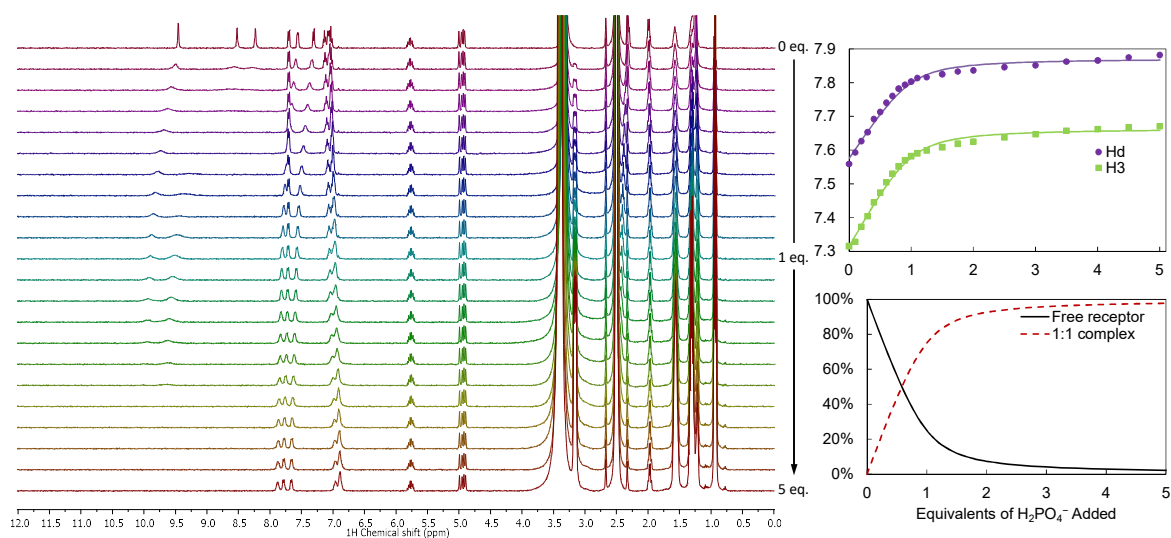
Figure A2.54. Titration of receptor **107** with $H_2PO_4^-$. Main: Stack plot (0–12 ppm) showing the change in resonances over $1 \rightarrow 5$ eq. Top right: Experimental data (points) and calculated fit (lines) for a 1:1 host-guest binding model. Bottom right: Speciation distribution diagram from the fit.

Table A2.62. Data output from the fitting of the above titration data.

|  | $\log\beta_{1:1}$ | Standard Deviation | Percentage error | $SE_y$ (ppb) |
|---|---|---|---|---|
| Titration 1 | 4.25 | 0.05 | 1% | 10.4 |

### A2.5.2.3  Receptor **106** and $H_2PO_4^-$ (0.7 mM)
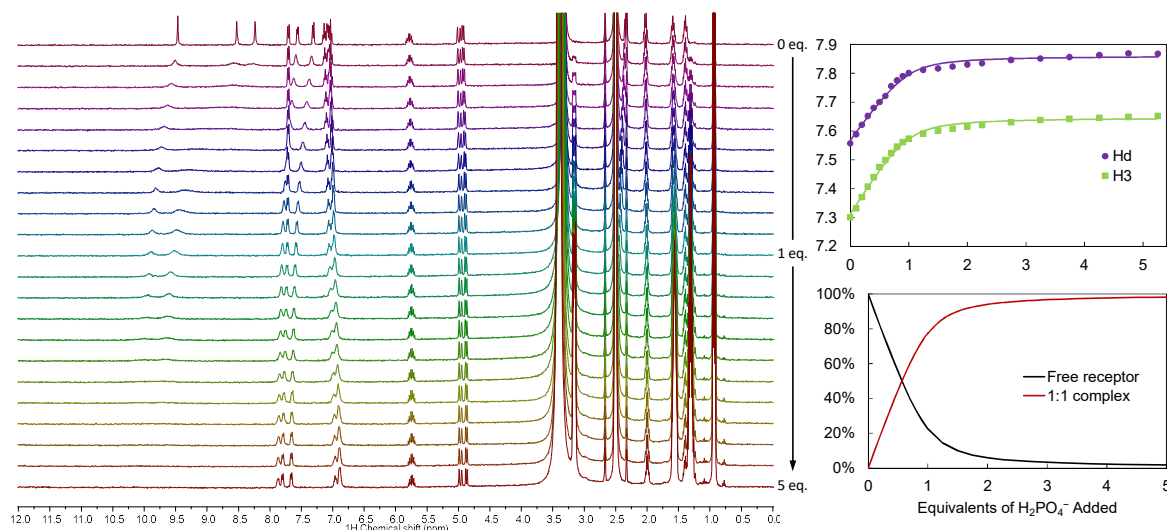


Figure A2.55. Titration of receptor **106** with $H_2PO_4^-$. Main: Stack plot (0–12 ppm) showing the change in resonances over $1 \rightarrow 5$ eq. Top right: Experimental data (points) and calculated fit (lines) for a 1:1 host-guest binding model. Bottom right: Speciation distribution diagram from the fit.

Table A2.63. Data output from the fitting of the above titration data.

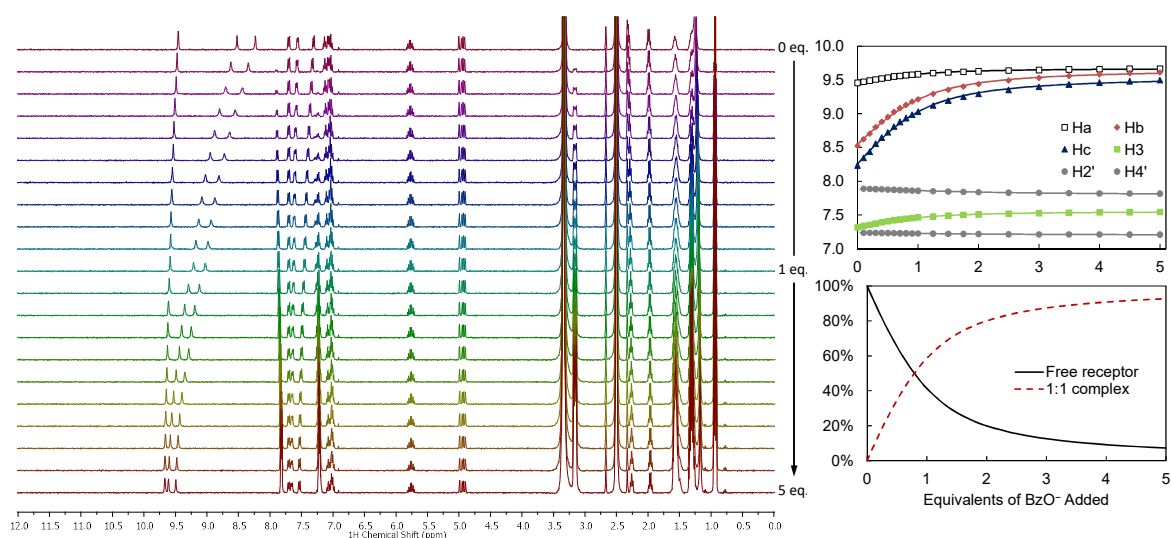|  | $\log\beta_{1:1}$ | Standard Deviation | Percentage error | $SE_y$ (ppb) |
|---|---|---|---|---|
| Titration 1 | 4.35 | 0.07 | 2% | 9.6 |

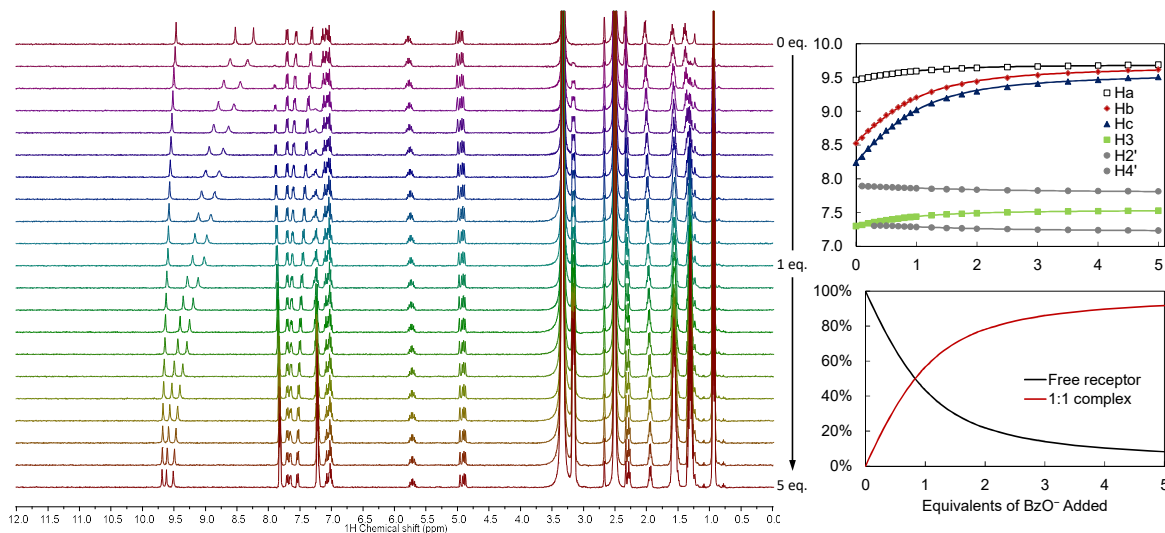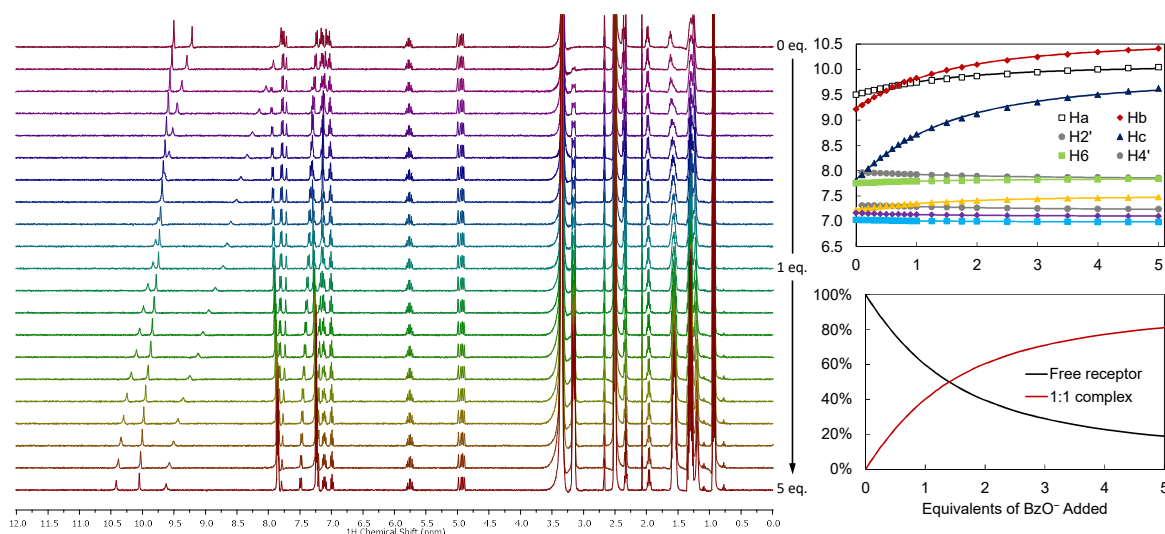## A2.5.2.4  Receptor **108** and $H_2PO_4^-$ (0.7 mM)
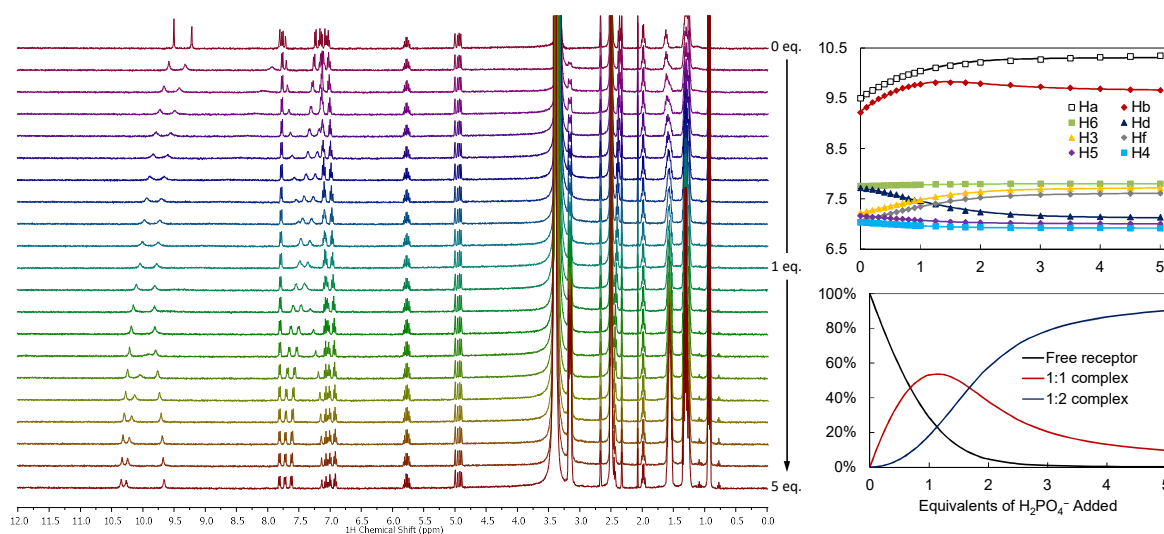


Figure A2.56. Titration of receptor **108** with $H_2PO_4^-$. Main: Stack plot (0–12 ppm) showing the change in resonances over $1 \rightarrow 5$ eq. Top right: Experimental data (points) and calculated fit (lines) for a 1:1 host-guest binding model. Bottom right: Speciation distribution diagram from the fit.

Table A2.64. Data output from the fitting of the above titration data.

|  | $\log\beta_{1:1}$ | Standard deviation | Percentage error | $\log\beta_{1:2}$ | Standard deviation | Percentage error | $SE_y$ (ppb) |
|---|---|---|---|---|---|---|---|
| Titration 1 | 4.42 | 0.10 | 2% | 8.10 | 0.12 | 2% | 10.6 |

Table A2.65. Further data output from the fitting of the above titration data, derived stepwise binding constant with propagated uncertainty, and calculated cooperativity parameter with associated propagated uncertainty.

|  | Correlation coefficient | $\log K_{1:2}$ | Standard deviation | Percentage error | $\log\alpha$ | Error |
|---|---|---|---|---|---|---|
| Titration 1 | 85% | 3.69 | 0.07 | 2% | -0.1 | 0.1 |

# A2.6 References

1.   Thordarson, P. *Chem. Soc. Rev.* **2011**, *40*, 1305.

2.   Hibbert, D. B.; Thordarson, P. *Chem. Commun.* **2016**, *52*, 12792.

3.   Frassineti, C.; Ghelli, S.; Gans, P.; Sabatini, A.; Moruzzi, M. S.; Vacca, A. *Anal. Biochem.* **1995**, *231*, 374.

4.   Gans, P.; Protonic Software: Leeds, United Kingdom, 2008.

5.   Boyle, E. M. PhD Thesis, Trinity College Dublin, the University of Dublin, 2012.

*'My name is Ozymandias, king of kings;*

*Look on my works, ye Mighty, and despair!'*

— Inscription on the ruins of the tomb of Rameses II, as quoted by P. B. Shelley:

Glirastes. Ozymandias. *The Examiner*, 1818, p 24.

Appendix 3.

Publications

# Solution-State Anion Recognition, and Structural Studies, of a Series of Electron-Rich *meta*-Phenylene Bis(phenylurea) Receptors and Their Self-Assembled Structures

Dermot M. Gillen,[†] Chris S. Hawes,[‡] and Thorfinnur Gunnlaugsson*,[†]

[†]School of Chemistry and Trinity Biomedical Sciences Institute (TBSI), Trinity College Dublin, The University of Dublin, 152−160 Pearse Street, Dublin 2, Ireland

[‡]School of Chemical and Physical Sciences, Keele University, Staffordshire ST5 5BG, United Kingdom

**S** Supporting Information

**ABSTRACT:** *meta*-Phenylene bis(phenylurea) receptors **1**−**4** were designed and synthesized to investigate the association between receptor shape, anion-selective binding and anion-directed self-assembly processes. Solution studies, performed through $^1$H NMR titrations with a variety of tetra-*N*-butylammonium salts, demonstrated strong binding of 2 equiv of $H_2PO_4^-$, $AcO^-$, $BzO^-$ anions and comparatively weak binding of $Cl^-$, $HSO_4^-$, and $SO_4^{2-}$ anions. Binding modes and stability constants (log $\beta$) were determined by regression analysis of the obtained $^1$H NMR titration data in DMSO-$d_6$, and the cooperativities of the binding interactions were probed. Host−guest complexes of receptors **1** and **2** were studied in the crystalline phase to further probe the anion-binding behavior of this motif. This included a triple-stranded helicate consisting of three strands of receptor **2** arranged around a mixed-phosphate anionic core, which was characterized by using X-ray crystallography.

## INTRODUCTION

The design and analysis of anion-binding receptors is an area of research that continues to grow, with applications that span organocatalysis, medicinal, and materials chemistry.[1−4] Synthetic receptors are often designed to mimic the selectivity of anion-binding proteins through the careful and methodical design of binding sites, creating a structured array 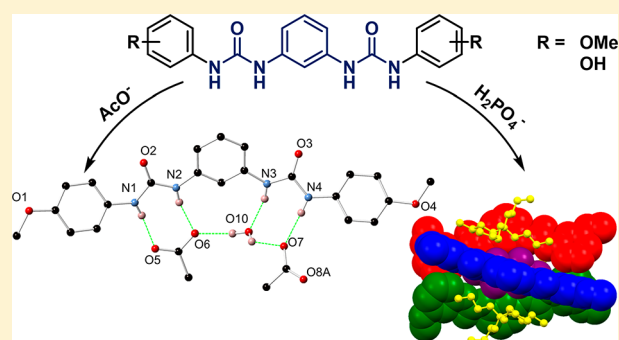of hydrogen bonds.[5] In particular, urea-based receptors have received much interest due to their rigidity and the directionality of their hydrogen bond donors.[6] Electron-poor receptors are an attractive option owing to the anticipated increase in anion-binding affinity to the relatively acidic hydrogen bond donor moieties.[6b,c] However, some of these receptors are merely deprotonated in the presence of anions, and the interaction between anion and receptor may be dominated by their acidity,[7d] a common feature often found for urea- and thiourea-based systems.[7b−d] Moreover, some highly acidic systems bind anions less strongly than their electron-rich counterparts,[8,9] in part due to dissociation of the host−guest complex in solution after proton transfer.

Structural effects have become much more important in the design of selective receptors in recent years, with the development of sophisticated anion-selective cages,[10] cyclic peptides,[5] and interlocked systems for the binding of simple anions,[11−13] and simple receptors for the differentiation of chiral anions.[14] We previously reported allosteric effects in the binding of several anions to a series of acetamido-substituted diphenylureas and thioureas, due to the presence of the additional hydrogen bonding group adjacent to the urea.[15,16] Similar effects in symmetric phenylene bisureas have been noted: *ortho*-phenylene bisureas have been established by Gale and co-workers as excellent hydrogen bonding receptors for carboxylate anions and tetrahedral oxoanions due to the four convergent hydrogen bonds, while the bis(urea)−carboxylate interaction displayed by these has been utilized as a supramolecular synthon.[17] Wu and co-workers have used bis(biurea) derivatives to form both $PO_4^{3-}$ templated helicates and cages,[18−21] while Das and co-workers have developed several electron-poor *meta*-phenylene bis(phenylurea) receptors, and studied their interactions with anions, with an emphasis on their crystalline adducts.[22−24] Others have extended the aromatic moieties of this framework: Ghosh et al. developed a series of coumarin-containing receptors and studied their interactions with mono- and dicarboxylate anions,[25] while the group of Caltagirone found that pyrophosphate binding in phenylene bis(arylurea) systems is promoted in asymmetric hosts bearing a naphthalene and an indole ring.[26]

Meanwhile, the effects of electron-rich substituents are not yet known. In such receptors, the relative affinity for various anions may be expected to differ to that described by others for simpler hydrogen bond donors, as has been suggested recently by Hunter and co-workers,[27] and by Fabbrizzi and co-workers,[28] as the contribution of receptor shape to the binding affinity may dominate over its acidity. This interest in electron-rich receptors is relevant to the wider study of anion-binding supramolecular systems, as electron-donating substituents such as alkoxy groups are commonly used to extend the receptor architecture. Herein, we report the anion-binding properties of *meta*-phenylene bis(phenylurea) receptors **1–4** (Scheme 1)

**Scheme 1. Synthesis of Compounds 1–4 Used in This Study To Investigate the Anion-Binding Properties and Anion-Templated Self-Assembly of the *meta*-Phenylene Bis(phenylurea) Motif[a]**
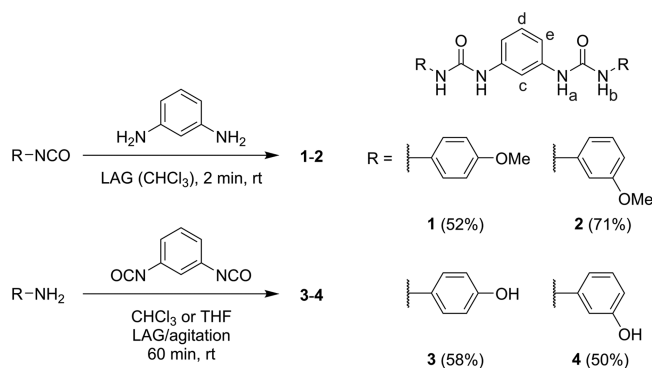


[a]Letters a–e indicate the protons of interest in the following ^{1}H NMR studies.

which feature either hydroxy or methoxy functionalities on the distal phenylene rings, and as such, these receptors are an important addition to the field. Receptors **1–4** were designed in order to investigate the anticipated synergistic effect of two urea binding sites; with the intention of incorporating the bisurea motif into large multicomponent systems, such as helicates and mechanically interlocked molecules. The compounds were characterized, and their anion recognition abilities quantified via ^{1}H NMR titrations with the tetra-*N*-butylammonium (TBA+) salts of $H_2PO_4^-$, AcO−, BzO−, Cl−, $HSO_4^-$, and $SO_4^{2-}$, where the emphasis was also on elucidating any cooperativity in the anion binding by these receptors. The use of these receptors in the formation of anion directed self-assembled structures was probed using X-ray crystallography, which included the solid-state characterization of a novel supramolecular self-assembled helicate, consisting of a mixed-phosphate anionic core. Relatively few such anion-directed helicates have been developed to date.

## ■ RESULTS

**Synthesis of Receptors 1–4.** The anion receptors **1–4** were initially synthesized via reaction of 1,3-phenylene diisocyanate with the corresponding aniline. 1,3-Phenylene diisocyanate proved to be an unsatisfactory starting material, due to an inability to ensure its complete removal from the host samples, and its tendency to form unpredictable mixtures of degradation products, oligomers, etc., upon dissolution in the titration solvent (DMSO-$d_6$). The alternate syntheses of **1–2** were, however, achieved by grinding *m*-phenylene

diamine with the corresponding commercially available methoxyphenyl isocyanate at room temperature for 2 min. This resulted in the formation of a paste, from which the ureas were isolated by successive trituration with methanol, acetonitrile, and diethyl ether, the products being separated from each solvent upon centrifugation, followed by drying *in vacuo*. This yielded receptors **1** and **2** as white solids in moderate yields (50−70%) and high purity, which were suitable for spectroscopic titration (Supporting Information). All products were analyzed using conventional methods (see Experimental Section), in addition to the use of X-ray crystallography in the case of the anion adducts of **1** and **2**; see below. Similarly, compounds **3−4** were produced by grinding or agitating commercially available 1,3-phenylene diisocyanate with an excess of the corresponding aminophenol in organic solvent (CHCl₃ or THF) at room temperature for 2 min (grinding) or 2 h (agitation). The precipitated ureas were collected using vacuum filtration and washed with CHCl₃ and MeOH and dried *in vacuo*. Receptors **3−4** were obtained as pale solids in moderate yields (50−58%) and were soluble in DMF and DMSO. For full characterization of receptors **1−4**, see Figures S1−S22 in the Supporting Information.

**Solution-State Anion-Binding Studies.** Anion titrations were performed with receptors **1−4** to gain insight into the anion recognition process for this family of structures. The binding constants were determined by using nonlinear regression analysis (see Discussion below). While compounds **3** and **4** could not be produced to the same degree of purity as **1** and **2** (as noted above), preliminary anion titrations were performed to complete the picture; the resulting values were largely in agreement with those obtained with hosts **1** and **2**, with an exception in the case of the titration of compound **4** with phosphate. This titration could not be fit to the same 1:1, 1:2 host−guest stoichiometric model expected for this kind of design, and consequently, the anion binding was not investigated further due to the aforementioned concerns.

**^{1}H NMR Titration of Receptors 1−4 with Dihydrogen Phosphate.** To investigate the anion binding of **1−4**, NMR titrations were carried out in competitive aprotic polar solvent (DMSO-$d_6$). Due to the nature of our design, where each receptor provides four hydrogen bonding donors, we anticipated that a variety of anions could be accommodated by such receptors, either as a simple 1:1 binding or through the formation of higher order self-assemblies, such as where the anion coordination requirement is met by a 1:2 anion:receptor stoichiometry. To investigate this, we initially carried out titrations using TBA+ $H_2PO_4^-$. The changes observed in the ^{1}H NMR spectrum are shown in Figure 1, and demonstrate significant changes in the chemical shifts of the resonances attributed to the urea protons (Ha, Hb), which were observed to increase in a monotonic and almost linear fashion during the addition of the first equivalent of anion (see Figure 1a,b). The aromatic resonance Hc was observed to move in a similar and opposite manner to the urea resonances (see Figure 1c).

An inflection in each trend was observed between the addition of 1 → 2 equiv of anion. The trends in chemical shift began to plateau, with more gradual changes observed in the region 2 → 5 equiv. This consistent change in gradient at 2 equiv for both resonances in all titrations was ascribed to the likely presence of a second binding equilibrium in solution. As such, each titration was fitted to a 1:1, 1:2 host−guest model, resulting in cumulative binding constants in the ranges log $\beta_{1:1}$ = 3.6−3.8 and log $\beta_{1:2}$ = 7.1−7.3 for receptors **1−2** (see Figure
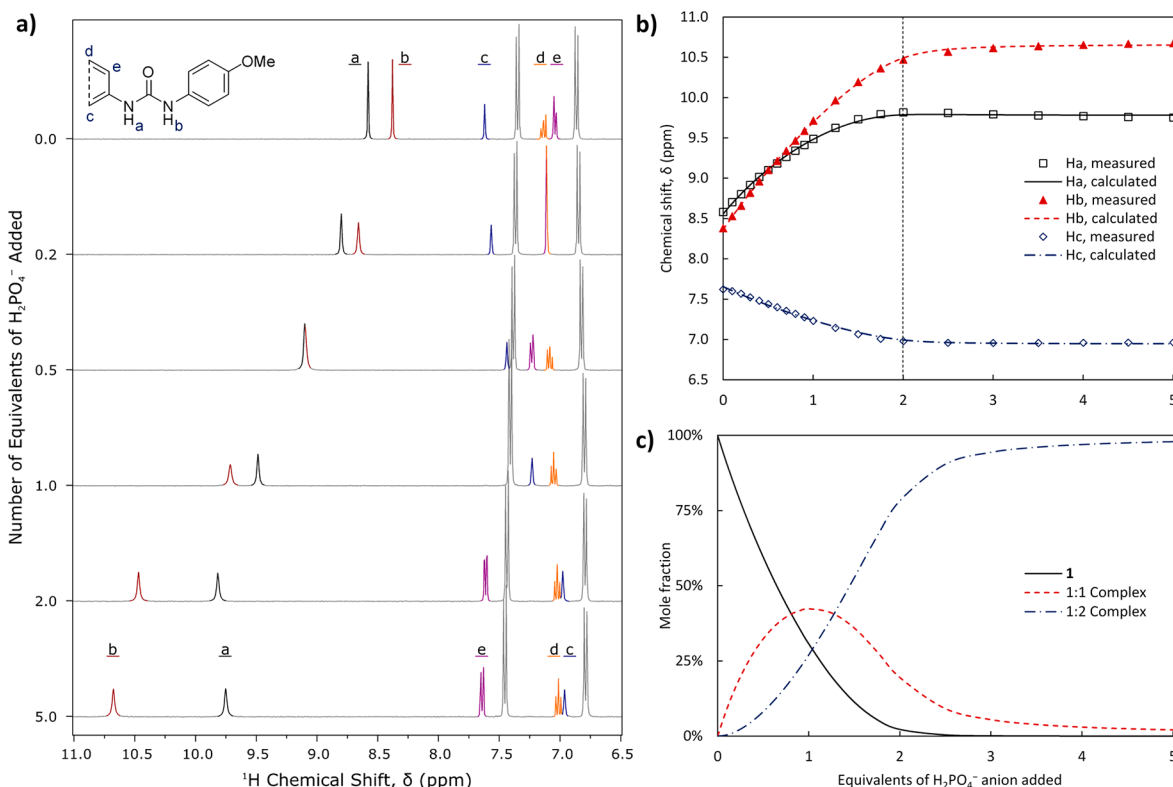
**Figure 1.** (a) Selected spectra (6.5−11.0 ppm) from the titration of **1** with $H_2PO_4^-$, with resonances of interest colored. (b) Experimentally measured chemical shifts (points) and calculated fit (lines) of resonances Ha−c of receptor **1**. (c) Speciation distribution diagram generated from the fitting of the experimental data. The concentrations are presented as mole-percentage values relative to the total host concentration.

1b and Table 1). The values of these constants for receptor **3** fell within the same range, supporting our hypothesis. As noted

**Table 1. Cumulative Logarithmic Binding Constants, log $\beta_{1:1}$ and log $\beta_{1:2}$, Assuming Both 1:1 and 1:2 Binding Modes As Determined from the Analysis of $^1$H NMR Titrations in DMSO-$d_6$ at 298.2 K**

| host | binding mode, m:n | $H_2PO_4^-$ log $\beta_{m:n}$ | AcO$^-$ log $\beta_{m:n}$ | BzO$^-$ log $\beta_{m:n}$ |
|---|---|---|---|---|
| **1**[a] | 1:1 | 3.74 ± 0.11 | 3.54 ± 0.23 | 3.18 ± 0.12 |
| | 1:2 | 7.14 ± 0.24 | 5.45 ± 0.33 | 4.75 ± 0.40 |
| **2**[a] | 1:1 | 3.63 ± 0.07 | 3.66 ± 0.28 | 3.13 ± 0.09 |
| | 1:2 | 7.24 ± 0.07 | 5.86 ± 0.49 | 4.88 ± 0.13 |
| **3**[b] | 1:1 | 3.77 ± 0.29 | 3.43 ± 0.06 | 3.37 ± 0.06 |
| | 1:2 | 7.13 ± 0.29 | 5.29 ± 0.08 | 5.08 ± 0.08 |
| **4**[b] | 1:1 | [c] | 3.40 ± 0.07 | 3.00 ± 0.10 |
| | 1:2 | | 5.44 ± 0.09 | 4.48 ± 0.20 |

[a]Association constants shown are averaged values; the errors shown are at the 95% confidence interval. [b]Association constants are as calculated from a single fit; the associated errors are the "standard deviation" parameter reported by HYPNMR.[30] [c]This titration could not be fit to a 1:1, 1:2 host−guest model. The TBA$^+$ salts of each anion were used in all cases.

above, it was not possible to fit the data from the titration of receptor **4** with phosphate, to a combined 1:1, 1:2 host−guest binding model. Logarithmic binding constants could be obtained from a 1:1, 1:2, 1:3 host−guest binding model; however, these values were unrealistically large given the titration concentration.[29]

The relative magnitudes of the 1:1 and 1:2 binding constants imply a strongly cooperative process, perhaps aided by phosphate−phosphate hydrogen bonding. Such an interaction has been described in MeCN and DMSO, and in aqueous solution,[31,32] and is commonly observed in solid-state structures.[33] The cooperativity of a system may be quantified by the interaction parameter $\alpha = 4K_{1:2}/K_{1:1}$, with values of $\alpha > 1$ implying cooperative binding, $\alpha = 1$ implying noncooperative binding, and $\alpha < 1$ implying anticooperative binding.[29] As the program used herein reports values of log $\beta$, in order to avoid the introduction of additional sources of error, the logarithm of the parameter $\alpha$ will be used. Thus, log $\alpha$ is positive in the case of positive cooperativity, and negative in the case of negative cooperativity. In this system, the value of log $\alpha$ was found to be in the range 0.2−0.6 (see Table 2, and Figure S54 in the Supporting Information). In a similar 1,2-*trans*-cyclohexyl derived system, weaker binding constants of log $\beta_{1:1} = 2.95$ and log $\beta_{1:2} = 6.39$ (averaged over both enantiomers) were reported for the 1:1 and 1:2 binding modes, respectively. The strongly cooperative binding in that system (log $\alpha = 1.1$) was explained as a result of phosphate−phosphate hydrogen bonding, as had been observed in the crystalline phase.[34]

**$^1$H NMR Titration of Receptors 1−4 with Acetate.** In contrast to the behavior shown by receptors **1−4** toward $H_2PO_4^-$, above, upon titration with AcO$^-$, the chemical shifts of the resonances Ha and Hb increased monotonically; with no inflection or other evidence from these trends of a 1:2 host−guest complex (Figure 2a). This is not surprising, as AcO$^-$ would be expected to bind through a planar or linear manner, unlike the tetrahedral $H_2PO_4^-$ anion. Nonlinear regression analysis with a 1:1 host−guest binding model afforded binding constants of log $\beta_{1:1} = 2.4$ (see Table 3). These constants are

**Table 2. Logarithmic Cooperativity Parameters, log $\alpha$, Assuming Both 1:1 and 1:2 Binding Modes As Determined from the Analysis of ^{1}H NMR Titrations in DMSO-$d_6$ at 298.2 K**

|      | $H_2PO_4^-$ | $AcO^-$ | $BzO^-$ |
|------|-------------|---------|---------|
| host | log $\alpha$ | log $\alpha$ | log $\alpha$ |
| **1**[a] | 0.27 ± 0.17 | −1.03 ± 0.25 | −1.01 ± 0.30 |
| **2**[a] | 0.59 ± 0.13 | −0.85 ± 0.36 | −0.78 ± 0.10 |
| **3**[b] | 0.21 ± 0.31 | −0.97 ± 0.05 | −1.06 ± 0.04 |
| **4**[b] | [c] | −0.75 ± 0.06 | −0.91 ± 0.05 |

[a]Cooperativity constants shown are averaged values; the errors shown are at the 95% confidence interval. [b]Cooperativity constants are as calculated from a single fit; the associated errors are as propagated from the "standard deviation" parameter and covariance reported by HYPNMR.[29] [c]This titration could not be fit to a 1:1, 1:2 host−guest model.

low for urea-based receptors: Kadam et al. determined a value of 3.3 for diphenylurea in DMSO-$d_6$/water (99.5:0.5), with log $\beta_{1:1}$ being in the range 2.5−4.9 for other aryl-substituted ureas.[35] Casula et al. reported binding constants in the range log $\beta$ = 3.1−3.9 for asymmetric phenylene bis(arylureas), with the corresponding *meta* isomer having the lowest binding affinity for acetate.[26]

In that and other works, the *ortho*-phenylene bis(phenylurea) receptor displayed especially strong binding, whereby one carboxylate anion forms hydrogen bonds to all four NH donors.[17] A similar saturation of all hydrogen bonding donors in the *meta* system by a single carboxylate ion is improbable, as the receptor binding site is not concave in shape and the outermost nitrogen atoms are more distant from each other. This would leave part of the receptor available for binding to a second anion.

While there was no evidence of a 1:2 host−guest complex in the trends of the NH resonances, such evidence came instead from the trends observed in the Hc resonances of each host, whereby the chemical shifts decreased up to the addition of 1 equiv of TBA$^+$ AcO$^-$, at which point an upward inflection (Figure 3a, indicative of an intermediate species; compare Figure 2b and Figure 3b), followed by a gentle plateau was observed. Fitting the data from all three resonances afforded binding constants of log $\beta_{1:1}$ = 3.5−3.7 and log $\beta_{1:2}$ = 5.4−5.9

(see Table 1). This fit also appears to suggest a strongly negative cooperative interaction, with log $\alpha$ between −1.1 and −0.8 (see Table 2) for receptors **1−2**. Similar values were determined for the phenolic receptors **3** and **4**.

**^{1}H NMR Titration of Receptors 1−4 with Benzoate.** In the titrations with TBA$^+$ BzO$^-$, the traces of the urea resonances follow a largely similar trend to that observed with the AcO$^-$ anion, above. The aromatic resonance Hc, meanwhile, followed a sigmoidal trend with positive curvature up to the addition of 1.5 equiv of anion, and a negative curvature thereafter. A larger overall change in chemical shift was observed for each receptor. Nonlinear regression analysis of these trends demonstrated that benzoate interacted in a similar manner to the acetate anions. As above, both the simple 1:1, and mixed 1:1/1:2 binding models were applied to the data from each titration (see Figure 4). The log $\beta_{1:1}$ values obtained by nonlinear regression analysis of the benzoate titrations are in the range 2.3−2.4 (see Table 3). Once again, the log $\beta_{1:1}$ values may be compared to the series of aryl-substituted urea receptors reported by Kadam et al. The binding for compounds **1−4** (2.3−2.4) appears to be relatively weak, and at the lower end of the scale reported in the literature (2.1−4.1).[35] While in that work the binding for the benzoate anion is weaker than for the acetate anion (by 0.3 log units or more), the 1:1 binding constants for **1−4** are equivalent within error. The ranges of log $\beta_{1:1}$ and log $\beta_{1:2}$ values obtained with a combined 1:1/1:2 host−guest binding model are 3.1−3.2 and 4.7−4.9, respectively (see Table 1). The logarithmic cooperativity parameters indicated a similar degree of anticooperativity to the above acetate titrations, with log $\alpha$ between −1.1 and −0.7 for receptors **1−4** (see Table 2).

**^{1}H NMR Titration of Receptors 1−2 with Chloride.** Small monotonic changes in chemical shift of less than 0.50 ppm were observed for each proton resonance over the addition of 5 equiv of TBA$^+$ Cl$^-$. These titrations were fitted to 1:1 models only as there was no evidence of other stoichiometries. The results obtained by nonlinear regression analysis for receptors **1** and **2** are equivalent, with log $\beta_{1:1}$ = 1.67 (see Table 3). This is comparable to similar *ortho*-phenylene receptors, which have log $\beta$ values in the range 1.1−1.6,[36] but recent electron-poor Cl$^-$ transporters based on that motif possess higher log $\beta_{1:1}$ values at ∼2.2.[37]
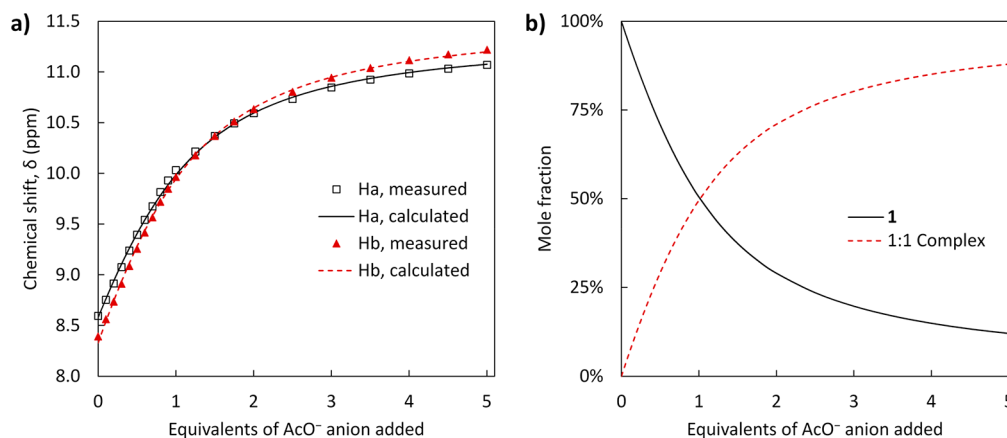


**Figure 2.** Titration of receptor **1** with AcO$^-$. (a) Experimentally measured chemical shifts (points) and calculated fit (lines) of resonances Ha and Hb of receptor **1**, as fitted to a 1:1 binding model. (b) Speciation diagram of this fit. The concentrations are presented as mole-percentage values relative to the total host concentration.

**Table 3. Logarithmic Binding Constants, log $\beta_{1:1}$, Assuming a 1:1 Binding Mode Only As Determined from the Analysis of $^1$H NMR Titrations in DMSO-$d_6$ at 298.2 K**

|  | AcO$^-$ | BzO$^-$ | Cl$^-$ | SO$_4$$^{2-}$ | HSO$_4$$^{-b}$ |
|---|---|---|---|---|---|
| host | log $\beta_{1:1}$ | log $\beta_{1:1}$ | log $\beta_{1:1}$ | log $\beta_{1:1}$ | log $\beta_{1:1}$ |
| **1**[a] | 2.43 ± 0.06 | 2.33 ± 0.06 | 1.67 ± 0.08 | 1.06 ± 0.62 | 0.52 ± 0.05 |
| **2**[a] | 2.44 ± 0.14 | 2.36 ± 0.03 | 1.67 ± 0.10 | 0.92 ± 0.19 | 1.43 ± 0.03 |
| **3**[b] | 2.39 ± 0.01 | 2.31 ± 0.01 | 1.64 ± 0.02 | 1.15 ± 0.03 | 0.39 ± 0.06 |
| **4**[b] | 2.49 ± 0.01 | 2.38 ± 0.01 | n.d.[c] | n.d.[c] | n.d.[c] |

[a]Association constants shown are averaged values (except for in the case of the HSO$_4$$^-$ titrations); the errors shown are at the 95% confidence interval. [b]Association constants are as calculated from a single fit; the associated errors are the "standard deviation" parameter reported by HYPNMR.[29] [c]Not determined. The TBA$^+$ salts of each anion were used in all cases.



**Figure 3.** Titration of receptor **1** with AcO$^-$. (a) Experimentally measured chemical shifts, $\delta$ (points), and calculated fit (lines) of resonances Ha−c of receptor **1**, as fitted to a 1:1, 1:2 binding model. (b) Speciation diagram of this fit. The concentrations are presented as mole-percentage values relative to the total host concentration.



**Figure 4.** Titration of receptor **1** with BzO$^-$. (a) Experimentally measured chemical shifts, $\delta$ (points), and calculated fit (lines) of resonances Ha−c of receptor **1**, as fitted to a 1:1, 1:2 binding model. (b) Speciation diagram of this fit. The concentrations are presented as mole-percentage values relative to the total host concentration.

**$^1$H NMR Titration of Receptors 1−2 with Sulfate and Bisulfate.** Titrations with TBA$^+$ SO$_4$$^{2-}$ and HSO$_4$$^-$ show small monotonic changes in chemical shift of less than 0.25 ppm for the urea resonances up to the addition of 5 equiv of anion, with little to no curvature observed in this trend. A greater curvature

was noted in the case of the aromatic resonance Hc. Nonlinear regression analysis produced log $\beta_{1:1}$ of 0.9−1.0 for SO$_4$$^{2-}$ and 0.5−1.4 for HSO$_4$$^-$ (see Table 3). The values of log $\beta_{1:1}$ should be viewed with some caution, due to poor fitting of the CH resonances, the lack of a curvature in the urea resonances,
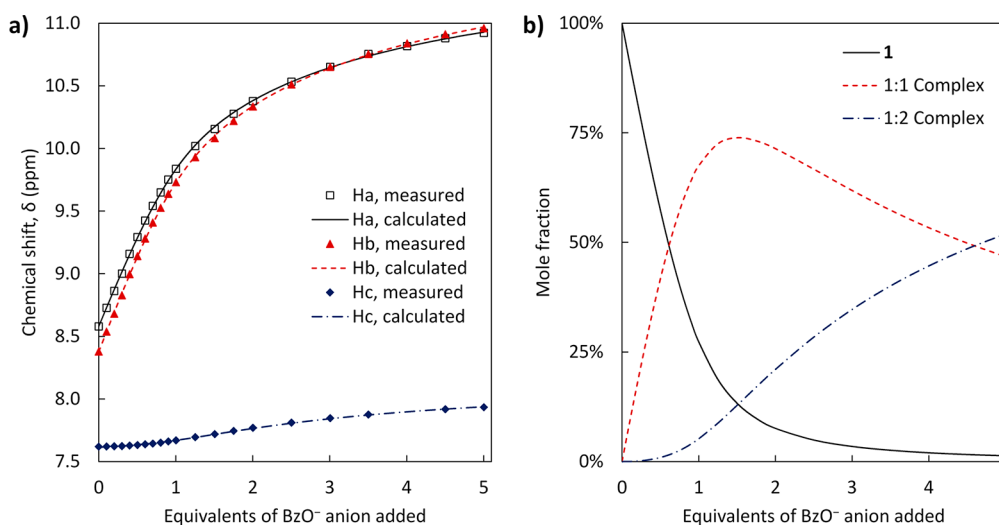
small overall change in chemical shift, and the expected binding affinities for these anions. It must also be noted that only preliminary titrations were performed with the $HSO_4^-$ salt. These values would indicate that **1**–**2** show a much lesser affinity for the strongly solvated sulfates compared to $H_2PO_4^-$, $BzO^-$, and $AcO^-$. This is unsurprising as hydrogen-bond-based receptors are generally expected to bind the $HSO_4^-$ anion least strongly of the anions studied.[27,28] In a similar study, the value of log $\beta_{1:1}$ for $HSO_4^-$ binding by *ortho*-phenylene bis(phenylurea) was determined to be less than 1.[36] However, more preorganized motifs bearing three urea,[38b,39] or *ortho*-phenylene diurea arms, bind $SO_4^{2-}$ much more strongly, with log $\beta_{1:1}$ for the latter in the range 5.5–5.9[40]

**Structural Studies in the Crystalline Phase.** As the ^{1}H NMR titrations of **1**–**4** showed stronger interactions with $AcO^-$ and $H_2PO_4^-$, cocrystallizations with these anions were considered. While the urea hosts **1**–**4** are poorly soluble in suitable crystallization solvents, they may be solubilized in $CHCl_3$, MeCN, and EtOAc by the addition of excess $AcO^-$ anion. Therefore, it must be noted that both the crystals of $1(TBAOAc)_2 \cdot 3H_2O$ and $2_3(TBA_3H_3P_2O_8) \cdot 0.5CHCl_3$ discussed below could only be prepared very sporadically as a product from a large excess of the mixed TBA salts, given the multitude of complex equilibria at play in such mixtures. As such, the structural data below are not intended as exhaustive descriptions of the binding modes available to these hosts, nor as supporting evidence of the binding models established by the solution studies (being prepared under different conditions). Rather, these data are provided as experimentally determined "snapshots", purely to visualize two of the many potential binding modes available to these hosts when crystallization is added as a further driving force to those equilibria.

**X-ray Crystallographic Analysis of $1(TBAOAc)_2 \cdot 3H_2O$.** The *para*-substituted derivative **1** was dissolved in a boiling mix of $CHCl_3$ and EtOAc in the presence of an excess of $AcO^-$ and $H_2PO_4^-$ as their $TBA^+$ salts. The solution was filtered hot, and small thin colorless crystals of $1(TBAOAc)_2 \cdot 3H_2O$ were obtained by slow evaporation of the solvent. In some instances, this was accompanied by various TBA OAc salts, hydrates, and adducts.

A crystal of $1(TBAOAc)_2 \cdot 3H_2O$ was analyzed by single-crystal X-ray diffraction, the diffraction data were solved, and the model was refined in the monoclinic space group *Cc*. Exhaustive searches were made for higher symmetry space groups, particularly the ubiquitous *C2/c*; although approximate 2-fold symmetry is present when considering the tetrabutylammonium cations and **1** molecules, the nonsymmetric arrangement of the acetate and water species prohibits a precise *C2/c* setting. The asymmetric unit of $1(TBAOAc)_2 \cdot 3H_2O$ contains one molecule of **1** in an acentric planar conformation, two acetate anions and associated tetrabutylammonium cations, two full-occupancy water molecules, and one disordered water molecule split across three sites. One of the two acetate moieties displayed minor rotational disorder and was modeled over two related orientations. The hydrogen bonding interactions in $1(TBAOAc)_2 \cdot 3H_2O$ are largely centered on the interaction of one molecule of **1** with two acetate anions, bridged by a water molecule (Figure 5a). One acetate anion is bound in the well-known $R_2^2(8)$ hydrogen bonding motif with a urea group,[41] with N···O distances 2.795(8) and 2.842(9) Å and N–H···O angles 166.6(4)° and 166.0(4)° for N1–H1···O5 and N2–H2···O6, respectively.
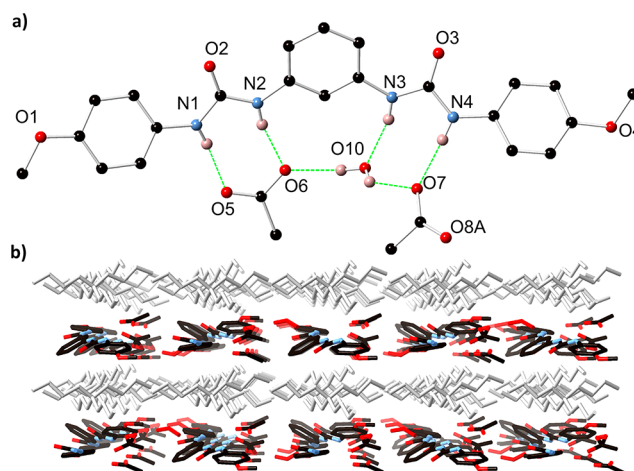


**Figure 5.** (a) Hydrogen bonding environment of the host species within the structure of $1(TBAOAc)_2 \cdot 3H_2O$ with heteroatom labeling scheme. Hydrogen atoms not involved in hydrogen bonding, tetrabutylammonium cations, and disordered solvent molecules omitted for clarity. (b) Extended structure of $1(TBAOAc)_2 \cdot 3H_2O$ showing alternating layers of tetrabutylammonium cations (gray) and anionic host-anion layers (colored).

The second acetate anion interacts with the remaining urea group *via* a single hydrogen bond, with the second potential interaction interrupted by the presence of a lattice water molecule O10, which donates a hydrogen bond to the acetate group and accepts a hydrogen bond from the inner urea N–H group, forming a cyclic assembly described by the $R_2^3(8)$ graph set. The two distinct hydrogen bonding environments involving the urea groups are further linked by hydrogen bonding from the lattice water molecule O10 to acetate oxygen atom O6, defining a further cyclic $R_2^3(10)$ motif edge-sharing with the two urea environments. Additional hydrogen bonding in the structure of $1(TBAOAc)_2 \cdot 3H_2O$ involves the remaining lattice water molecules; the well-defined water molecule O9 bridges adjacent **1**-acetate adducts through interactions with the acetate oxygen atom O5 and the urea oxygen atom O3 from an adjacent molecule of **1**. Although individual hydrogen atoms could not be assigned to the disordered water sites, their proximity to the disordered acetate anion suggests additional hydrogen bonding interactions are likely. The extended structure of $1(TBAOAc)_2 \cdot 3H_2O$ consists of alternating anionic $[1 \cdot 2OAc \cdot 3H_2O]^{2-}$ layers and cationic tetrabutylammonium layers, each extended in the *ac* plane (Figure 5b). No significant discrete interactions are visible between the cationic and anionic groups, and no $\pi$–$\pi$ interactions were evident between molecules of **1**.

**X-ray Crystallographic Analysis of the Triple Stranded Helicate $2_3(TBA_3H_3P_2O_8) \cdot 0.5CHCl_3$.** The 3′-methoxy substituted derivative **2** was dissolved in a boiling mixture of $CHCl_3$ and EtOAc in the presence of an excess of $AcO^-$ and $H_2PO_4^-$ as their $TBA^+$ salts. The orange solution was filtered hot, and crystals of $2_3(TBA_3H_3P_2O_8) \cdot 0.5CHCl_3$ were obtained by slow evaporation of the solvent. Despite exhaustive efforts, and owing to the practical difficulties described above, we were unable to optimize or repeat this crystallization process for larger-scale preparations.

A crystal of $2_3(TBA_3H_3P_2O_8) \cdot 0.5CHCl_3$ was analyzed by single-crystal X-ray diffraction, the data were solved, and the model was refined in the rhombohedral space group *R3c*. The asymmetric unit contains one complete molecule of **2** in a

planar acentric conformation, one tetrabutylammonium cation, a chloroform molecule overlapping the 3-fold axis with chemical occupancy of $^1/_2$, and fragments of two phosphate-derived anionic species. Expansion of the structure through crystallographic symmetry elements reveals a complete assembly containing three equivalent molecules of **2** encapsulating two anions, with three accompanying tetrabutylammonium cations (Figure 6). Charge balance considerations
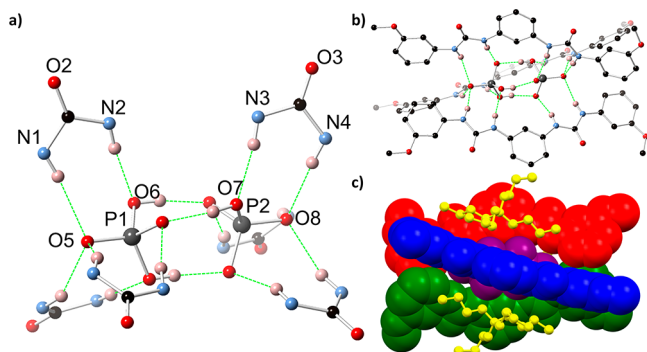


**Figure 6.** (a) Hydrogen bonding environment within the structure of $\mathbf{2}_3(TBA_3H_3P_2O_8)\cdot0.5CHCl_3$ with heteroatom labeling scheme, showing the encapsulation of the $(HPO_4)(H_2PO_4)$ moiety by six urea groups. Phosphate hydrogen atoms shown in representative positions. (b) Complete structure of the anionic assembly in the structure of $\mathbf{2}_3(TBA_3H_3P_2O_8)\cdot0.5CHCl_3$. Selected hydrogen atoms are omitted for clarity, and phosphate hydrogen atoms are shown in representative positions. (c) Interaction of tetrabutylammonium anions (yellow) with the external grooves of the anionic assembly in the structure of $\mathbf{2}_3(TBA_3H_3P_2O_8)\cdot0.5CHCl_3$. Individual host molecules and central anionic moiety colored separately.

require a total charge of $3^-$ for the dimeric anionic species, implying the presence of three protons per $(PO_4)_2$ moiety. The two phosphate groups share three crystallographically equivalent sites of hydrogen bonding, defined by a short $O\cdots O$ distance of 2.579(3) Å (Figure 6a). Commensurate with the overall crystallographic symmetry and expected chemical formula of $(H_2PO_4)(HPO_4)$, both oxygen atoms O6 and O7 were assigned riding hydrogen atoms at half occupancy, as a representation of the averaged configuration throughout the entire structure. The development of helicates from anions is relatively rare (particularly in comparison to the development of helicates from metal ions such as *d*- and *f*-metal ions), with some recent examples having been reported by Wu and co-workers.[18−20,42] The phosphate adduct closely resembles that observed by Burns and co-workers in a related system, in which a $(H_2PO_4)_2$ dimer lies encapsulated within the cavity of a tetra(urea)-substituted porphyrin, receiving seven hydrogen bonds from the surrounding urea groups.[43] The $(H_2PO_4)$-$(HPO_4)$ moiety presented is found in two structures reported by Didio et al.[44a] and Zhang et al.,[44b] respectively. In each a bis- or tris(urea) molecule hydrogen bonds to the ends of the dimer, but neither of these associated organic molecules encapsulate the anions. The structure also bears a strong resemblance to several adducts reported by Das and co-workers: those barrels consist of three or four molecules of a derivative of the *meta*-phenylene bis(phenylurea) scaffold around carbonate and sulfate cores, although these lack the helical manner of the structure presented in this work.[23,24]

The three molecules of **2** are arranged around each $H_3P_2O_8$ group in a triple-stranded helical fashion, with the helical axis

aligned with the crystallographic 3-fold axis in the $[0,0,1]$ direction. The encapsulated anions are supported by a series of hydrogen bonding interactions originating from the urea groups of **2**. The terminal oxygen atoms of each phosphate residue O5 and O8 each accept three symmetry-equivalent hydrogen bonds from the outermost urea nitrogen atoms N1 and N4, respectively, with $N\cdots O$ distances 3.117(4) and 3.029 Å, and $N-H\cdots O$ angles 153.8(2)° and 164.2(2)°, respectively. In addition to the $O-H\cdots O$ interactions supporting the two phosphate groups, each of the six central oxygen atoms accepts one hydrogen bond from the inner urea $N-H$ groups, with $N\cdots O$ distances 2.892(4) and 2.896(5) Å and $N-H\cdots O$ angles 173.2(2)° and 161.9(2)° for $N3-H3\cdots O7$ and $N2-H2\cdots O6$, respectively. The tetrabutylammonium cations associate with the outer grooves of the adduct, with two of the four butyl groups on each cation aligned parallel to the long axis of each molecule of **2** and interacting with the adduct *via* a series of $C-H\cdots\pi$ interactions. With the tetrabutylammonium cations occupying the interstitial regions, no substantial intermolecular interactions are observed between adjacent helicates in the structure of $\mathbf{2}_3(TBA_3H_3P_2O_8)\cdot0.5CHCl_3$, and no void space or additional guest molecules were detected.

The crystalline product $\mathbf{2}_3(TBA_3H_3P_2O_8)\cdot0.5CHCl_3$ was produced in sufficient quantities to perform analysis *via* powder FT-IR and $^1H$ NMR spectroscopy. In comparison to the solid host (**2**), the FT-IR spectrum of the above crystalline material shows suppression and broadening of the $N-H$ stretching bands (3400−3150 cm$^{-1}$), and a shift in the $C=O$ stretching frequency from 1635 to 1698 cm$^{-1}$ (see Supporting Information, Figure S61), which has been noted for ureas bound to such hydrogen bonding acceptor molecules in the solid state.[45] The helicate assembly was observed by $^1H$ NMR to degrade upon contact with CDCl$_3$ (see Supporting Information, Figure S60), due to the slow leaching of the phosphate salts into solution in a greater proportion to receptor **2**, which remained as a white powder. $^1H$ NMR in DMSO-$d_6$ showed the urea resonances to be shifted significantly more ($\Delta\delta \leq 2.5$ ppm) with regards to the host (**2**) than at 0.7 equiv of $H_2PO_4^-$ in the corresponding titration (see Supporting Information, Figures S58 and S59), due to the stronger interacting $HPO_4^{2-}$ ions present in the anionic assembly over the $H_2PO_4^-$ ions used in the titration. Thus, while the $H_2PO_4^-$ anion is known to form dimers in a "monodentate" and a less abundant "bidentate" form in solution,[31] we do not expect discrete helicates of the type described above to assemble spontaneously within solutions containing salts of the $H_2PO_4^-$ ion alone.

## ■ DISCUSSION

The similar values of cooperativity constants in the cases of AcO$^-$ and BzO$^-$ binding suggest that the manner of binding of these ions is not dependent on their steric bulk. As these are anticooperative processes, it is postulated either that there is a nonsteric interaction (i.e., electrostatic) between the binding anions or that the host−guest complex can adopt an alternate, less favored conformer to which the second anionic guest molecule may bind. In comparison, the positive cooperativity observed with $H_2PO_4^-$ leads to a binding, which is stronger than with AcO$^-$. This contrasts with a series previously derived for monourea-based anion receptors, in which phosphate was bound less strongly than the carboxylates (AcO$^- >$ BzO$^- >$ $H_2PO_4^- >$ HSO$_4^-$).[46] These positive cooperativity constants imply that phosphate−phosphate hydrogen may occur at the

binding site, allowing for two anions to be simultaneously bound by the receptor more easily. As noted above, such phosphate−phosphate binding is well-known to occur in solution.[30,31]

While it appears that the *meta* isomers **2** and **4** show differing binding strengths and cooperativities for $H_2PO_4^-$, $BzO^-$, and $AcO^-$, the associated errors are too large to draw any conclusions. Indeed, no meaningful correlation between the calculated binding affinities and the relevant Hammett values can be observed (see Supporting Information, Figure S55). While the values of log $\beta_{1:1}$ and log $\beta_{1:2}$ appear to be lower for receptors **2** and **4**, it must also be noted that the values calculated for the 1:1 fits are equivalent to or slightly higher than the values for the corresponding *para*-substituted receptors.

From the titration data, the importance of considering the behavior of all protons in the vicinity of the binding site can also be seen. While there are strong indications that the *meta*-phenylene bis(phenylurea) motif interacts with carboxylate anions in a 1:2 host−guest binding mode, this is only evident by considering the central aromatic proton Hc in the analysis. In our view, this provides a much more convincing probe for studying the solution-state association processes of these systems, as well as giving a spectroscopic handle which is less sensitive to pH. Nevertheless, to ensure comparability to the 1:1 binding constants reported for similar receptors in the literature, it was necessary to analyze **1−4** in the context of a purely 1:1 host−guest binding model.

## CONCLUSION

Herein, we have presented a family of neutral electron-rich *meta*-phenylene bis(phenylurea) receptors and investigate their anion-binding ability, complementing research performed on electron-poor urea receptors. The binding affinities of receptors **1−4** to several common anions of various geometries have been determined by nonlinear regression analysis of ^{1}H NMR trends in the solution state. Evidence of 1:2 host−guest binding was observed for the $H_2PO_4^-$, $AcO^-$, $BzO^-$ anions, and cooperativity parameters were derived to elucidate the processes occurring at the binding site. The acetate binding is anticooperative, and in comparison to similar urea-based receptors in the literature, appears relatively weak.[42] Meanwhile, the phosphate binding is the strongest of those studied in this work. The binding process is cooperative, and may be due to phosphate−phosphate hydrogen bonding at the receptor. A much lower affinity for $Cl^-$, $HSO_4^-$, and $SO_4^{2-}$ anions was observed. Attempts at producing solid state adducts of **1** and **2** with phosphate and acetate anions led to the discovery of a new helicate centered on a mixed-phosphate core. This adds to a somewhat limited set of anion-based helicates present in the literature. We envisage that this work will help drive further research in designed urea-based receptors, including those that take advantage of phosphate dimerization, and stress the need to look beyond the protons of the hydrogen bonding moiety in the binding site in determining binding behavior. We are in the process of exploring this, and the potential of the use of anions in general, to direct the formation of supramolecular self-assemblies in solution.

## EXPERIMENTAL SECTION

**General Experimental Details.** All solvents and chemicals were purchased from commercial sources and used without further purification. Mass spectrometry was carried out using HPLC grade solvents using electrospray mass spectrometry (ESI). High resolution ESI mass spectra were determined relative to a standard of leucine enkephalin. Infrared spectra were recorded on a PerkinElmer Spectrum One FT-IR spectrometer fitted with a universal ATR sampling accessory. Melting points were determined using an Electrothermal IA9100 digital melting point apparatus. Elemental analysis was carried out at the UCD School of Chemistry Microanalytical Laboratory, University College Dublin. ^{1}H NMR spectra were recorded at 400 MHz on a Bruker Avance III 400 NMR or Agilent 400-MR, or at 600 MHz on a Bruker Avance II 600 NMR. ^{13}C NMR spectra were recorded at either 150.9 or 100.6 MHz. All ^{13}C NMR spectra were decoupled from [1]H. Deuterated solvents used for NMR analysis (DMSO-$d_6$, CDCl$_3$) were purchased and used as received. Chemical shifts are reported in ppm with the residual solvent as internal reference, while 2D spectra were graphically referenced. All NMR spectra were carried out at 25.0 °C.

**^{1}H NMR Titration Experiments.** ^{1}H NMR titration experiments were performed in DMSO-$d_6$ at 25.0 °C on a 400 MHz Bruker Avance III 400 NMR spectrometer. A Norrell 507-HP NMR tube was charged with 0.8 mL of a 7.0 mM solution of the host being studied and the ^{1}H NMR spectrum obtained. Sequential additions of a 0.28 M stock solution in DMSO-$d_6$ of the appropriate TBA$^+$ salt were performed in 2−20 μL aliquots with a Gilson P20 pipette.

**Single-Crystal X-ray Crystallography.** Crystal and refinement data are presented in Table S40 (Supporting Information). CCDC 1840843−1840844. All data sets were collected on a Bruker APEX-II Duo dual-source instrument using Mo Kα ($\lambda$ = 0.71073 Å) using $\omega$ and $\varphi$ scans. Single crystals were mounted on Mitegen micromounts in NVH immersion oil, and maintained at a temperature of 100 K using a Cobra cryostream. The diffraction data were reduced and processed using the Bruker APEX suite of programs.[47] Multiscan absorption corrections were applied using SADABS.[48] The data were solved using the Intrinsic Phasing routine in SHELXT and refined with full-matrix least-squares procedures using SHELXL-2015 within the OLEX-2 GUI.[49−51] All non-hydrogen atoms were refined with anisotropic displacement parameters. All hydrogen atoms were placed in calculated positions and refined with a riding model, with isotropic displacement parameters equal to either 1.2 or 1.5 times the isotropic equivalent of their carrier atoms, unless involved in hydrogen bonding, in which case atoms were explicitly located from the Fourier residuals (where possible). Specific collection and refinement strategies, and treatment of the disorder in **1**(TBAOAc)$_2$·3H$_2$O, are further outlined in the combined crystallographic information file (CIF).

**Synthesis and Characterization.** *1,3-Phenylene-bis(3-(4′-methoxyphenyl)urea) (1).* *meta*-Phenylene diamine (56 mg, 0.52 mmol) and 4-methoxyphenyl isocyanate (0.15 mL, 1.2 mmol, 2.2 equiv) were ground together and CHCl$_3$ (5 mL) added as a solvent. The resulting white slurry was diluted with MeOH (10 mL), sonicated, and separated by centrifugation, and the process was repeated with MeOH (5 × 10 mL) and MeCN (3 × 10 mL). Compound **1** was obtained as a white powder in 52% yield (110 mg, 2.7 mmol). mp 294 °C dec HRMS−ESI (*m/z*): [M + H]$^+$ calcd for C$_{22}$H$_{23}$N$_4$O$_4$, 407.1714; found 407.1718. ^{1}H NMR (600 MHz, DMSO-$d_6$, $\delta$) 8.58 (s, 2H, NH, H*a*), 8.38 (s, 2H, NH, H*b*), 7.62 (t, *J* = 2.0 Hz, 1H, H*c*), 7.41−7.29 (m, 4H, H**2**′), 7.14 (dd, *J* = 8.8, 7.2 Hz, 1H, H*d*), 7.04 (dd, *J* = 7.5, 2.0 Hz, 2H, H*e*), 6.93−6.80 (m, 4H, H**3**′), 3.72 (s, 6H, CH$_3$). ^{13}C NMR (151 MHz, DMSO-$d_6$, $\delta$) 154.5 (quat., C**4**′), 152.7 (quat., C═O), 140.3 (quat., C−N), 132.8 (quat., C−N, C**1**′), 129.1 (C*d*), 120.0 (C**2**′), 114.0 (C**3**′), 111.5 (C*e*), 107.7 (C*c*), 55.2 (CH$_3$). FTIR (ATR, powder) $\nu_{max}$ (cm$^{-1}$): 3301 (m, N−H str.), 1638 (s, C═O str.), 1599 (m), 1560 (s, N−H vib.), 1510 (s), 1491 (s), 1403 (m), 1298 (m), 1218 (s, C−O str.), 1180 (m, N−C−N str.), 1108 (w), 1033 (m, C−O str.), 878 (w), 834 (m), 799 (m), 772 (m), 754 (m), 722 (m), 707 (m). Anal. Calcd for C$_{22}$H$_{22}$N$_4$O$_4$: C, 65.01; H, 5.46; N, 13.78. Found: C, 64.96; H, 5.49; N, 13.83.

*1(TBAOAc)$_2$·3H$_2$O.* The 4′-methoxy substituted derivative **1** was dissolved in a boiling mix of CHCl$_3$ and EtOAc in the presence of excess TBA$^+$ AcO$^-$ and H$_2$PO$_4^-$. The solution was filtered while hot,

and small thin white crystals of **1**(TBAOAc)$_2$·3H$_2$O were obtained by slow evaporation of the solvent. This material was then recrystallized from MeCN to yield crystals of a higher quality.

*1,3-Phenylene-bis(3-(3'-methoxyphenyl)urea) (2).* An alternate synthesis and the complete characterization of compound **2** has been previously reported.[52] *meta*-Phenylene diamine (53 mg, 0.49 mmol) and 3-methoxyphenyl isocyanate (0.15 mL, 1.1 mmol, 2.3 equiv) were ground together and CHCl$_3$ (5 mL) added as a solvent. The resulting white slurry was diluted with MeOH (10 mL), sonicated, and separated by centrifugation, and the process was repeated with MeOH (5 × 10 mL) and MeCN (3 × 10 mL). Compound **2** was obtained as a white powder in 71% yield (141 mg, 0.35 mmol). mp 276 °C dec (lit. 294−297 °C) HRMS−ESI (*m/z*): [M + H]$^+$ calcd for C$_{22}$H$_{23}$N$_4$O$_4$, 407.1714; found 407.1725. $^1$H NMR (400 MHz, DMSO-*d$_6$*, δ): 8.68 (s, 2H, NH, H*a*), 8.59 (s, 2H, NH, H*b*), 7.66 (t, *J* = 1.8 Hz, 1H, H*c*), 7.23−7.12 (m, 5H, H*d*, H**5'**, H**2'**), 7.06 (dd, *J* = 8.1, 1.5 Hz, 2H, H*e*), 6.91 (dd, *J* = 8.0, 1.2 Hz, 2H, H**6'**), 6.55 (dd, *J* = 8.1, 2.2 Hz, 2H, H**4'**), 3.73 (s, 6H, CH$_3$). $^{13}$C NMR (101 MHz, DMSO-*d$_6$*, δ): 159.8 (quat.), 152.4 (quat.), 141.0 (quat.), 140.1 (quat.), 129.6 (CH, C**5'**), 129.2 (CH, C*d*), 111.8 (CH, C*e*), 110.5 (CH, C**6'**), 107.9 (CH, C*c*), 107.3 (CH, C**4'**), 103.9 (CH, C**2'**), 55.0 (CH$_3$). FTIR (ATR, powder) ν$_{max}$ (cm$^{-1}$): 3274 (m, N−H str.), 1635 (s, C=O str.), 1600 (m), 1560 (s, N−H bend), 1490 (m), 1464 (m), 1402 (m), 1290 (m), 1269 (m), 1208 (m), 1167 (m, N−C−N str.), 1155 (m, N−C−N str.), 1080 (w), 1035 (m, C−O str.), 937 (w), 855 (m), 828 (w), 788 (m), 777 (m), 716 (m), 693 (m), 648 (s), 633 (s). Anal. Calcd for C$_{22}$H$_{22}$N$_4$O$_4$: C, 65.01; H, 5.46; N, 13.78. Found: C, 64.84; H, 5.33; N, 13.71.

**2**$_3$(TBA$_3$H$_3$P$_2$O$_8$)·0.5CHCl$_3$. The 3'-methoxy substituted derivative **2** was dissolved in a boiling mix of CHCl$_3$ and EtOAc in the presence of excess TBA$^+$ AcO$^-$ and H$_2$PO$_4$$^-$. The orange solution was filtered while hot, and crystals of **2**$_3$(TBA$_3$H$_3$P$_2$O$_8$)·0.5CHCl$_3$ were obtained by slow evaporation of the solvent. FTIR (ATR, microcrystalline) ν$_{max}$ (cm$^{-1}$): 3286 (w), 3210 (w), 2961 (m), 2874 (w), 2065 (w), 1697 (m), 1612 (m), 1598 (s), 1546 (s), 1479 (s), 1451 (s), 1436 (m), 1401 (w), 1380 (w), 1324 (m), 1292 (s), 1285 (m), 1264 (w), 1207 (s), 1155 (s), 1040 (s), 994 (m), 969 (m), 952 (m), 925 (m), 859 (m), 828 (m), 775 (s), 754 (m), 736 (m), 689 (s), 663 (w).

*1,3-Phenylene-bis(3-(4'-hydroxyphenyl)urea) (3).* 1,3-Phenylene diisocyanate (501 mg, 3.13 mmol) and *para*-aminophenol (884 mg, 8.10 mg, 2.6 equiv) were added to CHCl$_3$ (8 mL) and agitated; the thick mixture was ground together, filtered, triturated in MeOH, and filtered to obtain compound **3** as a brown solid in 58% yield (685 mg, 1.81 mmol). Decomp. 240−250 °C. HRMS−ESI (*m/z*): [M + H]$^+$ Calcd for C$_{20}$H$_{19}$N$_4$O$_4$, 379.1406; found 379.1404. $^1$H NMR (600 MHz, DMSO-*d$_6$*, δ): 9.06 (s, 2H, OH), 8.54 (s, 2H, NH, H*a*), 8.25 (s, 2H, NH, H*b*), 7.60 (s, 1H, H*c*), 7.21 (d, *J* = 8.8 Hz, 4H, H**2'**), 7.17−7.09 (m, 1H, H*d*), 7.09−6.97 (m, 2H, H*e*), 6.68 (d, *J* = 8.8 Hz, 4H, H**3'**). $^{13}$C NMR (101 MHz, DMSO-*d$_6$*, δ): 152.8 (quat.), 152.6 (quat.), 140.5 (quat., C−N), 131.2 (quat., C−N, C**1'**), 129.1 (C*d*), 120.5 (C**2'**), 115.3 (C**3'**), 111.4 (C*e*), 107.6 (C*c*). FTIR (ATR, powder) ν$_{max}$ (cm$^{-1}$): 3300 (m, N−H str.), 1638 (s, C=O str.), 1601 (m), 1561 (s, NH), 1509 (s), 1492 (s), 1460 (m), 1406 (w), 1298 (m), 1213 (s, C−O str.), 878 (w), 838 (m), 808 (m), 780 (m), 754 (m), 730 (w).

*1,3-Phenylene-bis(3-(3'-hydroxyphenyl)urea) (4).* 3-Aminophenol (712 mg, 6.53 mmol, 2.1 equiv) and 1,3-phenylene diisocyanate (501 mg, 3.13 mmol) were added to THF (15 mL) and agitated for 2 h. The resulting suspension was filtered and the solid was washed with THF. Compound **4** was obtained as an off-white solid and dried in air (587 mg, 1.55 mmol, 50% yield). mp c. 250 °C dec HRMS−ESI (*m/z*): [M + Na]$^+$ calcd for C$_{20}$H$_{18}$N$_4$O$_4$Na, 401.1226; found 401.1215. $^1$H NMR (400 MHz, DMSO-*d$_6$*, δ): 9.30 (s, 2H, OH), 8.61 (s, 2H, NH, H*a*), 8.48 (s, 2H, NH, H*b*), 7.66 (s, 1H, H*c*), 7.15 (t, *J* = 8.0 Hz, 1H, H*d*), 7.09−6.96 (m, 6H, H*e*, H**5'**, H**2'**), 6.78 (d, *J* = 8.1 Hz, 2H, H**6'**), 6.36 (d, *J* = 8.1 Hz, 2H, H**4'**). $^{13}$C NMR (101 MHz, DMSO-*d$_6$*, δ): 157.8 (quat.), 152.3 (quat.), 140.8 (quat.), 140.2 (quat.), 129.5 (C**5'**), 129.1 (C*d*), 111.6 (C*e*), 109.0 (C**4'**), 108.8 (C**6'**), 107.7 (C*c*), 105.2 (C**2'**). FTIR (ATR, powder) ν$_{max}$ (cm$^{-1}$): 3308 (m, N−H str.), 1647 (s, C=O str.), 1602 (m), 1560 (s, NH bend), 1489 (s), 1448

(m), 1407 (m), 1289 (m), 1218 (s, C−O str.), 1156 (s, N−C−N str.), 1049 (m, C−O str.), 947 (w), 883 (m), 855 (m), 836 (m), 787 (m), 748 (m), 731 (m), 686 (s).

## ASSOCIATED CONTENT

**ⓢ Supporting Information**

The Supporting Information is available free of charge on the ACS Publications website at DOI: 10.1021/acs.joc.8b01481.

> Crystallographic data for **1**(TBAOAc)$_2$·3H$_2$O (CIF)
> NMR spectra, IR spectra, MS data, NMR titration data, notes on calculations, and XRD data (PDF)

## AUTHOR INFORMATION

**Corresponding Author**
*E-mail: gunnlaut@tcd.ie.

**ORCID** ⓘ

Chris S. Hawes: 0000-0001-6902-7939
Thorfinnur Gunnlaugsson: 0000-0003-4814-6853

## ACKNOWLEDGMENTS

## REFERENCES

(1) Aletti, A. B.; Gillen, D. M.; Gunnlaugsson, T. Luminescent/colorimetric Probes and (Chemo-) Sensors for Detecting Anions based on Transition and Lanthanide Ion Receptor/binding Complexes. *Coord. Chem. Rev.* **2018**, *354*, 98−120.

(2) (a) Gale, P. A.; Caltagirone, C. Fluorescent and Colorimetric Sensors for Anionic Species. *Coord. Chem. Rev.* **2018**, *354*, 2−27. (b) Busschaert, N.; Caltagirone, C.; Van Rossom, W.; Gale, P. A. Applications of Supramolecular Anion Recognition. *Chem. Rev.* **2015**, *115*, 8038−8155. (c) Gale, P. A.; Howe, E. N.W.; Wu, X. Anion Receptor Chemistry. *Chem.* **2016**, *1*, 351−422.

(3) Evans, N. H.; Beer, P. D. Advances in Anion Supramolecular Chemistry: from Recognition to Chemical Applications. *Angew. Chem., Int. Ed.* **2014**, *53*, 11716−11754.

(4) (a) Yang, D.; Zhao, J.; Yang, X.-J.; Wu, B. Anion-coordination-directed Self-assemblies. *Org. Chem. Front.* **2018**, *5*, 662−690. (b) He, Q.; Tu, P.; Sessler, J. L. Supramolecular Chemistry of Anionic Dimers, Trimers, Tetramers, and Clusters. *Chem.* **2018**, *4*, 46−93.

(5) Elmes, R. B.; Jolliffe, K. A. Anion Recognition by Cyclic Peptides. *Chem. Commun.* **2015**, *51*, 4951−4968.

(6) (a) Blažek Bregović, V.; Basarić, N.; Mlinarić-Majerski, K. Anion Binding with Urea and Thiourea Derivatives. *Coord. Chem. Rev.* **2015**, *295*, 80−124. (b) Lowe, A. J.; Dyson, G. A.; Pfeffer, F. M. Steric and Electronic Factors Influencing Recognition by a Simple, Charge Neutral Norbornene Based Anion Receptor. *Org. Biomol. Chem.* **2006**, *5*, 1343−1346. (c) Lowe, A. J.; Dyson, G. A.; Pfeffer, F. M. Factors Influencing Anion Binding Stoichiometry: The Subtle Influence of Electronic Effects. *Eur. J. Org. Chem.* **2008**, *2008*, 1559−1567.

(7) (a) Pandurangan, K.; Aletti, A. B.; Montroni, D.; Kitchen, J. A.; Martínez-Calvo, M.; Blasco, S.; Gunnlaugsson, T.; Scanlan, E. M. Supramolecular Anion Recognition Mediates One-pot Synthesis of 3-Amino-[1,2,4]-Triazolo Pyridines from Thiosemicarbazides. *Org. Lett.* **2017**, *19*, 1068−1071. (b) Pandurangan, K.; Kitchen, J. A.;

Gunnlaugsson, T. Colorimetric 'Naked Eye' Sensing of Anions Using a Thiosemicarbazide Receptor: A Case Study of Recognition through Hydrogen Bonding vs Deprotonation. *Tetrahedron Lett.* **2013**, *54*, 2770−2775. (c) Pfeffer, F. M.; Kruger, P. E.; Gunnlaugsson, T. Anion Recognition and Anion-mediated Self-assembly with Thiourea-functionalised Fused [3]Polynorbornyl Frameworks. *Org. Biomol. Chem.* **2007**, *5*, 1894−1902. (d) Esteban-Gomez, D.; Fabbrizzi, L.; Licchelli, M.; Monzani, E. Urea vs Thiourea in Anion Recognition. *Org. Biomol. Chem.* **2005**, *3*, 1495−1500.

(8) (a) Gunnlaugsson, T.; Glynn, M.; Tocci, G. M.; Kruger, P. E.; Pfeffer, F. M. Anion Recognition and Sensing in Organic and Aqueous Media using Luminescent and Colorimetric Sensors. *Coord. Chem. Rev.* **2006**, *250*, 3094−3117. (b) Li, A.-F.; Wang, J.-H.; Wang, F.; Jiang, Y.-B. Anion Complexation and Sensing using Modified Urea and Thiourea-based Receptors. *Chem. Soc. Rev.* **2010**, *39*, 3729−3745. (c) Veale, E. B.; Gunnlaugsson, T. Fluorescent Sensors for Ions based on Organic Structures. *Annu. Rep. Prog. Chem., Sect. B: Org. Chem.* **2010**, *106*, 376−406.

(9) Busschaert, N.; Elmes, R. B. P.; Czech, D. D.; Wu, X.; Kirby, I. L.; Peck, E. M.; Hendzel, K. D.; Shaw, S. K.; Chan, B.; Smith, B. D.; Jolliffe, K. A.; Gale, P. A. Thiosquaramides: pH Switchable Anion Transporters. *Chem. Sci.* **2014**, *5*, 3617−3626.

(10) (a) Custelcean, R. Anion Encapsulation and Dynamics in Self-assembled Coordination Cages. *Chem. Soc. Rev.* **2014**, *43*, 1813−1824. (b) Johnstone, M. D.; Pfeffer, F. M. Bis-thiourea Macrocycles incorporating Fused [n]Polynorbornanes: Binding of Flexible versus Rigid Dicarboxylates. *Supramol. Chem.* **2014**, *26*, 202−206. (c) Lowe, A. J.; Long, B. M.; Pfeffer, F. M. Examples of Regioselective Anion Recognition among a Family of Two-, Three-, and Four-"armed" bis-, tris-, and tetrakis(Thioureido) [n]Polynorbornane hosts. *J. Org. Chem.* **2012**, *77*, 8507−8517. (d) Johnstone, M. D.; Schwarze, E. K.; Ahrens, J.; Schwarzer, D.; Holstein, J. J.; Dittrich, B.; Pfeffer, F. M.; Clever, G. H. Desymmetrization of an Octahedral Coordination Complex Inside a Self-Assembled Exoskeleton. *Chem. - Eur. J.* **2016**, *22*, 10791−10795.

(11) Langton, M. J.; Beer, P. D. Rotaxane and Catenane Host Structures for Sensing Charged Guest Species. *Acc. Chem. Res.* **2014**, *47*, 1935−1949.

(12) Ayme, J.-F.; Beves, J. E.; Campbell, C. J.; Gil-Ramírez, G.; Leigh, D. A.; Stephens, A. J. Strong and Selective Anion Binding within the Central Cavity of Molecular Knots and Links. *J. Am. Chem. Soc.* **2015**, *137*, 9812−9815.

(13) Byrne, J. P.; Blasco, S.; Aletti, A. B.; Hessman, G.; Gunnlaugsson, T. Formation of Self-Templated 2,6-Bis(1,2,3-triazol-4-yl)pyridine [2]Catenanes by Triazolyl Hydrogen Bonding: Selective Anion Hosts for Phosphate. *Angew. Chem., Int. Ed.* **2016**, *55*, 8938−8943.

(14) Ito, S.; Okuno, M.; Asami, M. Differentiation of Enantiomeric Anions by NMR Spectroscopy with Chiral Bisurea Receptors. *Org. Biomol. Chem.* **2018**, *16*, 213−222.

(15) (a) dos Santos, C. M.; McCabe, T.; Watson, G. W.; Kruger, P. E.; Gunnlaugsson, T. The Recognition and Sensing of Anions through "Positive Allosteric Effects" using Simple Urea-amide Receptors. *J. Org. Chem.* **2008**, *73*, 9235−9244. (b) Wu, F.-Y.; Li, Z.; Wen, Z.-C.; Zhou, N.; Zhao, Y.-F.; Jiang, Y.-B. A Novel Thiourea-based Dual Fluorescent Anion Receptor with a Rigid Hydrazine Spacer. *Org. Lett.* **2002**, *4*, 3203−3205.

(16) Boyle, E. M.; McCabe, T.; Gunnlaugsson, T. Synthesis, Photophysical and NMR Evaluations of Thiourea-based Anion Receptors Possessing an Acetamide Moiety. *Supramol. Chem.* **2010**, *22*, 586−597.

(17) Brooks, S. J.; Gale, P. A.; Light, M. E. *ortho*-Phenylenediamine bis-Urea-carboxylate: a New Reliable Supramolecular Synthon. *CrystComm* **2005**, *7*, 586−591.

(18) Wu, B.; Li, S.; Lei, Y.; Hu, H.; de Sousa Amadeu, N.; Janiak, C.; Mathieson, J. S.; Long, D.-L.; Cronin, L.; Yang, X.-J. The Effect of the Spacer of Bis(biurea) Ligands on the Structure of $A_2L_3$-type (A = anion) Phosphate Complexes. *Chem. - Eur. J.* **2015**, *21*, 2588−2593.

(19) Li, S.; Jia, C.; Wu, B.; Luo, Q.; Huang, X.; Yang, Z.; Li, Q.-S.; Yang, X.-J. A Triple Anion Helicate Assembled from a Bis(biurea) Ligand and Phosphate Ions. *Angew. Chem., Int. Ed.* **2011**, *50*, 5721−5724.

(20) Yang, D.; Zhao, J.; Zhao, Y.; Lei, Y.; Cao, L.; Yang, X. J.; Davi, M.; de Sousa Amadeu, N.; Janiak, C.; Zhang, Z.; Wang, Y. Y.; Wu, B. Encapsulation of Halocarbons in a Tetrahedral Anion Cage. *Angew. Chem., Int. Ed.* **2015**, *54*, 8658−8661.

(21) Jia, C.; Zuo, W.; Zhang, D.; Yang, X.-J.; Wu, B. Anion Recognition by oligo-(Thio)urea-based Receptors. *Chem. Commun.* **2016**, *52*, 9614−9627.

(22) Manna, U.; Das, G. Anion Binding Consistency by Influence of Aromatic *meta*-Disubstitution of a Simple Urea Receptor: Regular Entrapment of Hydrated Halide and Oxyanion Clusters. *CrystComm* **2017**, *19*, 5622−5634.

(23) Manna, U.; Chutia, R.; Das, G. Entrapment of Cyclic Fluoride-Water and Sulfate-Water-Sulfate Cluster Within the Self-assembled Structure of Linear *meta*-Phenylene Diamine Based Bis-Urea Receptors: Positional Isomeric effect. *Cryst. Growth Des.* **2016**, *16*, 2893−2903.

(24) Manna, U.; Kayal, S.; Samanta, S.; Das, G. Fixation of Atmospheric $CO_2$ as Novel carbonate-(water)$_2$-carbonate Cluster and Entrapment of Double Sulfate within a Linear Tetrameric Barrel of a Neutral bis-Urea Scaffold. *Dalton Trans* **2017**, *46*, 10374−10386.

(25) Ghosh, K.; Adhikari, S.; Fröhlich, R.; Petsalakis, I. D.; Theodorakopoulos, G. Experimental and Theoretical Anion Binding Studies on Coumarin Linked Thiourea and Urea Molecules. *J. Mol. Struct.* **2011**, *1004*, 193−203.

(26) Casula, A.; Bazzicalupi, C.; Bettoschi, A.; Cadoni, E.; Coles, S. J.; Horton, P. N.; Isaia, F.; Lippolis, V.; Mapp, L. K.; Marini, G. M.; Montis, R.; Scorciapino, M. A.; Caltagirone, C. Fluorescent Asymmetric bis-Ureas for Pyrophosphate Rcognition in Pure Water. *Dalton Trans* **2016**, *45*, 3078−3085.

(27) Pike, S. J.; Hutchinson, J. J.; Hunter, C. A. H-Bond Acceptor Parameters for Anions. *J. Am. Chem. Soc.* **2017**, *139*, 6700−6706.

(28) Boiocchi, M.; Del Boca, L.; Gomez, D. E.; Fabbrizzi, L.; Licchelli, M.; Monzani, E. Nature of Urea-fluoride Interaction: Incipient and Definitive Proton Transfer. *J. Am. Chem. Soc.* **2004**, *126*, 16507−16514.

(29) Thordarson, P. Determining Association Constants from Titration Experiments in Supramolecular Chemistry. *Chem. Soc. Rev.* **2011**, *40*, 1305−1323.

(30) Frassineti, C.; Ghelli, S.; Gans, P.; Sabatini, A.; Moruzzi, M. S.; Vacca, A. Nuclear Magnetic Resonance as a Tool for Determining Protonation Constants of Natural Polyprotic Bases in Solution. *Anal. Biochem.* **1995**, *231*, 374−382.

(31) Bregović, N.; Cindro, N.; Frkanec, L.; Užarević, K.; Tomišić, V. Thermodynamic Study of Dihydrogen Phosphate Dimerisation and Complexation with Novel Urea- and Thiourea-Based Receptors. *Chem. - Eur. J.* **2014**, *20*, 15863−15871.

(32) Rull, F.; Del Valle, A.; Sobron, F.; Veintemillas, S. Raman Study of Phosphate Dimerization in Aqueous $KH_2PO_4$ Solutions using a Self-deconvolution Method. *J. Raman Spectrosc.* **1989**, *20*, 625−631.

(33) Rajbanshi, A.; Wan, S.; Custelcean, R. Dihydrogen Phosphate Clusters: Trapping $H_2PO_4^-$ Tetramers and Hexamers in Urea-Functionalized Molecular Crystals. *Cryst. Growth Des.* **2013**, *13*, 2233−2237.

(34) Amendola, V.; Boiocchi, M.; Esteban-Gomez, D.; Fabbrizzi, L.; Monzani, E. Chiral Receptors for Phosphate Ions. *Org. Biomol. Chem.* **2005**, *3*, 2632−2639.

(35) Kadam, S. A.; Martin, K.; Haav, K.; Toom, L.; Mayeux, C.; Pung, A.; Gale, P. A.; Hiscock, J. R.; Brooks, S. J.; Kirby, I. L.; Busschaert, N.; Leito, I. Towards the Discrimination of Carboxylates by Hydrogen-Bond Donor Anion Receptors. *Chem. - Eur. J.* **2015**, *21*, 5145−5160.

(36) Brooks, S. J.; Gale, P. A.; Light, M. E. Carboxylate Complexation by 1,1'-(1,2-Phenylene)bis(3-phenylurea) in Solution and the Solid State. *Chem. Commun.* **2005**, *37*, 4696−4698.

(37) Dias, C. M.; Li, H.; Valkenier, H.; Karagiannidis, L. E.; Gale, P. A.; Sheppard, D. N.; Davis, A. P. Anion Transport by *ortho*-Phenylene bis-Ureas across Cell and Vesicle Membranes. *Org. Biomol. Chem.* **2018**, *16*, 1083−1087.

(38) (a) Pandurangan, K.; Kitchen, J. A.; Blasco, S.; Boyle, E. B.; Fitzpatrick, B.; Feeney, M.; Kruger, P. E.; Gunnlaugsson, T. Unexpected Self-Sorting Self-Assembly Formation of a [4:4] Sulfate:Ligand Cage from a Preorganized Tripodal Urea Ligand. *Angew. Chem., Int. Ed.* **2015**, *54*, 4566−4570. (b) dos Santos, C. M.; Boyle, E. M.; De Solis, S.; Kruger, P. E.; Gunnlaugsson, T. Selective and Tuneable Recognition of Anions using $C_{(3v)}$-symmetrical Tripodal Urea-amide Receptor Platforms. *Chem. Commun.* **2011**, *47*, 12176−12178.

(39) Brunetti, E.; Picron, J.-F.; Flidrova, K.; Bruylants, G.; Bartik, K.; Jabin, I. Fluorescent Chemosensors for Anions and Contact Ion Pairs with a Cavity-Based Selectivity. *J. Org. Chem.* **2014**, *79*, 6179−6188.

(40) Portis, B.; Mirchi, A.; Emami Khansari, M.; Pramanik, A.; Johnson, C. R.; Powell, D. R.; Leszczynski, J.; Hossain, M. A. An Ideal $C_3$-Symmetric Sulfate Complex: Molecular Recognition of Oxoanions by *m*-Nitrophenyl- and Pentafluorophenyl-Functionalized Hexaurea Receptors. *ACS Omega* **2017**, *2*, 5840−5849.

(41) Etter, M. C. Encoding and Decoding Hydrogen-bond Patterns of Organic Compounds. *Acc. Chem. Res.* **1990**, *23*, 120−126.

(42) Some examples include: (a) Keegan, J.; Kruger, P. E.; Nieuwenhuyzen, M.; O'Brien, J.; Martin, N. Anion Directed Assembly of a Dinuclear Double Helicate. *Chem. Commun.* **2001**, 2192−2193. (b) Coles, S. J.; Frey, J. G.; Gale, P. A.; Hursthouse, M. B.; Light, M. E.; Navakhun, K.; Thomas, G. L. Anion-directed Assembly: the First Fluoride-directed Double Helix. *Chem. Commun.* **2003**, 568−569. (c) Selvakumar, P. M.; Jebaraj, P. Y.; Sahoo, J.; Suresh, E.; Prathap, K. J.; Kureshy, R. I.; Subramanian, P. S. The First Bromide Ion Directed Double Helicate and its Role in Catalysis. *RSC Adv.* **2012**, *2*, 7689−7692. (d) Haketa, Y.; Maeda, H. From Helix to Macrocycle: Anion-Driven Conformation Control of *p*-Conjugated Acyclic Oligopyrroles. *Chem. - Eur. J.* **2011**, *17*, 1485−1492. (e) Jia, C.; Zuo, W.; Yang, D.; Chen, Y.; Cao, L.; Custelcean, R.; Hostaš, J.; Hobza, P.; Glaser, R.; Wang, Y.-Y.; Yang, X.-J.; Wu, B. Selective Binding of Choline by a Phosphate-coordination-based Triple Helicate featuring an Aomatic Box. *Nat. Commun.* **2017**, *8*, 938. (f) Sánchez-Quesada, J.; Seel, C.; Prados, P.; de Mendoza, J.; Dalcol, I.; Giralt, E. Anion Helicates: Double Strand Helical Self-Assembly of Chiral Bicyclic Guanidinium Dimers and Tetramers around Sulfate Templates. *J. Am. Chem. Soc.* **1996**, *118*, 277−278.

(43) Calderon-Kawasaki, K.; Kularatne, S.; Li, Y. H.; Noll, B. C.; Scheidt, W. R.; Burns, D. H. Synthesis of Urea Picket Porphyrins and Their Use in the Elucidation of the Role Buried Solvent Plays in the Selectivity and Stoichiometry of Anion Binding Receptors. *J. Org. Chem.* **2007**, *72*, 9081−9087.

(44) (a) Dydio, P.; Zieliński, T.; Jurczak, J. 7,7′-Diureido-2,2′-diindolylmethanes: Anion Receptors Effective in a Highly Competitive Solvent, Methanol. *Org. Lett.* **2010**, *12*, 1076−1078. (b) Zhang, Y.; Zhang, R.; Zhao, Y.; Ji, L.; Jia, C.; Wu, B. Anion Binding of tris-(Thio)urea Ligands. *New J. Chem.* **2013**, *37*, 2266−2270.

(45) Etter, M. C.; Panunto, T. W. 1,3-Bis(*m*-nitrophenyl)urea: an Exceptionally Good Complexing Agent for Proton Acceptors. *J. Am. Chem. Soc.* **1988**, *110*, 5896−5897.

(46) (a) Esteban-Gomez, D.; Fabbrizzi, L.; Licchelli, M. Why, on Interaction of Urea-based Receptors with Fluoride, Beautiful Colors Develop. *J. Org. Chem.* **2005**, *70*, 5717−5720. (b) Evans, L. S.; Gale, P. A.; Light, M. E.; Quesada, R. Anion Binding vs. Deprotonation in Colorimetric Pyrrolylamidothiourea Based Anion Sensors. *Chem. Commun.* **2006**, 965−967. (c) Gunnlaugsson, T.; Kruger, P. E.; Jensen, P.; Pfeffer, F. M.; Hussey, G. M. Simple Naphthalimide Based Anion Sensors: Deprotonation Induced Colour Changes and $CO_2$ Fixation. *Tetrahedron Lett.* **2003**, *44*, 8909−8913. (d) Pandurangan, K.; Kitchen, J. A.; Gunnlaugsson, T. Colorimetric 'Naked Eye' Sensing of Anions using a Thiosemicarbazide Receptor: A Case Study of Recognition through Hydrogen Bonding versus Deprotonation. *Tetrahedron Lett.* **2013**, *54*, 2770−2775.

(47) *APEX-3*; Bruker-AXS Inc.: Madison, WI, 2016.

(48) *SADABS*; Bruker-AXS Inc.: Madison, WI, 2016.

(49) Sheldrick, G. SHELXT - Integrated Space-group and Crystal-structure Determination. *Acta Crystallogr., Sect. A: Found. Adv.* **2015**, *71*, 3−8.

(50) Sheldrick, G. Crystal Structure Refinement with SHELXL. *Acta Crystallogr., Sect. C: Struct. Chem.* **2015**, *71*, 3−8.

(51) Dolomanov, O. V.; Bourhis, L. J.; Gildea, R. J.; Howard, J. A. K.; Puschmann, H. OLEX2: A Complete Structure Solution, Refinement and Analysis Program. *J. Appl. Crystallogr.* **2009**, *42*, 339−341.

(52) Easton, A.; Gould, P.; Marsh, A. Use of DDX3X Inhibitors for the Treatment of Pneumovirus Infections. Patent WO 2015136292 A1, 2014.

Review

# Luminescent/colorimetric probes and (chemo-) sensors for detecting anions based on transition and lanthanide ion receptor/binding complexes

Anna B. Aletti [1], Dermot M. Gillen [1], Thorfinnur Gunnlaugsson [*]

School of Chemistry and Trinity Biomedical Sciences Institute, Trinity College Dublin, The University of Dublin, Dublin 2, Ireland

ABSTRACT

Herein, some of the recent developments in the design and study of transition metal (d-metal) and lanthanide (f-metal) based sensors, probes and reagents for detecting anions in organic or competitive media will be reviewed. Some examples of main group and actinide-based sensors are also featured. In all cases, the anion recognition is probed by monitoring changes in the various photophysical properties of these complexes, with particular focus being paid to recent examples from the literature where the anion recognition event is communicated through colorimetric or luminescent (fluorescence or phosphorescence) changes. A select number of examples reported within the last 5 years (since 2011) are featured; the focus of this review is on those developed from organic ligands that can, in a synergetic manner with the metal ions, directly aid or enhance the anion recognition and sensing processes. Examples where such synergy is provided by hydrogen bonding interactions are particularly discussed.

© 2017 Published by Elsevier B.V.

## Contents

---

* Corresponding author.
    E-mail address: gunnlaut@tcd.ie (T. Gunnlaugsson).
[1] These authors contributed equally to the writing of this review.